Seismic Performance of Retrofitted Reinforced Concrete Bridge Piers

Laboratory Testing of the Proposed Thorndon Overbridge Retrofit Scheme

A thesis submitted in partial fulfilment of the requirements for the
Degree of Doctor of Philosophy in Civil Engineering
at the University of Canterbury

BY

ROBERT A. PRESLAND

SUPERVISED BY

J. I. RESTREPO

R. PARK

University of Canterbury,
Christchurch,
New Zealand

1999

ABSTRACT

This thesis describes the experimental set-up and testing of two scale models of particular piers of the Thorndon Overbridge incorporating the proposed retrofit measures to be included in the structure.

Each test specimen represented the structural model developed for the analysis of the Overbridge structure incorporating the proposed retrofit designs for each pier. Modelling of the boundary conditions of the structural model were incorporated into the test specimens by including elements to represent the variable stiffness properties of the piles in the structure under tension and compression.

Testing revealed potential deficiencies with the original structure and the proposed retrofit designs which would have limited the seismic performance of the retrofitted piers. Repairs to the test specimens showed improved seismic performance could be obtained and recommendations for the proposed retrofit designs are included.

A method for assessing the capacity of bridge columns containing curtailed longitudinal reinforcement is proposed following the results of the test programme. This method provides a lower bound strength for columns which compares well to the experimental results from the two test specimens.

Flexural strength enhancement over the ACI ideal moment is known to occur due to assumptions made when determining the ACI ideal moment. Expressions are presented which predict the ACI ideal moment and the maximum flexural strength of rectangular shaped columns. The observed shift in the critical section of a column, when confined by an adjacent member, and its influence on the flexural strength enhancement is investigated. A statistical analysis of a number of experimental column tests has indicated this to be a significant component of the flexural strength enhancement observed during testing.

ACKNOWLEDGEMENTS

The experimental research component of this project was carried out for Beca Carter Hollings and Ferner Ltd. (BCHF) on behalf of Transit New Zealand as part of the seismic retrofitting of the Thorndon Overbridge in Wellington. This research was completed at the Department of Civil Engineering, University of Canterbury under the supervision of Dr. Jose Restrepo and Professor Bob Park. I would like to thank both of my supervisors for their time, guidance, assistance and encouragement during my time spent on this project.

This test programme could not have been completed without the extensive involvement and co-operation of the technicians in the Department. Thank you to the number of technicians who were involved during various part of the project:- Ray Allen, George Clarke (now retired), Peter Coursey, Nigel Dixon, Gary Harvey, Norrie Hickey, John Maley, Russell McConchie, Paul Murphy, Richard Newton, Mark Stuart-Jones, Mike Weavers and Gavin Hill, who sadly passed away shortly after completion of the laboratory work. Thanks also to Val Grey and Melody Callahan for their part in preparing slides and figures for this project.

To the other graduate students of the Department during my time here, thank you for all the encouragement, advice, assistance, helping to keep things interesting and fun when not concentrating on work, getting me into trouble and keeping me out of trouble. Thanks especially to:- Chris Allington, Al Chambers, Jason Clements, Mark Ellis, Jeff Matthews, Dr. Nathan Schmidt and all the others who should be included here but escape me for the moment. Thanks also to Tony Parkes, long standing flatmate and friend, Roger Dawe who has kept me gainfully employed explaining the ins and outs of surveying and Des Bull for all his comments and advice, requested or not.

Lastly and importantly thank you to my family for all their support and encouragement over the years, often when not fully understanding what I've been up to. It's been of great importance knowing you were always there and that I could always fall back to you when I needed.

NOTATION

A_c = area of core enclosed by centreline of transverse reinforcement

A_{cc} = area of concrete enclosed by centreline of transverse reinforcement

A_e = area of effectively confined core concrete

A_g = gross cross-sectional area

A_s = area of tension reinforcement

A_{st} = total area of longitudinal steel

A_{sp} = area of transverse spiral or hoop reinforcing bar

A_{sx} = area of transverse reinforcement in x direction

A_{sy} = area of transverse reinforcement in y direction

A_v = total area of transverse reinforcement in a stirrup set crossing the critical crack in the direction of applied shear force

a_h = depth of horizontal arching in a column

a_v = depth of vertical arching in a column

B = width of square or rectangular concrete column

B_c = width of square or rectangular concrete core, measured to centreline of transverse reinforcement

c = neutral axis depth measured from compression face of member

D = diameter of circular column

D = depth of rectangular or square column

D_c = diameter of circular concrete core, measured to centreline of hoop or spiral

D_c = depth of square or rectangular concrete core, measured to centreline of transverse reinforcement

D_{cc} = depth of effectively confined concrete core

D′ = diameter of circular concrete core or depth of square or rectangular concrete core, measured to outside of transverse reinforcement

D″ = pitch of circular arrangement of longitudinal reinforcement, for circular columns, or distance between centrelines of reinforcing bars closest to faces of rectangular columns

d = distance from extreme compression fibre to the tension reinforcement

= effective depth of member

d_b = diameter of longitudinal reinforcing bar

d_{bh} = diameter of transverse reinforcing bar

E_c = initial Young's Modulus of Elasticity for concrete

E_{sec} = confined concrete secant modulus at peak stress

E_s = Young's Modulus of Elasticity for steel

E_{sh} = strain hardening modulus for steel

e_v = magnitude of tension shift

f_c = concrete stress

f'_c = 28 day compressive strength of concrete cylinder, specified concrete strength

f'_{cc} = confined concrete compressive strength

f'_{co} = unconfined concrete compressive strength

= $0.85\ f'_c$

f_l = lateral confining pressure

f_{lx} = lateral confining pressure in x direction

f_{ly} = lateral confining pressure in y direction

f'_l = effective lateral confining pressure

f'_{lx} = effective lateral confining pressure in x direction

f'_{ly} = effective lateral confining pressure in y direction

f'_{l1} = smallest effective lateral confining pressure

f'_{l2} = largest effective lateral confining pressure

f_s = steel tensile stress

f'_s = steel compressive stress

f'_{sp} = tensile splitting strength of concrete

f_{su} = ultimate stress of longitudinal reinforcement

f_u = ultimate stress of longitudinal reinforcement

f_y = yield stress of longitudinal reinforcement

f_{yh} = yield stress of transverse reinforcement

g = ratio of pitch of circular arrangement of longitudinal reinforcement to cross section diameter, for circular columns, or distance between reinforcing bars closest to faces of rectangular columns to section depth

H_a = theoretical lateral load to develop nominal flexural strength at base of column determined using moment-curvature analysis incorporating actual material properties measured at time of testing

H_y = theoretical lateral load to develop nominal flexural strength at base of column determined using moment-curvature analysis incorporating assumed material properties

jd = internal lever arm

= distance between compressive and tensile force resultants

k_e = confinement efficiency factor for Mander et al. model based on area

k^*_e = modified confinement efficiency factor for Mander et al. model based on first moment of area

l_c = distance to point of contraflexure

L_d = development length

L_p = plastic hinge length

M^* = maximum measured experimental moment

M_i = flexural strength determined using ACI method and actual material properties

M_n = predicted ACI flexural strength using Equation 8.29

M_o = predicted maximum flexural strength using Equation 8.31

M_y = nominal yield moment from moment-curvature analysis

m = mechanical reinforcement ratio

= $f_y / 0.85f'_c$

N^* = axial load acting on column

N_n = column axial load

P = power term to describe strain hardening region of Mander et al. stress-strain relationship for steel

p_{cc} = volumetric ratio of longitudinal reinforcement to core concrete

p_s = volumetric ratio of confining steel

p_{sx} = volumetric ratio of confining steel in x direction

p_{sy} = volumetric ratio of confining steel in y direction

p_t = longitudinal steel ratio

R = parameter in Mander et al. stress-strain model relating confinement effects on strain at peak stress to strength enhancement

r	=	parameter used in Mander et al. stress-strain model
S_{cc}	=	first moment of area of confined core
S_{ce}	=	first moment of area of effectively confined core
s	=	spacing of transverse reinforcement
s'	=	clear spacing between transverse reinforcement
T	=	resultant force acting in column from tensile longitudinal reinforcement
V	=	shear force
V_n	=	shear capacity of column
V_p	=	shear capacity of column provided by axial load component
V_s	=	shear capacity of column provided by transverse steel component
V_c	=	shear capacity of column provided by concrete component
v_g	=	vertical gap between jacket and supporting member, measured parallel to axis of column
w'	=	average of clear distances between restrained longitudinal bars in column section
y_m	=	maximum depth of arching, midway between hoop sets
α	=	constant used in Mander et al. stress-strain model for confined concrete
α	=	term relating position of compressive force resultant to centreline and internal lever arm of column
α_1	=	strength enhancement factor used in Mander et al. stress-strain model to evaluate peak confined concrete stress due to bi-equal confining stresses
α_1	=	factor defining effective stress in rectangular stress block
α_2	=	reduction factor used in Mander et al. stress-strain model to account for the effect of unequal confinement stresses on peak confined concrete stress
β	=	ratio of moment at the centre of mass at the top of a column to the base column moment
β_1	=	factor defining effective depth of rectangular stress block
β_2	=	ratio of specified concrete strength to confined concrete compressive strength
β_{shift}	=	ratio of shift of the critical section in a column to neutral axis depth of the column at spalling of the cover concrete

δ_{pT} = plastic displacement of test specimen in terms of actual pier

δ_{uT} = ultimate displacement of test specimen in terms of actual pier

δ_{yT} = first yield displacement of test specimen in terms of actual pier

Δ_y = yield displacement

Δ_{uS} = ultimate displacement of actual pier

Δ_{yS} = theoretical first yield displacement of actual pier

Δ_{pT} = plastic displacement of test specimen

Δ_{uT} = ultimate displacement of test specimen

Δ_{yT} = first yield displacement of test specimen

$\Delta_{0.75Hy}$ = average lateral displacement of test specimen from three load cycles to 0.75 H_y

ε_c = concrete strain

ε_{cc} = concrete strain at peak stress for confined concrete

ε_{co} = concrete strain at peak stress for unconfined concrete

ε_{spall} = strain at which cover concrete is considered to have spalled and ceased to carry any stress

ε_{sh} = strain at commencement of strain hardening

ε_{sy} = yield strain for steel

ε_y = yield strain for steel

ε_{su} = strain in steel corresponding to ultimate load

ε_u = strain in steel corresponding to ultimate load

ϕ_y = yield curvature obtained from moment-curvature analysis

η = ratio of shear resisted by stirrups to total shear

η = column width reduction factor to account for loss of cover concrete

= 0.85

λ_e = confined concrete efficiency factor

λ_C = overstrength factor for reinforcing steel in compression

λ_T = overstrength factor for reinforcing steel in tension

μ_Δ = displacement ductility factor

$\mu_{\Delta C}$ = displacement ductility factor of column

$\mu_{\Delta S}$ = displacement ductility factor of actual pier

$\mu_{\Delta T}$ = displacement ductility factor of test specimen

μ_{ϕ} = curvature ductility factor

$\mu_{\phi,f}$ = curvature ductility factor when limited by flexural ductility capacity of column

$\mu_{\phi,s}$ = curvature ductility factor when limited by shear strength capacity of column

ζ = factor depending on number and distribution of longitudinal bars in column

ψ = ratio of number of bars on one end face of a column to the total number of longitudinal bars

TABLE OF CONTENTS

CHAPTER SEVEN - ASSESSMENT OF BRIDGE COLUMNS WITH CURTAILED LONGITUDINAL REINFORCEMENT

CHAPTER EIGHT - ALTERNATIVE MODELLING OF CONFINED CONCRETE STRESS-STRAIN BEHAVIOUR

CHAPTER 1

INTRODUCTION

1.1 BACKGROUND

Recent destructive earthquakes in California and in Japan have resulted in severe damage or collapse of many reinforced concrete bridge structures [E1, E2, E3, H1, J1, L1, N1, N2, N3, N4]. Many of these bridges were designed prior to 1970 and typically did not contain adequate reinforcing details which would have enabled them to perform satisfactorily during these large earthquakes. Following the Loma Prieta earthquake in 1989 much focus has been on assessing the risk of existing bridge structures to major damage and/or collapse during a large earthquake. Extensive seismic assessment and retrofit programs have been initiated in California after the Loma Prieta earthquake, the Northridge earthquake in 1994 and also in Japan following the 1995 Hyogo-ken Nanbu (Kobe) earthquake. In conjunction with the implementation of seismic assessment programs and construction of seismic retrofit measures, a number of research programs have been carried out which has resulted in improved methods of evaluating the seismic performance of existing bridges and designing retrofit measures.

Since the early 1960's there has been ongoing development of seismic design requirements for reinforced concrete structures. This has eventually led to ductile reinforced concrete and capacity design principles being introduced to earthquake design philosophy in New Zealand [P1, P2]. It is now recognised that many structures designed during this time, without modern capacity design philosophies and adequate detailing, are susceptible to severe damage and possible collapse during relatively moderate earthquakes.

Much of the emphasis for improving seismic assessment and retrofit techniques has come from recent Californian experience of the performance of reinforced concrete structures during earthquakes. This need to assess the likely performance of bridges

and other reinforced concrete structures, in New Zealand, has been recognised and methods to identify and prioritise assessment and retrofit of vulnerable structures have been proposed [M1]. Design and implementation of seismic retrofit measures for New Zealand bridge structures falls short of the work already undertaken in California and in Japan. Fortunately much of the research work undertaken overseas can be applied to New Zealand bridges and as a result much of the retrofit assessment techniques and retrofit measures used in New Zealand has come from recent Californian experience.

1.2 THORNDON OVERBRIDGE

1.2.1 Overview of Structure

The Thorndon Overbridge, in Wellington, consists of two parallel, independent reinforced concrete bridges, each approximately 1.3 km long and carrying three lanes of traffic. On and off ramps provide access to the Overbridge approximately halfway along the bridge.

The Overbridge is located on the edge of Wellington Harbour on land which has been progressively reclaimed from the harbour from 1882 to 1970. The structure carries the Wellington Urban Motorway over the reclaimed foreshore, railway yards, harbour facilities and local arterial roads.

Designed from 1960 to 1967 and completed in 1969, the Thorndon Overbridge forms part of State Highways 1 and 2 leading into and out of Wellington City. The Overbridge was designed in three distinct stages, and as ductile reinforced concrete and capacity design principles were undergoing significant development at this time, the later stages of the Overbridge project are better detailed for seismic resistance. Figure 1.1 shows an aerial view of the Thorndon Overbridge and the various stages of construction.

Figure 1.1 *Aerial View of the Thorndon Overbridge Looking South Toward Wellington City*

Stage One covers nine piers at the northern end of the Overbridge which consist of multi-column bents with four or five 600 mm diameter circular columns per bent. These columns are supported on a common pilecap founded on groups of 600 mm diameter, driven steel cased reinforced concrete piles. A common piercap joins the columns in each bent with the superstructure simply supported at each pier. Figure 1.2 shows Pier 3, a Stage One type pier, with the multiple columns, common piercap, simply supported superstructure I-beams, end diaphragms and linkage bolts.

Figure 1.2 *Stage One Pier - Pier 3*

Stage Two and Stage Three piers are typically single 2.44 m diameter circular reinforced concrete columns each supporting a large cast in place umbrella platform. The superstructure is simply supported at each pier on the umbrella platforms. Stage Two piers extend from the northern end of the Overbridge to approximately half way along the length to the access ramps. These piers are typically supported on octagonal reinforced concrete pilecaps, 7.93 m across and 1.37 m thick, supported on groups of 12 driven steel cased reinforced concrete piles, 600 mm in diameter. Stage Three piers, from the access ramps to the southern abutment, are supported on square

pilecaps 8.53 m square and 2.44 m thick, and four 1.52 m diameter steel cased reinforced concrete bored piles, belled at their bases. Pier heights and span lengths vary throughout the structure with a small number of umbrella platforms supported by multiple columns. Many of the Stage Two piers have their pilecaps interconnected underground by tie beams to restrain the seaward piers to the inland piers to provide against ground movements in the event of an earthquake. Figure 1.3 shows a view looking south toward Wellington City of the Stage Three piers from the Aotea Quay on ramp to the southern abutment at Thorndon.

Figure 1.3 *General View of Stage Three Piers Looking South*

The superstructure, which is common along the entire length of the Overbridge, consists of precast, post-tensioned reinforced concrete I-beams simply supported between each pier. The beams are 1.60 m deep for spans between 19.8 to 27.4 metres in length and 2.34 m deep for spans up to 41.5 metres. The change in beam depth was required over the southern portion of the Overbridge, Stage Three, where increased span lengths were required due to pier foundation locations being dictated by the positions of railway lines in the area. Typically six I-beams are used in each

span with a 150 mm thick deck slab and intermediate diaphragms used to share the loads through the beams comprising a span. End diaphragms are used to eliminate concentrated loads at the umbrella platforms by distributing them throughout the length of the diaphragm at the bearing line.

The on and off ramps are of continuous prestressed box girder construction supported on single stemmed columns, tapering from circular at the base to rectangular at the top, on piled foundations.

The Overbridge was designed to carry the increasing volumes of traffic coming into and out of Wellington City over an area congested with railway lines, local arterial roads and harbour facilities. This structure provides an important lifeline link in the transportation network, forming an essential element in the main highway access into and out of Wellington City.

The Overbridge site has been reclaimed from the edge of Wellington Harbour in several stages from 1882 to 1970. These reclamations have consisted of rock fill or hydraulic fill material overlying the original beach and marine sediments which are prone to liquefaction at relatively low levels of shaking [M2]. Adjacent to the northern segment of the Overbridge is an old concrete gravity seawall used to retain earlier reclamations and partially buried under following reclamations. Liquefaction of the surrounding ground could cause the seawall to collapse leading to lateral spreading of the ground and collapse of some of the piers immediately adjacent to the exposed section of the seawall.

The main earthquake fault for the Wellington region, the Wellington Fault, runs alongside the Thorndon Overbridge for most of its length and crosses beneath the structure at one point, between Piers 25 and 26 (southbound) and Piers 62 and 63 (northbound). A Wellington Fault event has been estimated to have a Richter magnitude of 7.5 and a return period of 600 years with permanent ground displacements of approximately 5 metres horizontally and 1.0 metre vertically at the point where the fault crosses under the Overbridge [B1]. This study also indicates there is a high chance that the next large magnitude earthquake in this area will result from an event on the Wellington Fault.

Due to the importance of this structure to the roading network in the Wellington region and the serious seismic vulnerabilities of the Thorndon Overbridge a seismic assessment and retrofit programme was initiated by Transit New Zealand, the controlling authority responsible for national roads in New Zealand. Beca Carter Hollings and Ferner Ltd. (BCHF), consulting engineers, were engaged to conduct the seismic assessment and seismic retrofit design phases of the Thorndon Overbridge seismic retrofit.

1.2.2 Review of Seismic Assessment

Detailed assessment of the existing structure, site seismicity and geotechnical conditions at the Thorndon Overbridge site were undertaken as part of the seismic assessment of the structure.

Seismicity studies were undertaken to determine the likely seismic hazard and likely effects from active faults in the region surrounding the Thorndon Overbridge site. Geotechnical aspects of the Thorndon Overbridge seismic retrofit programme are described by Marsh and Toan [M2]. The expected seismic performance of the Thorndon Overbridge has been described by Chapman and Kirkaldie [C1] and Billings and Powell [B1]. Retrofit concepts proposed by BCHF have been summarised by Maffei and Park [M1] and cover superstructure linkage retrofit, multi-column bent retrofit, retrofit of single column piers and other retrofit measures to prevent span unseating, ground improvement to prevent liquefaction and solutions to prevent the loss of the spans where the Wellington Fault crosses beneath the Overbridge. Only the aspects of the seismic retrofit relating to the experimental work undertaken as part of this study will be reviewed here.

An extensive retrofit scheme was selected for the Thorndon Overbridge, designed for a ground shaking level corresponding to a 500 year return period earthquake, and designed to mitigate against collapse of the Overbridge due to movement of the Wellington Fault.

1.2.2.1 Single Column Pier Retrofit

As capacity design principles were not applied in the original design of the Thorndon Overbridge, there is no "limiting link" to give a well defined failure mechanism in the lateral load resisting system for the structure. Therefore a procedure, largely based on Californian research, was used to determine the strength and ductility of the critical collapse mechanism for the structure.

For single column piers this revealed that typically the pilecaps of the single column piers would represent the weak link in the structure. It appears that the pilecaps were detailed primarily for gravity moments with an allowance for seismic lateral loading of 0.3g at ultimate limit state [B1]. Therefore the pilecap reinforcement is generally a two way mat in the top and bottom of the pilecap with significantly more steel provided in the bottom of the pilecap. Relatively light flexural reinforcement is provided in the top and no shear reinforcement is present in the pilecaps.

After retrofitting of the pilecaps the inelastic mechanism is typically forced to occur at the base of the columns in the single column piers. The later stages of the project sought to improve column performance by increasing the amounts of transverse reinforcement in the columns above that typically used in construction at the time. Despite the efforts of the designers there is still insufficient reinforcement to ensure adequate column ductility is available when compared to transverse reinforcement requirements using current evaluation methods.

1.2.2.2 Linkage Bolt Retrofit

Superstructure movement joints in the Thorndon Overbridge were better detailed than Californian bridges constructed at the same time: seating lengths for each span are significantly longer [M1]. Linkage bolts are provided at each superstructure joint to tie the adjacent spans together with thick rubber pads at the ends of each linkage bolt to absorb earthquake impact forces. For Stage Two and Stage Three piers the linkage bolts pass through the umbrella platforms at each pier, requiring linkage bolts up to 12.8 m in length. A welded end detail allows the full length of the linkage bolt

to yield giving excellent elongation capacity. Much shorter linkage bolts are used in the Stage One multi-column bent piers, with a threaded end detail, which will give much shorter elongation capacity as failure would occur in the threads. Vertical hold down bolts are also provided to help secure the individual I-beams to their seatings.

Prior to retrofit of the pier pilecaps, the linkage bolts generally will not yield because as failure would occur in the pilecaps themselves. There would be no unseating of the spans but failure of the pilecaps could lead to excessive settlements of the piers and possible collapse of the spans. After retrofitting of the piers, the columns and foundations would have sufficient capacity to cause yielding of the linkage bolts under the induced ground motions. This however could lead to a concentration of the elongation at a single movement joint, leading to collapse of this span. Permanent ground displacements are expected to occur from ground disturbance around the Wellington Fault trace and due to liquefaction of the surrounding site. Movements induced by offset of the Wellington Fault trace will result in large, permanent ground displacements which have been addressed as a separate retrofit measure outside the scope of this study.

1.2.3 Proposed Retrofit Designs

1.2.3.1 Single Column Pier Retrofit Designs

To ensure the reliable seismic performance of bridge structures they are usually designed to allow plastic hinging to occur in the base of the columns. As the pilecaps have been assessed as the weak link in the majority of the single column piers in the Thorndon Overbridge, much of the retrofit work is focused on increasing the strength of these parts of the structure to shift a brittle mode of failure from the pilecap and force inelastic action to concentrate at the base of the columns. This is generally achieved through the use of a new reinforced concrete overlay built over the existing pilecap, post-tensioning cored through the existing pilecap or a combination of both to increase the pilecap's flexural strength. The overlay is connected to the existing pilecap through dowels drilled and grouted into the top surface. Post-tensioning may be cored horizontally through the existing pilecap, where pilecap overlay depths are

limited, with new post-tensioning anchor blocks constructed on the sides of the existing pilecap. Dowels are also provided to overlap with the existing pile reinforcement to transfer the pile tensile load to the top of the new reinforced concrete overlay. Additional reinforcement is also provided in the overlay to increase, along with any post-tensioning present, the strength of the pilecap to induce a plastic hinge in the column.

Typically Stage Two piers require an overlay and post-tensioning to strengthen the pilecap and ensure column hinging will occur. Stage Three piers may be strengthened with the use of a new reinforced concrete overlay only where ground clearances permit. If insufficient clearance is available for an overlay retrofit only, due to the presence of railway tracks or similar services, an overlay and post-tensioning is used to boost the strength of the pilecap. Figure 1.4 shows the proposed retrofit measures for a typical Stage Two single column pier.

Once the pilecap has been strengthened to ensure the formation of a plastic hinge in the column, the available strength and ductility of the columns had to be addressed to ensure they could meet the seismic demands imposed on them. Stage Two piers generally had insufficient transverse reinforcement in the columns to achieve the assessed ductility demand, typically having 12 mm diameter hoops at 300 mm centres at the base of the columns. As a result, 12 mm thick mild steel jackets, 2.5 m high were specified for the bases of the columns over the potential plastic hinge region to provide additional confinement and restrain the column longitudinal bars against buckling.

Stage Three piers had much improved transverse reinforcement details at the base of the columns with typically 20 mm diameter hoops at 100 mm centres. This was believed to be sufficient to ensure ductile performance of the columns and no additional column retrofit was specified. With pilecap-only retrofits of Stage Three piers it is believed that inelastic action could occur in the pilecap and provide satisfactory performance to the pier. Laboratory testing was required to determine whether inelastic pilecap action would occur and the available ductility from any inelastic pilecap response.

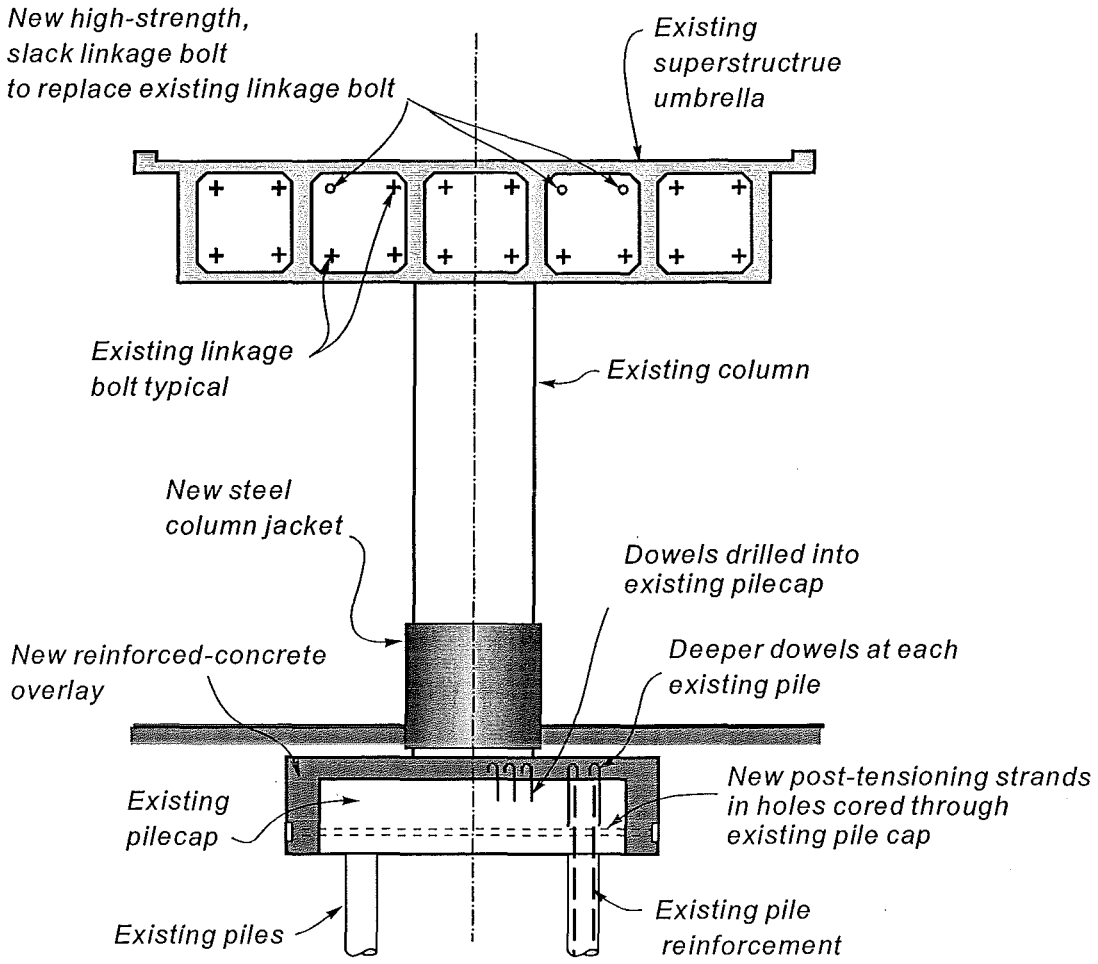

Figure 1.4 *Proposed Single Column Pier Retrofit Measures*

1.2.3.2 Linkage Bolt Retrofit

Retrofit of the linkage bolts requires replacement of some of the existing linkage bolts with new high strength slack linkage bolts at each superstructure umbrella location. This scheme is intended to prevent unseating of individual spans and spread the earthquake induced ground motions out over several span lengths. Yielding of the existing linkage bolts will occur but the new linkage bolts are designed to engage

before unseating of the spans occur, allowing the movements to be distributed over several spans.

Movements due to rupture of the Wellington Fault trace are also distributed through the use of new high strength slack linkage bolts at the piers, to distribute the ground movements over several spans. A support frame is provided to catch the superstructure once it is pulled off the pier umbrella seatings due to the large expected displacements across the fault trace.

1.3 SCOPE OF RESEARCH

1.3.1 Purpose of Laboratory Structural Testing

1.3.1.1 Previous Research Programs

The 1971 San Fernando earthquake in California led to urgent reviews of Californian design practice for the seismic design of bridge structures and initiated a staged programme for the seismic retrofit of existing bridges in California. This programme initially focused on linking adjacent spans to prevent their separation and loss of support during an earthquake. During this time New Zealand placed little emphasis on seismic retrofit of bridges as many bridges built after the 1931 Napier earthquake already had interlinked spans [C1]. The Loma Prieta earthquake in California during 1989 led to an increased commitment to evaluate and retrofit seismically deficient structures and brought further, international, attention to other vulnerable "lifeline" services. The need to maintain the integrity of bridges during an emergency stressed the importance of identifying vulnerable bridges and initiating investigation of what may be done to improve the reliability of these structures against earthquakes.

Assessment of a number of bridge structures has been undertaken since 1990 in New Zealand [C1, C2, C3] and led to a full assessment being undertaken on the Thorndon Overbridge after preliminary assessments indicated justification for a full seismic assessment. This eventually led to the proposal for the seismic retrofit details

outlined in Section 1.2.3. Although extensive research has been conducted, mainly in California, and has provided the theoretical and experimental background for assessing the seismic capacity of bridges, as well as effective and economic methods of retrofit, little seismic assessment and retrofit work has been undertaken on New Zealand bridges. Many of the retrofit measures tested overseas has already been applied to many Californian bridges and a number of Japanese bridges following the Hyogo-ken Nanbu earthquake in 1995.

1.3.1.2 Thorndon Overbridge

The proposed seismic retrofit provisions for the Thorndon Overbridge are similar to those already developed and used in California including the use of steel column jackets, reinforced concrete overlays on pilecaps and post-tensioning of existing pilecaps. These retrofit measures are intended to protect the bridge against collapse during severe ground shaking. Due to the significant number of piers to be retrofitted in the Thorndon Overbridge structural testing was required to investigate the performance of the various retrofit measures proposed. With the significance of the Thorndon Overbridge as a "lifeline structure" to the Wellington region and the scale of the retrofit required, testing was justified to ensure the retrofitted piers were capable of achieving the seismic performance levels required.

1.3.1.3 Pilecap Retrofit for Strength

Testing of the column/pilecap/pile assemblies serves two purposes. The first is to verify the use of a pilecap retrofit using a reinforced concrete overlay and post tensioning to force column hinging, similar to retrofits used in California and tested at the University of California, San Deigo [X1]. Testing will determine the actual test specimen behaviour which can be used to determine the likely performance of the actual structure during an earthquake. Modelling of the structure and the design of the pilecap retrofit details for the Thorndon Overbridge, including assumed mechanisms of load transfer, are different to previously tested retrofits.

The response of the structure is greatly influenced by the stiffness of the piles of each pier and the stiffness of the surrounding soil providing passive resistance to the lateral seismic loading. The loading rig for each test specimen must be able to adequately represent the boundary conditions as assumed for the structural analysis of the existing piers in the Thorndon Overbridge. Appropriate representation of the boundary conditions are necessary to give displacements and force distributions in the test specimens that are of similar magnitude to those obtained from scaling the results from structural analyses of the prototype piers. This requires the modelling of the piles in each pier and the effect of the passive lateral soil pressure on the side of the pilecap.

The stiffness of the piles and of the soil providing the passive pressure reaction have a significant influence on the force distribution through the pilecap. In order to properly model the influence of the piles, the stiffness coefficient of each pile needs to be different in tension and in compression to model the stiffness of the pile in tension and the stiffness of the pile due to end bearing when under compressive loads.

Typical early bridge footings were designed elastically using a relatively low lateral seismic force which often did not predict the pilecap negative moments, as seen in Figure 1.5, that occur when the column reaches flexural strength. As a result there is relatively little reinforcement provided in the top of the pilecaps of the Thorndon Overbridge and it is important to obtain a similar force distribution in the specimens as in the actual structure.

Testing without piles or with piles of equal tensile and compressive stiffness would give different force distributions through the pilecap and would not adequately represent the force distribution in the actual structure. Due to the piles having a smaller relative tension stiffness the positive moment generated in the bottom of the pilecap is significantly higher than the moment generated in the pilecap on the opposite side of the column.

1.3.1.4 Pilecap Retrofit for Ductility

The second purpose of testing is to verify whether inelastic action in the pilecap will occur and determine the available ductility from flexural behaviour of the pilecap. The pilecaps may not be able to sustain the required levels of ductility without suffering shear failure or buckling of the bottom reinforcement. As the seismic response of up to 75% of the Thorndon Overbridge piers rely on the retrofitted pilecap forcing ductile behaviour at the bases of the columns, testing must be carried out to verify the performance of the retrofitted pilecaps in forcing the ductile behaviour to occur in the columns. The possibility of inelastic pilecap action in Stage Three piers must be verified and evaluated as no previous retrofit has relied on pilecap flexural ductility for seismic performance.

While previous work has been done on bridge structure seismic retrofit, the design

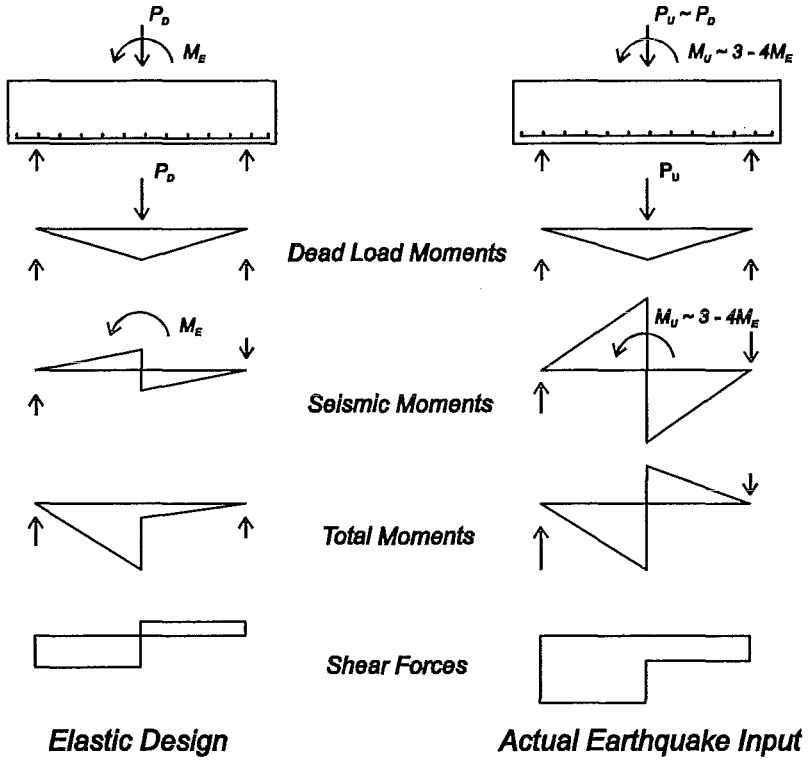

Figure 1.5 *Footing Moments Corresponding to Elastic Design Force, and Column Flexural Strength Under Seismic and Gravity Loads [X1]*

assumptions for the Thorndon Overbridge and behaviour required from the retrofitted structure are different to those previously tested. The significance of the Thorndon Overbridge and the need to retrofit this structure requires the testing of large scale models to evaluate their performance and the likely performance of the Thorndon Overbridge when subjected to severe ground motions from a large earthquake.

1.3.2 Laboratory Modelling of Test Specimens

1.3.2.1 Unit I-A and Unit I-B

Two scale models, Unit I-A and Unit I-B, of actual column/pilecap/pile assemblies from the Thorndon Overbridge, including the proposed retrofit details for each pier, were constructed and tested in the Department of Civil Engineering. Each specimen was constructed at 1:3.8 scale which was determined by scaled reinforcing bar sizes and strengths and the physical limits imposed by the laboratory and capacities of testing equipment.

Each of the test specimens modelled the pilecap and column of each pier with elements included to model the piles and represent the soil-structure interaction. Each specimen was subjected to constant axial compressive loading and simulated seismic lateral loading by applying quasi-static reversed cyclic lateral loading to the top of the column, at the equivalent centre of mass of the bridge deck. Simulated seismic reversed cyclic lateral loading was applied in one plan direction only due to constraints imposed in the laboratory and the practical difficulties in applying simulated multi-directional seismic loads. Loading was applied in the critical direction for each test specimen. For Unit I-A loading applied diagonally across the pilecap was assessed to be the critical loading direction. Unit I-B was loaded parallel to the longitudinal direction of the bridge. Performance of each specimen was observed up to failure and conclusions were drawn on the likely behaviour of the actual piers under severe ground motions resulting from a large earthquake. Design

of the test rig and each test specimen are described in Chapter 2. Chapters 3 and 4 present the results from the lateral load testing of Units I-B and I-A respectively.

Unit I-A represents Pier 68 of the Thorndon Overbridge, a typical Stage Three pier. A pilecap overlay only is proposed for this pier. A steel jacket is not proposed for this pier as the original column is believed to contain sufficient quantities of transverse reinforcement to provide adequate ductility to the column. Unit I-B represents Pier 46, a typical Stage Two pier. Retrofit of this pier includes a pilecap overlay, cored through post-tensioning and a steel jacket around the base of the column.

Each test specimen matches as closely as possible the as-built piers and the proposed retrofit measures as closely as possible with similitude laws. Each test specimen is designed as a simplified model representation of the actual pier. The specimens and the boundary conditions in the test rig, used for testing each specimen in the laboratory, are representative of the structural models used by BCHF in the analysis of the Thorndon Overbridge. In turn, components of the structural model are based on information supplied from geotechnical investigations and material testing carried out from the Overbridge.

1.3.2.2 Material Properties

As part of the seismic assessment and retrofit design stage, properties of materials used in the construction of the Overbridge were measured by removing samples of reinforcing steel, and by coring concrete cylinders from a number of columns and pilecaps. Material testing was used to obtain the probable material strengths to enable a realistic assessment of the bridge's seismic performance. Probable concrete strengths were determined from compressive tests on the concrete cores and correlated with Schmidt hammer tests. Steel yield strengths and maximum strains were obtained from test results obtained from the original steel supplier and testing of the removed steel samples.

The specified yield strength for the steel was 275 MPa. Tensile testing of the reinforcing steel gave an average yield strength of 318 MPa with a standard deviation of 19 MPa. Testing of the steel also gave the 95th percentile yield strength of the column longitudinal steel and the 5th percentile yield strengths for the column transverse steel and pilecap reinforcement which were used in the construction of the model specimens. The specified 28 day concrete strength for the Overbridge was 27.5 MPa. From compression tests on the cored concrete cylinders and correlation with Schmidt hammer readings an average concrete strength, nearly 30 years after construction, of 63 MPa was obtained with a standard deviation of 5.5 MPa [B1].

Steel reinforcement strengths for the design of test specimens with appropriate strength were taken as 350 MPa for the column longitudinal reinforcement and 286 MPa for the pilecap and column transverse reinforcement, being the 95th and 5th percentile yield strengths respectively, obtained from testing. Use of the 95^{th} percentile strength reinforcing for the column longitudinal steel and the 5^{th} percentile strength for column transverse and pilecap reinforcement is intended to represent the worst possible scenario with high column overstrength combined with low pilecap strength. Due to the pilecaps being the assessed weak link in the existing piers, retrofit of the pilecap for strength had to be capable of resisting the level of forces corresponding to development of overstrength actions at the base of the column.

A concrete compressive strength of 55 MPa at time of testing of the specimens was specified for the "as-built" part of the test specimens. Concrete compressive strengths of 40 MPa, for Unit I-A, and 30 MPa, for Unit I-B, at time of testing were specified for the retrofit parts of each specimen.

1.3.2.3 Modelling Soil-Structure Interaction

The main difference between the test specimens and the prototype is in the modelling of the soil-structure interaction. The tensile and compressive action of the piles in each specimen and the passive pressure provided to the side of the pilecap by the surrounding soil was carefully modelled in the test specimens. This was achieved through the use of mechanical "springs" which were able to provide the different

compressive and tensile stiffness values of each pile and supply the required passive pressure reaction to the pilecap.

Each pile or vertical spring was designed to provide different tension and compression stiffness values. The ratio of tension to compression stiffness was maintained at the same ratio as the stiffness ratio for the piles and the soil used in the structural model of the actual piers. By modelling the piles with the vertical springs and maintaining the same stiffness ratio, displacements in the test specimens could not be directly scaled to give those of the real structure. A mathematical relationship is used to relate the displacement ductilities in the test specimens and convert them to the displacement ductilities in the actual piers. Structural analyses of Unit I-A and Unit I-B indicated that the simplifications in the vertical spring design had an insignificant effect on the bending moment and shear forces in the pilecap as obtained from analyses of Pier 68 and Pier 46 respectively.

Schematic diagrams of the loading and spring arrangement for Unit I-A are shown in Figure 1.6. Figure 1.7 shows the loading arrangement for Unit I-B. Further details about the loading arrangement and spring design are provided in Chapter 2.

The action of the piles needed to be duplicated in order to produce the same bending moment distribution in the column and pilecap of each specimen which could not be duplicated by fixing the pilecap to the laboratory floor. The additional flexibility provided by the piles, through pilecap rotation, and the passive pressure reaction, allowing pilecap translation, also provides a significant component of the elastic displacement for each pier.

1.3.3 Expected Test Benefits

Laboratory testing of the two test specimens modelling piers from the Thorndon Overbridge is required to verify the assumed behaviour of the retrofitted piers.

Following the seismic assessment and retrofit design phase a number of proposed retrofit designs for various piers have been developed. Many aspects of these designs

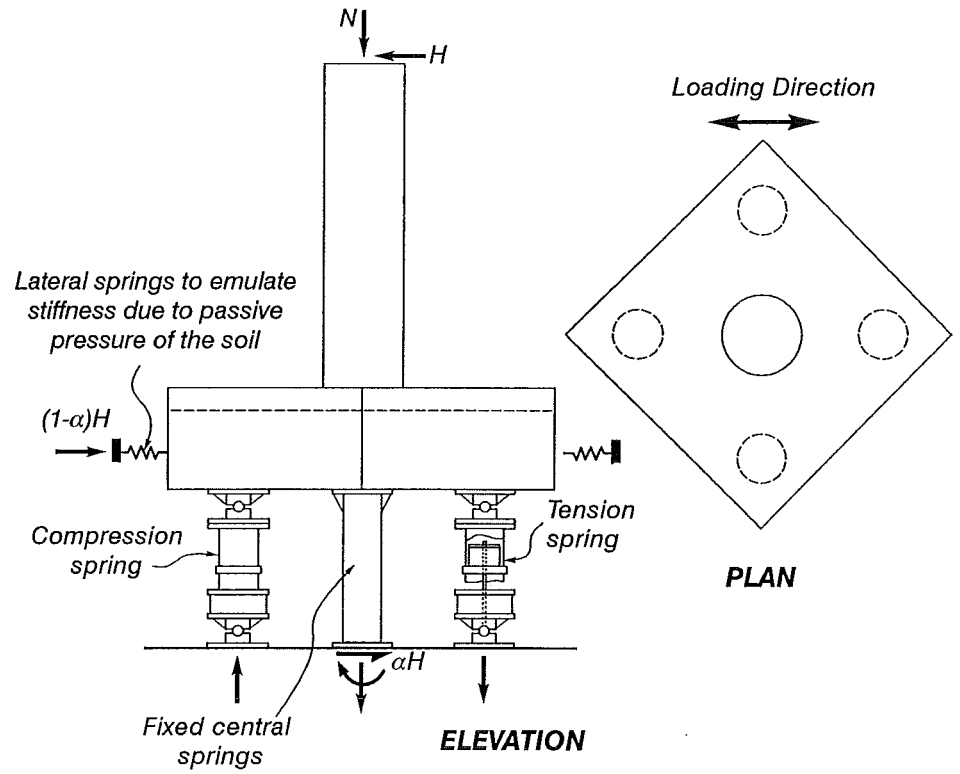

Figure 1.6 *Loading Arrangement of Unit I-A*

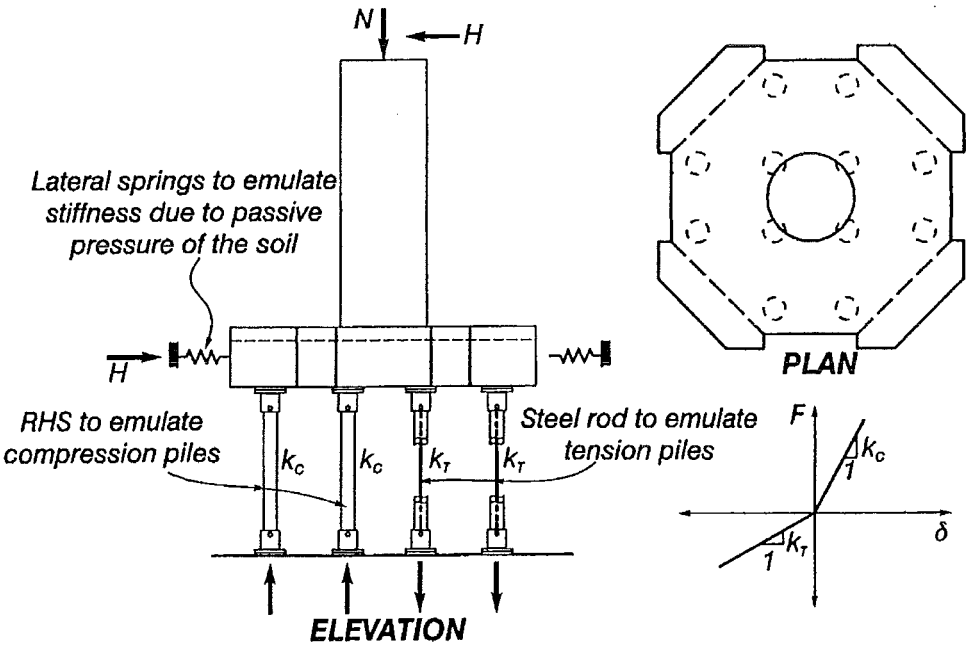

Figure 1.7 *Loading Arrangement of Unit I-B*

involve innovative design and state-of-the-art structural assessment methods. Use of this approach has the potential to save a considerable portion of the retrofit construction costs if more conservative and proven design methods must be used instead.

Testing is required to observe the behaviour of the retrofitted test specimens, verify the assumptions in load transfer mechanisms, design assumptions used in detailing of the retrofit measures and draw conclusions about the performance of the actual retrofitted piers under severe ground motions resulting from an earthquake.

Testing of the retrofit measures was proposed where potential retrofit-cost savings justify the need for testing to verify the design assumptions and expected structural performance. Engineering requirements, to provide verification of the assumed capacity of existing elements and integrity of existing details, has also provided the need to test other components of the proposed retrofit designs.

1.4 ANALYTICAL RESEARCH

1.4.1 Tension Shift Effect

As a result of the experimental testing of the two specimens investigations into the cause of the column failures were completed. These are outlined in Sections 3.5 and 4.5. Chapter 7 investigates the assessment and performance of bridge columns with curtailed longitudinal reinforcement and the potential for the tension shift effect to lead to brittle flexure-shear failures in columns.

Suitably conservative allowances for curtailing longitudinal reinforcement are included in design requirements to avoid the potential flexure-shear failures at curtailment points due to the tension shift effect. These rules, intended for design of new structures, may be overly conservative when used in a seismic assessment, and could lead to unnecessary and expensive retrofit.

Chapter 7 provides an explanation of the tension shift effect, which led to the observed test specimen column failures. A parametric study was conducted to determine the magnitude of the tension shift effect for older reinforced concrete bridge columns. A number of expressions are proposed which can be used for an initial assessment of potential failures at curtailment points due to the tension shift effect.

1.4.2 Alternative Modelling of Confined Concrete Stress-Strain Behaviour

In order to adequately describe the post-elastic behaviour of a reinforced concrete member, the moment-curvature response of the section must be determined. The stress-strain behaviour of the concrete confined within the core of the member must be known to determine the moment-curvature response.

The use of transverse reinforcement in reinforced concrete members provides confinement to the concrete core, prevents premature buckling of the longitudinal reinforcement, prevents shear failure of the member and ensures, when properly detailed, the member has adequate ductility to sustain the large inelastic deformations imposed during an earthquake.

Various stress-strain models for concrete confined with transverse reinforcement reflect the observed increase in peak compressive stress and strain as a result of the passive confining pressure provided by the reinforcement. A feature of commonly used confined concrete stress-strain models is the definition of an effectively confined core within the region bounded by the peripheral hoops. Arching between the transverse hoop sets and between restrained longitudinal bars produces a region of ineffectively confined concrete within the core.

Many stress-strain models account for the reduction of the concrete core, through arching, by using a reduced lateral confining pressure, through a confinement efficiency factor, and defining the core as having uniform stress-strain properties. Chapter 8 investigates the moment-curvature response of column subjected to axial load and flexure by using a confined concrete stress-strain model which employs a

confinement efficiency factor [M3, M4] and an approach which explicitly models the regions of effectively and ineffectively confined core concrete.

1.4.3 Flexural Strength Enhancement

Tests on columns at the University of Canterbury, under combined axial load and cyclic lateral loading, give measured experimental moments significantly higher than the predicted ACI flexural strengths of the sections. Some of this strength enhancement is expected due to conservative assumptions made to determine the ACI flexural strength. The column sections tested all had heavily reinforced stubs adjacent to the critical section of the column. This stub is provided to model the effect of adjacent members framing into the columns next the cricital section such as pilecaps, foundation beams, pier caps or beams.

It has been suggested that this stub is responsible for the observed strength enhancement seen in tests for columns tested at the University of Canterbury [S7]. Chapter 8 also includes an investigation into the components of flexural strength enhancement over the ACI predicted flexural strength. These components include strain hardening of longitudinal steel, effects of cyclic loading and confinement from adjacent members leading to a shift in the critical section away from the face of the adjacent member. Several case studies are used to compare theoretical moment-curvature responses to experimentally measured values.

CHAPTER 2

TEST SET-UP FOR UNITS I-A AND I-B

2.1 INTRODUCTION

This chapter discusses the different aspects in the design of the tests and the loading frame. Construction details for each of the test units follow the details of the existing structure and the proposed retrofit designs for each pier. In order to construct and test each specimen, an appropriate scale factor was required which would allow the existing and proposed structural details to be modelled with commercially available reinforcing bar sizes and concrete mixes as well as fit within the physical limits imposed by the laboratory and available testing equipment.

A scale factor of 1:3.8 was chosen for both test specimens as this gave the best match between the actual reinforcing bar sizes and the required scaled reinforcing bar sizes for the test specimens. All steel reinforcement bars in the as-built and retrofit parts of the test specimens could be modelled with commercially available reinforcing bar sizes using this scale factor. Steel reinforcement for the project was sourced from within New Zealand and from Japanese suppliers. The concrete aggregate used in the test specimen was scaled by the same factor, necessitating special mix designs to be prepared for construction of the test specimens due to the size of the aggregate required for the concrete mix.

A steel frame loading rig and concrete baseblock were constructed to apply the simulated lateral seismic loads to the specimens and provide the necessary reactions for each specimen.

2.2 DESIGN AND CONSTRUCTION OF TEST RIG

2.2.1 Baseblock Design and Construction

The concrete baseblock for the test rig was required to work in conjunction with the existing laboratory strong floor to resist the applied lateral and axial loads on the test specimens. The baseblock also provided an easy means of connecting the large number of components in each test specimen to the laboratory strong floor. As each specimen had different pile layouts, a number of large steel connection plates would be required to attach each pile to the laboratory strong floor bolts. With the baseblock the required number of connection points for each pile could be placed at the appropriate location for each test specimen and connections for each of the lateral springs and the axial load hold down points used for both specimens could be located without being restricted to the laboratory strong floor bolt arrangement.

2.2.1.1 Existing Strong Floor

The baseblock was constructed over the existing 750 mm thick Concrete Laboratory strong floor. The strong floor is 11.85 m long and 3.05 m wide with 1 $^1/_2$ inch (38 mm) diameter strong floor bolts placed at 15 inch (381 mm) centres in both directions. The floor is partially prestressed longitudinally. The baseblock for the test was constructed in four separate strips each measuring 900 mm wide, 4.8 m long and 600 mm thick to ease the demolition of the baseblock at the completion of testing. Each strip was match cast against the previous strip with vertical and horizontal shear keys cast into the side of each strip to key each adjacent strip together and ensure composite action from the four separate strips.

Due to the width and placement of the baseblock on the strong floor, as dictated by the strong floor bolt layout for bolting down the steel test rig, the baseblock extended off the side of the strong floor. Hold down bolts were provided at each end of the central strips to tie the baseblock to the strong floor but were not placed in the outer strips as the bolt arrangement will have been unsymmetrical and not matched with the strong floor bolt layout.

2.2.1.2 Analysis

The strong floor and baseblock were analysed together to obtain the maximum forces acting in the strong floor and in the baseblock under loading of the two test specimens. This was to ensure that the cracking capacity of the strong floor, in conjunction with the baseblock was not likely to be exceeded during testing and to provide design actions for reinforcement of the baseblock.

From Unit I-A was found to give the largest forces acting in the baseblock. For the design of the individual baseblock strips each of the two central strips were assumed to provide one-third of the total resistance with each outer strip contributing one-sixth of the total resistance. Each strip was designed with a factor of safety of 1.5 over the maximum analysed forces obtained from the analysis of Unit I-A to give the ultimate limit state forces for design of the baseblock.

2.2.1.3 Reinforcement

Conventional flexural reinforcement was placed along with longitudinal post-tensioning to resist the ultimate limit state forces acting in each of the two central strips. The configuration of the test rig introduces a horizontal force into the baseblock where the horizontal stay is attached. Figures 2.6 and 2.7 show the configuration of the test rig for the two test specimens. The effects of this force were accounted for in the design of the flexural reinforcement. The longitudinal post-tensioning was determined to allow cracking of the baseblock to occur when Unit I-A reached overstrength. The baseblock was post-tensioned transversely to hold the individual strips together and ensure composite action from the entire baseblock.

Design of the transverse reinforcement in the individual baseblock strips used a factor of safety of 1.5 times the analysed shear force acting in the baseblock. The transverse reinforcement required for each strip was determined assuming the design shear force was to be resisted by the two central strips only neglecting the

contribution of the post-tensioning to the concrete component of shear resistance. A design calculation error led to double the amount of transverse steel being provided in each baseblock strip. The reinforcement of all four baseblock strips were kept the same for simplicity during construction of the baseblock.

Figure 2.1 shows the reinforcement layout of the individual baseblock strips. Two HD28 bars and two HD24 bars were placed top and bottom of each baseblock strip. Longitudinal post-tensioning was placed at mid-depth and 200 mm below mid-depth of each strip. Transverse post-tensioning alternated top and bottom along the length of the baseblock. Eight legs of R16 stirrups were placed at nominal 325 mm centres along each baseblock strip. Stirrup sets and cross-ties were doubled up at each location to achieve the eight legs required. Care was taken to check the end zones of each baseblock strip where the post-tensioning was anchored. A simple strut and tie model was used to check the transverse steel requirements at the post-tensioning end-zone due to the eccentric post-tensioning layout and resulted in the spacing of the transverse reinforcement sets being reduced to a nominal 200 mm over the end 1000 mm at each end of each baseblock strip. Due to the congestion of the reinforcement in the baseblock, especially the central baseblock strips, the transverse reinforcement was adjusted accordingly to avoid clashes with post-tensioning ducts and fittings for the connection plates.

2.2.1.4 Hold Down Plates

Figure 2.2 shows the layout of the hold-down connection plates cast into the baseblock strips to provide the various connections for the piles in each of the two test specimens.

The twelve pile layout for Unit I-B dictated the positioning of plates within the baseblock to connect each pile. Each connection plate used a $7\ ^1/_2$ inch (190.5 mm) square bolt pitch arrangement. Additional plates were then placed to allow

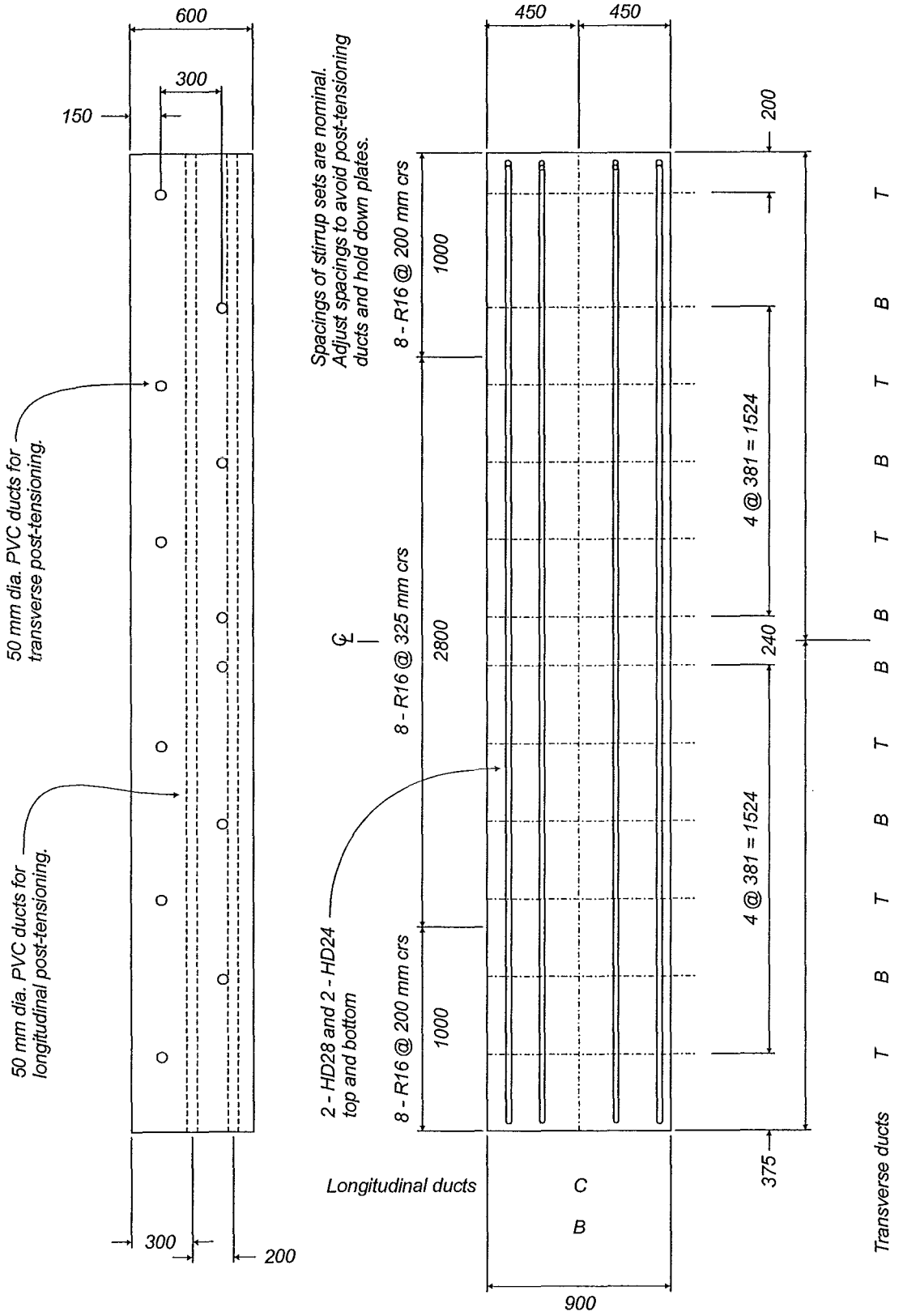

Figure 2.1 *Baseblock Strip Reinforcement Details*

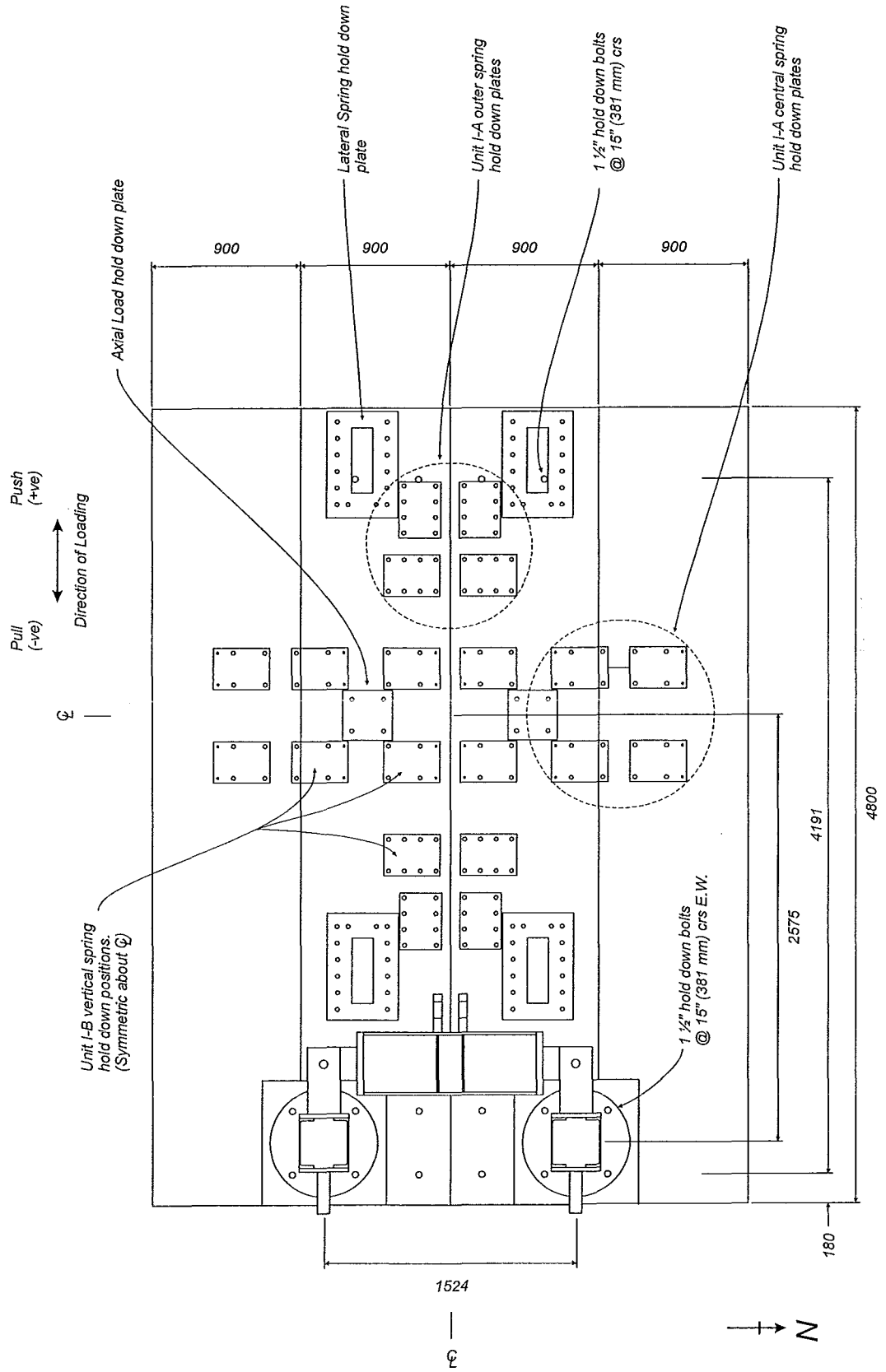

Figure 2.2 *Baseblock Hold-down Connection Point Layout*

connections to be made for the four piles in Unit I-A after casting of the baseblock. Plates were also provided for fittings to apply the axial load to each test unit and to connect the lateral spring units which were to resist the applied lateral loads at the pilecap level of each unit.

Each connection point was fabricated from 6 mm thick mild steel plate with holes for 24 mm diameter bolts at the appropriate location. Threaded couplers were tack welded to the underside of the plate at the position of each bolt hole. The plate was cast flush with the top surface of the baseblock with a 24 mm diameter deformed reinforcing rod screwed into the each threaded coupler. These deformed reinforcing rods were provided to transfer the bolt forces from each spring fitting into the baseblock.

Bolts with higher design forces also had threaded concrete inserts placed at the opposite ends of the reinforcing bar to aid the anchorage of the bar in the baseblock as the use of end hooks would have resulted in excessive congestion of the reinforcement.

The connection plates were positioned relative to one another and tack welded to lengths of steel flat to ensure they would remain in the correct position when cast into the baseblock. The reinforcing rods were screwed into the threaded couplers and the whole assembly lowered into the baseblock reinforcing cage in the mould. Figure 2.3 shows the connection plates being lowered into one of the central baseblock strips. From this photograph it can be seen how some of the rods had to be adjusted to avoid clashes with the post-tensioning ducts and reinforcement.

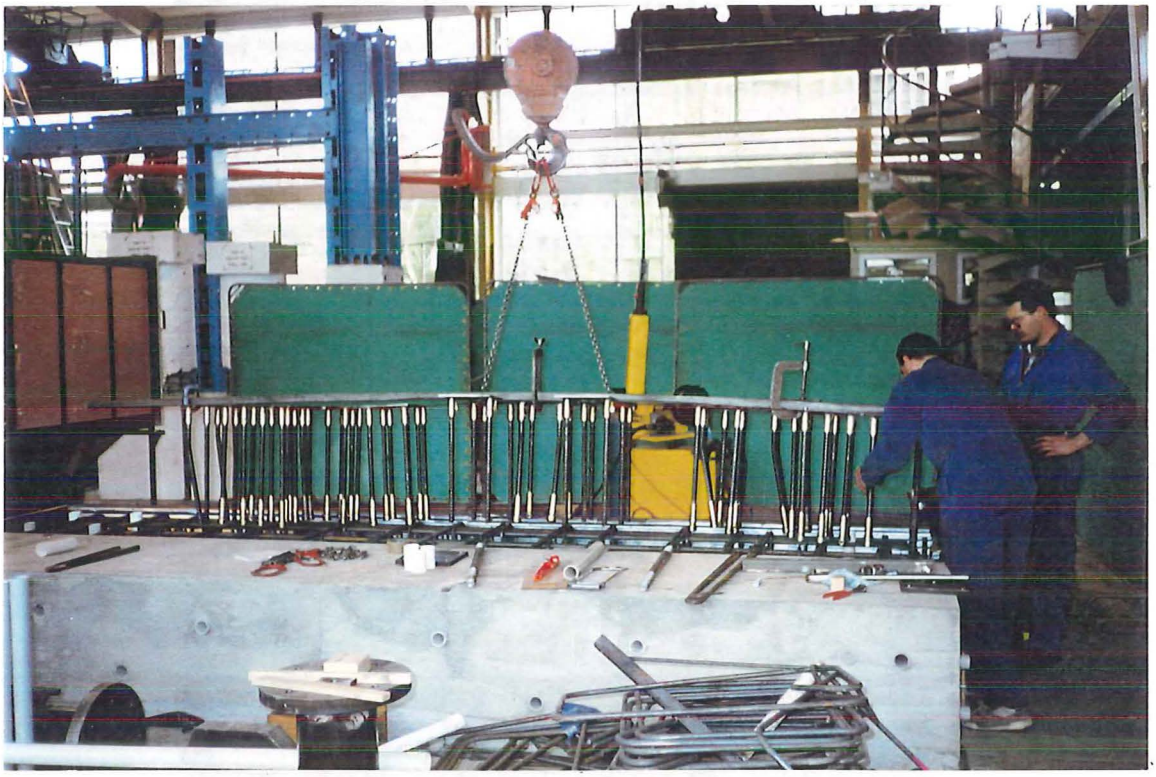

Figure 2.3 *Lowering of Connection Plates into Baseblock Reinforcing Cage*

2.2.1.5 Interconnection and Shear Keys

Post-tensioning ducts were made from 50 mm PVC pipe passed through the formwork and secured to the reinforcing cage to hold their position when the concrete was being cast. The transverse ducts projected slightly through the side of the formwork to allow the PVC duct to be slipped over the end for extending it through the next baseblock strip. Ducts for the hold down bolts were made from 50 mm PVC pipe running up from the strong floor and secured in position with a temporary bolt screwed into the strong floor. Figure 2.4 shows the final baseblock strip before casting of the concrete showing the reinforcing cage and the post-tensioning ducts.

The proximity of the lateral spring connection plates to one end of the baseblock required special detailing to prevent the reaction from the lateral springs pushing the reinforcing rods cast into the baseblock, from each of the bolts, through the end of

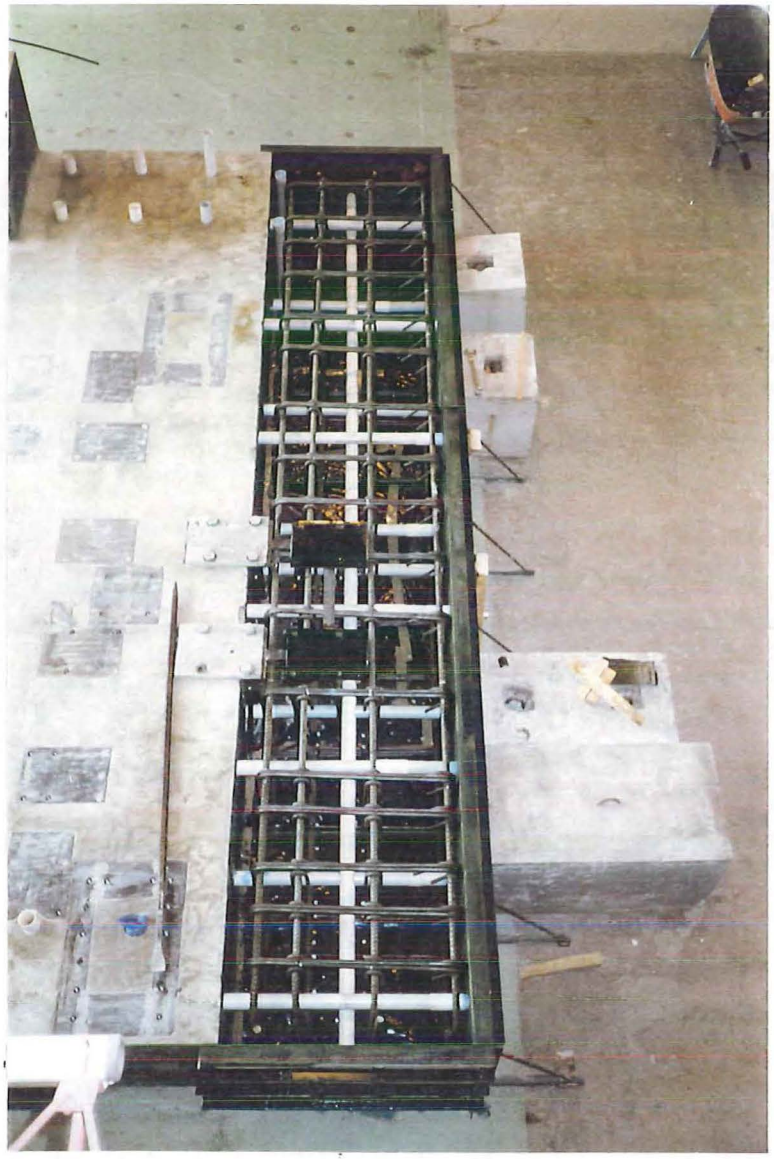

Figure 2.4 *Baseblock Strip Reinforcement and Post-Tensioning Ducts before Casting of Final Baseblock Strip*

the baseblock. Hairpins made from 16 mm deformed reinforcing bar were placed around the bolts holding the lateral springs directly under the connection plate to provide restraint to the reinforcing rods extending into the baseblock.

The shear keys in the side of each baseblock strip were formed by using "baby" corrugated roofing iron built into the formwork. Three sections of corrugated iron, each 150 mm deep, were fastened to the formwork to create the shear key. Figure 2.5 shows the shear key in the side of one of the baseblock strips before casting of the adjacent strip. The top and bottom corrugated strips ran horizontally with the middle corrugated strip oriented vertically providing shear keys for vertical and longitudinal

movement of the baseblock strips. The transverse post-tensioning ducts can also be seen in Figure 2.5.

2.2.1.6 Concrete Properties

As the concrete for each test specimen was to be made using a 6 mm round aggregate, scaled down from the maximum size aggregate used in the actual piers, several trial concrete mixes were required to come up with a suitable concrete mix design which would meet the required strengths using the small size aggregate. The baseblock strips provided an opportunity to trial several mixes before casting of the test specimens.

A mean concrete compressive strength of 63 MPa was recorded for the concrete compressive strength in the Thorndon Overbridge piers after nearly 30 years of natural strength gain and exposure to the atmosphere [B1]. This concrete strength was to be matched in the test specimens to realistically model the material properties of the actual piers. The concrete compressive strength for the retrofit of each pier was also required to be matched and this was trialed in the final baseblock strip.

Three concrete mix designs targeting a 60 MPa concrete compressive strength were used for the first three baseblock strips. For the final baseblock strip a concrete mix design targeting a 30 MPa concrete compressive strength was used. Details of the concrete mix design for each concrete batch are shown in Table 2.1.

2.2.1.7 Concrete Testing

Eight standard concrete test cylinders 100 mm diameter by 200 mm long were taken for each concrete pour. Two cylinders were tested each time to obtain the 7, 14, 28 and 56 day compressive strengths of each concrete mix. Concrete cylinders were cured in a fog room until removal for compression testing.

Table 2.2 shows the slump, specific density and compressive strength results for each concrete pour.

Figure 2.5 *Side of Baseblock Strip Showing Vertical and Horizontal Corrugated Shear Keys*

Table 2.1 *Baseblock Concrete Trial Mix Properties*

Baseblock Strip Pour		1	2	3	4
Target Strength	MPa	60	60	60	30
Ordinary Portland Cement (Pacific Cement)	kg / m^3	455	455	455	297
6 mm round aggregate	kg / m^3	1025	1025	1025	1059
Mortar Sand	kg / m^3	773	773	773	902
Total Water	kg / m^3	200	200	200	190
Water Cement Ratio		0.44	0.44	0.44	0.64

The concrete with the very high slump for the third baseblock strip was returned to the plant for the addition of further sand and cement to reduce the slump to the specified value. Partway through the pour the concrete mix became unworkable and a second batch of concrete was sent from the plant. As only eight test cylinders were made results are shown for the two batches at 7 days and 28 days only.

From these trial mixes and strength results a final concrete mix design was determined for use in the as-built and retrofit parts of the test specimens.

2.2.1.8 Post-tensioning

Post-tensioning of the baseblock was carried out using the VSL CT Stressbar post-tensioning system. The Stressbar was placed through the PVC ducting and anchored at the ends using the supplied bearing plates and nuts. Bars of 29 mm diameter were used for the longitudinal and transverse post-tensioning of the baseblock. Longitudinal and transverse bars were stressed using a centre-hole jack to a load of 330 kN giving 500 MPa stress in each bar immediately after stressing. Losses of 10 % were assumed for the post-tensioning of the baseblock. The bars were stressed shortly after casting of the first test specimen was completed and re-stressed to 330 kN prior to testing of the second test specimen. The Stressbar was left ungrouted in the PVC ducts to allow re-stressing of the bars during the test programme and removal and re-use of the bars in other projects following completion of the testing.

Table 2.2 *Baseblock Concrete Trial Mix Design Results*

Pour No.	Specified Slump (mm)	Slump (mm)	Specific Density	Compressive Strength[1] (MPa)			
				7 day	14 day	28 day	56 day
1	80 - 100	110	2.385	42.4	48.4	53.1	60.6
2	80 - 100	150	2.389	36.1	45.1	51.1	53.3
3[2]	80 - 100	180, 70[3]	2.363	38.1	-	52.2	-
		-	2.389	43.4	-	52.9	-
4	80 - 100	65, 40[4]	2.622	19.3	25.1	28.5	35.3

Notes:

[1] Based on average of two 100 mm diameter by 200 mm long cylinders cured in a fog room.

[2] Concrete received in two batches. Slump not recorded for Batch 2.

[3] Batch 1, 180 mm slump returned to plant for addition of sand and cement. 70 mm slump measured for Batch 1 after the addition.

[4] 65 mm slump measured at batching plant. 40 mm slump measured upon arrival of truck on site.

2.2.2 Reaction Frame Design

A triangulated steel frame loading rig was used to apply the simulated seismic lateral loads at the top of each of the two test specimens, see Figures 2.6 and 2.7. With the scale factor of 1:3.8, the lateral load applied to Unit I-A was going to be approximately 4.9 m above the top of the baseblock. The configuration of the reaction frame was designed so that it could be modified to accommodate either test specimen.

2.2.2.1 Steel members

Existing "meccano" multi-use column sections were used as part of the test rig with the diagonal brace members designed and fabricated specially for this test. The meccano columns were supported on concrete pedestals placed on top of the

baseblock to provide the necessary height for applying the lateral loads to Unit I-A. Maximum design actions for each element in the test rig were determined from analysis of the rig layout subjected to loads equivalent to developing the flexural strength of the columns in the full size piers.

Grade 350 219.1 x 8.2 CHS sections were used for the diagonal and horizontal braces in the test rig. Inclusion of the horizontal brace transfers the shear force from the lateral load applied to the top of the test specimen back into the baseblock requiring the brace connection to the strong floor to resist axial forces only. The connection of the horizontal CHS section to the baseblock was achieved by bolting the CHS section to a steel plate embedded in the end of the baseblock and transferring the forces into the baseblock using threaded couplers and reinforcing bars cast into the concrete. Pinned connections were used where the diagonal and horizontal braces meet and at the connection between the diagonal brace and meccano column.

2.2.2.2 Modifications for Each Test Unit

Testing of Unit I-B first set the initial layout of the test rig. In order to test Unit I-A the diagonal brace was extended to the top of the meccano columns with the use of a short extension piece. Each of the CHS members were connected with bolts through flanges at each end allowing the extension to the diagonal brace to be inserted easily. In order to minimise the eccentricity of the forces acting through the centreline of the members in the test rig additional holes were placed in the connection plate where the diagonal brace meets the meccano column. This plate was bolted through the meccano column into the connection used to mount the hydraulic actuator, which was used to apply the lateral loads to the specimens, using high strength threaded rods. This was to avoid application of forces to the flanges of the meccano column section and the undesirable effects this would have with attempting to transfer force through the flanges of the section.

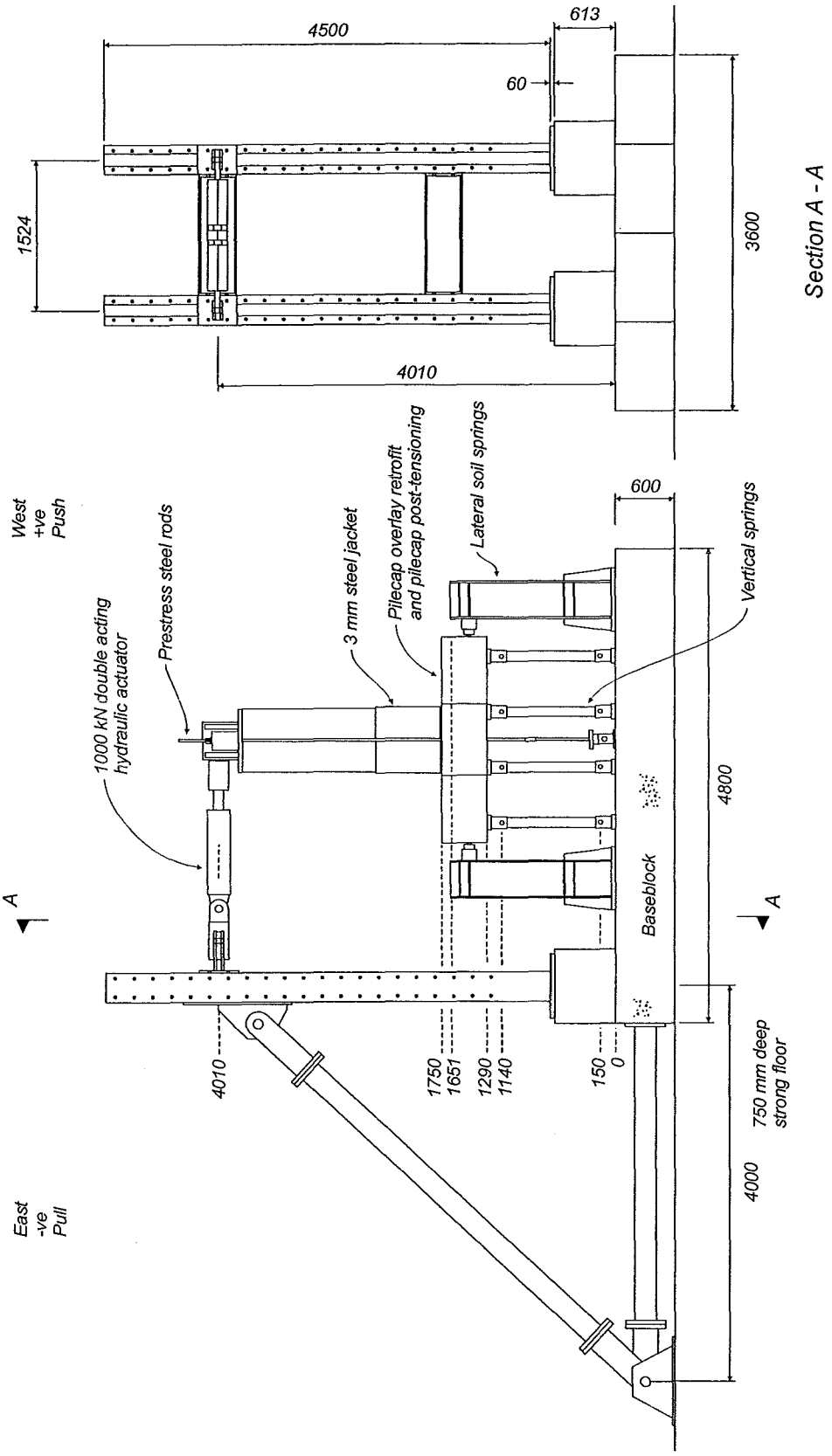

Figure 2.6 *Test Rig Layout for Testing of Unit I-B*

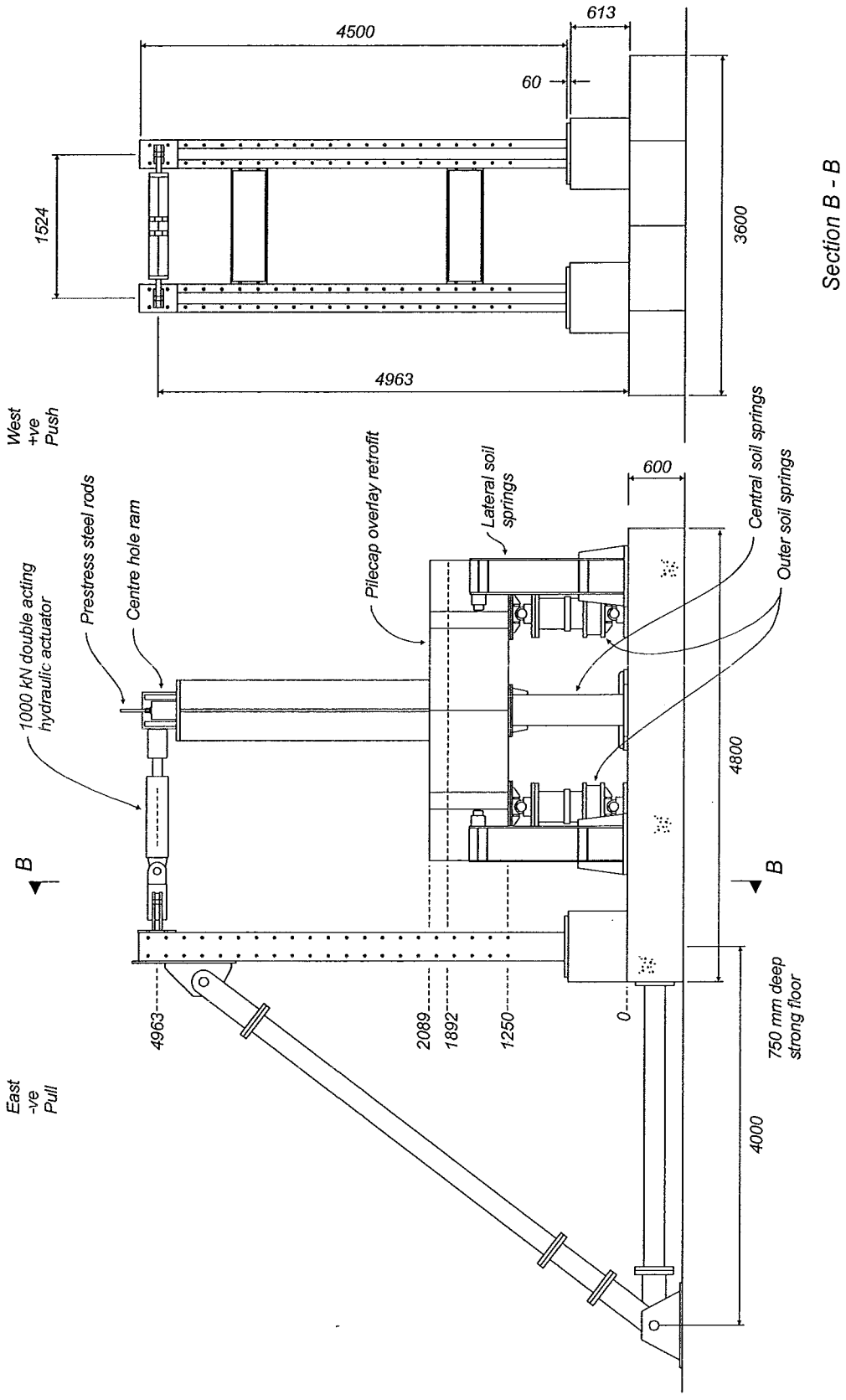

Figure 2.7 *Test Rig Layout for Testing of Unit I-A*

The mounting beam for the hydraulic actuator was pinned at both ends and sized to resist the loads from pushing and pulling the test specimens. Stiffeners were placed behind the connection with the hydraulic actuator to avoid crippling of the beam section when the point load from the actuator was applied. Stiff beams were placed between the two meccano columns to brace them against undesirable out of plane displacements when applying loads to the test rig.

Fabrication details of the test rig components can be found in Appendix F.

2.2.3 Lateral Spring Design

2.2.3.1 Lateral Spring Performance Requirements

The lateral springs used in the testing of each specimen simulated the passive pressure of the soil surrounding the pilecap of each pier. This passive pressure force, as modelled by the springs, is assumed to provide an major component of the lateral load resistance for each pier. Additional lateral force resistance is provided through bending and shear in each pile. Structural modelling of the actual piers assumed the presence of passive soil reactions against the side of the pilecap and distributed down the length of the piles. The test specimens were designed to represent the structural model of the actual piers. Providing for the entire length of pile, as in the structural model, and the surrounding soil would have been impossible using the proposed test rig. A length of pile and the tensile and compressive stiffness of each pile was modelled in the test specimen. Further details of the design and fabrication of the vertical springs in each specimen to model the action of the piles is included in Section 2.3.

The lateral spring units were placed at the mid-depth of the original pilecap of each test specimen. Two spring units were placed on each side of the pilecap to resist the lateral loads at the pilecap level. The lateral stiffness of these springs was designed to match the scaled stiffness of the pilecap spring used in the structural model of each pier. It was found during the analysis of Pier 46 that modelling of the pier with and without continuous piles made little difference to the actions in the pier. The

individual flexural resistance at the top of each pile is negligible compared to the resisting moment from the pile axial force. It was decided that Unit I-B, modelling Pier 46, would be built without modelling the flexural contribution of the piles to the lateral load resistance of the entire pier. This involved pinning the vertical springs top and bottom so they would carry no shear over their length requiring the full lateral load applied to the top of the column to be resisted by the lateral springs at pilecap level. Analysis of Unit I-B confirmed there was little difference in pilecap forces when modelled with or without piles. This analysis also showed that the stiffness of the lateral springs had little influence on the pilecap forces.

Analysis of Pier 68 showed a considerable contribution, from each pile, to the lateral force resistance of the pier. This required the modelling of the flexural contribution of the piles in Unit I-A and therefore some of the lateral load is resisted through shear and flexure in the piles. Analysis of Unit I-A showed that the stiffness of the lateral springs had a considerable influence on the distribution of forces within the pilecap of the test specimen. This required that the stiffness of the lateral springs for Unit I-A be matched as closely as possible to the scaled stiffness of the pilecap spring used in the analysis of Pier 68.

2.2.3.2 Design of Lateral Springs

The lateral springs were designed in steel, cantilevering from the baseblock. Two steel 380 x 100 PFC sections were used to provide the required lateral stiffness and to resist the loads imposed on the springs from the pilecap. The required stiffness of each spring was determined from the scaled stiffness of the pilecap spring used in the structural analysis of Pier 68. The size of the PFC sections were determined through strength requirements to prevent yielding of the sections when the lateral load was applied to the top of each spring unit. To determine the stiffness of the lateral spring unit various sources of flexibility were evaluated to give the displacement of the top of the lateral spring where the lateral load from the pilecap was applied. Flexibility sources included bending and shear deformation of the PFC sections and pullout of the bolts holding the lateral spring unit to the baseblock.

Stiffener plates at the base of the lateral spring unit and in each PFC section were used to limit the length of the spring which would contribute to the bending and shear deformations. As the stiffness of the lateral springs was not critical for Unit I-B the front row of hold down bolts were designed to reach yield under the design actions from Unit I-A. From the forces induced in the bolts the elastic bolt deformations were used to determine the rotation of the base of the lateral spring unit and the corresponding deflection at the top could be added to the total deflection of the lateral spring to determine its flexibility.

The deflections from bending and shear deformations of the steel PFC sections and additional rotations from pull out of the hold down bolts could not provide sufficient flexibility to match the required stiffness for Unit I-A. Additional flexibility was achieved through the use of rubber bearings placed between the steel PFC sections and the bearing plates on the side of the pilecap. These rubber bearings were used when testing Unit I-B. Determination of the experimental lateral stiffness of each spring unit showed previously unaccounted flexibilities in the test rig, thus the rubber bearings were not used for the subsequent testing of Unit I-A.

2.2.3.3 Details of Lateral Springs

Figure 2.8 shows the details for the lateral spring units. Each lateral spring unit was held down with 14-24 mm diameter bolts for resisting tension and shear from to the applied loads. The connections to the baseblock were the same as for the pile connections for each specimen, threaded couplers with reinforcing rods threaded into them and cast into the baseblock. The holes in the base plate of the lateral spring were profile cut to 40 mm diameter to allow adjustment when positioning the lateral spring unit for each test specimen. A layer of dental plaster was used to seat each lateral spring unit level in the appropriate position and to fill the space in the oversized holes around the threaded rod used to hold down each unit. The nuts on each threaded rod were done up and the excess plaster cleaned off and removed once the plaster had hardened sufficiently to allow the dental plaster to harden properly around the bolts. This process allowed sufficient tolerances for placement of the

lateral springs in the appropriate location and prevented any slipping of the lateral spring units when load was applied to them from the pilecap.

Rocker units were fabricated for each lateral spring to bear against a steel plate attached to the side of the pilecap transferring the force from the pilecap to the lateral spring. As the pilecap force is a passive reaction when the test specimen is displaced in the opposite direction a space forms between the rocker unit and the bearing plate on the pilecap. The bearing pin on the rocker unit was fabricated with a large radius to spread the force from the bearing pin over as larger area as possible to prevent localised yielding of the bearing plate. Figure 2.9 shows the rocker unit and rubber bearing used when testing Unit I-B. The same rocker unit and an additional rocker mechanism was devised for Unit I-A. Rotation of the pilecap caused vertical shear in the rubber bearing used in Unit I-B despite the provision of the rocker unit. The additional rocker mechanism, shown in Figure 2.10, for Unit I-A allowed the vertical displacements, caused by pilecap rotation, to be accommodated. Springs within the additional rocker mechanism returned the unit to its original position once the test specimen was displaced in the opposite direction.

2.2.3.4 Lateral Spring Calibration

To measure the lateral force being transferred into each lateral spring unit each spring was strain gauged to form a full bending bridge and calibrated using two 1000 kN hydraulic actuators connected through a load cell.

The actuators were placed between the two lateral springs at the height of application of the load from the pilecap, as shown in Figure 2.11, using one lateral spring to provide a reaction while calibrating the other. The load was increased in the actuator and the data from the strain gauges recorded using the data logger. The stiffness of the lateral springs were determined from a plot of the lateral displacement at the

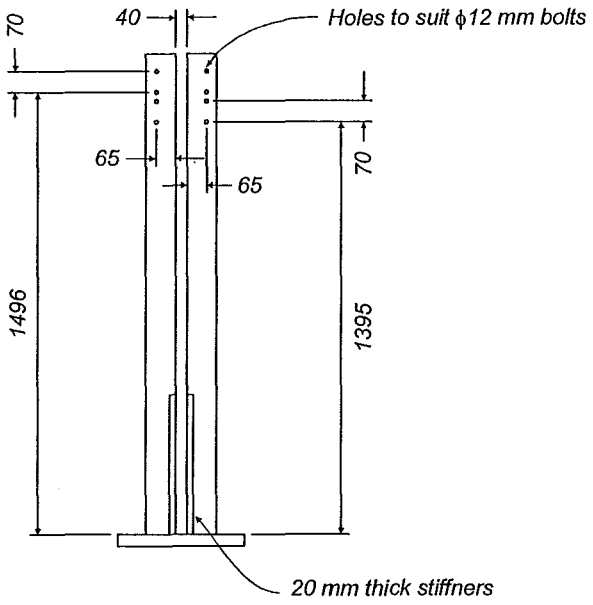

Lateral Spring End Elevation

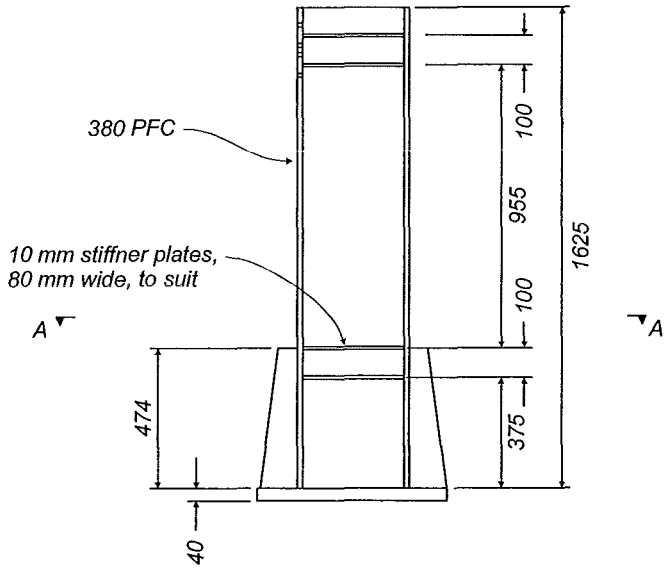

Lateral Spring Elevation

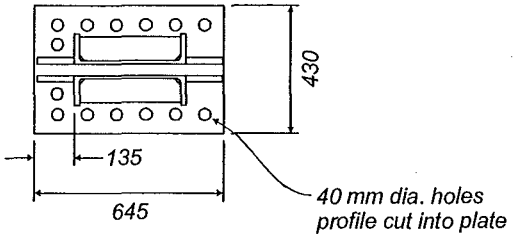

Section A-A

Figure 2.8 *Lateral Spring Unit Details*

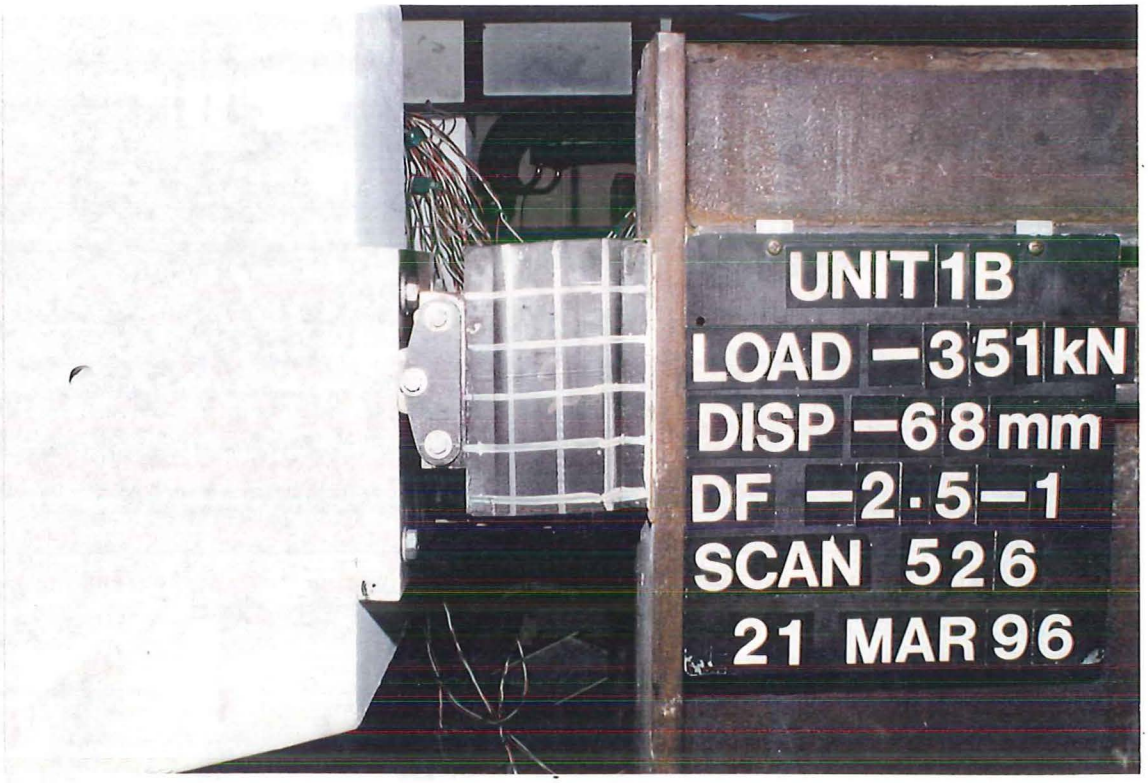

Figure 2.9 *Rocker Unit and Rubber Bearing for Transferring Pilecap Reaction to Lateral Spring for Testing of Unit I-B*

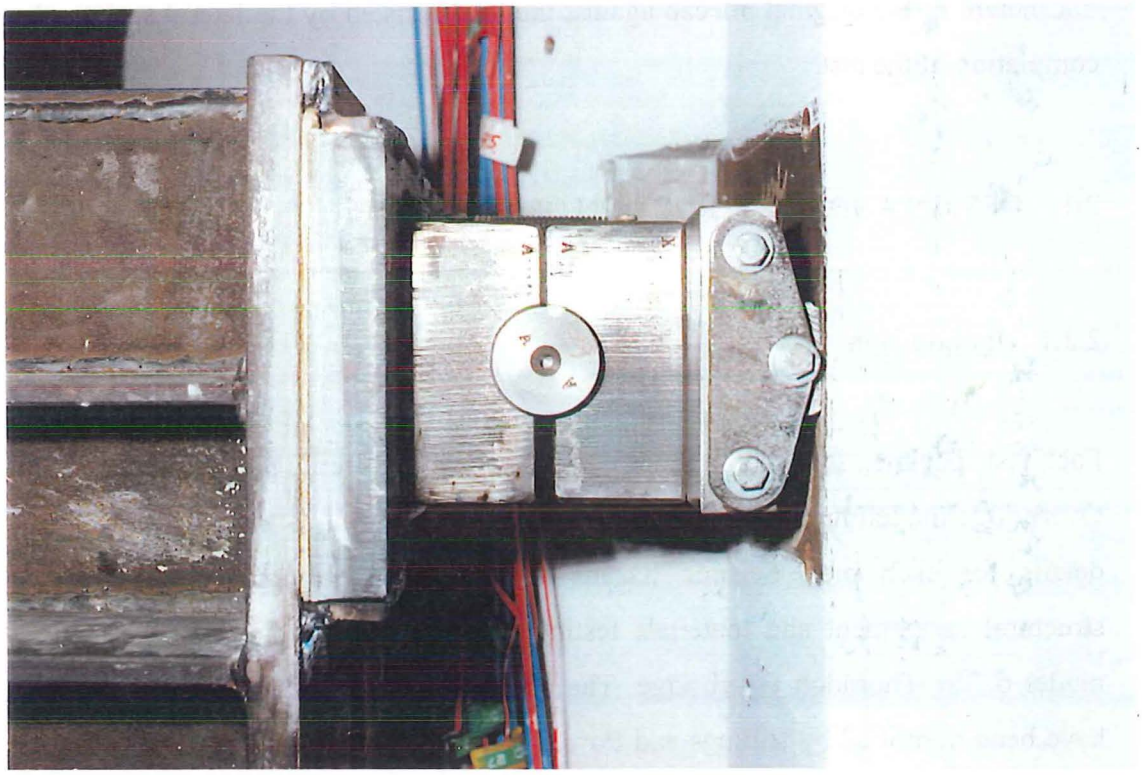

Figure 2.10 *Rocker Unit and Additional Mechanism for Transferring Pilecap Reaction To Lateral Spring for Testing of Unit I-A*

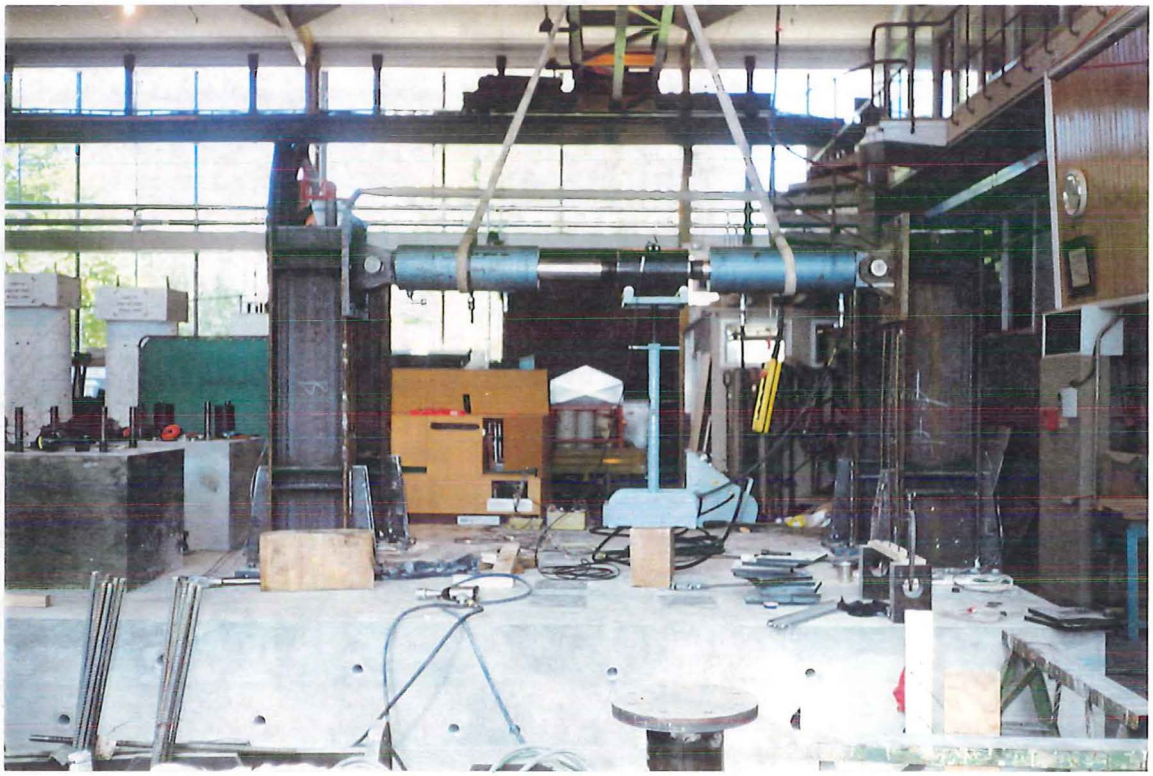

Figure 2.11 *Calibration of Lateral Springs*

mid-height of the original pilecap against the load resisted by the lateral spring after completion of the test.

2.3 DESIGN AND CONSTRUCTION OF TEST UNITS

2.3.1 Introduction

Each test specimen is based on the original details of a specific pier in the Thorndon Overbridge modelling the piles, pilecap and column as well as the proposed retrofit details for each pier. Seismic hazard assessment, geotechnical investigations, structural assessment and materials testing were required to develop a structural model of the Thorndon Overbridge. The assessment and findings from this phase have been described by Billings and Powell [B1], Chapman and Kirkaldie [C1] and Marsh and Toan [M2]. Information from the studies completed during the assessment phase went into developing a structural model of the Thorndon

Overbridge to investigate variation of different parameters on the likely performance of the structure. Details for Units I-A and I-B are based directly on the structural model of the respective piers of the Thorndon Overbridge. The two test specimens are simplified models of the structural model taking into consideration the effects of scale, modelling of the boundary conditions assumed in the structural model and duplicating the same structural actions in the test specimens as expected in the structural model.

2.3.2 Unit I-B

Unit I-B was the first of the two specimens to be tested. It is based on Pier 46 of the Thorndon Overbridge.

2.3.2.1 Pier 46 Retrofit Measures

Pier 46 contains a total of 76 1 $^1/_2$-inch (38 mm) diameter longitudinal bars arranged bundled in pairs at the base of the column. Transverse hoops $^1/_2$ inch (13 mm) diameter are spaced at 12 inch (305 mm) centres up the height of the column above the pilecap. The pilecap mats contained 39 bars in each direction top and bottom. The top pilecap mat bars are 1 inch (25 mm) in diameter and the bottom pilecap mat bars 1 $^1/_2$ inch (38 mm) in diameter.

The retrofit design proposed a new pilecap overlay 375 mm deep over the existing pilecap with HD20 hooked dowels embedded on a 450 mm grid in the original pilecap. Additional dowels were grouped around the outer piles to transfer the pile tension forces through the existing pilecap and to the top of the pilecap overlay. Top and bottom pilecap overlay mats were detailed along with new reinforced concrete anchor blocks for the post-tensioning to be cored longitudinally and transversely through the existing pilecap.

The pilecap overlay and the post-tensioning through the existing pilecap are intended to increase the flexural capacity of the pilecap to force the inelastic action to occur at the base of the column. The existing transverse reinforcement in the column of

Pier 46 was assessed to be insufficient to maintain the curvature ductility expected from a 500 year return period earthquake expected for the Thorndon Overbridge site. A 12 mm thick steel jacket, 2.5 m high, was proposed for the base of the column to improve the ductility capacity of the column at this point. The jacket was to be fabricated in two halves, brought together and welded on site leaving a gap of 50 mm between the base of the jacket and top of the pilecap overlay. A space of approximately 50 mm was to be left behind the jacket to the face of the column which was to be later filled with a cement grout.

Analysis of the forces acting in Pier 46 were based on $f_y = 350$ MPa for the column longitudinal reinforcing and $f_y = 286$ MPa for the column transverse and pilecap reinforcement [B1]. The chosen reinforcement strengths represent the 95th and 5th percentile strengths values, respectively, of steel reinforcement removed and tested from the Thorndon Overbridge and are used to determine the worst case scenario for the performance of the pier. An upper bound estimation of the column strength is needed as development of the column overstrength moment will induce larger forces into the pilecap. The pilecap is assessed to be the weak link in the original pier design and a lower bound for the strength is appropriate for this element.

2.3.2.2 Test Unit Design

The forces resulting from the estimated reinforcement strengths in Pier 46 were matched in Unit I-B by adjusting the number of bars required in the test specimen to achieve a scaled strength corresponding to the strength of the actual pier. With the scale factor of 1:3.8 the 1 $^1/_2$ inch diameter column and pilecap mat bars could be modelled with 10 mm diameter reinforcing bars. The 1-inch diameter pilecap mat bars were modelled using 6 mm diameter reinforcing bars. The proposed retrofit measures for Unit I-B specified HD20 bars which could not be modelled directly with commercially available reinforcing steel bars. HD6 bars were used to model the HD20 bars with allowances made for differences in the specified and actual yield strengths, spacings and embedment lengths of the HD6 bars as they were modelling bars of a larger size.

A moment-curvature analysis was used to match the flexural strength of the column in Unit I-B and the scaled flexural strength of the column of Pier 46. This resulted in 80 longitudinal column bars being required for Unit I-B compared to the 76 longitudinal bars in Pier 46. Pilecap mat reinforcing in Unit I-B was matched using an equivalent force criterion matching the yield force of the reinforcing bars in each mat compared to the scaled forces from yielding of the pilecap mat bars in Pier 46 with an assumed yield strength of $f_y = 286$ MPa.

Post-tensioning of Unit I-B was designed to give the same forces at transfer as will be present in Pier 46 after long term losses have occurred. It was found that the rather significant losses in Unit I-B due to pull in of the anchor wedges matched the losses through relaxation of the steel that will occur in Pier 46 after approximately 20 years. Two 15.6 mm diameter tendons longitudinally and two 12.7 mm diameter tendons transversely were placed through ducts cast into the original pilecap of Unit I-B.

The steel jacket for Pier 46 was designed to achieve the required curvature ductility in the column to exceed the expected ductility demands on the structure corresponding to a 500 year return period earthquake at the Thorndon Overbridge site. Design of the jacket for Unit I-B was carried out using a moment-curvature analysis of the test specimen column modelling a steel jacket to achieve the same ultimate concrete compressive strain in the test specimen as achieved with a 12 mm thick steel jacket in Pier 46. A 3 mm thick steel jacket for Unit I-B was found to be sufficient to model the 12 mm thick jacket proposed for Pier 46.

2.3.2.3 Materials

Steel for the reinforcement of Unit I-B was sourced from New Zealand and Japanese steel suppliers. Concrete for the as-built and retrofit part of the test specimen was supplied by a local ready-mix concrete supplier to a specific mix designed specially for the test program. The concrete mix design was determined from results from testing of the concrete used in the construction of the baseblock. A concrete compressive strength of 55 MPa, representing the lower characteristic strength of the concrete tested from the Thorndon Overbridge [B1], at time of testing was targeted

for the as-built part of Unit I-B with a compressive strength of 30 MPa specified for the concrete used in the pilecap overlay and anchor blocks.

Table 2.3 shows the mechanical properties of the reinforcing steel used in the construction of Unit I-B obtained from monotonic tensile testing of the steel.

Table 2.4 shows the concrete mix design for the as-built and retrofit parts of Unit I-B. Slump, compressive strength results, at 28 days and at time of testing, and splitting test results are shown for the pilecap, column and overlay concrete in Table 2.5. All concrete mixes for the test specimen were designed with the requirement that the mix be suitable for placement using a standard concrete grout pump. This involved the addition of superplasticiser on site, after an initial slump test was conducted, until the concrete had sufficient workability to be placed by pumping.

Table 2.3 *Mechanical Properties for Reinforcing Steel in Unit I-B*

Location	Description	f_y	f_u	f_u / f_y	E_s	ε_y	ε_{sh}	ε_u
		MPa	MPa		GPa	%	%	%
Column longitudinal bars	D10	320	463	1.45	197.7	0.16	2.6	21.5
Column transverse spirals	3.2 wire	261	375	1.44	200.0	0.13	2.4	14.5
Pilecap bottom mat	D10	320	463	1.45	197.7	0.16	2.6	21.5
Pilecap top mat	D6	340	509	1.50	242.5	0.14	2.3	24.5
Pilecap overlay and dowels[1]	HD6	440[2]	585	1.33	178.7	0.25	-	12.2

Notes:

[1] HD6 bars did not show a well defined yield plateau.

[2] Stress measured at 0.2% offset strain.

Table 2.4 *Concrete Mix Design for Unit I-B*

		As-built concrete	Retrofit concrete
Target Strength	MPa	55	30
Ordinary Portland Cement (Pacific Cement)	kg / m^3	455	323
Mortar Sand	kg / m^3	773	864
6 mm round aggregate	kg / m^3	1025	1056
Total Water	kg / m^3	200	200
Water Cement Ratio		0.44	0.62

Table 2.5 *Concrete Properties for Unit I-B*

			Compressive Strength (MPa)					Tensile Strength (MPa)
Location	Slump[1] (mm)	Age at time of testing (days)	Target Strength	Ambient[2] f'_c[4]		Fog Room[3] f'_c[4]		Fog Room f'_{sp}[5]
			At testing	28 day	At testing	28 day	At testing	At testing
Pilecap	70	109	55	43.6[6]	45.5	46.8[6]	59.2	4.1
Column	60	98	55	43.9	45.5	48.0	61.8	4.0
Overlay	50	49	30	25.5	31.4	28.9	41.7	3.2

Notes:

1. Slump recorded before addition of superplasticiser.
2. Test cylinders cured under same conditions and stored with test unit until time of testing.
3. Test cylinders cured and stored in fog room until time of testing.
4. Average of three 100 mm diameter by 200 mm high test cylinders.
5. Splitting test results average of two 100 mm diameter by 200 mm high test cylinders.
6. Pilecap cylinders tested at 34 days of age.

2.3.2.4 Construction of Unit I-B - Pilecap

The construction sequence of Unit I-B followed the same sequence as for Pier 46. The vertical spring units, representing the piles, were placed on the baseblock and bolted down. Restrainers and cross-bracing were put in place to prevent the vertical springs, which were pinned top and bottom, from moving while the test specimen was being constructed. The pilecap mould was placed on the vertical springs and the reinforcing cage for the column and pilecap mats fabricated. The pilecap bottom mat is placed over the top of the column reinforcing bars which are bent outward at the base. Reinforcement which would have carried up from the piles was modelled by welding HD6 reinforcing steel into a 20 mm plate which also served to anchor the bolts from the vertical springs to the bottom of the test specimen. The presence of these "pile brushes" required that some of the column bars be rearranged where they clashed. The column bars were placed so that the bars were resting on the top of the 20 mm plates of the "pile brushes". The presence of slots for applying the axial load to the specimen required adjustment of the diagonal trimmer bars around the column reinforcing cage, bundling the bars together instead of placing them as detailed for Pier 46. Some adjustment of the column longitudinal bars around the axial load slots was also required. The presence of a stormwater drain down the centre of the column in Pier 46 into the pilecap required some of the column longitudinal bars to be offset higher. These bars, marked C3 and C4, were also modelled in Unit I-B.

Figures 2.12 to 2.15 show the reinforcing layout for the column and pilecap of Unit I-B. The transverse reinforcement for the column was increased at the top to prevent any failure occurring at the top of the column where the lateral loading was applied. The transverse reinforcement was changed to 5.5 mm diameter wire, from the 3.2 mm wire, and the pitch reduced to 30 mm from 67 mm.

Figure 2.16 shows the pilecap reinforcement before casting of the concrete. Visible in the photograph are the pile brushes above the location of the vertical springs, slots for the axial load rods to pass through the pilecap and rubber tubing placed to form

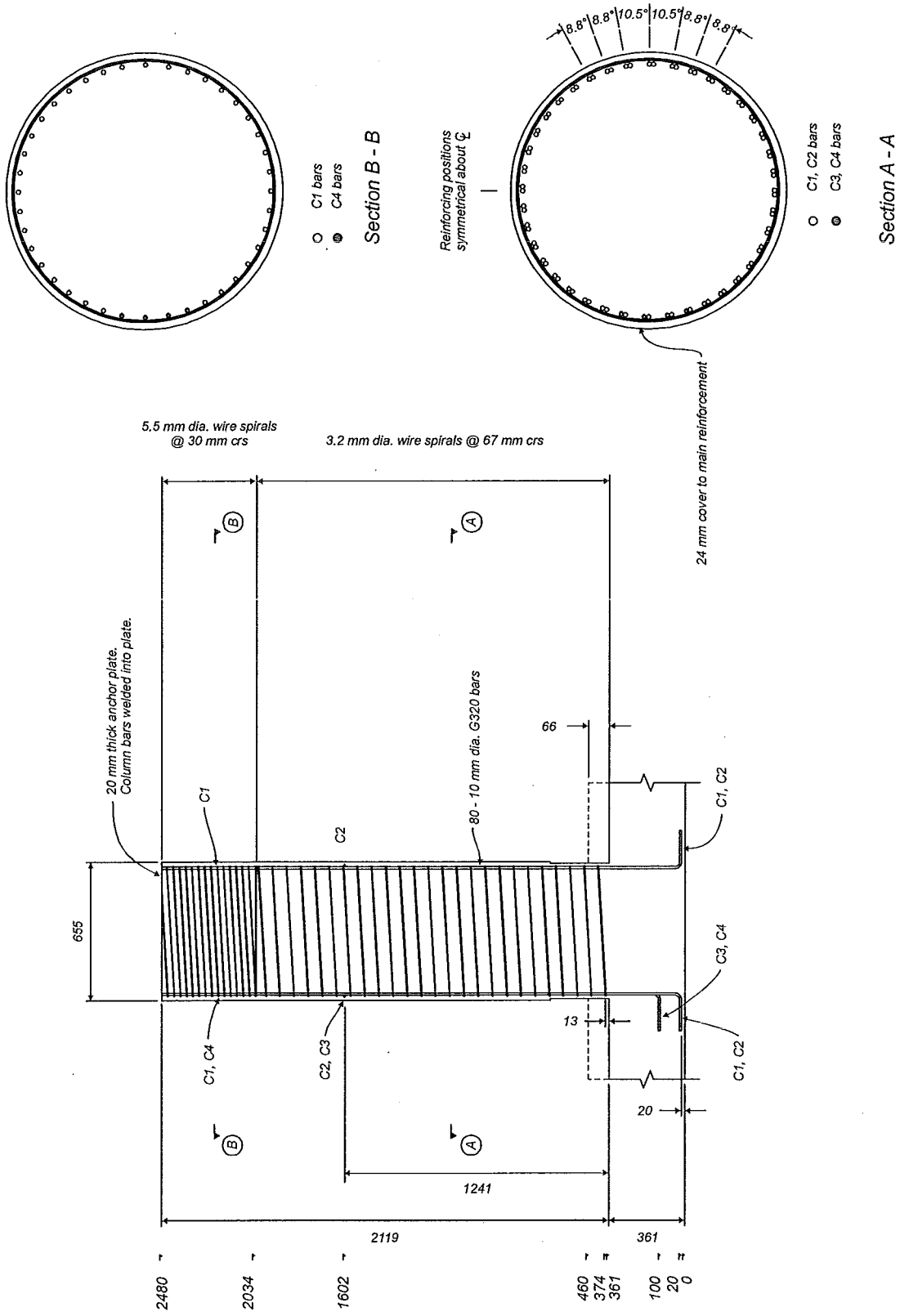

Figure 2.12 *Unit I-B Column Reinforcement*

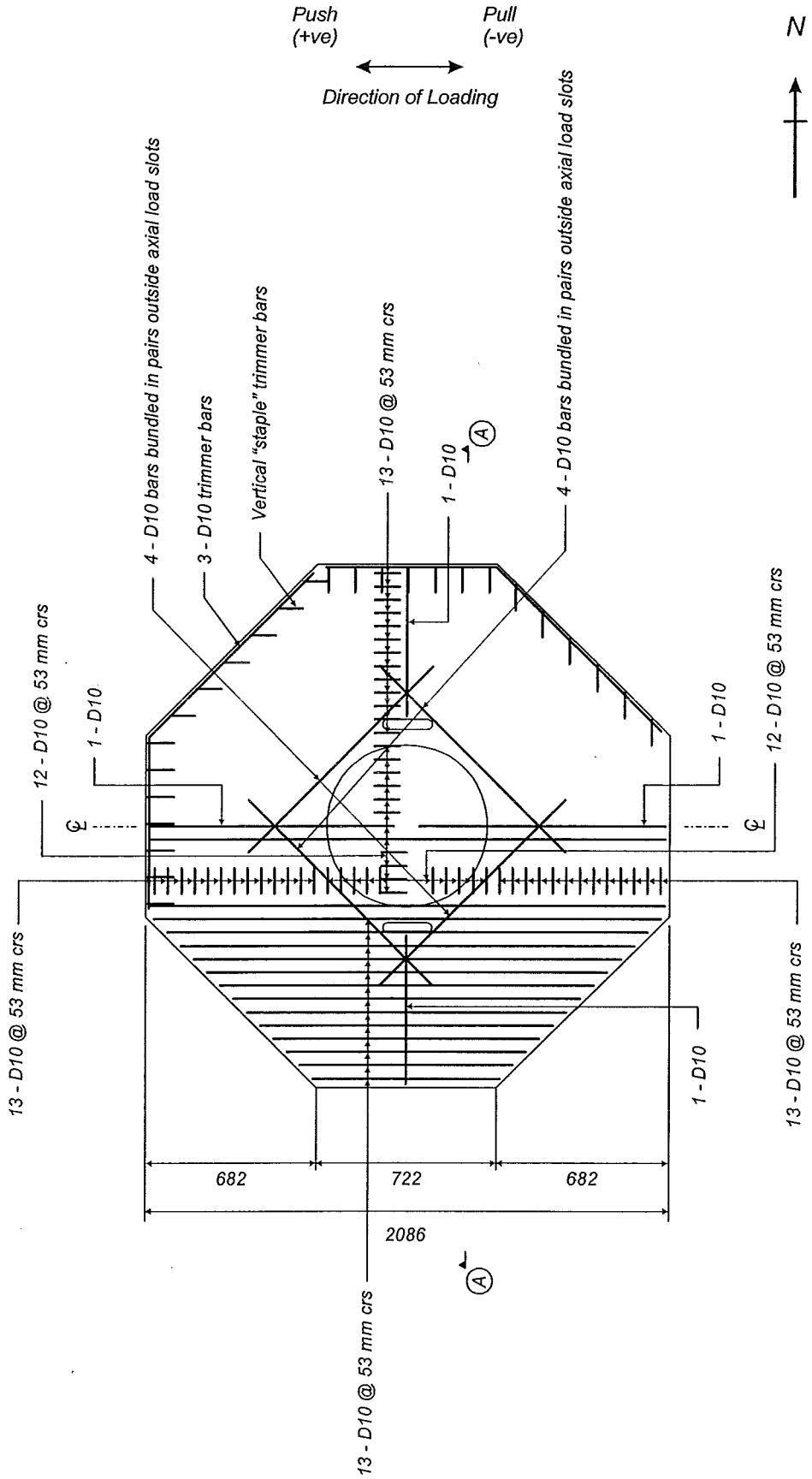

UNIT I-B TOP PILECAP MAT REINFORCEMENT

Figure 2.13 *Unit I-B Top Pilecap Mat Reinforcement*

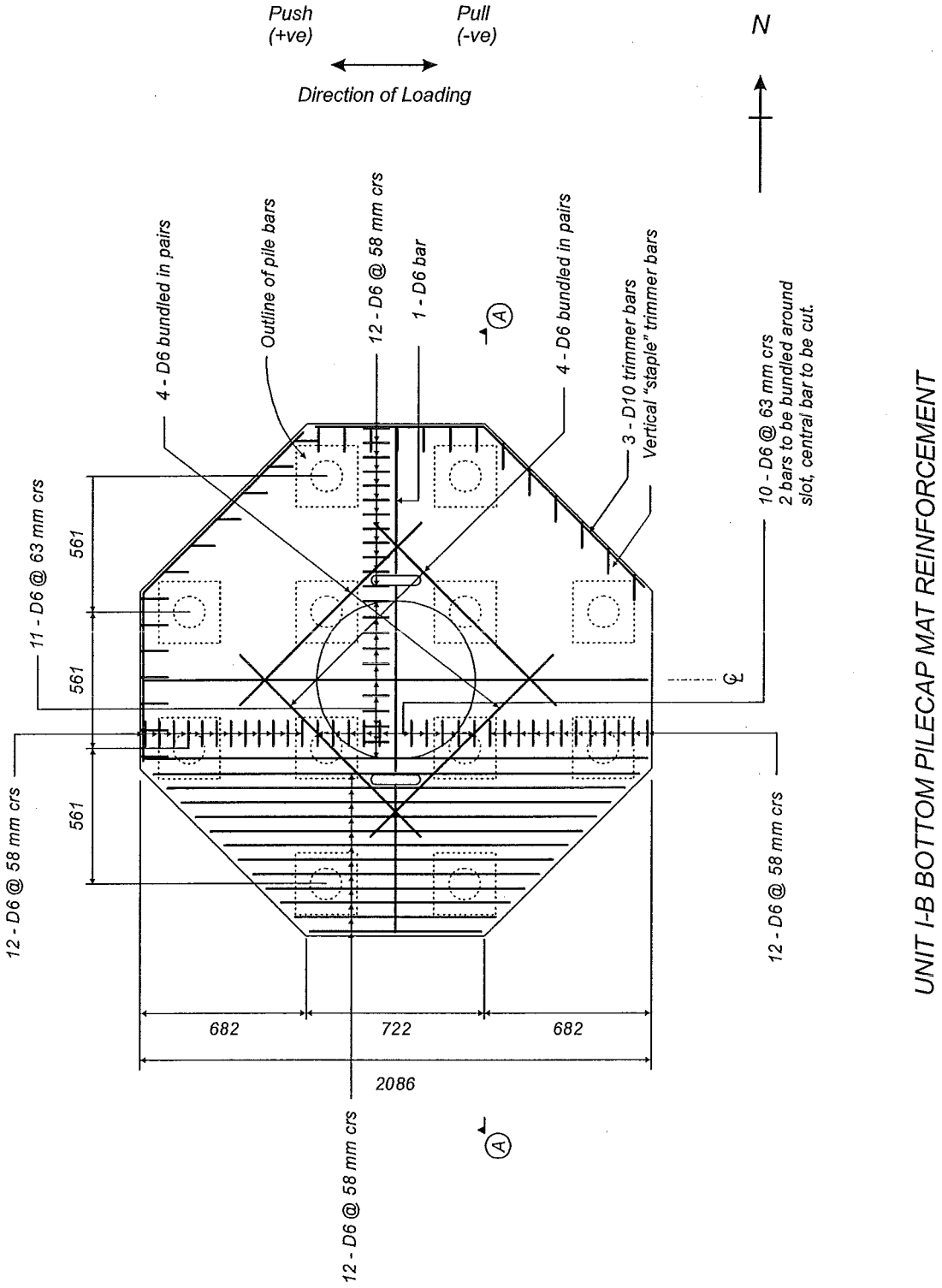

Figure 2.14 *Unit I-B Bottom Pilecap Mat Reinforcement*

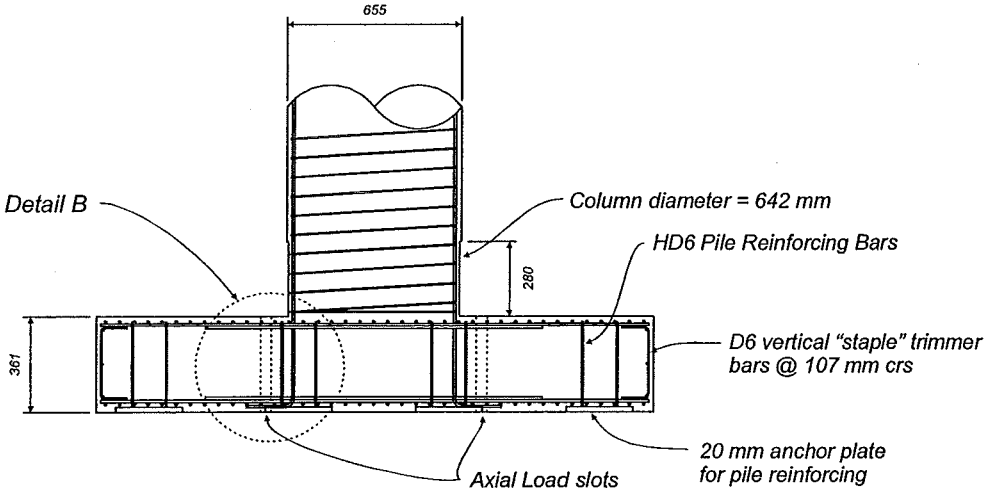

Section A- A

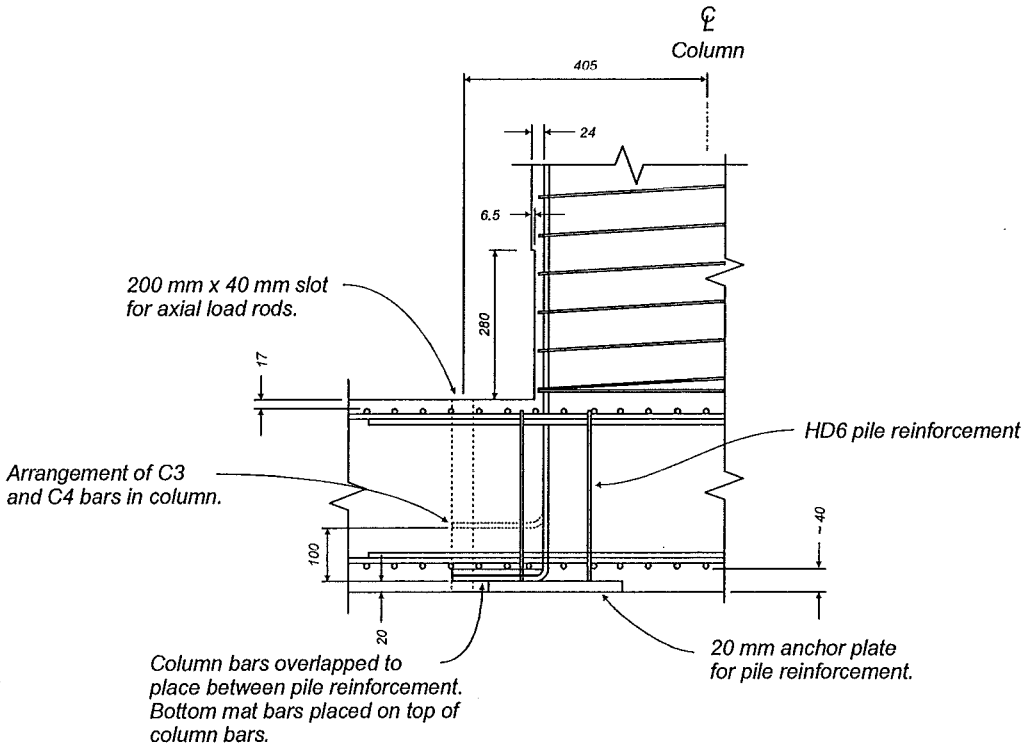

AS BUILT DETAIL B

Figure 2.15 *As-built Reinforcement Details at Base of Column for Unit I-B*

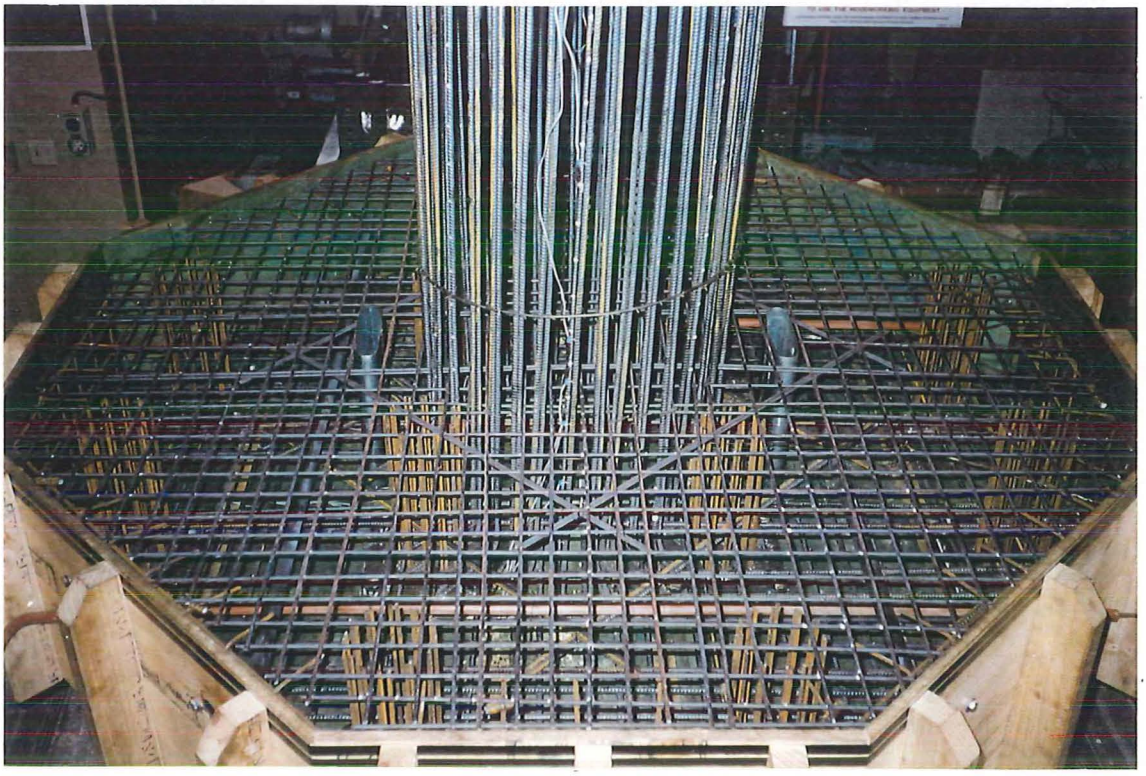

Figure 2.16 *Unit I-B Pilecap Reinforcement*

the ducts for placement of the cored through post-tensioning tendons for retrofit of the pilecap. The rubber tubing was cast into the pilecap and removed forming a duct through which the post-tensioning would be placed. This was easier to construct rather than coring holes through the pilecap after casting, as will have to be done in the actual piers.

The top surface of the pilecap was screed level and wood floated. A concrete retardant was applied to the area inside the column reinforcing cage to form a construction joint at the level of the pilecap. An acrylic curing compound, Sika Antisol-A, was applied to the top surface of the pilecap for curing purposes.

2.3.2.5 Construction of Unit I-B - Column

Casting of the pilecap was followed by casting of the column. The Thorndon Overbridge columns have a fluted architectural finish applied to the outside of the 8 foot (2.438 m) diameter circular columns. This finish was modelled in each of the

test specimens by increasing the diameter of the finished column by two-thirds of the scaled thickness of the fluted architectural finish. This architectural finish was applied from the ground level up so the column reverts to its original diameter where it is below the level of the ground.

The column mould was made in two semi-circular halves from 3 mm thick mild steel plate rolled to 655 mm diameter representing the column plus the architectural finish. A section at the base of the column 280 mm high, below the equivalent ground level for the test specimen, was reduced to 642 mm diameter by gluing a 6.5 mm thick rubber liner inside the column mould. The mould was bolted together around the column and sealed at the base and up the joins to prevent water and concrete fines leaking out of the mould.

2.3.2.6 Construction of Unit I-B – Retrofit Measures

Construction of the retrofit measures involved marking out and drilling of the holes for the hooked dowels in the pilecap. Figure 2.17 shows the location of the HD6 dowels in pilecap of Unit I-B. Nominal offset of the dowels was permitted to avoid clashes between the dowel holes and the top pilecap mat reinforcement. Each dowel was grouted into a 10 mm diameter hole using Conbextra GP, a proprietary cementious grout mix specified for the project. Each vertical dowel was hooked over the top pilecap overlay mat following the details of the retrofit design. Horizontal dowels were placed in the side of the pilecap to form the reinforcing cages of the new anchor blocks for the post-tensioning.

Tests on the grouting procedure, conducted by grouting a number of HD6 bars into the baseblock using the same procedures as for the overlay dowels, showed that the fracture strength of the bars could be reached without failing the grout. Construction specifications required a number of the vertical and horizontal dowels in the pilecap to be load tested before pouring of the overlay. Testing involved loading each dowel to 75% of its yield load and monitoring the load over a five minute period. The dowels were loaded to the specified load and the displacement held constant for five

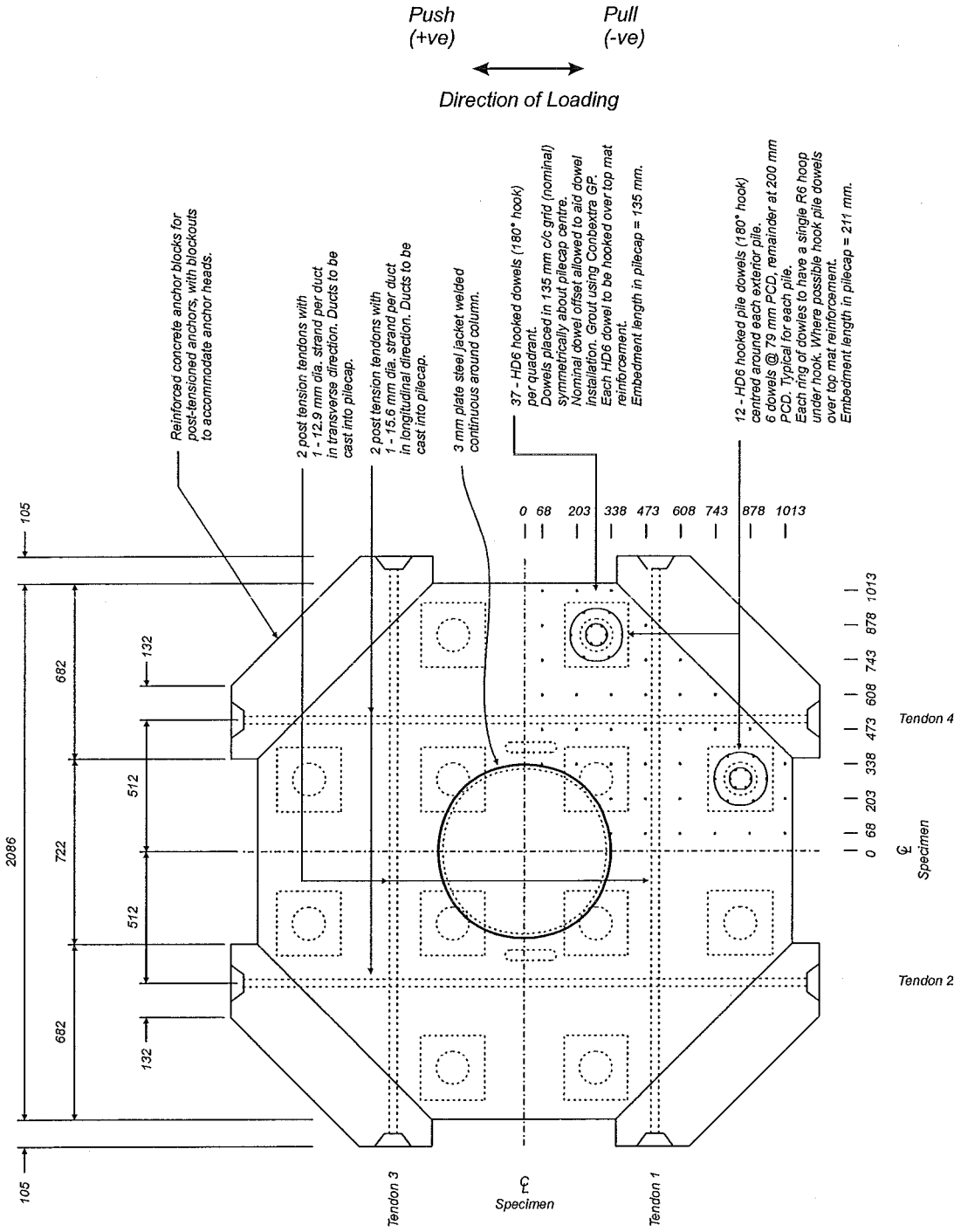

Figure 2.17 *Unit I-B Pilecap Overlay and Pile Dowel Layout*

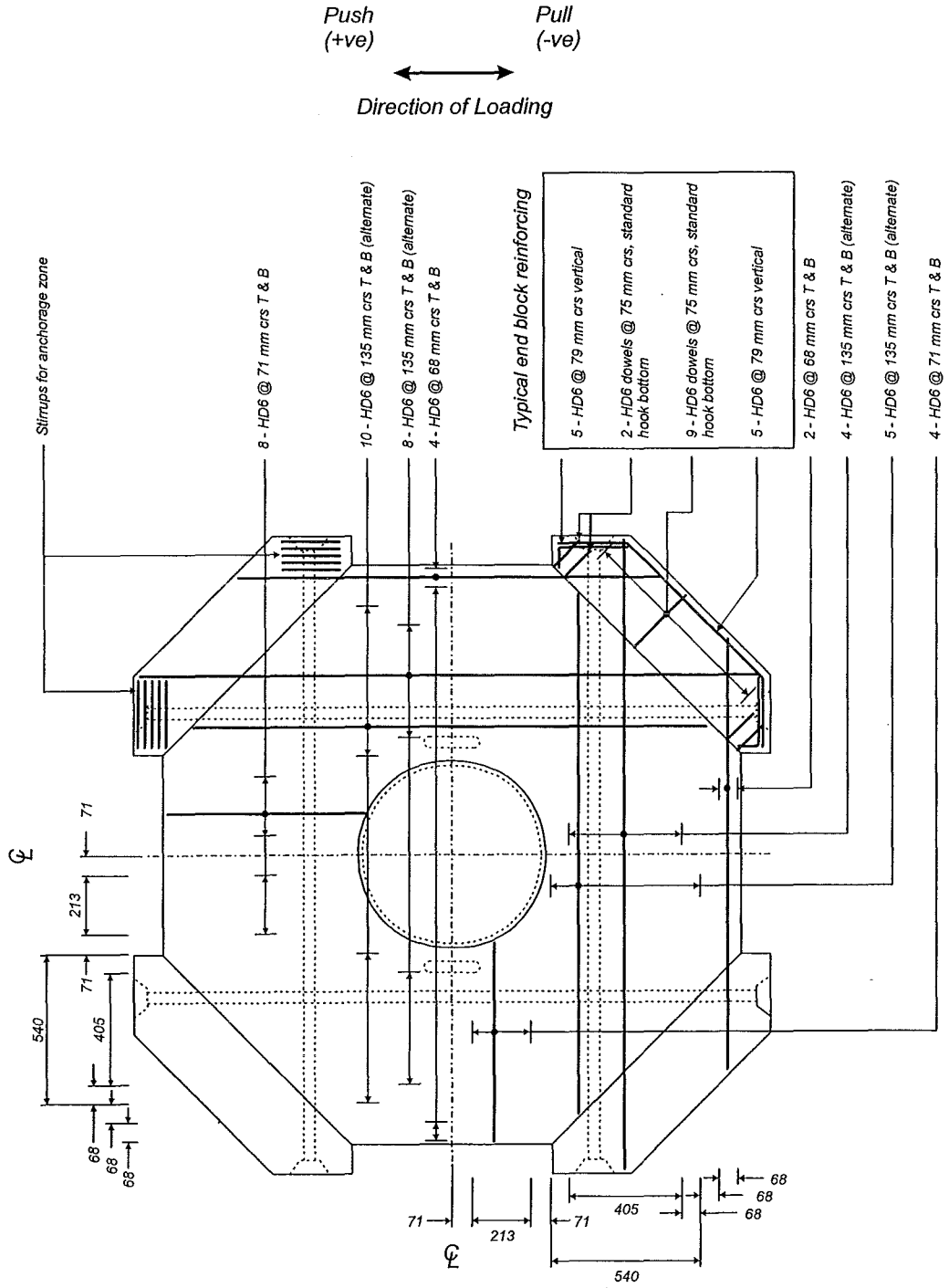

Figure 2.18 *Unit I-B Pilecap Overlay Reinforcement*

minutes while the load was monitored. All dowels maintained at least 95% of the initial applied load after a period of five minutes.

Figure 2.18 shows the layout of the pilecap overlay mat reinforcement and details for the anchor blocks at each corner of the pilecap. Additional spiral reinforcement and stirrup cages were placed around the anchorages for the post-tension tendons to contain the forces around each anchorage zone from the application of the post-tensioning force.

Figure 2.19 shows the pilecap overlay reinforcement before casting of the overlay concrete. After casting of the pilecap overlay, curing was effected by the application of Sika Antisol-A acrylic curing compound. The steel jacket around the base of the column was fitted by bringing the two semi-circular halves of the jacket around the column and welding them together. Ports were placed at the bottom of the jacket to allow the fitting of grout tubes to grout the jacket to the column once it was welded

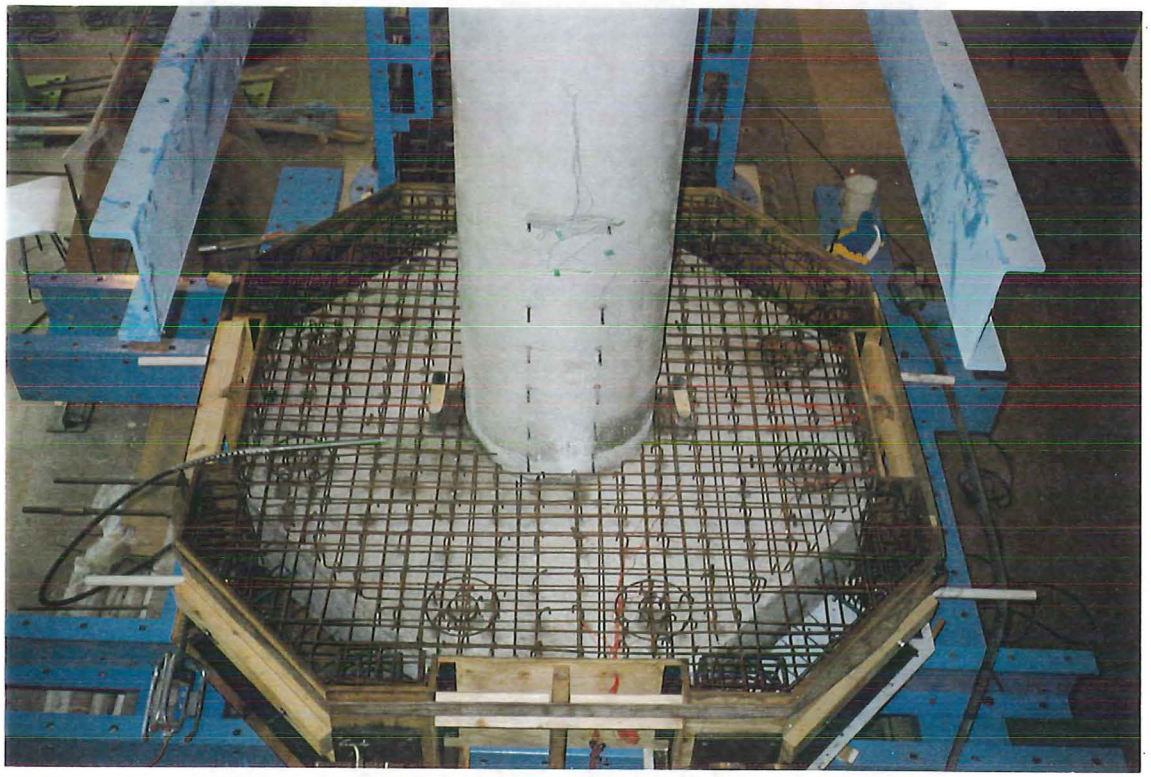

Figure 2.19 *Unit I-B Pilecap Overlay Reinforcement Before Pouring of Concrete*

in place. A 13 mm gap was left between the bottom of the jacket and the top surface of the pilecap overlay with an approximately 13 mm gap between the jacket and the surface of the column. Conbextra GP was used to grout the space behind the steel jacket. Figure 2.20 shows welding of the two steel jacket halves around the column.

Post-tensioning of the pilecap was carried out following the fitting of the column steel jacket. Transfer forces in the post-tensioning in Unit I-B were equivalent to the forces in Pier 46 after long term time dependent losses have occurred. Allowing for losses, including anchorage pull-in, transfer forces of 183 kN for the 15.6 mm diameter longitudinal strands and 132 kN for the 12.7 mm diameter transverse

Figure 2.20 *Welding of Steel Jacket Halves Around Column*

strands were used to provide the prestress force in the pilecap at transfer.

The axial load applied to the top of the column in Unit I-B, to represent the dead weight of the umbrella platform and adjacent suspended spans, was determined to apply the same compressive stress at the base of the column of the test specimen as acting at the base of the column in Pier 46. Two 500 kN centrehole rams were used to apply a total axial load of 600 kN to Unit I-B. The axial load was transferred through two 29 mm diameter VSL CT Stressbar rods from the rams at the top of the column to pinned fittings bolted to the baseblock. Both hydraulic rams were connected to a single pump through a manifold to ensure the same load was maintained in each ram. The axial load was monitored throughout the test through a calibrated pressure gauge and held constant during the test.

2.3.2.7 Vertical Spring Design

The function of the vertical springs in each of the test specimens is critical as the flexibilities of each of the vertical springs affect the bending moment and shear force distribution through the pilecap. As the piles in each pier are built into the pilecap they will influence the pilecap force distribution as some flexure will be carried in each pile. The piles used for Pier 46 are steel-cased reinforced concrete piles 2 feet (610 mm) in diameter. Structural analysis of Pier 46 modelling the pier with and without the flexural resistance of the piles showed little difference in the pilecap force distribution due to the relatively small flexural contribution from each pile. Subsequent analysis of Unit I-B also showed little difference in the pilecap force distribution when modelled with and without pile flexural resistance. This allowed the vertical springs in Unit I-B to be designed as pinned top and bottom thus carrying no shear or bending over their height.

The vertical stiffness of each pile still had to be modelled in Unit I-B, representing the combined soil-pile stiffness, to achieve the correct bending moment pattern through the pilecap under the application of lateral loads. The combined soil-pile stiffness from the structural analysis of Pier 46 was determined for compressive and

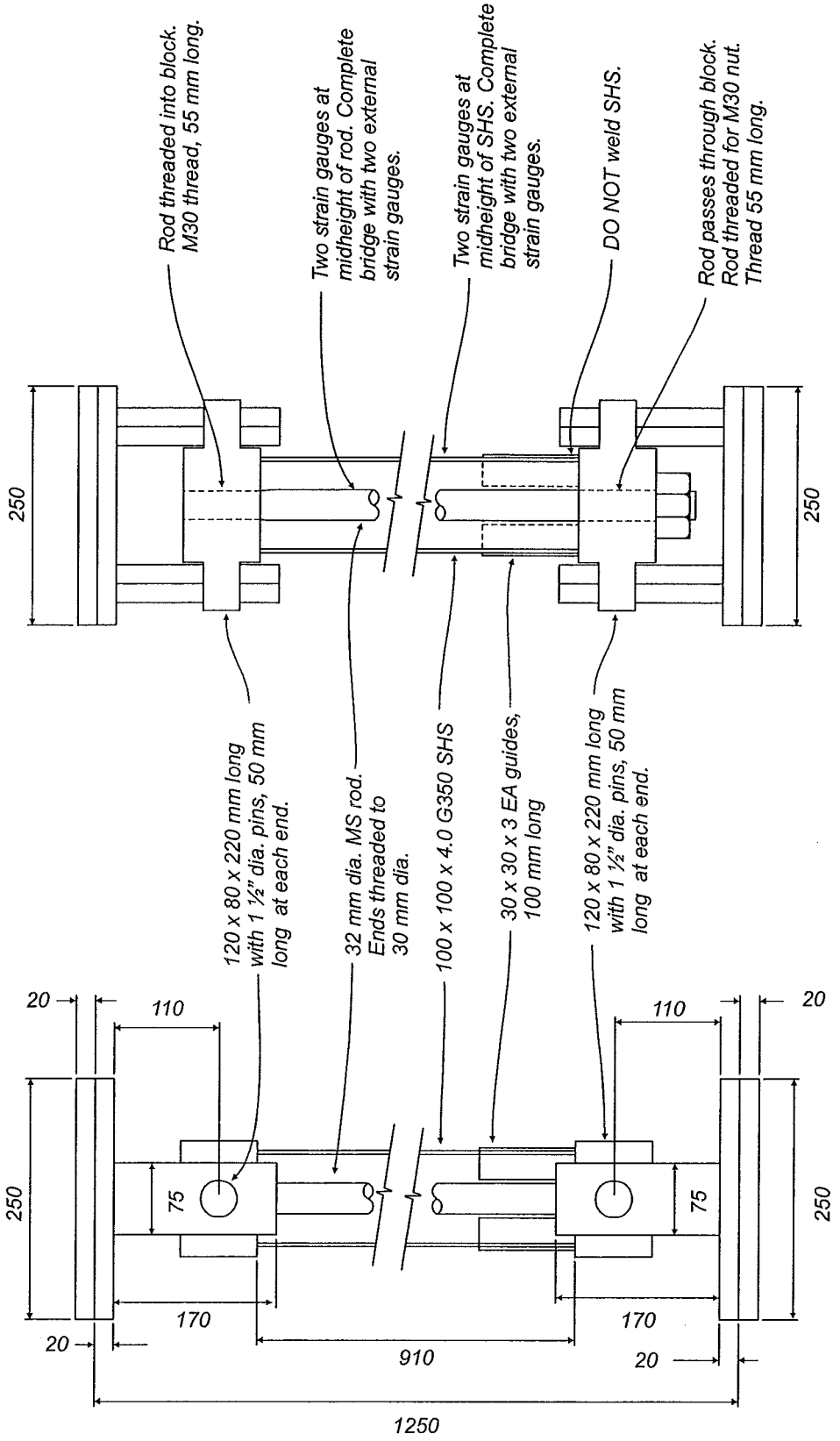

Figure 2.21 *Unit I-B Vertical Spring Details*

tensile loading of each pile. Matching the compression and tension stiffness values, as used in the structural analysis, for use in the vertical springs proved to be too difficult to achieve in the test specimen. In order to reproduce the same bending moment and shear force distribution in the pilecap the *relative* compression-to-tension stiffness ratio had to be maintained. Using different stiffness values in the vertical springs, as compared to the soil-pile stiffness used in the structural analysis of Pier 46, would affect the lateral displacement of the test specimen compared to the actual pier. By maintaining the same tension to compression stiffness ratio in the vertical springs for Unit I-B the same force distribution pattern would be achieved and a mathematical relationship can be developed to translate test specimen displacements to the equivalent displacements in Pier 46.

A compressive soil spring stiffness of 225 kN/mm and a tensile soil spring stiffness of 95 kN/mm per pile were taken as average soil stiffness in the structural analysis of Pier 46. Including the contribution of the axial flexibility of the individual piles gave a tensile stiffness of 81.5 kN/mm and a compressive stiffness of 161.6 kN/mm for each pile. The required stiffness of the vertical springs, with a scale factor of 1:3.8, is then 21.4 kN/mm in tension and 42.5 kN/mm in compression giving a compression-to-tension stiffness ratio of 1.99 for each vertical spring.

Stresses in each vertical spring were limited to approximately 60% of the yield stress of the material. A 100 x 100 x 4.0 Grade 350 cold-formed SHS (square hollow section) section was selected to resist the compressive loads in the spring. In order to maintain the stiffness ratio of 1.99 a 32 mm diameter mild steel rod was required to transfer the tensile forces in each vertical spring. Figure 2.21 shows a schematic layout of a vertical spring used in Unit I-B. The compressive forces are taken by bearing of the SHS section on the bottom bracket containing the pin connection. The SHS section is not welded to the bottom bracket, which allows it to separate when the vertical spring goes into tension. The rod, inside the SHS section, is threaded into the top bracket and passing through and secured by a nut at the bottom bracket.

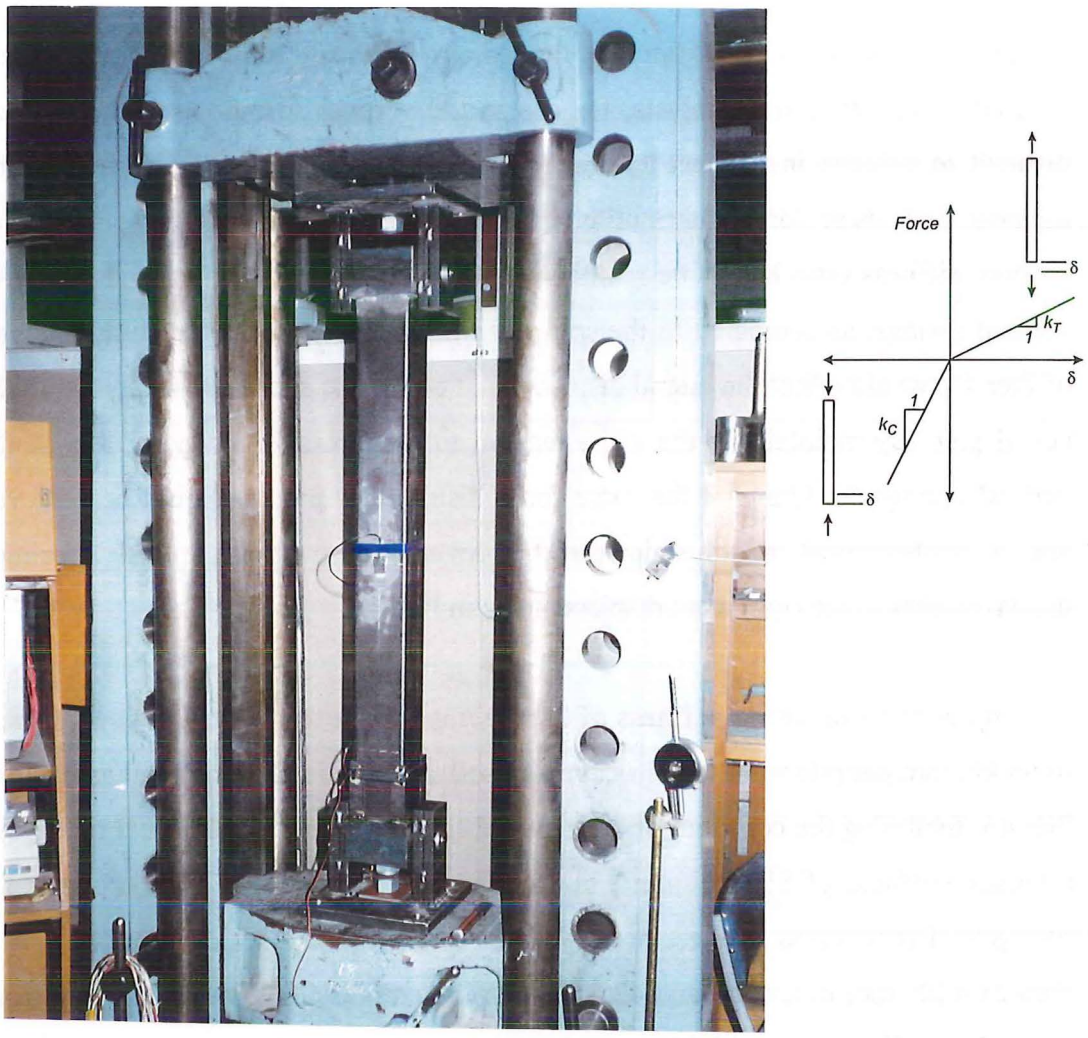

Figure 2.22 *Unit I-B Vertical Spring Ready for Calibration*

The nut is tightened by hand until it just contacts the bottom bracket. This is to ensure there is no slip of the rod through the bottom bracket so that the tension force is taken up by the rod immediately.

Each vertical spring was calibrated for load in compression and tension, before being placed into the test rig, using a 1000 kN Avery Universal Testing Machine. The SHS section and the steel rod were both strain gauged to form, in conjunction with two external dummy strain gauges, a full bridge for recording the loads in each section. Two channels per spring recorded the compressive and tensile loads in each spring during the test. Figure 2.22 shows a vertical spring unit placed in the Avery UTM for calibration.

2.3.3 Unit I-A

Unit I-A was the second of the two test specimens tested. It is based on Pier 68 of the Thorndon Overbridge.

2.3.3.1 Pier 68 Retrofit Measures

Pier 68 is a typical Stage 3 pier with an 8 feet (2.438 m) thick reinforced concrete pilecap 28 feet (8.534 m) square supporting a single 8 feet (2.438 m) diameter circular reinforced concrete column. The pilecap is supported on four 5 feet (1.524 m) diameter steel cased reinforced concrete bored piles at each corner of the pilecap. The column is reinforced at the base with a total of 93 2 $^1/_4$-inch (57 mm) diameter longitudinal bars bundled in groups of three. Transverse reinforcement consists of $^3/_4$ inch (19 mm) diameter circular hoops at 4 inch (102 mm) centres at the base of the column, extending to 6 inch (152 mm) spacings over the remainder of the column height.

The bottom pilecap mat consisted of 1 $^1/_2$ inch (38 mm) diameter bars arranged in two layers. The top pilecap mat is made up of a single layer of 1 $^1/_4$ inch (32 mm) diameter bars.

The retrofit design involved the construction of a new 750 mm thick reinforced concrete pilecap overlay. HD20 hooked dowels are placed on a 390 mm grid over the top surface of the original pilecap. Additional HD24 dowels are grouped around each pile to transfer the pile tension forces up to the top of the pilecap overlay. A single reinforcing mat of HD20 bars is placed at the top of the overlay.

The new pilecap overlay is designed to strengthen the pilecap and force all inelastic action to take place at the base of the column. Due to the increased quantities of transverse reinforcement at the base of the column in Pier 68, as compared to Pier 46, no additional column retrofit is required to meet the expected ductility demands on the column.

Analysis of the forces acting in Pier 68 were also based on $f_y = 350$ MPa for the column longitudinal reinforcing and $f_y = 286$ MPa for the column transverse and pilecap reinforcement to determine the worst case with high column strength and low pilecap strength. The assessed flexural strength of the retrofitted pilecap is approximately 5 % greater than the flexural strength demand caused by the column overstrength moment. Original concepts for the retrofit design centred on the possibility of the pilecap hinging before, or at approximately the same time as, the base of the column developing its flexural strength. Testing was required to determine whether this case would be likely and to assess the available ductility of a pilecap hinging mechanism. Further analysis and design refinements found that the retrofitted pilecap would have a margin of flexural strength over the column overstrength, and thus the pilecap would be unlikely to yield.

2.3.3.2 Test Unit Design

The forces resulting from the assumed reinforcement strengths in Pier 68 were matched in Unit I-A by adjusting the number of bars required in the test specimen to achieve a scaled strength corresponding to strength of the actual pier. With the scale factor of 1:3.8 the 2 $^1/_4$ inch diameter column bars could not be modelled directly with commercially available reinforcing bar sizes. The use 16 mm diameter bars and the measured yield strength of the bars required a total of 93 longitudinal bars to be provided in the column of Unit I-A, the same number of column bars as for Pier 68. The 1 $^1/_2$ inch diameter pilecap bottom mat bars were modelled using 9.6 mm diameter reinforcing bars with 6 mm diameter bars used to model the 1 $^1/_4$ inch diameter pilecap top mat bars. The number of bars in the pilecap mats were adjusted to match the scaled yield force in the pilecap mats of Pier 68. The proposed retrofit measures for Unit I-A specified HD20 bars which could not be modelled directly with commercially available reinforcing steel bars. HD6 bars were used to model the HD20 bars with allowances made for differences in the specified and actual yield strengths, and the spacings and embedment lengths of the HD6 bars as they were modelling bars of a larger size.

2.3.3.3 Materials

Steel reinforcement and concrete used for Unit I-A were sourced from the same suppliers as for Unit I-B. A concrete compressive strength of 55 MPa, representing the lower characteristic strength of the concrete tested from the Thorndon Overbridge [B1], at time of testing was targeted for the as-built part of Unit I-A with a compressive strength of 40 MPa specified for the concrete used in the pilecap overlay.

Table 2.6 shows the mechanical properties of the reinforcing steel used in the construction of Unit I-A, obtained from monotonic tensile testing of the steel. Table 2.7 shows the concrete mix design for the as-built and retrofit parts of Unit I-A. Slump, compressive strength results at 28 days and at time of testing, and splitting test results are shown for the pilecap, column and overlay concrete in Table 2.8. Higher concrete compressive strengths were noted for the test cylinders stored with the test unit compared to the cylinders cured in the fog room.

2.3.3.4 Construction of Unit I-A - Pilecap and Column

The construction sequence of Unit I-A followed the same sequence as for Pier 68. The as-built part of Unit I-A was constructed on top of the baseblock while the vertical spring units for this specimen were being fabricated. The column cage was fabricated and positioned in the centre of the pilecap mould so that the pilecap bottom mat could be placed over the top of the column reinforcing bars which are bent outward at the base. Reinforcement from each of the four piles were modelled by welding D10 reinforcing steel into a 20 mm plate which also served to anchor the bolts from the vertical springs to the bottom of the test specimen. The transverse reinforcement in each pile reinforcement unit was also detailed.

Table 2.6 *Mechanical Properties for Reinforcing Steel in Unit I-A*

Location	Description	f_y	f_u	f_u / f_y	E_s	ε_y	ε_{sh}	ε_u
		MPa	MPa		GPa	%	%	%
Column longitudinal bars	D16	311	468	1.50	207.8	0.15	2.7	22.9
Column transverse spirals	5.5 wire	269	407	1.51	171.0	0.16	2.5	24.3
Pilecap bottom mat	D9.6	341	516	1.51	195.9	0.17	2.0	18.5
Pilecap top mat[1]	HD6	440[2]	585	1.33	178.7	0.25	-	12.2
Pilecap overlay and dowels[1]	HD6	440[2]	585	1.33	178.7	0.25	-	12.2

Notes:

[1] HD6 bars did not show a well defined yield plateau.

[2] Stress measured at 0.2% offset strain.

Table 2.7 *Concrete Mix Design for Unit I-A*

		As-built concrete	Retrofit concrete
Target Strength	MPa	55	40
Ordinary Portland Cement (Pacific Cement)	kg / m^3	444	426
Mortar Sand	kg / m^3	742	802
6 mm round aggregate	kg / m^3	1024	980
Total Water	kg / m^3	200	200
Water Cement Ratio		0.45	0.47

Table 2.8 *Concrete Properties for Unit I-A*

Location	Slump[1] (mm)	Age at time of testing (days)	Compressive Strength (MPa)					Tensile Strength (MPa)
			Target Strength	Ambient[2] f'_c[4]		Fog Room[3] f'_c[4]		Fog Room f'_{sp}[5]
			At testing	28 day	At testing	28 day	At testing	At testing
Pilecap	90	130	55	50.5	55.6	39.1	47.8	3.4
Column	80	123	55	49.5	57.8	41.7	47.7	3.6
Overlay	90	60	40	45.7	47.7	35.6	38.7	3.0

Notes:

1 Slump recorded before addition of superplasticiser.

2 Test cylinders cured under same conditions and stored with test unit until time of testing.

3 Test cylinders cured and stored in fog room until time of testing.

4 Average of three 100 mm diameter by 200 mm high test cylinders.

5 Splitting test results average of two 100 mm diameter by 200 mm high test cylinders.

Figures 2.23 to 2.25 show the reinforcing layout for the column and pilecap of Unit I-A. The transverse reinforcement for the column of Unit I-A was determined directly from scaling the spacings from the column of Pier 68 without consideration of the difference in yield strength between the assumed 286 MPa for the $^3/_4$ inch (19 mm) diameter transverse reinforcement in Pier 68 and the 269 MPa of the 5.5 mm wire in Unit I-A. This resulted in an approximately 12 % increase in the shear strength provided by the transverse steel in Unit I-A as compared to Pier 68. This increase in steel shear strength contribution is not regarded as significant as the column shear strength is dominated by the concrete contribution to shear resistance.

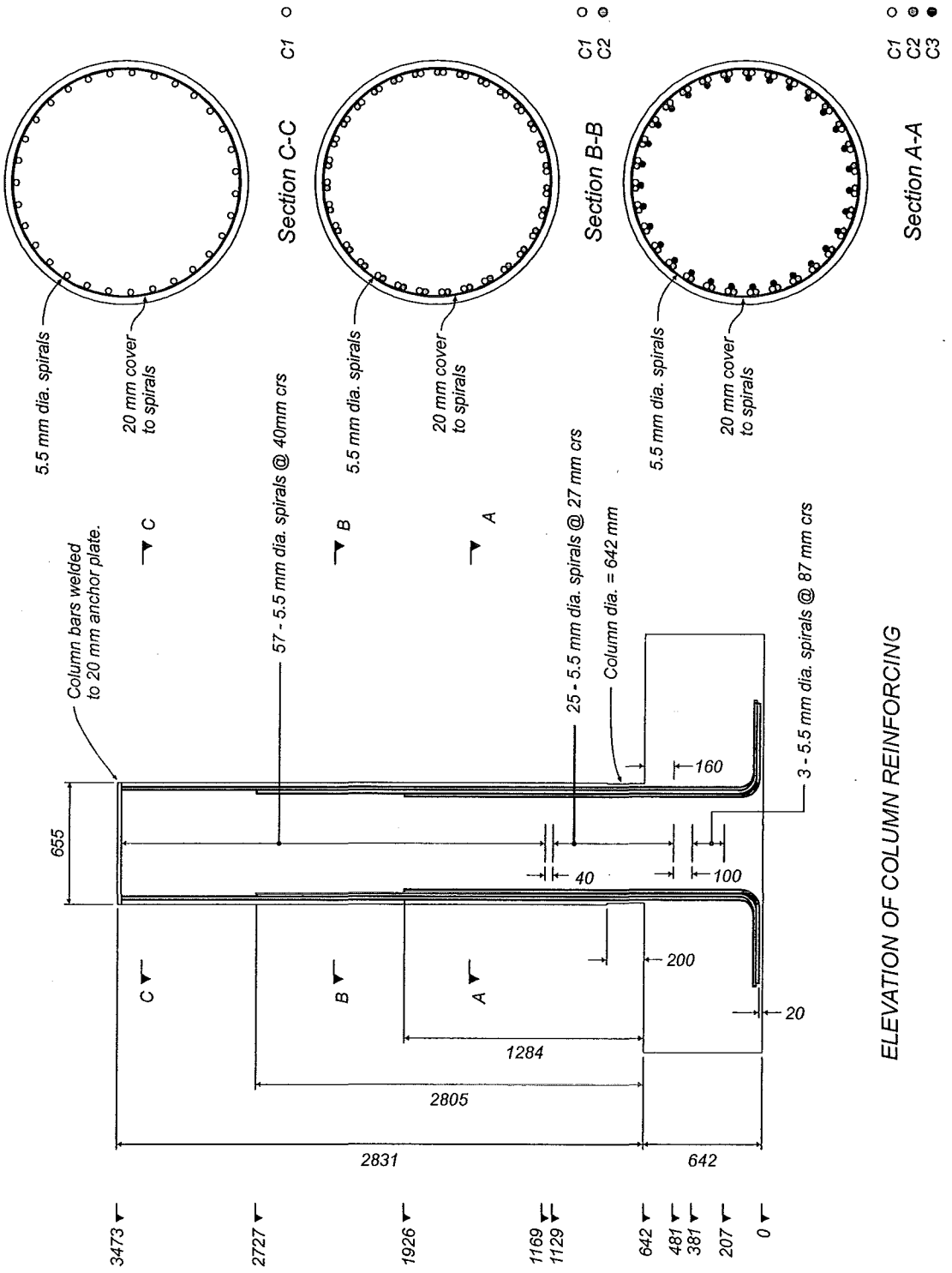

Figure 2.23 *Unit I-A Column Reinforcement*

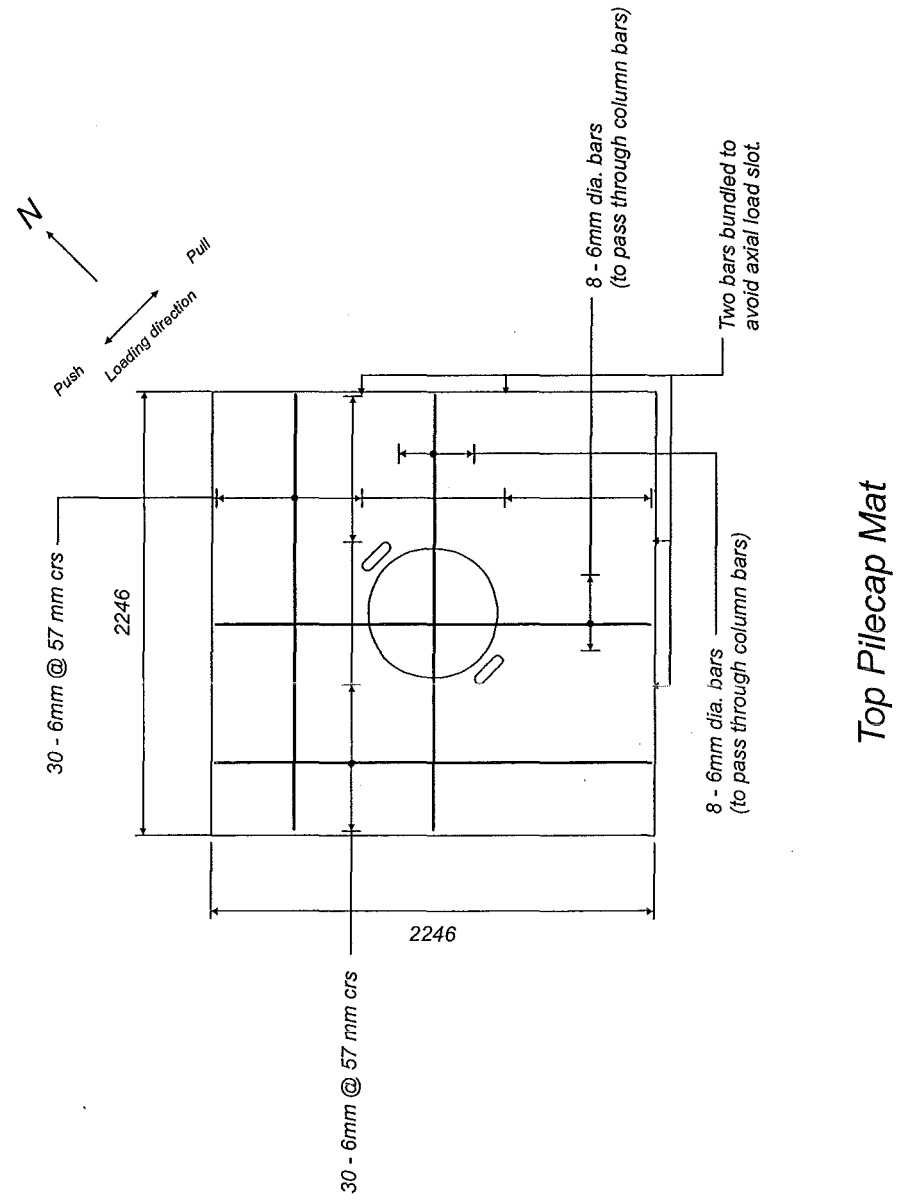

Figure 2.24 *Unit I-A Top Pilecap Mat Reinforcement*

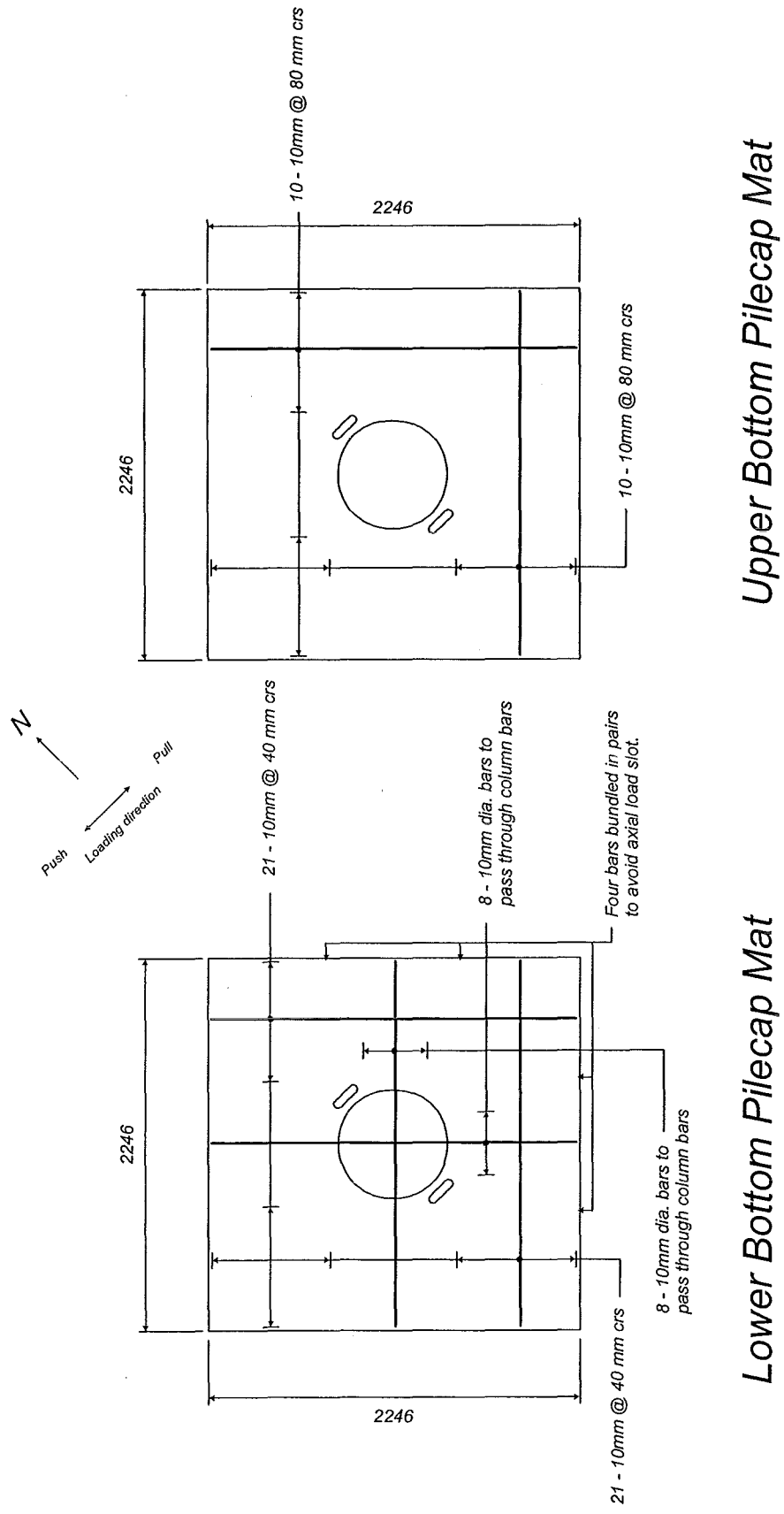

Figure 2.25 *Unit I-A Bottom Pilecap Mat Reinforcement*

Figure 2.26 shows the pilecap reinforcement before casting of the concrete. Visible in the photograph are the pile reinforcement, slots for the axial load rods to pass through the pilecap and corrugated post-tensioning ducts. These ducts were placed to allow post-tensioning of the pilecap in case yielding of the pilecap occurred and insufficient ductility capacity was available during testing. The post-tensioning would allow the pilecap to be strengthened and testing continued to force inelastic action to concentrate in the column. The angled corners in the pilecap provided reaction points for bearing of the lateral springs on the side of the pilecap during testing.

The top surface of the pilecap was screed level and wood floated. A concrete retardant was applied to the area inside the column reinforcing cage to form a construction joint at the level of the pilecap. Due to the poor results from use of the acrylic curing compound in Unit I-B, the top surface of the pilecap was wet cured for seven days in the traditional manner.

The fluted architectural finish on the columns was modelled in Unit I-A by increasing the diameter of the column by two-thirds the scaled thickness of the fluted finish. Below ground level the column reverted back to the original diameter of 8 feet (2.438 m) which corresponds to the bottom 200 mm of the column in Unit I-A.

2.3.3.5 Construction of Unit I-A - Retrofit Measures

The as-built part of Unit I-A was lifted up on to the vertical spring units after pouring of the column in order to complete the construction of the pilecap overlay. Figure 2.27 shows the pilecap overlay reinforcement before pouring of the overlay concrete. Figure 2.28 shows the layout of the hooked dowels in the top of the pilecap and Figure 2.29 shows the layout of the reinforcing mat in the top of the overlay.

Nominal offset of the dowels was permitted to avoid clashes between the dowel holes and the top pilecap mat reinforcement. Each dowel was grouted into 10 mm diameter holes using Conbextra GP as specified for the project. Each vertical dowel

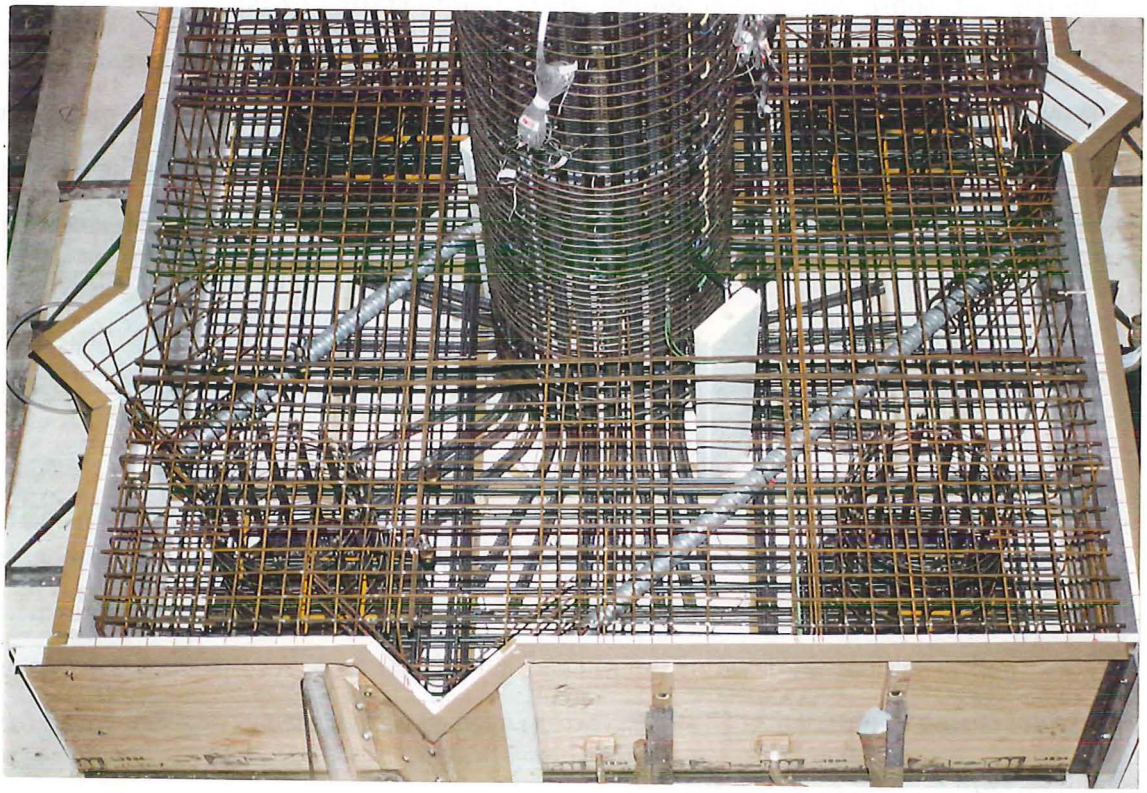

Figure 2.26 *Unit I-A Pilecap Reinforcement*

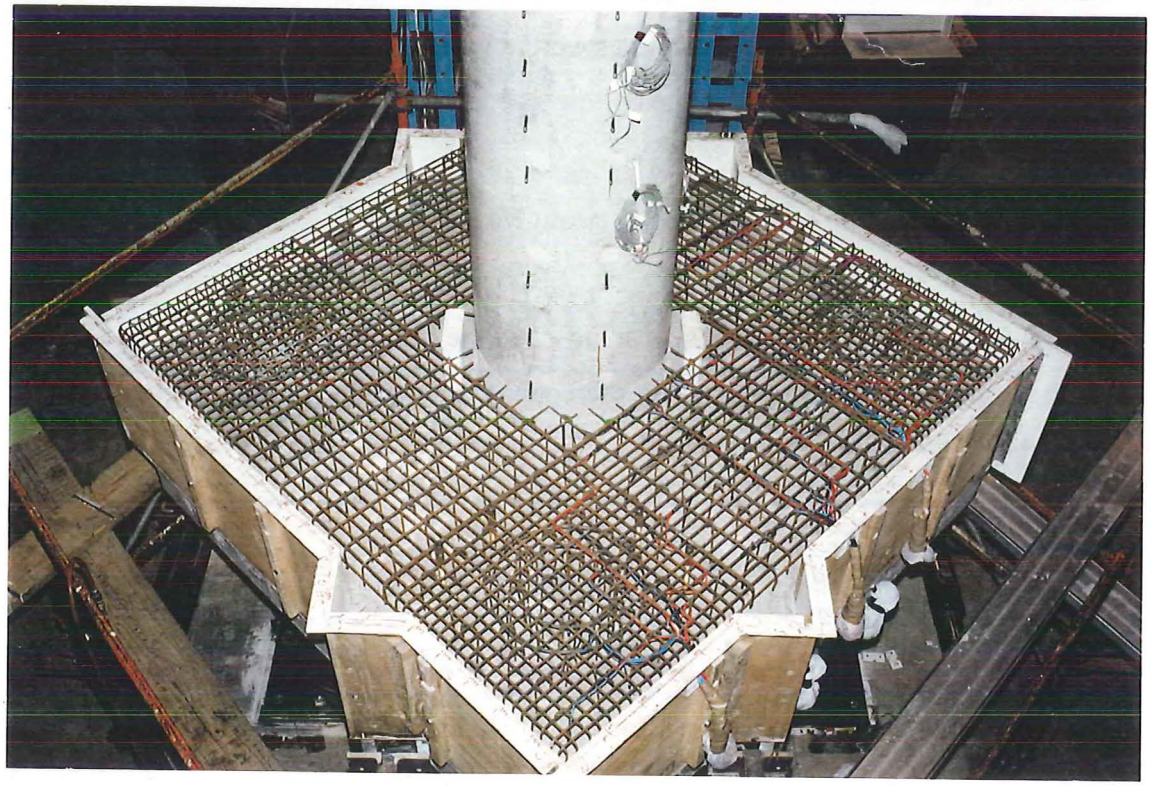

Figure 2.27 *Unit I-A Pilecap Overlay Reinforcement*

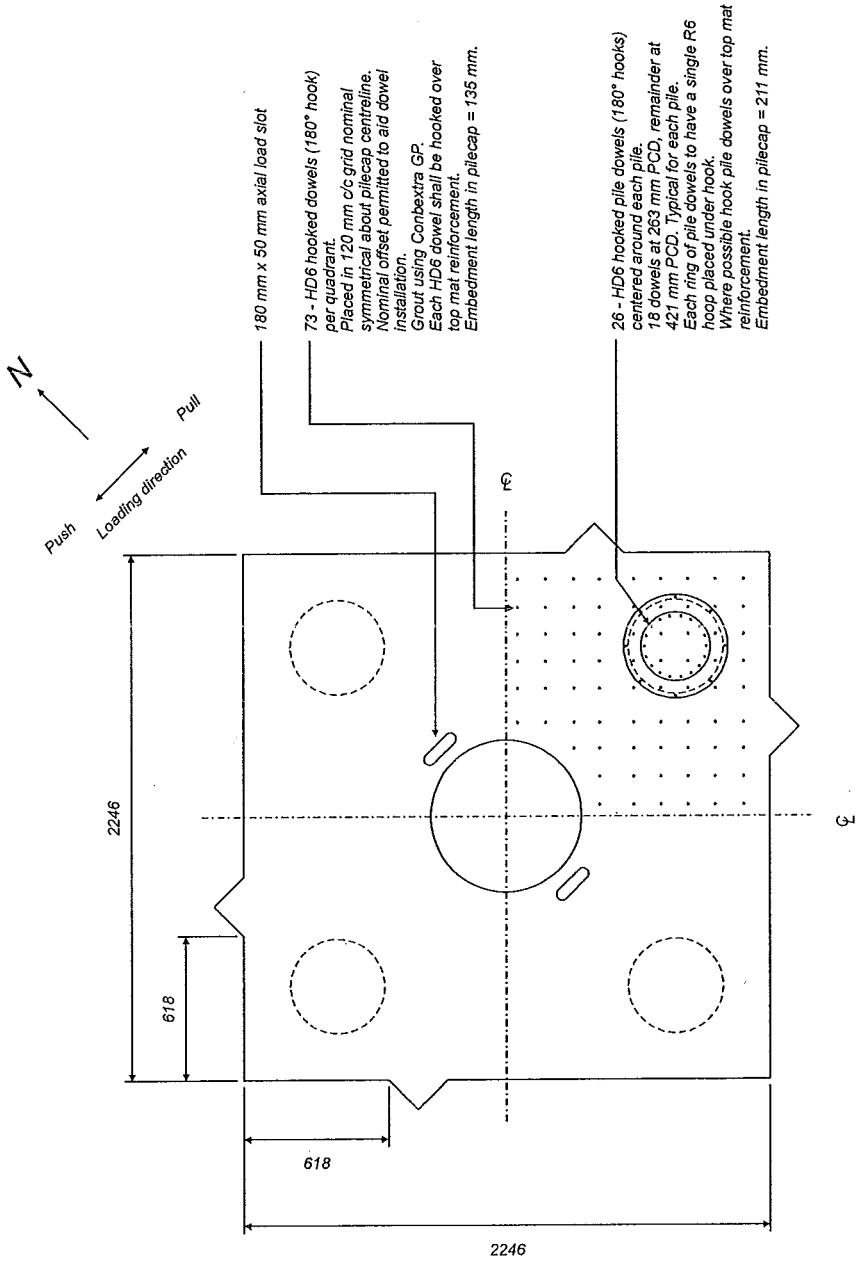

Figure 2.28 *Unit I-A Overlay and Pile Dowel Layout*

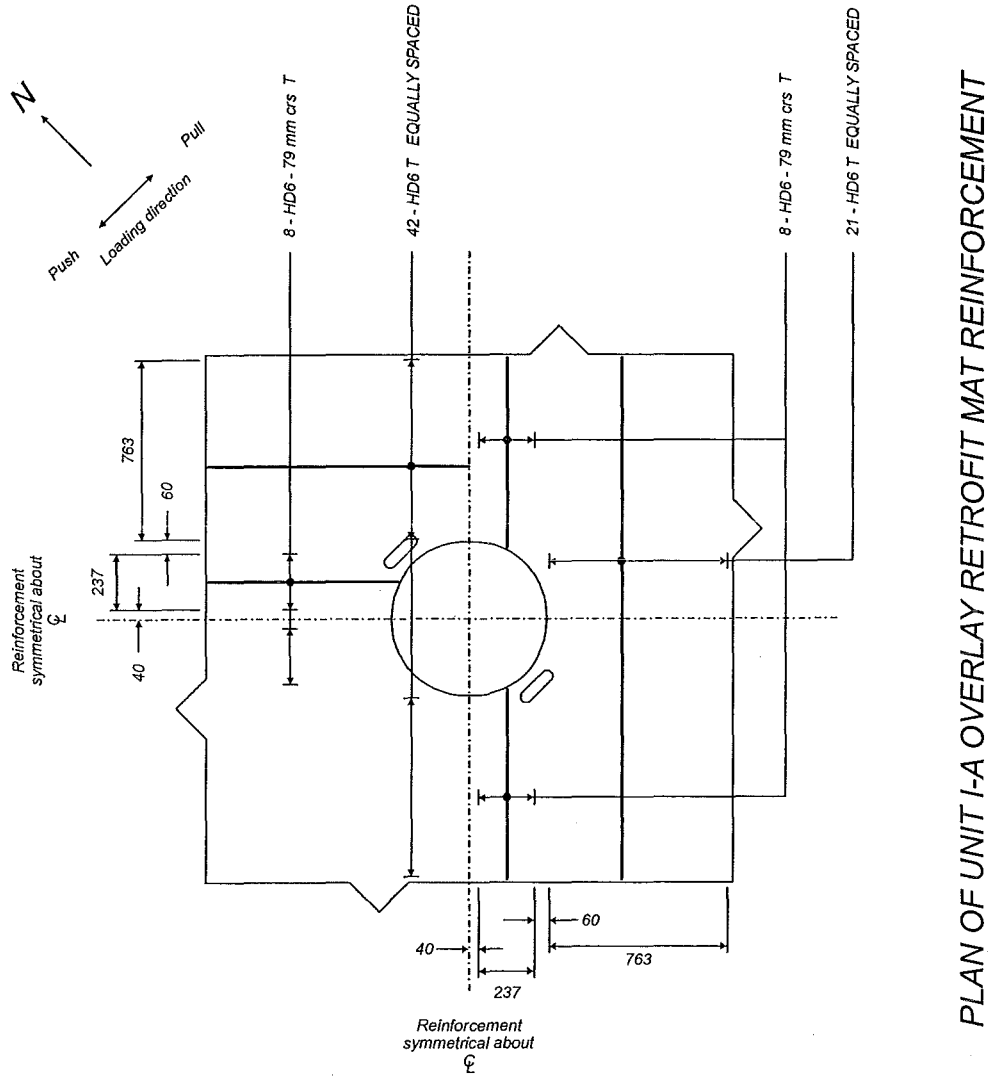

Figure 2.29 *Unit I-A Pilecap Overlay Mat Reinforcement*

was hooked over the pilecap overlay mat with allowance for off setting the overlay mat bars to be hooked under a dowel bar.

Construction specifications required a number of the hooked dowels in the pilecap to be load tested before pouring of the overlay. Testing involved loading each dowel to 75% of its yield load and monitoring the load over a five minute period. The dowels were loaded to the specified load and the displacement held constant for five minutes while the load was monitored. All dowels showed no significant drop in load after a period of five minutes.

Wet curing of the pilecap overlay was carried out instead of using an acrylic curing compound.

2.3.3.6 Design of Vertical Springs

Pier 68 is supported on four large diameter bored steel cased reinforced concrete piles each 5 feet (1.520 m) in diameter. When the pier is subjected to lateral loads a portion of the lateral load resistance is provided through shear and bending carried in each pile and the remainder through passive pressure on the side of the pilecap. Loading of the pier across the diagonal causes the bending carried in the two central piles to reduce the bending moment carried in the pilecap. As these piles are relatively large, the contribution of each pile to resisting flexure cannot be neglected. For Unit I-A, the force distribution through the pilecap of the test specimen would not match the force distribution from the structural analysis of Pier 68 if all of the vertical springs were pinned top and bottom.

The vertical springs for Unit I-A had to provide appropriate tension and compression stiffness and provide some means of resisting bending and shear to achieve the appropriate pilecap force distribution. The contribution of the two central vertical springs to flexure were modelled by fixing the top and bottom of each spring to allow them to resist shear and bending over their height. The two outer springs were to be pinned top and bottom and provide different tension and compression stiffness. Providing a vertical spring stiffness equivalent to the combined soil-pile stiffness

used in the structural analysis was not possible. It is necessary to model the different stiffness of the piles in tension and compression to correctly model the force distribution in the pilecaps of each test specimen, as achieved in the structural analysis of each pier but the relative forces and displacements were not able to be accommodated using structural steel elements. An approach where the "relative" compression to tension stiffness ratio was maintained allowed the pilecap force distribution to be matched between the test units and the structural analyses of Pier 68.

The influence of the lateral spring stiffness was not significant for Unit I-B but was significant to the pilecap force distribution in Unit I-A. The vertical spring stiffness for Unit I-A was adjusted to achieve the required pilecap force distribution to match the force distribution from the structural analysis whilst maintaining the same compression to tension stiffness ratio.

Adjusting the stiffness of the vertical springs in the test specimens affected the lateral displacement of the test units so that the displacement ductilities achieved in the test specimens could not be directly scaled to those of the prototype piers. A mathematical relationship is derived to relate the test specimen displacements to equivalent displacements in the actual structure.

A compressive soil spring stiffness of 2338 kN/mm and a tensile soil spring stiffness of 213 kN/mm per pile were taken as average soil stiffness in the structural analysis of Pier 68. The contribution of the axial stiffness of the individual piles gave a tensile stiffness of 203 kN/mm and a compressive stiffness of 1397 kN/mm for each pile. The required stiffness of the vertical springs, with a scale factor of 1:3.8, is then 53.4 kN/mm in tension and 367.6 kN/mm in compression giving a compression-to-tension stiffness ratio of 6.88 for each vertical spring. This ratio was maintained for the two outer springs in order to provide for the rotational displacement of the pilecap. As the central springs were designed to provide a certain flexural stiffness changing the axial stiffness of these springs for compressive or tensile loading would be impossible. This meant the central springs would provide the same axial stiffness for compressive or tensile loads.

A structural analysis of Unit I-A modelling the test specimen, baseblock, lateral springs and interaction with the strong floor was carried out to establish the appropriate stiffness for each of the vertical springs. The different stiffness provided by the lateral springs, due to one pair of lateral springs being located close to the end of the baseblock, required the properties for the elements modelling the outer springs be determined for each direction of loading. Properties for the central springs were also determined so that the same bending moment and shear force would be generated at the top of the central springs and within the pilecap for each direction of loading. Analysis of the average outside spring properties gave the design stiffness for the compression and tension springs. Sensitivity studies on the average outside spring stiffness values showed these had to be within ±5 % of the calculated values in order to maintain the desired force distribution through the test specimen.

2.3.3.7 Outer Springs

With the magnitude of the forces involved it was decided to provide all of the flexibility in the outer springs through rubber bearings. A bearing would be required to accommodate the compressive displacements in the outer springs and a separate bearing to provide the tensile displacements. The layout of the outer springs is similar to the vertical springs used in Unit I-B but with the inclusion of the rubber bearings with the hollow steel section and with the tension rod. Figure 2.30 shows the schematic layout of the outer springs when acting in compression and in tension.

Each bearing has a hole through the centre of the bearing to allow the rod for carrying tension loads to pass through. The compression reaction on the outer springs are taken through the hollow circular steel section and into the bearing at the base. The rod, which is threaded into the bottom pin, remains slack where it passes through the smaller bearing inside the hollow steel section. When the spring goes into tension the large bearing is separated from the bottom plate, engaging the steel rod through the centre of the spring, and compresses the smaller bearing inside the spring.

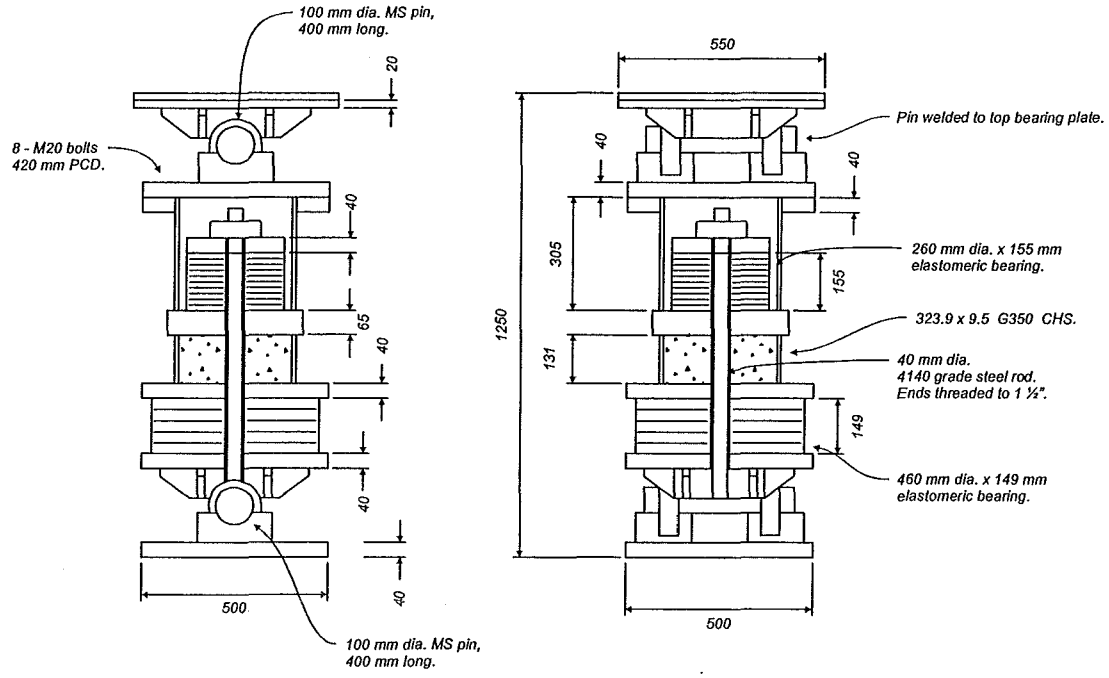

(a) *Construction Details*

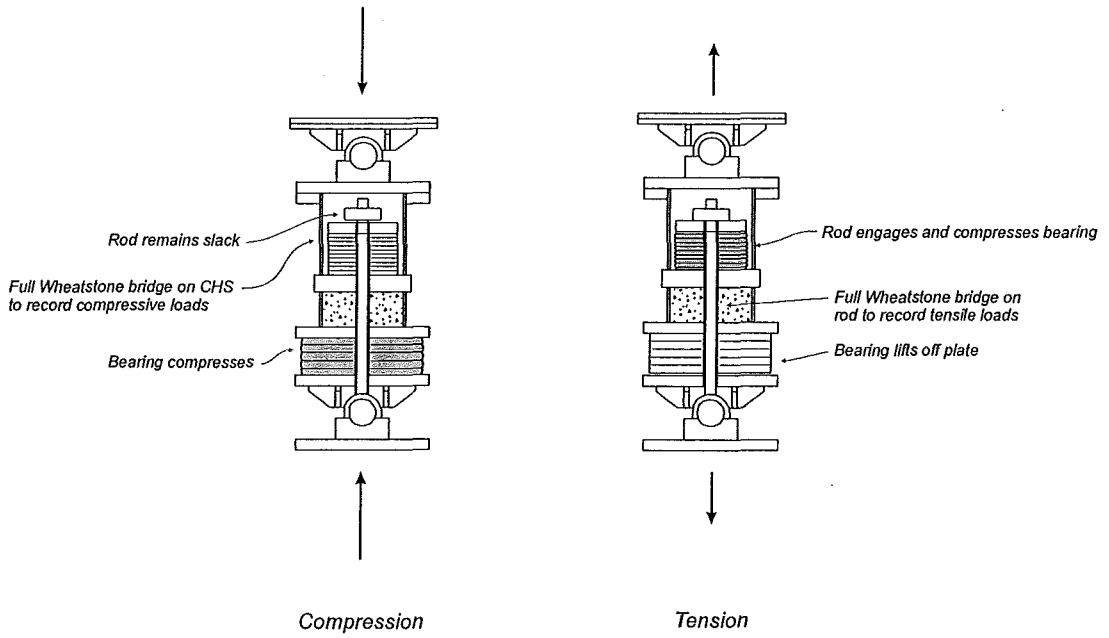

(b) *Load Paths*

Figure 2.30 *Unit I-A Outer Spring Details*

A Grade 350 323.9 x 9.5 CHS section was selected for the vertical spring units. This section allowed a smaller 260 mm diameter by 155 mm high rubber bearing to be fitted inside the CHS to provide the tension flexibility in the outer spring units. A 450 mm diameter by 149 mm high bearing provided the compression flexibility for the outer springs.

In order to provide an even distribution of bearing forces from the CHS on to the 450 mm diameter bearing the CHS section was filled with a non-shrink cement grout with a 50 mm diameter PVC tube to allow the steel rod to pass through.

The steel rod to transfer the tension force into the smaller bearing was made from 40 mm diameter AS4140 high strength steel. The ends of the rod were threaded to fit a 1 $^{1}/_{2}$ inch (38 mm) diameter nut.

2.3.3.8 Central Springs

The central springs were fabricated from the same Grade 350 323.9 x 9.5 CHS section with gusset plates top and bottom to adjust the flexural stiffness of each of the spring units to generate the required force distribution in the central piles. Figure 2.31 shows the central spring details.

As the compressive stiffness of the outer springs is much smaller than the compressive stiffness of the central springs the static reactions supported by the central springs are much larger than the static reactions supported by the outer springs. In order to obtain equal reactions in each spring, additional forces had to be induced into the outer springs to reduce the reactions supported by the central springs. This was achieved by shimming the outer springs so that they were higher than the central springs creating additional displacements into the outer spring and inducing larger reactions in these units.

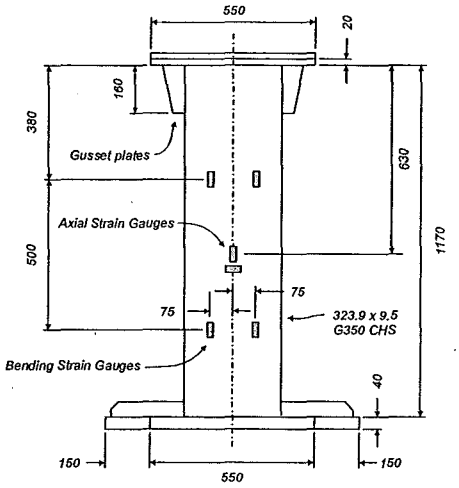

Elevation

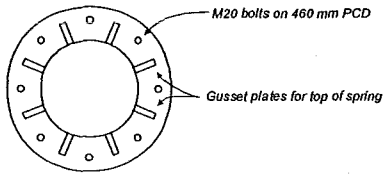

Top Plate Detail

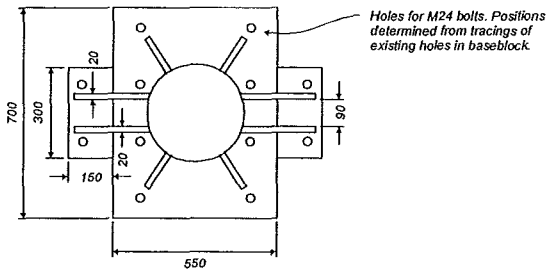

Bottom Plate Detail

Figure 2.31 *Unit I-A Central Spring Details*

The target dead load reaction in each vertical spring is one quarter of the test specimen's self-weight plus the axial load applied to the top of the column. As the combined compressive stiffness of each vertical spring is known the displacement under the ideal reaction can be obtained. The vertical displacement of the test specimen will be limited by the displacement of the stiffest vertical springs, the two central springs. Therefore the difference between the displacement of each of the

central springs and the two outer springs is required to be induced into the outer springs to increase the reaction taken by these springs.

An additional displacement of 1.3 mm was induced in each of the outer springs through the use of levelling screws mounted on the base of each spring unit which were used to raise each spring unit off the baseblock before placing shims between the bottom plate of the spring and the surface of the baseblock. Dental plaster was used to ensure even contact with the baseblock surface and bottom plate of the spring unit before bolting them down.

2.3.3.9 Rubber Bearings for Outer Springs

The sensitivity of the structural analysis of Unit I-A to the outer spring stiffness required the rubber bearings meet extremely tight stiffness specifications. With the usual manufacturing tolerances for the stiffness of rubber bearings being ±25 % the requirements for the rubber bearings for use in the test involved close collaboration with personnel at Skellerup Base Isolation Systems, the suppliers of the rubber bearings.

Each bearing required a nominal 50 mm diameter hole through the centre to accommodate the 40 mm diameter steel rod. Each bearing was manufactured without the hole initially and its compressive stiffness determined before drilling out a hole in the bearing to accommodate the steel rod and lower the bearing stiffness. The diameter of the hole would be sized to bring the bearing's compressive stiffness to within the targeted stiffness required for each bearing.

The combined compressive stiffness of the bearings and 40 mm diameter rod, when the outer spring is in tension, had to be 26.1 kN/mm. Compressive stiffness specifications for the manufacture of these bearings, containing a 50 mm diameter hole, targeted this value. The maximum compressive working force on the bearing is 280 kN requiring a linear response up to 11 mm vertical displacement. The 260 mm diameter by 155 mm high bearings supplied have 10 mm thick steel plates top and bottom, 11 internal layers of rubber each 10 mm thick and 10 internal steel plates 2.5 mm thick.

The combined compressive stiffness of the bearings and CHS section had to be 179.2 kN/mm. This was the stiffness specified for the manufacture of the rubber bearings complete with a hole through the bearing along with a maximum compression force of 1800 kN and a linear response up to 10 mm vertical displacement. The 450 mm diameter by 149 mm high bearings supplied have 10 mm thick top and bottom steel plates, 8 internal layers of rubber each 13.5 mm thick and 7 internal steel plates each 3 mm thick.

Accounting for additional displacements in the CHS and steel rod required the bearings be slightly stiffer than specified. The target stiffness for the 260 mm diameter bearings is 29.7 kN/mm in order to achieve the combined stiffness value of 26.1 kN/mm with the steel rod and CHS flexibilities included. The required stiffness of the 450 mm diameter bearings were determined after calibration of the 260 mm diameter bearings to keep the compression-to-tension stiffness ratio constant for both springs.

To determine the compressive stiffness of each bearing the bearings were loaded up to the rated load three times before completing two further load cycles recording the load and displacement of the bearing. The 260 mm diameter bearings were calibrated in the 2500 kN Avery Compression Testing Machine and the 450 mm diameter bearings using the DARTEC Universal Testing Machine. Once the bearing compressive stiffness had been obtained 50 mm diameter holes were bored through the centre of each bearing and the bearings re-calibrated.

The 50 mm diameter holes through the 260 mm diameter bearings lowered the compressive stiffness to within the targeted stiffness required for these bearings. A linear relationship exists between the hole diameter and compressive stiffness of the rubber bearing. From the compressive stiffness of the 450 mm diameter bearings with a 50 mm diameter hole through the centre extrapolation of the compressive stiffness versus hole diameter relationship showed that a 70 mm diameter hole would lower the bearing stiffness to within the allowed stiffness range.

Due to bulging of the rubber bearing, when subjected to compression, the rubber inside the 50 mm diameter holes of the 260 mm diameter bearings bears against the 40 mm diameter steel rod. This increases the stiffness of the bearing slightly results in non-linear load-displacement behaviour of the bearing at a lower load. Each bearing was calibrated again with a 40 mm diameter rod, 140 mm long, inside the hole through the bearing. Table 2.9 shows the compressive stiffness determined for the 260 mm diameter by 155 mm high bearings. The stiffness value given is the secant stiffness taken between the load-displacement readings at 20 kN and 280 kN.

From the stiffness of each bearing with the 40 mm diameter rod in the hole and accounting for the flexibility of the steel rod in the spring unit the stiffness of the

Table 2.9 *Compressive Stiffness of 260 mm diameter by 155 mm high Rubber Bearings*

	T1	T2
	kN/mm	kN/mm
Target Stiffness, with hole	29.7	29.7
No Hole	54.2	50.0
50 mm Hole	25.7	27.4
50 mm Hole and 40 mm rod	27.1	29.2

Table 2.10 *Compressive Stiffness of 450 mm diameter by 149 mm high Rubber Bearings*

	C1	C2
	kN/mm	kN/mm
Target Stiffness, with hole	175.3	185.9
No Hole	286.7	296.0
50 mm Hole	-	213.2
70 mm Hole	181.6	185.4

outer spring in tension containing bearing T1 is 24.3 kN/mm. For the outer spring containing bearing T2 the combined spring stiffness in tension is 25.7 kN/mm.

This gives combined spring stiffness values in compression of 167.2 kN/mm and 176.8 kN/mm for the springs containing bearing T1 and bearing T2 respectively. The flexibility of the CHS section in compression requires stiffness of 175.3 kN/mm and 185.9 kN/mm to be targeted for the 450 mm diameter bearings. Table 2.10 shows the compressive stiffness of the 450 mm diameter by 149 mm diameter bearings. The stiffness values given are the secant stiffness taken between load-displacement readings at 50 kN and 1800 kN.

The combined stiffness of the outer springs in compression, accounting for the bearing and CHS stiffness are 172.9 kN/mm and 176.3 kN/mm for the springs containing bearings C1 and C2 respectively. Bearings C1 and T1 were placed together in the outer spring at the eastern side of the test specimen with bearings C2 and T2 paired together in the outer spring at the western side of the test specimen. This gives compression-to-tension stiffness ratios for the outer springs of 7.12 for the eastern outer spring and 6.86 for the western outer spring.

2.3.3.10 Vertical Spring Calibration

Each vertical spring was calibrated in compression using the DARTEC UTM to determine the load calibration factor of each channel for the data logger. Each outer spring contained strain gauges arranged to form two axial full bridges to record the axial compression in each spring. Two axial full bridges were also placed on the steel rod inside each spring to record the tensile axial load taken by each spring. Each central spring had a full bridge placed at mid height of the CHS section to record axial loads and two bending full bridges placed 500 mm apart to measure bending induced strains at different heights and obtain the shear force carried by each central spring.

Calibration was carried out after completion of the test on Unit I-A as time did not permit the calibration to be carried out before placement of the vertical springs and

test specimen into the test rig. The central springs were calibrated in bending by inducing a constant moment over the height of the spring through the use of a hydraulic ram and strong beam. Figure 2.32 shows the loading arrangement for calibration of the bending channels in each of the central springs. The difference in

Figure 2.32 *Calibration of Central Springs for Bending*

the amount of bending recorded in each channel divided by the distance between the points where the strain gauges were placed gave the shear force carried by each central spring.

The 40 mm diameter steel rods for resisting the tensile loads in the outer springs were calibrated using the 1000 kN Avery UTM.

2.4 LINKAGE BOLT TESTS

2.4.1 Introduction

The use of simply supported spans in the Thorndon Overbridge requires the use of a large number of linkage and hold-down bolts at each pier location. Typically the linkage bolts extend the full width of the umbrella platform at each of the single column piers, from 25 to 40 feet (8 to 12 m) long. Shorter linkage bolts are used at the multi-column piers used in Stage One of the Overbridge.

Due to the possibility of liquefaction and permanent sliding movements of the surrounding ground unseating collapses of the suspended spans may occur within the length of the bridge. Permanent ground deformations of approximately 5 m horizontally and 1.0 m vertically are expected to occur where the Wellington Fault crosses beneath the axis of the bridge [B1, M1]. A retrofit scheme to prevent unseating of the spans of the Thorndon Overbridge involves the replacement of some of the existing linkage bolts with high strength, slack bolts to prevent the concentration of displacements in the superstructure to one movement joint. Additional retrofit measures are also proposed for preventing collapse of the spans across the Wellington Fault [M1].

Tests on linkage bolts removed from the Thorndon Overbridge are required to determine the capacity of hold-down bolts under shear loading and the strength and elongation capacity of the linkage bolt details at the umbrella platforms.

2.4.2 Linkage Bolt Tensile Tests

Substantial linkage bolts are provided at each movement joint in the Thorndon Overbridge to tie the adjacent spans together along with conventional hold-down bolts for each span. Each linkage bolt contains welded end anchorage details along with thick rubber buffer pads to reduce earthquake impact forces. Stage Two of the construction used 1 $^1/_8$ inch (28 mm) diameter linkage bolts with 1 $^1/_2$ inch (38 mm)

diameter linkage bolts used in Stage Three. Typically 20 linkage bolts are provided through the umbrella platform at each of the single column piers. Figure 2.33 shows the typical layout of linkage bolts through the umbrella platforms of Stage Two and Stage Three piers. Stage One linkage bolts were 1 $^1/_2$ inch (38 mm) diameter, approximately 1.0 m long, with a threaded end detail. Due to the short length and the threaded end detail, little elongation capacity from these bolts is expected.

Design of the superstructure retrofit measures required a accurate estimation of the dependable strength, overstrength and elongation capacity of the linkage bolts. Two linkage bolts were removed from the Thorndon Overbridge, one of 1 $^1/_8$ inch diameter and one of 1 $^1/_2$ inch diameter, including the welded end anchorage details.

Monotonic tensile tests, up to fracture of the bolts, were conducted using the 1000 kN Avery UTM recording the load and elongation of each test specimen.

2.4.3 Hold Down Bolt Tests

As each simply supported I-beam is restrained through the use of conventional hold-down bolts as well as the linkage bolts through the umbrella platform the force required to unseat a particular span is dependent on the shear capacity of the hold-down bolts and tensile capacity of the linkage bolts. Two different hold-down bolt details are used in the Thorndon Overbridge for the multi-column piers of Stage One and the simply supported spans at the umbrella platforms of Stages Two and Three. Bolts of 1 $^1/_4$ inch (32 mm) diameter cast into the cap beam and end diaphragms of the I-beams are used at each of the multi-column piers in Stage One. Stage Two and Three hold-down bolts use 1 $^3/_8$ inch (35 mm) diameter bolts with a threaded coupling cast into the umbrella platform and passing through the end diaphragm.

Two hold-down bolt details were tested, Unit 1 modelling the Stage Two and Three bolts and Unit 2 modelling the Stage One hold-down bolts.

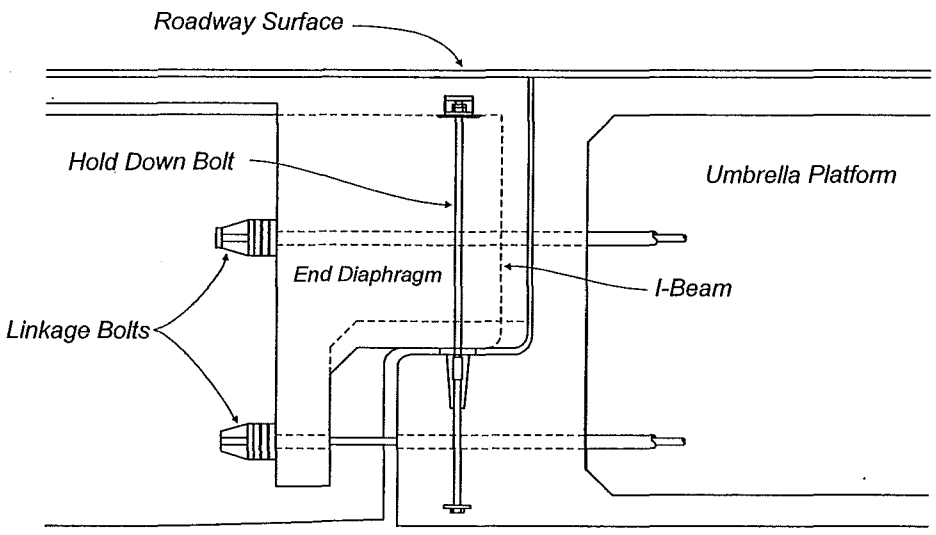

Figure 2.33 *Linkage Bolt Details at Umbrella Platforms*

2.4.3.1 Unit 1 Hold Down Bolt Test

Unit 1 models the 1 $^{3}/_{8}$ inch (35 mm) diameter hold-down bolt detail as used in the Stage Two and Three piers. These hold-down bolts incorporate a threaded coupler which is used to connect two halves of the bolt, one end cast into the umbrella platform and the other end passed through the end diaphragm of the I-beams. Figure 2.34 shows the layout of hold down bolts in Stage Two and Stage Three piers. As these hold-down bolts connect the notched end of the I-beams at each umbrella platform they are only subjected to loading in one direction as movement in the opposite direction is prevented by the I-beam bearing against the umbrella platform.

Unit 1 replicated the conical movement pocket, threaded coupler detail and separation between the I-beam and the umbrella platform. Two concrete blocks were connected using the hold-down bolt detail in order to obtain the strength of this bolt detail under shear loading. The loading rig used to test this hold-down bolt incorporated three reinforced concrete blocks, the outer blocks representing the end

diaphragm connecting the ends of the I-beams and the central block representing the umbrella platform. The central block incorporated two hold-down bolt details, one at each end, with the steel rod representing the bolt continuous through the central block. Figure 2.35 shows the layout of Unit 1 and the details of the hold-down bolt. The hold-down bolt details were loaded monotonically in double shear using the DARTEC UTM until failure of the bolt.

2.4.3.2 Unit 2 Hold Down Bolt Test

Unit 2 models the 1 $^{1}/_{4}$ inch (32 mm) diameter hold-down bolts at the multi-column piers of Stage One. These bolts are capable of loading in both longitudinal directions and they were tested under cyclic loading until failure of the bolt. Each hold-down bolt is continuous, cast into the cap beam of the pier and extending through a steel pipe cast into the end diaphragms connecting the I-beams together. Figure 2.36 shows the hold-down bolt detail used in the Stage One piers.

Unit 2 replicated the hold-down bolt, conical movement pocket and the connection between the cap beam of the pier and end diaphragm which the bolt was cast into. Figure 2.37 shows the details of Unit 2 and the hold-down bolt tested.

2.4.4 Linkage Bolt End Detail Tests

Each of the linkage bolts in Stage Two and Stage Three pier had welded end details for installation of the linkage bolts. The dead end was shop welded with the tightening end welded on site after installation of the linkage bolt through the umbrella platform. Figure 2.38 shows the details of the welded end details used in these linkage bolts.

The welded end details were removed from the linkage bolts prior to the tensile testing of the bolts for testing in compression to determine the likely strength of the welded details. If the end details were weaker than the tensile strength of the linkage bolt failure could occur in these details, affecting the strength and elongation capacity available from the linkage bolts.

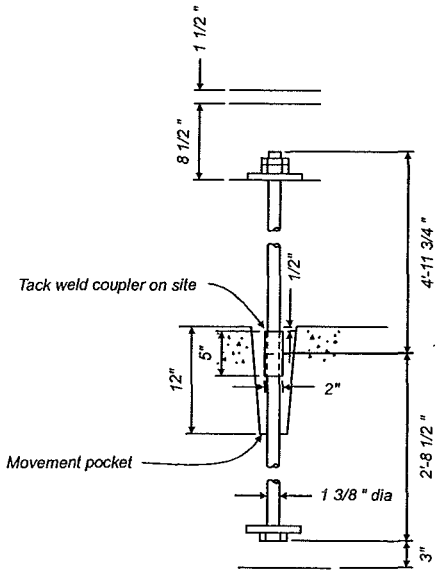

Figure 2.34 *Stage Two and Stage Three Hold Down Bolt Details*

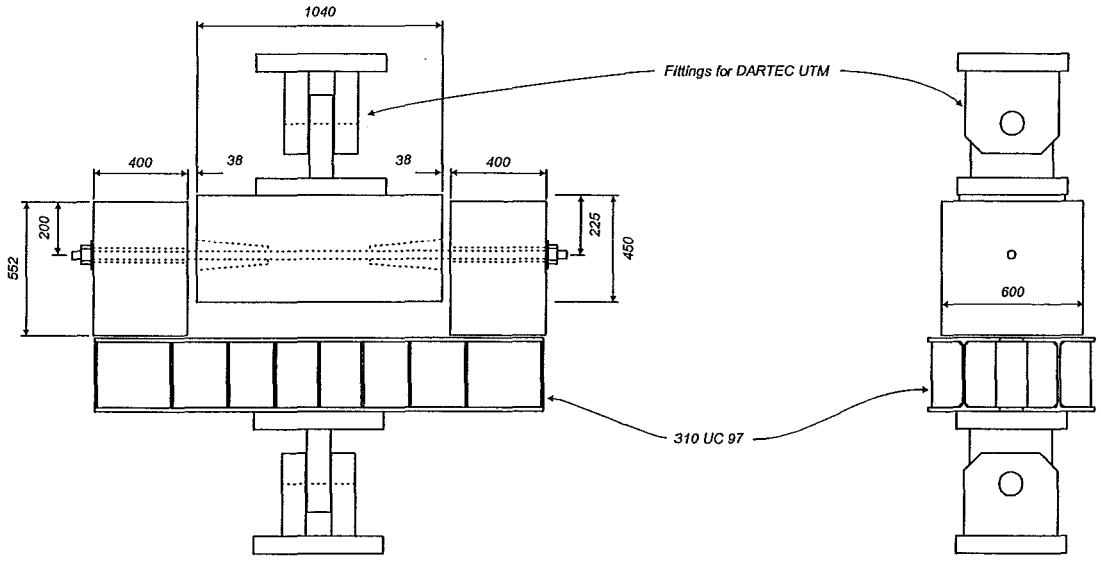

Figure 2.35 *Unit 1 Hold Down Bolt Test Rig Layout*

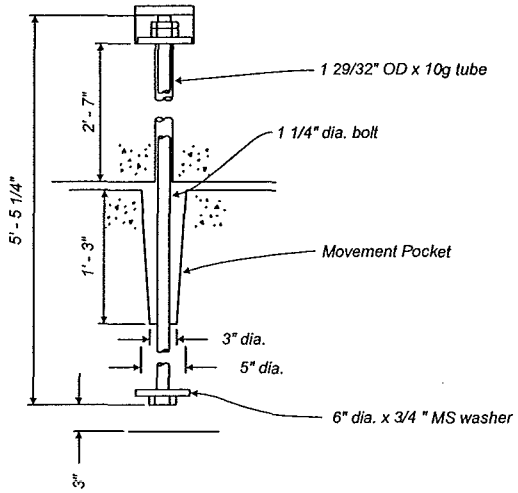

Figure 2.36 *Stage One Pier Hold Down Bolt Details*

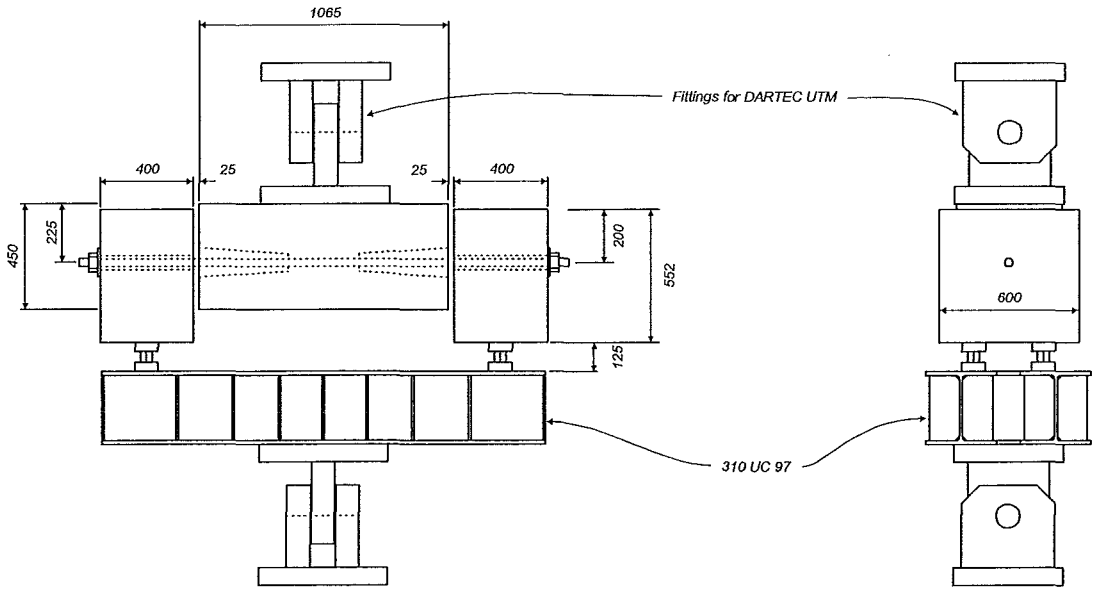

Figure 2.37 *Unit 2 Hold Down Bolt Test Rig Details*

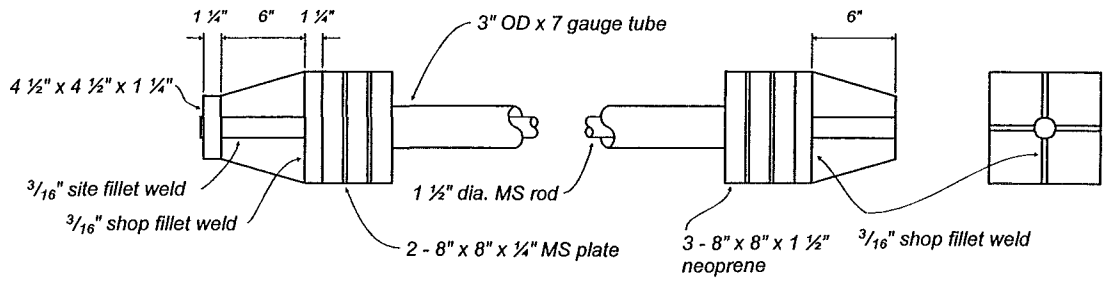

1 ½" dia. Linkage Bolt

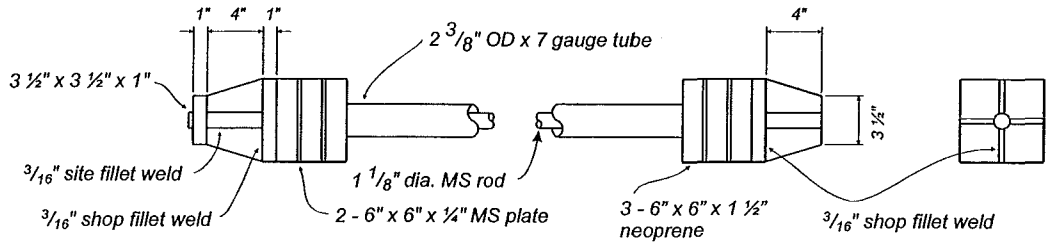

1 1/8" dia. Linkage Bolt

Figure 2.38 *Linkage Bolt End Details*

Each welded end detail was tested using the 2500 kN Avery UTM in compression in an attempt to fail the end details through the welds.

2.5 TEST PROCEDURES

2.5.1 Lateral Loading History for Units I-A and I-B

Both test specimens, Units I-A and I-B were subjected to simulated earthquake loading through reversed cyclic lateral loading. The units were under constant axial compression during testing, simulating the superstructure dead load. Lateral loading and displacements to the west were denoted as push cycles and defined as positive. The first three cycles of lateral loading in each direction were load-controlled to 0.5 times the load to develop the flexural strength at the base of the column, H_y. Three further load-controlled cycles were completed to 0.75 H_y in each direction. The

global experimental yield displacement of the test specimen, Δ_y, measured at the top of the column was calculated as:-

$$\Delta_y = \frac{4}{3}\left(\frac{\left|\Delta_{0.75H_y}\right| + \left|\Delta_{-0.75H_y}\right|}{2}\right) \qquad (2.1)$$

where $\Delta_{0.75H_y}$ and $\Delta_{-0.75H_y}$ are the average lateral displacements recorded at the top of the column during the three cycles to $0.75H_y$.

Displacement controlled cycles followed applied to increasing levels of displacement ductility, $\mu_\Delta = \Delta/\Delta_y$, where Δ is the lateral displacement at the top of the column. Three cycles each to $\mu_\Delta = 1$, $\mu_\Delta = 1.5$, $\mu_\Delta = 2$, $\mu_\Delta = 3$, $\mu_\Delta = 4$ and so on, in each direction were applied. Testing was stopped when the absolute value of the applied lateral load during the first cycle to a new displacement increment dropped to less than 60 % of the maximum recorded lateral load or until the travel of the hydraulic actuator is exhausted.

2.5.2 Determination of Theoretical First Yield Displacement

The configuration of each test specimen and the test rig was intended to model the various components of foundation flexibility present in the actual structure. The piles of each pier, and the vertical springs of the test specimen, allow rotation of the pilecap to occur under applied seismic lateral loading. End bearing of the compression piles and pull out of the tension piles allow the pilecap to rotate, causing additional displacement at the top of the column. Passive pressure from the soil surrounding the pilecap allows a rigid body translation of the entire pier which was modelled through the use of the lateral springs at the pilecap level. Lateral loading applied at the top of the column causes flexural deformations in the column itself. Rigid body deformations of the column occur through strains developed in the reinforcing bars and pull out of these bars from the base.

Figure 2.39 shows the main components of lateral displacement at the top of the column of the test specimens. Other sources of displacement from flexure and shear in the pilecap and shear in the column are small and can be neglected.

In order to predict the theoretical displacement at the top of the column, corresponding to the development of the flexural strength of the base of the column, all these components of lateral displacement had to be accounted for. Flexural deformations and rigid body displacements of the column were determined from moment-curvature analysis of the section, using actual material properties. The equivalent flexural stiffness of the column, EI_e, was used for analysis of the complete test specimen, which modelled the column, pilecap, vertical and lateral springs. This analysis used the equivalent column flexural stiffness and tested stiffness properties for the vertical and lateral springs in order to determine the lateral displacement components at the top of the column due to rotation and translation of the pilecap and displacements in the column.

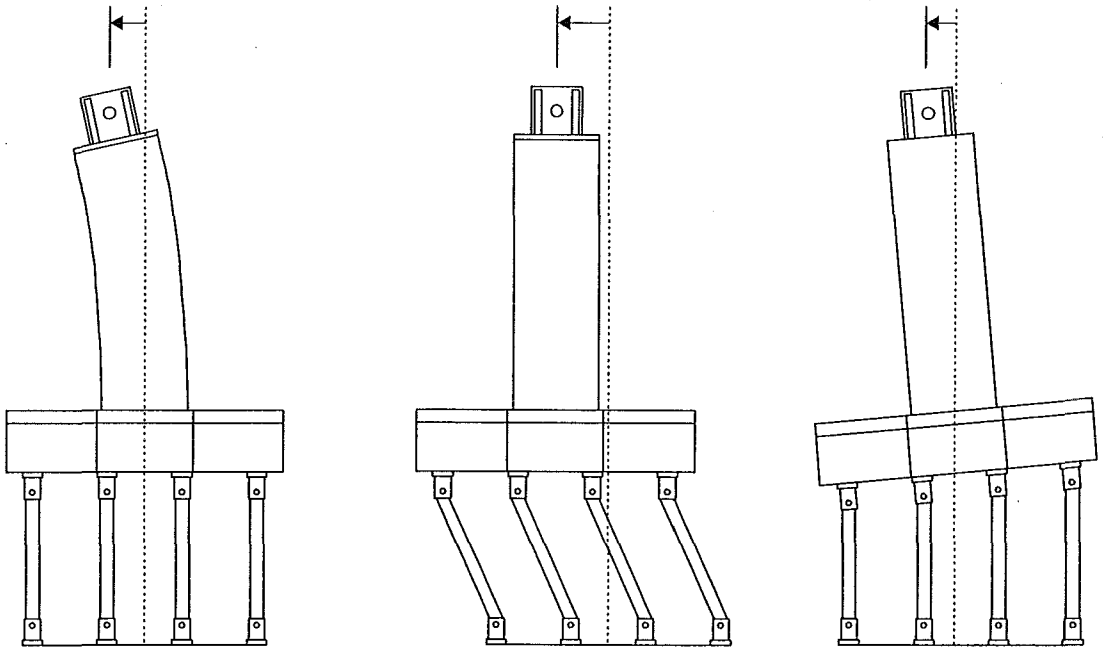

(a) Column Flexure *(b) Pilecap Translation* *(c) Pilecap Rotation*

Figure 2.39 *Components of Lateral Displacement at the Top of the Column*

As some of the vertical springs go from compression to tension during the lateral loading an incremental analysis had to be used. The test specimen was analysed under full gravity loading with compression vertical spring stiffness properties. Lateral load was applied until the trailing vertical springs are at zero axial force. The trailing vertical spring stiffness was changed to the appropriate tension stiffness and the gravity load removed and lateral load applied until the second vertical spring reaches zero axial force under the combined actions of the previous analyses. The second vertical spring stiffness was changed to the appropriate tension stiffness and lateral load applied until the column overstrength is reached.

The results from each analysis can be superimposed and the non-linear effects of different tension and compression vertical spring stiffness accounted for. Displacements at the top of the column and at the level of the lateral springs can be then compared to results from lateral load cycles to a displacement ductility $\mu_\Delta = 1$.

2.5.3 Displacement Ductility of Test Specimens Compared to Displacement Ductility of Actual Piers

As the actual vertical spring stiffness was not matched between the structural analysis of Pier 68 and Unit I-A, and Pier 46 and Unit I-B, the components of displacement in the test specimen could not be directly scaled to give the same components of displacement in the actual pier. Elastic displacements, such as rotation and translation of the pilecap, could not be directly scaled from the test specimens as the stiffness of the springs used were not scaled from the structural analysis. This affects the first yield displacement of the test specimen and the definition of displacement ductility used to define the displacement controlled cycles of each test.

The theoretical first yield displacement of the actual pier, Δ_{yS}, was obtained from the structural analysis along with the ultimate displacement of the actual pier, Δ_{uS}. The yield displacement, Δ_{yT}, ultimate, Δ_{uT}, and plastic displacement, Δ_{pT}, of the test specimen are known from the experimental results. These can be expressed as

equivalent displacements in the actual structure, δ_{yT}, δ_{uT} and δ_{pT}, by multiplying by the scale factor used for the test.

$$\begin{aligned} \delta_{pT} &= \delta_{uT} - \delta_{yT} \\ &= \mu_{\Delta T}\delta_{yT} - \delta_{yT} \\ &= (\mu_{\Delta T} - 1)\,\delta_{yT} \end{aligned} \qquad (2.2)$$

The plastic displacement recorded for the test specimen, in terms of the actual structure, δ_{pT}, remains the same as that determined from the structural analysis.

Therefore:-

$$\begin{aligned} \Delta_{uS} &= \Delta_{yS} + \Delta_{pS} \\ &= \Delta_{yS} + \delta_{pT} \\ &= \Delta_{yS} + (\mu_{\Delta T} - 1)\,\delta_{yT} \end{aligned} \qquad (2.3)$$

The displacement ductility of the actual pier, expressed in terms of the displacement ductility of the test specimen becomes:-

$$\mu_{\Delta S} = 1 + (\mu_{\Delta T} - 1)\,\frac{\delta_{yT}}{\Delta_{yS}} \qquad (2.4)$$

Equation 2.4 is used to convert the displacement ductilities reached in the test specimens to the equivalent displacement ductilities of the actual piers. This enables a comparison between the ductility capacity and the expected ductility demand on the piers of the Thorndon Overbridge.

CHAPTER 3

CYCLIC LATERAL LOADING OF UNIT I-B

3.1 INTRODUCTION

Unit I-B is a 1:3.8 scale model of Pier 46 of the Thorndon Overbridge incorporating the existing and the proposed retrofit details for the pier. The test specimen was be subjected to simulated seismic loading by applying a constant compressive axial load and reversed cyclic lateral loads at the top of the column, representing the centre of mass of the bridge deck. Reinforcing details and the test specimen layout for Unit I-B are shown in Section 2.3.2. The lateral loading history used for testing of Unit I-B is described in Section 2.5.

Unit I-B was instrumented over one half of the test specimen, using symmetry about the centre of the test specimen in line with the direction of loading. Electrical resistance strain gauges were used to record strains on the reinforcing steel in the column, bottom pilecap mat bars, pile and overlay retrofit dowels and pilecap overlay retrofit mat bars. Linear potentiometers were used to record external displacements of the test specimen and internal displacements at the base of the column. Loads were recorded as applied by the 1000 kN hydraulic actuator, through a 1000 kN loadcell, in each vertical spring and in the lateral springs which resisted the applied lateral load, through calibrated strain gauge circuits.

All circuits from loadcells, strain gauges and linear potentiometers were monitored and recorded using the Department's PCLAB data logger. This data logger allowed up to 256 separate channels to be monitored, scanned and recorded. The scanning of the channels is controlled using a computer program, which allows the scan to be taken at any instant as directed from the computer keyboard. Data from the channels is written to a file which enables the data to be reduced, using calibration factors determined for each channel, to give loads, strains or displacements.

3.2 TEST UNIT INSTRUMENTATION

3.2.1 Measurement of Loads

The loads measured during the testing of Unit I-B are the force applied by the hydraulic actuator at the top of the column, the tensile or compressive reaction in each of the vertical springs, the lateral load resisted by each of the lateral springs at pilecap level and the level of axial load applied to the specimen. The 1000 kN loadcell attached to the hydraulic actuator has two independent full bridge circuits. One circuit is monitored by the data logger and the other connected to a digital strain indicator. Each circuit was calibrated in compression using the 2500 kN Avery Compression Testing Machine. Output from the digital strain indicator was used to control the lateral loading of the specimen during the initial load controlled cycles and provide a separate measure of load during the remaining cycles. Figure 3.1 shows the measurement of loads in Unit I-B.

Each vertical spring in Unit I-B contained two axial half bridge circuits for measuring the tensile and compressive forces resisted by each spring. Two 120Ω resistance 5 mm foil strain gauges were placed on the steel rod to measure tensile forces and another two gauges placed on the SHS section to measure compressive forces. A full bridge circuit was completed for each channel, for input into the data logger, by using external dummy gauges, similar type strain gauges mounted on a steel plate and wired together to complete the circuit. It was found that the dummy gauges and strain gauges on the springs were affected by daily temperature fluctuations causing the channel readings to drift with no change in load. To offset the channel drift a dummy vertical spring was strain gauged and wired to form a full bridge circuit using external dummy gauges on monitored during testing. This dummy spring was fabricated using the same steel rod and SHS section as used in the test specimen and was not subjected to any load during testing. Any offset in readings recorded in the channels of the dummy spring would be due to temperature variations only and could be removed from the readings taken during the test for the other vertical spring channels.

The axial load applied to Unit I-B was monitored by a calibrated pressure gauge attached to the hydraulic rams used to apply the load. The pressure gauge was calibrated using each hydraulic ram against the 2500 kN Avery Compression Testing Machine and connected to a motor driven pump to apply the load. A manifold was used to ensure the same pressure was maintained in each of the hydraulic rams at all times. After the axial load was applied the displacement of the rams was held constant by shutting off a valve between the pump and the rams. During testing the pressure gauge was monitored and kept at the same pressure by manually relieving the excess pressure, due to elongation of the column during loading, or increasing the pressure by starting the pump, caused by shortening of the column during unloading.

3.2.2 Measurement of Test Unit Displacements

Column lateral displacements measured during the test programme were the gross horizontal displacement at the top of the column at the point of application of the lateral load, midway between the top of the column and the top of the steel jacket and at the top of the steel jacket. Lateral displacements of the pilecap were measured at the mid depth of the original pilecap with vertical displacements recorded adjacent to the position of each vertical spring. Figure 3.2 shows the location of the linear potentiometers for recording external test specimen displacements.

All external test specimen lateral displacements were taken relative to a fixed reference point located on a wall separate from the strong floor area. Light gauge aramid wire was used to connect the linear potentiometers mounted on the wall, via a pulley system, to the test specimen. Weights on the linear potentiometers were used to ensure the aramid wire remained taut during displacement of the test specimen. Linear potentiometers to measure vertical displacements of the pilecap, at each vertical spring location, were mounted on lengths of steel angle sections tack welded to the connection plates used to connect the vertical springs to the baseblock. A 15 mm linear potentiometer was mounted on the top column fitting to measure any

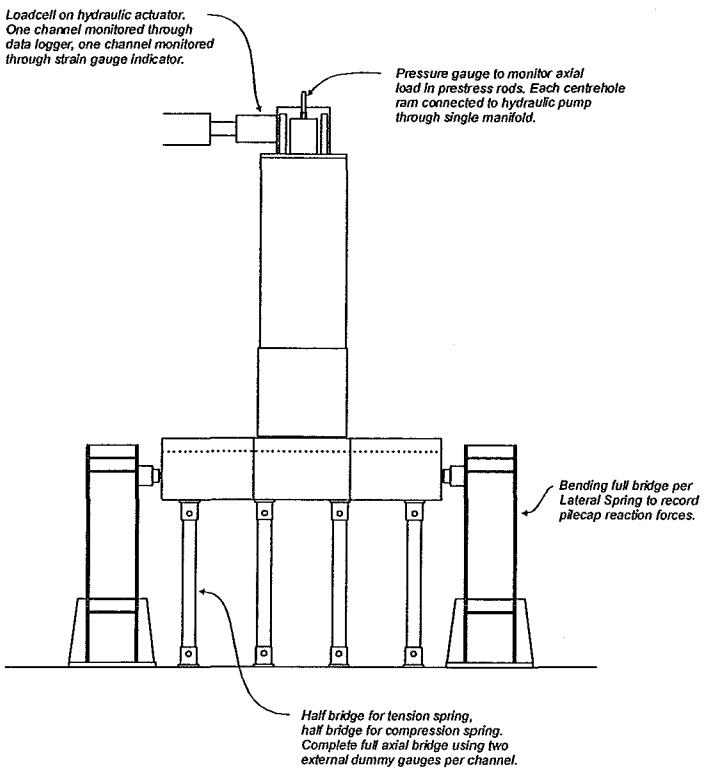

Figure 3.1 *Measurement of Loads in Unit I-B*

relative movement of the top column fitting, containing the axial load hydraulic rams, connection for applying the lateral loading and measurement point for the gross column top displacement, to the column. Additional displacements recorded at the top of the column are also due to rotation of the baseblock and strong floor during application of the lateral load to the specimen. These were recorded using a calibrated precise level bubble mounted on the baseblock under the centre of the test specimen and read at the peak of each load increment.

Internal displacements of the column due to flexure were recorded using linear potentiometers attached to the base of the column covering the region of the column retrofitted with the steel jacket.

Figure 3.3 shows the location of the linear potentiometers to measure internal displacements. The linear potentiometers are mounted on steel brackets screwed into 10 mm diameter plain round reinforcing rods which were cast into and passed through the column.

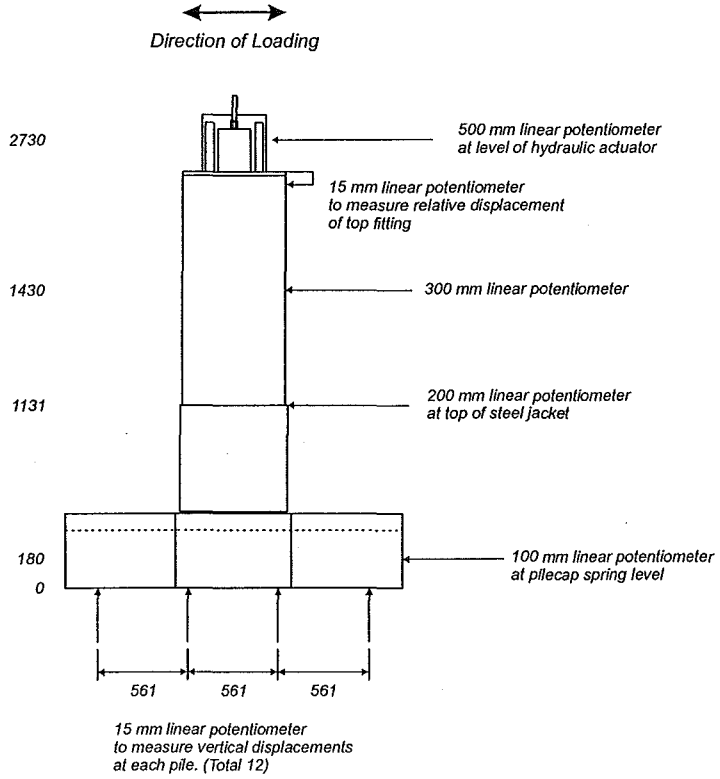

Figure 3.2 *Measurement of External Test Specimen Displacements*

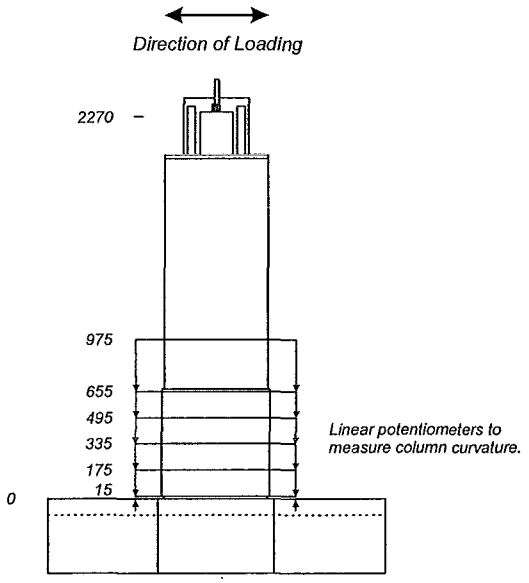

Figure 3.3 *Measurement of Internal Test Specimen Displacements*

All linear potentiometers were calibrated before testing using steel spacer blocks machined to known depths to obtain calibration factors for the data logger. Displacement measurements from the linear potentiometer at the point of application of the lateral load was monitored through the data logger and through a digital voltmeter. This voltmeter was used to control the lateral loading during the displacement controlled cycles.

These displacement measurements were recorded to determine the components of lateral displacement recorded at the top of the column due to rigid body translation of the test specimen, rigid body rotation of the pilecap and flexure in the column.

Displacements recorded from the top of the column and the applied load from the strain indicator attached to the loadcell were used as inputs to an X-Y plotter to give a visual record of load and displacement during testing.

3.2.3 Reinforcement Strains

Local strains on reinforcing bars in the specimen were measured using 120Ω resistance 5 mm foil strain gauges on the pilecap bottom mat and column bars. Strains in the pilecap overlay retrofit mat bars and dowels were measured using 120Ω resistance 1 mm foil strain gauges. All of the strain gauges supplied had the strain gauge leads already connected to the gauges removing the need to place separate terminal blocks to complete the strain gauge circuit.

Strain gauges were attached to the reinforcing bars before fabrication of the reinforcing cages. All strain gauges were protected with several layers of waterproofing cement and a piece of vinyl mastic tape for additional protection against physical damage.

3.2.3.1 Column Strain Gauges

Five longitudinal column bars were strain gauged in Unit I-B as shown in Figure 3.4. Three bars were strain gauged from the bottom of the pilecap to 890 mm above the level of the pilecap overlay retrofit. The other two bars were strain gauged over the original pilecap and overlay retrofit depth only. As inelastic action in the specimen was assumed to occur at the base of the column strain gauges were concentrated around the pilecap retrofit overlay surface and down into the original pilecap.

3.2.3.2 Pilecap Bottom Mat Strain Gauges

Strain gauges on the pilecap bottom mat were concentrated on the bars arranged in the longitudinal direction, parallel with the loading direction of the test specimen. Two transverse pilecap bottom mat bars were also strain gauged. Figure 3.5 shows the position and identification of the strain gauges on the bottom pilecap mat bars.

3.2.3.3 Pilecap Overlay Retrofit Mat Strain Gauges

The top mat of HD6 pilecap overlay retrofit mat bars were gauged with the strain gauge positions mirroring the position of gauges in the bottom pilecap mat. The position of these gauges is shown in Figure 3.6. Gauge OL8, on the longitudinal pilecap overlay retrofit mat bars, was damaged during construction and no readings were obtained from this gauge during the test.

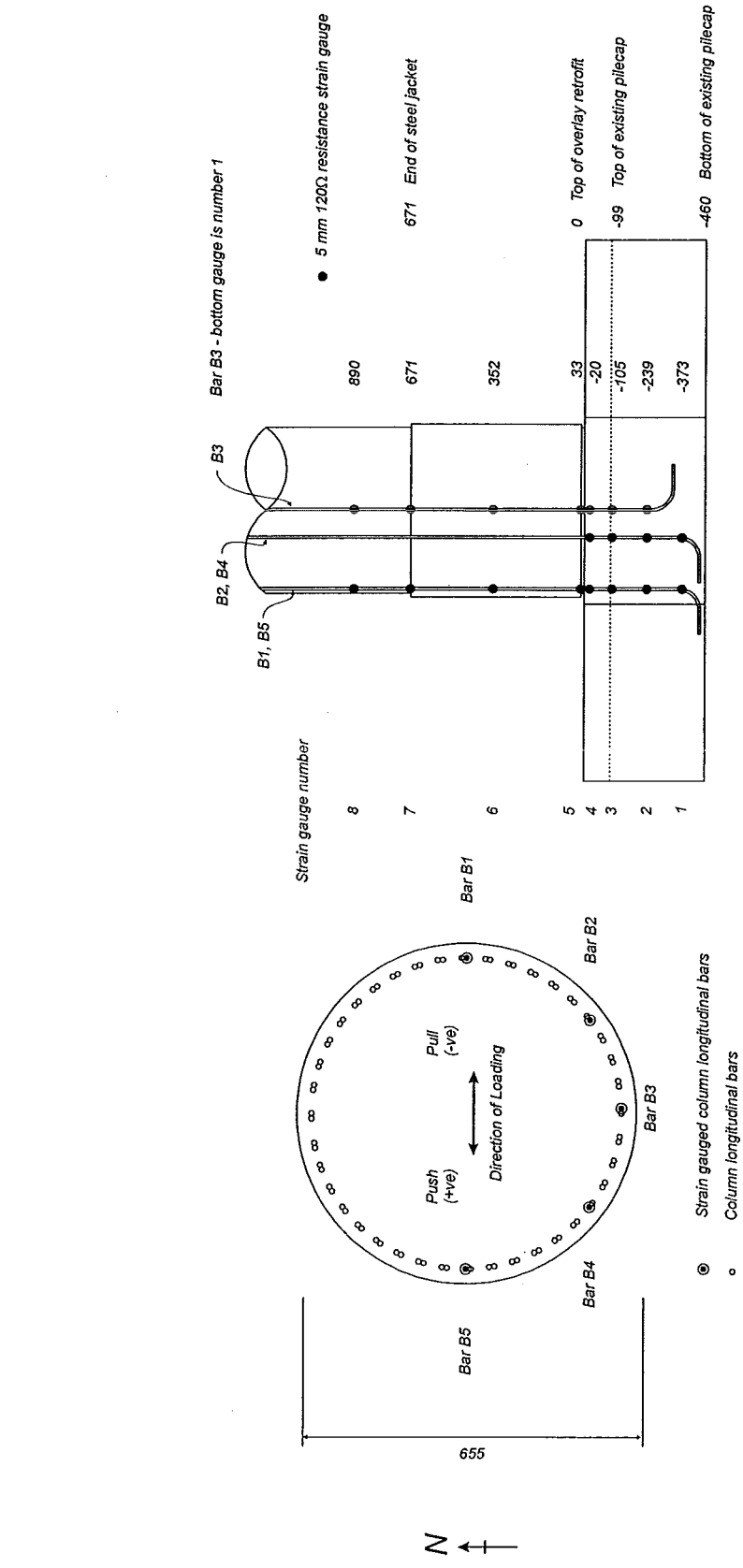

Figure 3.4 *Position of Column Longitudinal Bar Strain Gauges*

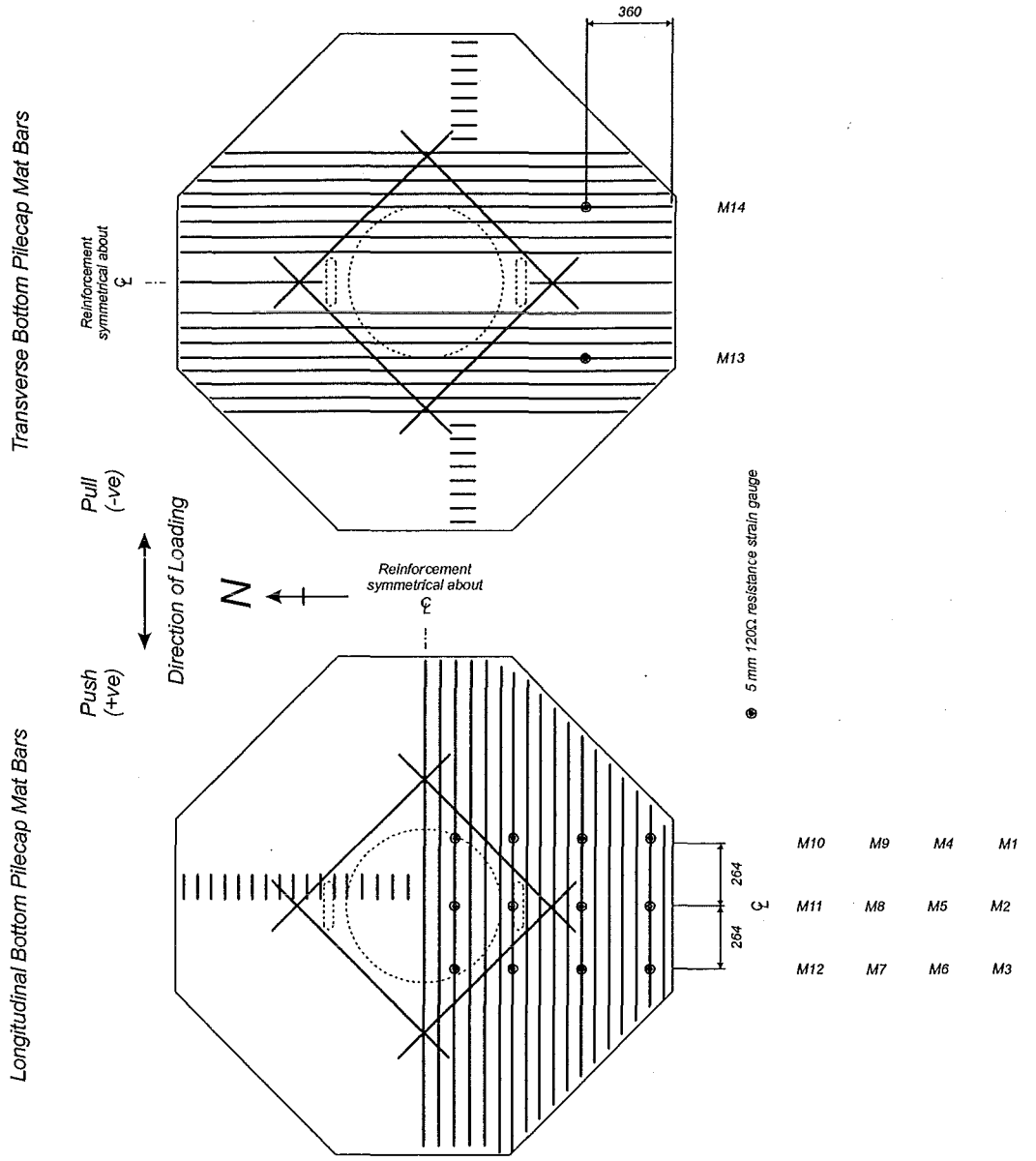

Figure 3.5 *Position of Bottom Pilecap Mat Strain Gauges*

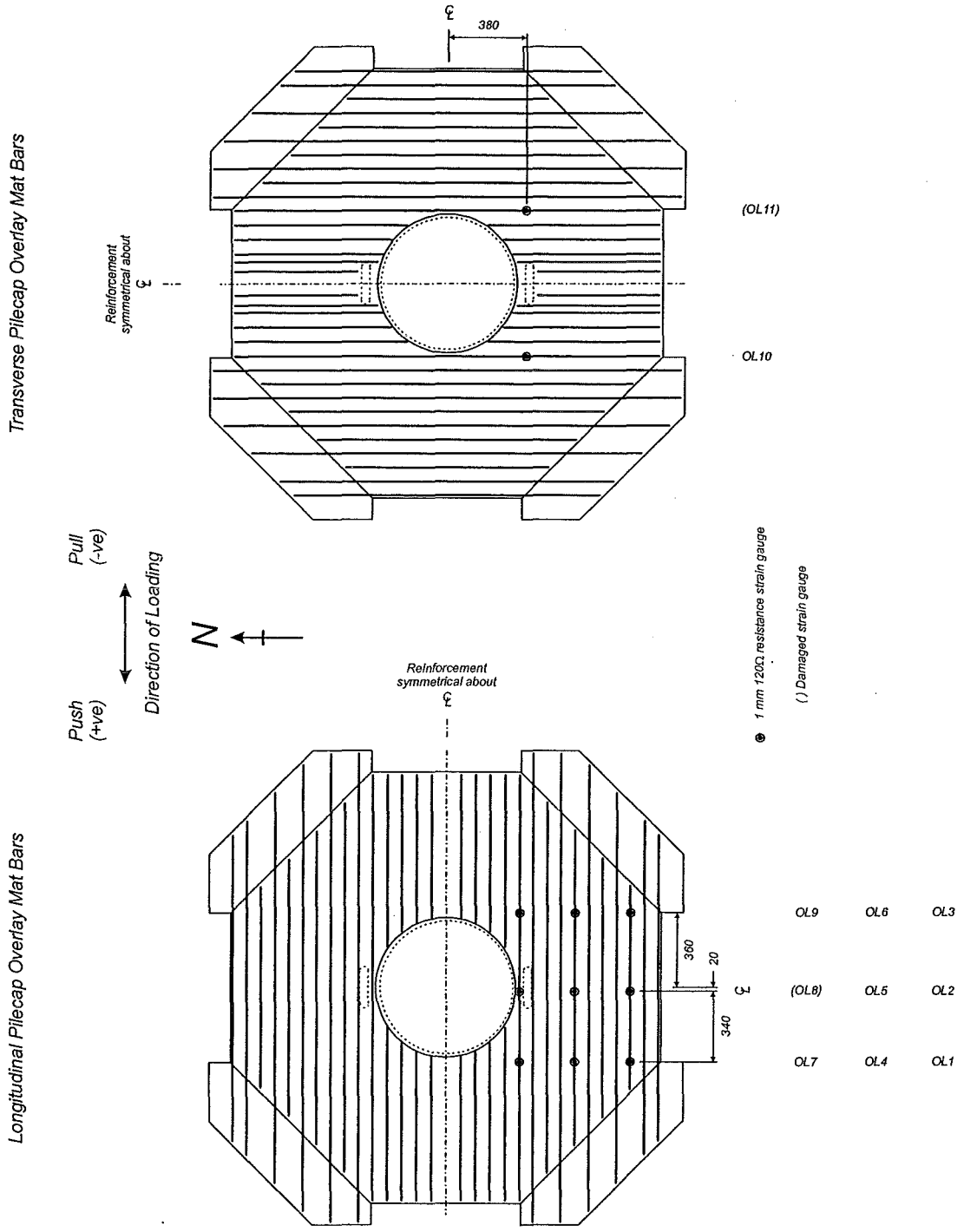

Figure 3.6 *Position of Pilecap Overlay Retrofit Mat Strain Gauges*

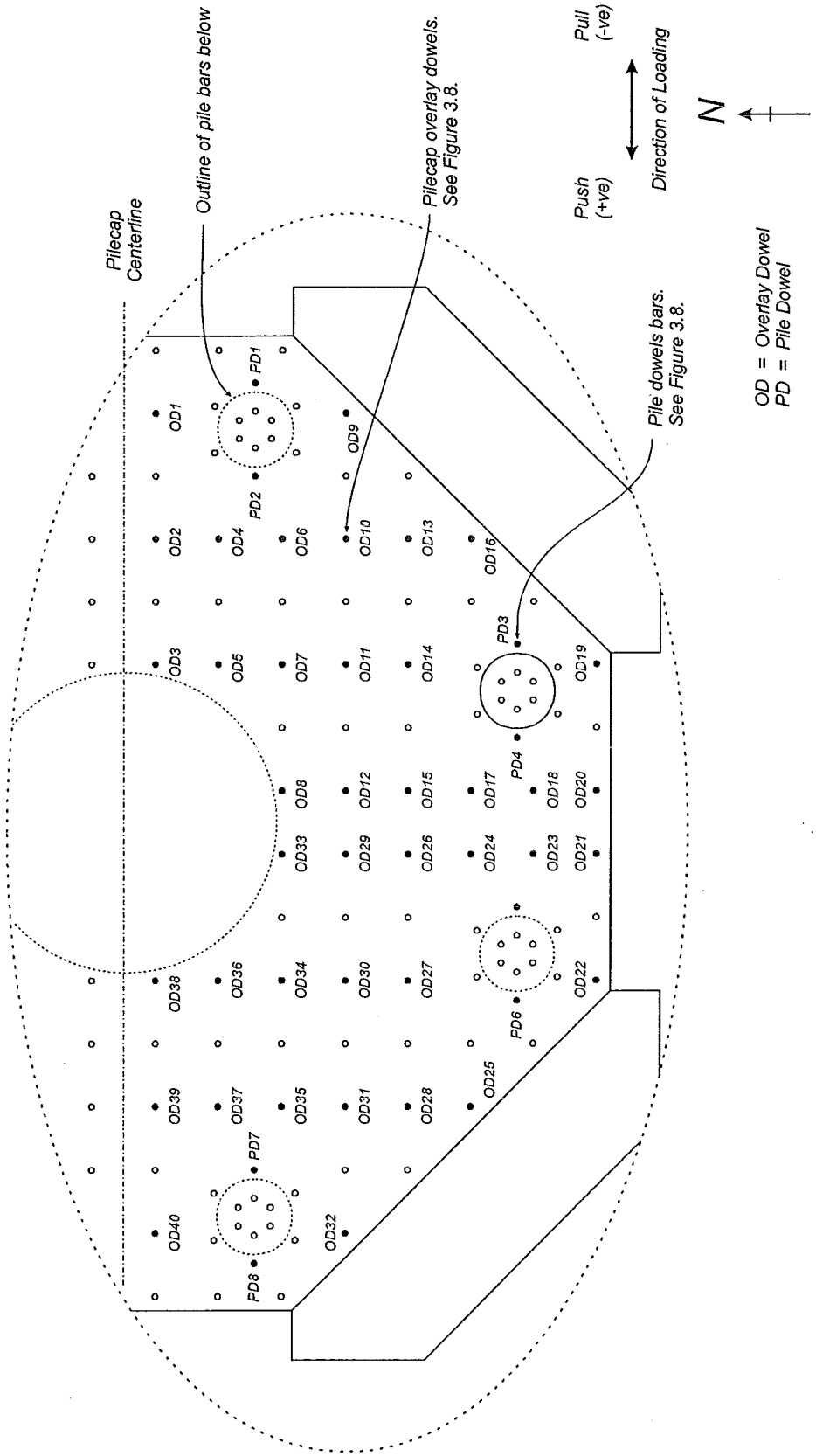

Figure 3.7 *Position of Strain Gauged Pilecap Overlay Dowel and Pile Dowel Bars*

3.2.3.4 Pilecap Overlay Retrofit Dowel and Pile Dowel Strain Gauges

The pilecap overlay retrofit dowels were placed on a nominal 135 mm square grid. The position of the strain gauged dowels are shown in Figure 3.7. Alternate overlay dowels were strain gauged to measure the strains developed in each dowel across the pilecap overlay. Longer pile dowels, at the location of each of the outer piles, were also strain gauged to see the development of strains and forces transferred through these longer dowels. Each strain gauged dowel had the gauge positioned 10 mm above the surface of the original pilecap as shown in Figure 3.8.

3.2.3.5 Steel Jacket Strain Gauges

Four strain gauges were also placed at the base of the steel jacket to measure transverse strains developed in the jacket during the test. The position of these gauges is shown in Figure 3.9.

3.3 LATERAL LOAD TESTING OF UNIT I-B

3.3.1 Lateral Loading History

The lateral loading history used for testing of Unit I-B followed the procedure outlined in Section 2.5.1. Three cycles to each level of load were carried out with a full set of readings, marking of cracks and photographs of the test specimen completed at the peak of each cycle. Push cycles are loading with the loadcell on the hydraulic actuator in compression are denoted as positive loads and positive displacements. Pull cycles are denoted with negative forces and displacements.

The force, H_y, used to determine the level of lateral loading applied during the force controlled cycles was determined from a moment-curvature analysis [K1] of the base of the column, using a nominal concrete strength of 60 MPa and a steel yield strength of 320 MPa and accounting for the confining effects of the steel jacket. This gave a

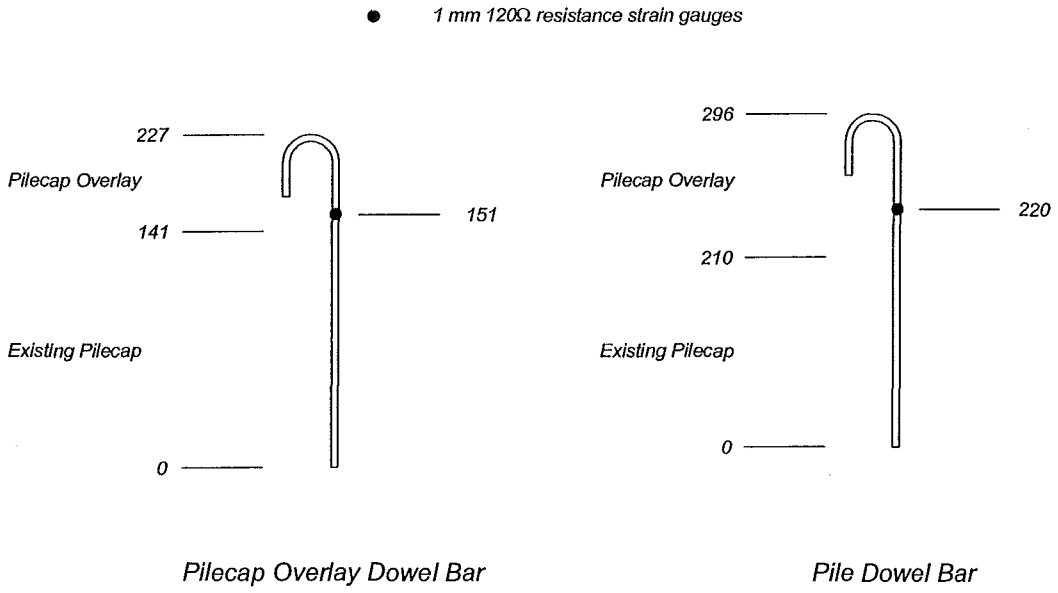

Figure 3.8 *Detail of Strain Gauge Positions for Pilecap Overlay Dowel and Pile Dowel Bars*

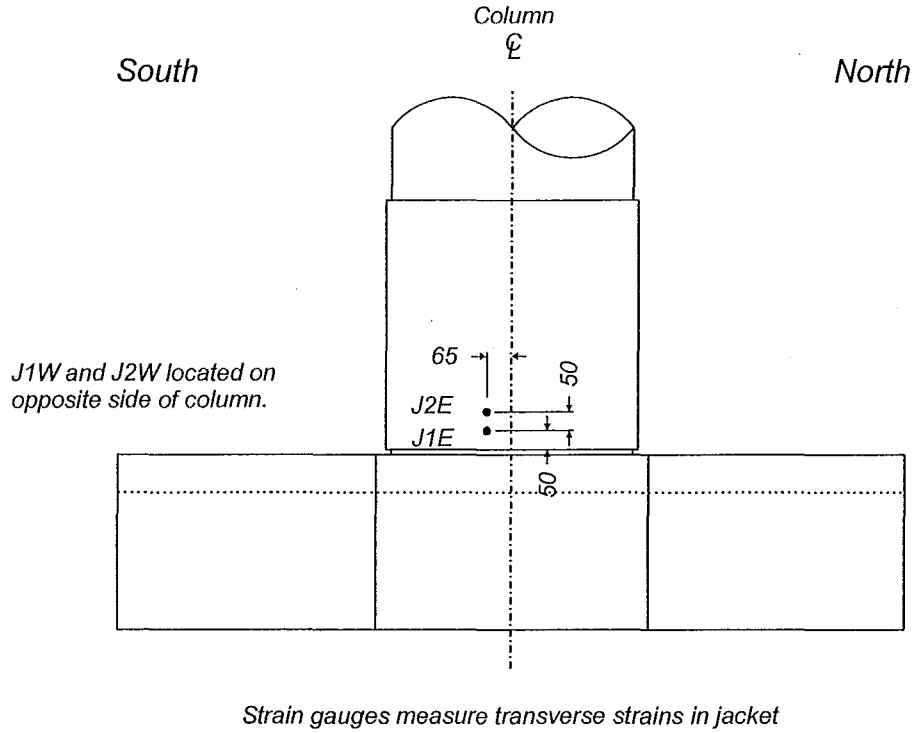

Figure 3.9 *Position of Strain Gauges on Steel Jacket*

value for $H_y = 309$ kN to develop the flexural strength at the base of the column using nominal material strengths. The actual lateral force corresponding to the development of the nominal flexural strength at the base of the column, H_a, was determined from a moment-curvature analysis of the base of the column using the actual concrete and reinforcing steel strengths, measured at time of testing for Unit I-B, and accounting for the confinement provided by the steel jacket. This lateral load was determined to be $H_a = 303$ kN, approximately 2 % less than the lateral load, H_y, used to control the force displacement cycles. The effect of this difference in lateral load on displacements, displacement ductilities and the test results is negligible.

The initial analysis [K1] used to determine the level of lateral load during the force controlled cycles uses a steel stress-strain relationship which does not accurately represent the stress-strain relationship measured for the column longitudinal steel. The value assumed for the ultimate stress of the steel and function used to describe the variation in steel stress over the strain hardening region over estimate the actual ultimate stress and stresses through this part of the steel stress-strain relationship. Subsequent analysis using the appropriate steel stress-strain relationship yields a lower lateral force required to develop the flexural strength at the base of the column.

Three force controlled cycles were completed in both directions to 0.5 H_y (±155 kN) and 0.75 H_y (±232 kN). The yield displacement of Unit I-B, Δ_{yT}, was determined from Equation 2.1 to be $\Delta_{yT} = 27$ mm.

As the tensile and compressive stiffness of the vertical springs do not match the scaled stiffness of the combined soil-pile stiffness used in the structural analysis the test specimen displacement ductilities, $\mu_{\Delta T}$, are not the same for Pier 46. The yield displacement of Unit I-B, Δ_{yT}, cannot be directly scaled to give the yield displacement of Pier 46, Δ_{yS}, due to different amounts of elastic displacement occurring in the test specimen as a result of the different vertical spring stiffness. Displacement ductilities achieved in the test specimen can be related to displacement ductilities in Pier 46 through Equation 2.4.

The theoretical yield displacement of Pier 46 was determined from a structural analysis of the pier to be $\Delta_{yS} = 150$ mm. The displacement of Unit I-B in terms of the actual structure can be obtained by multiplying the test yield displacement, Δ_{yT}, by the scale factor of 3.8. This gives $\delta_{yT} = 102.6$ mm for the yield displacement of Unit I-B in terms of the actual structure allowing the displacement ductility reached in the actual structure, $\mu_{\Delta T}$, to be determined using Equation 3.1.

$$\mu_{\Delta S} = 1 + (\mu_{\Delta T} - 1)\frac{102.6}{150} \qquad (3.1)$$

3.3.2 General Behaviour of Unit I-B

Cracking between the top of the pilecap and bottom of the steel jacket commenced during the cycles to 0.5 H_y. Cracks in the column occurred up to halfway between the top of the steel jacket and top of the column during the cycles to 0.75 H_y. These cracks remained horizontal extending almost halfway around the diameter of the column. The first cracks in the bottom of the pilecap formed between the two central vertical springs, under the edge of the column, during the first cycles to 0.75 H_y. By the completion of the third cycle to this lateral load another crack had formed perpendicular to the first crack on the bottom of the pilecap extending to the edge of the pilecap. Yielding at the base of an extreme column longitudinal bar occurred during these cycles, in both directions of loading.

Following the force controlled cycles it was planned to apply displacement controlled cycles to peaks of $\mu_{\Delta T} = 1.0$, 1.5, 2.0, 3.0 until failure of the test specimen, where $\mu_{\Delta T}$ = maximum lateral displacement divided by Δ_y. Three cycles were successfully completed to displacement ductility factors of $\mu_{\Delta T} = 1.0$, 1.5 and 2.0. Figure 3.10 shows the lateral load-lateral displacement response measured for Unit I-B up to the first cycle of $\mu_{\Delta T} = 3.0$ ($\mu_{\Delta S} = 2.37$). Slight pinching of the hysteresis loops can be seen during the displacement controlled cycles with a slight decrease in lateral load carrying capacity between successive cycles to the same displacement.

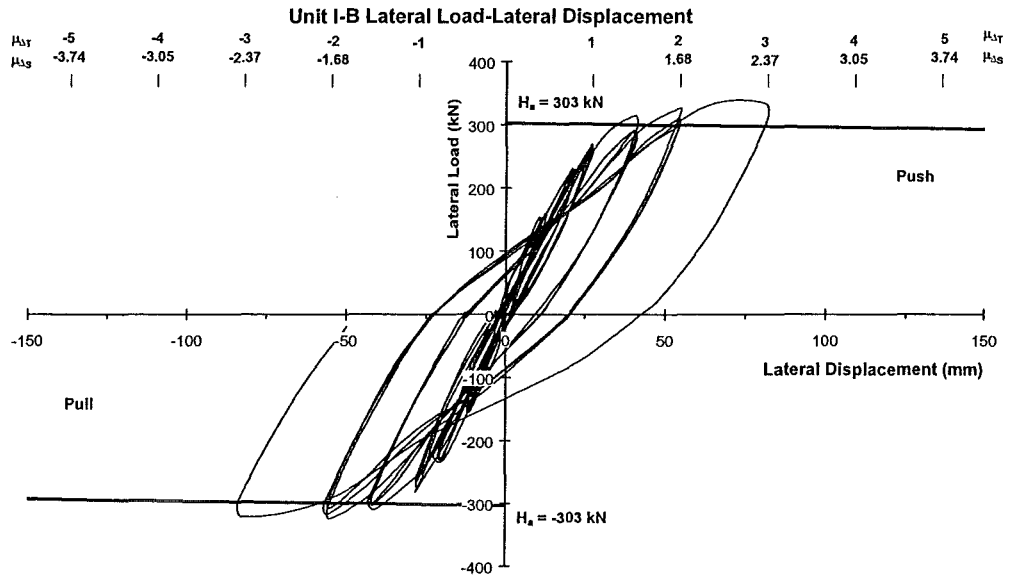

Figure 3.10 *Lateral Load-Lateral Displacement Response for Unit I-B up to* $\mu_{\Delta T} = 3$ *(*$\mu_{\Delta S} = 2.37$*)*

During the first loading cycle to $\mu_{\Delta T} = 3.0$ ($\mu_{\Delta S} = 2.37$) a large diagonal tension crack formed in the column above the steel jacket, where the longitudinal column bars had been curtailed.

The crack initially formed horizontally at the point where the longitudinal bars were curtailed, changing direction to a 30° angle to the column longitudinal axis when it crossed the column centreline. This crack extended down to terminate at the top of the steel jacket and extended back up the column at a 45° angle. Figure 3.11 shows the diagonal cracks in the column after completion of both cycles of loading to $\mu_{\Delta T} = 3$ ($\mu_{\Delta S} = 2.37$). The lateral load-lateral displacement plot can be seen to maintain a constant lateral load of 341 kN from a lateral displacement of approximately 66 mm to the peak lateral displacement of 82 mm at $\mu_{\Delta T} = 3$ ($\mu_{\Delta S} = 2.37$). It was decided to complete the reverse cycle of loading to the same displacement, to observe the formation of the diagonal tension crack in the opposite direction and assess the condition of the column. Development of the diagonal tension crack in the reverse direction of loading was similar, the crack initiating

Figure 3.11 *Unit I-B Showing Diagonal Tension Cracks in Column After Loading to* $\mu_{\Delta T} = 3$ *(*$\mu_{\Delta S} = 2.37$*)*

horizontally and changing direction to terminate at the top of the steel jacket. A maximum lateral load of -325 kN was attained at a displacement of -82 mm. Maximum crack widths were of the order of 4-5 mm in the column.

Buckling of the compressive longitudinal reinforcement occurred during the reverse loading cycle over three transverse hoop spacings causing spalling of the cover

concrete. Spalling also occurred on the opposite side of the column due to buckling of the column longitudinal reinforcement. No strain gauges were placed on column bars around the curtailment point but it is clear that the column longitudinal bars had yielded at this point. Figure 3.12 shows a close up of the column at the curtailment point with the large crack widths, curtailed and buckled longitudinal bars before repair of the column.

Only one cycle to a displacement ductility of at $\mu_{\Delta T} = 3$ ($\mu_{\Delta S} = 2.37$), in each direction, was completed before halting the test, even though the test unit maintained the peak loads attained in each cycle. Application of further load cycles to this level of ductility could have resulted in a quick degradation of the column's strength. The failure of the column at this location was unexpected and a continuation of testing was required to investigate the pilecap overlay retrofit performance. Very little damage to the pilecap and pilecap overlay retrofit had occurred up to this point so repair of the column and extension of the test was required.

The retrofit measures outlined in Chapter 1 and covered in more detail by Maffei and Park [M1] for the Thorndon Overbridge are intended to prevent collapse of the Overbridge during a seismic event corresponding to a 500 year return period earthquake. The assessed structural ductility demand on Pier 46 corresponding to this level of shaking is $\mu_{\Delta} = 2.36$, equivalent to the structural ductility reached in Unit I-B at the formation of the large diagonal tension cracks in the column. Due to the undesirable potential brittle mode of failure that occurred at this point, repair of the column was necessary to continue the test and determine the likely performance of other components of the test specimen.

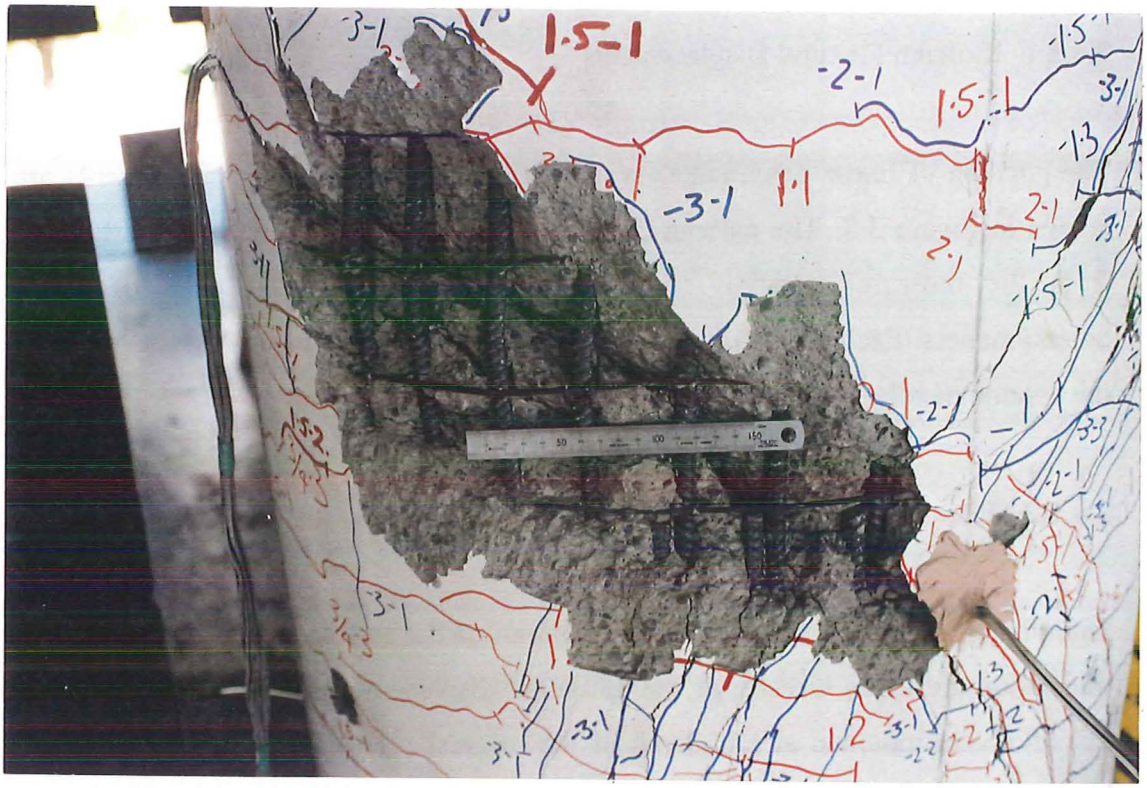

Figure 3.12 *Curtailment Point of Column Showing Diagonal Cracks and Curtailed Longitudinal Bars*

3.4 COMPONENTS OF LATERAL DISPLACEMENT

3.4.1 Displacement Components

Displacements measured at the top of the column can be decomposed into the different components of lateral displacement that occur in the test specimen. A significant component of the overall test specimen displacement is provided by the elastic displacements that occur in the pilecap, through translation against the lateral springs and rotation of the pilecap due to the tensile and compressive reactions in the vertical springs.

3.4.1.1 Column Flexural Displacements

The position of linear potentiometers measuring column internal displacements are shown in Figure 3.3. The column flexural displacement components are estimated from the measured rotation of a column segment between pairs of linear potentiometers. Each pair of linear potentiometers are mounted on opposite sides of the column parallel with the direction of loading.

3.4.1.2 Pilecap Translation

Lateral displacements at the top of the column of the test specimen due to pilecap translation are taken directly as the measured displacement recorded by the linear potentiometer mounted at mid-depth of the original pilecap. Figure 3.2 shows the location of this linear potentiometer.

3.4.1.3 Pilecap Rotation

Displacements at the top of the column due to pilecap rotation are determined from the average rotation of the test specimen pilecap as measured by the vertical displacements of the linear potentiometers at the extreme compression and tension vertical springs. The position of the linear potentiometers measuring the vertical displacements at each vertical spring are shown in Figure 3.2.

3.4.2 Overall Test Unit Displacements

Figures 3.13 and 3.14 show the components of displacement measured as a percentage of the lateral displacement measured by the linear potentiometer mounted at the top of the column for each direction of loading. Up to 60 % of the lateral displacement at the top of the column is provided by pilecap translation and rotation during the load controlled cycles. The contribution of these components reduces during the displacement controlled cycles as the contribution of the flexural

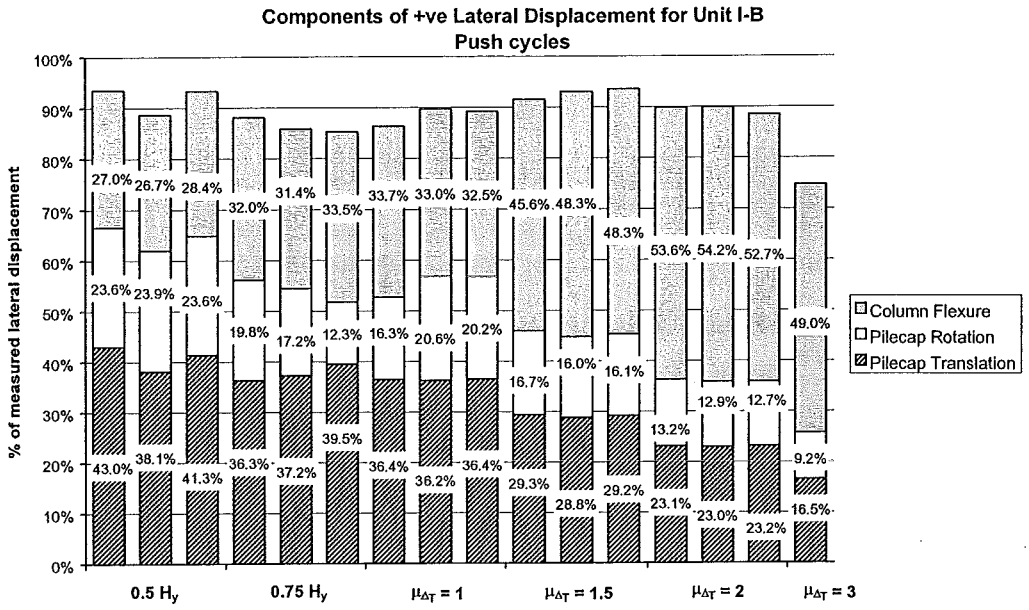

Figure 3.13 *Components of Lateral Displacement of Unit I-B for Push Cycles*

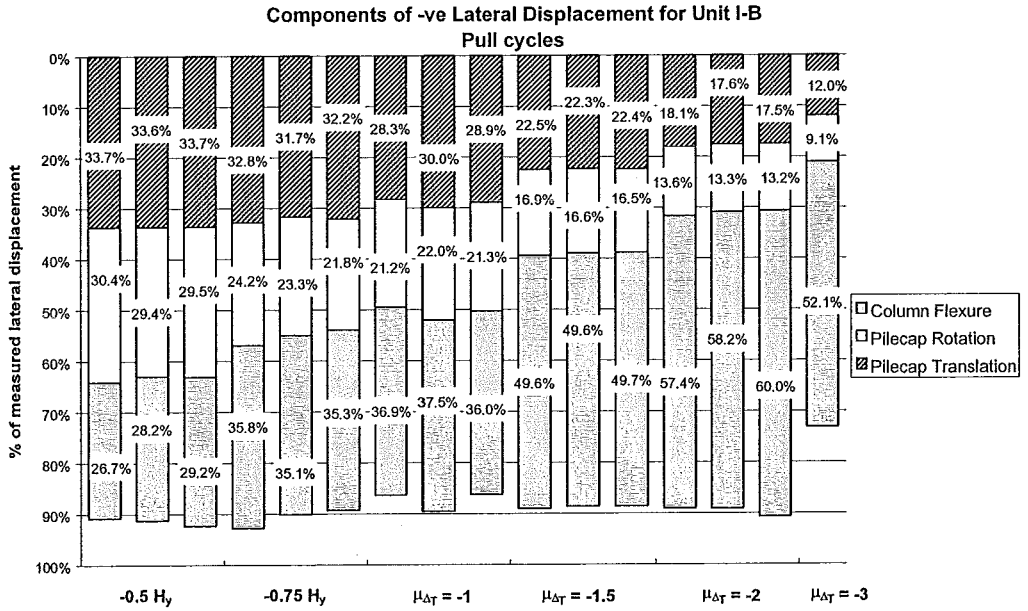

Figure 3.14 *Components of Lateral Displacement of Unit I-B for Pull Cycles*

displacements in the column increase to 50 % of the total measured lateral displacement at the top of the column.

Approximately 90 % of the overall displacement was recovered through measurement of the individual displacement components for both directions of loading which represents the major sources of displacement in the test specimen. The remaining 10 % of unrecovered displacements are due to curvature in the column around the curtailment point, where no instrumentation was placed to record the deformations. The large discrepancy between the measured lateral displacement and the sum of the displacement components at $\mu_{\Delta T} = 3.0$ ($\mu_{\Delta S} = 2.37$) is due to the formation of the large diagonal cracks and resulting shear displacement in the column at this point.

The lateral springs for the push cycle of loading are located directly at the end of the baseblock and strong floor and are affected by rotations induced in the baseblock and strong floor during loading. The lateral springs for the pull cycle are located within the baseblock away from the end of the strong floor and are not influenced by flexibility of the baseblock and/or strong floor. Investigation following completion of testing of Unit I-B also showed the plates in the baseblock on which the push lateral springs were mounted had been dented during the test. Air pockets left after pouring of the baseblock were present under these plates and allowed these plates to be deformed during loading resulting in additional displacements from these lateral springs during the test. The plates for the pull lateral springs were also affected although to a lesser extent. Epoxy resin was injected through holes drilled into each plate to fill the void left under the affected plates before testing of Unit I-A.

Placement of the push lateral springs at the end of the baseblock and the air voids beneath the plates results in a greater flexibility for the lateral springs in the push direction of loading and a greater contribution of this component of displacement to the overall test unit lateral displacement.

3.5 ANALYSIS OF POTENTIAL MODE OF FAILURE

3.5.1 Potential Failure Mode of Unit I-B

The development of the large diagonal tension cracks in the column of Unit I-B at the curtailment point was unexpected. Predictions on the performance of Unit I-B and Pier 46 were based on the assumption that all inelastic action was expected to be confined to the base of the column.

The development of these cracks would have resulted in the rapid degradation of the column's lateral load carrying capacity if further cycles were carried out to this level of displacement. These cracks indicate the development of a brittle flexure-shear failure in the column at the curtailment point. This points to the flexural and shear strength of the column being reached at this point during loading of the test specimen. The consequences of the flexure-shear failure developing in the column could lead to loss of axial load carrying capacity and collapse of the structure. The axial load applied to the test specimen was monitored through a pressure gauge on the manifold connecting the two rams to the hydraulic pump. This pump was not load controlled, the displacement of each ram being held constant throughout the test instead, so the axial load was not being actively controlled. The axial load increased to a maximum of 745 kN and 690 kN at the peak displacements at $\mu_{\Delta T} = 3.0$ ($\mu_{\Delta S} = 2.37$) and $\mu_{\Delta T} = -3.0$ ($\mu_{\Delta S} = -2.37$) due to extension of the column through opening of the diagonal cracks. This gives a 24 % and 15 % increase respectively over the initially applied axial load to the column. With the initial axial load ratio for this column being $0.04\, f'_c A_g$ this increase in axial load will not influence the performance of the column as the axial load ratios are lo, even with the increased load applied during the test.

The longitudinal reinforcement in the column of Pier 46 was curtailed just above the mid-height of the column, closely following the elastic bending moment demand as was the standard practice for curtailment of longitudinal steel reinforcement at the time. The designers attempted to provide adequate length of bar beyond the

calculated theoretical level, approximately equal to the effective depth of the section which is also equal to 40 bar diameters, for the anchorage of the reinforcement [H2]. Although attempts were made to provide some additional length of reinforcing bar beyond the theoretical cut off point it appears that this was not adequate. In addition the shortening of the column through the addition of the reinforced concrete pilecap overlay in Pier 46 and in Unit I-B the curtailment point of the longitudinal bars is moved closer to mid-height of the column of the retrofitted pier.

3.5.2 Moment-Curvature Analysis

The interaction of flexure and shear in a column leads to increased forces carried in the longitudinal reinforcement, compared to the internal forces required for equilibrium at a section, and is referred to here as the tension shift effect. This can be expressed as a fictional increase in the bending moment demand in the column and was responsible for the flexural strength at the curtailment point being reached during the testing of Unit I-B. This occurrence combined with the shear strength of the column in Unit I-B being reached led to the development of the large diagonal tension cracks in the column. A comparison of the bending moment demand versus the moment capacity for the column of Unit I-B was carried out by conducting moment-curvature analyses for the base of the column, with and without the steel jacket, and for the column at the curtailment point, where half the column longitudinal bars were curtailed, using the measured material strength properties. These gave the flexural strengths of the base of the column and at the curtailment point and an estimation of the ultimate available curvature of each section. Figure 3.15 shows the moment-curvature responses for the base of the column, modelled with and without the steel jacket, and the curtailment point of the column. The beneficial effects of the additional confinement provided by the steel jacket enhancing the available curvature ductility of the column and allowing the development of column overstrength can be clearly seen.

Table 3.1 gives the nominal yield moment and yield curvature for each section of the column of Unit I-B which can be used to define a bi-linear moment-curvature approximation for each section. This bi-linear approximation can be used to

determine the curvature distribution following the bending moment diagram to determine elastic displacements of the column of Unit I-B.

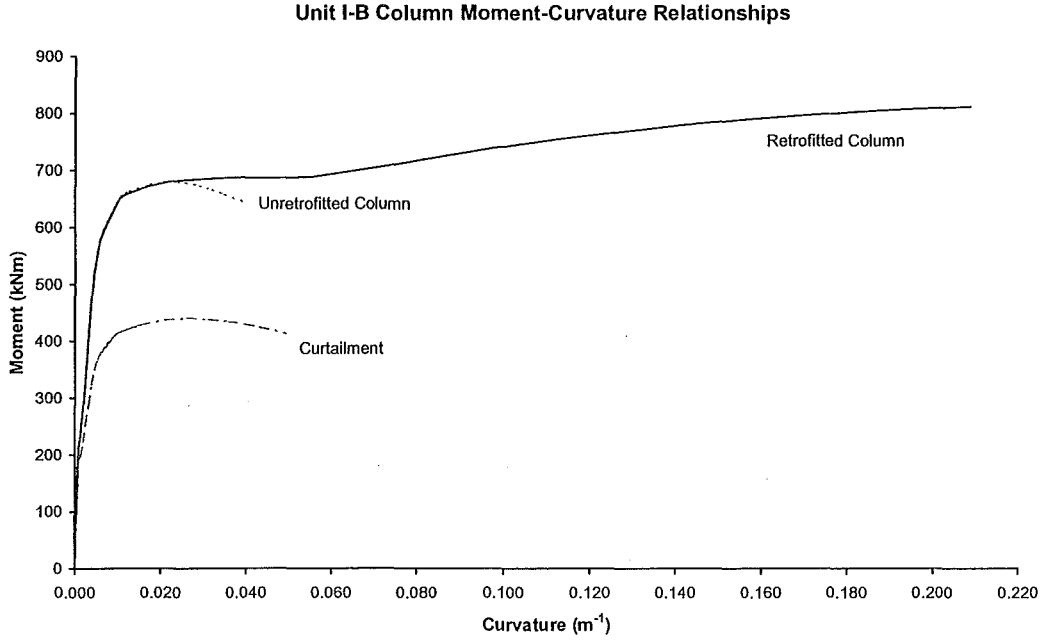

Figure 3.15 *Moment-Curvature Relationships for Column of Unit I-B*

Table 3.1 *Nominal Yield Moment and Yield Curvature for Unit I-B*

	M_y kNm	ϕ_y m^{-1}
Retrofitted Column	683.9	0.00564
Unretrofitted Column	674.4	0.00553
Curtailment	440.2	0.00519

The lateral loads at development of the diagonal tension cracks in the column were 341 kN and -325 kN at $\mu_{\Delta T}$ = 3.0 and -3.0 respectively ($\mu_{\Delta S} = \pm 2.37$) which correspond to moments at the base of the column of 774 kNm for the push (positive load) direction and 738 kNm for the pull (negative load) direction. This is greater

than the yield moment for the retrofitted base of the column and indicate that the flexural strength at the base of the column was reached and strain hardening occurred leading to the flexural strength at the curtailment point being reached.

3.5.3 Column Shear Capacity Assessment

The shear capacity of the column in Unit I-B is assessed following the procedure proposed by Priestley et al. [P3, P4] and outlined in Section 6.4.2. The three components of shear resistance; concrete, transverse steel and axial load, are assessed to provide a total shear resistance of:-

$$
\begin{aligned}
V_n &= V_s + V_p + V_c \\
&= 52 + 79 + 542 \\
&= 673\ kN \qquad \text{for } k = 0.29 \\
&= 52 + 79 + 187 \qquad (3.2) \\
&= 318\ kN \qquad \text{for } k = 0.10 \\
&= 52 + 79 + 93 \\
&= 224\ kN \qquad \text{for } k = 0.05
\end{aligned}
$$

3.5.4 Comparison of Assessed Column Shear Strength and Failure Loads

The shear strength of a column decreases with increasing column curvature ductility due to the degradation of the concrete component of shear resistance [P3, P4]. This allows the shear strength envelope for the column to be plotted against the column curvature ductility and the equivalent column shear force-curvature relationship, derived from a moment-curvature relationship, to be plotted for comparison. Where the shear force-curvature relationship intersects the shear strength envelope indicates the development of a flexure-shear failure in the column and a limit for the available ultimate column curvature. The column may possess further residual strength and displacement capacity but the reliance on shear strength and shear deformation capacity of a column is not recommended for ductile seismic response [P1, P2, P3].

From moment-curvature analyses of the column of Unit I-B an assessment of the base moment and corresponding column shear force can be made to determine the moment reached when the tension shift effect causes the bending moment demand to reach the flexural strength at the curtailment point. The method used here to assess columns with curtailed longitudinal reinforcement is presented in Chapter 6.

The flexural strength envelope for the column can be plotted against the column height from the results of the moment-curvature analyses for each section. The procedure proposed in Chapter 6 assumes the flexural strength at the critical section, the base of the column, is attained and the tension shift is calculated based on the shear force required to develop the column's flexural strength, V, and an angle of the inclined compression fields in the column of $\theta = 30°$.

The bending moment demand corresponding to the development of the flexural strength at the base of the column including the fictional increase in the bending moment demand due to tension shift effect and the flexural strength envelope are shown in Figure 3.16. The fictional increase in the bending moment demand is shown dashed, parallel to the bending moment demand acting on the column, and can be seen to be just below the flexural strength envelope at the curtailment point. This plot suggests it is likely that the flexural strength of the base and the curtailment point will be reached at the same time with a tension shift based on an angle of $\theta = 30$.

With the point of application of the lateral load 2.270 m above the top of the pilecap overlay the shear force corresponding to the development of the flexural strength at the base of the column is 303 kN. As the lateral load at the development of the diagonal shear cracks in the column were 341 kN and -325 kN the tension shift occurring in Unit I-B would have to be less to allow the flexural strength at the base of the column and some overstrength to be developed before the tension shift led to the flexural strength at the curtailment point being developed. This approach neglects the contribution of the concrete tensile stresses developed in the region around the curtailment point. Once the tensile stress contribution of the concrete is exceeded, when the diagonal cracks increased in width, the full tension shift is able to develop.

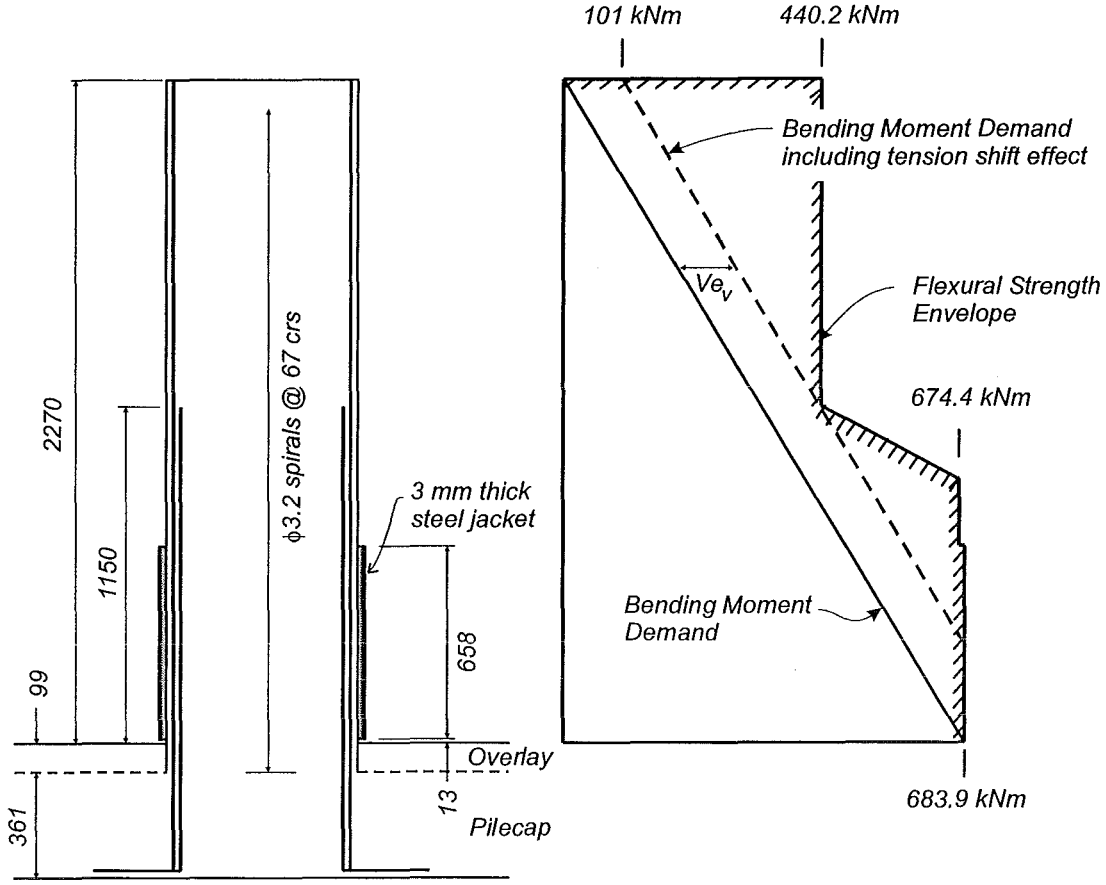

Figure 3.16 *Flexural Strength Envelope and Bending Moment Demand for Unit I-B*

The angle of the diagonal compressive stress fields, θ, when the flexural strength at the curtailment point was reached can be determined using the column shear force corresponding to development of the diagonal cracks. This would give larger angles for the diagonal compressive stress field as the tensile capacity of the concrete is neglected. The assessment procedure, outlined in Chapter 6, will give a lower base

moment attainable before the tension shift leads to the flexural strength at the curtailment point being reached.

The formation of the diagonal crack at approximately 45° to the column axis above the curtailment point indicates the inclined parallel compressive fields had probably formed at an angle of close to 45° before the diagonal cracks increased in width and the tensile capacity of the concrete was exceeded allowing the full tension shift to develop. The steeper inclination of the cracks where they terminated at the top of the steel jacket probably results from the forces in the column seeking a load path that provides adequate resistance after cracking forms in the column.

3.6 REPAIR AND TESTING OF UNIT I-B

3.6.1 Repair of Unit I-B

Following the development of the large diagonal cracks in the column of Unit I-B around the curtailment point of the longitudinal reinforcement the column had to be repaired in order to continue testing. The failure at the curtailment point was not expected during testing as all inelastic action was expected to be confined to the base of the column behind the steel jacket. Very little damage had occurred to the pilecap and pilecap overlay retrofit so a continuation of testing was required to observe the performance of the pilecap overlay retrofit to strengthen the existing pilecap and the steel jacket to confine the plastic hinge region expected at the base of the column.

Repair of the column comprised removal of all loose, spalled cover concrete from the damaged region around the curtailment point and the extension of the existing 3 mm thick steel jacket by 1.200 m above the top of the existing jacket. This extended the steel jacket 705 mm above the curtailment point of the longitudinal column bars, to practically the full height of the column. This jacket was fabricated in two halves and welded together in place and to the existing steel jacket.

Prior to the installation of the steel jacket, provision was made for injecting the cracks in the column with epoxy resin. Small tubes were placed to allow the epoxy to be injected into the cracks in the column and act as breather holes during the injection process. Usually cracks to be epoxy injected are sealed at the surface using an automotive body filler compound to prevent the epoxy resin, which is being injected under a low pressure, from leaking out from the surface. The filler compound is ground off the surface after the injection is completed and the epoxy hardened. Sealing of the cracks at the surface of the column before injection of the epoxy was impractical due to the large width and total length of the cracks so the steel jacket was fitted and the space behind the jacket filled with cement grout. This grout also sealed the cracks in the column preventing the epoxy resin from leaking out during the injection process. Holes were placed in the new steel jacket to pass the tubes out and the epoxy injected into the column.

The epoxy injection was carried out a day after the cement grout was placed behind the new steel jacket and a period of seven days was allowed to give time for the epoxy resin to cure and the cement grout to gain sufficient strength before testing recommenced. Figure 3.17 shows the repaired Unit I-B with the full height steel jacket.

3.6.2 Lateral Loading History for Repaired Unit I-B

After completion of the repair to the column two load controlled cycles were completed to $0.75\,H_y$ to observe the change in stiffness of the repaired column. Further cycles were displacement controlled with two cycles completed to $\mu_{\Delta T} = 2.5$ and three cycles completed to $\mu_{\Delta T} = 3.0$, 4.0 and 5.0 completing the test programme. The yield displacement of the test specimen from the initial cycles was used to define the displacement ductility for the load cycles following repair of the specimen.

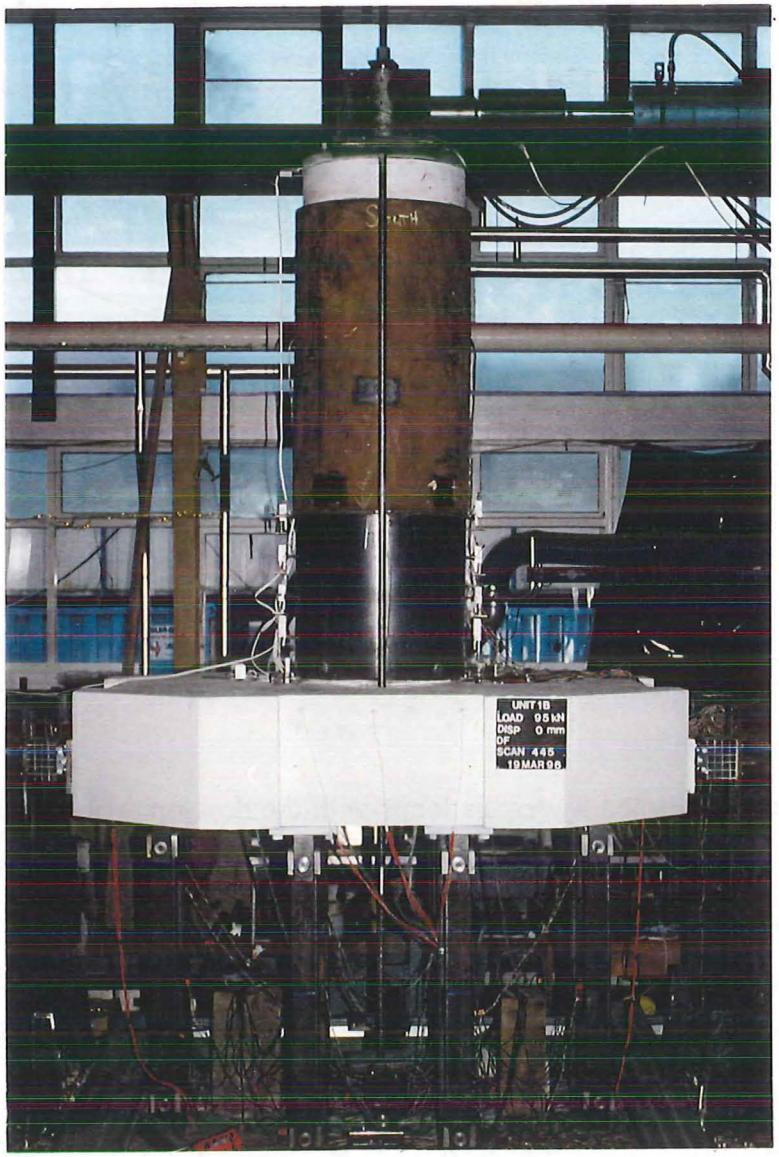

Figure 3.17 *Repaired Unit I-B with Full Height Steel Jacket*

3.6.3 General Behaviour of Repaired Unit I-B

As expected the column had a markedly reduced stiffness during the cycles to 0.75 H_y mainly due to the softening of the column caused by the plasticity at the column base during the inelastic cycles of the first part of the test. Figure 3.18 shows the lateral load-lateral displacement response of the repaired Unit I-B. This plot

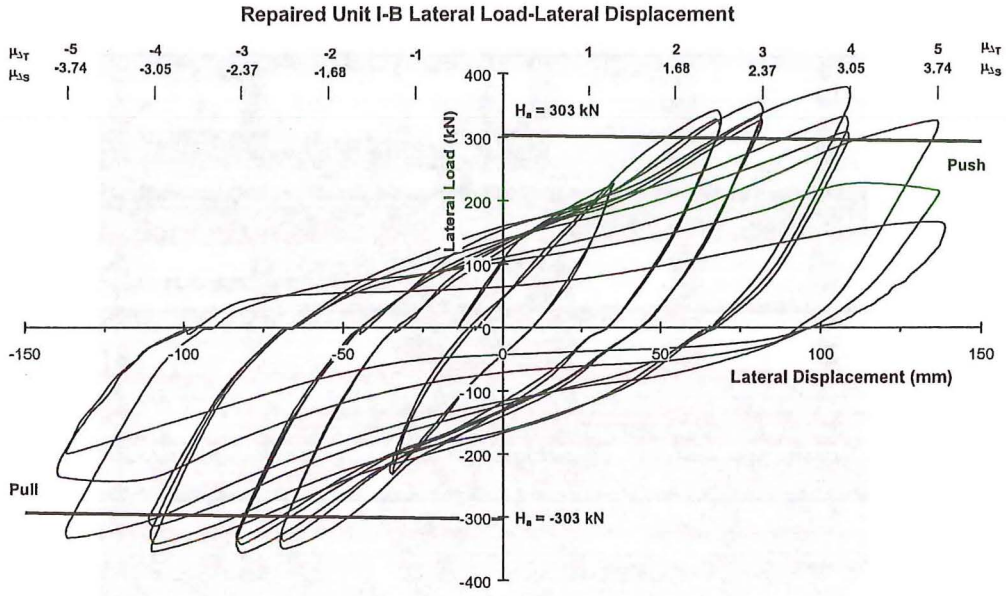

Figure 3.18 *Lateral Load-Lateral Displacement Response for Repaired Unit I-B*

shows stable but pinched hysteresis loops with the development of a large column lateral load overstrength. A decrease in lateral load carrying capacity is seen in the first cycles to $\mu_{\Delta T} = 5.0$ ($\mu_{\Delta S} = 3.74$) which was followed by fracture of up to half the column longitudinal bars at the base of the column during the second and third cycles to this displacement ductility, ending the test. Maximum lateral loads of 386 kN and -358 kN were obtained during the first displacement cycles to $\mu_{\Delta T} = 4.0$ ($\mu_{\Delta S} = 3.05$) and $\mu_{\Delta T} = -4.0$ ($\mu_{\Delta S} = 3.05$) respectively. A significant decrease in the lateral load carrying capacity during the second and third cycles to $\mu_{\Delta T} = 4.0$ ($\mu_{\Delta S} = 3.05$) indicated imminent failure of the test specimen but three displacement cycles to $\mu_{\Delta T} = 5.0$ ($\mu_{\Delta S} = 3.74$) were completed before stopping the test. Fracture of the longitudinal column bars commenced during the second cycle to $\mu_{\Delta T} = 5.0$ ($\mu_{\Delta S} = 3.74$) and resulted in a very rapid decrease in lateral load carrying capacity.

Strain gauges recording the transverse strain at the base of the original steel jacket indicated yielding of the jacket occurred during the cycles to $\mu_{\Delta T} = 2.5$ ($\mu_{\Delta S} = 2.03$) after repair of the column. Noticeable bulging of the base of the steel jacket was seen

during the cycles to $\mu_{\Delta T} = 4.0$ ($\mu_{\Delta S} = 3.05$) with considerable crushing of the grout and concrete behind the jacket. Buckling of the longitudinal column bars increased the bulging behind the jacket until fracture of the bars ended the test.

In additional to allowing the test specimen to achieve a large lateral load overstrength and increased structural ductility the extension of the steel jacket successfully prevented the shear failure from occurring in the column around the curtailment point. Removal of the steel jacket following the completion of the test revealed no cracking in the grout around the column at the curtailment point or sign of the diagonal tension cracks which had formed earlier in the test. All cracking and damage was confined to the base of the column in the lower half of the original steel jacket.

The pilecap and pilecap overlay retrofit transferred the forces induced from the repaired column with restricted cracking only and limited yielding of some bottom pilecap mat bars. Data from strain gauges in the pilecap overlay retrofit indicated the reinforcement remained within the elastic range throughout the entire test. Several pilecap overlay dowels immediately adjacent to the base of the column yielded through dowel action caused by the pull-out of a cone shaped wedge of concrete. Overlay dowels away from the column showed decreasing peak strains with distance away from the column.

3.7 REPAIRED UNIT LATERAL DISPLACEMENTS

3.7.1 Repaired Overall Test Unit Displacement Components

The measured lateral displacement of the top of the column of the repaired Unit I-B can be decomposed into the components of lateral displacement due to pilecap translation, pilecap rotation and column flexure. The upper set of linear potentiometers placed above the original steel jacket to measure internal column displacements were removed with the installation of the steel jacket for the repair of the specimen. The remaining linear potentiometers were used to determine the

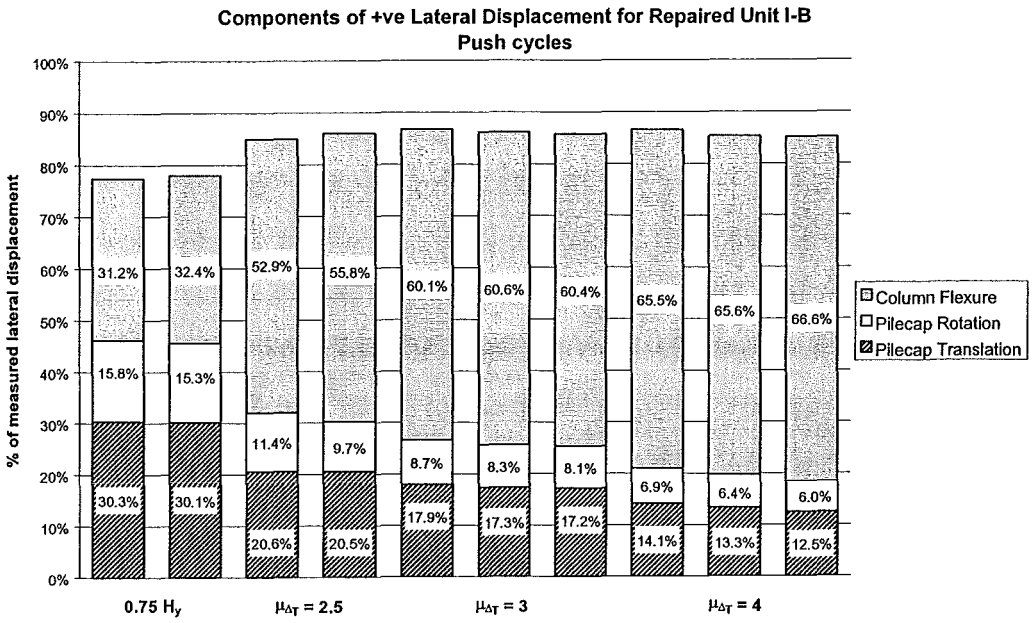

Figure 3.19 *Components of Displacement for Repaired Unit I-B for Push Cycles*

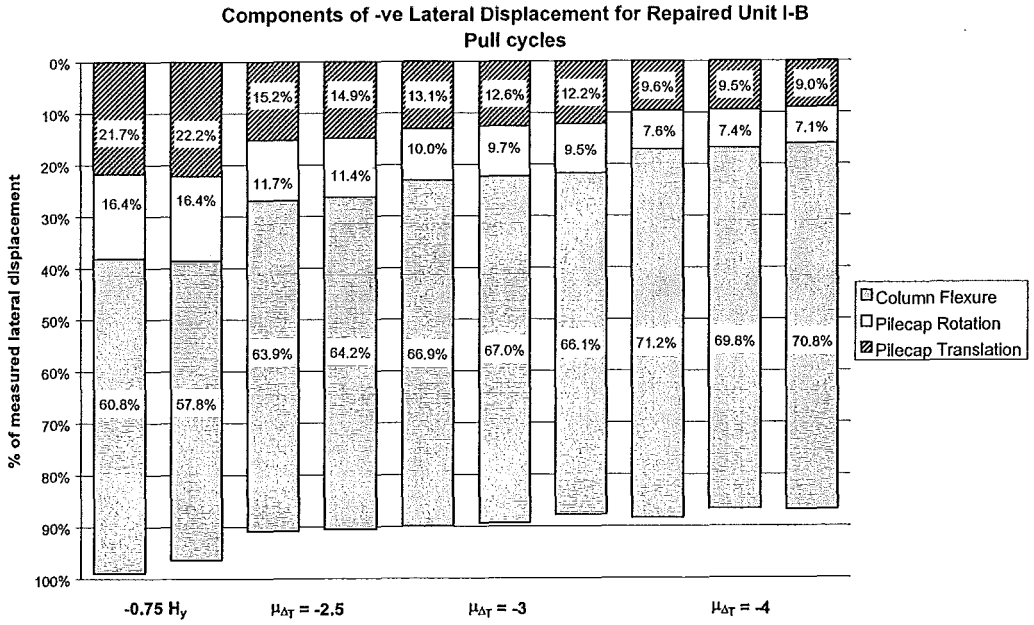

Figure 3.20 *Components of Lateral Displacement of Repaired Unit I-B for Pull Cycles*

component of lateral displacement due to column flexure. After completion of the lateral load cycles to $\mu_{\Delta T}$ = 4.0 ($\mu_{\Delta S}$ = 3.05) the bottom two sets of linear potentiometers were removed as they were clashing with the top surface of the pilecap overlay. Displacements at the base of the column were also large, greater than the travel of the linear potentiometers at that position, rendering the readings unreliable.

Figures 3.19 and 3.20 show the components of displacement as a percentage of the measured lateral displacement at the top of the column for the push and pull cycles for the repaired test specimen. Again the greater flexibility of the lateral springs in the push direction show a greater component of translational displacement in this direction of loading. Column flexure is the dominant component of lateral displacement for this part of the test with much of the flexure taking place at the base of the column.

3.8 BEHAVIOUR OF MEMBERS OF UNIT I-B DURING TESTING

3.8.1 General Observations

First cracking occurred at the base of the column between the top of the pilecap overlay and the bottom of the steel jacket at the first cycle to 0.5 H_y. Short horizontal cracks also formed just above the top of the steel jacket during the third cycle to 0.5 H_y. Further horizontal cracking occurred between the top of the steel jacket and up to the curtailment point during the cycles to 0.75 H_y extending across one third of the column diameter in each direction. These cracks extended horizontally to the column centreline during the cycles to $\mu_{\Delta T}$ = 1.0.

A long horizontal crack formed directly at the point where the longitudinal column bars are curtailed, extending to the column centreline, in both directions during the cycles to $\mu_{\Delta T}$ = 1.0. This crack extended during cycles to higher displacement ductilities developing at a 45° angle to the axis of the column as it passed the

centreline. The remaining cracks in the column remained essentially horizontal until the development of the large diagonal tension cracks at the curtailment point.

By $\mu_{\Delta T} = 2.0$ ($\mu_{\Delta S} = 1.68$) the crack at the base of the column, due to yield and strain penetration of the longitudinal bars, opened up to 3 mm. The steel jacket was seen to debond from the column over the height with considerable slip at the base of the jacket reducing to negligible slip at the top. Crushing and spalling of the grout occurred at the later stages of this part of the test.

Although no strain gauges were placed on the longitudinal reinforcement around the curtailment point it is apparent from the buckled reinforcement that the longitudinal bars must have yielded at this point.

Following repair of the column the steel jacket prevented any observation of column crack patterns. Dilation of the concrete at the base of the column forced the steel jacket to bulge outwards from $\mu_{\Delta T} = 4.0$ ($\mu_{\Delta S} = 3.05$) leading to spalling of the grout and concrete from the base of the column, buckling and eventual fracture of the longitudinal bars at the base. Up to half the longitudinal bars fractured during the second and third cycles to $\mu_{\Delta T} = 5.0$ ($\mu_{\Delta S} = 3.74$) ending the test.

3.8.2 Column Displacements

Lateral displacements of the column of Unit I-B can be derived from measuring the total lateral displacement at the top of the column and removing the components of displacement due to rotation and translation of the of the pilecap.

Figure 3.21 shows the lateral load-lateral column displacement plot for Unit I-B up to the development of the diagonal cracks in the column at $\mu_{\Delta T} = 3.0$ ($\mu_{\Delta S} = 2.37$). Also shown is the column displacement ductility based on the yield displacement of the column measured during the test. The yield displacement of the column is established using Equation 2.1 where $\Delta_{0.75Hy}$ and $\Delta_{-0.75Hy}$ are taken as the average measured column lateral displacements from the three cycles to $0.75H_y$. This gives a column yield displacement $\Delta_{y,\,c} = 11.6$ mm which compares well to the calculated

theoretical yield displacement for the column of 10.0 mm, accounting for the difference in the column EI_e values for the region of column behind the steel jacket and above the curtailment point, strain penetration at the base of the column, top and bottom of the steel jacket and at the curtailment point.

The column developed its flexural strength at the base of the column during the cycles to $\mu_{\Delta T} = \pm 1.0$ and continued to develop further lateral load overstrength during the following cycles. The last load cycle is marked by the flattening of the load-displacement plot as the diagonal tension cracks developed in the column corresponding to a column displacement ductility $\mu_{\Delta C}$ of approximately 5.

The lateral load-lateral column displacements for the repaired Unit I-B are shown in Figure 3.22. The extension of the steel jacket allowed the development of a large lateral load overstrength until the loss of confinement caused by bulging of the steel jacket led to a drop in the load carrying capacity and eventual fracture of the longitudinal bars. Column displacement ductilities in excess of 10 were achieved with the use of the full height steel jacket.

3.8.3 Column Curvature Distribution

The measured curvature distribution for the base of the column of Unit I-B is shown in Figure 3.23. No instrumentation was provided further up the height of the column, around the curtailment point, as failure was not expected to occur at this point. The curvature values plotted were obtained from the measurements of the linear potentiometers at each level and are plotted at the mid-points of the gauge lengths between each of the potentiometer positions. Shown on each plot is the position of the steel jacket and the position of the curtailment point of the longitudinal reinforcement in the column. The theoretical yield curvature, ϕ_y, obtained from a moment-curvature analysis of the base of the column, modelling the steel jacket and using measured material properties is also shown. The chart legend shows the global structural displacement ductility $\mu_{\Delta T}$ along with corresponding measured column displacement ductility $\mu_{\Delta C}$.

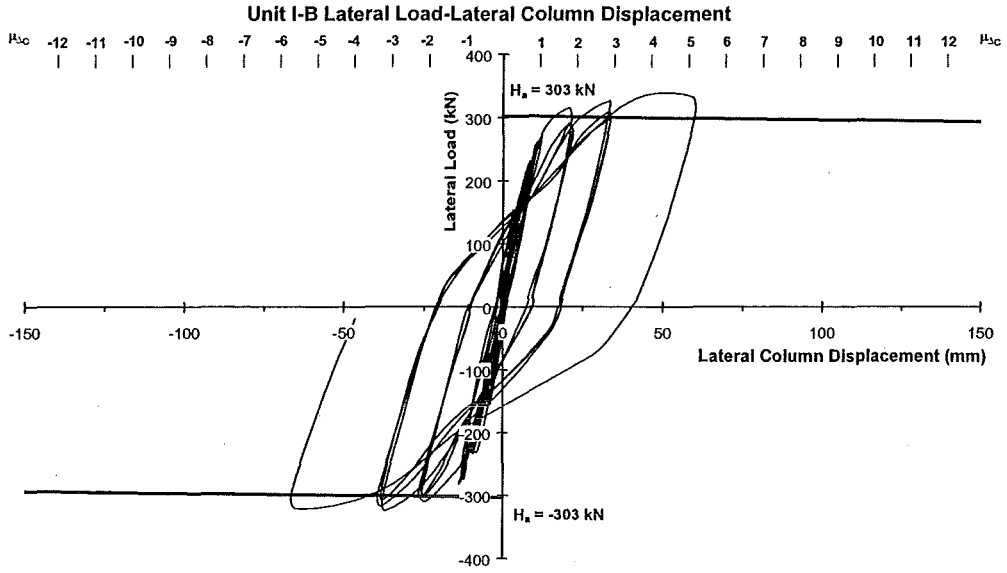

Figure 3.21 *Lateral Load-Lateral Column Displacements for Unit I-B up to* $\mu_{\Delta T}$ = *3.0* ($\mu_{\Delta S}$ = *2.37)*

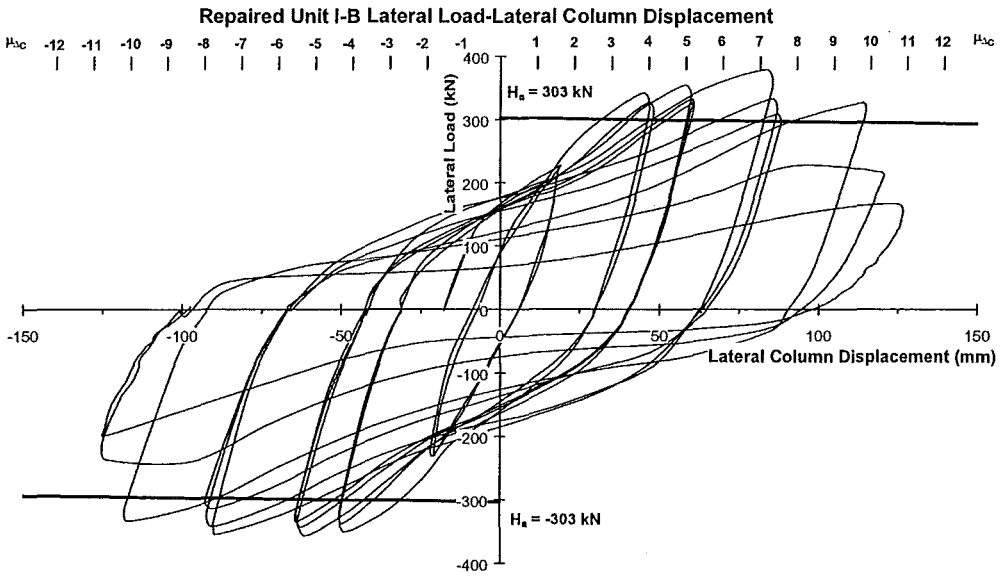

Figure 3.22 *Lateral Load-Lateral Column Displacements for Repaired Unit I-B*

The effect of the steel jacket is to concentrate the plasticity in the column to the gap between the bottom of the steel jacket and the top surface of the pilecap overlay. Plasticity in the column can be seen spreading to the top of the steel jacket 671 mm above the top of the pilecap overlay surface by $\mu_{\Delta T} = 3.0$ ($\mu_{\Delta S} = 2.37$) corresponding to a column displacement ductility of 5.3.

The plastic hinge length for columns retrofitted by jacketing can be expressed as the gap between the supporting member and the steel jacket plus a term to account for the strain penetration in the longitudinal reinforcement.

$$L_p = v_g + 0.044 f_y d_b \qquad (3.3)$$

where L_p = plastic hinge length
v_g = gap between jacket and supporting member
f_y = yield strength of longitudinal reinforcement
d_b = longitudinal bar diameter

Equation 3.3 has been taken from Reference [P3]. Similar expressions for the plastic hinge length for columns retrofitted by jacketing have been proposed by different researchers [C4, P5]. For Unit I-B the plastic hinge length from Equation 3.3 would be equal to 154 mm which appears smaller than the observed spread of plasticity in the column as shown in Figure 3.23(b).

A finite bond transfer length from the top and bottom of the jacket is required to achieve full composite action of the steel jacket. Chai et al. [C5] developed an analytical model for steel jacketed reinforced concrete circular bridge columns which proposes a method to determine the bond transfer length at first yield of the column.

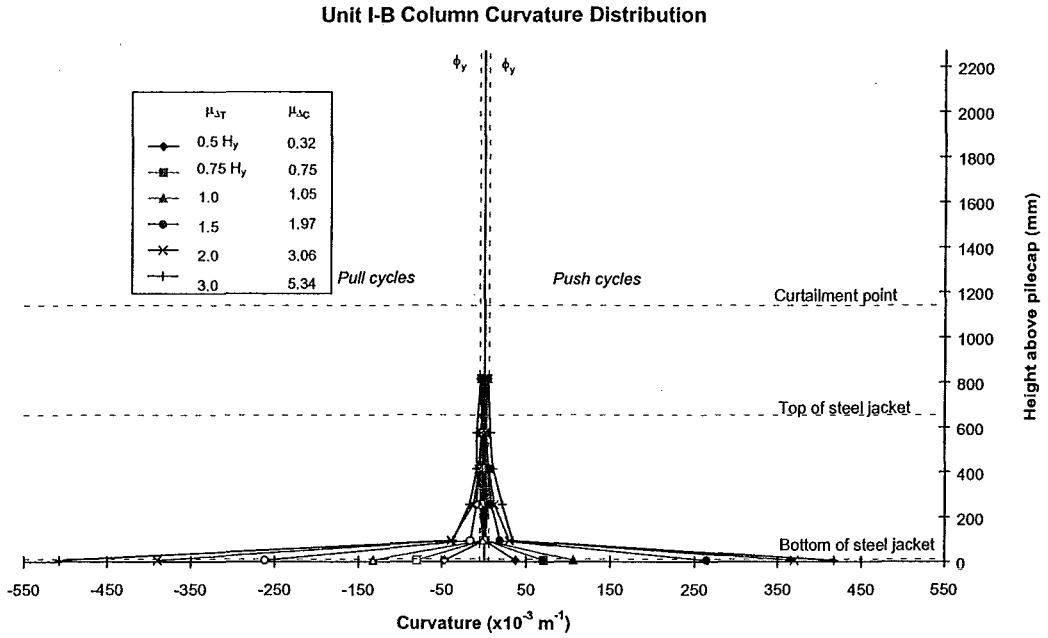

Figure 3.23(a) *Unit I-B Column Curvature Distribution up to* $\mu_{\Delta T} = 3.0$ *(*$\mu_{\Delta S} = 2.37$*)*

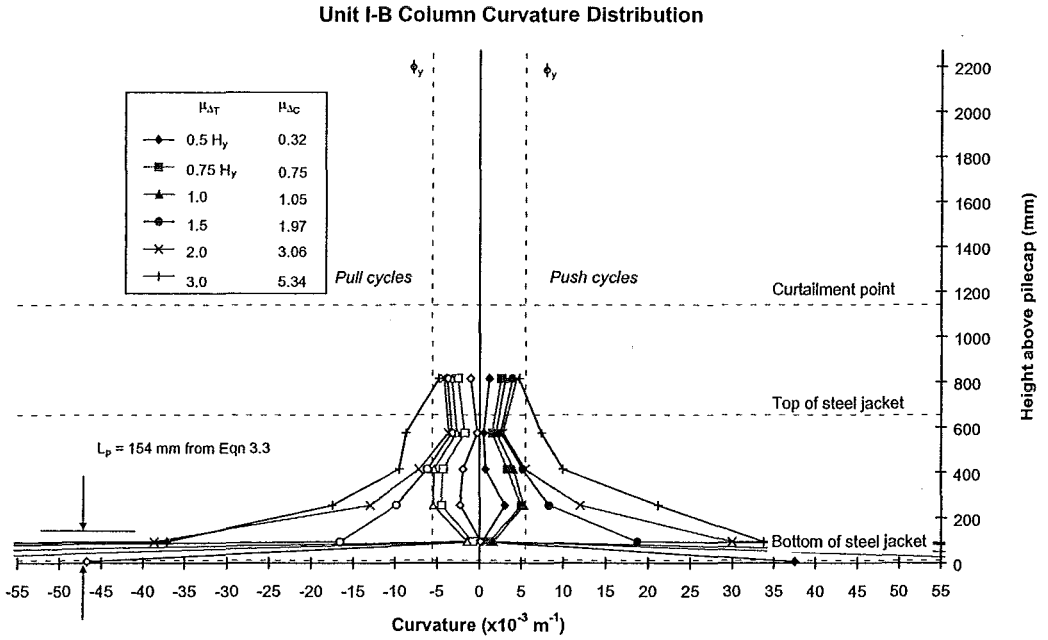

Figure 3.23(b) *Unit I-B Column Curvature Distribution up to* $\mu_{\Delta T} = 3.0$ *(*$\mu_{\Delta S} = 2.37$*), Detail at Low Curvatures*

This transfer length is dependent on the length of the steel jacket and the bond strength between the grout and the jacket and if the steel jacket is of sufficient length to provide for the bond transfer a central region of full composite action can be developed. If a relatively short jacket is provided full composite action of the jacket cannot be developed.

Composite action of the jacket and column can be seen in the early cycles of testing of Unit I-B. The spread of plasticity in the column agrees well with the plastic hinge length as determined using Equation 3.3 up to $\mu_{\Delta T} = 2.0$ ($\mu_{\Delta C} = 3.06$). The formation of the critical section at the curtailment point leads to the sudden increase in curvature distribution over the column height during the cycle to $\mu_{\Delta T} = 3.0$ ($\mu_{\Delta C} = 5.34$) due to strain penetration and the spread of plasticity down the column from the curtailment point at this point in loading.

Figure 3.24 shows the column curvature distribution for the repaired Unit I-B. Debonding of the jacket at the base had occurred during the earlier cycles in the test and this can be seen through the lack of composite action during the cycle to 0.75 H_y. During the cycles to $\mu_{\Delta T} = 2.5$ ($\mu_{\Delta C} = 4.09$) crushing and spalling of the grout behind the jacket was noticed and continued until the end of the test. Cracks in the column were noticed behind the steel jacket through the holes in the potentiometer rods and a slip of approximately 4 mm at the base of the column was distributed over three-quarters of the original jacket height. Yielding of the steel jacket at the base occurred at $\mu_{\Delta T} = 4.0$ ($\mu_{\Delta S} = 3.05$, $\mu_{\Delta C} = 4.09$) with the base of the jacket commencing to bulge outwards. Considerable crushing of the grout and cover concrete from behind the base of the jacket continued until the end of the test.

3.8.4 Column Strain Gauges

Bars 1, 3 and 5 have strain gauges distributed from the bottom of the original pilecap up to 890 mm above the top surface of the pilecap overlay. Bars 2 and 4 only had strain gauges placed over the depth of the original pilecap. Instrumentation on the

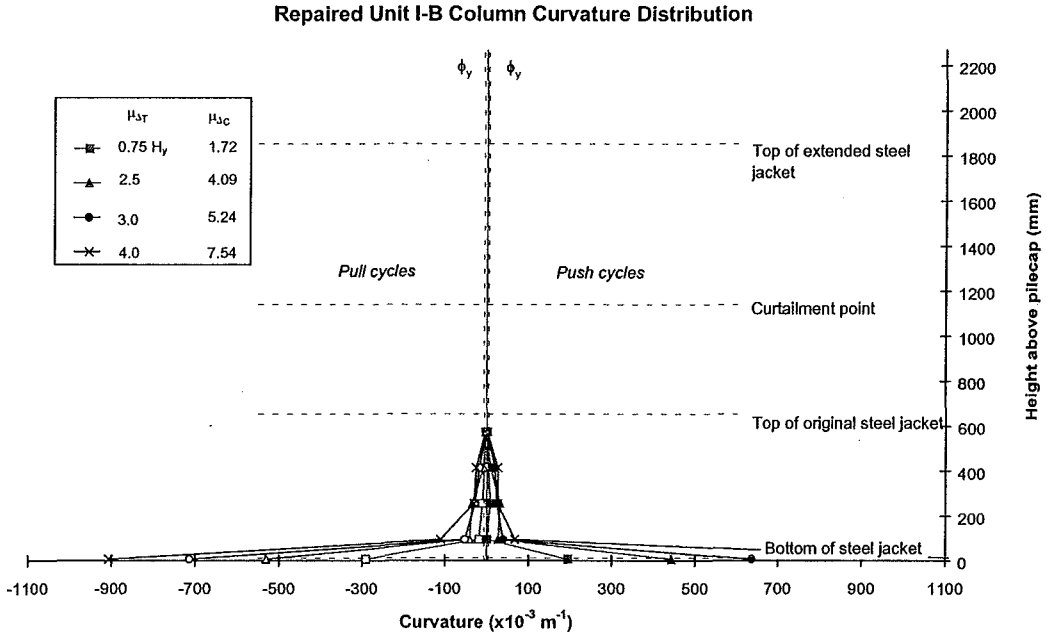

Figure 3.24(a) *Repaired Unit I-B Column Curvature Distribution*

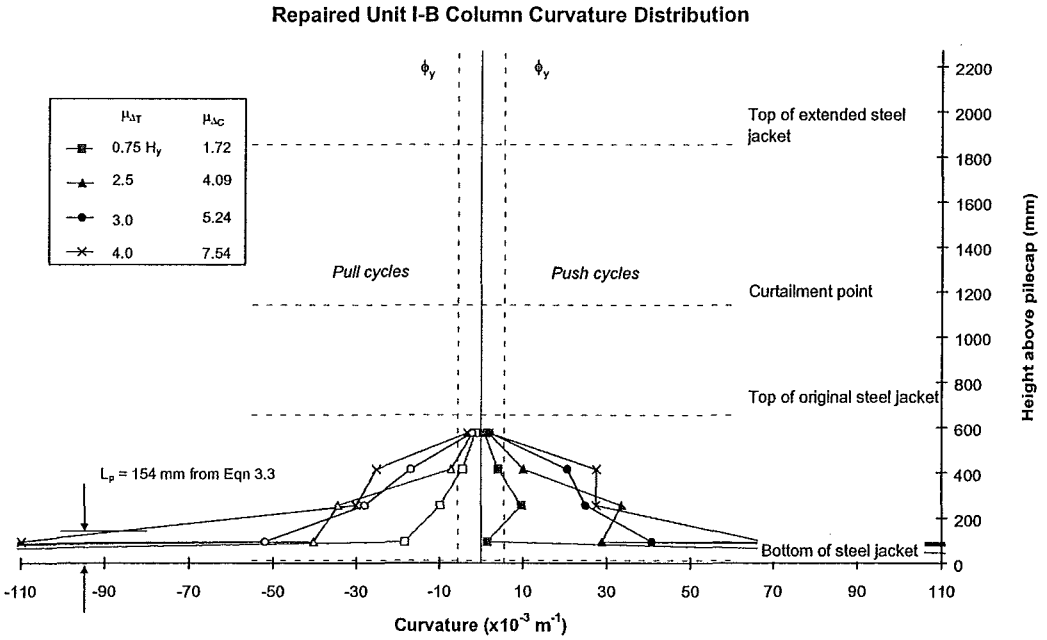

Figure 3.24(b) *Repaired Unit I-B Column Curvature Distribution, Detail at Low Curvatures*

column longitudinal bars did not extend up to the curtailment point, 1150 mm above the top of the pilecap overlay, as failure was not expected to occur in this region when the commenced.

Strain gauges are numbered consecutively starting from 1 at the bottom-most gauge on each bar and identified with the bar number and the gauge number eg. B1-3 being gauge number 3 on Bar 1.

Figures 3.25 to 3.30 show the maximum recorded strain in each gauge against position of the gauge within the column for the three cycles of loading to each level. Solid symbols indicate readings from Push (positive loading) cycles with hollow symbols indicating Pull (negative loading) cycles. Tensile strains are taken as positive. Shown on each plot is the position of the steel jacket, curtailment point and yield strain of the column longitudinal reinforcement. The top of the vertical axis, 2270 mm above the top of the pilecap overlay is the point of application of the simulated seismic load to the test specimen.

Strain gauges on the extreme column longitudinal bars indicate yielding of these bars (B1-4, B1-5 and B5-4) at the base of the column took place during the cycles to 0.75 $H_y = \pm 232$ kN. Strains of up to 2 % were recorded in gauges at these positions before debonding of the strain gauges from the reinforcement and possible mechanical damage to the gauge rendered further readings unreliable.

Yield penetration into the pilecap up to strain gauges 239 mm below the pilecap overlay surface can be seen in Bars 1, 2, 4 and 5 up to the cycles to $\mu_{\Delta T} = 3.0$ ($\mu_{\Delta S} = 2.37$). Yield in tension extended half way up the steel jacket on the extreme bars, B1 and B5. Strains in the reinforcement in these two bars approach the yield strain in tension above the top of the steel jacket during the cycles to $\mu_{\Delta T} = 1.5$ ($\mu_{\Delta S} = 1.34$).

By the development of the large diagonal tension cracks in the column at $\mu_{\Delta T} = 3.0$ ($\mu_{\Delta S} = 2.37$) the strain gauges indicate the extreme column bars had yielded from

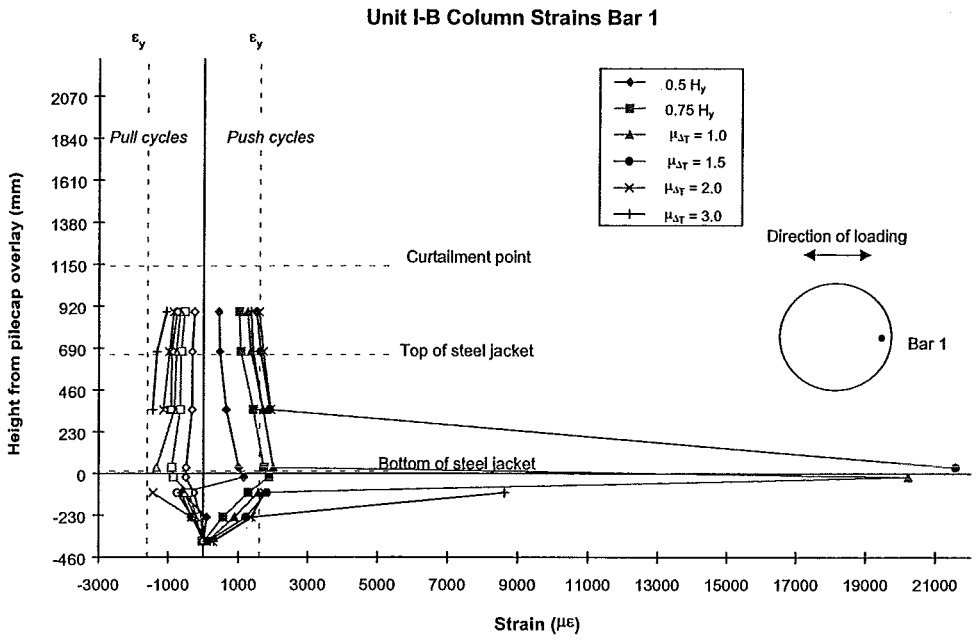

Figure 3.25 *Unit I-B Column Longitudinal Bar 1 Strain Profile*

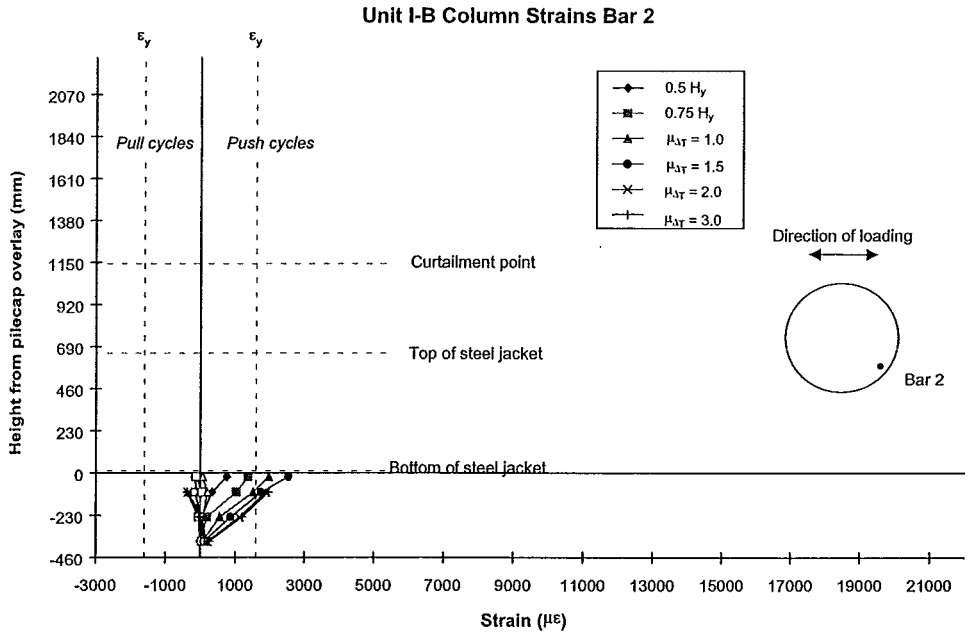

Figure 3.26 *Unit I-B Column Longitudinal Bar 2 Strain Profile*

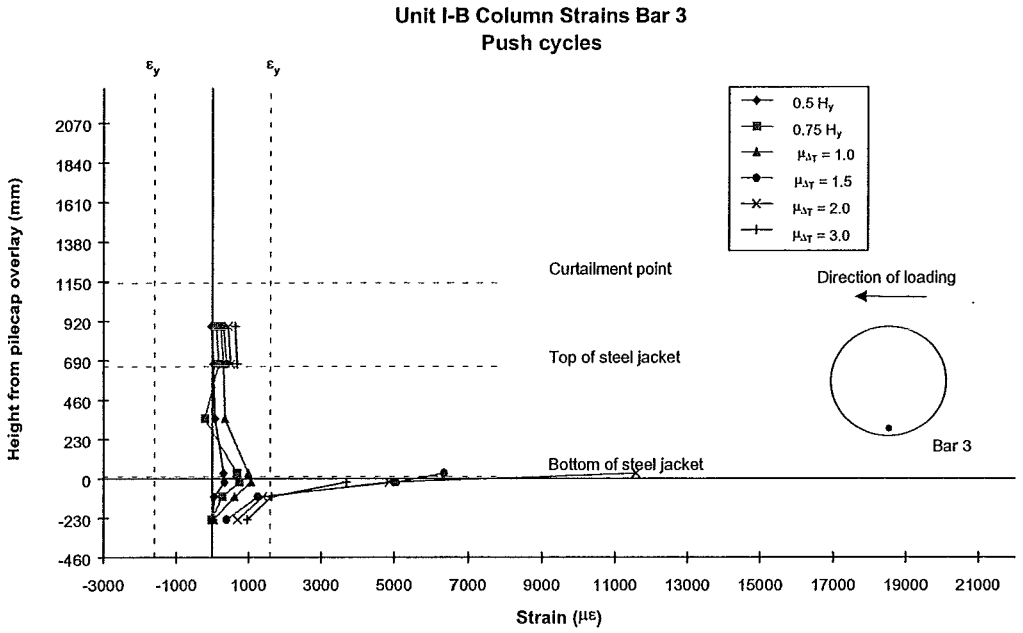

Figure 3.27 *Unit I-B Column Longitudinal Bar 3 Strain Profile for Push Cycles*

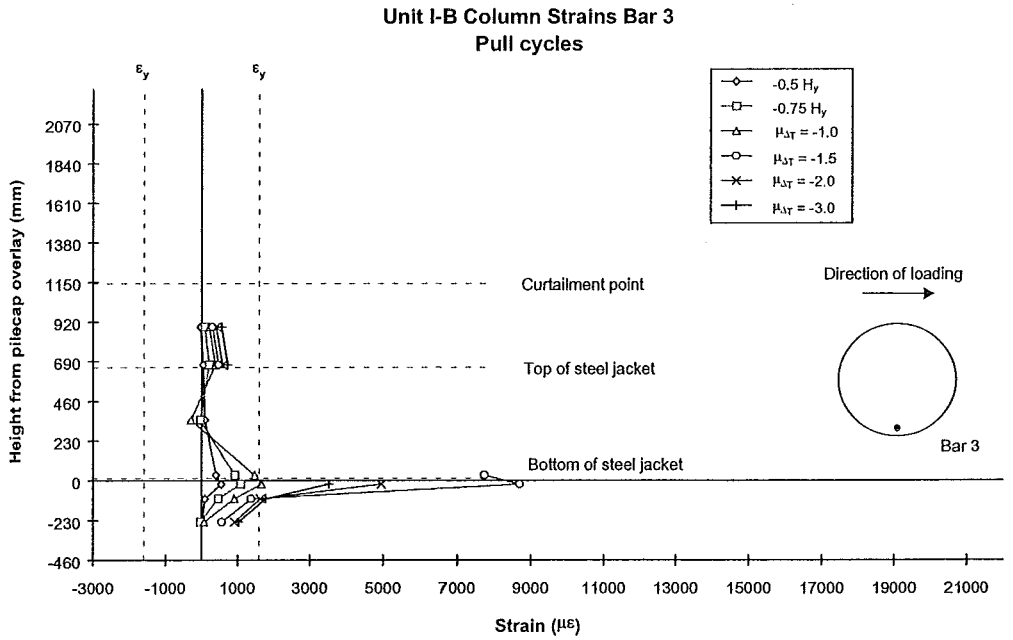

Figure 3.28 *Unit I-B Column Longitudinal Bar 3 Strain Profile for Pull Cycles*

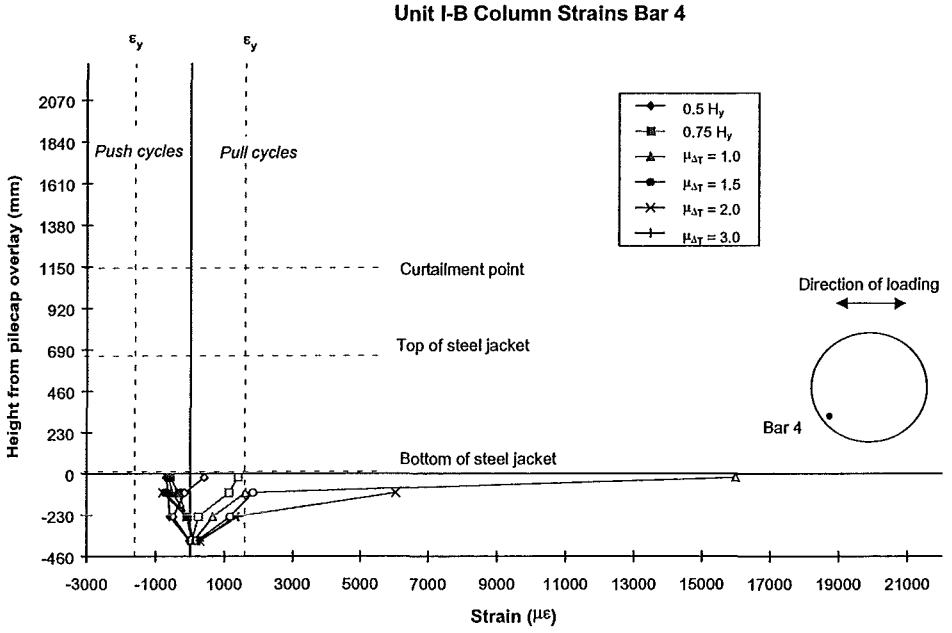

Figure 3.29 *Unit I-B Column Longitudinal Bar 4 Strain Profile*

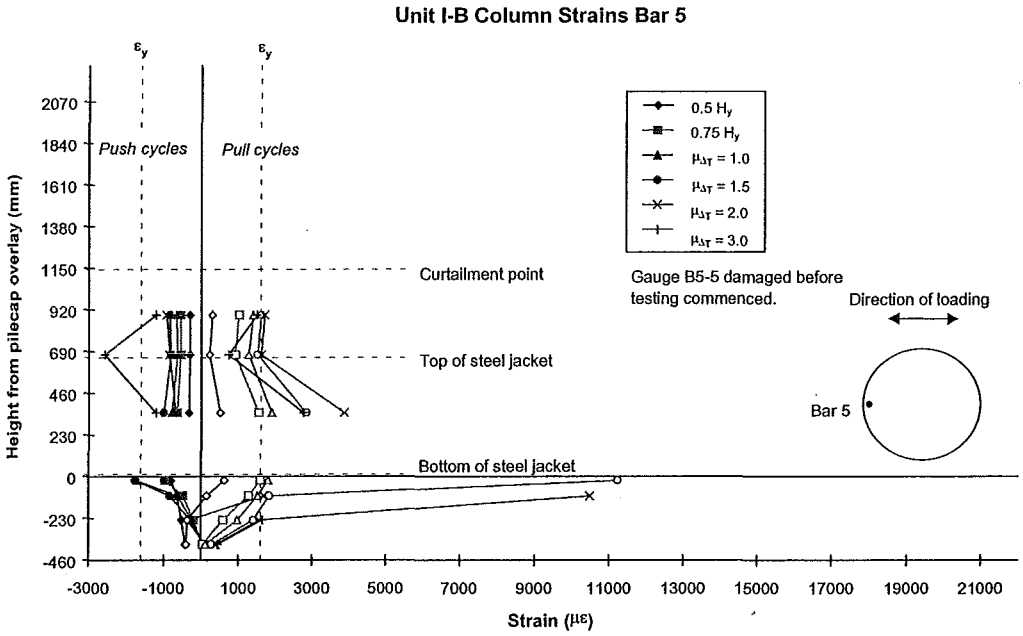

Figure 3.30 *Unit I-B Column Longitudinal Bar 5 Strain Profile*

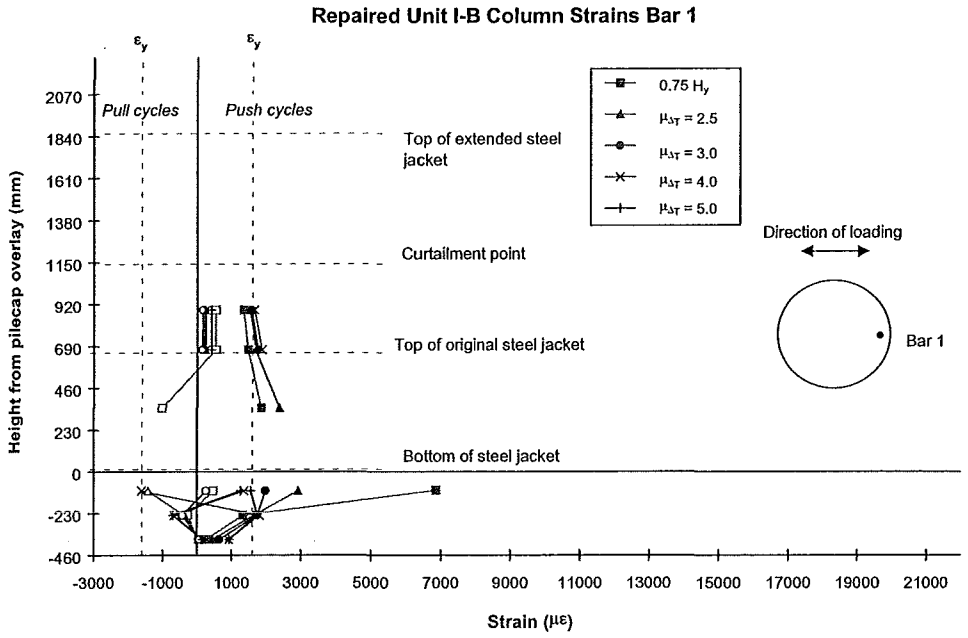

Figure 3.31 *Repaired Unit I-B Column Longitudinal Bar 1 Strain Profile*

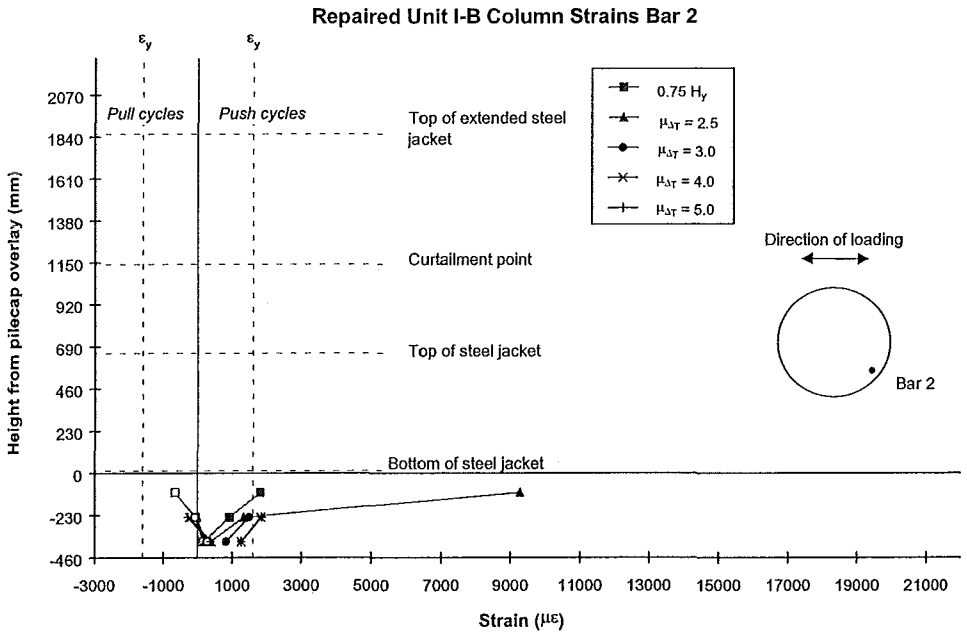

Figure 3.32 *Repaired Unit I-B Column Longitudinal Bar 2 Strain Profile*

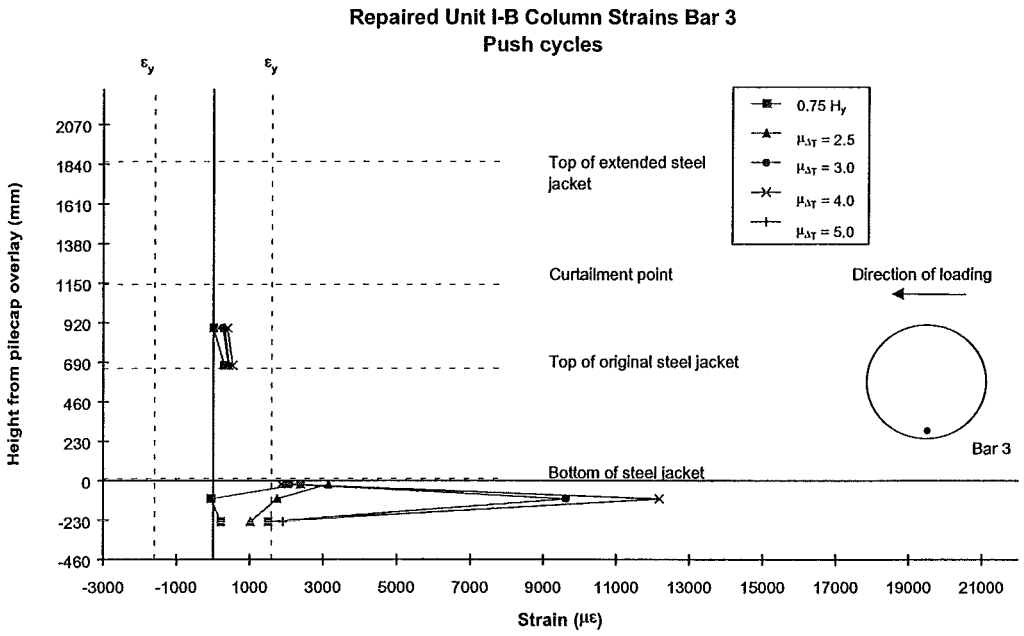

Figure 3.33 *Repaired Unit I-B Column Longitudinal Bar 3 Strain Profile for Push Cycles*

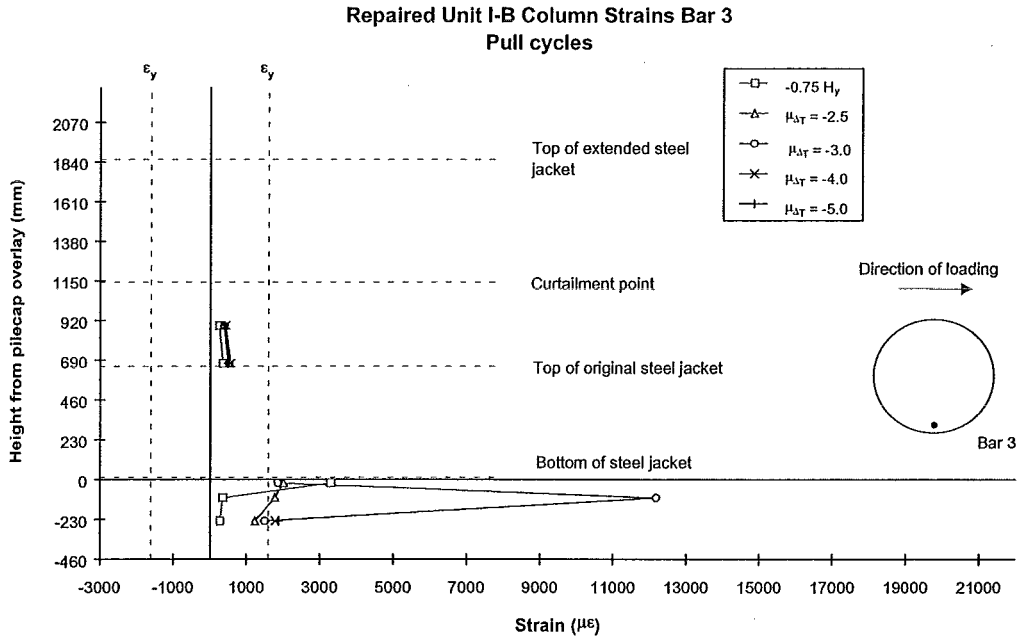

Figure 3.34 *Repaired Unit I-B Column Longitudinal Bar 3 Strain Profile for Pull Cycles*

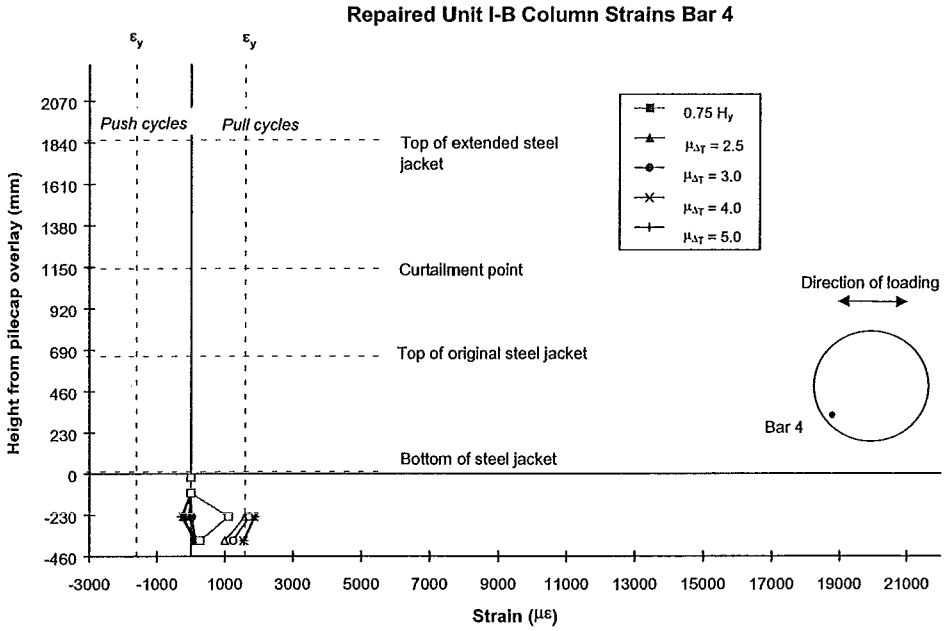

Figure 3.35 *Repaired Unit I-B Column Longitudinal Bar 4 Strain Profile*

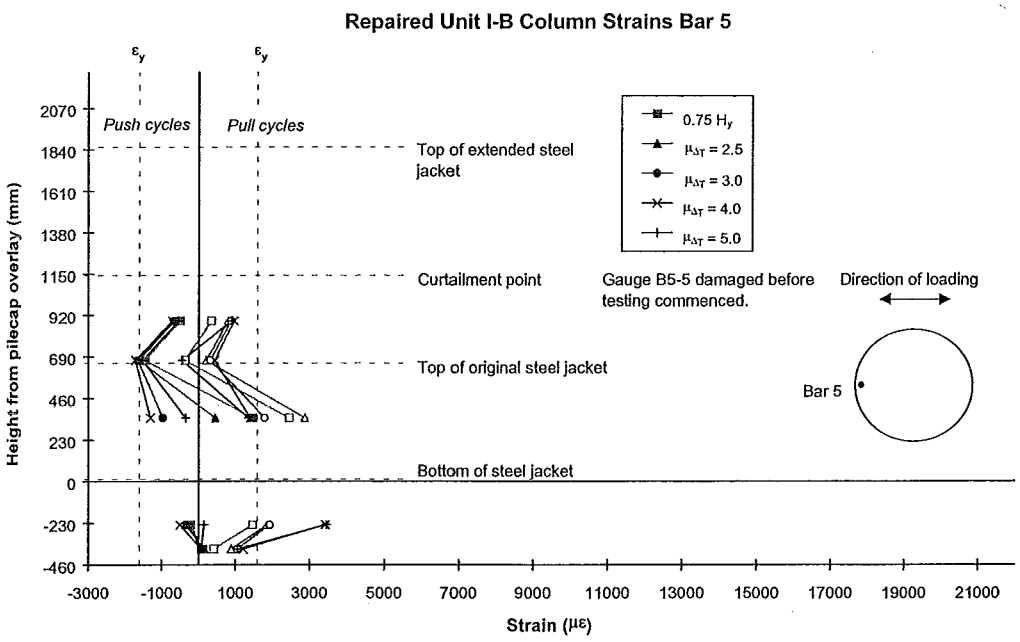

Figure 3.36 *Repaired Unit I-B Column Longitudinal Bar 5 Strain Profile*

mid-depth of the original pilecap to the upper most strain gauge in the column. Evidence from the buckled longitudinal reinforcement at the curtailment point indicates the column longitudinal reinforcement had yielded at this location when the large cracks developed in the column.

Strain gauge B5-7 shows a large compressive strain, -2566 με, during the Push cycle to $\mu_{\Delta T} = 3.0$ ($\mu_{\Delta S} = 2.37$) due to the steep diagonal cracks which terminated at the top of the steel jacket, near the position of this strain gauge.

Continuation of the test after repair of the column shows yield of all the strain gauged longitudinal bars extended down past mid-depth of the original pilecap at $\mu_{\Delta T} = 4.0$ ($\mu_{\Delta S} = 3.05$). Strains in the reinforcement at mid-depth of the original pilecap remained low, in the order of 2000 με. Strain gauges -373 mm from the top of the pilecap overlay recorded maximum strains less than 1500 με during the entire test. Results are shown in Figures 3.31 - 3.36.

3.8.5 Pilecap and Pilecap Overlay

Modelling of the different stiffness of the piles under tension and compression was required to match the force distribution in Unit I-B to the forces from the structural analysis of Pier 46. The BCHF analysis for Pier 46 was conducted using average values for the soil springs at the side of the pilecap and for each row of piles. This pier was analysed with and without piles to observe any difference in the pilecap force distribution. Comparison between the bending moments from testing of Unit I-B and the scaled BCHF Pier 46 "no piles" analysis is shown. The bending moment is drawn for the centreline of the original pilecap, in Figure 3.37, at ductility $\mu_{\Delta T} = 1.0$, at development of the diagonal cracks in the column at $\mu_{\Delta T} = 3.0$ ($\mu_{\Delta S} = 2.37$) and at the peak lateral load corresponding to the first cycle to $\mu_{\Delta T} = 4.0$ ($\mu_{\Delta S} = 3.05$).

The main difference between the BCHF Pier 46 structural analysis and Unit I-B is the application of 10 % of the column base moment to the top of the column,

representing the centre of mass of the bridge deck, to account for the effects of the rotational inertia of the umbrella platform. From the pilecap bending moment profiles the influence of the compressive soil-pile stiffness and the lesser tensile soil-pile stiffness can be seen. The negative bending moment, on the trailing side of the pilecap is much less than the positive bending moment developed underneath the pilecap.

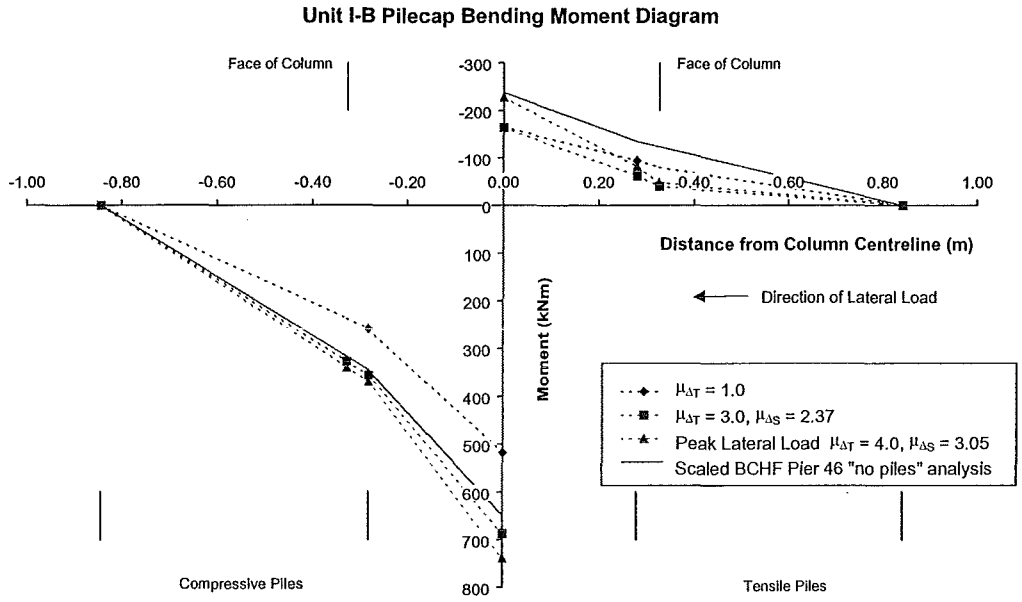

Figure 3.37 *Unit I-B Pilecap Bending Moment Diagram*

Comparison between the bending moments developed in the pilecap during the test to the scaled BCHF Pier 46 "no piles" analysis shows the same bending moment profile was developed during testing. The positive bending moment, underneath the pilecap, was reached during testing due to the development of column overstrength during the test, after repair of the column with extension of the steel jacket.

First cracking occurred on the bottom of the pilecap running transversely between the two central compressive piles directly beneath the edge of the column during the

cycles to 0.75 H_y. Cracking propagated perpendicular to this crack, extending along the pilecap centreline to the edge of the pilecap during further load cycles.

Extension of this crack up the side of the pilecap continued throughout the test. The longitudinal crack along the pilecap centreline is created as a result of the boundary conditions of the test specimen. The reaction from the lateral springs is assumed to act through two inclined struts from the compression zone of the column to the point of application of the reaction from each lateral spring. The resulting tension field created between the two struts results in the formation of the longitudinal cracks along the centreline of the pilecap.

A 45° - 150 mm long crack formed on the top surface of the pilecap overlay retrofit extending away from the tension edge of the column during the first cycles to $\mu_{\Delta T} = 1.0$. These cracks continued to extend during the following load cycles.

Strain gauges in the pilecap bottom mat indicate yield of the bottom mat bars occurred directly beneath the compression edge of the column during the cycles to $\mu_{\Delta T} = 2.0$ ($\mu_{\Delta S} = 1.68$). Maximum strains in the pilecap bottom mat bars did not exceed 2300 $\mu\varepsilon$ in the bars that yielded while all other strain gauges showed the bars remained well within the elastic range during the entire test.

In the final cycles prior to stopping the test when the diagonal tension cracks formed in the column, a small concrete cone pulled out of the pilecap overlay retrofit around the circumference of the column. This cone is due to the yield penetration of the longitudinal bars developing into the pilecap and pulling out as the bars went into tension. This was evident from the cracking of the column base at the pilecap overlay retrofit surface. A small region of the overlay surface had a hollow sound when tapped, indicating that a wedge shaped section was lifting out from the surface. Figure 3.38 shows the wedge of concrete pulling away from the pilecap overlay

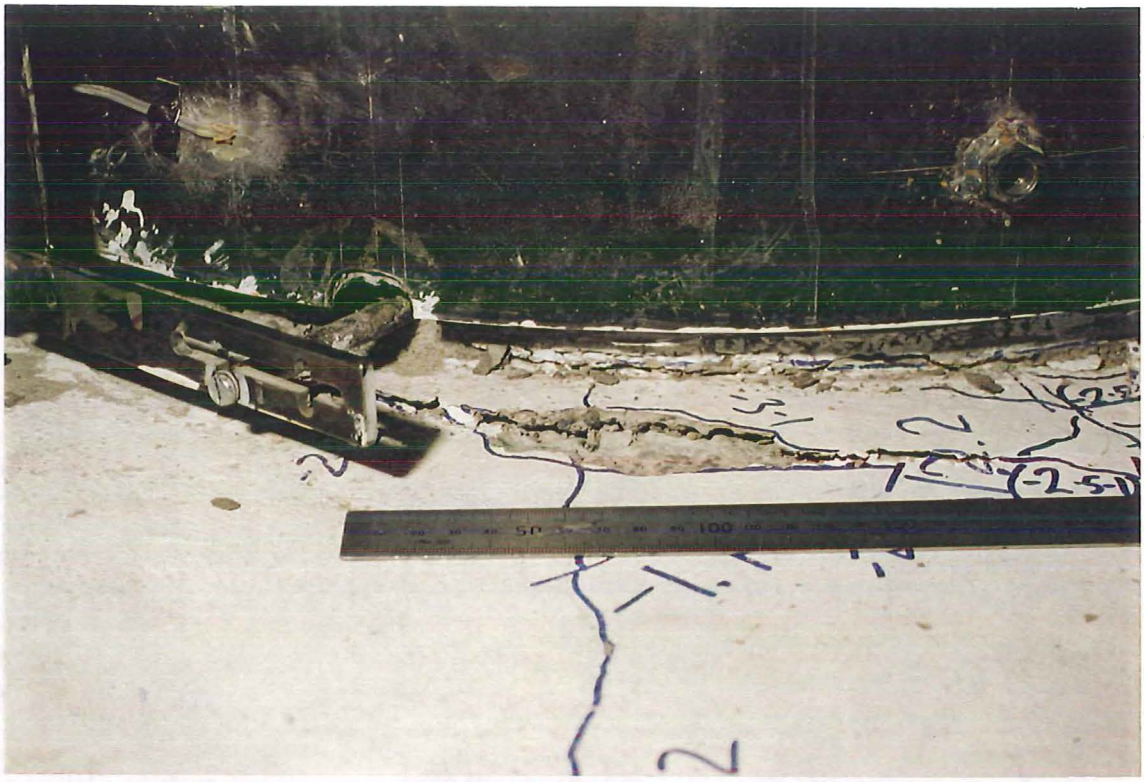

Figure 3.38 *Pullout of Concrete Wedge at Base of Column*

retrofit surface. Lifting of the pilecap overlay retrofit surface resulted in dowel action through the overlay mat reinforcing engaging the pilecap overlay vertical dowels, in turn causing those dowel bars immediately adjacent to the base of the column to yield.

Following repair of the column and continuation of testing the cracks underneath the pilecap continued to extend. Cracks were formed at 45° to the pilecap longitudinal axis and extended to the edge of the original pilecap. Diagonal tension cracks on the top surface, at the side of the column, and underneath the pilecap extended out from the axial load slots. The longitudinal crack underneath the pilecap extended up the side of the pilecap and on to the top edge of the pilecap overlay. This crack then extended from the edge of the column toward the column during loading to $\mu_{\Delta T} = 3.0$ ($\mu_{\Delta S} = 2.37$). At $\mu_{\Delta T} = 4.0$ ($\mu_{\Delta S} = 3.05$) the 45° cracks underneath the pilecap extended through the post-tension anchor blocks and continued up the side of the pilecap. Diagonal shear cracks also developed on the sides of the pilecap in both

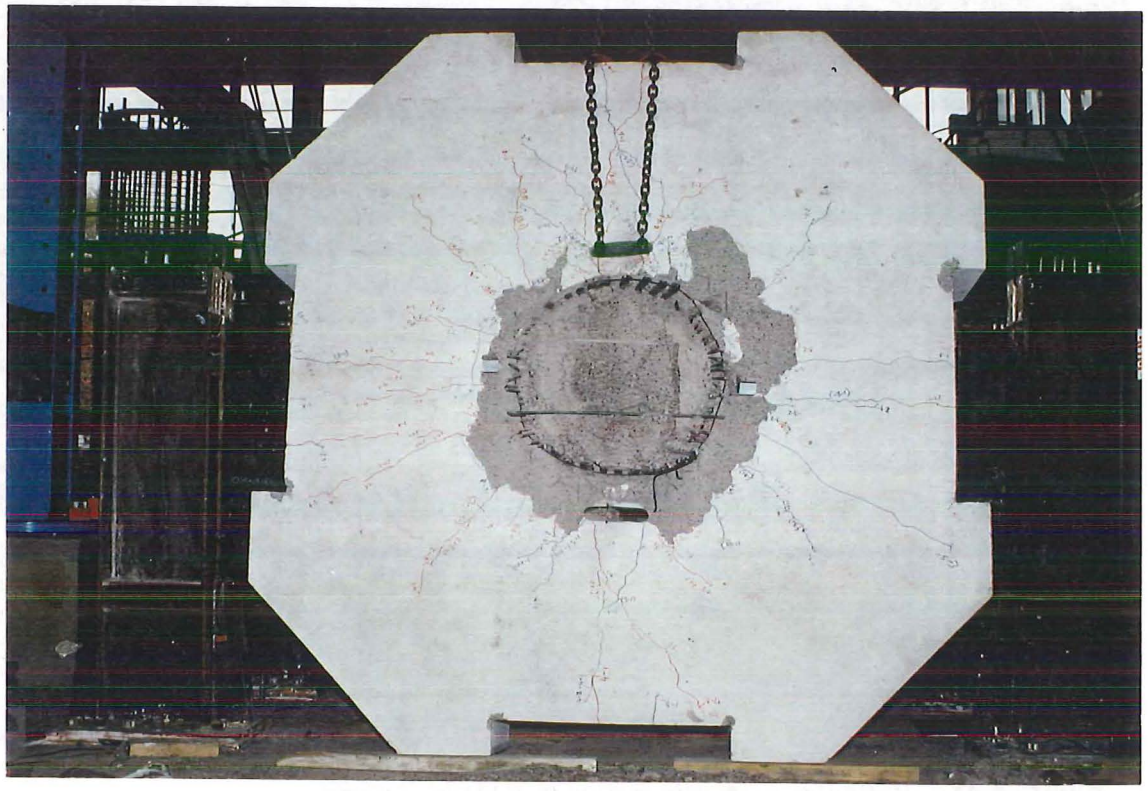

Figure 3.39 *Cracking in Top Surface of Pilecap Overlay Retrofit of Unit I-B at End of Test*

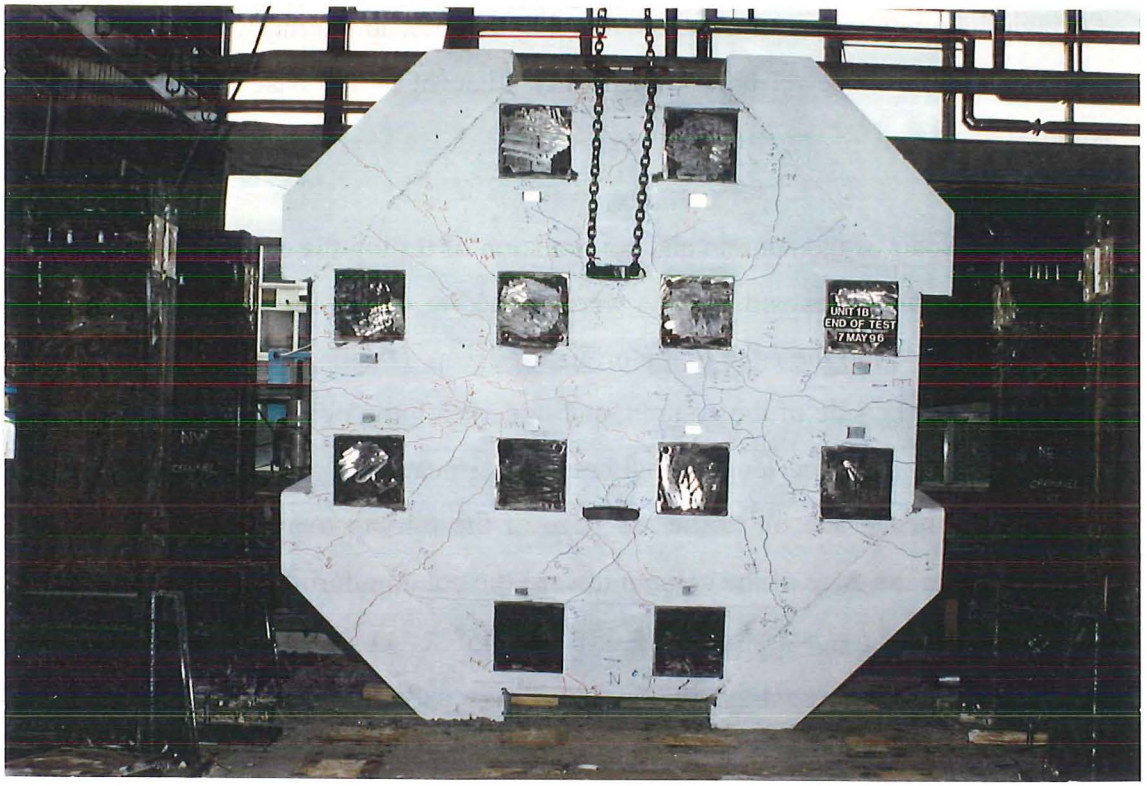

Figure 3.40 *Cracking in Bottom Surface of Pilecap of Unit I-B at End of Test*

directions of loading to $\mu_{\Delta T} = 4.0$ ($\mu_{\Delta S} = 3.05$). Figures 3.38 and 3.39 illustrate the crack patterns developed in the top and bottom of the pilecap, respectively, after demolition of Unit I-B. This shows the limited amount of cracking that occurred in the pilecap and pilecap overlay retrofit during the entire test. The loading direction is from left-to-right in Figure 3.39 for Push (positive) loading cycles with the northern edge of the pilecap at the bottom of the figure. Push (positive) loading cycles are from right-to-left in Figure 3.40.

Data from strain gauges on the overlay retrofit mat reinforcement show these bars remained well within the elastic range during the test. A maximum strain of 1300 με was recorded from a strain gauge on a longitudinal overlay mat bar close to the column.

Several vertical dowels, immediately adjacent to the base of the column, yielded through dowel action as the overlay retrofit mat engaged the dowels as the overlay lifted off. The position of these dowels corresponds roughly to the region of spalled concrete from the pilecap overlay retrofit in Figure 3.39. Maximum strains in these dowels were recorded in the order of 5000 με. Immediately outside the group of dowels which yielded a maximum strain of 1100 με was recorded with lower strains seen in dowels further from the column.

The longer pile dowel bars, placed at the positions of the outer vertical springs, remained elastic throughout the entire test. Maximum strains of 900 με were recorded in one pile dowel bar during the first cycle to $\mu_{\Delta T} = 5.0$ ($\mu_{\Delta S} = 3.74$).

3.8.6 Steel Jacket

The steel jacket proposed for Pier 46 is provided to enhance the available ultimate concrete compressive strain of the column in order to increase the available displacement and curvature ductility of the base of the column. The column surface behind the region of the steel jacket was not roughened to limit the bond that would

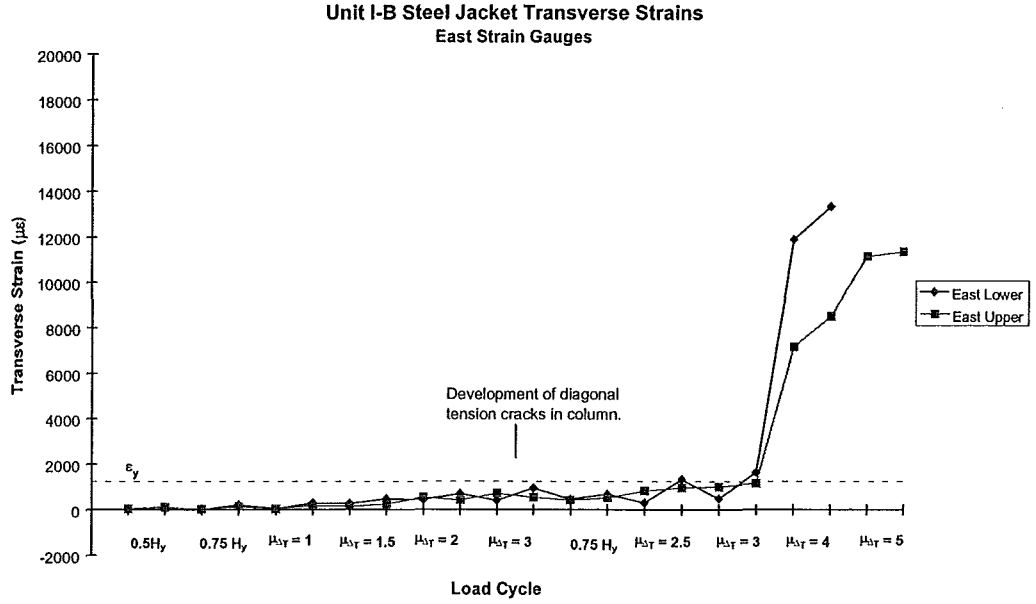

Figure 3.41 *Unit I-B Steel Jacket Transverse Strain, East Strain Gauges*

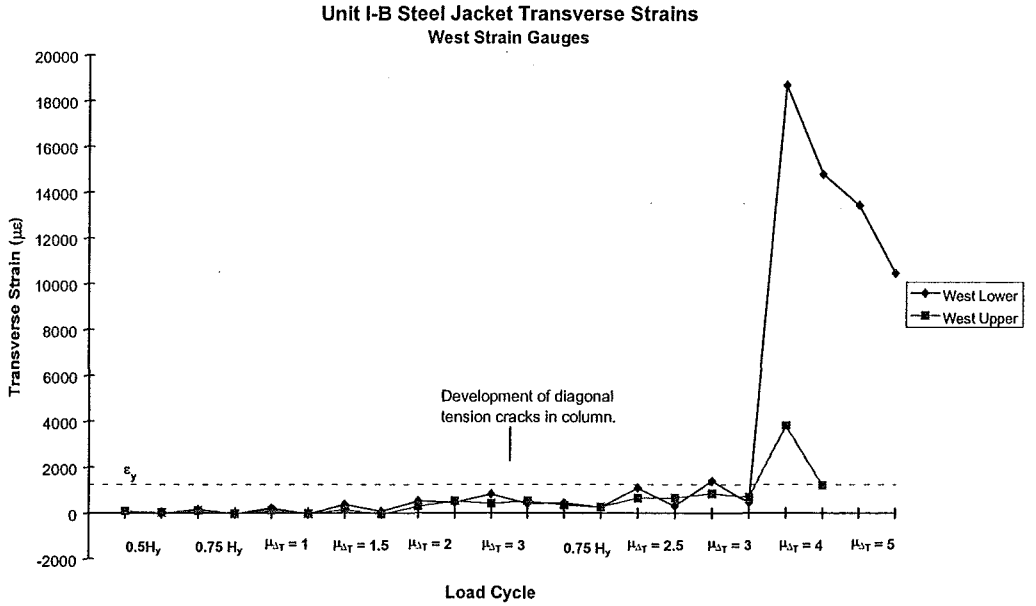

Figure 3.42 *Unit I-B Steel Jacket Transverse Strains, West Strain Gauges*

develop between the column and the grout behind the steel jacket. During the early stages of the test, creaking could be heard from behind the jacket suggesting debonding of the jacket from the grout. Debonding, as seen by cracks between the grout and the top of the steel jacket, became apparent during the third cycle to 0.5 H_y and could be presumed to have occurred over the full height of the jacket. Composite action between the column and the jacket appears to have been maintained up to the $\mu_{\Delta T} = 1.0$ as indicated by the column curvature distribution shown in Figure 3.23.

Slip of the steel jacket over the grout became noticeable at $\mu_{\Delta T} = 2.0$ ($\mu_{\Delta S} = 1.68$). Limited crushing and spalling of the grout from behind the steel jacket was observed and continued throughout the test. The slip of the jacket could clearly be seen distributed over the height of the steel jacket through holes provided in the jacket for the column curvature potentiometer rods. Up to 4 mm slip at the base of the jacket along the column centreline was observed by the end of the test. The slip in the jacket reduced up the height of the jacket with negligible slip at the top of the original jacket. Slip of the jacket along with the formation of flexural cracks in the column, behind the jacket, required the holes for the column curvature potentiometer rods to be enlarged to accommodate the jacket slip during the later stages of the test.

Strain gauges were placed on the East and West faces of the steel jacket, at the base, to record transverse strains developed in the steel jacket during the test. Strain readings from these gauges are shown in Figures 3.40 and 3.41. The lower strain gauges show yielding of the jacket took place near the base at $\mu_{\Delta T} = 2.5$ ($\mu_{\Delta S} = 2.03$) after development of the diagonal cracks and subsequent repair of the column. The upper strain gauges, 50 mm above the lower gauges, indicate yielding at $\mu_{\Delta T} = 4.0$ ($\mu_{\Delta S} = 3.05$). Bulging of the steel jacket at the base was noticed after the second cycle to $\mu_{\Delta T} = 4.0$ ($\mu_{\Delta S} = 3.05$) which continued until the end of the test and is responsible for the large increase in strains recorded by the strain gauges. Considerable crushing of the grout and column concrete behind the jacket along with buckling of the column bars increased the bulging of the steel jacket around the base up to $\mu_{\Delta T} = 5.0$ ($\mu_{\Delta S} = 3.74$) when the longitudinal bars

began fracturing. Figure 3.43 shows the bulging of the steel jacket commencing at the base after the second cycle to $\mu_{\Delta T} = 4.0$ ($\mu_{\Delta S} = 3.05$). Figure 3.44 shows the base of the column at the end of the test with the fractured longitudinal reinforcement, crushed concrete and grout coming out from behind the bulged steel jacket.

The steel jacket was successful in providing the required ductility capacity or the column, after repair of the diagonal cracks which formed at the curtailment point. The damage to the base of the column is concentrated in a small region as seen in

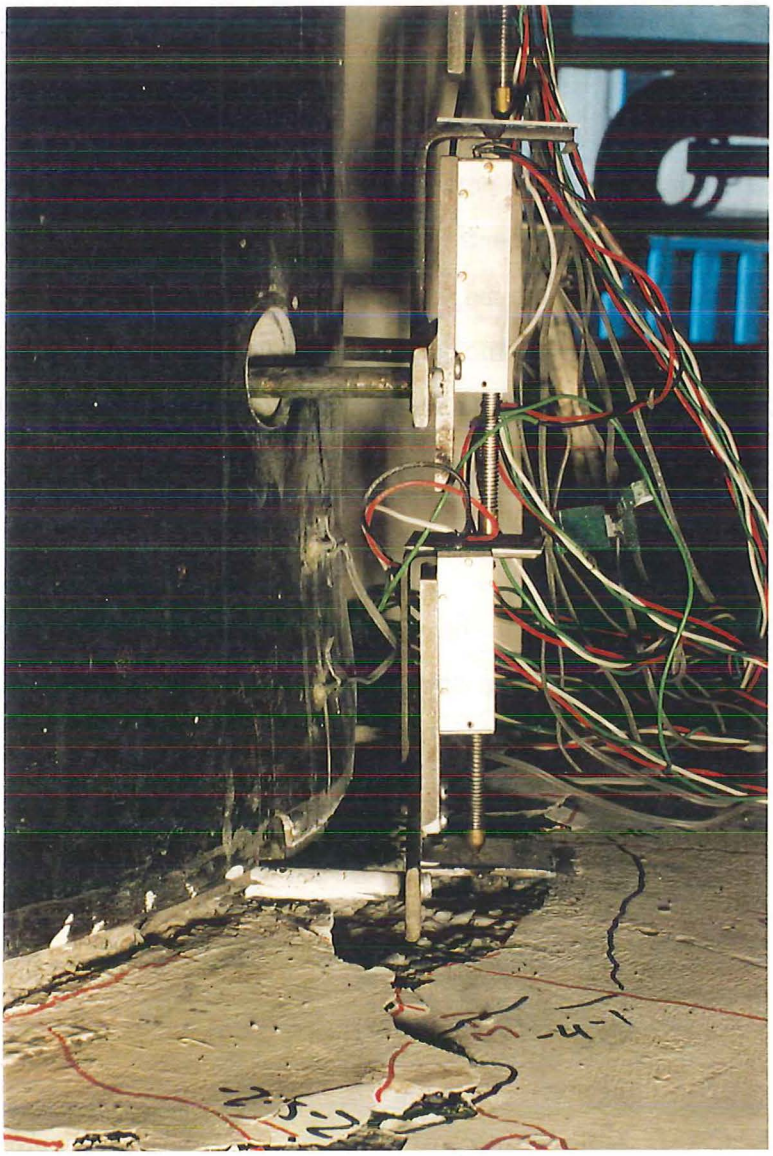

Figure 3.43 *Bulging of Base of Steel Jacket after Second Cycle to* $\mu_{\Delta T} = 4.0$ *(*$\mu_{\Delta S} = 3.05$*)*

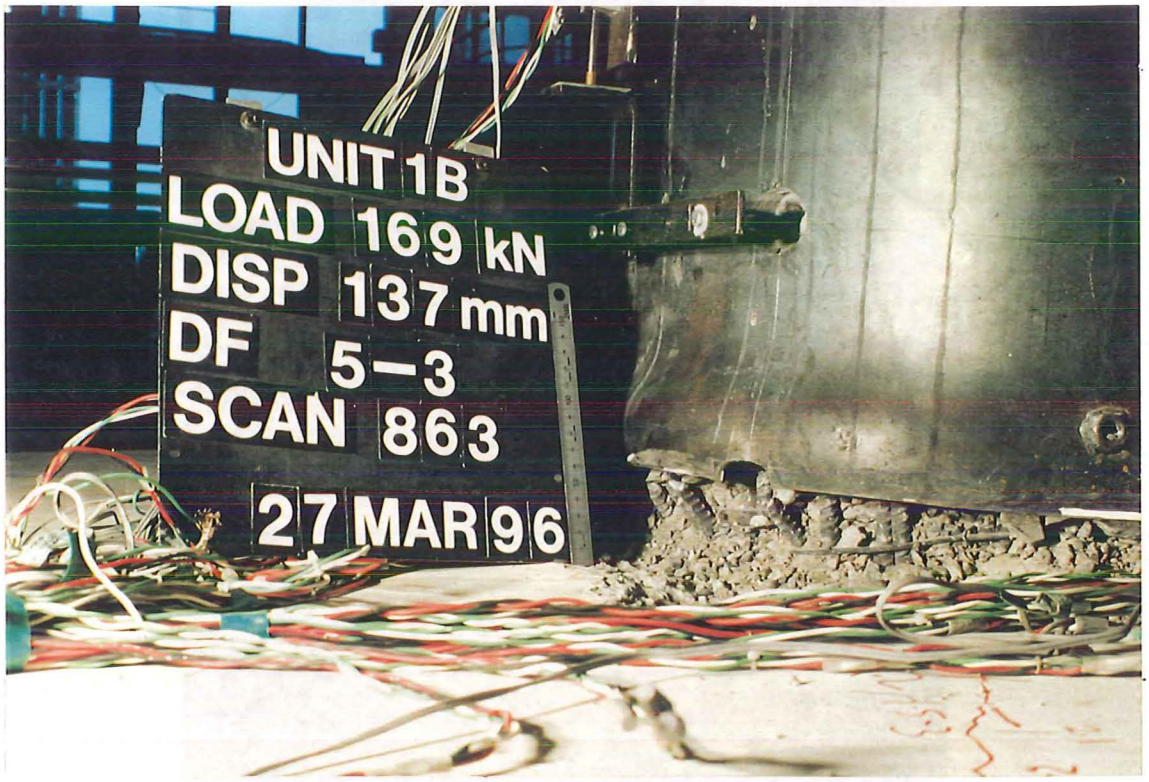

Figure 3.44 *Base of Steel Jacket at End of Test*

Figure 3.45 where the steel jacket has been removed after the end of the test. Cracking in the grout is marked in this figure and is concentrated within one-half of the column diameter from the base. Inspection of the column following removal of the full height steel jacket showed no sign of the original diagonal cracks at the curtailment point appearing in the grout showing the extended steel jacket was successful in precluding a shear failure in the column at this point, as well as enhancing the available ductility of the test specimen.

3.9 RECOMMENDATIONS FROM TESTING OF UNIT I-B

The simulated seismic loading test of Unit I-B showed that the test specimen had an available structural ductility capacity approximately equal to the ductility demand expected to arise in Pier 46 from a 500 year return period earthquake at the Thorndon Overbridge site.

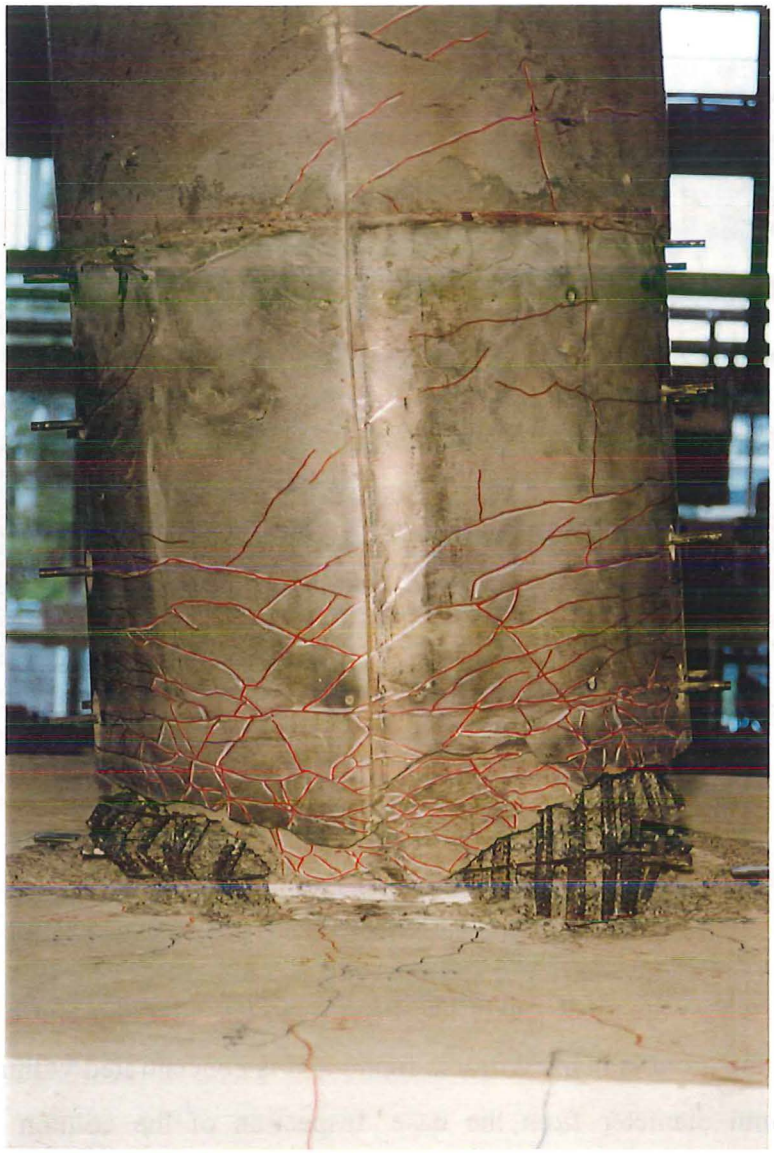

Figure 3.45 *Cracking and Damage Behind Steel Jacket at Base of Column of Unit I-B at End of Test*

At this imposed level of ductility two large diagonal tension cracks developed in the column, initiated at the point where 50 % of the column longitudinal reinforcement are curtailed. This undesirable mode of failure occurred when loading Unit I-B to $\mu_{\Delta T} = 3.0$, which relates to a structural ductility factor in Pier 46 of $\mu_{\Delta S} = 2.37$. A theoretical analysis, described in Section 3.5, using moment-curvature analysis and assessment of the available shear resistance of the column, was used to predict the likelihood of a shear failure in the column at the curtailment point by taking into account the tension shift effect.

Observation of the damage sustained in the rest of the test specimen showed very minor damage was suffered by the pilecap and retrofit measures at this stage of loading. All inelastic action was concentrated at the base of the column, initially behind the steel jacket at the base of the column, and later in the column around the curtailment point of the longitudinal bars.

As the test specimen indicated a potentially brittle mode of failure, with very little ductility reserve, the test specimen was repaired and the test was continued to observe the performance of the repaired column, pilecap and other retrofit measures.

The extension of the steel jacket was successful in achieving the objective of enhancing the available ductility of the column and precluding a shear failure around the curtailment point. The pilecap retrofit showed excellent behaviour, transferring the forces from the repaired column, with only limited yield of some bottom pilecap mat reinforcing bars and limited cracking occurring in the pilecap and pilecap overlay retrofit. Comparison of the expected pilecap bending moments from the BCHF structural analysis of Pier 46 showed a good match with the bending moment distribution achieved during testing of Unit I-B. The maximum, scaled, pilecap bending moment from the structural analysis was reached during the test as a result of column overstrength developing after repair of the column. A small number of pilecap overlay retrofit dowels, immediately adjacent to the base of the column, yielded through dowel action with dowels further away from the base of the column remaining well within the elastic range. Pile dowel bars, provided to transfer the pile tension force through to the top of the pilecap overlay retrofit, remained elastic throughout the test. The pilecap overlay mat reinforcing bars also remained within the elastic range up to completion of the test.

The detailing of Pier 46, and Unit I-B, with the column longitudinal bars curtailed following the bending moment diagram, without adequate regard for the tension shift, led to the development of the large diagonal tension cracks in the column, at the curtailment point, and a potentially brittle shear failure with limited ductility. Provision of the pilecap overlay, at the base of the column, further increased the

likelihood of failure by shortening the column and shifting the critical section closer to the curtailment point.

The provision of the steel jacket at the base of the column allowed inelastic action to commence at this point. The additional ductility provided by the steel jacket at the base of the column allowed the development of a degree of column overstrength in the test specimen which contributed to the flexural strength of the curtailment point being reached. Inelastic action began to concentrate at the curtailment point and eventually overstrength at the base of the column led to the available shear strength of the column at the curtailment point above the steel jacket being exceeded.

Extension of the steel jacket to above the curtailment point in the column successfully prevented the formation of further shear failure in the column and increased the available ductility capacity of the repaired column in Unit I-B. This indicates the use of a full height steel jacket in Pier 46 will prevent any shear failure from occurring in the column at the curtailment point and provide adequate ductility reserve to meet the expected ductility demands on this pier.

The other retrofit measures, pilecap overlay retrofit and pilecap post-tensioning, ensured the pilecap was capable of ensuring inelastic action would occur at the base of the column, after extension of the original steel jacket to a full height steel jacket, and resist the imposed forces from these actions.

CHAPTER 4

CYCLIC LATERAL LOADING OF UNIT I-A

4.1 INTRODUCTION

Unit I-A was a 1:3.8 scale model of Pier 68 of the Thorndon Overbridge incorporating the existing and the proposed retrofit details for the pier. The test specimen was subjected to simulated seismic loading by applying a constant compressive axial load and reversed cyclic lateral loads at the top of the column, representing the centre of mass of the bridge deck. Reinforcing details and the test specimen layout for Unit I-A are shown in Section 2.3.3. The lateral loading history used for testing of Unit I-A is described in Section 2.5.

Unit I-A was instrumented over one half of the test specimen, using symmetry about the centre of the test specimen in line with the direction of loading. Electrical resistance strain gauges were used to record strains on the reinforcing steel in the column, bottom pilecap mat bars, pile and overlay retrofit dowels and pilecap overlay retrofit mat bars. Linear potentiometers were used to record external displacements of the test specimen and internal displacements of the column. Loads were recorded as applied by the 1000 kN hydraulic actuator, through a 1000 kN loadcell, in each vertical spring and in the lateral springs which resisted the applied lateral load, through calibrated strain gauge circuits.

All circuits from loadcells, strain gauges and linear potentiometers were monitored and recorded using the Department's PCLAB and the BURR BROWN data loggers. The PCLAB data logger allowed up to 256 channels to be monitored, scanned and recorded, including all loadcells, linear potentiometers and most of the specimen's strain gauges. The BURR BROWN data logger was used to monitor and record an overflow of approximately 100 strain gauge channels. The scanning of the channels is controlled using a computer program on each data logger, which allows the scan to be taken at any instant as directed from the computer keyboard.

4.2 TEST UNIT INSTRUMENTATION

4.2.1 Measurement of Loads

The loads measured during the testing of Unit I-A were the force applied by the hydraulic actuator at the top of the column, the tensile or compressive reaction in each of the outer vertical springs, the axial reaction and amount of bending in each central spring, the lateral load resisted by each of the lateral springs at pilecap level and the level of axial load applied to the specimen. The 1000 kN loadcell attached to the hydraulic actuator has two independent full bridge circuits. One circuit was monitored by the data logger and the other connected to a digital strain indicator. Each circuit was calibrated in compression using the 2500 kN Avery Compressive Testing Machine. Output from the digital strain indicator was used to control the lateral loading of the specimen during the initial load controlled cycles and provide a separate measure of load during the remaining cycles. Figure 4.1 shows the measurement of loads in Unit I-A.

Each outer vertical spring in Unit I-A contained two axial full bridge circuits for measuring the tensile and compressive forces resisted by each spring. Two complete full bridge circuits using 120Ω resistance 5 mm foil strain gauges were placed on the steel rod to measure tensile forces and another two complete full bridge circuits using 120Ω resistance 5 mm foil strain gauges placed on the CHS section to measure compressive forces. The central spring contained three full bridge circuits, one at mid-height to measure the axial reaction and two bending full bridge circuits spaced 250 mm above and below the axial gauges to derive the shear force carried in each central spring.

The axial load applied to Unit I-A was monitored by a calibrated pressure gauge attached through a manifold to the hydraulic rams used to apply the load. During testing the pressure gauge was monitored and kept at the same pressure by manually relieving the excess pressure, due to elongation of the column during loading, or increasing the pressure by starting the pump, caused by shortening of the column during unloading.

4.2.2 Measurement of Test Unit Displacements

Column lateral displacements measured during the test programme include the gross horizontal displacement at the top of the column, at the point of application of the lateral load, at the upper and lower curtailment points. Lateral displacements of the pilecap were measured at the mid depth of the original pilecap with vertical displacements recorded adjacent to the position of each outer vertical spring and either side of the central vertical springs. Figure 4.2 shows the location of the linear potentiometers for recording external test specimen displacements.

All external test specimen lateral displacements were taken relative to a fixed reference point located on a wall separate from the strong floor area as used with Unit I-B.

Linear potentiometers to measure vertical displacements of the pilecap, at each vertical spring location, were mounted on lengths of steel angle sections tack welded to the connection plates used to connect the vertical springs to the baseblock. A calibrated precise level bubble mounted on the baseblock under the centre of the test specimen provided a measure of additional displacements through rotation of the baseblock at the peak of each load increment.

Internal displacements of the column due to flexure were recorded using linear potentiometers mounted on steel brackets screwed into 10 mm diameter plain round reinforcing rods which were cast into and passed through the column.

Figure 4.3 shows the location of the linear potentiometers to measure internal displacements. Following the experience with Unit I-B with the failure around the curtailment point it was decided to monitor the internal column displacements over the full height of the column.

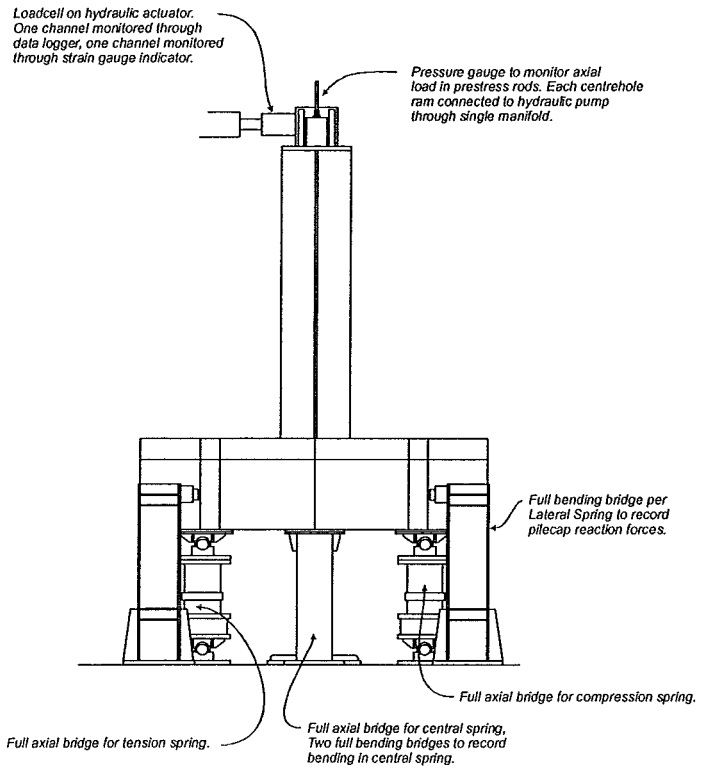

Figure 4.1 *Measurement of Loads in Unit I-A*

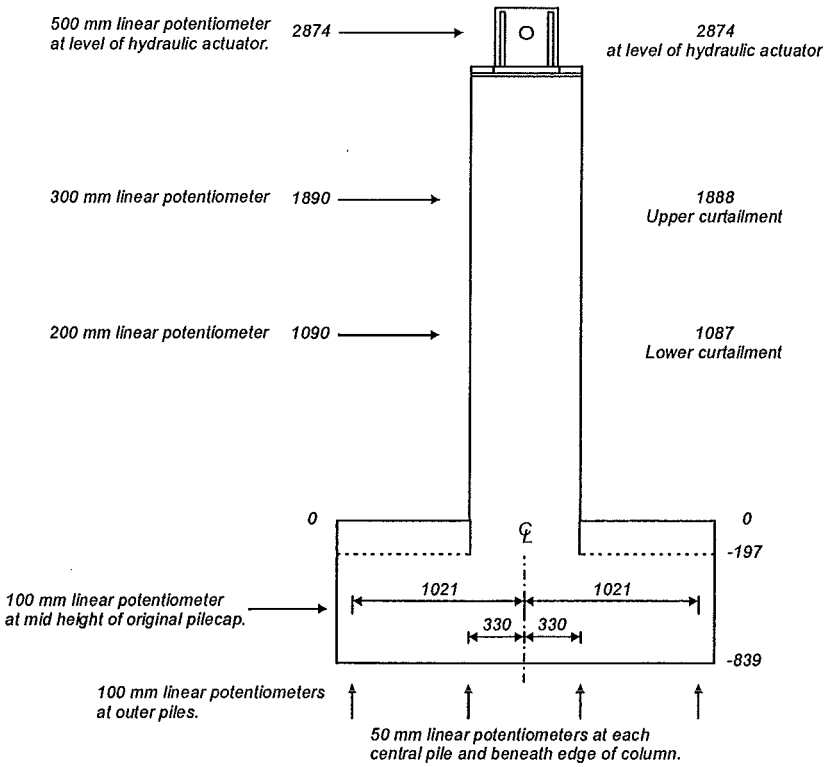

Figure 4.2 *Measurement of External Test Specimen Displacements*

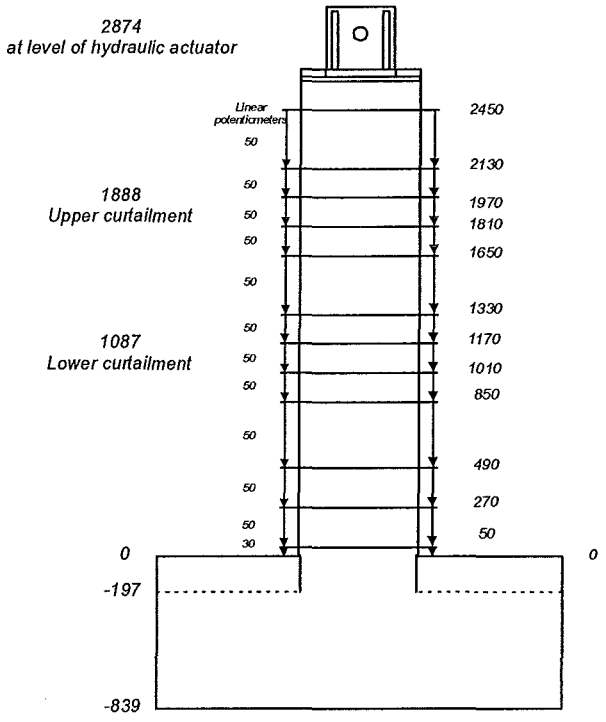

Figure 4.3 *Measurement of Internal Test Specimen Displacements*

Displacement measurements from the linear potentiometer at the point of application of the lateral load was monitored through the data logger and through a digital voltmeter. This voltmeter was used to control the lateral loading during the displacement controlled cycles. Displacements recorded from the top of the column and the applied load from the strain indicator attached to the loadcell were used as inputs to an X-Y plotter to give a visual record of load and displacement during testing.

4.2.3 Reinforcement Strains

Local strains on column longitudinal and pilecap bottom mat reinforcing bars in the specimen were measured using 120Ω resistance 5 mm foil strain gauges on the pilecap bottom mat and column bars. Strains in the pilecap overlay retrofit mat bars and dowels and the column spiral reinforcement were measured using 120Ω 1 mm foil strain gauges.

Strain gauges were attached to the reinforcing bars before fabrication of the reinforcing cages. All strain gauges were protected with several layers of waterproofing cement and a piece of vinyl mastic tape for additional protection against physical damage.

4.2.3.1 Column Strain Gauges

Five longitudinal column bars were strain gauged over the full height of the bar as shown in Figure 4.4. Following testing of Unit I-B strain gauges were distributed over the full column height to record strain data from these bars around the upper and lower curtailment points, from around the pilecap retrofit overlay surface and down into the original pilecap.

4.2.3.2 Pilecap Bottom Mat Strain Gauges

Strain gauges on the pilecap bottom mat were placed on the longitudinal and transverse mat bars. Figure 4.5 shows the position and identification of the strain gauges on the bottom pilecap mat bars.

4.2.3.3 Pilecap Overlay Retrofit Mat Strain Gauges

The top mat of HD6 pilecap overlay retrofit mat bars were gauged with the strain gauge positions mirroring the position of gauges in the bottom pilecap mat. The position of these gauges is shown in Figure 4.6.

4.2.3.4 Pilecap Overlay Retrofit Dowel and Pile Dowel Strain Gauges

The pilecap overlay retrofit dowels were placed on a nominal 120 mm square grid. The position of the strain gauged dowels are shown in Figure 4.7. Alternate overlay dowels were strain gauged to measure the strains developed in each dowel across the pilecap overlay. Longer pile dowels, at the location of each of the outer piles, were also strain gauged to see the development of strains and forces transferred through

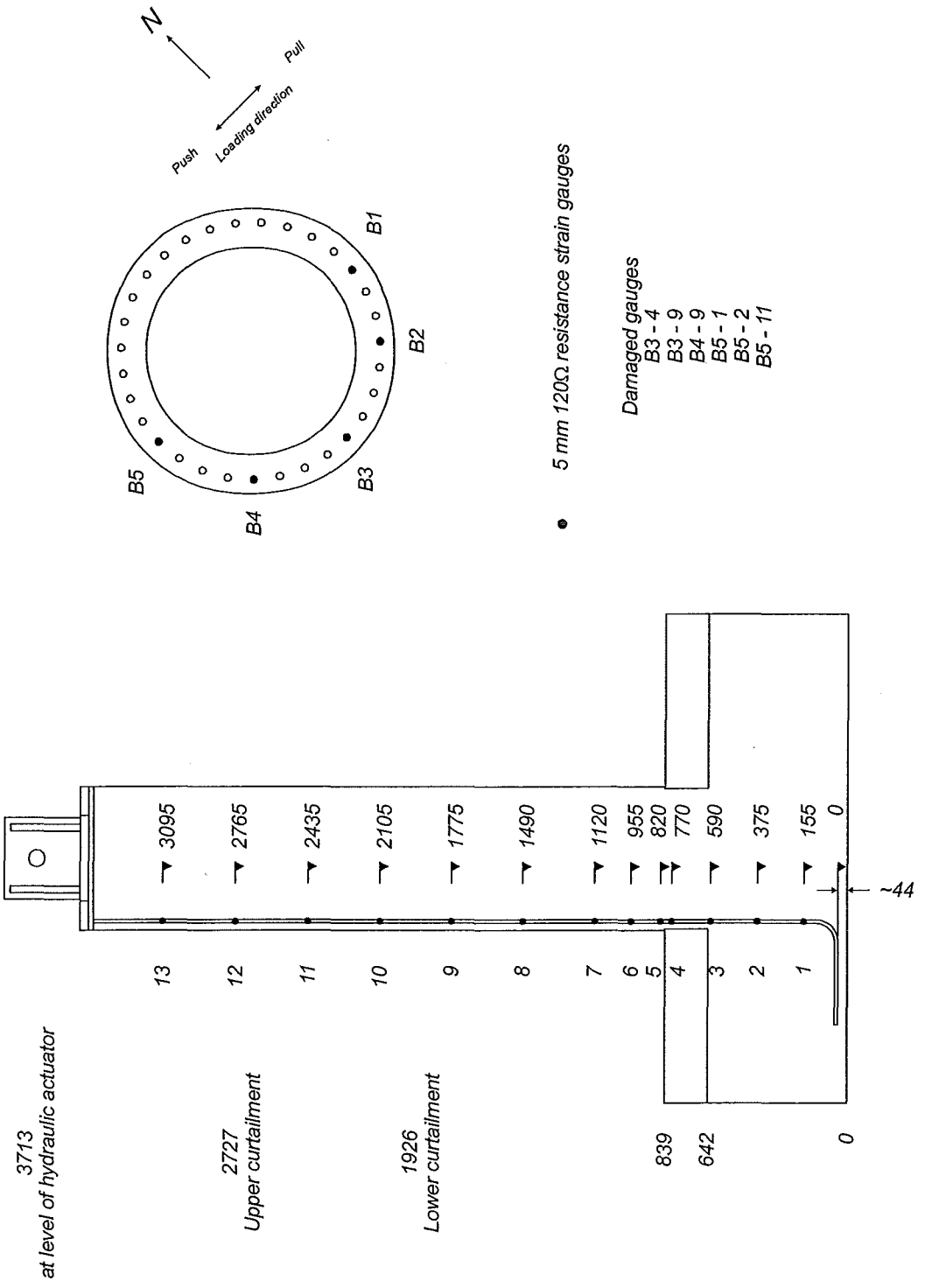

Figure 4.4 *Position of Column Longitudinal Bar Strain Gauges*

Figure 4.5 *Position of Bottom Pilecap Mat Strain Gauges*

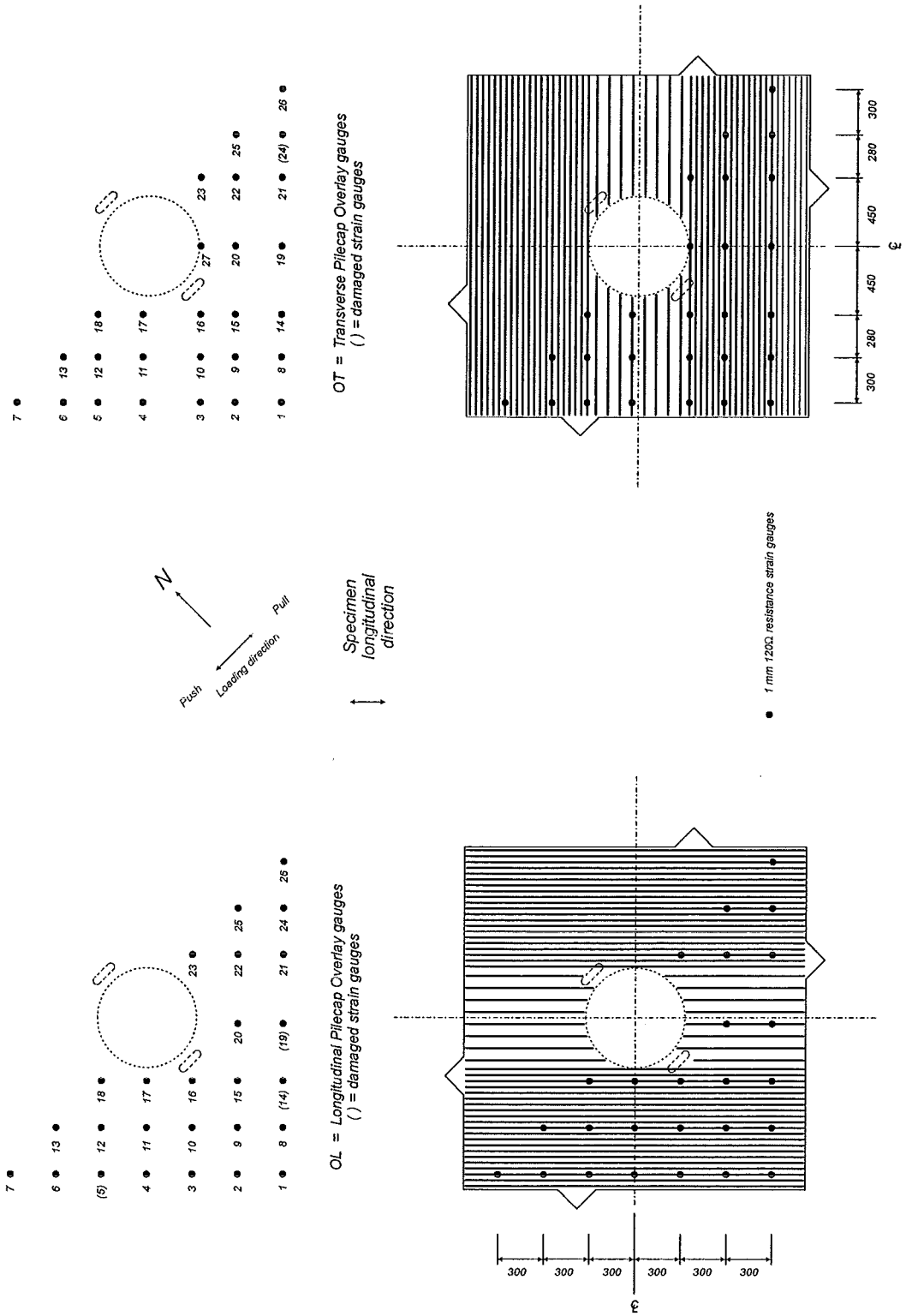

Figure 4.6 *Position of Pilecap Overlay Retrofit Mat Strain Gauges*

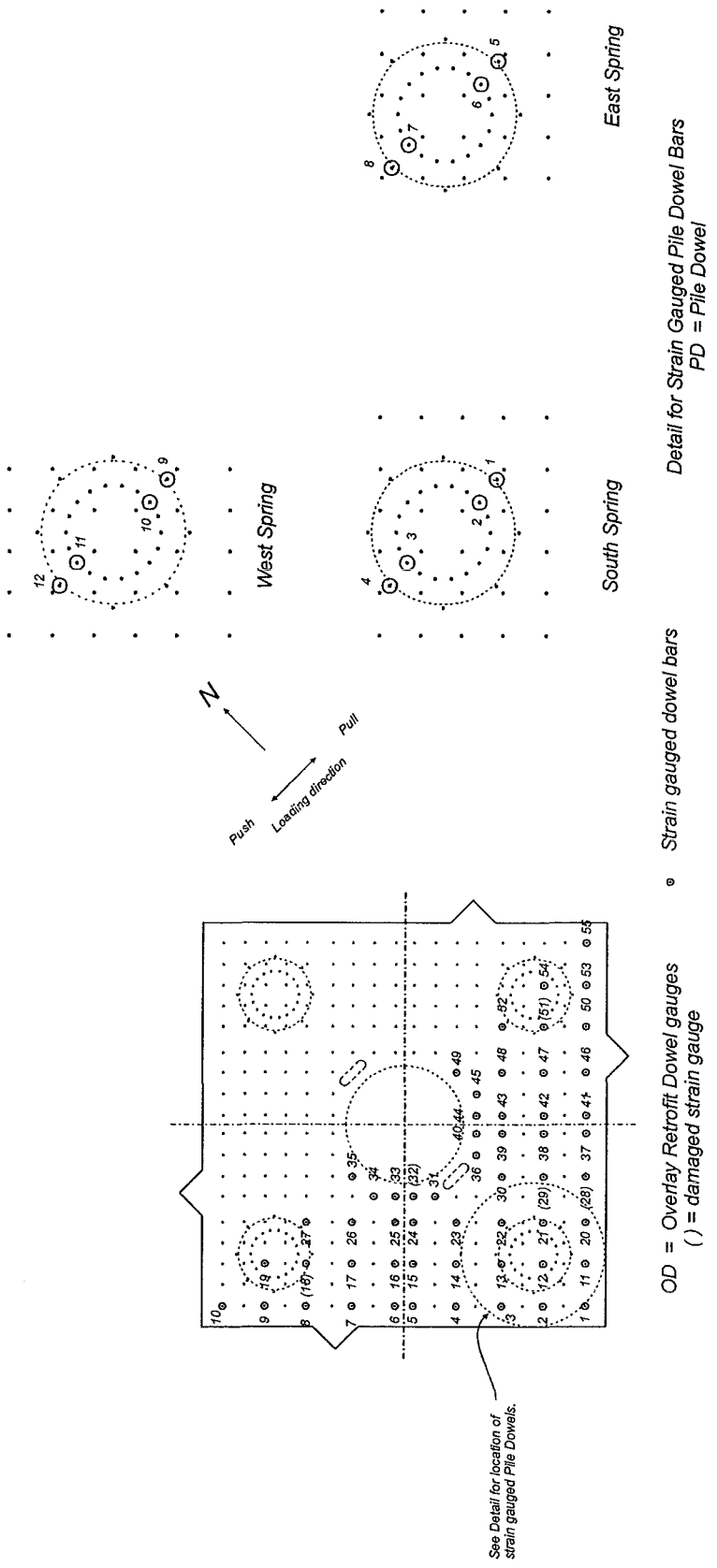

Figure 4.7 *Position of Strain Gauged Pilecap Overlay Dowel and Pile Dowel Bars*

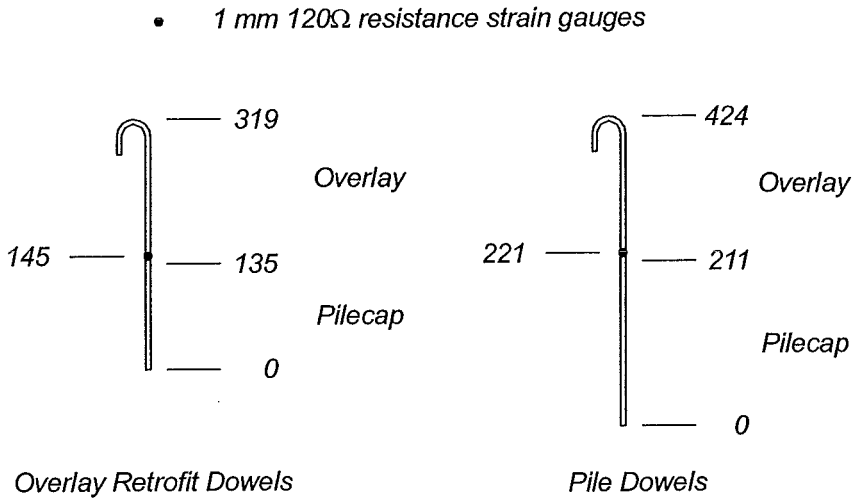

Figure 4.8 *Detail of Strain Gauge Positions for Pilecap Overlay Dowel and Pile Dowel Bars*

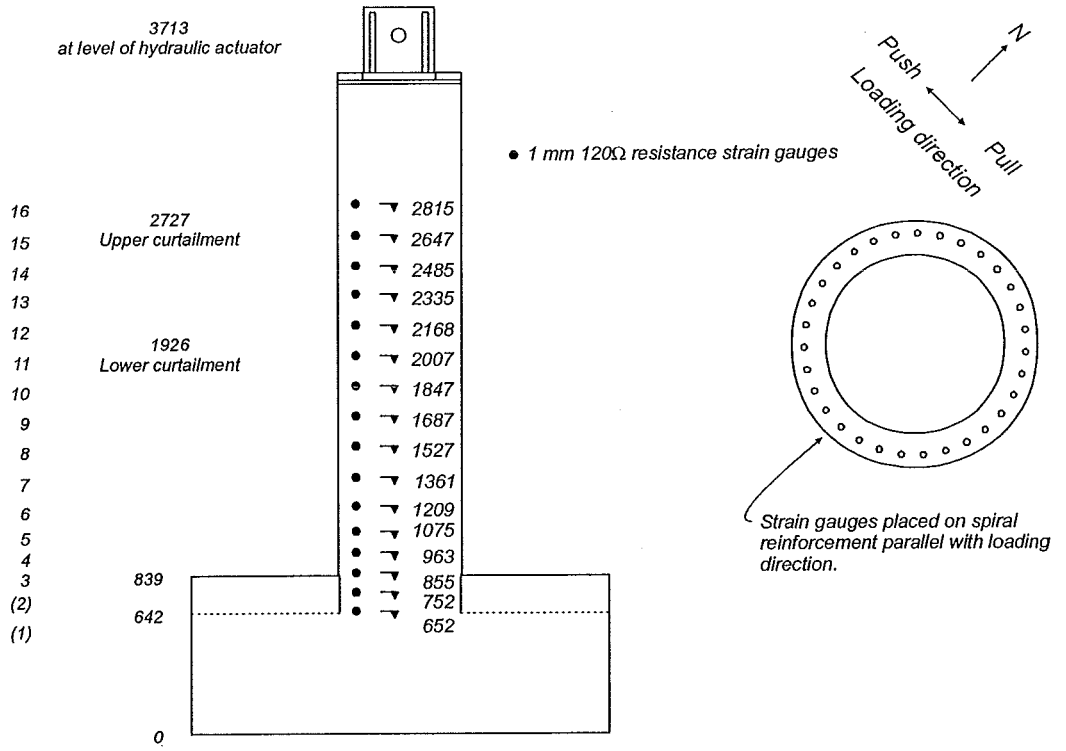

Figure 4.9 *Position of Column Spiral Strain Gauges*

these longer dowels. Each strain gauged dowel had the gauge positioned 10 mm above the surface of the original pilecap as shown in Figure 4.8.

4.2.3.5 Column Spiral Strain Gauges

Strain gauges were placed on the column spiral reinforcement distributed over the full height of the column to measure strains developed in the transverse reinforcement during the test. The position of these gauges is shown in Figure 4.9.

4.3 LATERAL LOAD TESTING OF UNIT I-A

4.3.1 Lateral Loading History

The lateral loading history used for testing of Unit I-A followed the procedure outlined in Section 2.5.1. Three cycles to each level of load were carried out with a full set of readings, marking of cracks and photographs of the test specimen completed at the peak of each cycle. Push cycles are loading with the loadcell on the hydraulic actuator in compression are denoted as positive loads and positive displacements. Pull cycles are denoted with negative forces and displacements.

The force, H_y, used to determine the level of lateral loading applied during the force controlled cycles was determined from a moment-curvature analysis of the base of the column using approximate concrete and steel strengths of 55 MPa for the concrete compressive strength and a steel yield strength of 310 MPa. The lateral force corresponding to the development of the nominal flexural strength at the base of the column, H_y, was determined to be $H_y = 546$ kN. The actual lateral force required to develop the flexural strength at the base of the column, H_a, determined using actual the concrete compressive strength and the measured steel stress-strain relationship for the longitudinal column steel was determined to be $H_a = 527$ kN. This is approximately 4 % lower than the lateral force used to control the force controlled cycles of the test. The influence of the higher lateral force on the response

of the test specimen and definition of specimen yield displacement and displacement ductility is negligible.

The initial analysis [K1] used to determine the level of lateral load during the force controlled cycles uses a steel stress-strain relationship which does not accurately represent the stress-strain relationship measured for the column longitudinal steel. The value assumed for the ultimate stress of the steel and function used to describe the variation in steel stress over the strain hardening region over estimate the actual ultimate stress and stresses through this part of the steel stress-strain relationship. Subsequent analysis using the appropriate steel stress-strain relationship yields a lower lateral force required to develop the flexural strength at the base of the column.

Three force controlled cycles were completed in both directions to 0.5 H_y (±273 kN) and 0.75 H_y (±410 kN). The yield displacement of Unit I-A, Δ_{yT}, was determined from Equation 2.1 to be $\Delta_{yT} = 73$ mm.

As the tensile and compressive stiffness of the vertical springs do not match the scaled stiffness of the combined soil-pile stiffness used in the structural analysis the test specimen displacement ductilities, $\mu_{\Delta T}$, are not the same for Pier 68. The yield displacement of Unit I-A, Δ_{yT}, cannot be directly scaled to give the yield displacement of Pier 68, Δ_{yS}, due to different amounts of elastic displacement occurring in the test specimen as a result of the different vertical spring stiffness. Displacement ductilities achieved in the test specimen can be related to displacement ductilities in Pier 68 through Equation 2.4.

The theoretical yield displacement of Pier 68 was determined from a structural analysis of the pier to be $\Delta_{yS} = 160$ mm. The displacement of Unit I-A in terms of the actual structure can be obtained by multiplying the test yield displacement, Δ_{yT}, by the scale factor of 3.8. This gives $\delta_{yT} = 277.4$ mm for the yield displacement of Unit I-A in terms of the actual structure allowing the displacement ductility reached in the actual structure, $\mu_{\Delta T}$, to be determined using Equation 4.1.

$$\mu_{\Delta S} = 1 + (\mu_{\Delta T} - 1)\frac{277.4}{160} \qquad (4.1)$$

4.3.2 General Behaviour of Unit I-A

Cracking at the base of the column of Unit I-A commenced during the cycles to 0.5 H_y (±273 kN). Horizontal cracking in the column extended up to the position of the upper curtailment point extending approximately one third of the way around the column. The first cracks in the bottom of the pilecap formed underneath the compression edge of the column, extending three-quarters of the column diameter across the pilecap. This crack extended across the full pilecap width during the cycles to 0.75 H_y (±410 kN) opening up to 0.2 mm width. Yield of the extreme longitudinal column bars took place a the base of the column immediately above and below the pilecap overlay surface during the cycles to 0.75 H_y. Column cracking around the curtailment points crossed diagonally through the column centreline with the horizontal crack initiated at the upper curtailment point opening up to 0.3 mm width at the peak of the loading cycle. Cracking at the base of the column remained horizontal. Figure 4.10 shows the column crack pattern after completion of three load cycles to 0.75 H_y.

A 45°-300 mm long crack developed on the top surface of the pilecap overlay away from the tension side of the column at 0.5 H_y, extending diagonally toward the edge of the pilecap near the "corners" where the reaction from the lateral springs are applied to the pilecap. Further cracks were developed from the compression zone at the base of the column toward the point where the lateral pilecap reaction is resisted by the lateral springs. The diagonal compressive stress field set up by the lateral spring reactions induced a splitting crack from the column to the corner of the test unit pilecap, along the direction of loading.

Following the force controlled cycles it was planned to apply displacement controlled cycles to peaks of $\mu_{\Delta T}$ = 1.0, 1.5, 2.0, 3.0 until failure of the test specimen, where $\mu_{\Delta T}$ = maximum lateral displacement divided by Δ_y. Three cycles were

Figure 4.10 *Cracking in Unit I-A Column After Cycles to 0.75 H_y*

successfully completed to displacement ductility factors of $\mu_{\Delta T} = 1.0$ and 1.5 and one cycle to $\mu_{\Delta T} = 2.0$.

Figure 4.11 shows the lateral load-lateral displacement response measured for Unit I-A up to the first cycle of $\mu_{\Delta T} = 2.0$ ($\mu_{\Delta S} = 2.74$). Slight pinching of the hysteresis loops can be seen during the cycle to $\mu_{\Delta T} = 2.0$ ($\mu_{\Delta S} = 2.74$). Fracture of a weld on one of the fittings used to connect the axial load rods to the baseblock

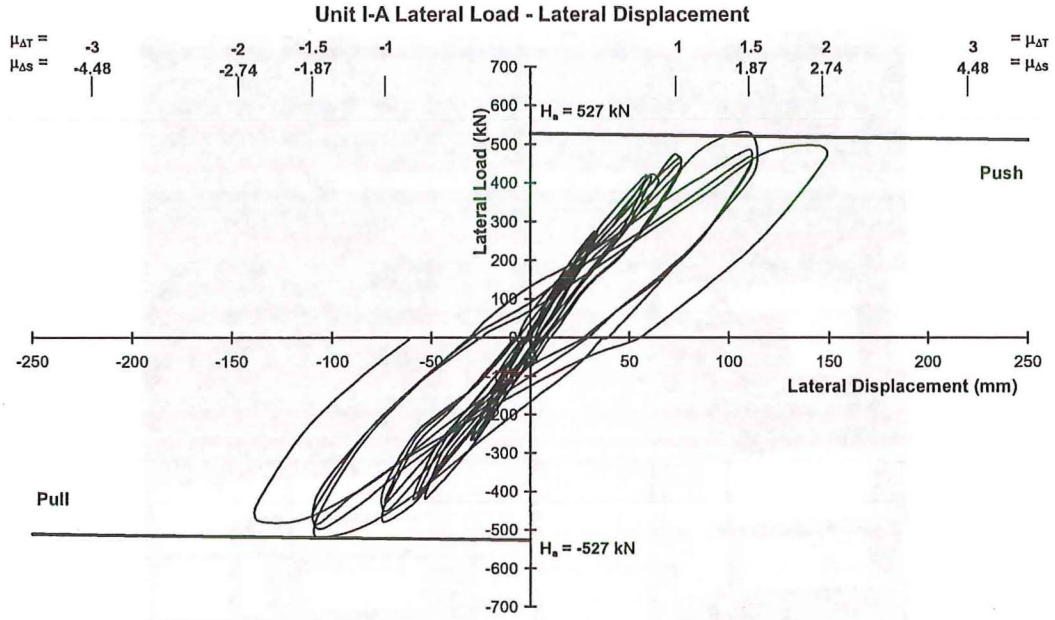

Figure 4.11 *Lateral Load-Lateral Displacement Response for Unit I-A up to* $\mu_{\Delta T} = 2$ *(*$\mu_{\Delta S} = 2.74$*)*

resulted in a full loss of the applied axial load on Unit I-A at the peak of the first cycle to $\mu_{\Delta T} = 1.5$ ($\mu_{\Delta S} = 1.87$). The use of a single hydraulic pump and manifold connecting the two rams used to apply the axial load to the prestress rods prevented any accidental eccentric loading being applied to the column. Unloading from the peak at $\mu_{\Delta T} = 1.5$ ($\mu_{\Delta S} = 1.87$) to zero lateral load was done with no applied axial load. The axial load fitting was repaired and testing was resumed.

Yielding of the column longitudinal bars in tension was seen to occur over the full height of the column at $\mu_{\Delta T} = 1.0$ and yielding in compression as the lateral load is reversed. Yield penetration extended down to the top of the original pilecap in the extreme longitudinal column bars at $\mu_{\Delta T} = 1.0$ and down to mid-depth of the original pilecap during the cycles to $\mu_{\Delta T} = 1.5$ ($\mu_{\Delta S} = 1.87$).

Figure 4.12 *Unit I-A Showing Column Cracking At* $\mu_{\Delta T} = 1.0$

Tensile strains in excess of 2.5 % were being developed in the extreme column longitudinal bars at the upper curtailment point and to the order of 1 % at the base of the column during the cycles to $\mu_{\Delta T} = 1.5$ ($\mu_{\Delta S} = 1.87$). These cycles also resulted in significant widening of the cracks at the upper curtailment point. The main horizontal crack at the point of curtailment of the longitudinal bars had increased in width to 3 - 4 mm with 1 - 2 mm diagonal cracks around the column. Cracking at the lower curtailment point did not increase in width as the main damage and cracking was taking place at the upper curtailment point.

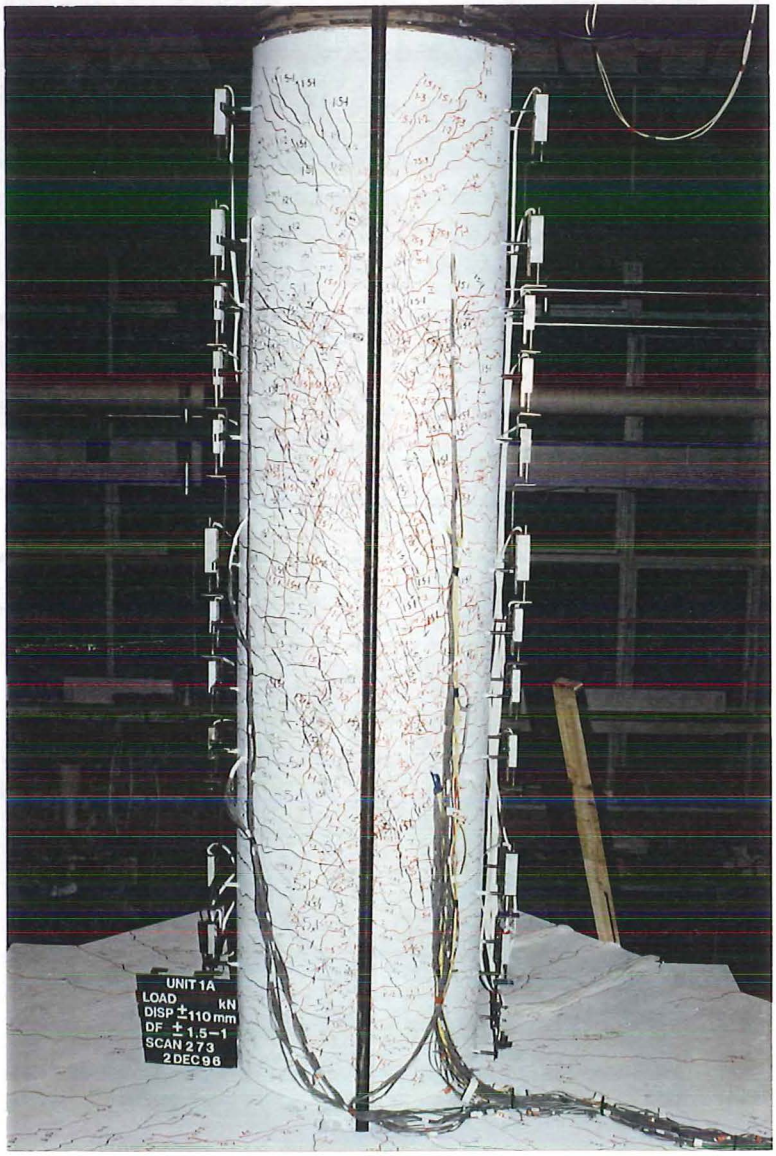

Figure 4.13 *Unit I-A Showing Column Cracking At* $\mu_{\Delta T} = 1.5$ *(*$\mu_{\Delta S} = 1.87$*)*

Figures 4.12 and 4.13 show the crack pattern in the column of Unit I-A at different stages of loading.

Cracking on the bottom of the pilecap extended across the full pilecap width with an additional crack beneath the column centreline, running perpendicular to the direction of loading, developing during cycles to $\mu_{\Delta T} = 1.0$. Cracks developed at 45° to the initial transverse cracks under the pilecap, extending toward the position of the lateral springs. These cracks extended diagonally up the side of the pilecap, back

toward the column, eventually joining with the 45° cracks developed on the top of the pilecap overlay, from the tension side of the column from the opposite direction of loading.

Due to the loading arrangement used in testing of this specimen the concentrated point loads applied at the side of the pilecap, representing the lateral reaction provided by passive soil pressure, induced diagonal splitting cracks which extended up the side of the pilecap and vertically up onto the top surface of the pilecap overlay. The passive soil pressure from the soil surrounding the pilecap would create a distributed loading almost perpendicular to the edge of the pilecap and would not develop the crack pattern seen on the side of the pilecap in Unit I-A.

Three cycles to $\mu_{\Delta T} = 1.5$ ($\mu_{\Delta S} = 1.87$) were successfully completed with maximum lateral loads of +527 kN and -518 kN developed during the first cycle to this displacement ductility. The lateral load had degraded to +469 kN and -485 kN by the third cycle to this displacement. A further cycle to $\mu_{\Delta T} = 2.0$ ($\mu_{\Delta S} = 2.74$) was attempted after completion of cycles to $\mu_{\Delta T} = 1.5$ ($\mu_{\Delta S} = 1.87$). Buckling of the compression column longitudinal bars caused spalling of the cover concrete around the upper curtailment point. The test unit was clearly in poor condition with the lateral load only reaching maximums of +496 kN and -476 kN at peak displacement of +145 mm and -137 mm respectively. Loading to $\mu_{\Delta T} = -2.0$ ($\mu_{\Delta S} = -2.74$) was halted early as the lateral load was degrading as the peak displacement was approached.

Figure 4.14 shows Unit I-A after completion of the cycles to $\mu_{\Delta T} = 2.0$ ($\mu_{\Delta S} = 2.74$) and removal of the loose cover concrete around the upper curtailment point. Extensive diagonal cracking is seen to extend the full column height especially around the upper and lower curtailment points. Cracking at the base of the column is seen to have remained essentially horizontal up to this point in the test.

Only one cycle to a displacement ductility of at $\mu_{\Delta T} = 2.0$ ($\mu_{\Delta S} = 2.74$), in each direction, was completed before halting the test, due to buckling of the longitudinal column bars, spalling of cover concrete and degradation of lateral load carrying

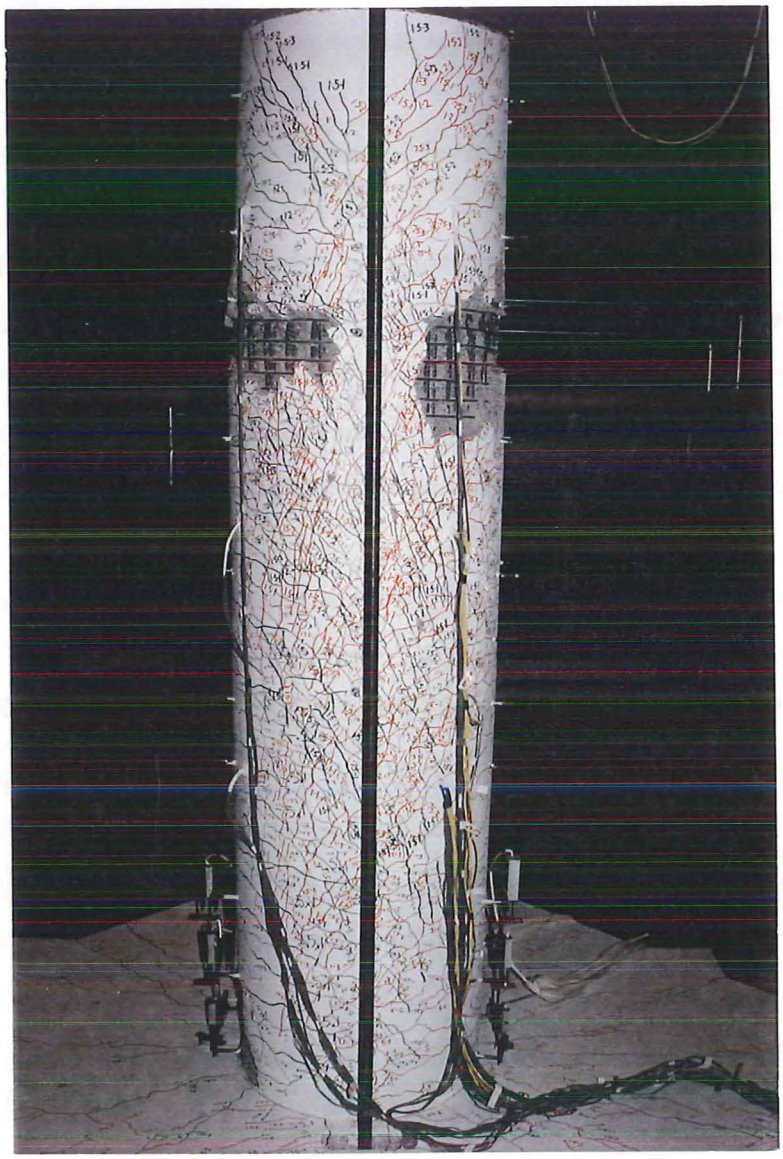

Figure 4.14 *Unit I-A Showing Column Cracking After Completion of Cycles to* $\mu_{\Delta T} = 2.0$ *(*$\mu_{\Delta S} = 2.74$*)*

capacity. From Figure 4.11 it can be seen that the test specimen just developed the nominal flexural strength of the base of the column in the first cycle to $\mu_{\Delta T} = +1.5$ ($\mu_{\Delta S} = +1.87$). Following this the flexural strength at the lower and upper curtailment points were reached, due to the tension shift effect, with inelastic action in the column concentrated at the upper curtailment point position.

Very little damage to the pilecap and pilecap overlay retrofit had occurred up to this point so assessment and repair of the column and extension of the test could be carried out.

The retrofit measures proposed by BCHF for the Thorndon Overbridge are intended to prevent collapse of the Overbridge during a seismic event corresponding to a 500 year return period earthquake. The assessed structural ductility demand on Pier 68 corresponding to this level of shaking is $\mu_{\Delta} = 1.78$, equivalent to a structural ductility of $\mu_{\Delta T} = 1.45$ in Unit I-A. Due to the undesirable potential brittle mode of failure that occurred in Unit I-A in the following load cycles to $\mu_{\Delta T} = 2.0$ ($\mu_{\Delta S} = 2.74$), repair of the column was necessary to improve performance of the test specimen, continue the test and determine the likely performance of other components of the test specimen.

4.4 COMPONENTS OF LATERAL DISPLACEMENT

4.4.1 Displacement Components

Displacements measured at the top of the column can be decomposed into the different components of lateral displacement that occur in the test specimen. A significant component of the overall test specimen displacement is provided by the elastic displacements that occur in the pilecap, through translation against the lateral springs and rotation of the pilecap due to the tensile and compressive reactions in the vertical springs.

4.4.1.1 Column Flexural Displacements

The position of linear potentiometers measuring column internal displacements are shown in Figure 4.3. The column flexural displacement components are estimated from the measured rotation of a column segment between pairs of linear potentiometers. Each pair of linear potentiometers are mounted on opposite sides of the column parallel with the direction of loading.

4.4.1.2 Pilecap Translation

Lateral displacements at the top of the column of the test specimen due to pilecap translation are taken directly as the measured displacement recorded by the linear potentiometer mounted at mid-depth of the original pilecap. Figure 4.2 shows the location of this linear potentiometer.

4.4.1.3 Pilecap Rotation

Displacements at the top of the column due to pilecap rotation are determined from the rotation of the test specimen pilecap as measured by the vertical displacements of the linear potentiometers at the extreme compression and tension vertical springs. Rigid body rotation of the pilecap between these two points is assumed. The position of the linear potentiometers measuring the vertical displacements at each vertical spring are shown in Figure 4.2.

4.4.2 Overall Test Unit Displacements

Figures 4.15 and 4.16 show the components of displacement measured as a percentage of the lateral displacement measured by the linear potentiometer mounted at the top of the column for each direction of loading.

Discovery of air pockets left under the plates used to attach the lateral springs to the baseblock following the testing of Unit I-B were remedied before testing of Unit I-A. Epoxy resin was injected through holes drilled into each plate to fill the void left under the affected plates and appears to remove the apparent additional flexibility in the Push direction due to lateral displacements of the pilecap.

Decomposition of the measured lateral displacements show that up to 50 % of the lateral displacement at the top of the column came through flexure in the column. The remaining displacements are provided predominantly through rotation of the pilecap with pilecap translation providing 10 - 15 % of the total lateral displacement.

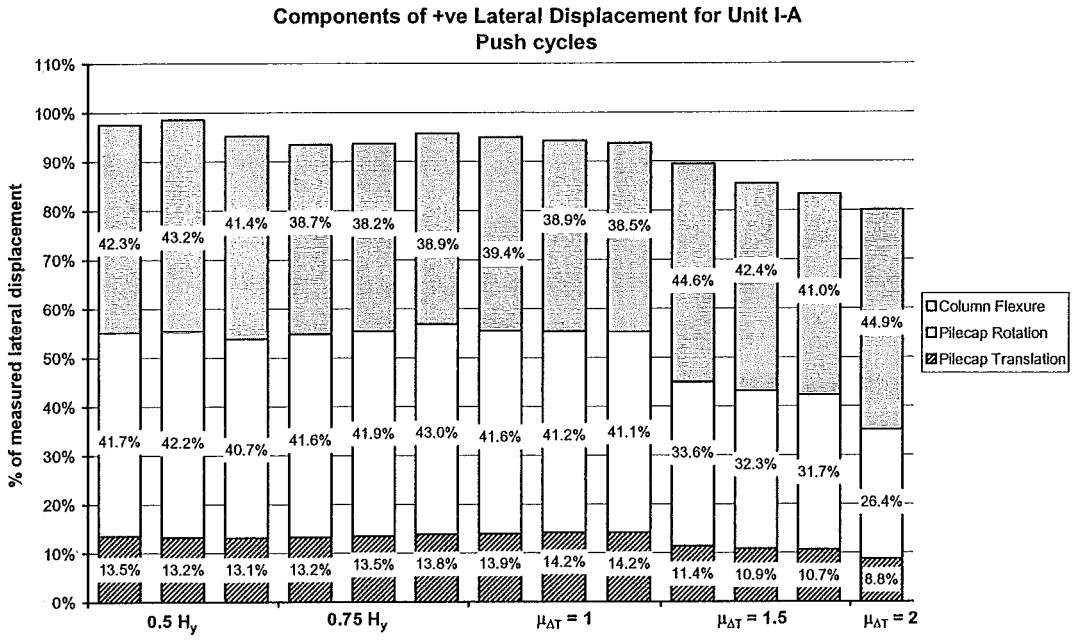

Figure 4.15 *Components of Lateral Displacement of Unit I-A for Push Cycles*

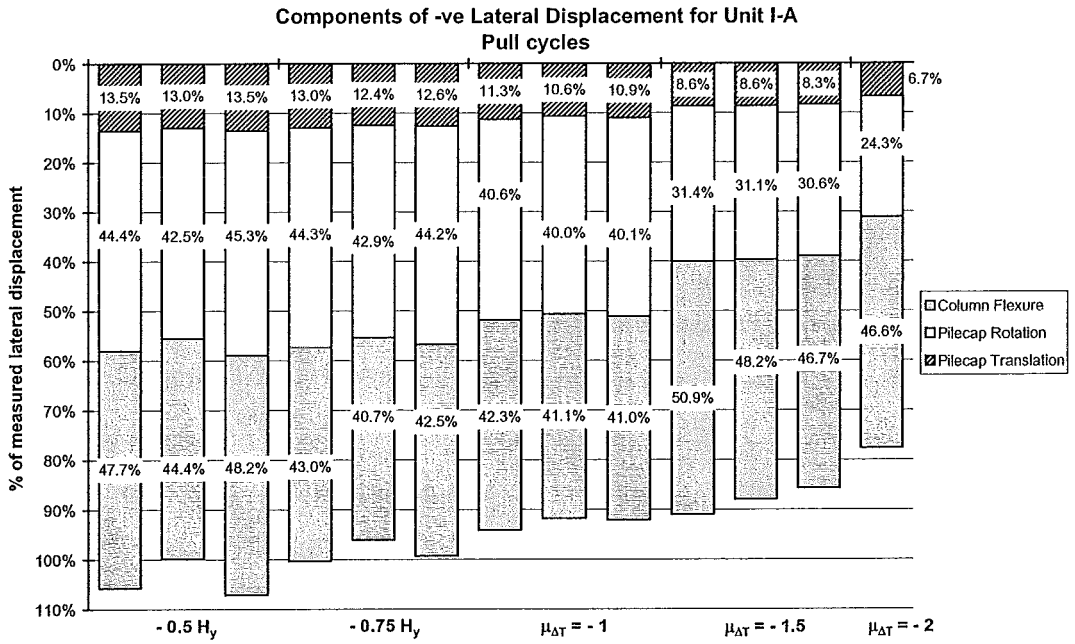

Figure 4.16 *Components of Lateral Displacement of Unit I-A for Pull Cycles*

During the later load cycles the discrepancy between the sum of the measured lateral displacement components and the lateral displacement measured at the top of the column can be attributed to the extensive diagonal cracking in the column and the resulting shear displacements in the column at the upper curtailment point.

4.5 ANALYSIS OF POTENTIAL MODE OF FAILURE

4.5.1 Potential Failure Mode of Unit I-A

Following the testing of Unit I-B failure of Unit I-A around the curtailment points was expected. Preliminary assessment of Unit I-A was carried out at the same time as Unit I-B following the failure of that test specimen. This indicated that the flexural strength of the upper and lower curtailment points could be reached when the flexural strength at the base was achieved, due to the tension shift effect. Assessment of the column's shear strength indicated that shear failure around the curtailment points was possible when the flexural strength at the base of the column was attained. Predictions on the performance of Unit I-A were based on the assumption that if inelastic action were to occur in the column it would be confined to the base of the column, ignoring the likelihood that inelastic action could occur higher in the column.

The extensive diagonal cracking in the column of Unit I-A and concentration of inelastic action at the upper curtailment point did not allow the flexural strength of the base of the column to be maintained. Developing the flexural strengths of both curtailment points limited the lateral force resisted by the column preventing it increasing to a level which would exceed the flexural strength of the base of the column. Inelastic displacements in the column were occurring at the upper and lower curtailment points and further cycles to higher structural displacement ductilities were placing increasingly larger curvature demands at the upper curtailment point due to the smaller lever arm between this point and the top of the column. Figure 4.17 shows clearly the displacement profile distributed up the height of the column at

$\mu_{\Delta T} = +2.0$ ($\mu_{\Delta S} = +2.74$) when the top of the column has been displaced a total of +147 mm. Noticeable rotation of the column is seen at the lower curtailment point with a smaller rotation occurring in the column at the upper curtailment point.

The cracking clearly indicates the development of a brittle flexure-shear failure in the column at the curtailment point due to the flexural and shear strength of the column

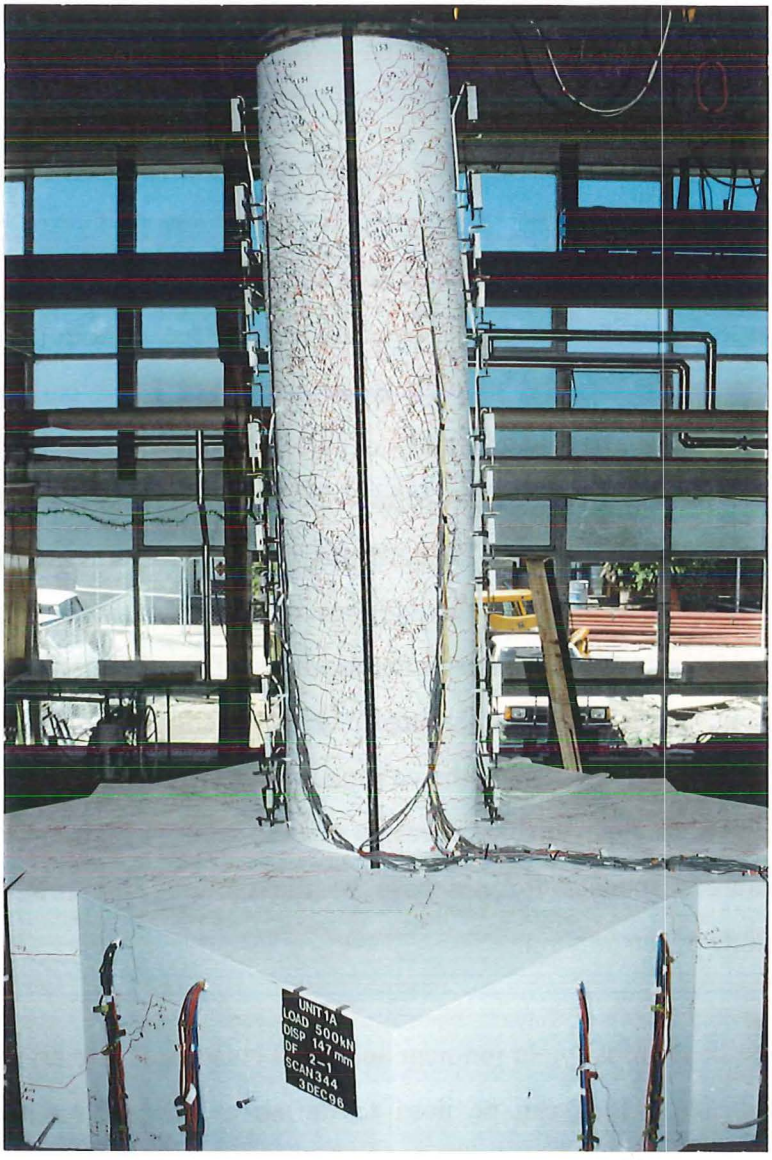

Figure 4.17 *Unit I-A Column Displacement Profile at* $\mu_{\Delta T} = 2.0$ ($\mu_{\Delta S} = 2.74$)

being reached at this point during loading of the test specimen. The consequences of the flexure-shear failure developing in a column could lead to loss of axial load carrying capacity and collapse of the structure. The axial load applied to the test specimen was monitored through a pressure gauge on the manifold connecting the two rams to the hydraulic pump. This pump was not load controlled, the displacement of each ram being held constant throughout the test instead. Close monitoring of the axial load throughout each load cycle prevented any large increases in axial load over the required 876 kN axial load applied.

4.5.2 Moment-Curvature Analysis

The interaction of flexure and shear in a column leads to increased forces carried in the longitudinal reinforcement, compared to the internal forces required for equilibrium at a section, and is referred to here as the tension shift effect. This can be expressed as a fictional increase in the bending moment demand in the column and was responsible for the flexural strength at the upper and lower curtailment points being reached during the testing of Unit I-A. This occurrence led to the development of extensive diagonal cracking in the column of Unit I-A concentrated around the upper and lower curtailment points. A comparison of the bending moment demand versus the moment capacity for the column of Unit I-A was carried out by conducting moment-curvature analyses for the base of the column, the upper and lower curtailment points using the measured material strength properties. These gave the flexural strengths of the base of the column and at the curtailment points and an estimation of the ultimate available curvature of each section. Figure 4.18 shows the moment-curvature responses for the base of the column, the lower and upper curtailment points of the column.

Table 4.1 gives the nominal yield moment and yield curvature for each section of the column of Unit I-A which can be used to define a bi-linear moment-curvature approximation for each section. This bi-linear approximation can be used to determine the curvature distribution following the bending moment diagram to determine elastic displacements of the column of Unit I-A.

The lateral loads in the column when the test was halted were +496 kN and -476 kN at $\mu_{\Delta T}$ = +2.0 and -2.0 respectively ($\mu_{\Delta S} = \pm 2.74$) which correspond to moments at the base of the column of 1426 kNm for the push (positive load) direction and 1368 kNm for the pull (negative load) direction.

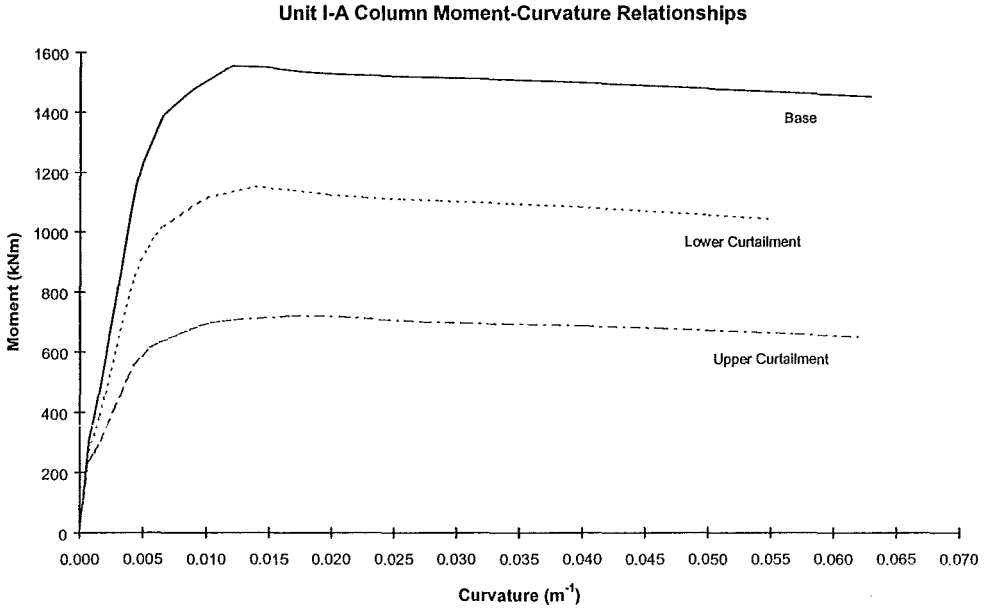

Figure 4.18 *Moment-Curvature Relationships for Column of Unit I-A*

Table 4.1 *Nominal Yield Moment and Yield Curvature for Unit I-A*

	M_y	ϕ_y
	kNm	m^{-1}
Base	1513.8	0.00581
Lower Curtailment	1104.2	0.00553
Upper Curtailment	700.4	0.00521

4.5.3 Column Shear Capacity Assessment

The shear capacity of the column in Unit I-A is assessed following the procedure proposed by Priestley et al. [P3, P4] and outlined in Section 6.4.2. The three components of shear resistance; concrete, transverse steel and axial load, are assessed to provide a total shear resistance at the base of:-

$$\begin{aligned} V_n &= V_s + V_p + V_c \\ &= 390 + 84 + 595 \\ &= 1069\ kN \qquad \text{for } k = 0.29 \\ &= 390 + 84 + 368 \\ &= 842\ kN \qquad \text{for } k = 0.10 \\ &= 390 + 84 + 184 \\ &= 658\ kN \qquad \text{for } k = 0.05 \end{aligned} \tag{4.2}$$

and at the curtailment points of:-

$$\begin{aligned} V_n &= V_s + V_p + V_c \\ &= 263 + 84 + 595 \\ &= 942\ kN \qquad \text{for } k = 0.29 \\ &= 263 + 84 + 368 \\ &= 715\ kN \qquad \text{for } k = 0.10 \\ &= 263 + 84 + 184 \\ &= 531\ kN \qquad \text{for } k = 0.05 \end{aligned} \tag{4.3}$$

The assessed shear strength of the column at the curtailment points at k = 0.05 is close to the lateral force corresponding to the development of the nominal flexural strength at the base of the column, H_a.

4.5.4 Comparison of Assessed Column Shear Strength and Failure Loads

The shear strength of a column decreases with increasing column curvature ductility due to the degradation of the concrete component of shear resistance [P3, P4]. This allows the shear strength envelope for the column to be plotted against the column

curvature ductility and the equivalent column shear force-curvature relationship, derived from a moment-curvature relationship including the tension shift effect, to be plotted for comparison. Where the shear force-curvature relationship intersects the shear strength envelope indicates the development of a flexure-shear failure in the column and a limit for the available ultimate column curvature. The column may possess further residual strength and displacement capacity but the reliance on shear strength and shear deformation capacity of a column is not recommended for ductile seismic response [P1, P2, P3].

From moment-curvature analyses of the column of Unit I-A an assessment of the base moment and corresponding column shear force can be made to determine the moment reached when the tension shift effect causes the bending moment demand to reach the flexural strength at the curtailment point. The method used here to assess columns with curtailed longitudinal reinforcement is presented in Chapter 6.

The flexural strength envelope for the column can be plotted against the column height from the results of the moment-curvature analyses for each section. The procedure proposed in Chapter 6 assumes the flexural strength at the critical section, the base of the column, is attained and the tension shift is calculated based on the shear force required to develop the column's flexural strength, V, and an angle of the inclined compression fields in the column of $\theta = 30°$.

The bending moment demand corresponding to the development of the flexural strength at the base of the column including the fictional increase in the bending moment demand due to tension shift effect and the flexural strength envelope are shown in Figure 4.19. The fictional increase in the bending moment demand is shown dashed, parallel to the bending moment demand acting on the column, and can be seen to be just below the flexural strength envelope at the upper curtailment point and just exceeding the flexural strength envelope at the lower curtailment point. This plot suggests it is likely that the flexural strength of the base and both of the curtailment points will be reached at the same time with a tension shift based on an angle of $\theta = 30°$. This angle compares well with the angle of diagonal crack pattern seen to have developed in the column of Unit I-A.

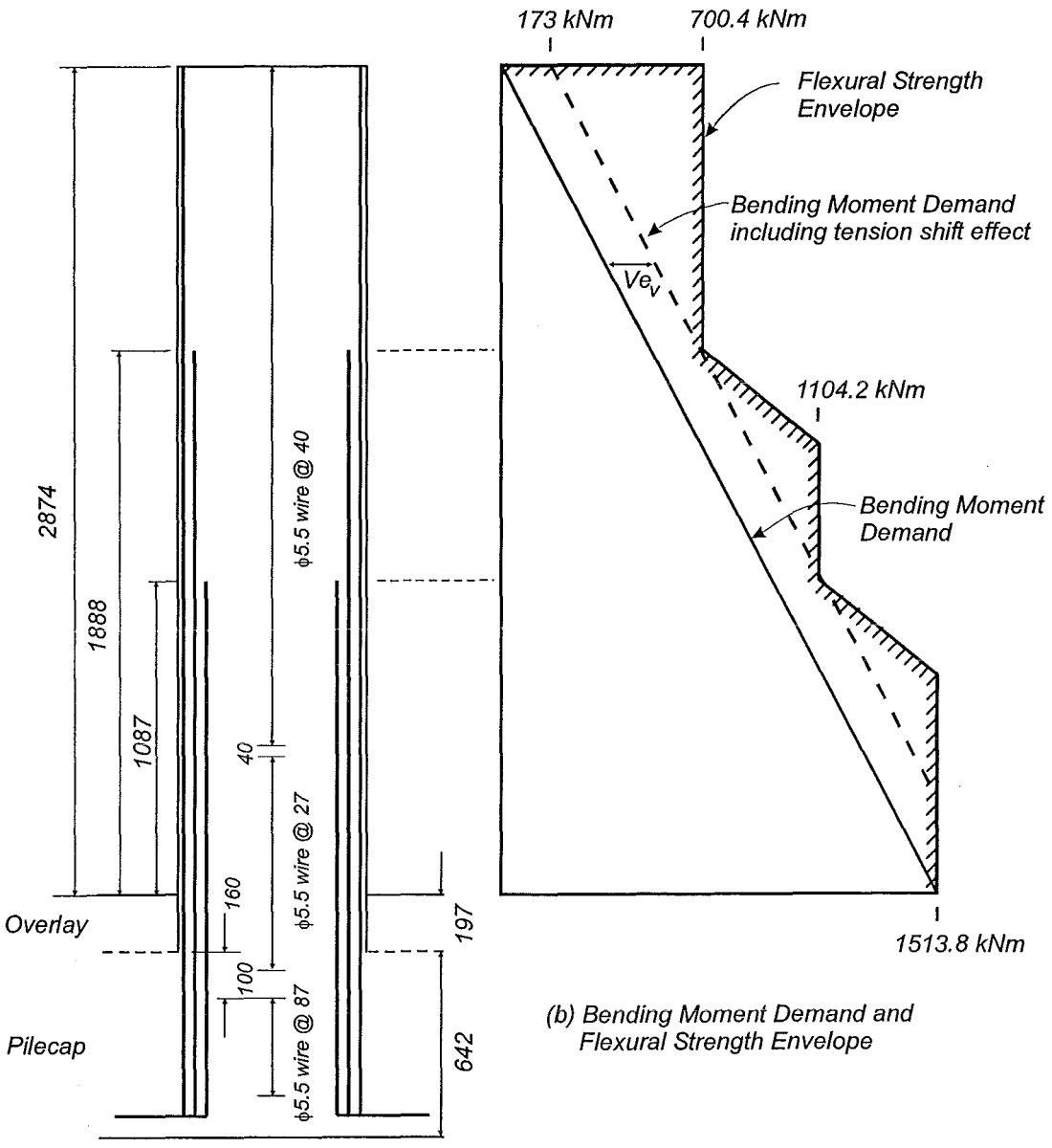

Figure 4.19 *Flexural Strength Envelope and Bending Moment Demand for Unit I-A*

4.6 REPAIR AND TESTING OF UNIT I-A

4.6.1 Repair of Unit I-A

Very little damage had occurred to the pilecap and pilecap overlay retrofit so a continuation of testing was required to observe the performance of the pilecap overlay retrofit to strengthen the existing pilecap and force inelastic action to occur at the base of the column. With the extensive damage to the column of Unit I-A occurring during testing up to $\mu_{\Delta T} = 2.0$ ($\mu_{\Delta S} = 2.74$) the column had to be repaired and strengthened in order to continue testing of the specimen.

Repair of the column comprised removal of all loose, spalled cover concrete from the damaged region around the curtailment point and the installation of a new 3 mm thick steel jacket, 2.400 m tall around the column. This steel jacket extended 527 mm above the upper curtailment point in the column, to practically the full height of the column. The jacket was fabricated in two halves and welded together in place around the column.

Epoxy injection of the cracks in the column of Unit I-A was conducted in a similar manner to Unit I-B with fitting of the steel jacket and grouting the space behind the jacket with a cement based grout first. Holes were placed in the new steel jacket for the tubes for injection of the epoxy to pass out and sealed so that the cement grout could be placed.

The epoxy injection was carried out a day after the cement grout was placed behind the new steel jacket and a period of seven days was allowed to give time for the epoxy resin to cure and the cement grout to gain sufficient strength before testing recommenced. The epoxy was injected through a tube located at the base of the column and the epoxy was able to penetrate through the cracks in the column up the full height, requiring approximately 15 litres of epoxy resin. Figure 4.20 shows the repaired Unit I-A with the full height steel jacket.

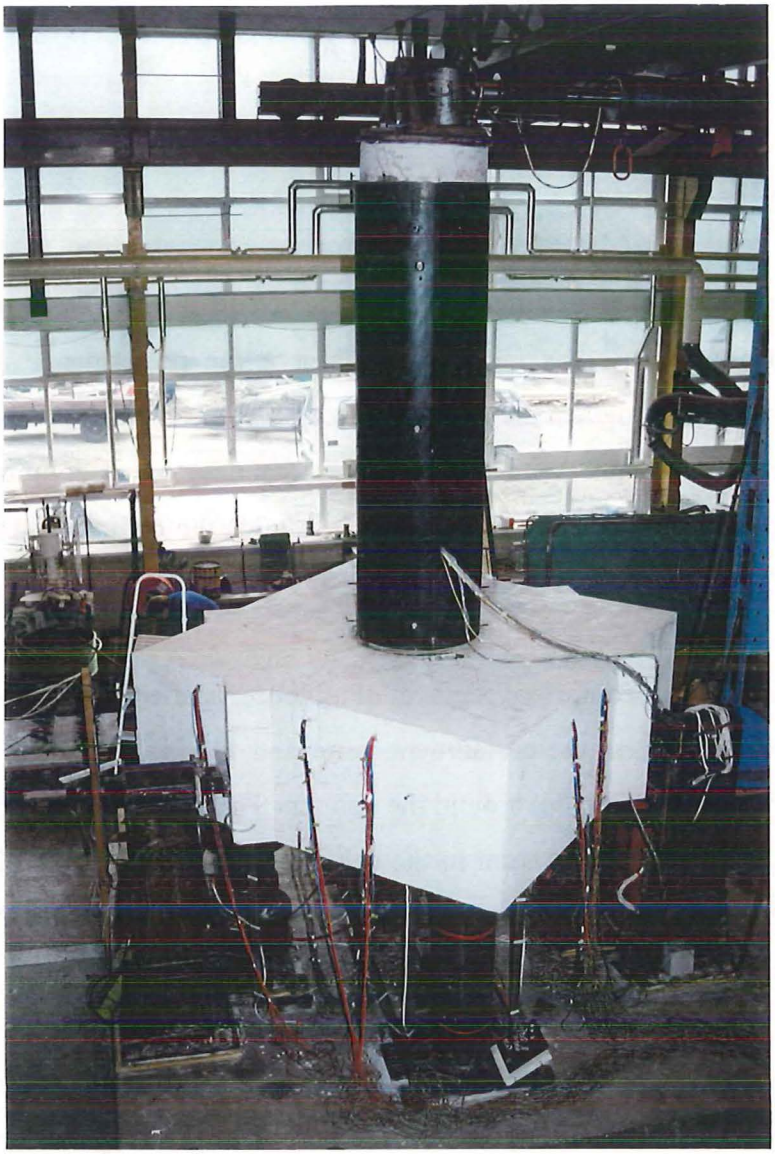

Figure 4.20 *Repaired Unit I-A with Full Height Steel Jacket*

4.6.2 Lateral Loading History for Repaired Unit I-A

After completion of the repair to the column two load controlled cycles were completed to 0.75 H_y to observe the change in stiffness of the repaired column. Further cycles were displacement controlled with two cycles completed to $\mu_{\Delta T} = 1.0$ and three cycles completed to $\mu_{\Delta T} = 1.5$, 2.0 and to the full extension of the hydraulic actuator completing the test programme. The yield displacement of the test specimen from the initial cycles was used to define the displacement ductility for the load cycles following repair of the specimen.

4.6.3 General Behaviour of Repaired Unit I-A

After repair of Unit I-A the column returned to its original stiffness during the cycles to 0.75 H_y. This can be attributed to there being little inelastic action occurring at the base of the column, before the repair, as inelastic action was taking place higher in the column. The stiffening effect of the steel jacket and epoxy injection of the cracks in the column will also have contributed to regaining the original column stiffness. Figure 4.21 shows the lateral load-lateral displacement response of the repaired Unit I-A. This plot shows stable hysteresis loops with the development of a large column lateral load overstrength. The limits of extension on the hydraulic actuator meant the final three load cycles were repeated to $\mu_{\Delta T} = +2.0$ ($\mu_{\Delta S} = +2.74$) and extended to approximately $\mu_{\Delta T} = -3.0$ ($\mu_{\Delta S} = -4.48$).

Maximum lateral displacements of +143 mm and -202 mm were possible to the full extension of the hydraulic actuator corresponding to displacement ductilities of $\mu_{\Delta T} = +2.0$ ($\mu_{\Delta S} = +2.74$) and approximately $\mu_{\Delta T} = -3.0$ ($\mu_{\Delta S} = -4.48$) respectively. Performance of this part of the test was excellent, exhausting the limits of the travel on the hydraulic actuator without failing the test unit. Unit I-A showed an increase in the lateral load carrying capacity, developing the flexural strength at the base of the column and a large lateral load overstrength.

Fitting of the steel jacket to Unit I-A resulted in the removal of strain gauges and column curvature potentiometers over the upper region of the column. Data from the remaining strain gauges indicated that yield in all the instrumented column longitudinal bars penetrated down to mid-depth of the original pilecap recording strains in the order of 2000 $\mu\varepsilon$.

Loading to $\mu_{\Delta T} = 1.5$ ($\mu_{\Delta S} = 1.87$) led to the development of a wedge shaped section of the pilecap overlay retrofit pulling out from around the base of the column. This pullout of the overlay concrete is due to yielding of the column longitudinal bars and pulling out of the pilecap where the crack at the column-overlay interface forms. During loading to $\mu_{\Delta T} = 2.0$ ($\mu_{\Delta S} = 2.74$) crushing of the overlay concrete at the compression edge of the column contributed to the damage created by pullout of the

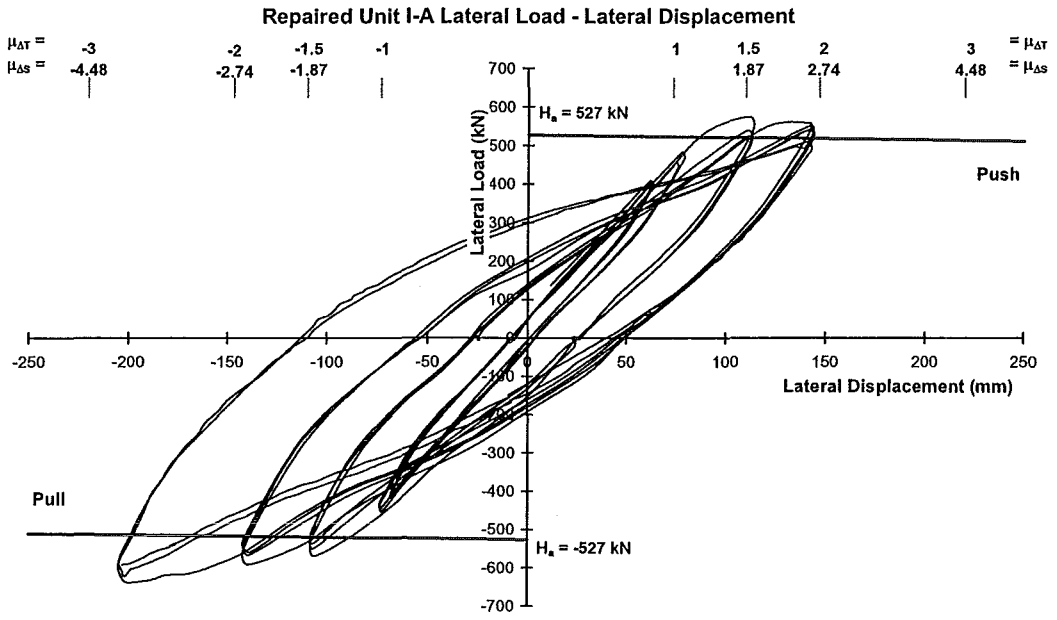

Figure 4.21 *Lateral Load-Lateral Displacement Response for Repaired Unit I-A*

column bars.

The initial transverse cracks underneath the pilecap continued to open during loading after repair of the test specimen. Cracks widths of up to 3 mm were observed in one crack during loading up to the final cycles of $\mu_{\Delta T} = -3.0$ ($\mu_{\Delta S} = -4.48$).

The pilecap and pilecap overlay retrofit transferred the forces induced from the repaired column with restricted cracking only and limited yielding of some reinforcement. Tension only yielding of the bottom pilecap mat bars was seen after repair of the column. High strains are also observed in some overlay mat strain gauges which are in the wedge pullout region of the overlay, near the base of the column. The pullout of the concrete will have engaged the overlay mat and dowels around this location leading to the high strains recorded in the reinforcement.

Pullout of the reinforcement at the central piles indicates yielding of the pile reinforcement during the last cycles to $\mu_{\Delta T} = -3.0$ ($\mu_{\Delta S} = -4.48$) although no increase

in strains in the pile dowel bars at the central pile locations, lapped with the existing pile reinforcement, was recorded.

4.7 REPAIRED UNIT LATERAL DISPLACEMENTS

4.7.1 Repaired Overall Test Unit Displacement Components

The measured lateral displacement of the top of the column of the repaired Unit I-A can be decomposed into the components of lateral displacement due to pilecap translation, pilecap rotation and column flexure. The three lowest sets of linear potentiometers placed on the column to measure column curvatures were left after fitting the steel jacket to repair Unit I-A, the remaining linear potentiometers were removed and not refitted. The remaining linear potentiometers were used to determine the component of lateral displacement due to column flexure. During completion of the lateral load cycles to $\mu_{\Delta T} = -3.0$ ($\mu_{\Delta S} = -4.48$) the travel of the bottom two sets of linear potentiometers were exceeded rendering the readings unreliable for this load cycle. Therefore displacement components for this load cycle are not shown.

Figures 4.22 and 4.23 show the components of displacement as a percentage of the measured lateral displacement at the top of the column for the push and pull cycles for the repaired test specimen. Pilecap translation and rotation are the major displacement components during the load controlled cycles with column flexure becoming more dominant as the test specimen is loaded to higher displacement ductilities. The apparent loss in measured displacement components is due to increase in the width of the transverse cracks under the pilecap as the bottom pilecap mat bars started yielding. The assumed rigid body rotation of the pilecap as measured between the extreme tension and compression piles is reduced as the cracks open during each load cycle. Using the rigid body rotation of the column, as measured by the two linear potentiometers mounted under pilecap beneath the edges of the column, allows some of the lost displacement components to be recovered.

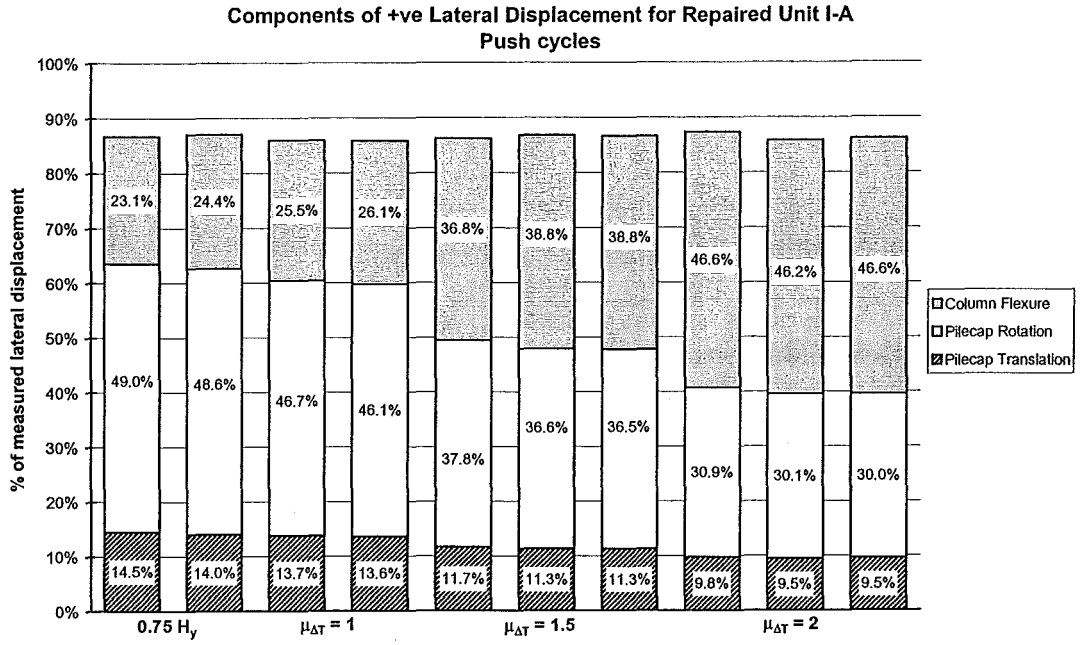

Figure 4.22 *Components of Displacement for Repaired Unit I-A for Push Cycles*

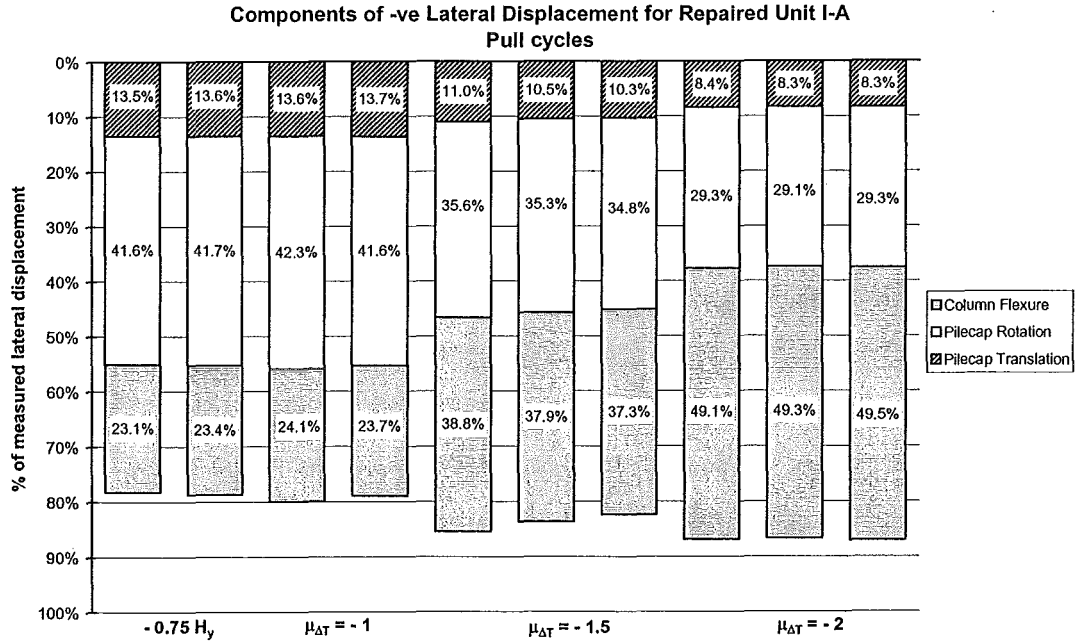

Figure 4.23 *Components of Lateral Displacement of Repaired Unit I-A for Pull Cycles*

4.8 BEHAVIOUR OF MEMBERS OF UNIT I-A DURING TESTING

4.8.1 General Observations

First cracking occurred at the base of the column between the top of the pilecap overlay and the bottom of the steel jacket at the first cycle to 0.5 H_y. Cracking extended up to the upper curtailment point and during the cycles to 0.75 H_y crossed diagonally through the column centreline at this point. Diagonal cracking was also seen to form at the lower curtailment point with much of the cracking at the base of the column remaining essentially horizontal.

By $\mu_{\Delta T} = 1.5$ ($\mu_{\Delta S} = 1.87$) the crack at the upper curtailment point had increased in width to 3 mm. Spalling of the cover concrete, due to buckling of the column longitudinal bars at the upper curtailment point, occurred at $\mu_{\Delta T} = 2.0$ ($\mu_{\Delta S} = 2.84$). Spalling of the cover concrete at the base of the column on the western side of the test specimen was also seen at this stage of the test. Pullout of approximately 10 mm of the column longitudinal bars at the upper curtailment point was visible after removal of the cover concrete.

Following repair of the column the steel jacket prevented any observation of column crack patterns. Only a small amount of grout crushing was seen at the bottom of the steel jacket by the end of the test.

4.8.2 Column Displacements

Lateral displacements of the column of Unit I-A can be derived from measuring the total lateral displacement at the top of the column and removing the components of displacement due to rotation and translation of the pilecap.

Figure 4.24 shows the lateral load-lateral column displacement plot for Unit I-A up to halting the test at $\mu_{\Delta T} = 2.0$ ($\mu_{\Delta S} = 2.84$). Also shown on this plot is the column displacement ductility, $\mu_{\Delta C}$, as determined from the yield displacement calculated for

the column, measured during the experiment. The column yield displacement was determined from Equation 2.1 where $\Delta_{0.75\,Hy}$ and $\Delta_{-0.75\,Hy}$ are the average of the column displacements measured during the cycles to 0.75 H_y. The yield displacement of the column was determined to be $\Delta_{y,c} = 32.7$ mm from the experiment, compared to the theoretical displacement of 32.3 mm including the effecs of curvature distribution over the height of the column, strain penetration at the base and at the curtailment points.

The column only just developed its flexural strength at the base due to the combined lateral load and P-Δ effect during the first cycle to $\mu_{\Delta T} = +1.5$ ($\mu_{\Delta S} = +1.87$). Reaching the flexural strength at the upper and lower curtailment points at this stage, due to the tension shift effect, prevented the lateral load from increasing to exceed the flexural strength at the base of the column. The last load cycle is marked by the flattening off of the load-displacement plot as the column started to fail at the upper curtailment point.

The lateral load-lateral column displacements for the repaired Unit I-A are shown in Figure 4.25. The fitting of a full height steel jacket allowed the development of a large lateral load overstrength until the travel was exhausted on the hydraulic actuator.

4.8.3 Column Curvature Distribution

The measured curvature distribution for the column of Unit I-A is shown in Figure 4.26. The curvature values plotted were obtained from the measurements of the linear potentiometers at each level and are plotted at the mid-points of the gauge lengths between each of the potentiometer positions. Shown on each plot is the position of the upper and lower curtailment points of the longitudinal reinforcement in the column and the measured column displacement ductility, $\mu_{\Delta C}$, is indicated alongside the structural displacement ductility, $\mu_{\Delta T}$. The theoretical yield curvature for the base of the column, ϕ_y, obtained from a moment-curvature analysis of the base of the column and using measured material properties is also shown. Theoretical

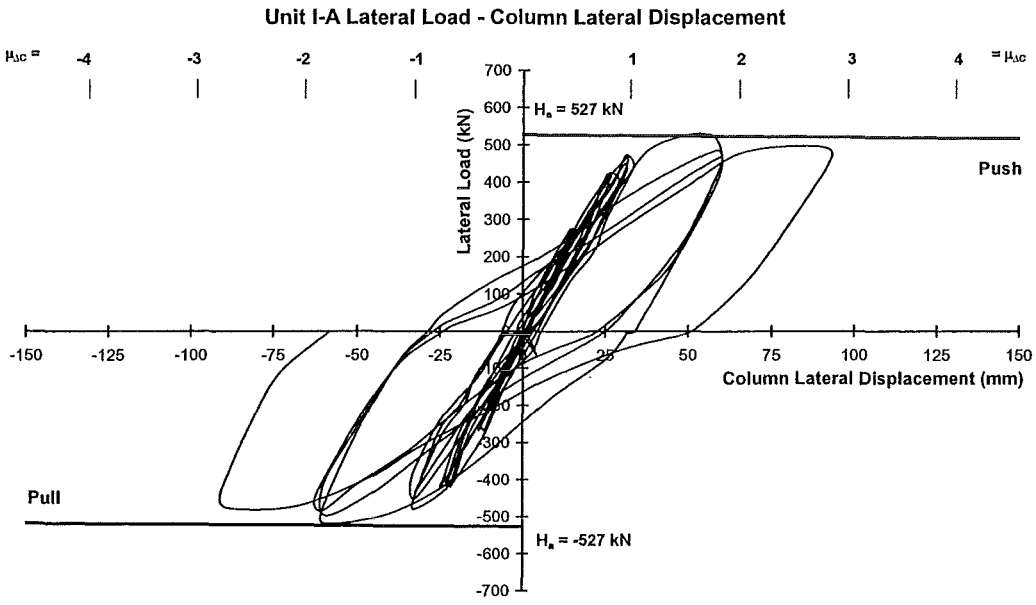

Figure 4.24 *Lateral Load-Lateral Column Displacements for Unit I-A up to* $\mu_{\Delta T} = 2.0$ *(*$\mu_{\Delta S} = 2.84$*)*

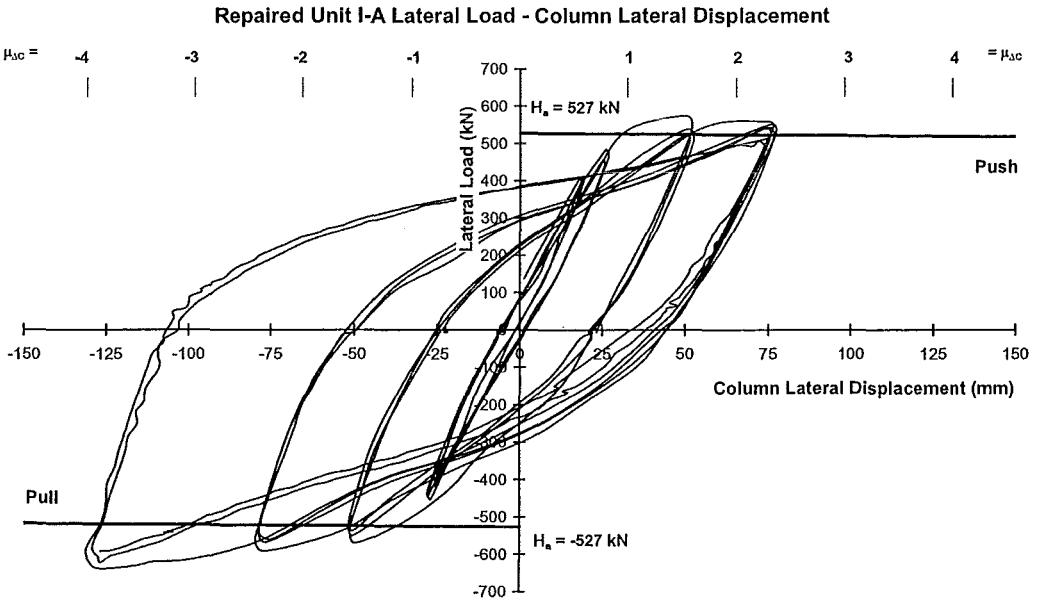

Figure 4.25 *Lateral Load-Lateral Column Displacements for Repaired Unit I-A*

yield curvatures for the upper and lower curtailment points are of the same order of magnitude as can be seen in Table 4.1 and Figure 4.18.

It can be seen that the column curvature distribution was exceeding the yield curvature at the base, lower and upper curtailment points during the cycles to $\mu_{\Delta T} = 1.0$. A substantial increase in curvatures around the upper and lower curtailment points is seen during the cycles to $\mu_{\Delta T} = 1.5$ ($\mu_{\Delta S} = 1.87$) and at the upper curtailment point during the cycle to $\mu_{\Delta T} = 2.0$ ($\mu_{\Delta S} = 2.84$). The spread of plasticity at the upper and lower curtailment points appears to be over a distance of D / 2 above and below the curtailment point of the longitudinal reinforcement, where D is the overall column diameter.

Although the major damage to the column of Unit I-A occurred at the upper curtailment point, significant rotations were taking place at the lower curtailment point. The significantly smaller lever arm between the top of the column and the upper curtailment point placed large curvature ductility demands on the column at this location. Large rotations were allowed to develop at the lower curtailment point due to the larger lever arm to the top of the column reducing the curvature demand on the column at this point. This is illustrated in Figure 4.17 where it can be seen that there is a larger rotation occurring in the column at the lower curtailment point than at the upper curtailment point when the photo was taken at $\mu_{\Delta T} = +2.0$ ($\mu_{\Delta S} = +2.87$).

Figure 4.27 shows the column curvatures recorded for the repaired Unit I-A. As expected they show the concentration of curvatures occurring at the base of the column, between the top of the pilecap overlay and bottom of the steel jacket.

4.8.4 Column Strain Gauges

Unit I-A had five column longitudinal bars strain gauged over their full height. Strain gauges are numbered consecutively starting from 1 at the bottom-most gauge on each bar and identified with the bar number and the gauge number eg. B1-3 being gauge number 3 on Bar 1.

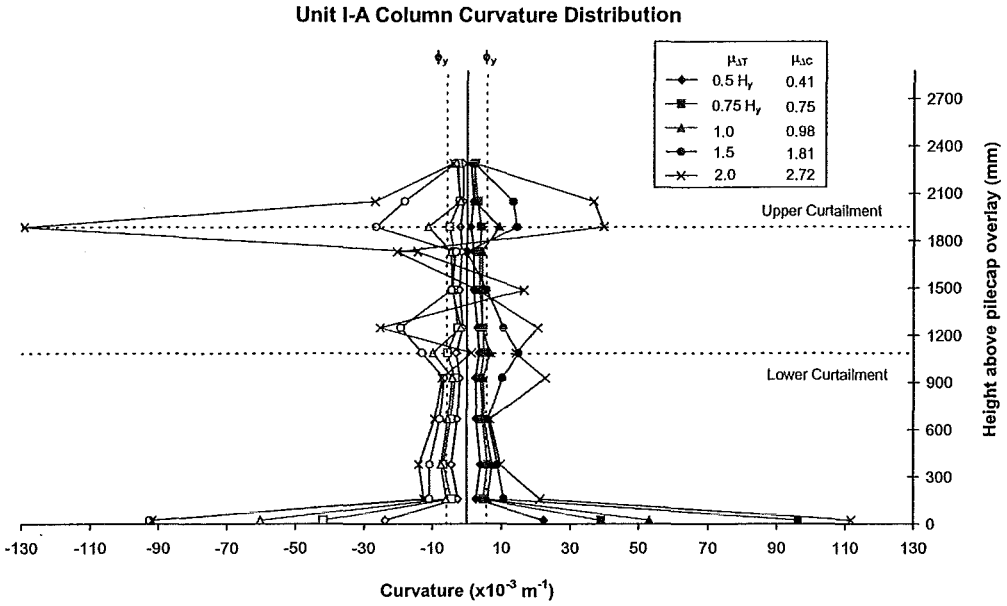

Figure 4.26 *Unit I-A Column Curvature Distribution up to* $\mu_{\Delta T} = 2.0$ *(*$\mu_{\Delta S} = 2.84$*)*

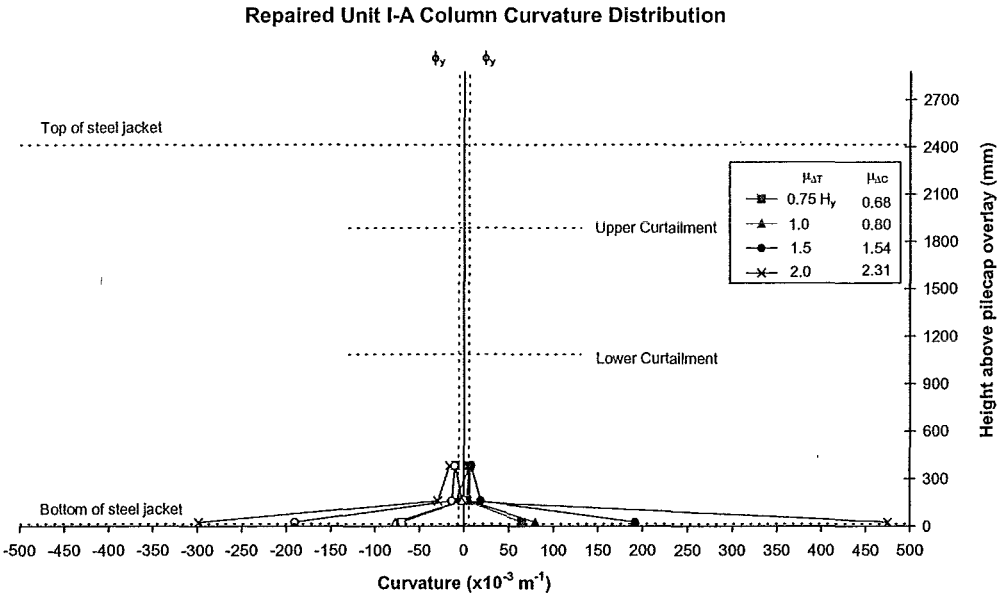

Figure 4.27 *Repaired Unit I-A Column Curvature Distribution*

Figures 4.28 to 4.33 show the maximum recorded strain in each gauge against position of the gauge within the column for the three cycles of loading to each level. Solid symbols indicate readings from Push (positive loading) cycles with hollow symbols indicating Pull (negative loading) cycles. Tensile strains are taken as positive. Shown on each plot is the position of the curtailment points and yield strain of the column longitudinal reinforcement. The top of the vertical axis, 2874 mm above the top of the pilecap overlay is the point of application of the simulated seismic load to the test specimen.

Strain gauges on the extreme column longitudinal bars indicate yielding of these bars at the base of the column took place during the cycles to $0.75\,H_y = \pm 410$ kN in tension and compression. Yield in tension of the extreme longitudinal bars also extended over the full height of the column at this stage of loading. Bars 2 and 4 show tension yielding over the full column height during the cycles to $\mu_{\Delta T} = 1.0$. A significant increase in strains is seen when the test specimen is loaded to $\mu_{\Delta T} = 1.5$ ($\mu_{\Delta S} = 1.87$) at the base of the column, in Bars 1, 2, 4 and 5, and around the upper curtailment point for all bars. The high tensile strains developed at the upper curtailment point, in excess of 2 % strain, are probably due to the start of buckling of the longitudinal reinforcement at this position. Increases in tensile strains can also be seen at the lower curtailment point for the extreme column bars (Bars 1 and 5) at this level of loading. High compressive strains are seen to develop at the base of the column in these bars also.

Peaks in strains appear in the Bar 3 strain profile below the curtailment points at $\mu_{\Delta T} = 2.0$ ($\mu_{\Delta T} = 2.84$). This bar is located at the column centreline and the strain peaks below the curtailment point are as a result of the inclined compressive stress field developed in the column.

Tensile yield penetration into the pilecap up to approximately 300 mm below the pilecap overlay surface can be seen in Bars 1, 2, 4 and 5 up to the cycles to $\mu_{\Delta T} = 1.5$ ($\mu_{\Delta S} = 1.87$).

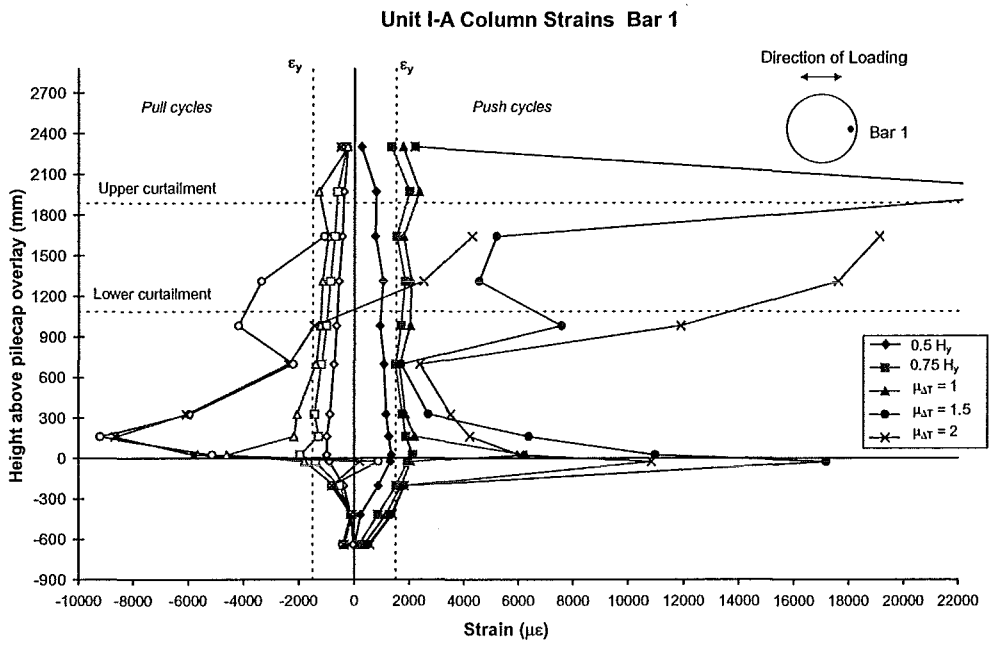

Figure 4.28 *Unit I-A Column Longitudinal Bar 1 Strain Profile*

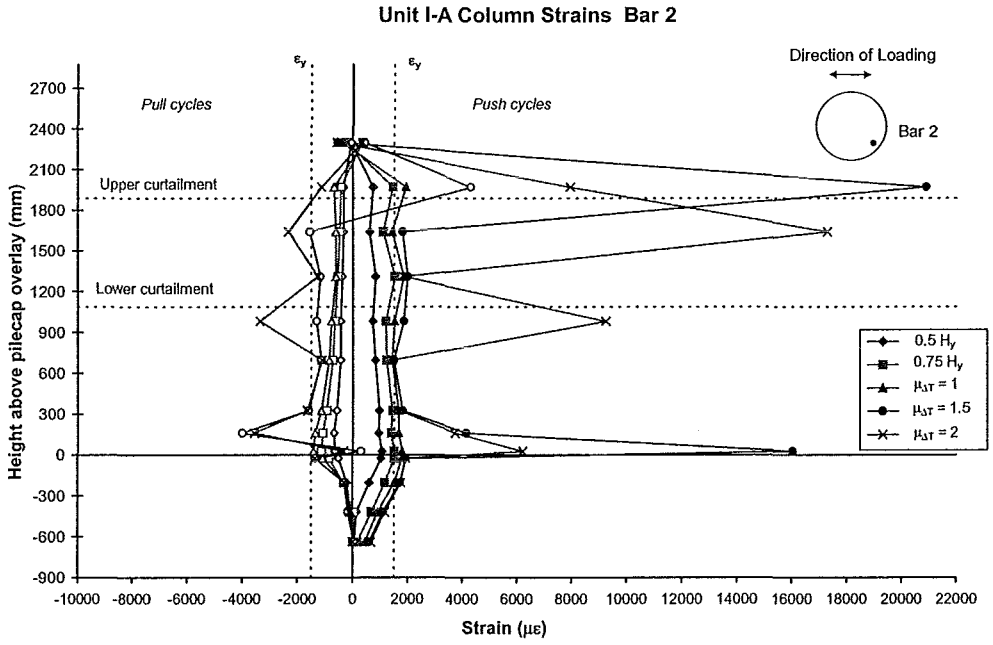

Figure 4.29 *Unit I-A Column Longitudinal Bar 2 Strain Profile*

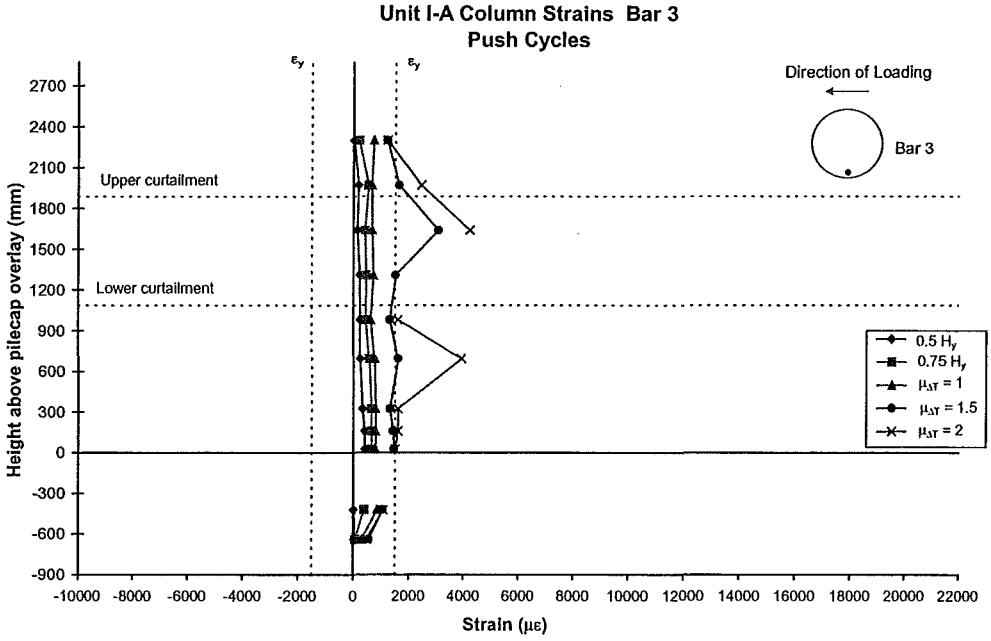

Figure 4.30 *Unit I-A Column Longitudinal Bar 3 Strain Profile for Push Cycles*

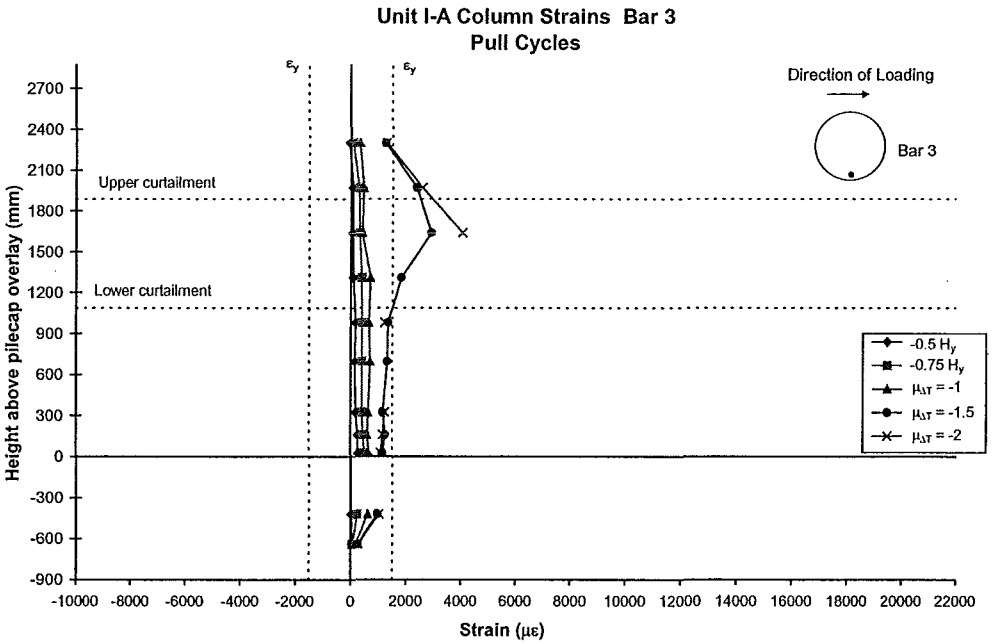

Figure 4.31 *Unit I-A Column Longitudinal Bar 3 Strain Profile for Pull Cycles*

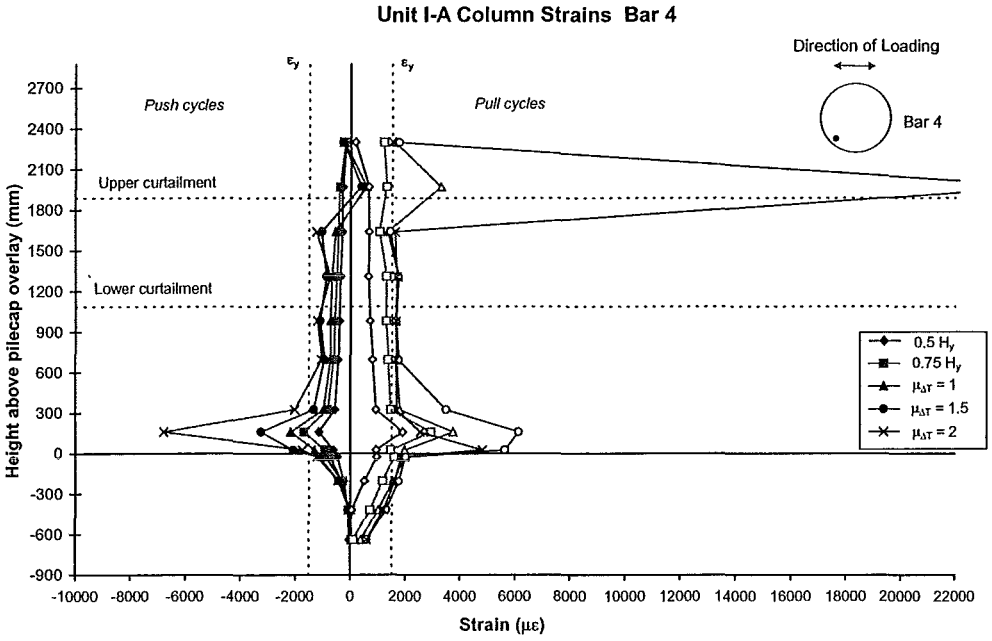

Figure 4.32 *Unit I-A Column Longitudinal Bar 4 Strain Profile*

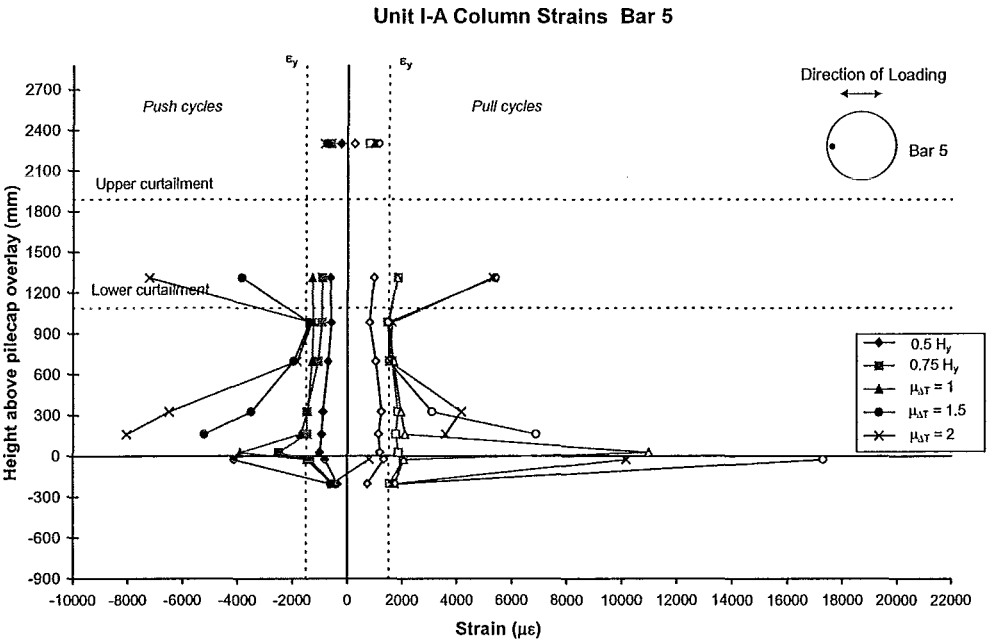

Figure 4.33 *Unit I-A Column Longitudinal Bar 5 Strain Profile*

The strain profiles from these bars show the yield strain is exceeded for a distance of approximately D / 2 above and below the curtailment points. Along with the readings from the column curvature linear potentiometers it appears that a reasonable value for the plastic hinge length, where the flexural strength of a member is reached at a point where the longitudinal reinforcement is curtailed, is half the diameter, or depth of the member.

Residual strains in the column bars after buckling at the upper curtailment point skew the strain profiles for Bars 1 and 5 for the opposite cycle of loading after $\mu_{\Delta T} = 1.5$ ($\mu_{\Delta S} = 1.87$).

Leads for all the strain gauges above the lower curtailment point were removed during the fitting of the steel jacket to repair the column of Unit I-A and strain readings were only recorded for the remaining strain gauges. Continuation of the test after repair of the column show that yield penetrated down into mid-depth of the original pilecap by the end of the test. Yield also extended up to the last remaining strain gauge, close to the lower curtailment point.

4.8.5 Column Transverse Spiral Strain Gauges

Strain gauges placed on the column transverse spiral reinforcement show peaks in the recorded transverse spiral strains corresponding to the upper and lower curtailment points during the cycles to $\mu_{\Delta T} = 1.0$, Figures 4.34 and 4.35. These peaks in strain appear below the curtailment points due to the formation of the inclined compressive stress fields in the column and the strain gauges being located on the column centreline parallel to the direction of loading. Yielding of the transverse spirals is seen during both cycles to $\mu_{\Delta T} = 1.5$ ($\mu_{\Delta S} = 1.87$) corresponding to the upper curtailment point. Yielding corresponding to the lower curtailment point is seen during both cycles to $\mu_{\Delta T} = 2.0$ ($\mu_{\Delta S} = 2.84$). The high strains recorded are also probably due to buckling of the longitudinal reinforcement inducing high local strains in the transverse spirals.

4.8.6 Pilecap and Pilecap Overlay

Modelling of the different stiffness of the piles under tension and compression and fixing of the central piles top and bottom were required to match the force distribution in Unit I-A to the forces from the structural analysis of Pier 68. The BCHF analysis for Pier 68 was conducted using values for the soil spring stiffness 25 % less than the average stiffness values at the side of the pilecap and 25 % greater than the average stiffness values for each of the piles. This pier was analysed with elements to model the existing piles including soil springs distributed along the length of the pile to model the bearing of the pile on to the surrounding soil. Comparison between the bending moments from testing of Unit I-A and the scaled BCHF Pier 68 analysis is shown. The bending moment is drawn for the centreline of the original pilecap, in Figure 4.36, at ductility $\mu_{\Delta T} = 1.0$, at development of the diagonal cracks in the column at $\mu_{\Delta T} = 2.0$ ($\mu_{\Delta S} = 2.74$) and at the peak lateral load corresponding to the first cycle to $\mu_{\Delta T} = -3.0$ ($\mu_{\Delta S} = -4.48$). The bending moment diagram for the cycle to $\mu_{\Delta T} = -3.0$ ($\mu_{\Delta S} = -4.48$) has been plotted taking the direction of application of the lateral load as for the other bending moment profiles.

The main difference between the BCHF Pier 68 structural analysis and Unit I-A is the application of 10 % of the column base moment to the top of the column, representing the centre of mass of the bridge deck, to account for the effects of the rotational inertia of the umbrella platform. From the pilecap bending moment profiles the influence of the compressive soil-pile stiffness and the lesser tensile soil-pile stiffness can be seen. The negative bending moment, on the trailing side of the pilecap is much less than the positive bending moment developed underneath the pilecap.

Comparison between the bending moments developed in the pilecap during the test to the scaled BCHF Pier 68 analysis shows the same bending moment profile was developed during testing. The positive bending moment, underneath the pilecap, was reached during testing due to the development of column overstrength during the test, after repair of the column was fitted with a full height steel jacket.

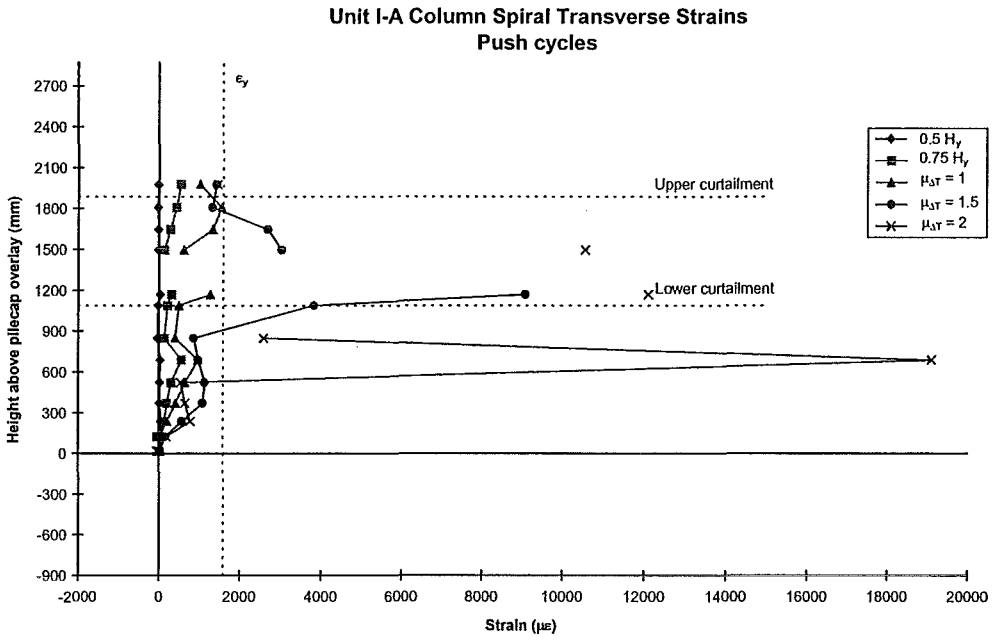

Figure 4.34 *Unit I-A Column Transverse Spiral Strain Profile for Push Cycles*

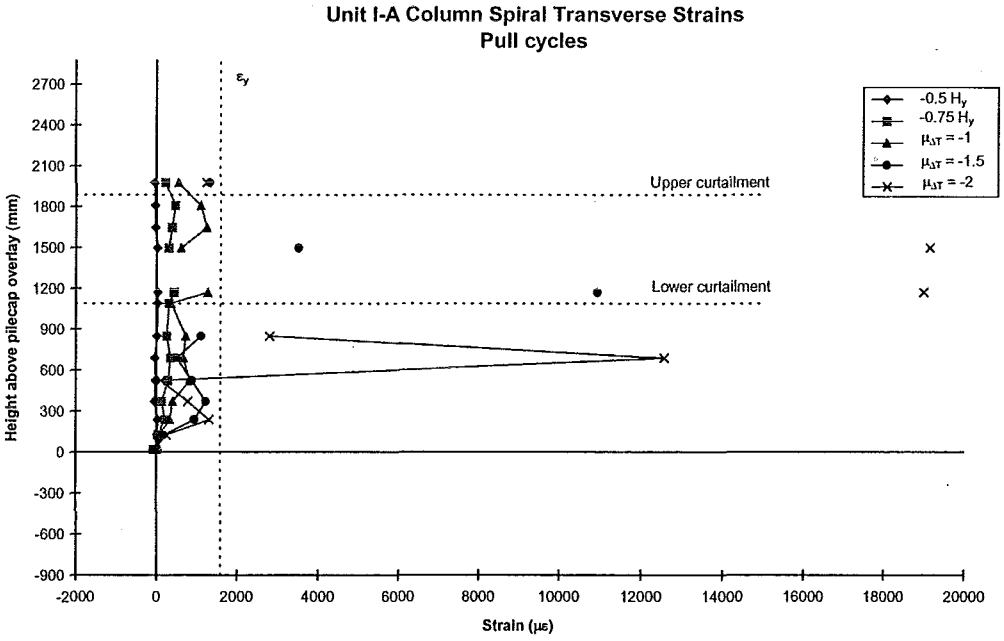

Figure 4.35 *Unit I-A Column Transverse Spiral Strain Profile for Pull Cycles*

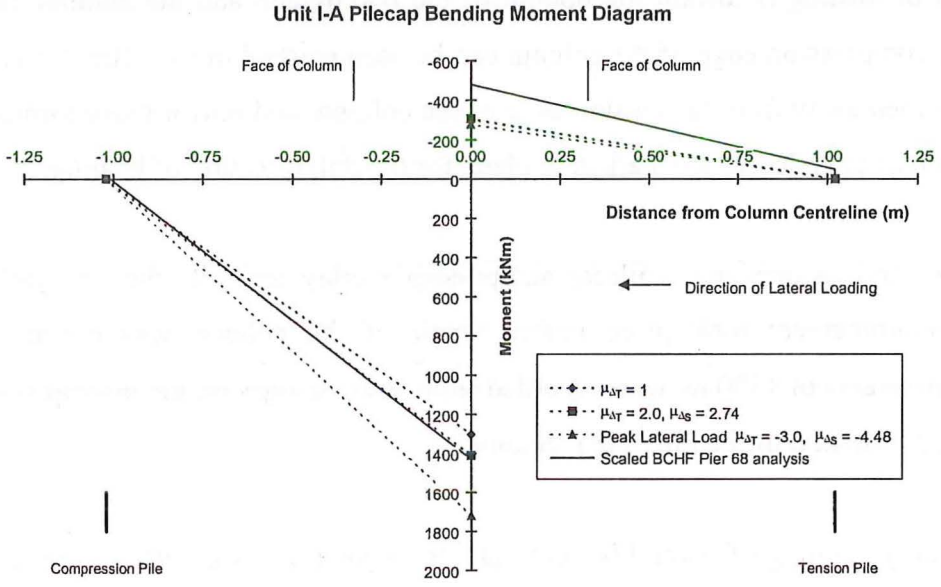

Figure 4.36 *Unit I-A Pilecap Bending Moment Diagram*

First cracking occurred on the bottom of the pilecap running transversely directly beneath the compression edge of the column during the cycles to 0.5 H_y (±273 kN). Cracking extended transversely across the full column diameter underneath the pilecap during the cycles to 0.75 H_y (±410 kN) and extended across the full pilecap width during the cycles to $\mu_{\Delta T} = 1.0$. Three main transverse cracks formed underneath the pilecap, beneath the edges of the column and across the column centreline, which crossed the full pilecap width perpendicular to the direction of loading. These cracks continued to open up during testing of the specimen, due to yield of the bottom mat bars close to these locations.

Cracks also developed at 45° to these transverse pilecap cracks extending away toward the trailing tension pile. The 45° cracks eventually extended up the edge of the pilecap to join with the 45° cracks forming on the top of the pilecap overlay surface away from the tension edge of the column. A series of almost parallel cracks appeared on the top of the pilecap overlay running from the compression edge of the column to

the position of the lateral springs where the pilecap reaction is provided by the lateral springs. Figure 4.37 shows the pilecap overlay surface at the end of the test. The Push direction of loading is toward the bottom of the photograph and the parallel cracks from the compression edge of the column can be seen marked in red. The 45° cracks which formed away from the tension edge of the column, and mirror those formed on the bottom of the pilecap, are marked in black for the Pull direction of loading.

Data from strain gauges in the pilecap and pilecap overlay generally show no yielding of the reinforcement took place before repair of the column was carried out. Maximum strains of 1500 με were recorded from strain gauges on the pilecap bottom mat directly beneath the centre of the column.

Tension only yielding of several bottom mat strain gauges is seen after repair of the column was carried out during the cycles to $\mu_{\Delta T} = 1.5$ ($\mu_{\Delta S} = 1.87$) in the central region of the pilecap parallel with the direction of loading. Maximum strains, of 2200 με, were again recorded directly beneath the column. Figures 4.38 and 4.39

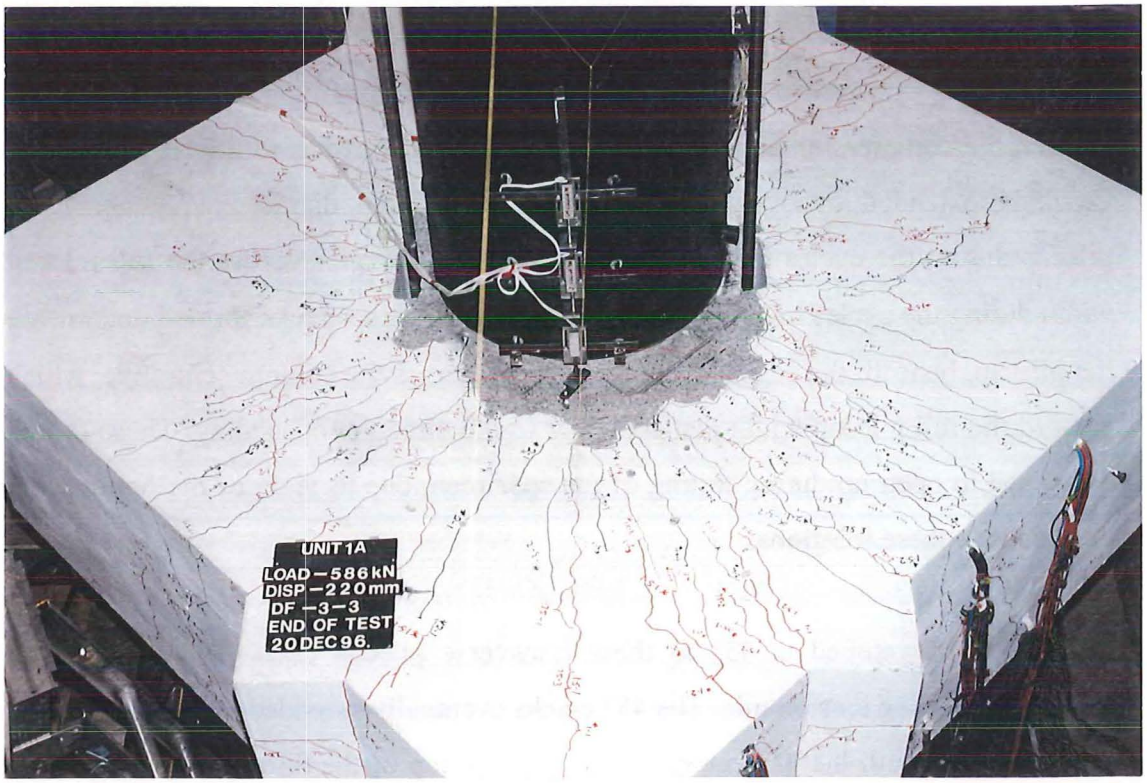

Figure 4.37 *Unit I-A Pilecap Overlay Crack Pattern at End of Test*

show the maximum recorded strain envelope for the pilecap bottom mat bars during the test against their position along the reinforcing bar.

The overlay mat remained elastic throughout the initial part of the test with maximum recorded strains in the order of 1400 με. Yielding did occur in some gauges after repair of the column at $\mu_{\Delta T} = 1.5$ ($\mu_{\Delta S} = 1.87$) and $\mu_{\Delta T} = 2.0$ ($\mu_{\Delta S} = 2.74$) again in the central region of the pilecap parallel with the direction of loading. Figures 4.40 and 4.41 show the maximum recorded strain envelope against the position of the strain gauges on the reinforcement for the pilecap overlay mat reinforcement. The location of the yielding overlay mat reinforcing bars coincides with locations of overlay dowels which yielded or showed high strains by the end of the test. The wedge pullout of concrete at the base of the column will have engaged some of the overlay dowel bars and the overlay mat bars leading to high strains recorded in some of the overlay retrofit reinforcement located close to the base of the column.

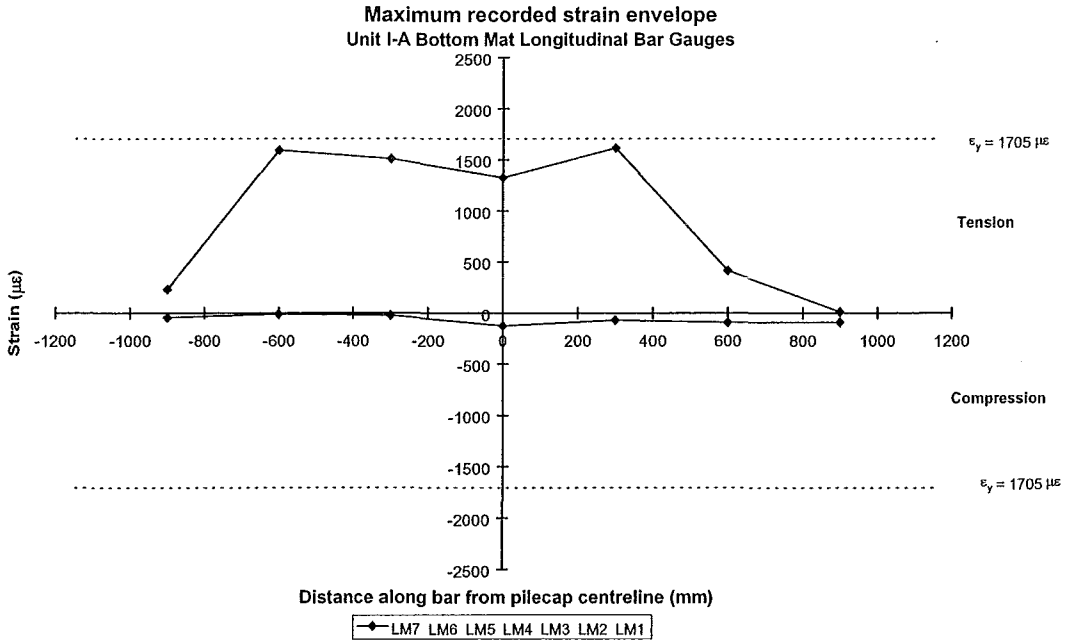

Figure 4.38(a) *Unit I-A Pilecap Longitudinal Bottom Mat Maximum Strain Envelope*

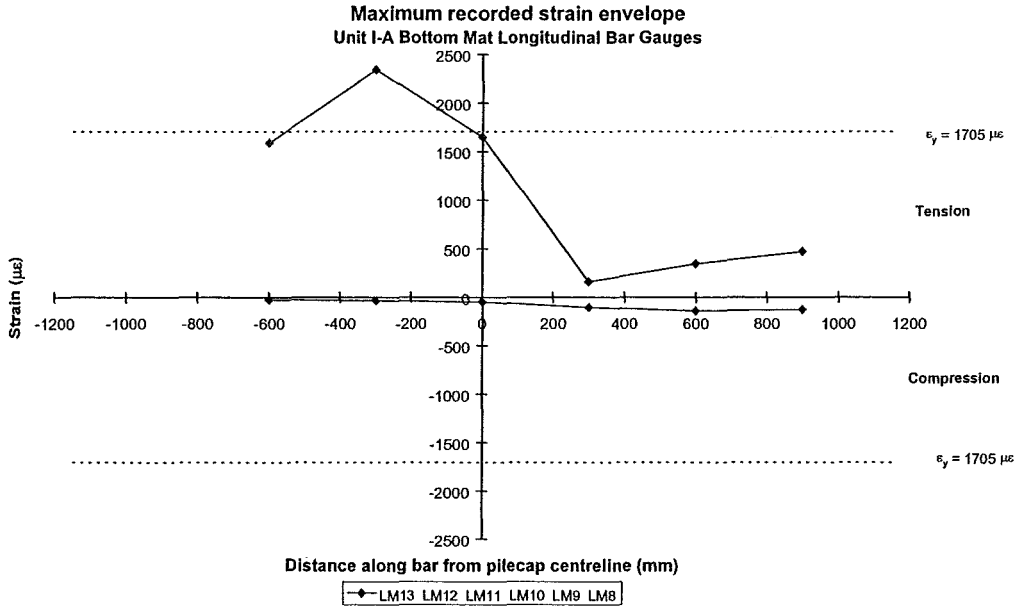

Figure 4.38(b) *Unit I-A Pilecap Longitudinal Bottom Mat Maximum Strain Envelope*

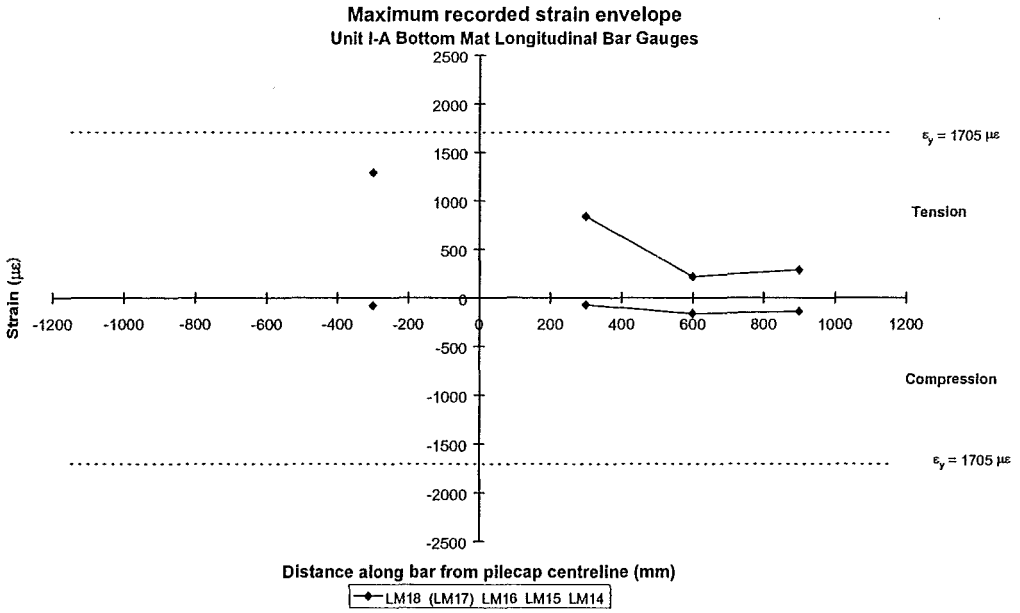

Figure 4.38(c) *Unit I-A Pilecap Longitudinal Bottom Mat Maximum Strain Envelope*

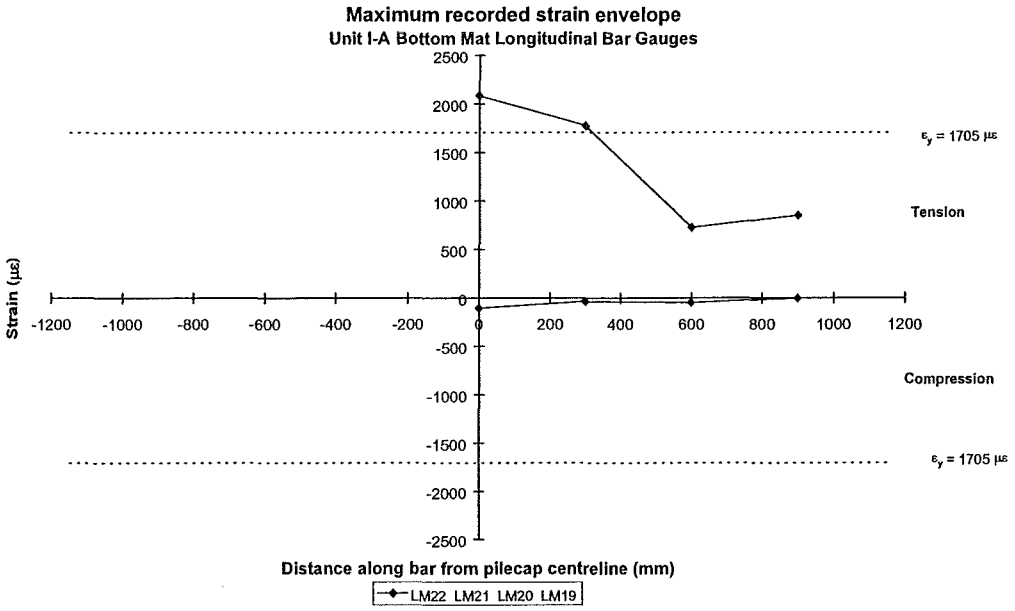

Figure 4.38(d) *Unit I-A Pilecap Longitudinal Bottom Mat Maximum Strain Envelope*

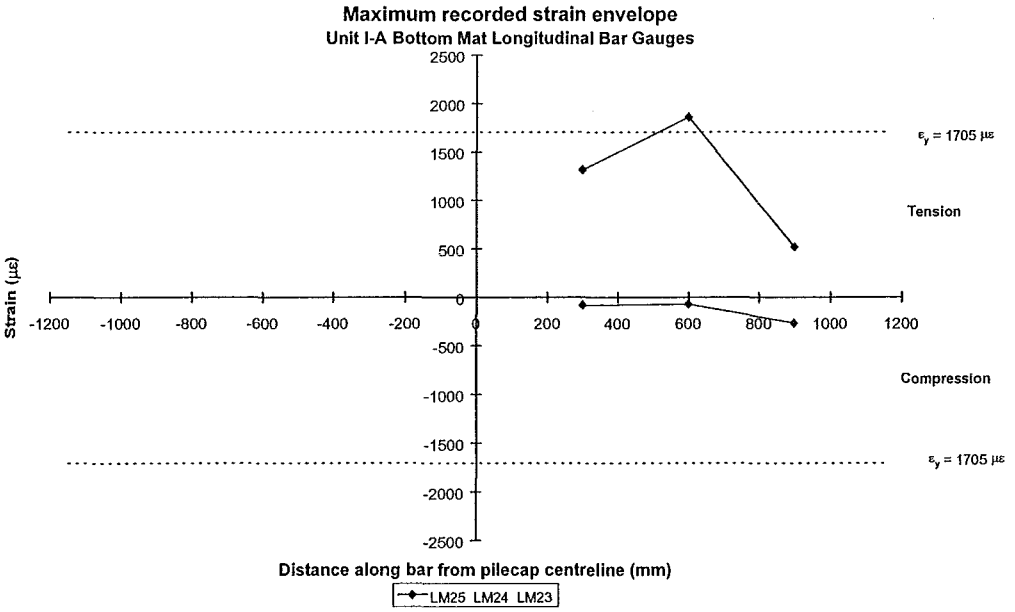

Figure 4.38(e) *Unit I-A Pilecap Longitudinal Bottom Mat Maximum Strain Envelope*

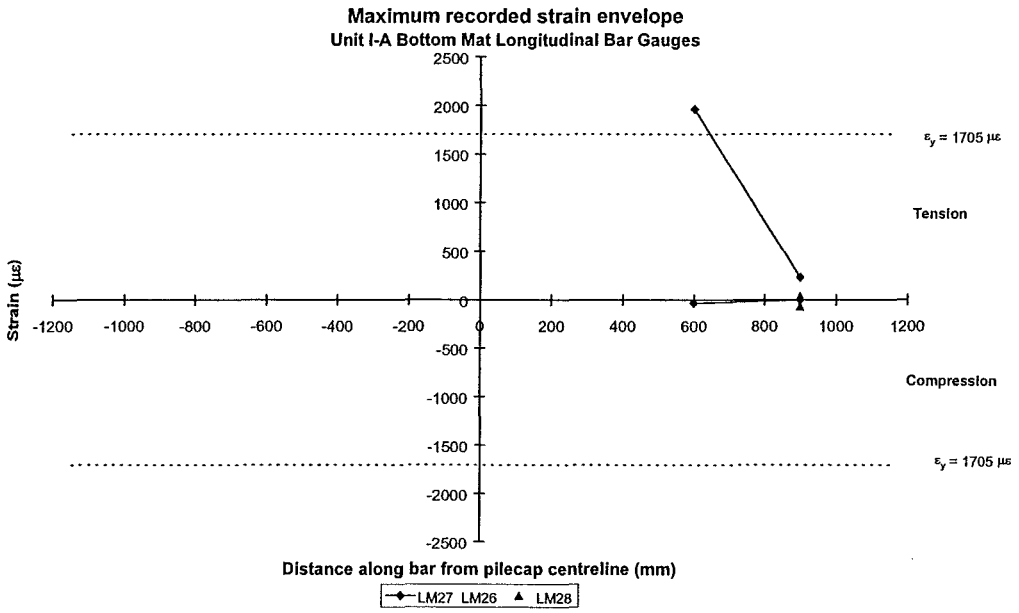

Figure 4.38(f) *Unit I-A Pilecap Longitudinal Bottom Mat Maximum Strain Envelope*

Figure 4.39(a) *Unit I-A Pilecap Transverse Bottom Mat Maximum Strain Envelope*

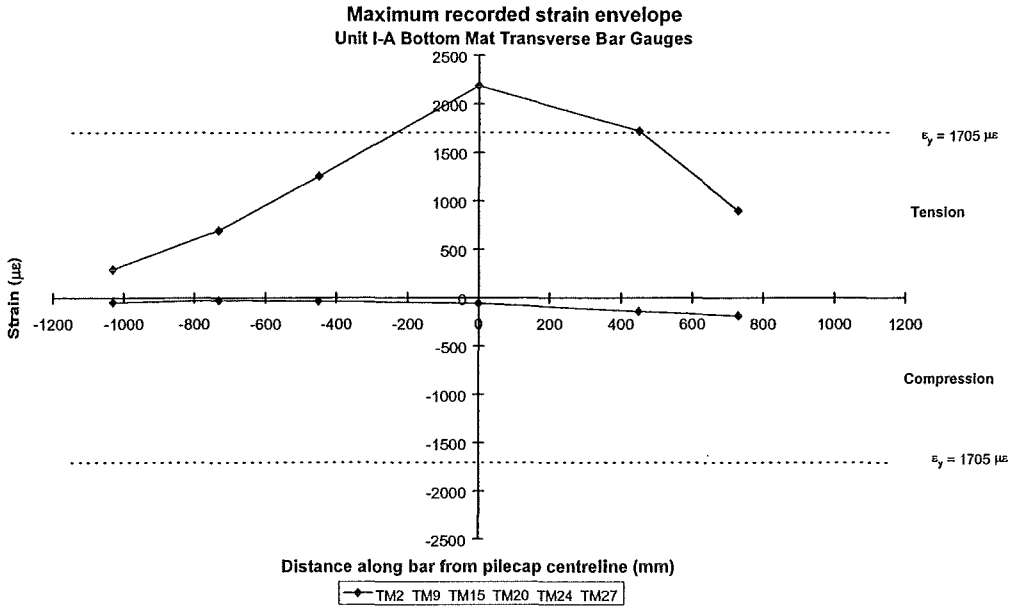

Figure 4.39(b) *Unit I-A Pilecap Transverse Bottom Mat Maximum Strain Envelope*

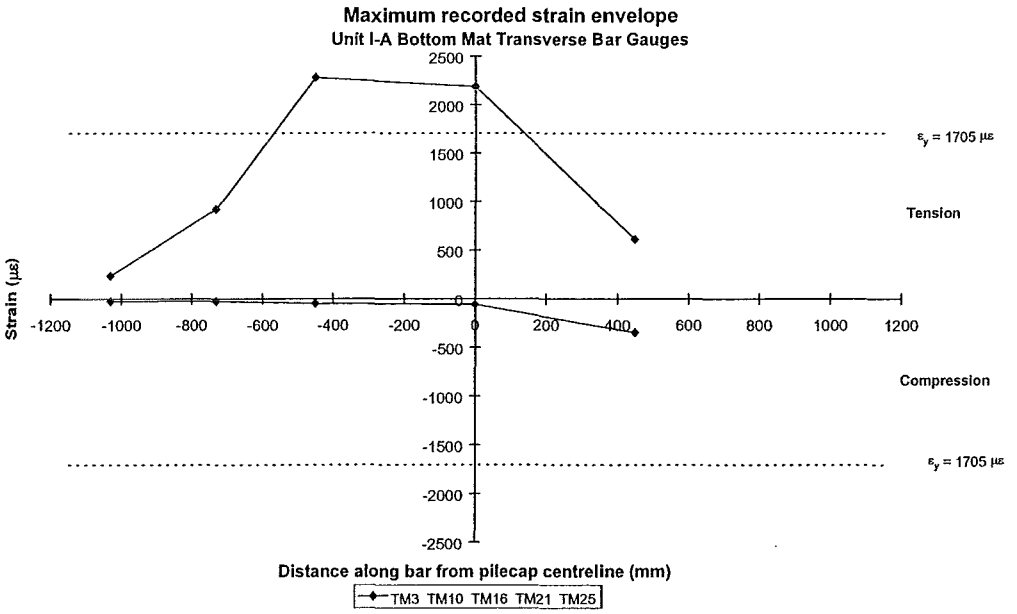

Figure 4.39(c) *Unit I-A Pilecap Transverse Bottom Mat Maximum Strain Envelope*

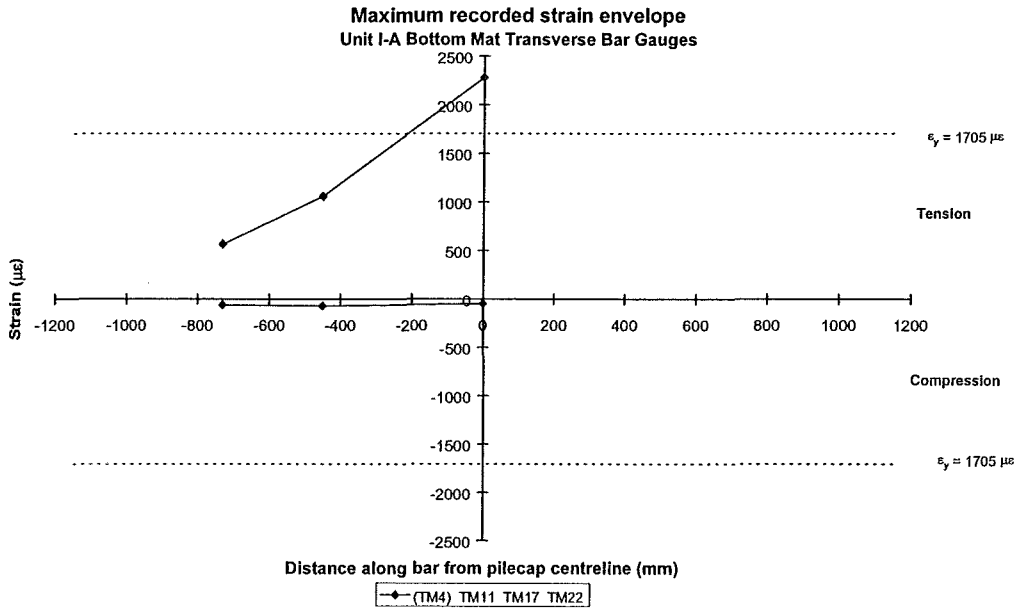

Figure 4.39(d) *Unit I-A Pilecap Transverse Bottom Mat Maximum Strain Envelope*

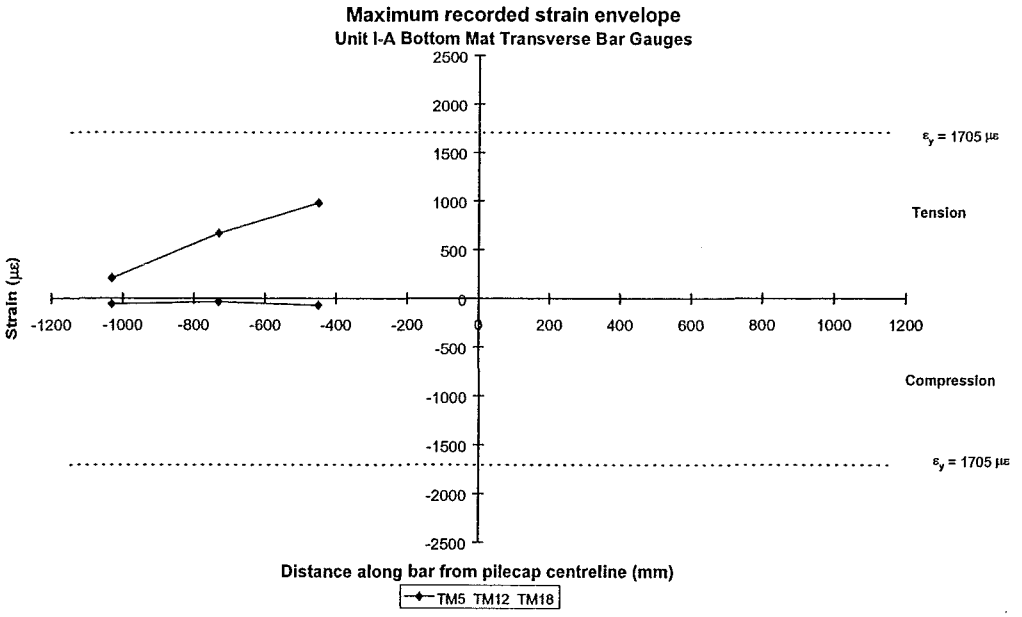

Figure 4.39(e) *Unit I-A Pilecap Transverse Bottom Mat Maximum Strain Envelope*

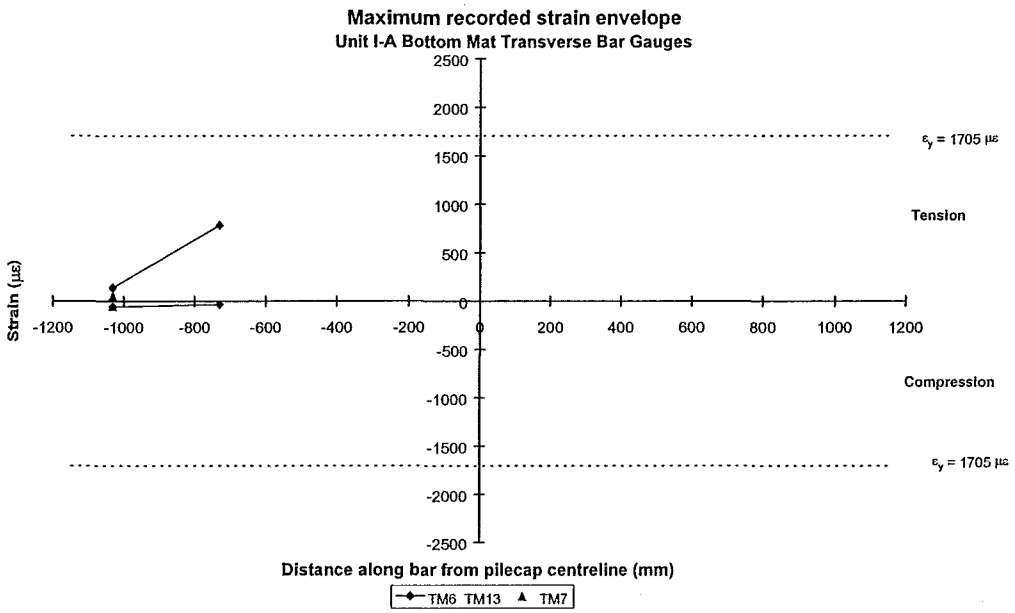

Figure 4.39(f) *Unit I-A Pilecap Transverse Bottom Mat Maximum Strain Envelope*

Other than the overlay dowels located at the base of the column, which yielded due to pullout of the column longitudinal bars engaging a wedge of concrete, the overlay mat reinforcement and all other dowels remained elastic throughout the test. Dowels located further away from the column showed lower maximum strains during the test. The longer pile dowels, placed at the location of each of the piles to overlap with the existing pile reinforcement, showed low strains throughout the test. This was also seen in the overlay dowels grouped around each pile location. Pile dowel bars at the outer piles show peak strains of around 700 με while the pile dowel bars at the central pile showed low strains throughout the test. This is despite evidence suggesting the pile reinforcement at the central piles had yielded during the final load cycles to $\mu_{\Delta T} = -3.0$ ($\mu_{\Delta S} = -4.48$). Observation at the location of the central piles showed the pile reinforcement, and the plate to which they were welded to, had pulled out of the pilecap by 1 - 2 mm yet no increase in pile dowel strains at this location was recorded.

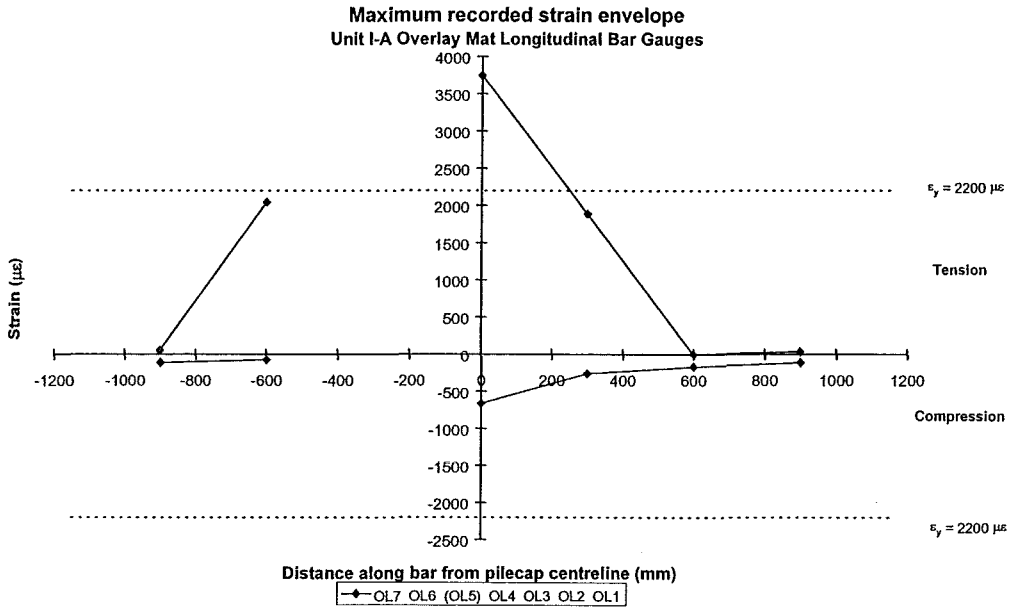

Figure 4.40(a) *Unit I-A Pilecap Overlay Mat Longitudinal Bar Maximum Strain Envelope*

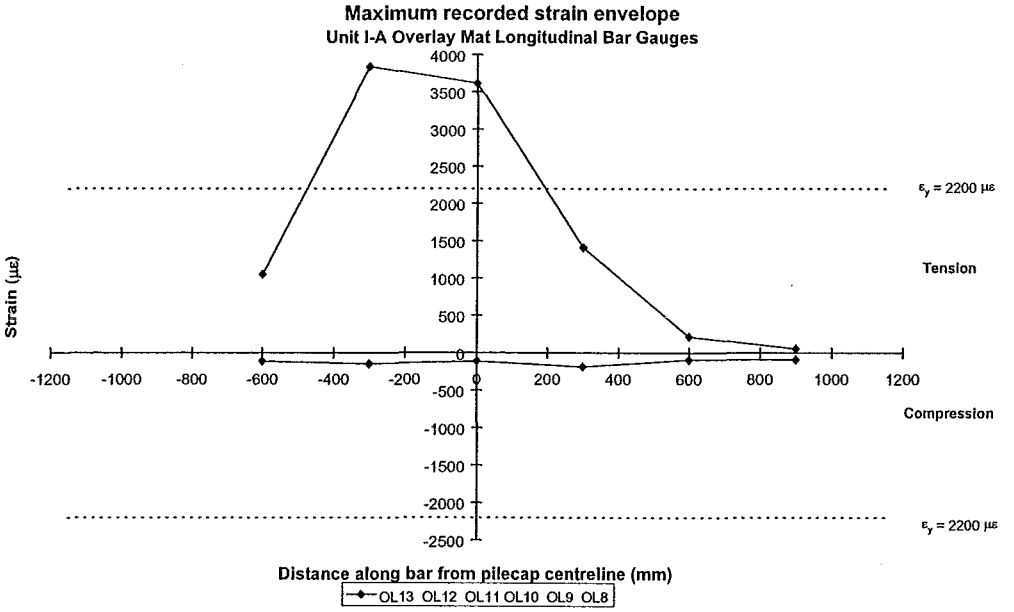

Figure 4.40(b) *Unit I-A Pilecap Overlay Mat Longitudinal Bar Maximum Strain Envelope*

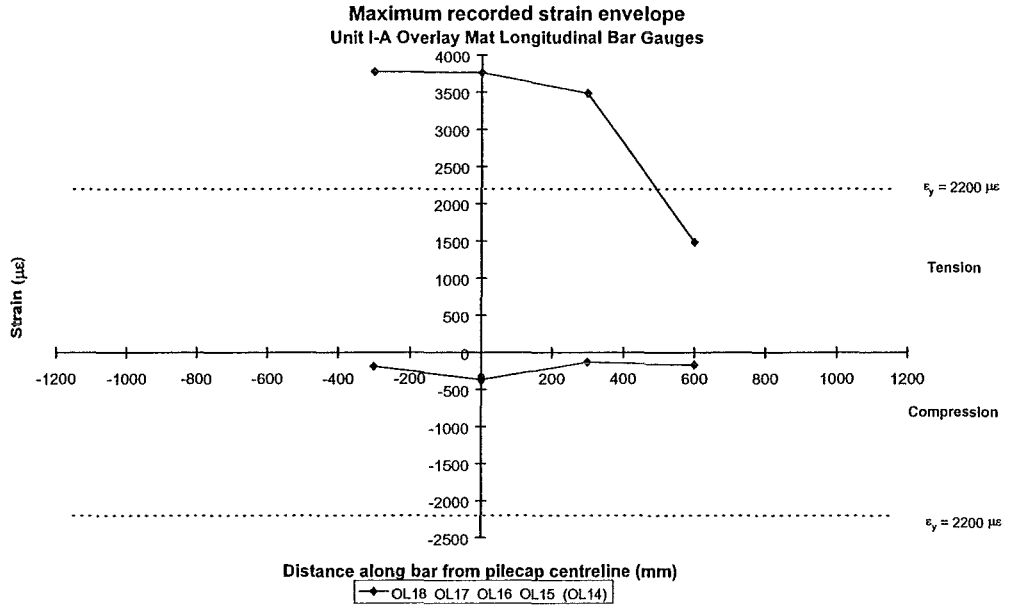

Figure 4.40(c) *Unit I-A Pilecap Overlay Mat Longitudinal Bar Maximum Strain Envelope*

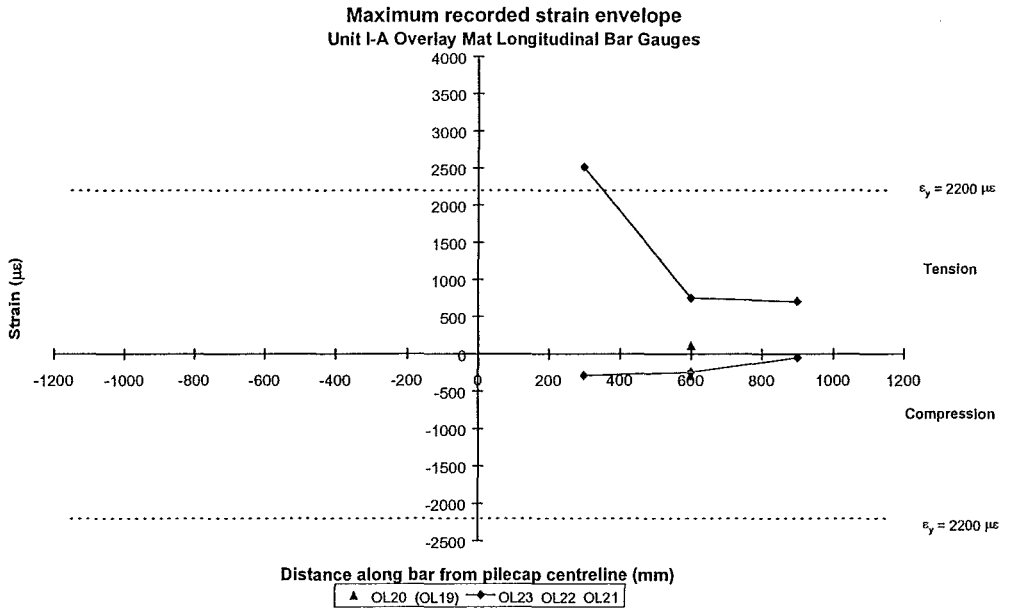

Figure 4.40(d) *Unit I-A Pilecap Overlay Mat Longitudinal Bar Maximum Strain Envelope*

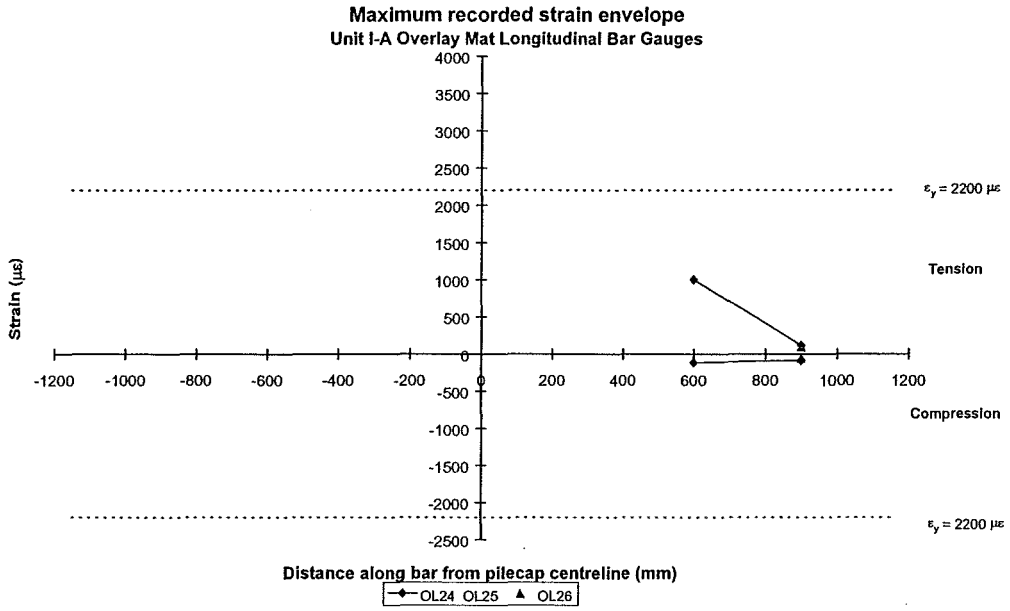

Figure 4.40(e) *Unit I-A Pilecap Overlay Mat Longitudinal Bar Maximum Strain Envelope*

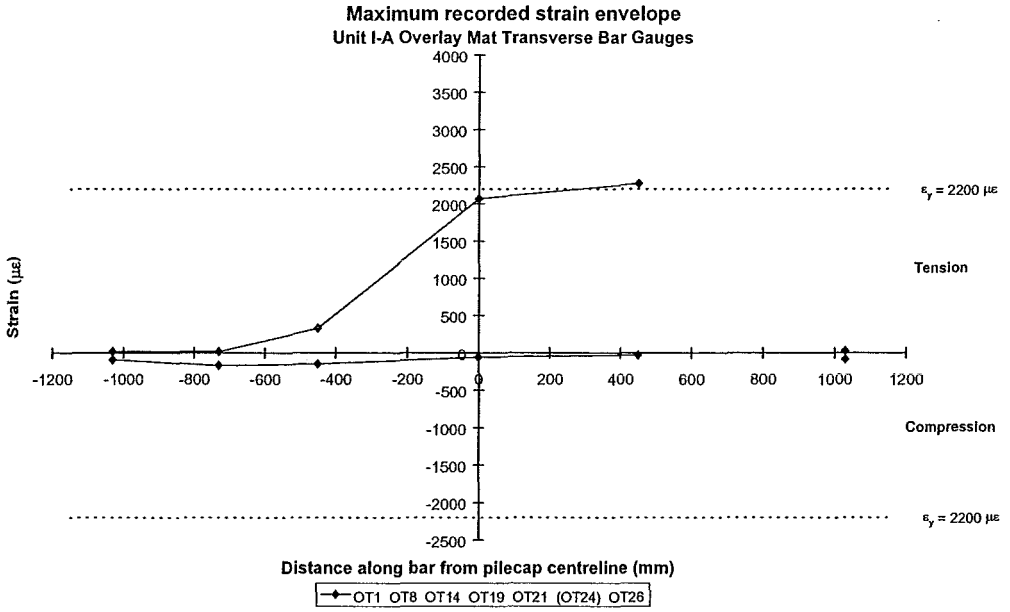

Figure 4.41(a) *Unit I-A Pilecap Overlay Mat Transverse Bar Maximum Strain Envelope*

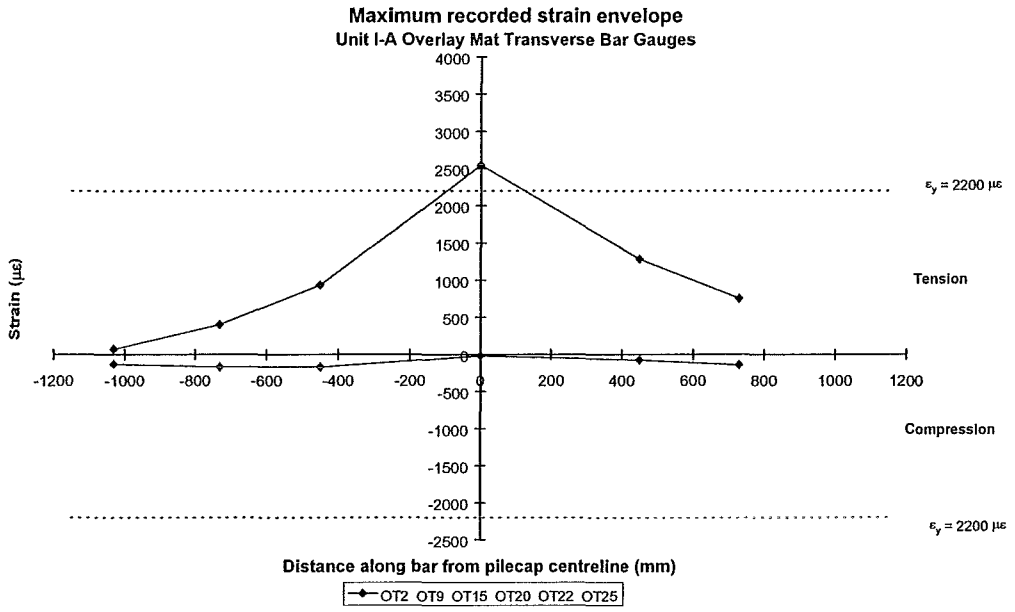

Figure 4.41(b) *Unit I-A Pilecap Overlay Mat Transverse Bar Maximum Strain Envelope*

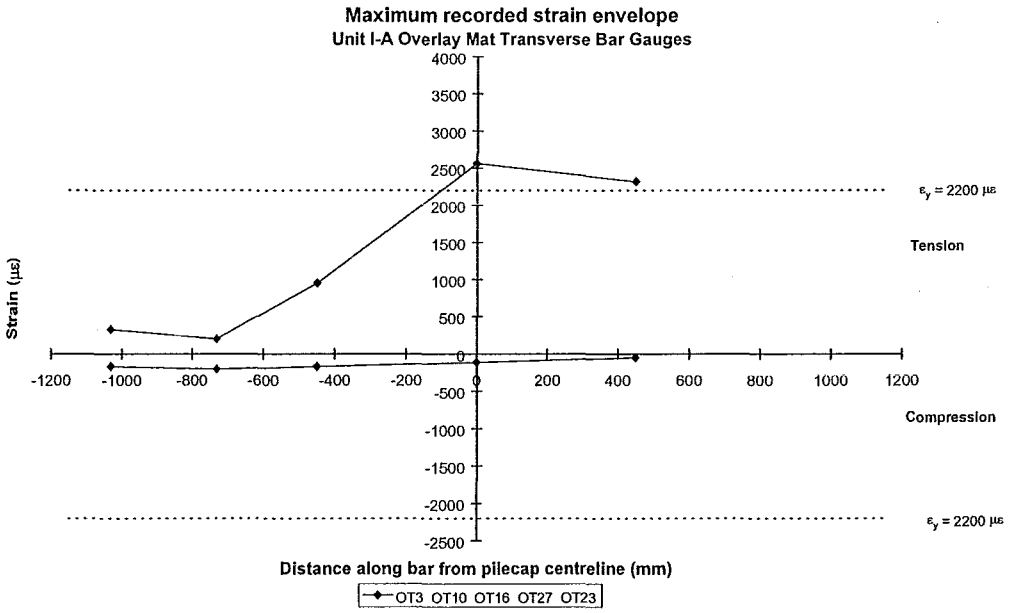

Figure 4.41(c) *Unit I-A Pilecap Overlay Mat Transverse Bar Maximum Strain Envelope*

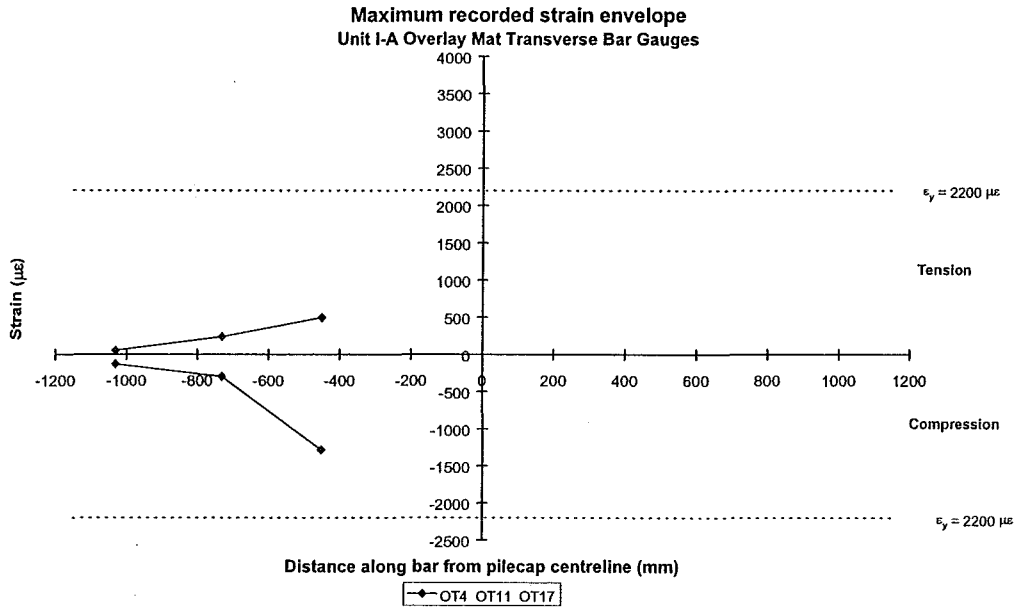

Figure 4.41(d) *Unit I-A Pilecap Overlay Mat Transverse Bar Maximum Strain Envelope*

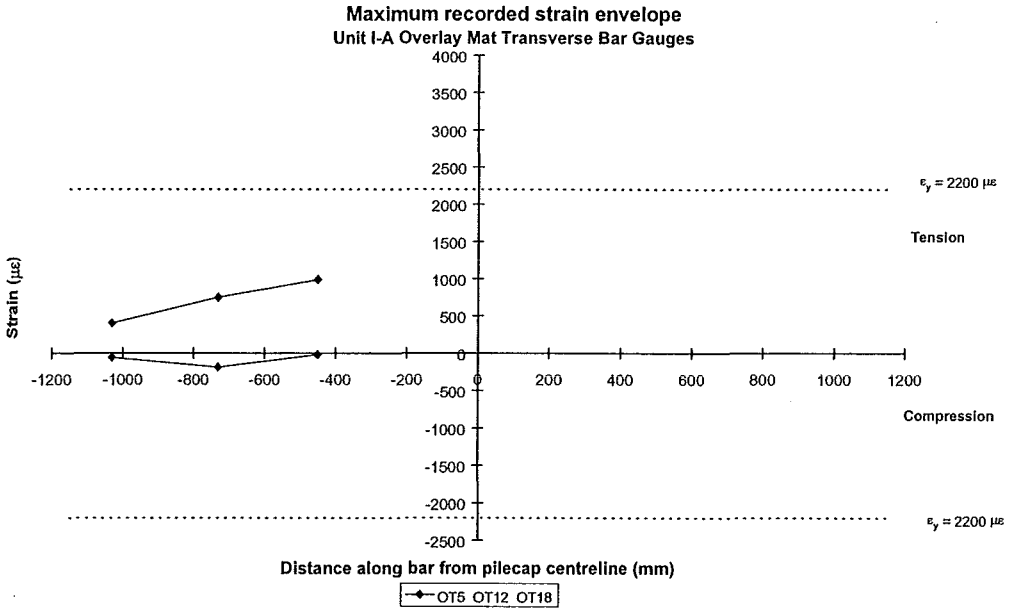

Figure 4.41(e) *Unit I-A Pilecap Overlay Mat Transverse Bar Maximum Strain Envelope*

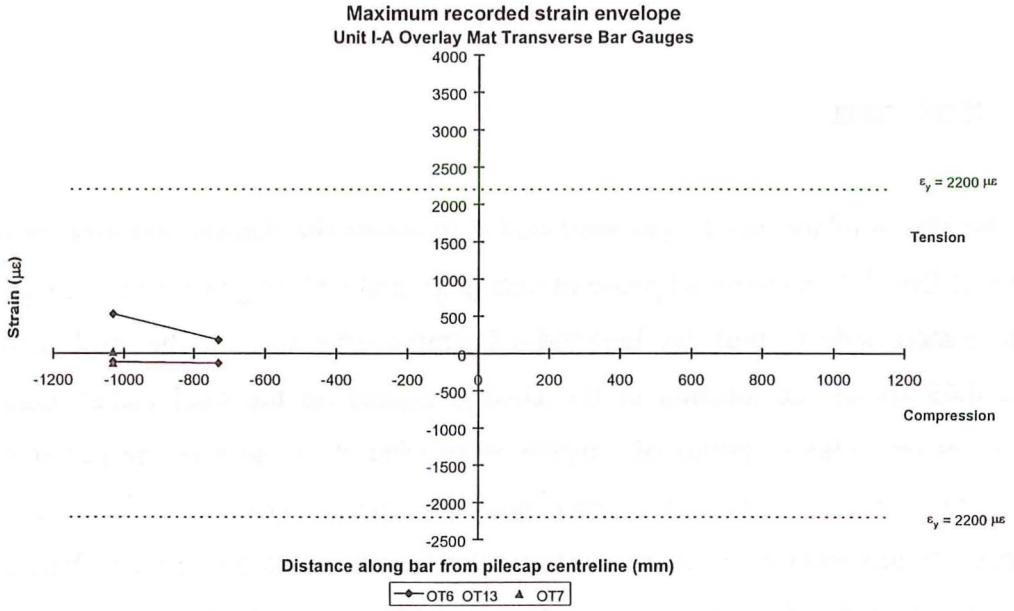

Figure 4.41(f) *Unit I-A Pilecap Overlay Mat Transverse Bar Maximum Strain Envelope*

Figure 4.42 *Unit I-A Pilecap Overlay Surface After Demolition of Column*

Figure 4.42 shows the pilecap of Unit I-A and the final crack pattern developed in the overlay surface after demolition of the column at the end of the test.

4.8.7 Steel Jacket

With the fitting of the full height steel jacket to repair the damage suffered in the column of Unit I-A in the initial phase of testing several DEMEC gauges were installed on the eastern side to measure longitudinal strains developed in the steel jacket. Figure 4.43 shows the location of the DEMEC gauges on the steel jacket. Gauge lengths between DEMEC points of 4 inches were used at the base of the jacket and 8 inches were used, centred around the curtailment points higher in the column. The maximum strains recorded at the peak of each load cycle are plotted midway between the positions of the DEMEC gauges in Figure 4.44 to give the longitudinal strain profile developed over the height of the column.

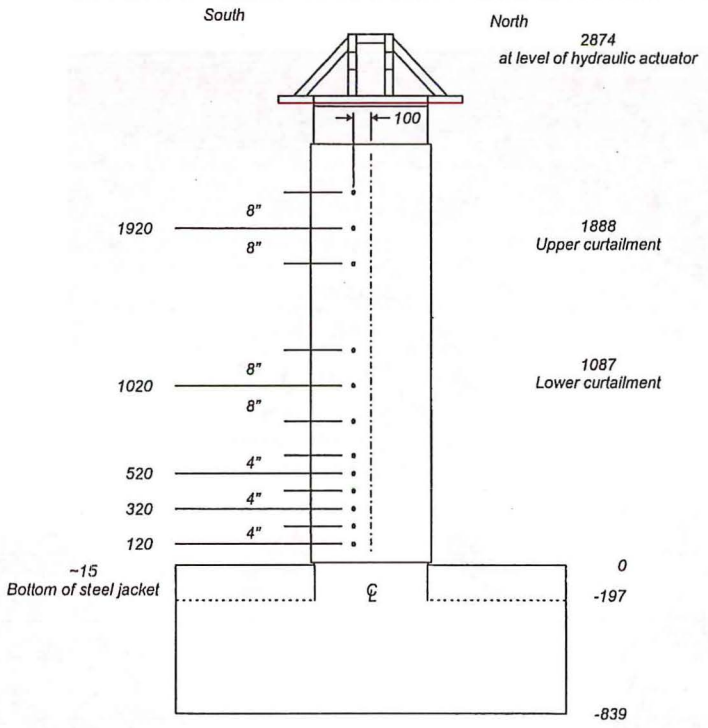

Figure 4.43 *Position of DEMEC Gauges on Steel Jacket of Repaired Unit I-A*

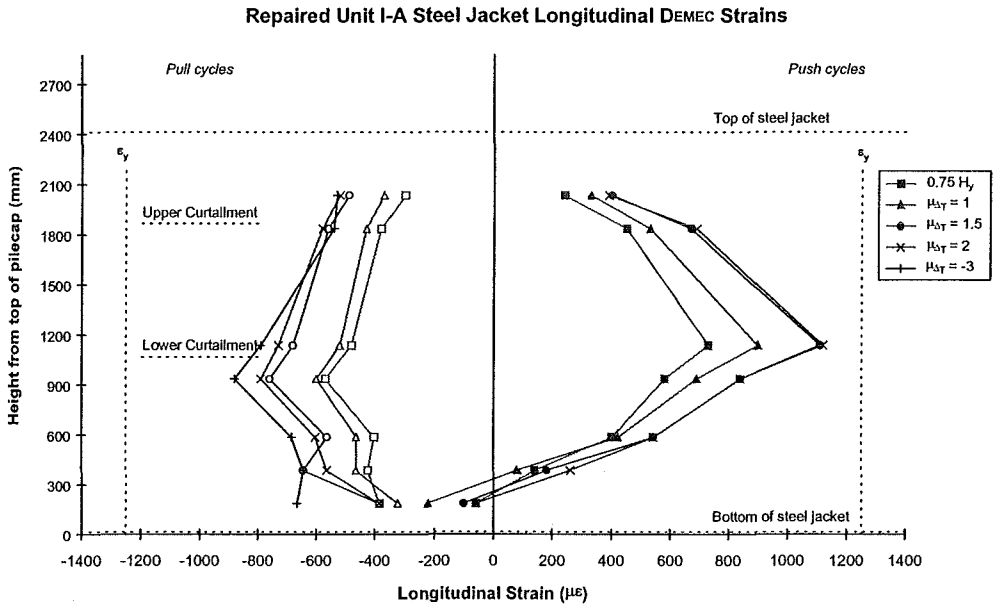

Figure 4.44 *Longitudinal Strain Profiles in Steel Jacket of Repaired Unit I-A*

Maximum strains developed in the steel jacket by the end of the test on Unit I-A remained less than the yield strain of the steel. When loaded in the Push direction the DEMEC gauges record tensile longitudinal strains in the steel jacket which peak around the lower curtailment point. This indicates the steel jacket is acting to provide additional longitudinal reinforcement at the lower curtailment point making up for the flexural strength shortfall at this point and at the upper curtailment point due to the premature curtailment of the column longitudinal reinforcement. Longitudinal strain profiles from the Pull cycles show a more uniform strain profile over the column height with a smaller peak in strains seen at the lower curtailment point.

Assessment of Unit I-A, described in Section 4.5.4, after failure of the column at the upper curtailment point, shows that the flexural strength of the upper and lower curtailment points would have been reached due to the tension shift effect when the base of the column developed its flexural strength. The lower peak longitudinal strains seen in the steel jacket at the upper curtailment point may be due to there being insufficient length of jacket above the curtailment point to provide adequate bond transfer between the column and the jacket. The steel jacket is also providing

additional transverse reinforcement to the column acting as both additional shear reinforcement and as confining reinforcement enhancing the available curvature ductility of the column.

Removal of the steel jacket after completion of the test showed no signs of diagonal cracking around the curtailment points showing the jacket was successful in confining the column and preventing any form of shear failure around the curtailment points. Provision of the steel jacket enabled the column to achieve the flexural strength at the base of the column and develop a large lateral load overstrength by preventing failure at the curtailment points. Some cracking at the base of the column was apparent due to the concentration of plastic hinging at this point.

4.9 RECOMMENDATIONS FROM TESTING OF UNIT I-A

The simulated seismic load testing of Unit I-A showed that this test specimen was able to sustain a structural displacement ductility of $\mu_{\Delta T} = 1.5$. The expected structural displacement ductility demand expected to arise in Pier 68 from a 500 year return period earthquake at the Thorndon Overbridge site is $\mu_{\Delta} = 1.78$. The structural displacement ductility sustained in Unit I-A is equivalent to a structural displacement ductility of $\mu_{\Delta S} = 1.87$.

At this level of ductility the column showed extensive diagonal cracking over the full height of the column concentrated around the upper and lower curtailment points. Cracking at the base of the column remained essentially horizontal and the test specimen was maintaining its lateral load carrying capacity. Performance of the retrofitted pilecap showed that no significant inelastic action took place in the pilecap, as was expected from the assesment of Pier 68. All inelastic action, up to this stage of loading, was limited to the column at the upper and lower curtailment points.

A further load cycle was attempted to $\mu_{\Delta T} = 2.0$ ($\mu_{\Delta S} = 2.74$) where buckling of the column longitudinal reinforcement and spalling of the cover concrete at the upper curtailment point led to a degradation of the load carrying capacity of the test specimen.

A theoretical analysis, using moment-curvature analysis and assessment of the available shear resistance of the column, was used to show that a shear failure in the column around the curtailment points was predicted when the base of the column developed its flexural strength. Accounting for the tension shift effect also showed that the flexural strength of the upper and lower curtailment points would be reached once the base of the column developed its flexural strength.

Observation of the damage sustained by the rest of the test specimen showed very minor cracking in the pilecap and pilecap overlay retrofit. Inelastic action had been limited to the upper regions of the column where the longitudinal reinforcement had been curtailed.

As the test specimen showed considerable damage to the column, a potentially brittle mode of failure and little ductility reserve over the expected ductility demand, the test specimen was repaired and the test was continued to observe the performance of the repaired column, the pilecap and other retrofit measures. Repair of the column involved fitting of a new 3 mm thick steel jacket, 2.40 m tall around the existing column and epoxy injection of the column cracks.

Placement of a new steel jacket on the existing column was successful in allowing the test specimen to develop the flexural strength of the base of the column, preventing failure of the column around the two curtailment points, enhancing the available structural displacement ductility and developing a large lateral load overstrength. The extension limits of the hydraulic actuator used to apply the lateral loads to the top of the column of Unit I-A prevented testing continuing until failure of the test specimen. Three load cycles to displacement ductilities of $\mu_{\Delta T} = +2.0$ ($\mu_{\Delta S} = +2.74$) and approximately $\mu_{\Delta T} = -3.0$ ($\mu_{\Delta S} = -4.48$) were completed without failure of the specimen.

The retrofitted pilecap showed excellent behaviour, transferring the forces from the repaired column, with limited cracking of the pilecap and pilecap overlay. Comparison of the expected pilecap bending moments from the BCHF structural

analysis of Pier 68 showed a good match with the bending moment distribution achieved during the testing of Unit I-A. Yielding of some of the pilecap bottom mat bars allowed the development of cracks underneath the pilecap, 2 - 3 mm wide by the end of the test. Yielding of some pilecap overlay retrofit mat bars occurred after repair of the column was completed along with development of high strains or yielding of pilecap overlay dowel bars at the same location. Some pilecap overlay reinforcement, around the base of the column, yielded through the pilecap overlay mat engaging the overlay dowels with the pullout of the column longitudinal bars. Pilecap overlay dowels further from the column generally exhibited lower strains, remaining well within the elastic range. Pile dowel bars, provided to transfer the pile tension force to the top of the pilecap overlay, remained elastic throughout the entire test. This was despite observations indicating that the pile reinforcement at the central piles had yielded during the final load cycles and had pulled out of the bottom of the pilecap.

The detailing of Pier 68 and of Unit I-A with the column longitudinal bars curtailed closely following the elastic bending moment diagram, without regard for the tension shift and adequate anchorage length beyond the critical section, allowed the flexural strength of the upper and lower curtailment points to be reached when the base of the column developed its flexural strength. Provision of the pilecap overlay retrofit, to strengthen the pilecap and force inelastic action to occur at the base of the column, shortened the column and increased the chances of the flexural strengths of the curtailment points being reached.

The much reduced lever arm between the upper curtailment point and the top of the column placed large curvature demands on the column at this point leading to buckling of the column longitudinal reinforcement and spalling of the cover concrete at this location.

Fitting of the full height steel jacket to the column of Unit I-A prevented any failure of the column around the curtailment points and increased the available structural ductility of the specimen. This indicates that the use of a full height steel jacket on Pier 68 should prevent the observed failure of the column at the curtailment points seen in Unit I-A. The steel jacket is able to act as additional longitudinal reinforcement in the column, increasing the flexural strength of the column at the

curtailment points, and providing additional transverse reinforcement to provide confinement and act as shear reinforcement in the column. Provision of a full height steel jacket to Pier 68 should provide adequate ductility reserve to meet the expected structural ductility demands on this pier.

The other retrofit measures namely the pilecap overlay were capable of ensuring inelastic action would occur at the base of the column, after fitting of the full height steel jacket, resisting the imposed forces from these actions with only limited yielding of some of the pilecap and pilecap overlay reinforcement.

CHAPTER 5

LINKAGE BOLT TESTS

5.1 LINKAGE BOLT TENSILE TESTS

5.1.1 Results From Tensile Tests

Linkage bolts from a Stage Two pier and a Stage Three pier were removed from the Thorndon Overbridge for testing. A single $1\ ^1/_8$ inch (29 mm) diameter linkage bolt was removed from Pier 12 and a single $1\ ^1/_2$ inch (38 mm) diameter linkage bolt was removed from Pier 23 and shipped to the University of Canterbury for tensile testing. Each linkage bolt was cut to approximately 4 m in length and included both of the welded end details.

Monotonic tensile tests were conducted up to fracture of the linkage bolts to determine the upper and lower yield points, the ultimate tensile strength and available uniform elongation of each bolt. Force-elongation plots were obtained for each bolt tested.

The linkage bolts were plain round mild steel rods specified to NZSS 197 in the original contract documents. This specification gives $f_y = 276$ MPa and $f_u = 410$ to 510 MPa. The welded end details were removed from each linkage bolt and test specimens cut to approximately 1.6 m in length. Each specimen was gripped using standard jaws for testing in the 1000 kN Avery UTM. Elongation of the specimens were measured using a rotary encoder device attached to the bolt over a 750 mm gauge length. Outputs from the Avery UTM and the rotary encoder were recorded on an X-Y plotter to give force-elongation plots for each specimen.

Table 5.1 shows the results from testing of the $1\ ^1/_8$ inch diameter linkage bolts removed from Pier 12. Figure 5.1 shows the force-elongation plots obtained from these tensile tests.

Table 5.1 *1 1/8 inch Diameter Linkage Bolt Tensile Test Results*

	Yield		Ultimate		ε_{sh}		ε_u	
	kN	MPa	kN	MPa	mm	%	mm	%
Bar 1	188	293	300	467	11.25	1.50	86	11.4
Bar 2	193	300	306	477	11.25	1.50	145	19.3

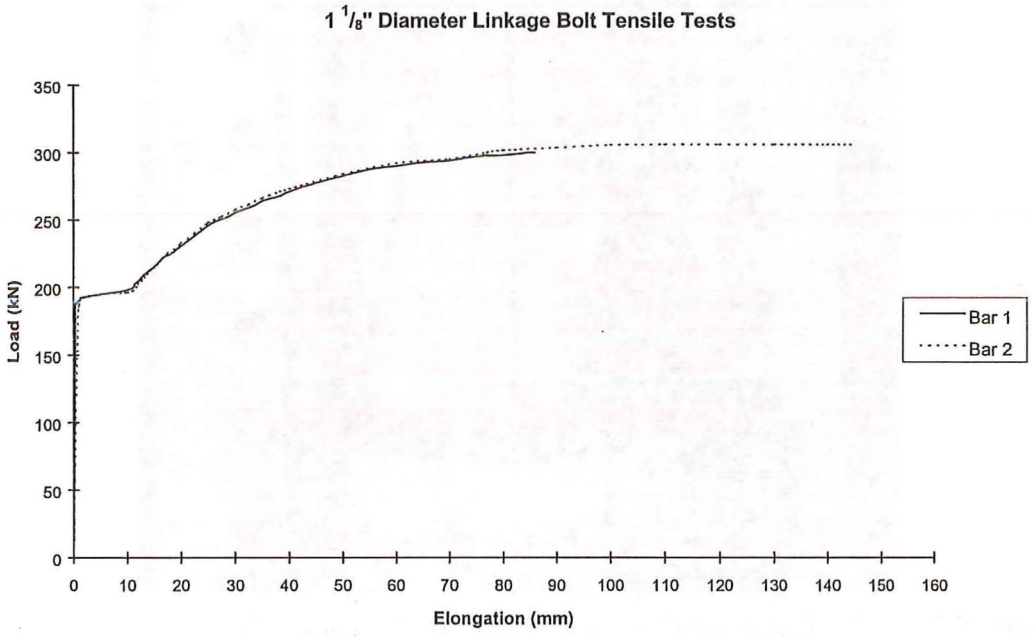

Figure 5.1 *Force-Elongation Plots for 1 1/8 inch Diameter Linkage Bolt Tensile Tests*

Bar 1 contained a region of corrosion and noticeable pitting within the gauge length. This corrosion reduced the cross sectional area of the bar and had a marked effect on the available total elongation of the bar. Eventual necking and fracture took place through the corroded region. No noticeable corrosion was noticed on Bar 2. Figure 5.2 shows Bar 1 in the Avery UTM showing the rotary encoder setup for measuring the specimen elongation and the corroded region on the bar.

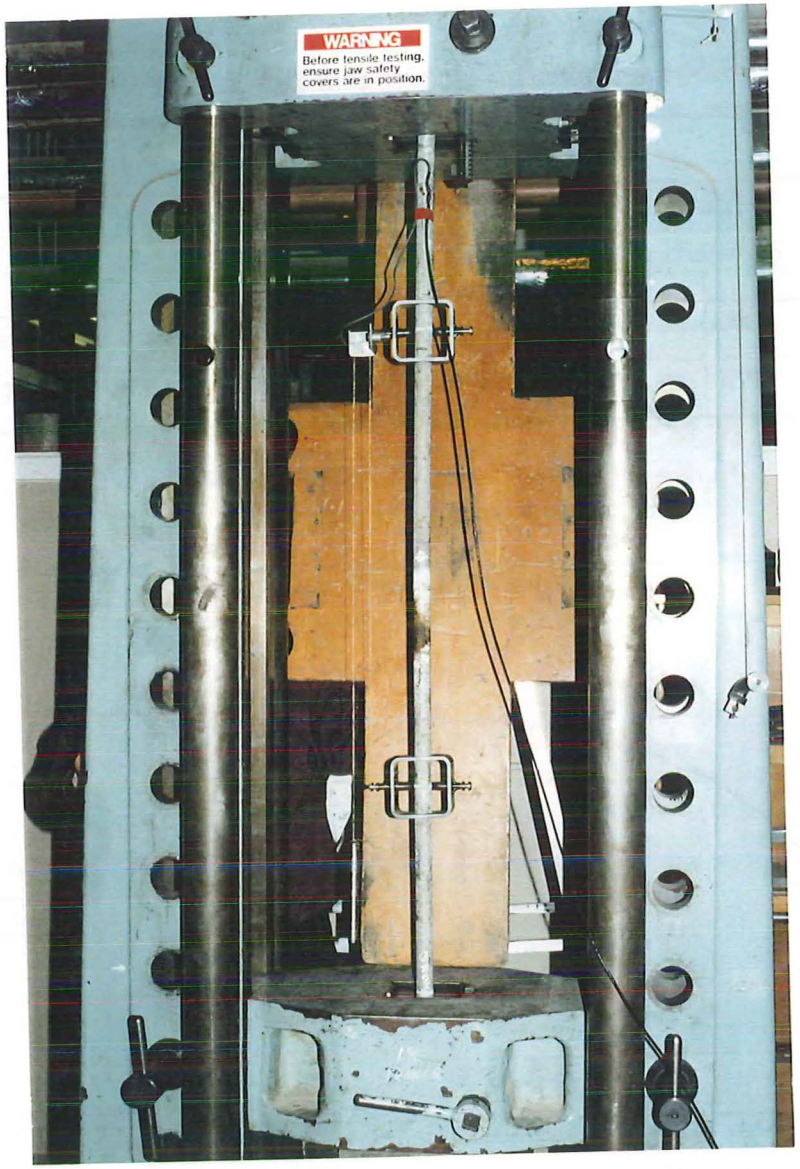

Figure 5.2 *Bar 1 showing Corroded Region Within Gauge Length*

Table 5.2 shows the tensile test results for the $1\,{}^{1}/_{2}$ inch diameter linkage bolts. Figure 5.3 shows the force-elongation plots for each bar tested.

Table 5.2 *1 1/2 inch Diameter Linkage Bolt Tensile Test Results*

	Yield		Ultimate		ε_{sh}		ε_u	
	kN	MPa	kN	MPa	mm	%	mm	%
Bar 3	318	279	527	462	11.0	1.47	140	18.7
Bar 4	324	284	526	461	12.0	1.60	135	18.0
Bar 5	332	291	538	472	11.0	1.47	140	18.7

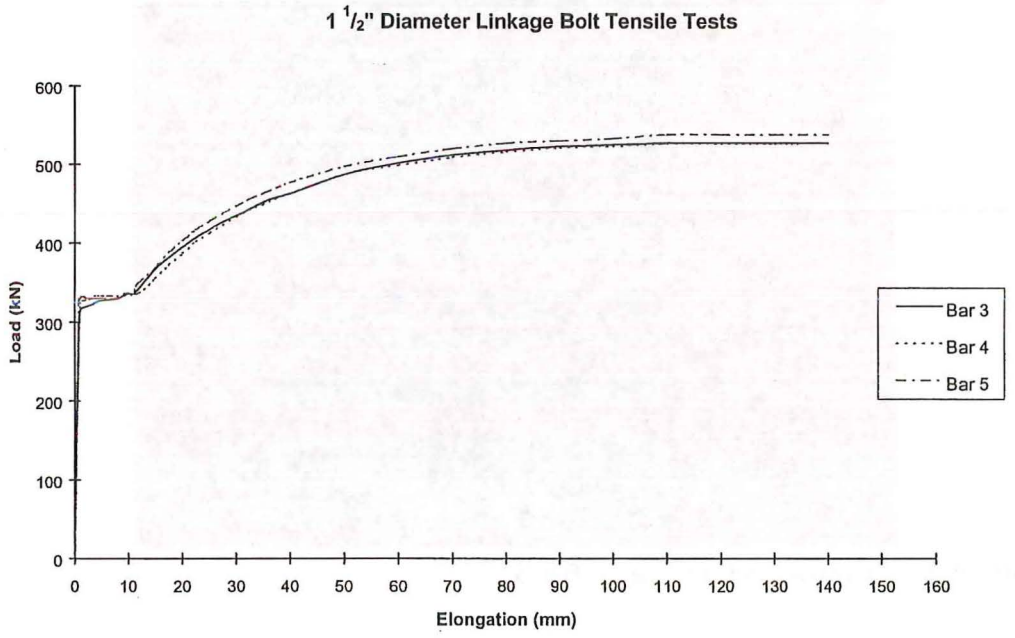

Figure 5.3 *Force-Elongation Plots for 1 1/2 inch Diameter Linkage Bolt Tensile Tests*

Bar 3 and Bar 4 contained no corrosion or visible damage within their length. Bar 5 contained a small region of corrosion on the bar and some pitting reducing the cross-sectional area of the bar. This reduction in bar area appeared to have no effect on the available elongation capacity of this bar despite necking and fracture of the bar occurring at this position. Figure 5.4 shows the corrosion damage on Bar 5 before testing of this specimen.

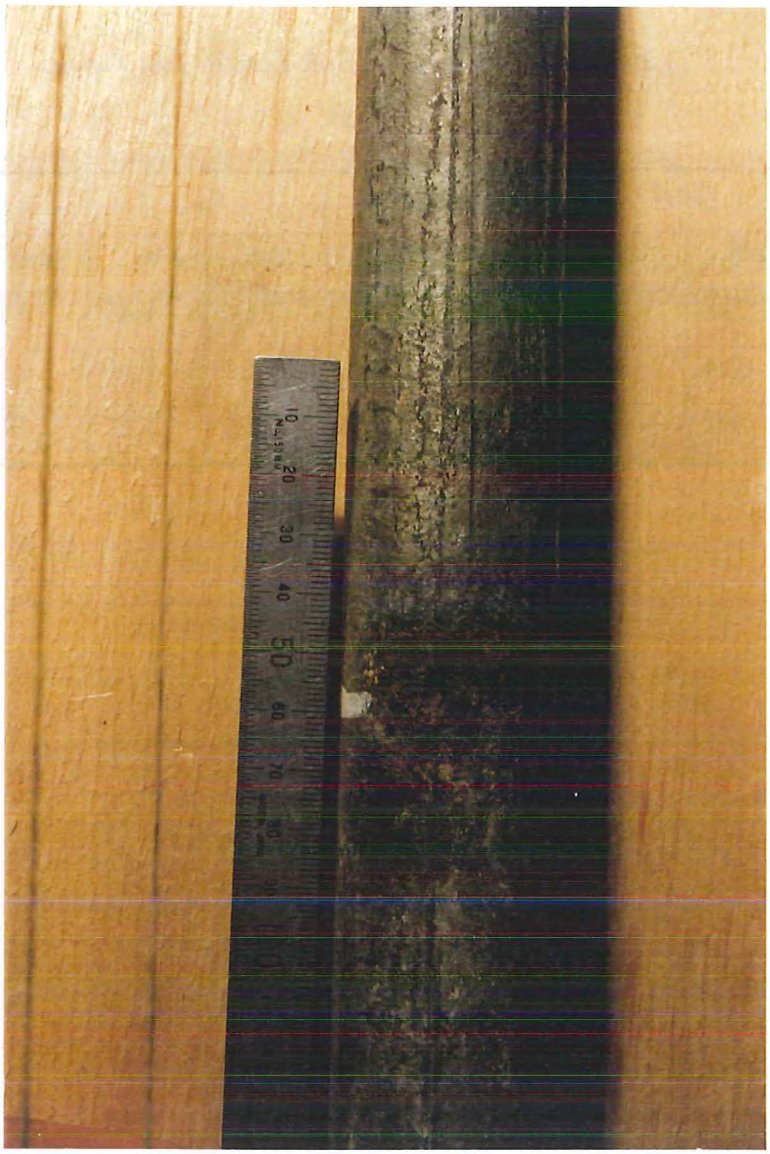

Figure 5.4 Corrosion Damage on Bar 5

5.1.2 Observed Corrosion Damage to Linkage Bolts

Each of the linkage bolts supplied for tensile testing contained a region of corrosion toward the ends of the bolts. For the 1 $^{1}/_{8}$ inch (29 mm) diameter bolts the region of corrosion appears approximately 1.2 m from the welded end details. The galvanised coating on the bar appears to have been rubbed off the bolts with corrosion and pitting of the steel taking place as a result. The distance from the welded end details appears to be where the linkage bolt passes through the gap between the I-beam end diaphragm and the umbrella platform. It was noted that one end of the 1 $^{1}/_{8}$ inch diameter bolts had a bituminous type material around the region of corrosion,

possibly the material used to fill the space between the umbrella platform and the I-beam end diaphragm.

The 1 $^{1}/_{2}$ inch (38 mm) diameter linkage bolts also showed a small region of corrosion approximately 1.5 m from the welded end detail. Again this appears to be the position where the linkage bolt passes from the I-beam end diaphragm and the umbrella platform.

Figure 5.5 shows the layout of the linkage bolts at an umbrella platform and the position where it is believed the corrosion of the linkage bolts is occurring. The linkage bolts are contained in steel tubes where they pass through the I-beam end diaphragm and where they enter the umbrella platform. Whether this steel tube is continuous where the top set of linkage bolts pass from the umbrella platform and the I-beam end diaphragm cannot be ascertained from the original construction drawings. With the corrosion damage on these linkage bolts corresponding so closely to this position it could be assumed that the bolt is exposed at this location.

The lower set of linkage bolts are also exposed over an approximately 375 mm length where they pass from the I-beam end diaphragm and the umbrella platform.

With these linkage bolts being exposed to the environment some corrosion of these bolts at the point where they enter the steel tube through the umbrella platform may have occurred.

Figure 5.6 shows the corroded region of the 1 $^{1}/_{8}$ inch and 1 $^{1}/_{2}$ inch diameter linkage bolts and the approximate distance from the welded end details for each bolt.

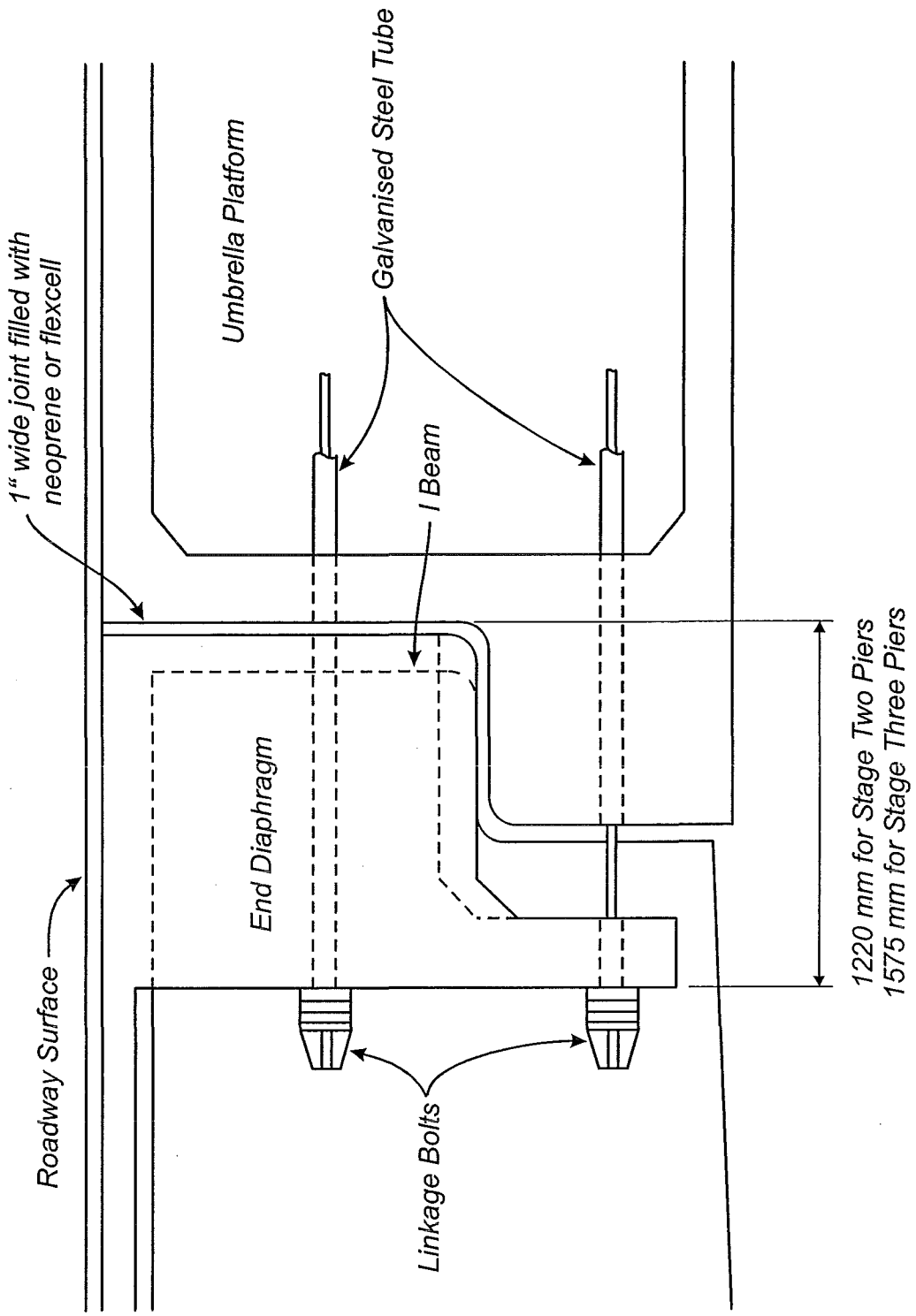

Figure 5.5 *Linkage Bolt Detail at I-Beam End Diaphragm and Umbrella Platform*

5.1.3 Influence of Cross Section Reduction on Available Uniform Elongation

The presence of corrosion on the linkage bolts can have a significant effect on the available uniform elongation capacity of the linkage bolt. The reduction in cross section due to the corrosion and pitting on the 1 $^{1}/_{8}$ inch (29 mm) diameter linkage bolt reduced the uniform elongation capacity of the bar from 19.3 % to 11.4 %. The yield and ultimate strengths for Bar 1 given in Table 5.1 are based on the nominal cross-sectional area of a 1 $^{1}/_{8}$ inch diameter bar. Bar 2, which was cut from the same linkage bolt as Bar 1, allows an estimation of the amount of reduction in cross-sectional area that has occurred in Bar 1 and the influence this reduction in bar area has on the elongation capacity of the linkage bolt.

From a bar of cross-sectional area, A, length, L, and containing a section of bar with a reduced cross-sectional area, βA, of length, αL, the influence of the reduced cross section can be analytically established (Figure 5.7). It is assumed that the reduced

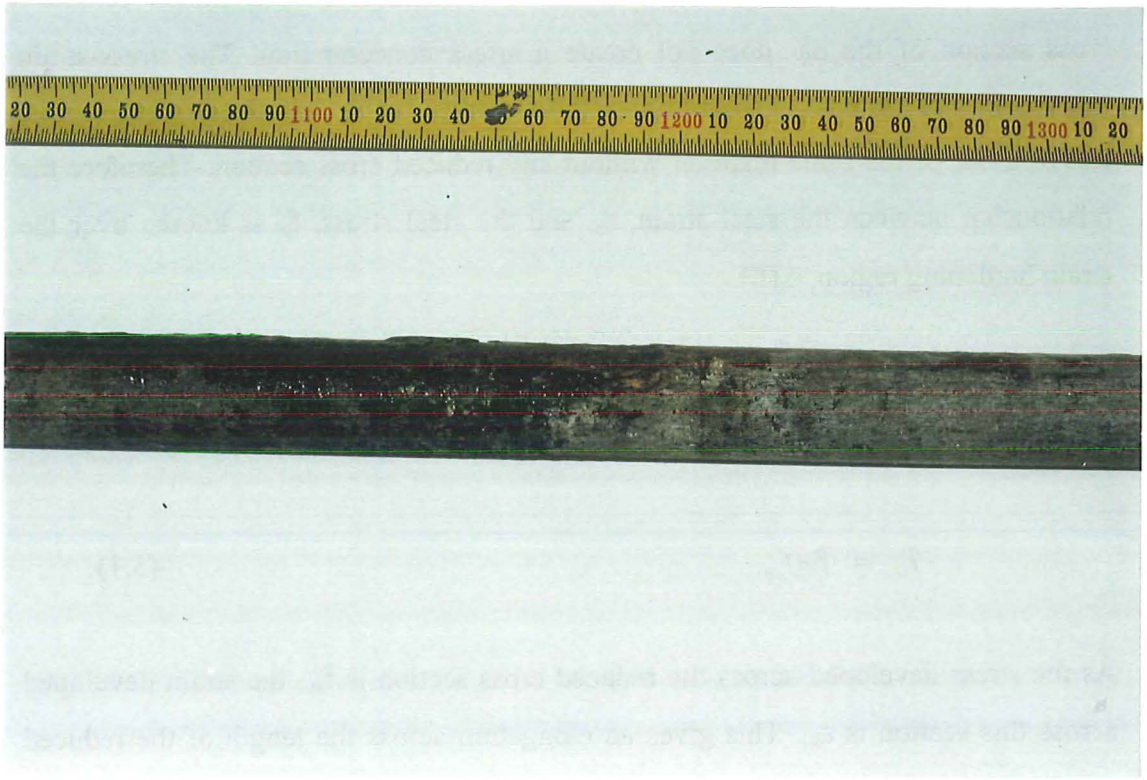

Figure 5.6(a) *Corroded Region of 1 $^{1}/_{8}$ inch Diameter Linkage Bolt*

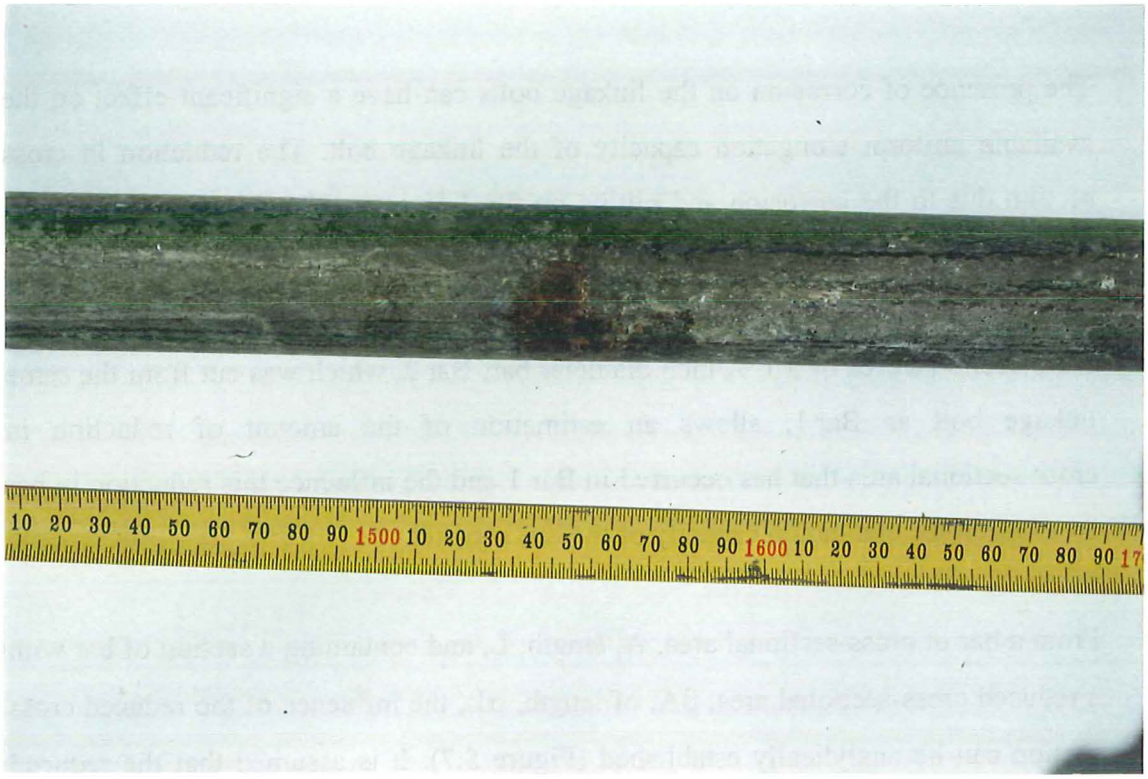

Figure 5.6(b) *Corroded Region of 1 ½ inch Diameter Linkage Bolt*

cross section of the bar does not create a stress concentration. The stress-strain relationship for the bar is known from a force-elongation plot obtained from a tensile test of a bar of the same material without any reduced cross section. Therefore the relationship between the steel strain, ε_s, and the steel stress, f_s, is known over the strain hardening region, $\varepsilon_s(f_s)$.

The ultimate tensile force for the specimen is controlled by the ultimate tensile steel stress, f_{su}, and the reduced cross-sectional area, βA.

$$T_u = \beta A f_{su} \qquad (5.1)$$

As the stress developed across the reduced cross section is f_{su}, the strain developed across this section is ε_{su}. This gives an elongation across the length of the reduced cross section of $\varepsilon_{su}\alpha L$.

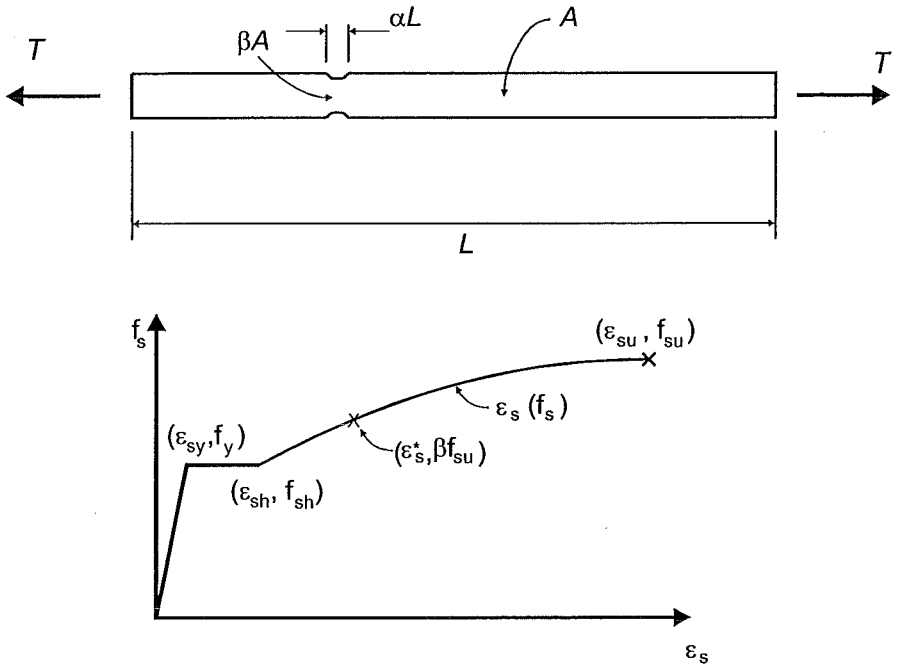

Figure 5.7 *Bar with Reduced Cross Section*

The stress developed across the full section of the bar is βf_{su} with a corresponding strain across the full section of ε_s^* which is less than ε_{su}.

As the length of the reduced cross section, αL, is small the elongation of this section can be neglected. Therefore the elongation of the entire bar can be expressed as:-

$$\Delta L = \varepsilon_s^* (1-\alpha) L \qquad (5.2)$$

where ε_s^* = strain corresponding to a stress of βf_{su}

The term β can be approximated from the ratio of forces obtained from a test on a bar with a reduced cross section and a test on a bar without any reduced cross section. As the stress-strain relationship for a bar without any reduced cross section is known the elongation, ε_{so}, corresponding to a stress of βf_{su} can be obtained. The strain ε_{so} is also the strain developed across a length of bar which contains a reduced cross section.

From the results of tensile tests on Bar 1 and Bar 2 the ratio of forces indicates that the corrosion damage has reduced the cross section of Bar 1 by approximately 2 %. From the force-elongation plot of Bar 2 (Figure 5.3) the elongation of this bar at a force corresponding to a load of 98 % of the maximum tensile force in Bar 2 can be found to be equal to 77 mm. Over a gauge length of 750 mm this corresponds to a strain of:-

$$\varepsilon_{so} = \frac{77}{750} \times \frac{100}{1} \% \qquad (5.3)$$
$$= 10.3 \%$$

The value of ε_{so} compares to an available uniform elongation capacity of Bar 2 of 19.3 % and is equivalent to the strain developed in Bar 1 at maximum load. The calculated value of $\varepsilon_{so} = 10.3$ % compares well to the measured uniform elongation of Bar 1 of 11.4 %.

From these two tests it can be seen that a small reduction in the cross-sectional area of the linkage bolt can reduce the available elongation capacity of the bolt from 19 % to approximately 10 % depending on the amount of cross section reduction that has occurred. The tests on the 1 $^1/_2$ inch (38 mm) diameter linkage bolt containing a region of corrosion, Bar 5, did not produce the same reduction in elongation capacity due to the smaller amount of corrosion and larger diameter of the bar.

Should this type and extent of corrosion be common to a large number of linkage bolts in the Thorndon Overbridge, it may be possible only to rely on about 10 % elongation capacity of these bolts. Inspection of the linkage bolts, to determine their condition at the critical section, is unfortunately difficult and probably impossible without complete removal of the linkage bolts.

At 10 % available uniform elongation, the length of the linkage bolts, 7.6 metres to 12.8 metres, at Stage Two and Stage Three piers allows significant displacements to be achieved through yielding of the linkage bolts. In conjunction with other linkage bolt retrofit measures this should allow the distribution of permanent ground

displacements between several spans where the Wellington Fault crosses beneath the bridge structure.

5.2 HOLD DOWN BOLT TESTS

5.2.1 Unit 1 Test Results

The Unit 1 hold down bolt specimen modelled the hold down bolt detail used in the Stage Two and Stage Three piers. This detail used a $1\ ^{3}/_{8}$ inch (35 mm) diameter linkage bolt with a 5 inch (127 mm) long threaded coupler joining two lengths of the bolt at the interface of the umbrella platform and the I-beam end diaphragm. A conical movement pocket, 5 inch (127 mm) diameter at the top and 3 inch (76 mm) diameter at the bottom, 12 inches (305 mm) long is provided in the umbrella platform for each bolt. The linkage bolt then passes into a steel tube which extends up through the I-beam end diaphragm where it is secured by a nut and washer at the top of the I-beam.

Unit 1 incorporated two full-scale hold down bolt details so that the entire test rig could be subjected to double shear using the DARTEC UTM. Figure 5.8 shows the schematic layout of Unit 1 for testing of this hold down bolt detail. Figure 5.9 shows the threaded coupler detail. The original construction specifications called for the coupler to be tack welded at both ends, on site, to the hold down bolt to prevent the coupler from turning. As the bottom of the coupler, inside the movement pocket, cannot be accessed after the hold down bolt is cast into the umbrella platform the coupler can only be tack welded at one end only.

The central block of the test rig represents the umbrella platform with the outer blocks representing the I-beam end diaphragm which the hold down bolt passes through. As the ends of the I-beams in the Stage Two and Stage Three piers are tight to the umbrella platform these hold down bolts are subjected to loading in one direction only during an earthquake. The outer blocks were secured to two

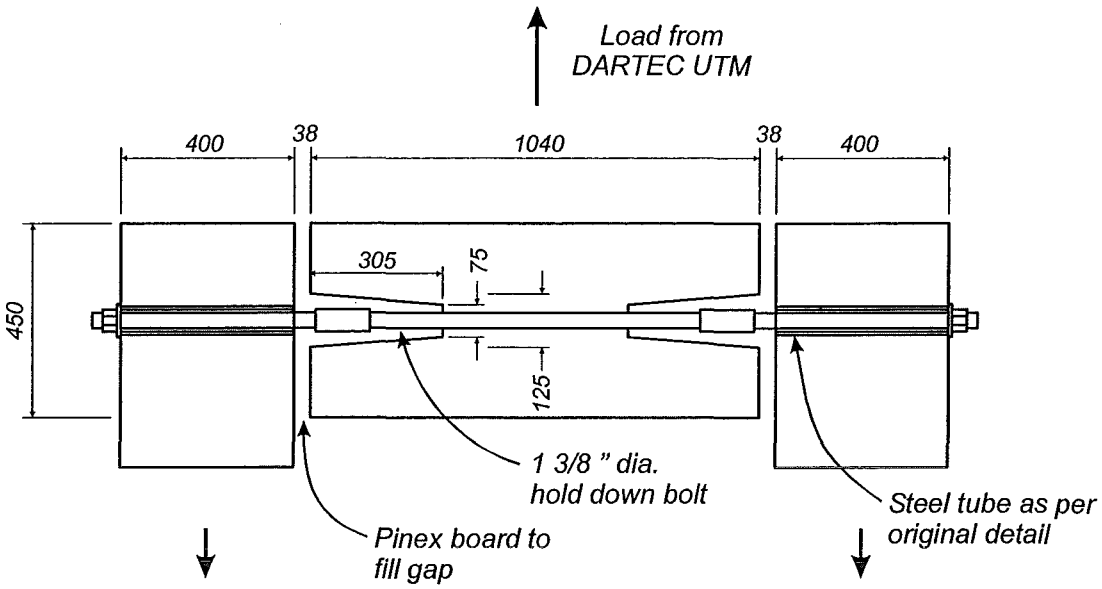

Figure 5.8 *Unit 1 Hold Down Bolt Test Rig Schematic*

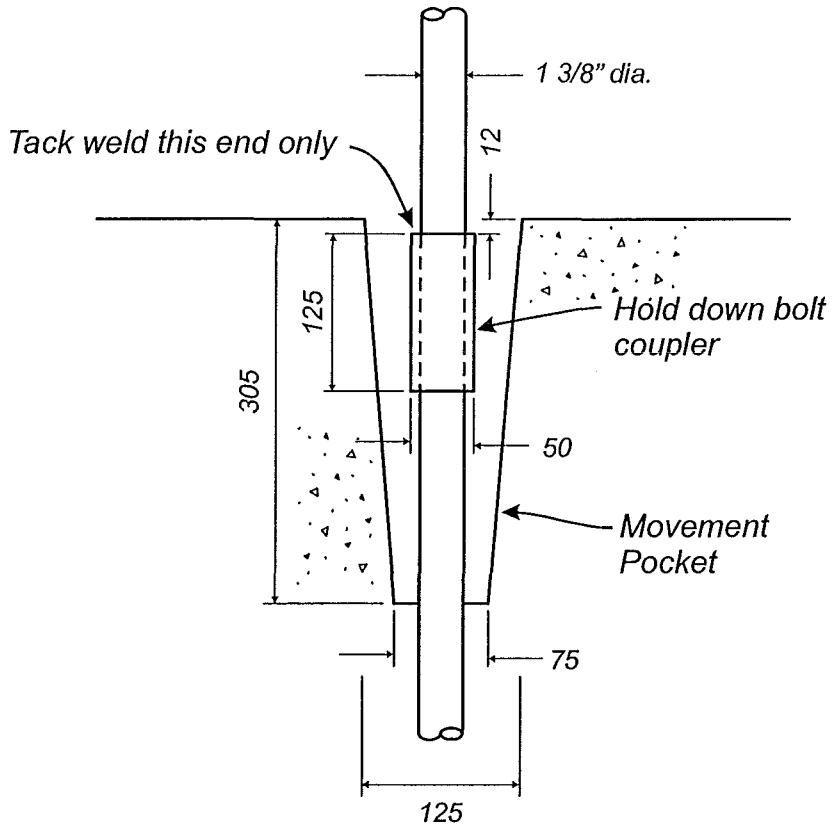

Figure 5.9 *Unit 1 Hold Down Bolt Threaded Coupler Detail*

supporting steel 310 UC 97 sections using two 29 mm diameter VSL CT Stressbar rods with spherical seated washers and nuts at both ends. This allowed the outer blocks to rotate during the loading replicating the rotation of the suspended I-beam spans which could occur in the Thorndon Overbridge. Existing pinned fittings were used to transfer the load from the DARTEC UTM to the central block and through the steel UC sections.

The hold down bolt was fabricated from a 40 mm diameter plain round Grade 300 steel bar. This bar was turned down to 1 $^{3}/_{8}$ inch diameter where it passed thorough the movement pocket and outer blocks. The bar was left at the original 40 mm diameter where it was cast into the central block. The ends of the bar were threaded for the coupler and nuts to secure the bolt to the end of the outer blocks. The space between the central and outer blocks was packed with Pinex board as was done for the original construction.

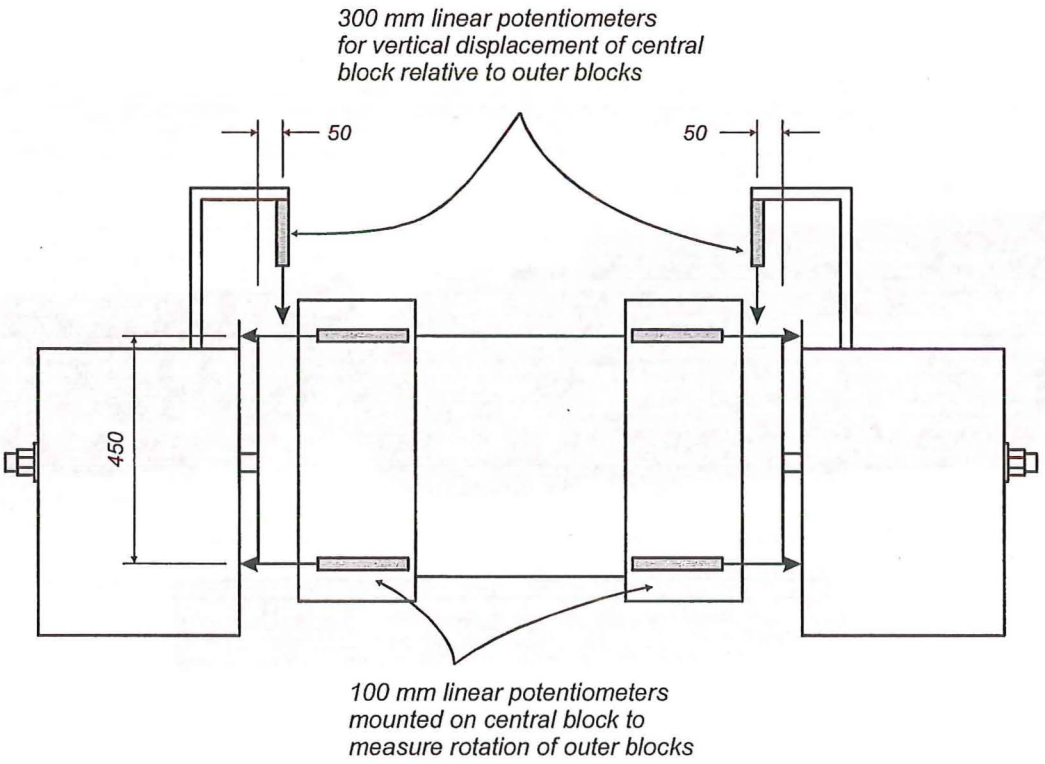

Figure 5.10 *Measurement of Displacements in Hold Down Bolt Test Rig*

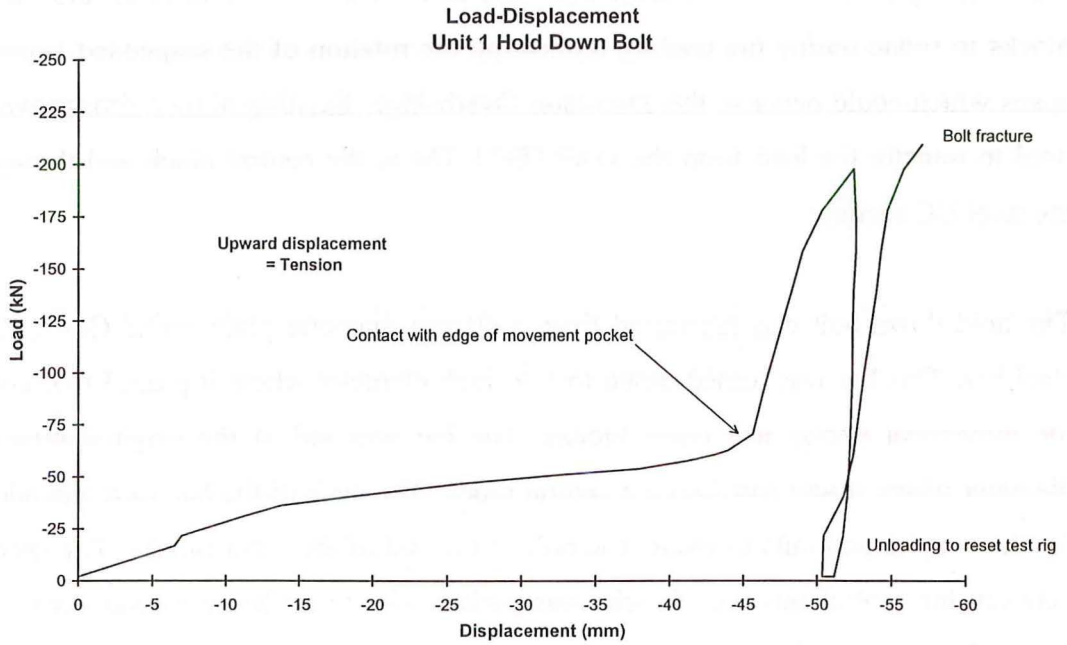

Figure 5.11 *Unit 1 Hold Down Bolt Load-Displacement Results*

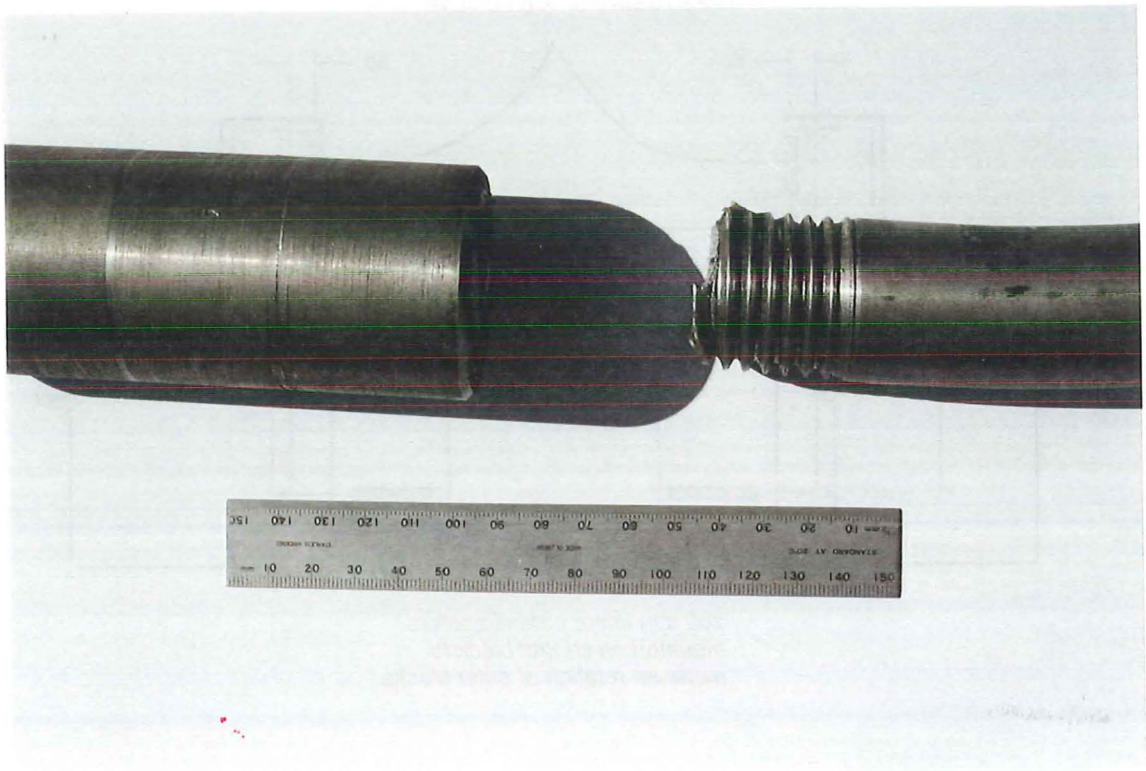

Figure 5.12 *Fractured Hold Down Bolt and Coupler From Unit 1*

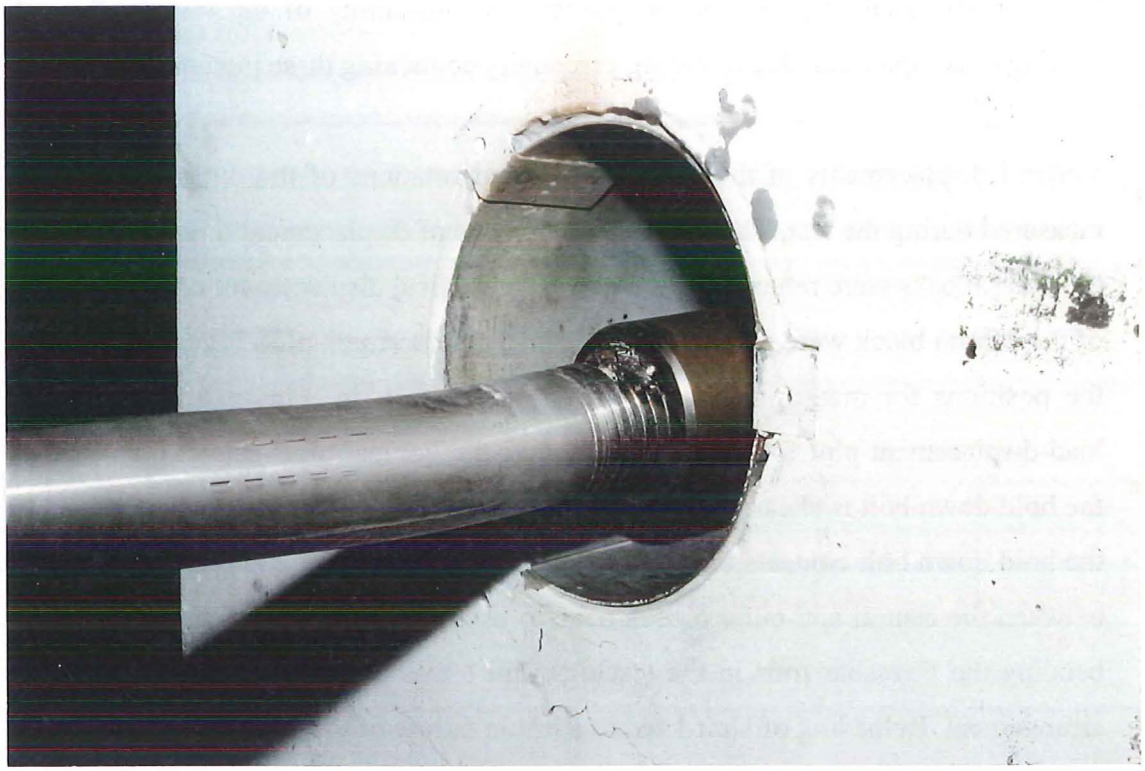

Figure 5.13 *Undamaged Hold Down Bolt and Threaded Coupler Detail From Unit 1*

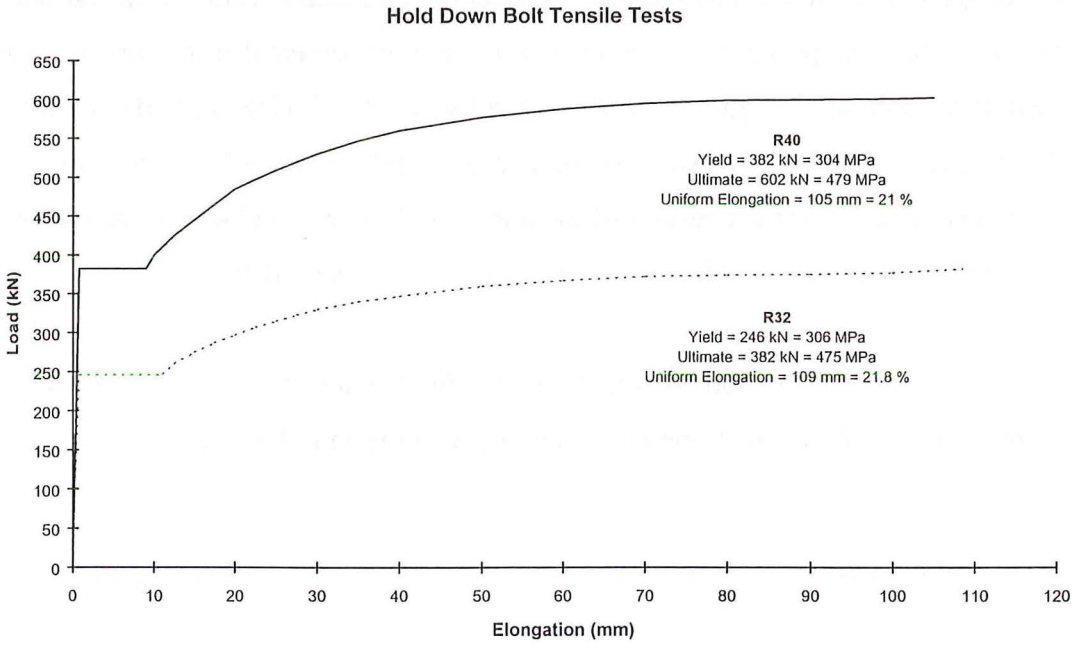

Figure 5.14 *Force-Elongation Plots for Unit 1 and Unit 2 Hold Down Bolts*

Loading was applied in tension to prevent any instability of the test rig through loading in compression due to the rig essentially containing three pin connections.

Vertical displacements of the central block and rotations of the outer blocks were measured during the test. The vertical components of displacement due to rotation of the outer blocks were removed and the average vertical displacement of the two ends of the central block were plotted to give a load-displacement plot. Figure 5.10 shows the positions for measuring displacements in the test rig. Figure 5.11 shows the load-displacement plot for Unit 1. This shows the vertical block moving upward as the hold down bolt is sheared inside the movement pocket. The unit picks up load as the hold down bolt contacts the edge of the movement pocket and the bolt is caught between the central and outer blocks. Due to excessive rotations of the outer blocks bending the Stressbar rods in the test rig, Unit 1 was unloaded to reset the test rig arrangement. Reloading of Unit 1 led to a brittle failure of the hold down bolt shortly after reaching the load attained during the initial loading.

The bolt failed at a load of 209 kN in double shear and a vertical displacement of 57 mm by fracture of the bolt through the thread at the position of the tack weld on the coupler. The presence of the tack weld on the threaded portion of the bar and its affect on the steel properties at this location were instrumental in the failure of this hold down bolt detail. Figure 5.12 shows the fractured end of the hold down bolt and the coupler. Figure 5.13 shows the undamaged end of the hold down bolt in the movement pocket. Tensile testing of the a length of the original 40 mm diameter bar gave a yield stress of 304 MPa and an ultimate stress of 479 MPa.

Figure 5.14 shows the force-elongation plot for the tensile testing of the 40 mm diameter rod used in Unit 1 and the 32 mm diameter rod used in Unit 2.

5.2.2 Unit 2 Test Results

The Unit 2 hold down bolt duplicates the hold down bolt detail used in the Stage One multi-column bents. These hold down bolts are 1 $^1/_4$ inch (32 mm) diameter and are continuous from the multi-column bent cap beam through the I-beam end diaphragm.

The detailing of the superstructure connection at the Stage One piers allows the hold down bolts to be subjected to cyclic loading during an earthquake. Unit 2 was tested using the same test rig as Unit 1 applying a cyclic loading pattern up to fracture of the hold down bolt.

A conical movement pocket, 5 inch (127 mm) diameter at the top and 3 inch (76 mm) diameter at the bottom, 15 inches (381 mm) long is provided in the cap beam of the multi-column bent for each bolt. The linkage bolt then passes into a steel tube which extends up into the I-beam end diaphragm where it is secured by a nut and washer cast into the diaphragm.

Figure 5.15 shows the schematic layout of Unit 2 for testing of this hold down bolt detail. Two cycles of loading were applied to each level of loading. Cycles were controlled by displacement until the hold down bolt contacted the edge of the movement pocket when the load was used to control the testing. Figure 5.16 shows the unit picking up load at approximately 50 mm vertical displacement where the hold down bolt contacts the edge of the movement pocket. Some cracking of the central block was noticed at around this level of loading along with crushing of the concrete around the edge of the movement pocket. Further loading up to 65 mm vertical displacement led to slipping of the nut securing the bolt at the end of the outer block.

Instability of the test rig when loading in compression, due to the formation of a mechanism between the pinned connections top and bottom and a "pin" at the hold down bolt required the test be completed by loading in tension up to fracture of the bolt. This loading led to considerable crushing and spalling of the concrete around the end of the movement pocket and where the bolt enters the steel tube through the outer blocks. Unloading of the test rig was done to remove the steel plates under the outer blocks to prevent them rotating further by bolting them directly to the steel UC sections of the test rig.

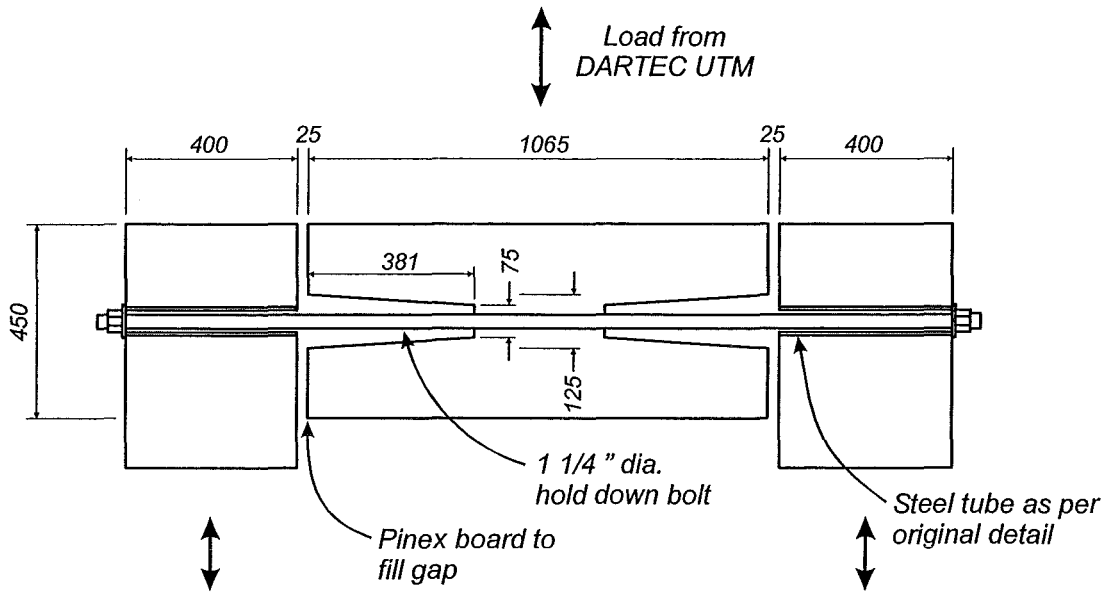

Figure 5.15 *Unit 2 Hold Down Bolt Test Rig Schematic*

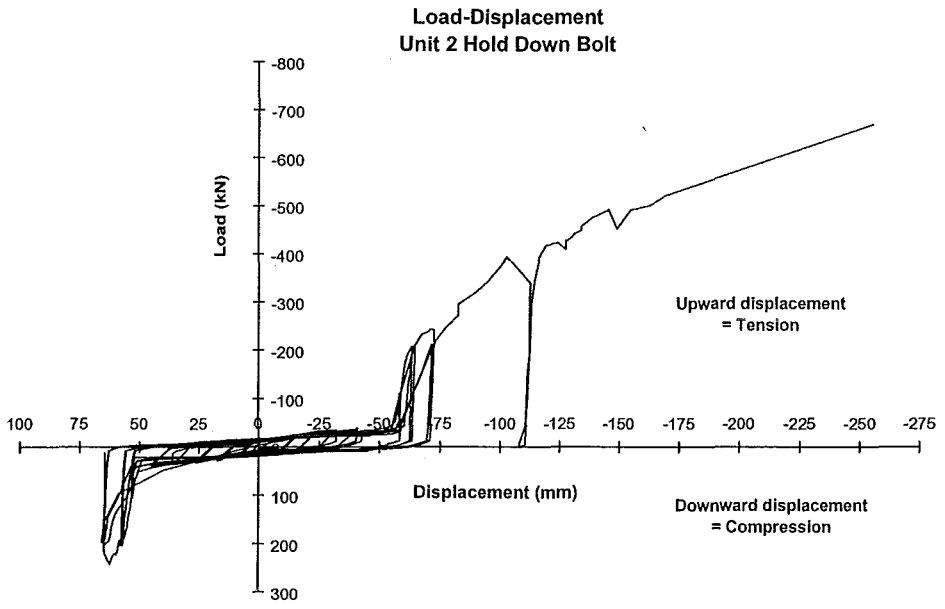

Figure 5.16 *Unit 2 Hold Down Bolt Load-Displacement Results*

Failure of this hold down bolt detail was eventually through a tensile fracture of the bolt as it was deformed through the movement pocket and steel tube. The hold down bolt developed a significant kink through the movement pocket and the steel tube causing spalling of concrete from the bottom of the central block and top of the outer blocks. Fracture occurred with the bolt at load of 668 kN in double shear and a vertical displacement of 255 mm. Figure 5.17 shows the end of the fractured hold down bolt in the central block after testing.

Figure 5.18 shows the fractured end of the hold down bolt in the outer block. From the classic "cup and cone" failure surface of the steel bolt it is obvious that the mode of failure was tensile rather than through shear.

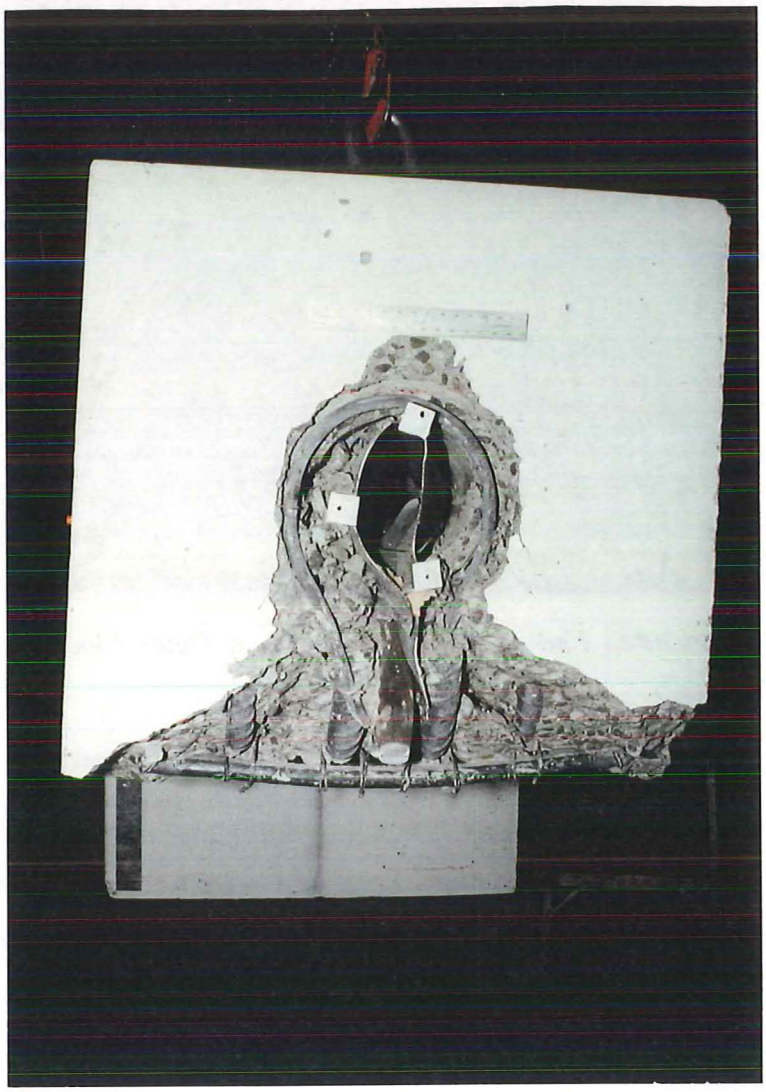

Figure 5.17 *Fractured End of Hold Down Bolt in Central Block After Testing of Unit 2*

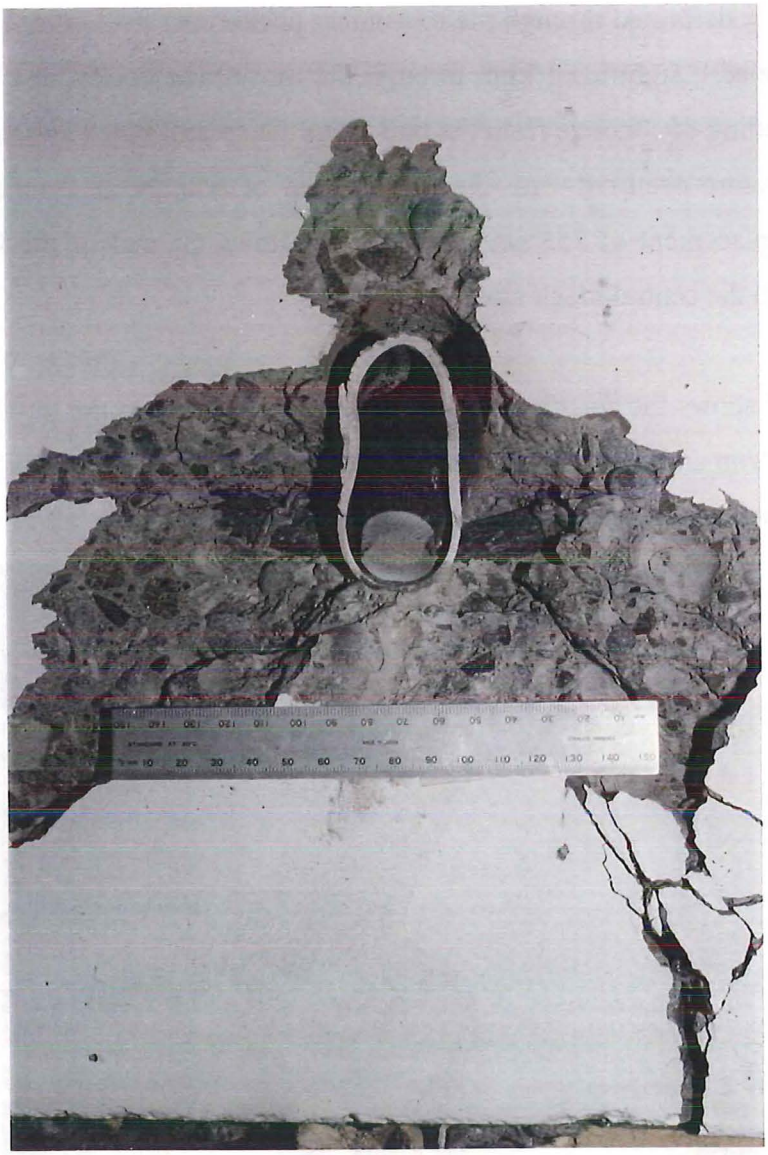

Figure 5.18 *Fractured End of Hold Down Bolt in Outer Block After Testing of Unit 2*

The tensile test of the 32 mm diameter bolt used for this hold down bolt detail gave a yield stress of 306 MPa and an ultimate stress of 475 MPa. The angle of deformation of the hold down bolt at fracture was 60° to the original bolt axis and it can be shown that at development of the ultimate tensile strength of the bar, and the angle of the bar to the vertical, that a load of 662 kN would be obtained for this test configuration. This corresponds closely with the failure load obtained during the test.

5.3 WELDED END DETAIL TEST RESULTS

The welded end details from the 1 $^1/_8$ and 1 $^1/_2$ inch diameter linkage bolts were cut from the specimens before tensile testing of the linkage bolts. Each end detail was left with a 40 mm length of bolt protruding from the face of the detail. Each end detail was then tested in compression using the 2500 kN Avery UTM to determine the strength of the welded details. Should the strength of the welds be less than the strength of the linkage bolts failure of the linkage bolts will take place in the end details which will affect the available elongation capacity of the linkage bolts.

Figure 5.19 shows the dead end welded detail for the 1 $^1/_2$ inch diameter linkage bolts with the tightening end detail shown in Figure 5.20. The tightening end detail was site welded following installation of the linkage bolts in the umbrella platforms.

Loading of each welded end detail was applied directly to the cut off end of the bolt. Each end detail was loaded to approximately 20 % strain in compression without failure of the end details. The stub of the bar that was loaded yielded in compression at forces comparable to those obtained from the tensile tests. Buckling of the gusset plates on the end details occurred during the test, after yielding of the bar stub. Continued loading of the bar stub causes it to bulge and lock up in the hole where it passes through the end plate. Once this had occurred the load was transferred directly to the gusset plates which caused them to yield and buckle.

Figure 5.21 shows a welded end detail near the end of testing in the Avery UTM. No failure of the welds in any details were noted during testing. Figures 5.22 and 5.23 show the load-displacement plots from the compression testing of the welded end details.

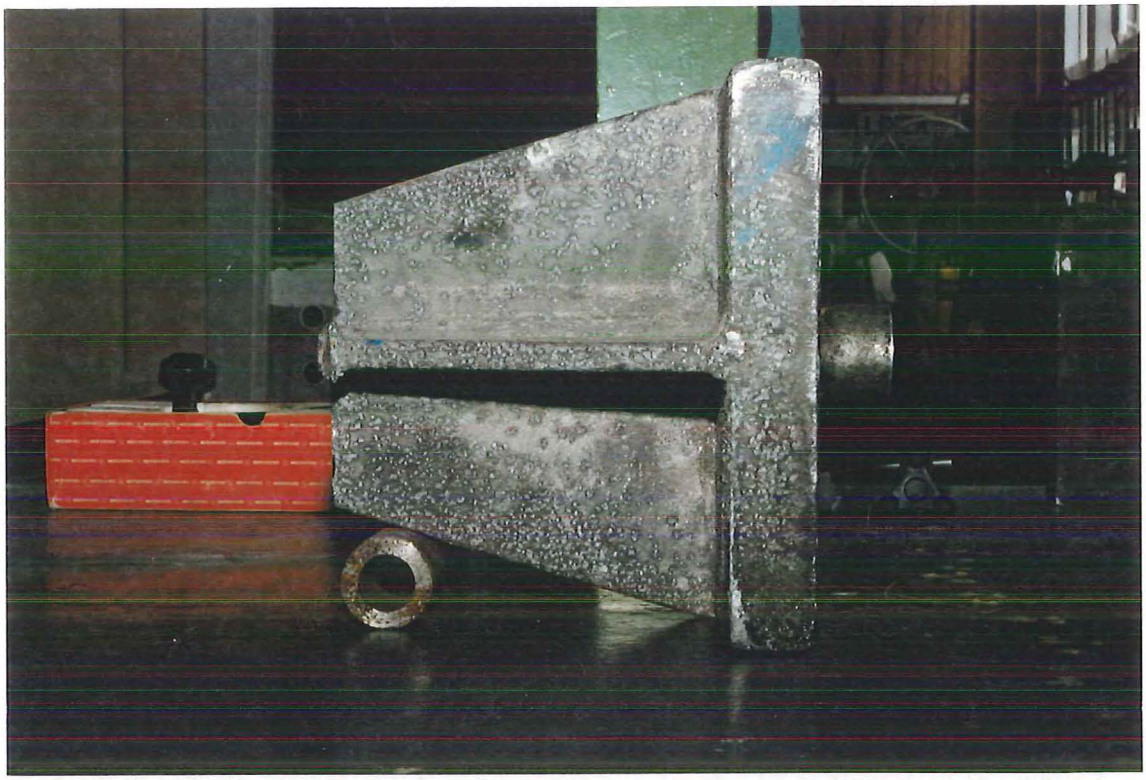

Figure 5.19 *Linkage Bolt Dead End Welded Detail*

Figure 5.20 *Linkage Bolt Tightening End Welded Detail*

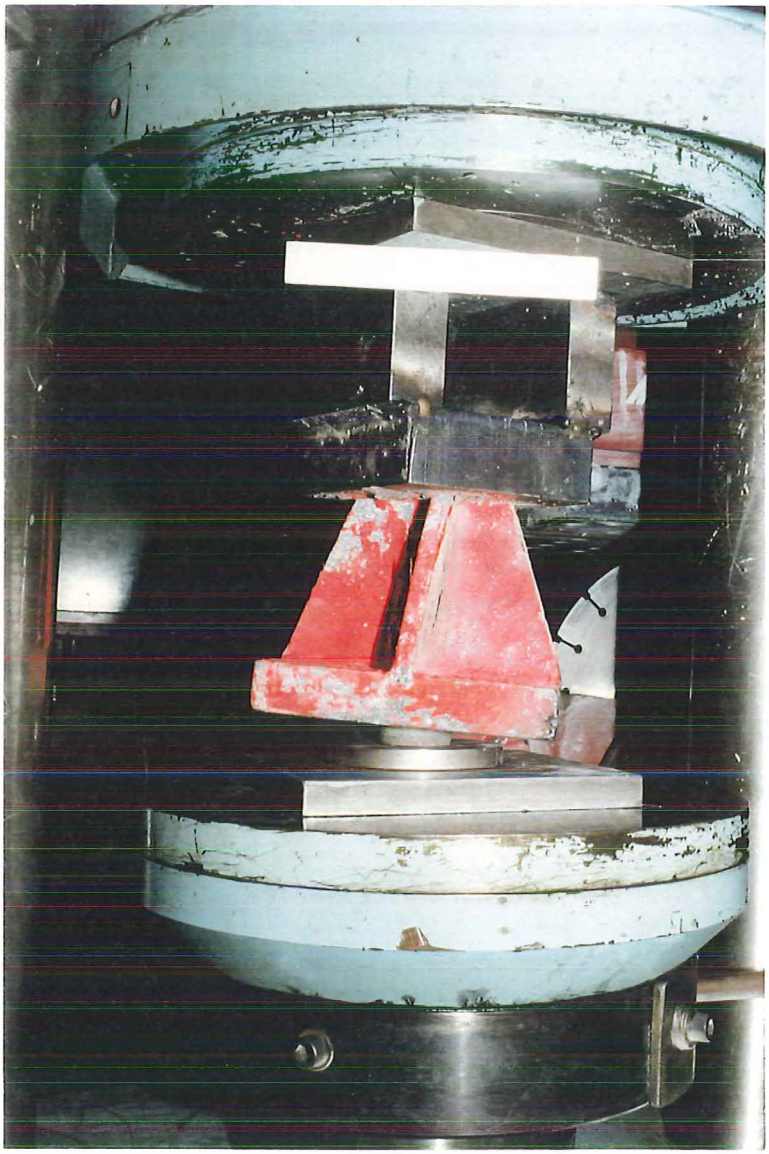

Figure 5.21 *Welded End Detail at End of Compression Testing*

5.4 RECOMMENDATIONS FROM LINKAGE BOLT TESTING

5.4.1 Linkage Bolts

Monotonic tensile tests on a single 1 $^{1}/_{8}$ inch and a single 1 $^{1}/_{2}$ inch diameter linkage bolt removed from a Stage Two and a Stage Three pier, respectively, of the

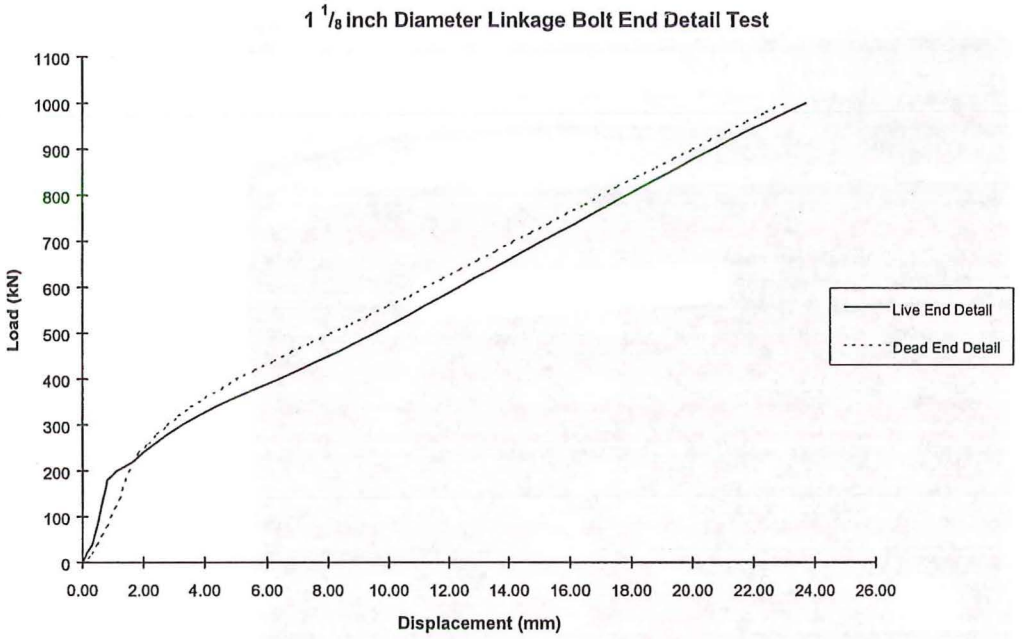

Figure 5.22 *Load-Displacement Plots From Compression Testing of 1 1/8 inch Diameter Linkage Bolt End Details*

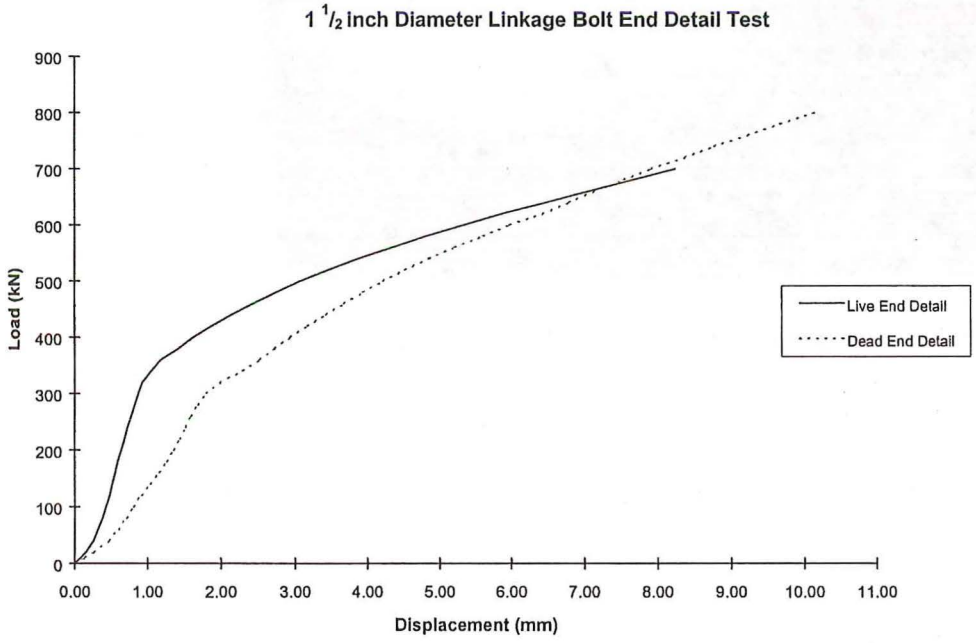

Figure 5.23 *Load-Displacement Plots From Compression Testing of 1 1/2 inch Diameter Linkage Bolt End Details*

Thorndon Overbridge show an average yield strength, for all bolts tested of 289 MPa and an average ultimate tensile strength of 466 MPa.

The average measured uniform elongation of these bolts is 18.7 % for bolts tested without any corrosion damage present within their lengths. The appearance of corrosion damage on the linkage bolts supplied for testing can drastically reduce the available elongation capacity of the linkage bolts, depending on the amount of reduction in the bolt cross section. The corrosion damage on the supplied linkage bolts suggests that the damage is taking place where the upper set of linkage bolts pass through the umbrella platform and into the I-beam end diaphragm. This is probably due to the linkage bolts being in contact with the steel tube, where it enters the concrete, and movements of the superstructure causing the protective galvanising coating to be rubbed off the bolt.

The lower set of linkage bolts are also exposed to the environment where they pass from the I-beam end diaphragm into the umbrella platform. Should this type and extent of corrosion damage be common and present in a large number of linkage bolts the available elongation capacity of the bolts may be limited to approximately 10 %. The length of the linkage bolts, 7.6 – 12.8 metres, will permit significant elongation of the linkage bolts and displacements to occur, in conjunction with other linkage bolt retrofit measures.

Compression testing of the welded end details from the supplied linkage bolts showed that these details are stronger than the linkage bolts. Failure of the linkage bolts should take place through yielding and fracture of the bolts themselves.

5.4.2 Hold Down Bolts

Shear testing of two hold down bolt details, used in Stage One piers and in Stage Two and Three piers show two different modes of failure. Cyclic testing of the continuous Stage One pier hold down bolt detail, Unit 2, showed that the hold down bolt kinked through the movement pocket causing extensive crushing and spalling of the surrounding concrete. The failure of the hold down bolt occurred through the bolt

developing its ultimate tensile capacity after pulling through the concrete surrounding the movement pocket. This hold down bolt detail tested was capable of accommodating 255 mm displacement between the central and outer blocks at fracture of the bolt.

Detailing of the Stage Two and Three hold down bolts incorporate a threaded coupler to join the two ends of the hold down bolt together. The coupler is located in the movement pocket and is tack welded to the bolt on site. The presence of the weld on the threaded portion of the bolt was instrumental in leading to the brittle fracture of the hold down bolt through the thread. A displacement of 57 mm was recorded between the outer and central block when the bolt failed. This hold down bolt detail indicates limited displacement capacity and strength due to the detailing measures used.

CHAPTER 6

RECOMMENDATIONS

6.1 RECOMMENDATIONS FROM TESTING OF UNITS I-A AND I-B

Two test specimens were constructed to model the as-built column, pilecap and piles of two particular piers in the Thorndon Overbridge. Due to the staged nature of the design and construction of the Overbridge different retrofit details were proposed for each stage. Based on a previous seismic assessment [B1] of the existing structure the chosen level of retrofit corresponds to the expected seismic demand resulting from an earthquake with a 500 year return period at the Thorndon Overbridge site. Design of the proposed retrofit details are intended to prevent collapse of the structure and loss of life on and near the Overbridge for this level of earthquake. Testing and evaluation of the performance of a typical Stage Two and a typical Stage Three pier, incorporating the proposed retrofit details for each pier, were carried out during this study. Each specimen was subjected to simulated seismic lateral loading by applying constant axial compression and reversed cyclic lateral loads at the top of the column, representing the centre of mass of the bridge deck.

The proposed retrofit details are designed to prevent premature failure of the pilecaps of each pier, by strengthening them through the use of a pilecap overlay retrofit, and/or pilecap post-tensioning. This is intended to force inelastic action into the base of the column where behaviour of each pier can be easily determined. The base of the columns in the Stage Two piers do not contain sufficient transverse reinforcement to provide the required ductility capacity to the pier for the chosen level of retrofit and steel jackets are proposed for the base of each column. The columns of the Stage Three piers are deemed to contain sufficient transverse reinforcement at the base to meet the expected ductility demands and these piers are retrofitted with a pilecap overlay retrofit only.

Cyclic lateral load testing of Units I-A and I-B showed that the available structural ductility of each test specimen was equivalent to the structural ductility demand expected to occur in Piers 68 and 46, respectively, during a 500 year return period earthquake at the Thorndon Overbridge site, corresponding to the chosen level of retrofit. At this level of imposed ductility both specimens exhibited signs of an imminent brittle flexure-shear failure in the column at the point where the longitudinal column reinforcement had been curtailed.

Failure of the specimens around the curtailment points in the column were not expected, as all inelastic action was assumed to take place at the base of the column. Subsequent analysis of each test specimen showed the flexural strength at the curtailment points had been exceeded during testing due to the tension shift effect. The tension shift effect, caused by the formation of diagonal flexure-shear cracks, in the column, led to the yield stress in the column longitudinal reinforcement being exceeded at the curtailment point and yielding of the column section at this location. Assessment of the available shear strength of each column showed that the applied shear force, corresponding to the formation of a critical section at the curtailment point(s), exceeded the available shear strength, leading to the initiation of a brittle flexure-shear failure at these locations.

Review of the detailing of Piers 68 and 46 and of Units I-A and I-B showed the column longitudinal bars were curtailed closely following the bending moment diagram, following the design practice of the time. No allowance was made to extend the curtailment point further to allow for the tension shift effect and provide for the required anchorage length beyond the critical section. This column detailing led to the development of the large diagonal tension cracks in the columns and the initiation of a potentially brittle shear failure of limited ductility in the column. Provision of the pilecap overlay retrofit in both piers further increased the likelihood of failure by shortening the columns and shifting the critical section at the base closer to the curtailment point.

Unit I-B showed one large diagonal tension crack in the column for each direction of loading. Results from the lateral load testing show that the column initially yielded at the base of the column, behind the steel jacket, allowing inelastic action to take

place. The additional ductility provided by the steel jacket at the base of the column allowed the development of a degree of column overstrength in the test specimen. This then led to the flexural strength at the curtailment point being reached. Concentration of inelastic action at the curtailment point and column overstrength being developed at the base of the column led to the available shear strength of the column at the curtailment point, above the steel jacket, being exceeded.

Extensive diagonal column cracking occurred in Unit I-A over the full column height. It was apparent from the behaviour of Unit I-A that the flexural strength at the base of the column was not achieved and inelastic action was concentrating at the curtailment points higher in the column. Due the decreased lever arm between the upper curtailment point and the top of the column a majority of the inelastic action was concentrated at this location with significant damage occurring due the large curvature demands from the imposed loading displacements.

Theoretical analyses, using moment-curvature analysis and assessment of the available shear strength of the column, of each test specimen are able to show that a shear failure around the curtailment points can be predicted when the base of the column reaches its flexural strength. The development of the flexural strength at the curtailment points of each column can also be shown when the tension shift effect is accounted for.

Observations from both Unit I-A and I-B showed relatively little damage was sustained in the pilecap and pilecap overlay at development of the diagonal cracking in the columns. Minor cracking and limited yielding of some of the pilecap reinforcement occurred in both specimens. Repair of each column was achieved by fitting of a full height steel jacket to Unit I-A and extension of the existing jacket in Unit I-B over the full column height. Epoxy injection of the cracks in each column was also done after fitting and grouting of the full height steel jackets.

Placement of the full height steel jackets on both test specimens were successful in allowing each test specimen to develop the flexural strength at the base of the columns and prevent the failure of the columns around the curtailment points. This allowed enhancement of the available structural displacement ductility of each

specimen and the development of a large lateral load overstrength for each column. Testing of the repaired Unit I-A was limited by the extension of the hydraulic actuator used to apply the lateral loads to the top of the column without failing the specimen. The repaired Unit I-B failed through fracture of the column longitudinal steel at the base of the column and the resulting drop in lateral load carrying capacity.

Modelling of the different pile tensile and compressive stiffness ratios for each specimen allowed the same bending moment patterns to be achieved in the pilecaps of each test unit as obtained from the structural analysis of the respective piers. The maximum, scaled, pilecap moments from the structural analyses of each pier were reached during the test of each specimen, largely due to the development of column overstrength after repair of the columns. The pilecap and pilecap overlay retrofits of each test specimen were able to resist the imposed forces from the repaired columns with little distress. Limited yielding of some of the bottom pilecap mat bars occurred in the repaired Units I-A and I-B along with limited cracking of the pilecap and pilecap overlay retrofit. Pilecap overlay dowels placed close to the base of the columns yielded through dowel action as they were engaged by the column longitudinal bars pulling out of the pilecap overlay surface. Lower strains were observed in overlay dowels further from the column. Longer pile dowels placed to overlap with the existing pile reinforcement remained within the elastic range up to the end of the tests for both Unit I-A and I-B. This was despite observations indicating yielding of the existing pile reinforcement at the central piles of Unit I-A by the end of that test.

Lateral load testing of the repaired Units I-A and I-B showed the provision of a full height steel jacket to the columns of both test specimens would prevent premature failure of the columns at the curtailment points. Design and provision of full height steel jackets for Piers 46 and 68 will prevent the occurrence of a potentially brittle shear failure in the columns initiated by the curtailment of the column longitudinal reinforcement due to the tension shift effect and inadequate column shear strength around the curtailment points. The full height steel jackets proved successful in increasing the available structural displacement ductility of the columns in Units I-A

and I-B well beyond the expected equivalent structural displacement ductility demand for the level of retrofit chosen for the Thorndon Overbridge.

6.2 RECOMMENDATIONS FROM LINKAGE BOLT TESTING

Monotonic tensile testing of two linkage bolts removed from the Thorndon Overbridge showed the average tensile strength, for all the bolts tested, of 289 MPa and an average ultimate tensile strength of 466 MPa.

An average measure uniform elongation of 18.7 % was measured for the undamaged linkage bolts. Removal of the bolts from the Overbridge revealed a region of corrosion damage within their length which corresponds closely to the location where the linkage bolts pass through the I-beam superstructure end diaphragm into the umbrella platform. This damage can drastically reduce the available uniform elongation of these linkage bolts, depending on the reduction in cross section resulting from the corrosion. Tensile testing of a linkage bolt containing corrosion damage within its length indicated an available uniform elongation for this specimen of 11.4 %. Should the observed type and extent of corrosion damage be common and present in a large number of linkage bolts in the Thorndon Overbridge then the available elongation capacity of these bolts should be limited to approximately 10 %.

Compression testing of the welded end details from the supplied linkage bolts showed these details are stronger than the linkage bolts. Failure of the linkage bolts should take place through yielding and fracture of the linkage bolts themselves.

Shear testing of two hold bolt details, used in Stage One piers and Stage Two and Three piers, showed two different modes of failure. Cyclic testing of the Stage One pier hold down bolt detail showed the bolt failed after developing its ultimate tensile capacity after pulling through the concrete surrounding the bolt detail. Failure occurred at a shear displacement of 255 mm across the bolt.

Detailing of the Stage Two and Three pier hold down bolt details incorporate a threaded coupler detail which is tack welded to the hold down bolt. Failure of this

detail occurred through a brittle fracture of the bolt at the thread where it was tack welded. A shear displacement of 57 mm was recorded for this hold down bolt detail indicating limited displacement capacity and strength due to the detailing measures used.

CHAPTER 7

ASSESSMENT OF BRIDGE COLUMNS WITH CURTAILED LONGITUDINAL REINFORCEMENT

7.1 INTRODUCTION

The curtailment of column longitudinal reinforcement in frame buildings, following the bending moment pattern, is often impractical due to the flexural demands imposed at the top and bottom of the columns from a typical bending moment distribution resulting from the lateral forces being resisted by the frame structure. Column longitudinal bars are carried over the full story height necessitating splicing of column bars at some point over the column height. For bridge structures it is often possible to curtail some of the longitudinal reinforcement in the column where the bending moment has reduced. The practice of longitudinal column bar cut-off was common in the construction of bridge columns in New Zealand. This practice was done for economy and ease of construction.

A reinforced concrete member subjected to flexure and shear behaves before cracking as if homogeneous and isotropic, and conventional beam-column theory is applicable. After diagonal cracking takes place in the member significant redistribution of stresses take place and the members behave more like trusses. As a result, the tensile force in the longitudinal reinforcement at a section is not proportional to the bending moment at that section but is proportional to the bending moment at a distance of e_v from that section. This phenomenon is known, and referred to in this study, as the tension shift [P1].

Previous common design practice was to curtail longitudinal reinforcement closely following the bending moment diagram, which makes no allowance for the development of the tension shift effect. This may lead to the column reaching its flexural strength at the point of curtailment and ultimately failing at this point. Testing of Unit I-A and Unit I-B showed that the early curtailment of the

longitudinal reinforcement led to the development of a brittle flexure-shear failure at the point of curtailment. The failure resulted from the tension shift effect and the inadequate shear strength of the column. Shear failures of any kind should be precluded in columns as they jeopardise the gravity-load-carrying capacity and could lead to catastrophic structural collapse.

As the tension shift has been recognised as an important effect to be considered when curtailing longitudinal reinforcement in reinforced concrete members, suitable allowances have been included in design requirements to sufficiently extend the point of reinforcement curtailment so that premature failure does not occur at the curtailment point. For existing columns, with curtailed reinforcement, the potential for the tension shift to cause a flexure-shear failure of the column at the curtailment point needs to be identified during the assessment phase of a retrofit programme. Appropriate retrofit measures should then be detailed and put in place if such a potential failure is identified. A measure of the actual tension shift that will occur in a column is required to assess its potential for leading to premature failure. The use of rules intended for the design of new structures may be overly conservative when used in a seismic assessment, and could lead to an unnecessary and expensive retrofit.

7.2 TENSION SHIFT EFFECT

7.2.1 Beam Theory

Four basic assumptions are made when deriving a general theory for the flexural strength of reinforced concrete sections [P1, P2]:

Plane sections before bending remain plane after bending.
The stress-strain curve for steel is known.
The tensile strength of concrete may be neglected.
The stress-strain curve for concrete, defining the magnitude and distribution of compressive stress, is known.

These assumptions can be used to determine the strength of members subjected to flexure with or without axial load with reasonable accuracy for design purposes.

Few reinforced concrete members, or only short regions in the members, are subjected to flexure without the presence of shear. With the interaction of flexure and shear and the formation of inclined flexure-shear cracks in a reinforced concrete member, beam theory is no longer able to determine the magnitude of the internal forces acting within a member at a particular section.

If applied to a member with inclined flexure-shear cracks, the plane sections hypothesis would give tensile reinforcement stresses, corresponding to the moment at a section, which are smaller than the stresses in the reinforcement that are required for equilibrium. Stresses in the tensile reinforcement at a particular section will be larger than those given by beam theory due to the tension shift effect.

7.2.2 Truss Analogy and the Tension Shift

A truss analogy can be used to describe the internal forces within a reinforced concrete member after diagonal cracking develops. This analogy, when applied to prismatic members, considers equilibrium of a parallel chord truss where the chords carry the concrete compressive force and the tensile force in the longitudinal reinforcement. The transverse reinforcement in the member and diagonal concrete struts complete the elements in the truss. With this simple analogy the tension shift effect can be quantified.

Figure 7.1 shows a beam subjected to flexure and shear, after formation of inclined flexure-shear cracks. The bending moment diagram from the imposed loading is illustrated along with the internal forces and truss analogy for the beam. Inclined parallel compression fields form at an angle of θ to the axis of the beam, in those regions of the beam which are not considered to have a disturbed stress field.

Internal forces acting in the beam at section A are shown in the free body diagram, flexural concrete compression, C_A, flexural tension in the longitudinal reinforcement, T_A, and the resultant force from the parallel diagonal compression fields, V/sinθ. Taking moments about point A′ it can be seen that,

$$Vx = M_A = T_A jd - \frac{Vjd}{2\tan\theta} \qquad (7.1)$$

where jd = internal lever arm

It can now be seen that the flexural tension force, T_A, at section A is not directly proportional to the moment, M_A, at section A but is somewhat larger,

$$T_A = \frac{M_A + Ve_v}{jd}$$
$$e_v = \frac{jd}{2\tan\theta} \qquad (7.2)$$

Thus the flexural tension force at section A, T_A, after formation of the inclined flexure-shear cracks is greater than that required to resist the external moment at section A. The flexural tension force, T_A, corresponds to a moment which occurs at a distance e_v beyond section A.

The distance e_v is known as the tension shift and is dependent on the angle of inclined flexure-shear cracking in the member. Therefore the additional moment at a section in a beam subjected to diagonal flexure-shear cracking, above the moment predicted by the plane sections hypothesis, is the shear force, V, times the tension shift, e_v.

Conservatively the angle of inclined flexure-shear cracking can be taken as $\theta = 45°$ giving a tension shift equal to jd / 2.

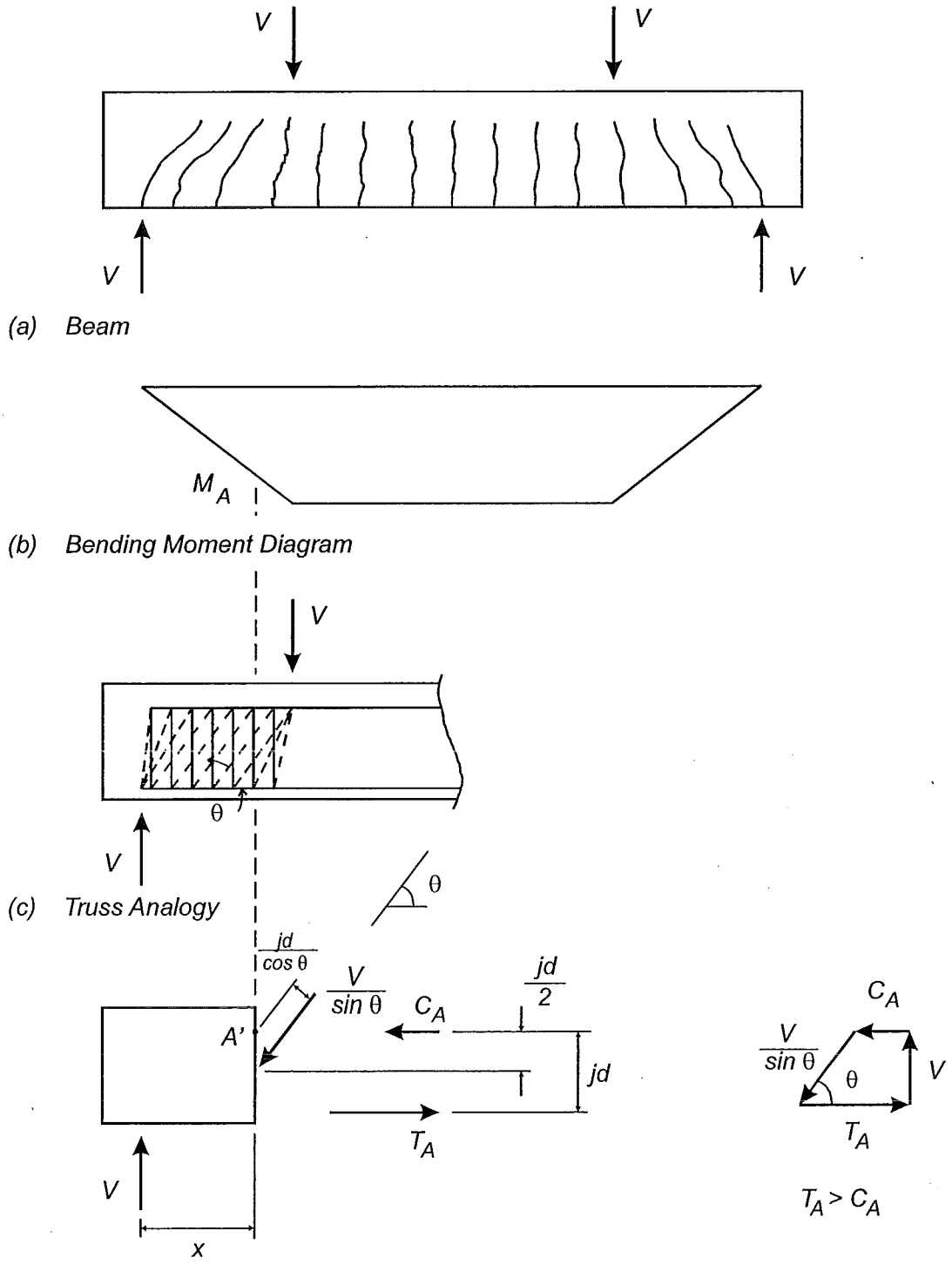

Figure 7.1 *Internal Forces and Truss Mechanism in Diagonally Cracked Reinforced Concrete Beam*

Figure 7.2 shows a column section subjected to low compressive axial load, bending and shear. The resultant internal forces and their positions are also shown. The resultant compression force, C, is made up of the compression carried in the concrete and in the longitudinal steel under compression. The tension force, T, results from the longitudinal steel reinforcement carrying tensile forces. The resultant force due to the diagonal compressive stress field acts through a strut in the section making an angle of θ with the axis of the column. The transverse reinforcement is placed perpendicular to the axis of the column and the inclined flexure-shear cracks have also formed at an angle of approximately θ to the axis of the column.

The critical angle of inclination, θ, of the diagonal compressive stress field developing in the truss between the compressive and tensile chords can be established assuming that the transverse reinforcement crossing the critical diagonal crack carries the entire shear force. In reality this assumption is conservative as a portion of the shear force is carried by a direct strut in a column subjected to axial compression [P3, P4]. The shear force in the column is then:-

$$V = \chi \frac{A_v f_{yh}}{s} \frac{jd}{\tan\theta} \qquad (7.3)$$

Where χ is equal to 1 for rectangular columns and $\pi/4$ for circular columns [A1, A2]. The term A_v is the total area of transverse reinforcement in a stirrup set crossing the critical crack in the direction of the applied shear force. This factor, χ, recognises that the horizontal component in the plane of loading in columns reinforced with circular spirals or hoops is less than one toward the ends of the critical cracks.

Rearranging Equation 7.3 gives the angle θ in terms of the shear force V.

$$\theta = \tan^{-1}\left[\frac{A_v f_{yh}}{V} \frac{\chi\, jd}{s}\right] \qquad (7.4)$$

Note that in Equations 7.3 and 7.4 it has been assumed that the transverse reinforcement yields before the diagonal compressive stress field crushes.

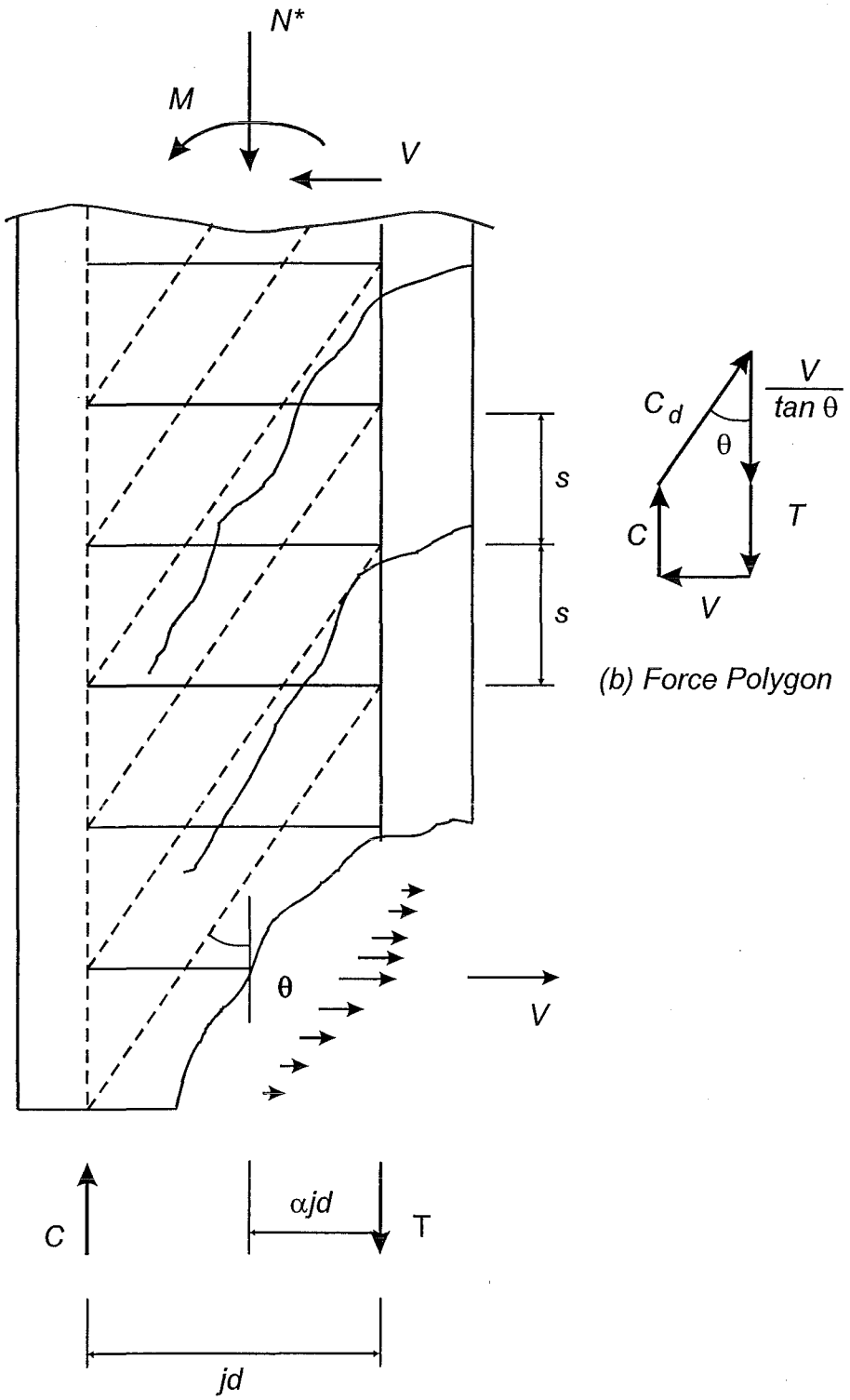

Figure 7.2 *Internal Forces and Truss Mechanism in Diagonally Cracked Reinforced Concrete Column*

Experimental work has shown that $\theta < 30°$ as the diagonally cracked concrete crushes before reaching the angle θ found from Equation 7.4 [P3]. The shear force V to be used in conjunction with Equation 7.4 should be that corresponding to the development of the plastic hinges in the retrofitted column. Nevertheless it is conservative, and simple, to use an angle $\theta = 30°$.

The distance between the resultant compression force, C, and the resultant tension force, T, is jd and the position of the latter force relative to the section centreline is αjd, as seen in Figure 7.2. By taking moments about the position of the resultant compression force the nominal moment due to the compression/tension force couple and the axial load is,

$$M_n = Tjd + (1-\alpha)jd\,N^* \qquad (7.5)$$

The influence of the diagonal concrete compressive field in the column, due to the interaction of bending and shear in the cracked concrete section, is to increase the tensile force in the longitudinal reinforcement at a particular section over that given by the plane sections hypothesis. Analogous to a beam, the actual tensile force in the longitudinal reinforcement can be determined through the use of a shifted or fictitious bending moment demand. Thus the fictitious moment at a section including the tension shift effect is,

$$M + Ve_v = \phi\left[Tjd + (1-\alpha)jd\,N^*\right] \qquad (7.6)$$

The term on the right hand side of Equation 7.6 is the dependable flexural strength of the section while the term on the left side of the equation represents the fictitious bending moment demand on the column to account for the tension shift effect with a shift of $e_v = jd/2tan\theta$ occurring in the column.

For beams the dependable flexural strength envelope is used to ensure that the bending moment demand does not exceed the dependable strength of the beam at any point. By taking the dependable flexural strength envelope for a column the same

principle can be applied to compare the moment demand, including the tension shift effect, to the flexural strength of the column section as expressed in Equation 7.6.

For a column the choice of a 30° crack angle and rounding up of the tension shift to the section diameter or depth is sufficient for design purposes as suitably conservative assumptions are used.

7.2.3 Curtailment of Flexural Reinforcement

Reinforced concrete members may have flexural reinforcement curtailed in order to economise on the use of reinforcing steel and to reduce possible congestion of bars at a particular section. The reinforcement is curtailed where the reduction in bending moment allows this to be done and it is possible and practical to do so. Often only beams and structural walls in buildings will have longitudinal reinforcement curtailed as it is seldom practicable to curtail reinforcement in columns.

7.2.3.1 New Zealand Code Requirements

The current New Zealand Concrete Structures Standard, NZS 3101:1995 [X2] requires that the longitudinal tension reinforcement extend beyond the point at which according to the design bending moment envelope it is,

- required at full strength for a distance equal to the development length, L_d, plus the effective depth, d, of the member and,
- no longer required to resist flexure for a distance of 1.3 times the effective depth, d, of the member.

Besides the tension shift the second requirement recognises that a small amount of moment redistribution can cause a shift in the bending moment demand due to changes in the loading, settlement of the supports and other causes.

The requirements of NZS 3101:1995 are intended to cover the tension shift and anchorage requirements in columns or beams in order to prevent premature

flexure-shear failures occurring within the member due to the curtailment of the longitudinal tension reinforcement. For circular columns 1.3d could be interpreted as the column depth, D.

The previously common practice of curtailing the longitudinal tension reinforcement closely following the bending moment diagram, without regard for the tension shift effect occurring, only provided the required development length for anchorage beyond the critical section. As mentioned before with the tension shift effect the stresses in the reinforcement at the critical section are higher than those that would be predicted from the bending moment diagram and the reinforcement is required to resist flexure for some distance beyond the critical section. As the development length for the reinforcement has been taken from the critical section there is often insufficient length of reinforcement past the point at which the steel is required to resist flexure to properly anchor the bar and develop the yield strength of the reinforcement.

From the tests of Units I-A and I-B the results show that the practice of curtailing reinforcement directly following the static bending moment diagram may lead to the development of shear failures with limited ductility at the curtailment sections. As columns are usually detailed for plastic hinging to occur at the base and/or the top of the column there would generally be insufficient transverse reinforcement provided at a curtailment point to ensure adequate rotational capacity of the column to accommodate the additional inelastic rotational demands generated at this point.

Design standard requirements for development lengths and requirements for extension past the point at which the reinforcement is theoretically required to resist flexure, to account for the tension shift effect, are appropriate for design of new structures but may be too conservative for use when assessing existing structures.

For an existing column with curtailed longitudinal reinforcing, which may not possess an adequate length of longitudinal reinforcement beyond the critical section to cover the tension shift effect and anchorage requirements, the amount of tension shift that will occur in the column must be determined. Columns with distributed longitudinal reinforcement often have internal lever arms, jd, somewhat smaller than

the effective depth of the section. Therefore the provisions used in the design of columns will overestimate the actual tension shift that occurs. Consequently a more rational value for the tension shift effect would be a more appropriate value to use when assessing the potential for exceeding the flexural strength of a column at a curtailment point.

7.3 QUANTIFYING THE SIZE OF THE TENSION SHIFT

7.3.1 Modelling of Column Sections

From Equation 7.2 it can be seen that the amount of tension shift, e_v, is dependent on the internal lever arm, jd, and the angle of diagonal compressive stress field, θ. The angle θ can be determined for a member from Equation 7.4 which depends on the amount of transverse reinforcement provided in the member. However it is simple to assume an angle for the diagonal compressive stress field of between 45° and 30°, with a common angle for flexure-shear cracking of 30° assumed for assessment of columns [P3].

By establishing the internal forces in a column and the position of their resultants the internal lever arm can be obtained. By using concrete stress-strain models that account for strength enhancement due to confinement of the concrete and steel stress-strain curves which account for strain hardening, the internal forces, position of their resultants, moment and curvature can be calculated for any level of concrete strain in the extreme compressive fibre. These results can be obtained as part of a full moment-curvature analysis of a section.

As well as the moment, curvature and extreme bar steel strain, the internal lever arm ratio, jd/D, neutral axis depth ratio, c/D, contribution of tension reinforcement, $T/A_{st}f_y$, and position of compression and tension force resultants, for a given column, can be determined at any extreme fibre compressive strain in a column for each step in a moment-curvature analysis.

7.3.2 Parameter Study

The variation of these parameters with different axial load ratios and longitudinal steel ratios for circular and rectangular columns was investigated by analysing a number of different sized columns to allow the development of expressions for each parameter. Each parameter was evaluated for each given column at an extreme compressive fibre strain of $\varepsilon_c = 0.004$ and the results used to derive expressions for each parameter. This extreme fibre strain has been taken as it is approximately the strain at which the nominal flexural strength of a column is reached.

Circular columns were modelled with the longitudinal reinforcement distributed equally around the circumference of the column. Rectangular columns were modelled with the longitudinal reinforcement distributed equally on all four faces of the column. Figure 7.3 shows the reinforcement layout of each type of column.

7.3.2.1 Range of Variables Used

The variables examined for the circular and rectangular columns include:

- compressive axial load ratio, N^*/f'_cA_g, from zero to 0.1
- longitudinal reinforcement ratio, p_t, from 0.8 % to 4 %
- mechanical ratio $m = f_y / 0.85\ f'_c$, from m = 6 to 16
- the concrete cover to column diameter or column depth ratio

Compressive loads and strains are defined as negative. The yield strength of the longitudinal and transverse steel was taken as 300 MPa.

The concrete cover to diameter ratio was changed through the use of the parameter g, where g is the ratio of pitch of circular arrangement of longitudinal reinforcement to cross section diameter, for circular columns, or distance between reinforcing bars closest to faces of rectangular columns to section depth. Column interaction design charts are often produced for different values of g or concrete cover to diameter

ratios and require interpolation between the two values. For this study columns were evaluated with g = 0.8, 0.9 and 1.0.

The values of the variables were chosen as many bridge columns are usually lightly loaded in compression and the chosen yield strength of the reinforcing steel more closely matches the probable yield strength of the steel used in older structures. Chapman [C2] reports that site sampling and testing of reinforcing steel from New Zealand structures built during the period 1930 - 1970 showed the reinforcement possessed a yield strength 15 - 20 % greater than the specified value. Typical specified yield strengths for reinforcement were 240 MPa which gives probable yield strengths of 276 to 288 MPa [M2].

The New Zealand Concrete Structures Standard [X2] allows longitudinal reinforcement ratios in columns from a minimum of 0.8 % to a maximum of 8 %. Since it is impractical to use longitudinal steel ratios as high as 8 % due to the difficulties in placing and lapping such large quantities of bars, an upper limit of 4 % is often adopted for columns designed for seismic resistance.

As the yield strength, f_y, was held constant at 300 MPa the variation of the mechanical ratio, m, is used to vary the concrete compressive strength from f'_c = 22 MPa to 59 MPa. This range of strengths covers concrete strengths assumed at the design stage through to higher concrete strengths that result from the natural strength gain of concrete over time. Older structures, those more likely to require seismic assessment and/or retrofit, will have in-situ concrete strengths which will be substantially higher then the concrete strengths assumed at the design stage.

Although expressions developed from this study used a constant longitudinal yield strength of f_y = 300 MPa the expressions can be applied with good confidence for steel strengths in the range of 250 MPa to 350 MPa with mechanical ratios in the range m = 6 to 16. For steel yield strengths significantly different from these values the appropriate values can be obtained from a moment-curvature analysis of the column section. Comparison of the data points used to derive these expressions with f_y = 300 MPa are included in Appendix E. Comparative analyses using f_y = 250 MPa

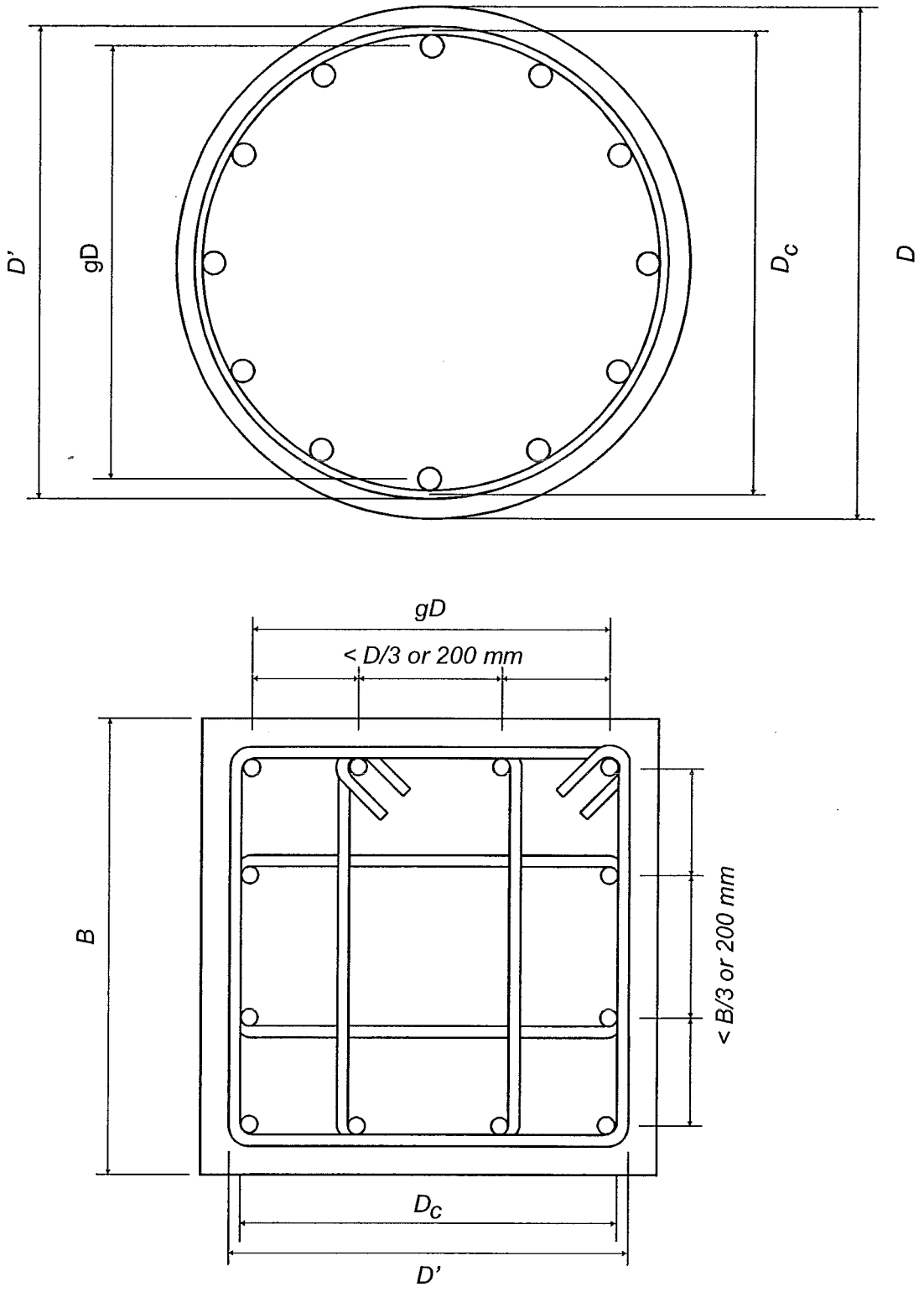

Figure 7.3 *Layout of Circular and Rectangular Columns Used to Evaluate Size of Tension Shift Effect*

and 350 MPa were also conducted and are plotted in Appendix E for comparison of the data points with the proposed expressions.

7.3.2.2 Column Detailing and Geometry

Transverse reinforcement for the columns was detailed so that the spacing between transverse hoop sets was approximately eight times the longitudinal bar diameter. The current New Zealand Concrete Structures Standard, NZS 3101:1995 [X2], specifies the transverse reinforcement spacing, for columns required to resist seismic actions, be no greater than one quarter of the least lateral dimension of the cross section or six times the diameter of the longitudinal bar restrained. This spacing requirement is relaxed to one third the least lateral dimension of the cross section or 10 times the longitudinal bar diameter for columns not required to resist seismic actions.

For the rectangular columns analysed the distance between longitudinal bars which are laterally restrained by a cross-tie or corner of a transverse hoop is set at the larger of 1/3 of the adjacent lateral dimension of the cross section or 200 mm. This is the same as the NZS 3101:1995 general requirements for columns while the lateral restraint spacing requirements for columns designed to resist seismic actions is decreased to the larger of 1/4 of the adjacent lateral dimension or 200 mm.

The analysed columns fall outside the current requirements for transverse reinforcement spacings in NZS 3101:1995 for columns designed to resist seismic actions. It is intended that the expressions derived can be applied to existing columns designed using previous, less stringent, transverse reinforcement spacing requirements and containing potential deficiencies with the curtailment of longitudinal reinforcement in the columns which will likely affect the seismic performance of the structure. It is unlikely to find longitudinal reinforcement which has been curtailed in building columns as the moment demands in a building frame would not allow or warrant any curtailment. Bridge columns however, especially large sections and tall piers, are more likely to have longitudinal reinforcement curtailed up the height of the column.

The transverse reinforcement ratio for the rectangular columns analysed ranged from $p_s = 0.30$ % to 1.08 % for a yield strength $f_{yh} = 300$ MPa. Circular columns analysed had transverse reinforcement ratios ranging from $p_s = 0.16$ % to 0.38 % for a yield strength $f_{yh} = 300$ MPa. The amount of transverse reinforcement provided in the column will influence the amount of confinement provided to the concrete, the compressive strength enhancement and hence the neutral axis depth required in the column at development of the nominal flexural strength. The range of p_s values for the rectangular and circular columns analysed do not significantly influence the c/D values obtained at an extreme compressive fibre strain of $\varepsilon_c = -0.004$. However the moment-curvature response after reaching the nominal flexural strength will be greatly influenced by the amount of transverse steel provided in the column.

7.3.3 Results of the Parameter Study

The truss analogy was used in Section 7.2.2 to derive an expression for the tension shift. Equation 7.2 shows that the shift depends on the internal lever arm, jd, and on the inclination of the diagonal compressive stress field, θ. An expression for θ was derived in Section 7.2.2.

The parametric analysis was employed to derive simple equations for jd for both circular and rectangular columns. In addition, the proportion of the force in the longitudinal reinforcement in tension to the total yield force $A_{st}f_y$ was obtained as this ratio enables a simple design of a retrofit scheme.

Investigations have shown that the internal lever arm in circular and rectangular columns remains constant for a range of longitudinal steel ratios, p_t, from 0.8 % to 4 % and compressive axial loads, N^*, from zero up to $-0.1f'_cA_g$. Results for both the rectangular and circular columns were found to be within ±10 % of the values given by the following equations. It was found that,

for rectangular columns:-

$$\frac{jd}{D} = 0.7 - 0.4(1 - g) \qquad (7.7)$$

and for circular columns:-

$$\frac{jd}{D} = 0.62 - 0.4(1 - g) \qquad (7.8)$$

where jd = internal lever arm

D = depth of rectangular section or diameter of circular section

g = ratio of pitch of circular arrangement of longitudinal reinforcement to cross section diameter, for circular columns, or distance between reinforcing bars closest to faces of rectangular columns to section depth

This shows that the internal lever arm, jd, for columns with distributed longitudinal reinforcement can be lower than 0.5 D, which would give tension shifts less than half of the value usually assumed for design purposes.

By taking a more rational value for the tension shift, the effects of premature curtailment of longitudinal reinforcement in existing columns can be evaluated and the possibility of attaining the flexural strength at the curtailed section can be assessed. The bending moment envelope for the column can be modified to take into account the tension shift effect which increases the moment demand over the column height. This can then be compared to the dependable flexural strength envelope obtained from the proposed equations, design charts or moment-curvature analyses at each section of the column. From this it can be easily seen if the bending moment demand, including the tension shift effect, exceeds the flexural strength envelope of the column.

The magnitude of resultant tension force to the total longitudinal steel is given for rectangular columns:-

$$\frac{T}{A_{st} f_y} = 1.2 \frac{N^*}{f_c' A_g} + 0.75 \qquad (7.9)$$

and for circular columns:-

$$\frac{T}{A_{st} f_y} = 1.9 \frac{N^*}{f_c' A_g} - 7.3 p_t + 1.08 - 0.2 g \qquad (7.10)$$

but $T/A_{st}f_y$ must not be taken less than 0.58 nor greater than 0.75.

where $N^* / f'_c A_g$ is negative for compressive axial loads

T	=	resultant tensile force in longitudinal steel
A_{st}	=	total area of longitudinal steel
f_y	=	yield strength of longitudinal steel
p_t	=	volumetric ratio of longitudinal steel

The results for all rectangular columns fell within ±10% of the values given by Equation 7.9 for the range of longitudinal steel ratios and axial load ratios investigated.

The position of the resultant forces within the column, with respect to the centreline of the column and the internal lever arm is found using the factor α, (see Figure 7.2). It was found that,

for rectangular columns:-

$$\alpha = -0.9 \frac{N^*}{f_c' A_g} + 0.29 - 0.15 (1 - g) \qquad (7.11)$$

but α should not be taken less than $0.34 - 0.15(1-g)$,

and for circular columns:-

$$\alpha = (15p_t - 2)\frac{N^*}{f_c' A_g} + 6p_t + 0.3g - 0.15 \qquad (7.12)$$

but α should not be taken less than $0.2g + 0.07$ nor greater than 0.40.

The neutral axis depth for rectangular and circular columns was also investigated and related to the axial load ratio and longitudinal steel ratio. The following expressions have been obtained from the range of columns analysed in order to obtain the expressions in Equations 7.7 to 7.12.

For rectangular columns:-

$$\frac{c}{D} = (18p_t - 1.4)\frac{N^*}{f_c' A_g} + 5p_t + 0.22(1-g) \qquad (7.13)$$

and for circular columns:-

$$\frac{c}{D} = (18p_t - 1.4)\frac{N^*}{f_c' A_g} + 4.6p_t + 0.10(1-g) + 0.07 \qquad (7.14)$$

where c = distance from extreme compressive fibre to position of neutral axis

By substituting typical values of p_t and g into Equations 7.13 and 7.14 a simplified expression for the neutral axis depth ratio can be obtained for both rectangular and circular columns when the extreme compressive fibre strain reaches $\varepsilon_c = -0.004$.

$$\frac{c}{D} = 0.18 - 0.95\frac{N^*}{f_c' A_g} \qquad (7.15)$$

Equation 7.15 provides a good approximation to the neutral axis depth ratios given by Equations 7.13 and 7.14 where the longitudinal steel ratio, p_t, lies between 1.5 % and 3 %.

7.4 ASSESSMENT OF THE STRENGTH AND LATERAL DEFORMATION CAPACITY IN COLUMNS WITH LONGITUDINAL BAR CURTAILMENT

7.4.1 Location of Plastic Hinges

As part of a seismic assessment of a structure, once the potential failure hierarchy and mechanism of inelastic deformation are identified, the critical sections would have to be determined and the overall strength and capacity of the structure assessed and compared to the force and displacement demands imposed on the structure. The presence of longitudinal bars that have been curtailed in a column because of decreased bending moment demand may become a critical region within the structure if insufficient provision for anchoring the longitudinal bars has been allowed. This is common in earlier structures where the longitudinal steel has been curtailed directly from the bending moment diagram. Other situations may arise where the dynamic response of the column exceeds the static bending moment demand over the height of the column or where the column has been shortened by use of an overlay at the base of the column moving the critical section closer to the curtailment point.

The formation of a critical section within the height of a column, due to the curtailment of longitudinal reinforcement, may affect the overall performance of a structure as this section would probably not have been adequately detailed to provide sufficient strength and/or ductility to match the demands imposed on the structure at this point.

Generally with structures requiring detailed seismic assessment and retrofit, the columns will not possess adequate transverse reinforcing to provide sufficient shear capacity and ductility to ensure satisfactory performance during a large earthquake. Assessment of the nominal flexural strength of a column up its height can easily be done by applying the proposed equations, use of column design charts or moment-curvature analyses at each point where the longitudinal tension reinforcing is curtailed. The moment capacity can then be compared directly to the bending moment demand in the column, including an allowance for the tension shift effect, to determine whether the flexural strength of the column will be reached at any point.

The proposed relationships with internal lever arm, tension steel contribution and position of the internal force resultants as functions of axial load ratio and longitudinal steel ratio allow the nominal flexural strength envelope of a column to be determined by applying these equations instead of conducting moment-curvature analyses for the column. Similarly column design charts will give the nominal flexural strength of a column. Application of the proposed equations or the use of design charts will determine the nominal flexural strength of the column section but a moment-curvature analysis is useful to determine any overstrength and the inelastic deformation capacity of the column.

Equations 7.7 - 7.12 can be used to determine the nominal flexural strength envelope for symmetric square or circular columns where the area of longitudinal steel at each section is used to determine the magnitude of Tjd up the height of the column and added to the axial load contribution to flexural strength, $(1-\alpha)jd\,N^*$. This can then be represented graphically and the bending moment demand, including the tension shift effect, can be plotted over the dependable flexural strength envelope to determine any potential flexural strength shortfall at the curtailment point(s). Examples of the application of Equations 7.6 – 7.12 are included in Appendix A.

If the retrofit scheme is based on the principles underlying capacity design the strength reduction factor can be taken as $\phi = 1$. This implies that the concrete compressive strength and the yield strengths of the longitudinal and transverse reinforcement are determined with accuracy. However, destructive testing methods are required to establish the yield strength of the reinforcement. In lieu of such tests, if the typical values of the yield strengths of the reinforcement can be traced, the yield strength of the transverse reinforcement can be taken as the lower 5^{th} percentile value whereas the longitudinal reinforcement yield strength can be taken as the 95^{th} percentile strength.

Figure 7.4(a) shows a column containing longitudinal reinforcement which has been curtailed part way up the height of the column. This curtailment has been done following the bending moment diagram without adequate allowance for the tension

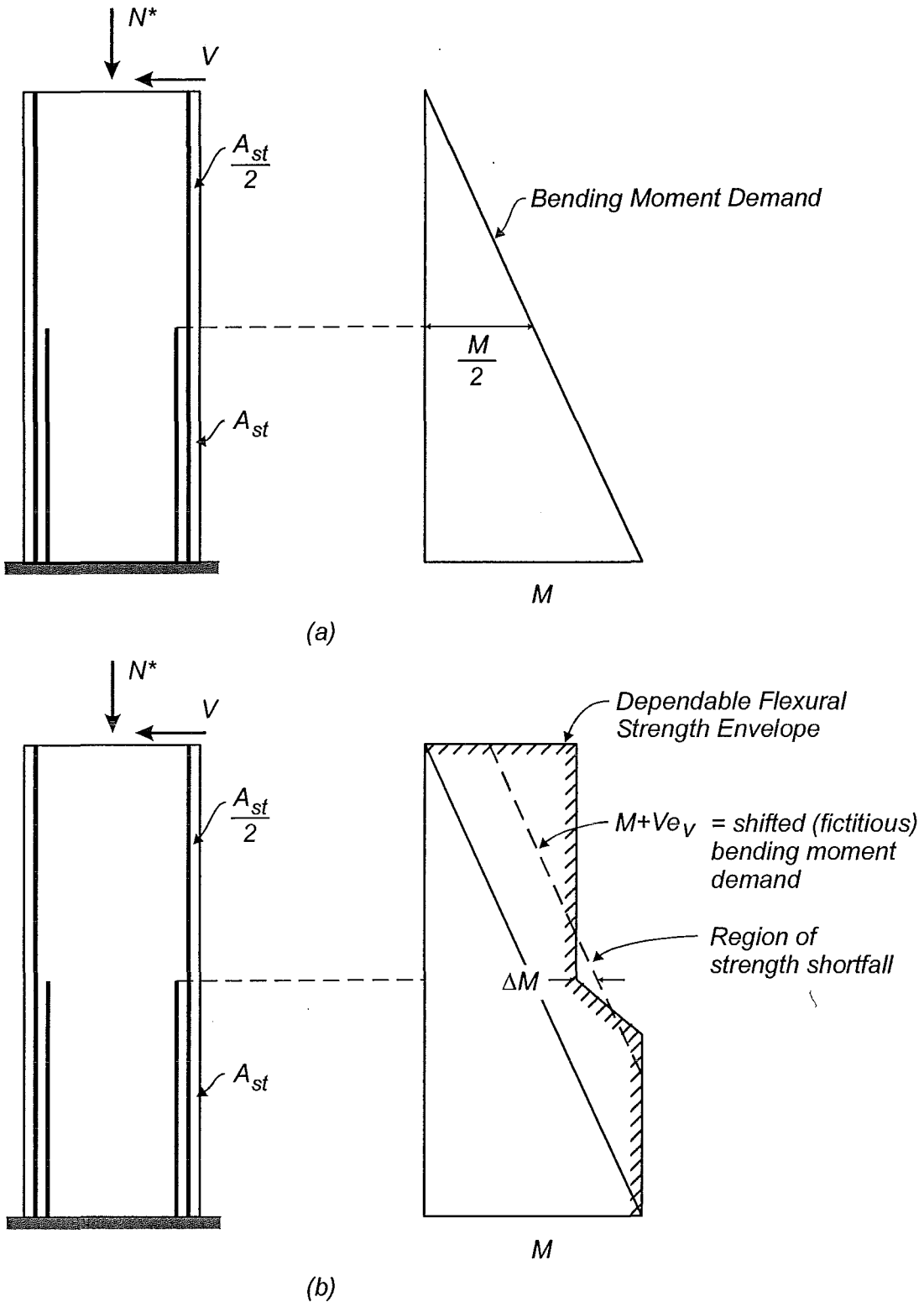

Figure 7.4 *Flexural Strength and Bending Moment Demand Envelopes*

shift to occur. Figure 7.4(b) illustrates the dependable flexural strength and bending moment diagram as expressed in Equation 7.6. From this diagram it can be seen that the flexural strength of the column is exceeded at the curtailment point when the tension shift effect is taken into account. Where the moment demand has exceeded the dependable flexural strength envelope, any flexural strength shortfall at the curtailment point can be determined from the diagram. If the retrofit scheme is solely based on enhancing the flexural strength of the column, the flexural strength shortfall, ΔM_n, can be expressed as:-

$$\Delta M_n = \phi \left[\Delta \left(Tjd + (1-\alpha) jd\, N^* \right) \right] \qquad (7.16)$$

A column would need to be assessed at the moment corresponding to development of the nominal flexural strength at the base of the column and at higher column base moments resulting from any strength increase due to strain hardening of the reinforcement at higher curvatures in the column. This will indicate whether there is any potential for exceeding the flexural strength at the curtailment points in the column when the base of the column reaches its nominal flexural strength and to ensure that increased flexural demands at the base of the column do not lead to excessive flexural strength demands on the column at the curtailment point(s).

If the column's flexural strength is exceeded at the curtailment point(s) the inelastic deformations will concentrate at the curtailment point. This will then place large curvature demands on the column at the curtailment point due to the concentration of the inelastic deformations in the column at this point. Often the curtailment points up the height of the column will not contain sufficient quantities of transverse reinforcement as only the base of the column will have been detailed for inelastic action. Therefore the large inelastic displacement demands on the column at the curtailment point are not able to be sustained and the column is likely to fail after limited ductility response at this point.

7.4.1.1 Effect of Dynamic Response on Bending Moment Pattern

The bending moment demand on a column will be influenced by the dynamic response of the structure. Figure 7.5 illustrates the static and dynamic bending moment demand for a bridge pier with a large superstructure rotational inertia due to the presence of a column cap. The assumed static bending moment demand has zero bending moment at the centre of mass of the superstructure where the equivalent lateral seismic force is assumed to act. If the superstructure has a large rotational inertia the bending moment demand at the centre of mass of the superstructure corresponding to the first mode of vibration will be increased giving a worst case for the evaluation of bar curtailment effects in a bridge pier.

The amount of flexural strength shortfall can be obtained from a graphical representation of the dependable flexural strength envelope, the bending moment demand, including dynamic effects, and the "fictitious" bending moment demand due to the tension shift effect.

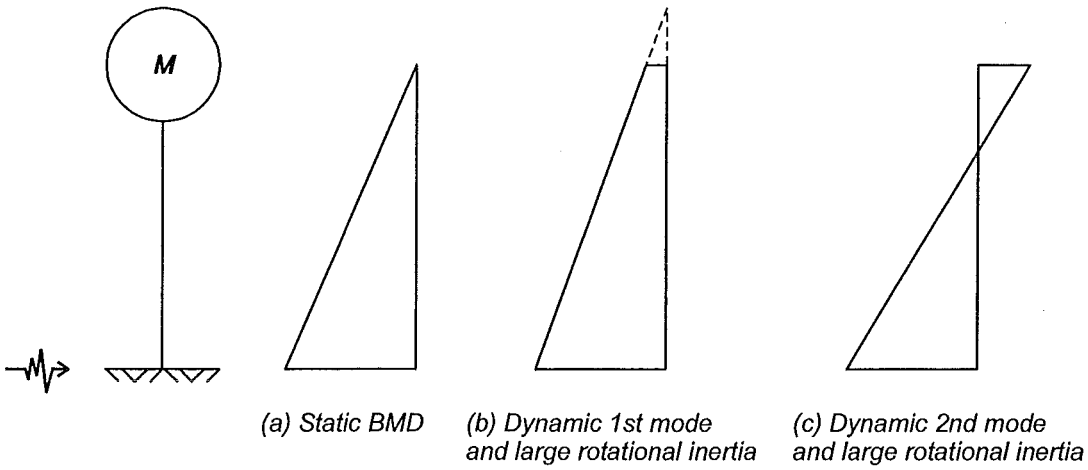

Figure 7.5 *Bending Moment Demand for Static and Dynamic Response*

7.4.2 Deformation Capacity of Plastic Hinges in Regions of Bar Curtailment

A method for evaluating the shear capacity of an existing column is proposed by Priestley et al. [P3, P4] which accounts for the transverse reinforcing, axial load and concrete contributions to shear resistance.

$$V_n = V_c + V_s + V_p \tag{7.17}$$

where

$$V_c = 0.8\,k\sqrt{f_c'}\,A_g \tag{7.18}$$

$$V_s = \frac{\pi}{2}\frac{A_{sp} f_{yh} D_c}{s \tan\theta} \quad \text{circular columns} \tag{7.19a}$$

$$V_s = \frac{A_v f_{yh} D_c}{s \tan\theta} \quad \text{rectangular columns or beams} \tag{7.19b}$$

$$V_p = -N^* \tan\alpha \tag{7.20}$$

The concrete shear resisting mechanism, V_c, degrades with increasing curvature ductility demand. The term k varies with curvature ductility as shown in Figure 7.6 and is dependent on whether the column is subjected to uniaxial or biaxial ductility.

The contribution of the transverse steel to shear resistance, V_s, is based on a truss mechanism with an angle θ of 30° between the compression diagonals and the axis of the column unless the corner-to-corner diagonal subtends a larger angle with the axis of the member. The distance D_c is taken as the distance between centres of the peripheral hoops or spirals in the column as shown in Figure 7.3.

The axial load, N^*, is taken as negative for compressive axial loads and compressive axial loads are considered to enhance the shear strength of the column. The axial load component, V_p, is provided through the formation of an inclined strut joining the centres of flexural compression at the top and bottom of the column as shown in Figure 7.7.

In the event of a plastic hinge forming at a curtailment point within the height of a column, this component of shear resistance must be neglected. Once a plastic hinge has developed at a curtailment point the inclined strut can no longer develop between the top of the column and the base, as indicated in Figure 7.7. The inclined strut will form between the top of the column and the compression zone at the curtailment point. Below the curtailment point the strut is no longer inclined offering no horizontal component to resist shear and thus must be neglected.

Due to the low axial load applied to many bridge columns, much of the shear resistance is provided by the concrete and transverse steel mechanisms. Where there is insufficient contribution to the shear resisting mechanism from the transverse reinforcement the column will fail through shear when the capacity for the concrete shear resistance contribution is reached.

Since the total shear strength of a column may be expressed in terms of curvature ductility the comparison of the flexural strength-curvature ductility and the shear strength-curvature ductility for the column can be made. The flexural moment-curvature relationship can be expressed as an equivalent shear force-curvature relationship and compared to the shear strength-curvature ductility relationship. Figure 7.8 shows three different moment-curvature responses, expressed as equivalent shear force-curvature relationships, which may be applicable to three different levels of longitudinal reinforcement ratio. Relationship 1 shows the column developing a flexural strength, $V_1 > V_i$, the initial nominal shear strength, and a brittle shear failure occurs. Relationship 3 develops a maximum shear force corresponding to a fully ductile response which is inside the shear strength envelope. Shear failure does not occur and the column fails when the flexural ductility capacity, $\mu_{\phi,f}$ is reached. Relationship 2 has a shear force corresponding to an ideal flexural strength lower than the shear strength envelope. As the ductility develops the increasing shear force intersects the decreasing shear strength envelope developing a limited ductile shear failure at $\mu_{\phi,s}$, less than the limit to flexural ductility.

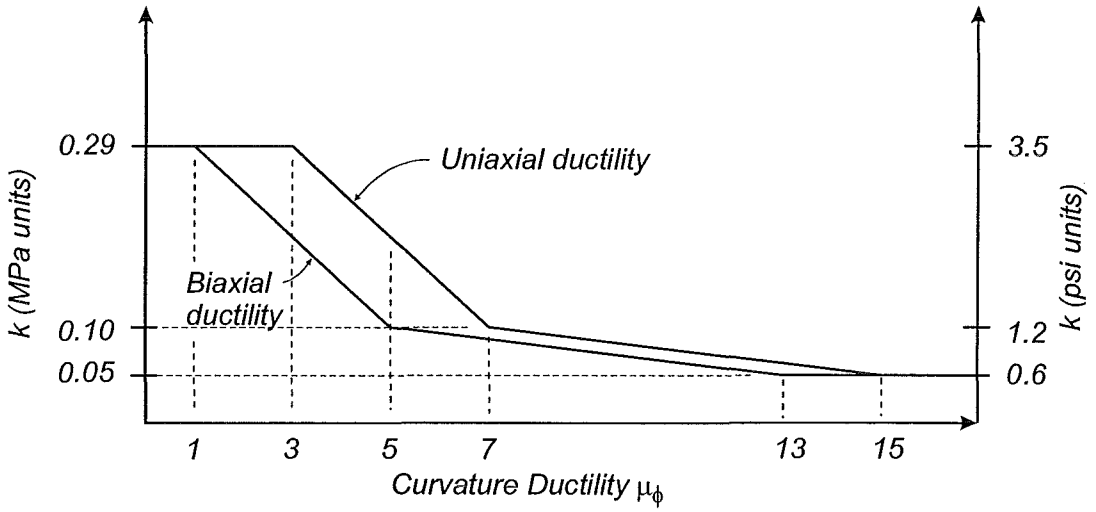

Figure 7.6 *Variation of Concrete Component of Shear Resisting Mechanism with Curvature Ductility for Assessment Purposes [P3]*

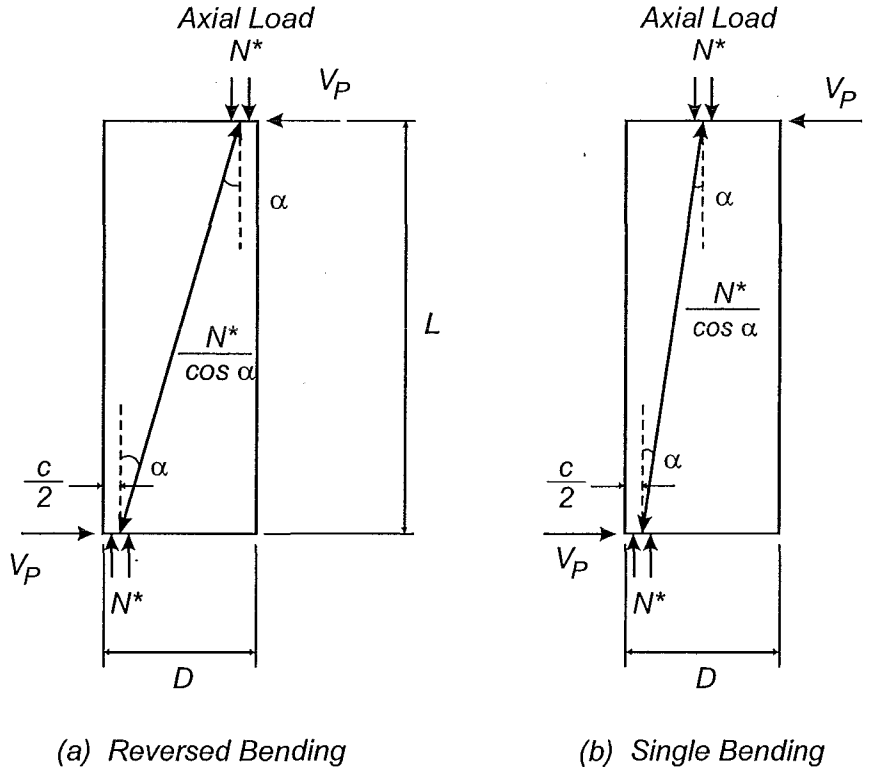

Figure 7.7 *Contribution of Axial Load to Column Shear Resistance [P3]*

The ultimate curvature corresponding to this premature shear failure is used as a limit to the amount of plastic rotation of a hinge during a plastic collapse analysis. Further displacement capacity may be available from the column through shear deformations but the definition of curvature and curvature ductility is lost as the displacement is not taking place through rotation but due to shear distortion of the column. Displacements of the tip of a column due to rotation (curvature) are dependent on the distance from the top of the column to the plastic hinge. When displacement is controlled by shear the displacement of the top of the column is independent of the distance from the top of the column to the plastic hinge. As a result large shear displacements are required to satisfy the lateral displacement demand and it is unlikely that the available shear displacements will be adequate. Thus it is conservative to take the curvature when the flexure and shear envelopes intersect, corresponding to $\mu_{\phi, s}$, as the maximum available curvature in the column.

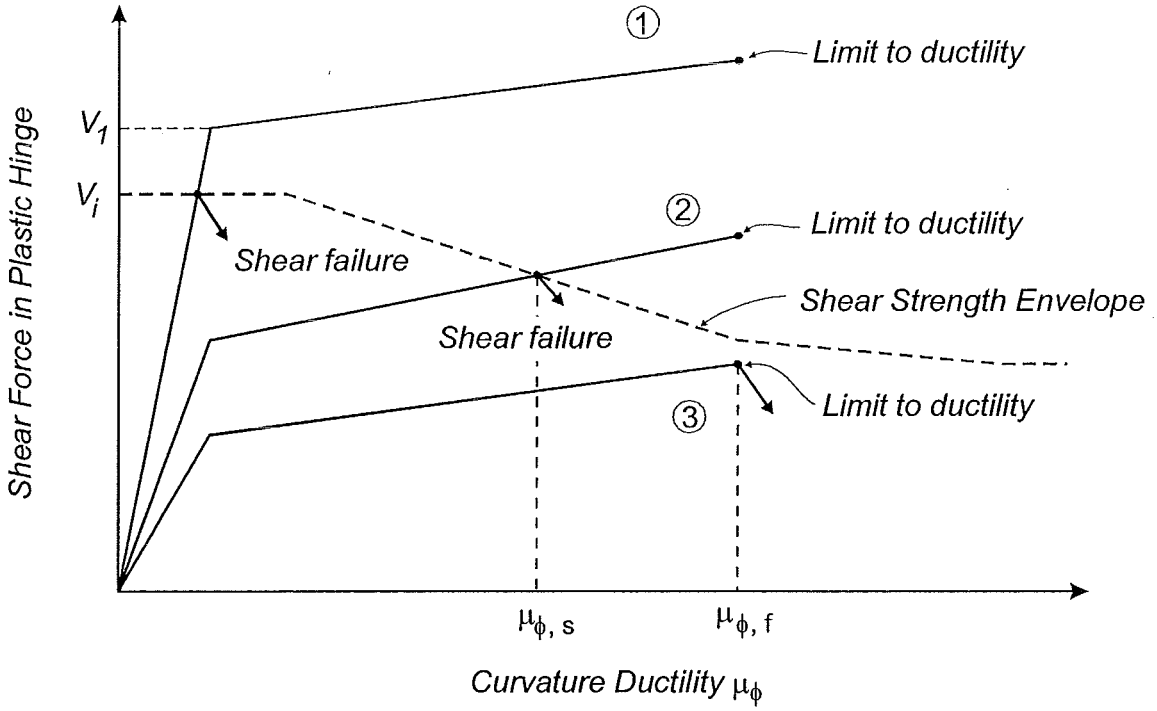

Figure 7.8 *Ductility at Failure for Columns with Different Longitudinal Reinforcement Ratios [P3]*

7.4.3 Retrofit of Columns with Deficient Strength at the Curtailment Points

Should a column have insufficient flexural strength to resist the flexural demand, when the tension shift effect is included, the column should be retrofitted to improve its performance to meet the expected demands. This shortfall can be corrected by:-

- Enhancing the flexural strength through the use of a reinforced concrete, steel or fibre reinforced polymer (FRP) jacket.
- Enhancing the shear strength through the use of a reinforced concrete, steel or FRP jacket.
- By a combination of (a) and (b)

If retrofit is required to improve the flexural strength of the column at a curtailment point, the additional flexural strength required can be obtained from the flexural strength envelope diagram and expressed as in Equation 7.16. This indicates that the flexural strength of a section can be improved by increasing the contribution of the tensile longitudinal steel to the flexural strength and/or increasing the axial load contribution to the flexural strength. This could be achieved by increasing the amount of longitudinal steel in the column or increasing the axial load acting on the column to overcome the flexural strength shortfall.

The simplest method of achieving the required flexural strength shortfall is to increase the amount of longitudinal reinforcement in a column by equating the flexural strength shortfall to $\phi \Delta Tjd$ and determining the additional area of longitudinal reinforcement required in the column at the curtailment point(s) from this. Yield of the longitudinal reinforcement placed in reinforced concrete and steel jackets are appropriate to determine the required additional area of longitudinal reinforcement. Strain compatibility and the choice of an appropriate longitudinal strain is required when using an elastic FRP jacket [W1].

7.5 TENSION SHIFT NUMERICAL EXAMPLES

Numerical examples are included in Appendix A demonstrating the use of the proposed relationships to determine the possibility of reaching the flexural strength of a column containing longitudinal reinforcement which has been curtailed up the height of the column. The proposed relationships are used along with a graphical approach to compare the flexural strength envelope of a column and the bending moment demand, including the tension shift effect.

The original "as-built" designs for Piers 46 and 68 are analysed along with an example rectangular column.

CHAPTER 8

ALTERNATIVE MODELLING OF CONFINED CONCRETE STRESS-STRAIN BEHAVIOUR

8.1 INTRODUCTION

8.1.1 Outline

This Chapter presents the model used to describe the stress-strain behaviour of unconfined concrete and concrete confined with the use of transverse steel, developed by Mander et al. [M3, M4]. This model is presented here as it has been widely accepted and used in New Zealand and is used as a benchmark stress-strain relationship for confined and unconfined concrete. Moment-curvature analyses are conducted for columns subjected to axial load and flexure. Results obtained using the original Mander et al. stress-strain model are compared to an approach which explicitly models the effectively confined core and the regions defined within the concrete core, outside the effectively confined core, instead of smearing the effectively confined core over the entire core area. As the confinement efficiency factor depends on the effectively confined core area, the choice of arch profile assumed to act in the section will influence this value. This study will investigate the sensitivity of the initial tangent angle chosen for the arch profile for columns subjected to flexural and axial load. A statistical approach comparing maximum moments obtained from experimental results to predicted maximum moments while varying the arch profile is included.

Sakai and Sheikh [S7] suggest that the presence of a heavily reinforced stub adjacent to the critical section of columns tested at the University of Canterbury are responsible for the observed strength enhancement seen in test results for these columns. This stub is provided in University of Canterbury column tests to model the effects of members framing into the columns of buildings or bridge structures adjacent to the critical section. Gill et al. [G1, P6] first noted the effect of the stub on

the moment-curvature response of a column, yet despite much research into the moment-curvature behaviour of columns in the last 20 years there has been no attempt to quantify this effect. Ang et al. [A1] suggested an expression to account for the observed flexural strength enhancement, for University of Canterbury column tests, as a function of axial load ratio. The flexural strength enhancement has been attributed to the increased contribution of the concrete compressive force to flexural strength at high axial load ratios, resulting from the influence of the enhanced compressive strength due to the presence of confining reinforcement. An investigation into the influence of the confining stub on the amount of flexural strength enhancement and moment-curvature response of a column is included in this Chapter.

Derivation of a simple moment-curvature analysis to account for the effects of reversed cyclic loading of a column is also included here.

8.1.2 Stress-Strain Behaviour of Confined Concrete

In the seismic design of reinforced concrete members in structures, the behaviour of the member, when undergoing large displacements in the inelastic range, can be highly influenced by the behaviour of the confined concrete within the core. Potential plastic hinge regions of these members must be carefully detailed for ductility to ensure that the members can sustain the large inelastic deformations imposed during an earthquake and prevent collapse of the structure. The most important part of ensuring adequate ductility of a member is the provision of sufficient transverse reinforcement in the form of circular hoops or spirals, for circular members, or of overlapping rectangular hoops and cross-ties in rectangular members. Transverse reinforcement is required to confine the compressed concrete within the core, to prevent premature buckling of longitudinal steel and prevent failure of the member through shear.

To adequately describe the behaviour of a member, the stress-strain behaviour of the confined concrete within the core of the member must be known, in terms of the

peak stress attained, the strain at which this stress is reached and the amount of ultimate strain available from the concrete.

The peak stress and ultimate strain of concrete has been observed to increase when concrete is placed under a triaxial compression stress state compared to values for a uniaxial stress state. As the concrete approaches its uniaxial strength, internal cracking and crushing causes dilation, which is resisted by the lateral confining pressure acting on the concrete. The result is a significant enhancement of the peak stress and ductility of the concrete [B2, R1].

The use of transverse reinforcement can also lead to a significant increase in the strength and ductility of the compressed concrete. Concrete is generally confined with the use of closely spaced transverse steel hoops or spirals. As the concrete dilates, as it reaches its uniaxial (unconfined) strength, it bears outward against the transverse reinforcement which supplies a passive confining pressure.

Stress-strain models for confined concrete have been proposed by various researchers to quantify the degree of strength enhancement and increase in ductility. Comprehensive literature reviews of research to model the stress-strain behaviour of concrete confined with circular hoops or spirals and rectangular hoops, with or without supplementary cross-ties have been conducted by Zahn et al. [Z1], Tanaka and Park [T1], and Dodd and Cooke [D1]. These reviews present a number of different studies into describing the effect of confinement on the strength and ductility of concrete. Many of these models are based on experimental results obtained from compression testing of cylinders or prisms containing transverse reinforcement for confinement with or without longitudinal reinforcement present.

A feature of the commonly used confined concrete stress-strain models is the definition of a region of effectively confined core concrete within the region bounded by the peripheral hoops. Sheikh and Uzumeri [S1] first proposed the concept of an effectively confined core which is smaller than the concrete core, within the peripheral hoops because of vertical arching of the concrete between the transverse hoop sets and horizontal arching between the restrained longitudinal bars, as shown in Figures 8.1 and 8.2 for rectangular sections. The area of the effectively confined

core is determined by the spacing and arrangement of the transverse reinforcement and the arrangement of the longitudinal reinforcement in the section.

Although the effectively confined core area is defined, many stress-strain models smear the effectively confined core area over the entire concrete core through the use of a confinement efficiency factor. The confinement efficiency factor is usually based on the ratio of effectively confined core area to the concrete core area and is used to reduce the assumed lateral confining pressure provided by the transverse reinforcement. This reduced, or effective, lateral pressure is then assumed to act uniformly across the entire core area of the column and is used as the basis for determining the amount of strength enhancement provided to the confined concrete. This procedure essentially defines the concrete core of the column as having uniform stress-strain properties.

8.2 MANDER ET AL. STRESS-STRAIN MODEL

Mander et al. [M3, M4] proposed a model that describes the stress-strain behaviour of unconfined concrete and concrete confined with circular hoops, spirals or rectangular hoops. This model has the advantage that it describes the complete stress-strain curve as a single function, can be applied to circular and rectangular sections, and can also account for column or wall sections with different quantities of confining steel in the two perpendicular directions.

The compressive strength of unconfined concrete is denoted f'_{co}. This value is usually assumed to be 0.85 times the concrete cylinder strength, f'_c, due to size effects between concrete control cylinders and concrete within large members.

The strength of the confined concrete is calculated by using the concept of an effectively confined core within the nominal concrete core, as measured between the centreline of the peripheral hoops. The area of effectively confined core is determined by the spacing of transverse reinforcement, arrangement of longitudinal reinforcement in the section and the corresponding transverse reinforcement arrangement.

Rectangular hoops effectively confine the concrete only at and near the corners of the hoops. The sides of the rectangular hoops tend to bow outwards due to their small flexural stiffness and cannot effectively confine the concrete. Therefore confinement of the concrete is only achieved at the corners of the rectangular hoops or at locations where a longitudinal bar is laterally restrained by a hoop corner or cross-tie.

This leads to an area of concrete at the surface of the core which is not effectively confined as the concrete arches between each restrained longitudinal bar. In Figure 8.1 this area is shown shaded for various transverse hoop arrangements. It can be seen that the area of ineffectively confined concrete reduces when a greater number of restrained longitudinal bars are present in the section. Beyond the shaded area, over the effectively confined core, the confining stresses are assumed to be applied uniformly.

Mander et al. assumed that the confined concrete arches in the form of a parabola horizontally between restrained longitudinal bars, at the level of the transverse hoop sets, and vertically between the transverse hoop sets up the height of the column as shown in Figure 8.2. Arching is assumed to take place over the clear spacings between restrained longitudinal bars and transverse hoop sets. The boundary between the unconfined and confined concrete was assumed to have a parabolic shape with an initial tangent angle, θ, of 45°. The effectively confined core is then the total core area less the sum of the core areas which are not effectively confined.

Full details of the Mander et al. concrete stress-strain model can be found in the original references [M3, M4] and are well covered by literature reviews by Zahn et al. [Z1], Tanaka and Park [T1], and Dodd and Cooke [D1].

Circular columns reinforced with circular hoops or spirals are only affected by vertical arching as the hoops or spirals apply a uniform pressure due to hoop tension in the transverse reinforcement.

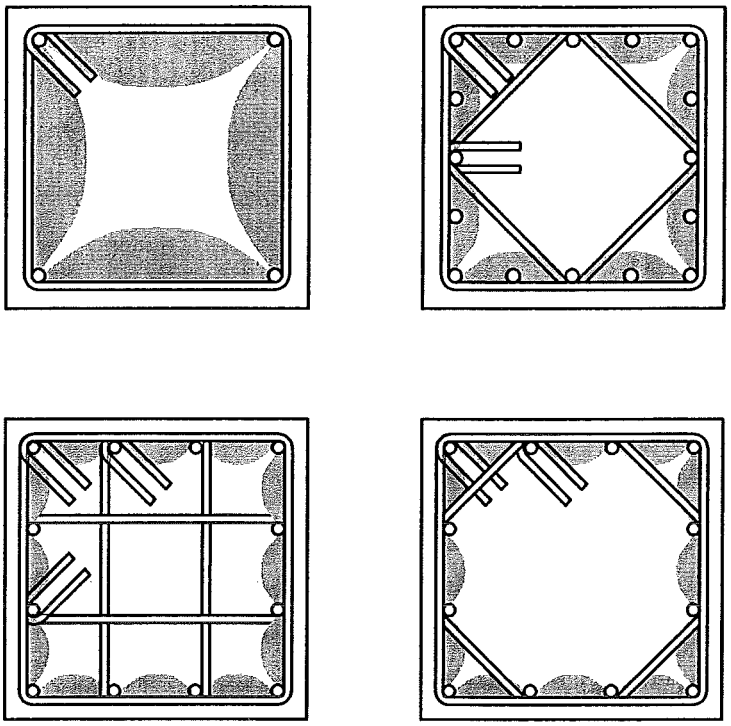

Figure 8.1 *Arching between Restrained Longitudinal Bars for Various Hoop Arrangements for Rectangular Columns [P1]*

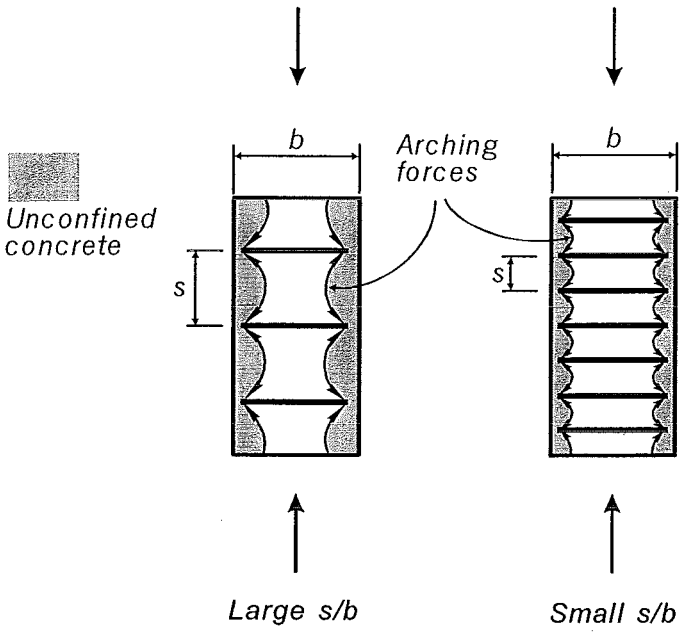

Figure 8.2 *Arching Between Transverse Hoop Sets [P1]*

The confinement efficiency factor, k_e, is defined as the ratio between the effectively confined core area, A_e, midway between transverse hoop sets and the total concrete area of the core, as measured between the centreline of the peripheral hoops.

The lateral confining pressure provided by the transverse reinforcement is taken at yielding of the transverse reinforcement. This is evaluated for each of the two perpendicular directions in the case of unequal transverse reinforcement.

$$f_{lx} = p_{sx} f_{yh}$$
$$f_{ly} = p_{sy} f_{yh} \qquad (8.1)$$

where p_{sx} and p_{sy} are the volumetric ratios of effective transverse reinforcement in the x and y directions for rectangular sections,

$$p_{sx} = \frac{A_{sx}}{sD_c}$$
$$p_{sy} = \frac{A_{sy}}{sB_c} \qquad (8.2)$$

where A_{sx} and A_{sy} = total area of transverse steel running in the x and y directions respectively.

For circular sections p_{sx} and p_{sy} are replaced by the volumetric ratio of the confining hoop or spiral reinforcement, p_s,

$$p_s = \frac{4A_{sp}}{sD_c} \qquad (8.3)$$

and

$$f_l = \frac{1}{2} p_s f_{yh} \qquad (8.4)$$

As the effectively confined core area, A_e, is less than the area of concrete within the centrelines of the peripheral spiral or hoop, A_{cc}, an effective lateral confining pressure, f'_l, is assumed to act uniformly over the total core area,

$$f_l' = k_e f_l \tag{8.5}$$

To evaluate the compressive strength of the confined concrete, Mander et al. evaluated the ultimate strength surface following the "five parameter" model proposed by William and Warnke [W2]. When the confined concrete core is placed under triaxial compression with equal effective lateral confining pressures the compressive strength of the confined concrete, f'_{cc}, can be given by:-

$$f_{cc}' = \alpha_1 \alpha_2 f_{co}' \tag{8.6}$$

The factor α_1 increases the compressive strength as a function of lateral confining pressure.

$$\alpha_1 = \left(2.254 \sqrt{1 + \frac{7.94 f_{l2}'}{f_{co}'}} - 2\left(\frac{f_{l2}'}{f_{co}'}\right) - 1.254 \right) \tag{8.7}$$

f'_{co} = unconfined concrete strength

f'_{l2} = maximum effective lateral confining pressure

The effect on the compressive strength of concrete which is confined with unequal effective lateral confining pressures, in two perpendicular directions, is given by the reduction factor α_2 which can be evaluated from Figure 8.3 in terms of the maximum and minimum effective lateral confining pressures. The effective lateral confining pressure f'_{l1} is taken as the minimum of f'_{lx} and f'_{ly}, and f'_{l2} is taken as the maximum of f'_{lx} and f'_{ly}. Restrepo and Wang [R2] proposed an approximate closed form solution for α_2, in lieu of using Figure 8.3, to evaluate the confined concrete strength.

$$\alpha_2 = \left[1.4 \frac{f_{l1}'}{f_{l2}'} - 0.6\left(\frac{f_{l1}'}{f_{l2}'}\right)^2 - 0.8 \right] \sqrt{\frac{f_{l2}'}{f_{co}'}} + 1 \tag{8.8}$$

Once the compressive strength of the confined concrete, f'_{cc}, has been established, Mander et al. proposed that the other parameters for the stress-strain relationship may be determined from:

$$\varepsilon_{cc} = \varepsilon_{co}\left(1 + R\left(\frac{f'_{cc}}{f'_{co}} - 1\right)\right) \tag{8.9}$$

$$E_c = 4700\sqrt{f'_{co}} \tag{8.10}$$

$$E_{sec} = \frac{f'_{cc}}{\varepsilon_{cc}} \tag{8.11}$$

$$r = \frac{E_c}{E_c - E_{sec}} \tag{8.12}$$

$$x = \frac{\varepsilon_c}{\varepsilon_{cc}} \tag{8.13}$$

where ε_c = variable concrete strain

ε_{cc} = concrete strain at confined concrete strength, f'_{cc}

ε_{co} = concrete strain at unconfined concrete strength, f'_{co}

= 0.002

The parameter R in Equation 8.9 is used to determine the strain at which the peak confined concrete stress is reached. This was calibrated using experimental results and was assumed by Mander et al. to be R = 5. The complete stress-strain curve, shown in Figure 8.4, is then given by Popovic's [P7] equation,

$$f_c = \frac{f'_{cc}\, x\, r}{r - 1 + x^r} \tag{8.14}$$

The stress-strain relationship for unconfined concrete can be obtained from the same set of equations using a lateral confining pressure, $f_l = 0$. To define the stress-strain behaviour of cover concrete, the descending portion of the unconfined concrete stress-strain relationship is assumed to decrease linearly from a strain of $2\varepsilon_{co}$ to reach zero stress at the spalling strain, ε_{spall}.

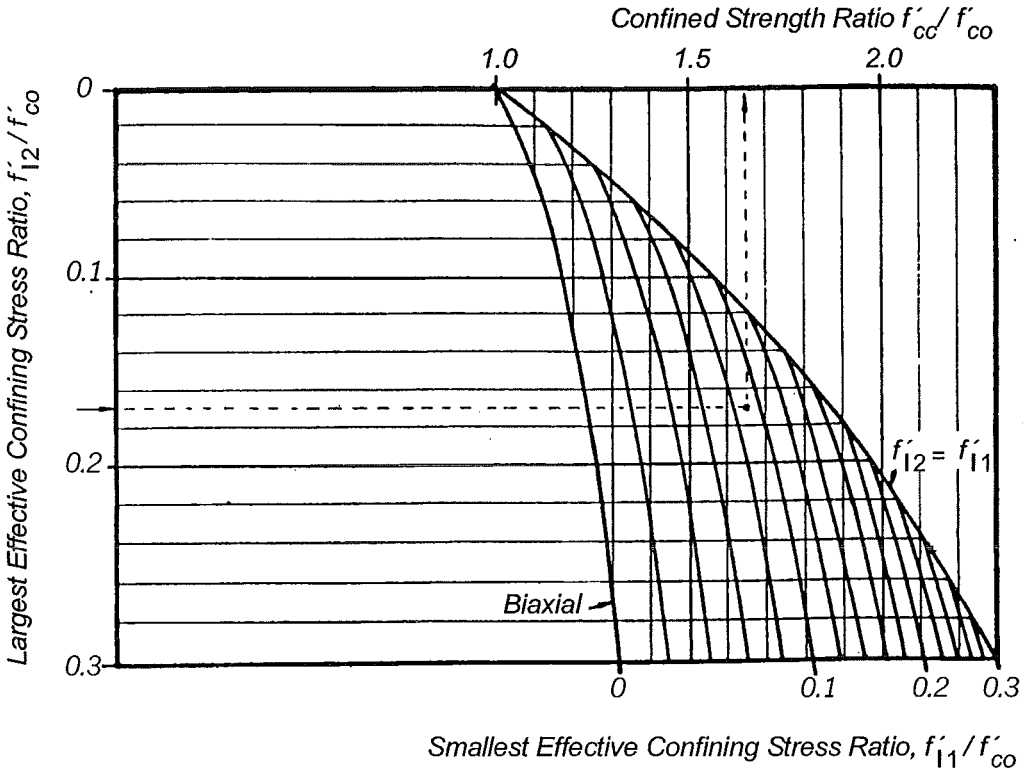

Figure 8.3 *Determination of Confined Concrete Strength from Lateral Confining Stresses for Rectangular Sections [M3]*

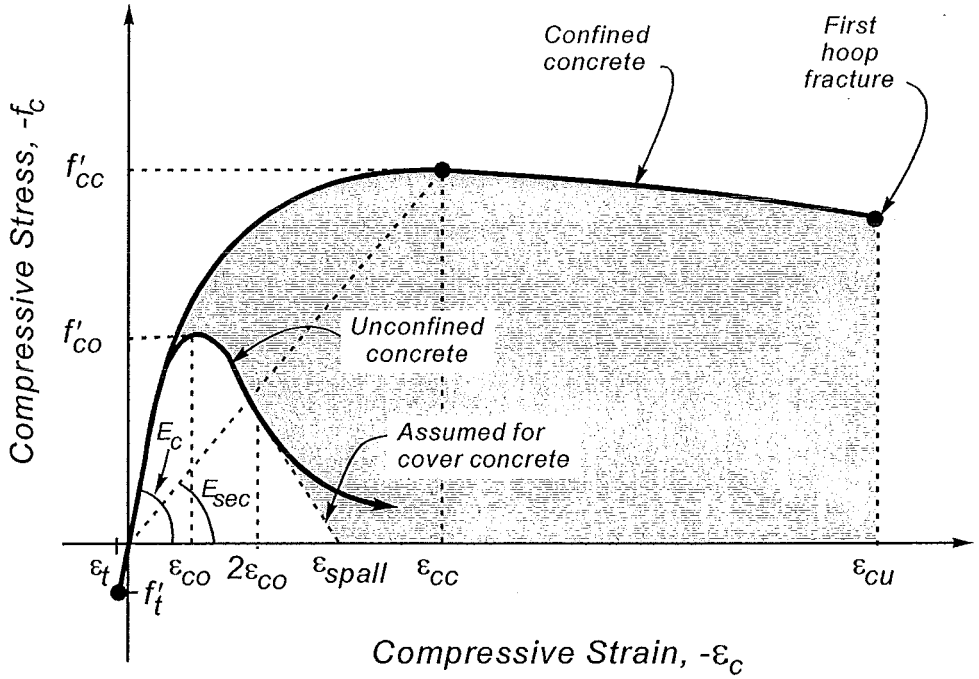

Figure 8.4 *Mander et al. [M3] Stress-Strain Model for Confined and Unconfined Concrete*

Mander et al. tested under concentric compression a number of realistically sized circular, square and rectangular columns with various arrangements of longitudinal and transverse reinforcement. They found that the most significant parameters affecting the shape of the stress-strain curve of confined concrete were the amount and configuration of the transverse reinforcement. An increased quantity of transverse reinforcement led to improved strength and ductility of the confined concrete and the effect of the transverse reinforcement configuration could be predicted through the confinement efficiency factor, k_e. The longitudinal steel layout only influences stress-strain behaviour through its effect on k_e.

The performance of columns confined with circular spirals or hoops was considerably better than columns confined with rectangular hoops. Rectangular hoops have a reduced confinement efficiency when compared to circular hoops as the steel is placed in hoop tension by dilation of the core concrete and apply a uniform radial pressure to the core. Therefore the confinement efficiency factor, k_e, for circular hoops or spirals is close to 1.0 and is only affected by vertical arching of the concrete between sets of hoops or spirals. Rectangular hoops only efficiently confine the concrete located near the corners of each hoop or near a bar restrained by a cross-tie. Thus the confinement efficiency factor, k_e, for rectangular hoops with or without supplementary cross-ties is usually much less than 1.0.

In a column subjected to axial load and flexure the strain gradient present will give decreasing strains for the fibres further from the extreme compressive fibre. As the extreme compressive fibres are not effectively confined, due to arching within the column core, they will not follow the assumed stress-strain relationship for the effectively confined concrete. These fibres will achieve lower peak stresses, for a given strain, compared to the effectively confined concrete. As illustrated in Figure 8.5 the ineffectively confined concrete region supports the lower stress, as given by the stress-strain relationship assumed for the concrete in this region while the effectively confined core is still supporting a high compressive stress, following the effectively confined concrete stress-strain relationship. This results in a decrease in the moment capacity of the section as the concrete compressive force is supplied mostly by the effectively confined concrete core. In addition the position of the

concrete compressive force resultant is limited to the region between the neutral axis and the edge of the effectively confined core.

The decrease in moment capacity is not seen in current stress-strain models where the smearing of the effectively confined core across the column core is done. Each compressive fibre is capable of supporting the same peak stress, and the position of the concrete compressive force resultant can lie anywhere between the neutral axis and the edge of the column core at the position of the peripheral hoop. Under concentric axial load the concrete compressive force resultant will lie at the centroid of the section. For current stress-strain models each fibre will contribute equally to the concrete compressive force resultant due the constant strain applied over the entire section. Assuming different behaviour of effectively and ineffectively confined concrete in the core region will not influence the results where the section is subjected to a concentric axial load as the compressive stresses in each fibre still all contribute to the resultant concrete force.

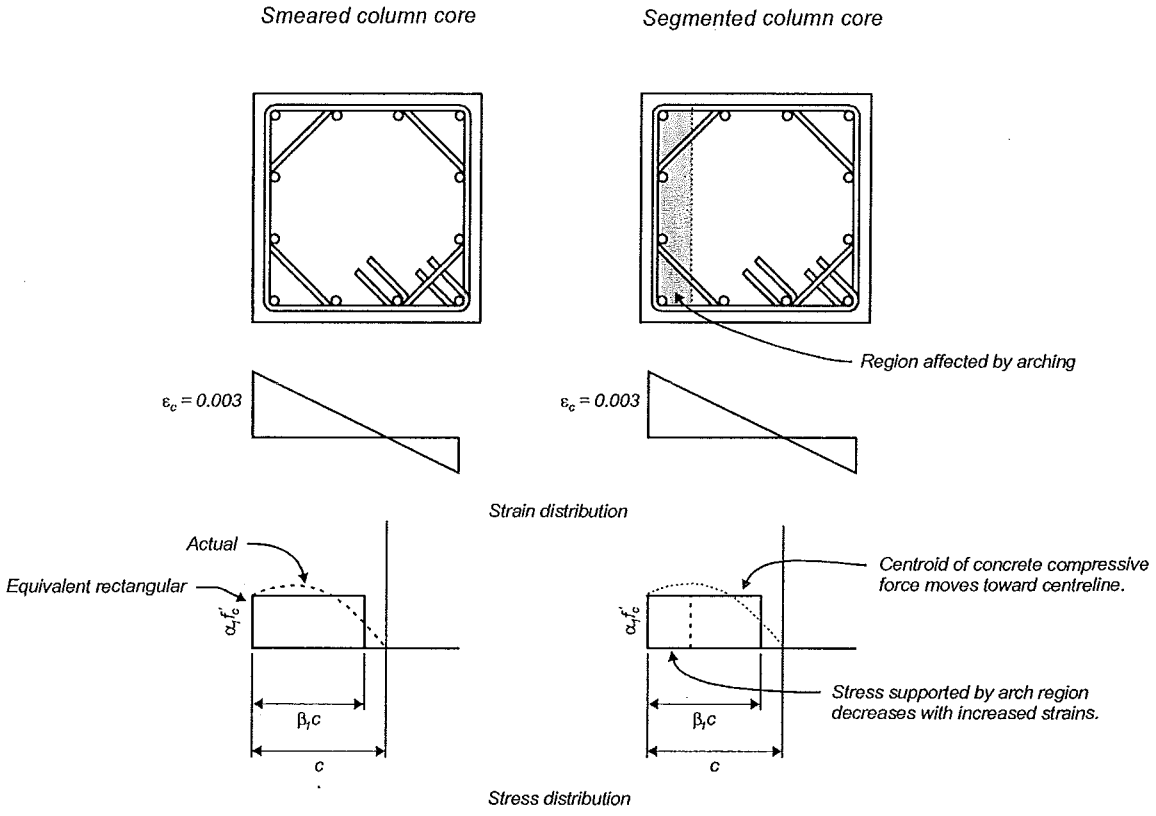

Figure 8.5 *Column Sections Subjected to Combined Axial Load and Flexure with Smeared and Segmented Column Core Regions*

For a significant strain gradient across the section, when a column is subjected to flexure, the concrete located closer to the extreme compression fibre contributes more to the bending moment. A more appropriate definition of the efficiency factor should weight the efficiency of the individual concrete strips according to their distance from the neutral axis. Zahn et al. [Z1] proposed that when only part of the section is in compression the efficiency factor should be redefined as the ratio of the first moments of area of the effectively confined core to the concrete in the core.

$$k_e^* = \frac{S_{ce}}{S_{cc}} \tag{8.15}$$

where S_{ce} = first moment of area of effectively confined core area, A_e

S_{cc} = first moment of area of confined core area, A_{cc}

Zahn et al. [Z1] used the approach suggested by Mander et al. to calculate the theoretical behaviour of a number of columns subjected to axial and lateral loads. The strain at which the peak stress is attained was evaluated using R = 5 as proposed by Mander et al. Results generally showed poor agreement between experimental moments and theoretical moment-curvature envelopes for the square sections tested by Zahn et al. By using a value of R = 3 in the Mander et al. stress-strain model, better agreement was obtained between experimental and theoretical results for these columns. Analysis of columns tested by Ang et al. [A3], Gill et al. [G1] and Potangaroa et al. [P8] showed similar results between experimental and theoretical results. Zahn et al. proposed that the poor agreement for some test units may have been due to an overestimation of the confinement efficiency factor, k_e as defined by Mander et al.

By using the modified efficiency factor, k^*_e, Zahn et al. found that a better agreement could be obtained between experimental and theoretical results using the value of R = 5 as originally proposed by Mander et al. Although better agreement between experimental and theoretical moment-curvature results can be obtained the properties of the effectively confined core are still smeared over the entire column core region.

8.3 STRENGTH ENHANCEMENT FROM MANDER ET AL. MODEL

From early tests on the effects of providing confinement to plain concrete the increase in compressive strength over the unconfined compressive strength, f'_{co}, has been noted [R1, B2]. The general trend is for the confined concrete strength to continue increasing for increasing lateral confining pressures. Early tests were conducted with an active hydrostatic fluid pressure providing the confinement followed by experiments using closely spaced transverse steel reinforcement to provide passive confinement to the concrete.

The expression proposed by Mander et al. [M3], shown in Equation 8.7, does not show an indefinite increase in the confined concrete compressive strength with increasing lateral confining pressures. From the derivative of α_1 in Equation 8.7 a maximum strength enhancement can be found,

$$\frac{d\alpha_1}{du} = \frac{1}{7.94}\left[\frac{2.254}{2\sqrt{1 + 7.94u}} - \frac{2}{7.94}\right] \qquad (8.16)$$

$$u = \frac{f_l'}{f_{co}'}$$

By setting Equation 8.16 to zero a maximum strength enhancement of 4.3 times the unconfined concrete strength can be found at a confining stress ratio, $f'_l / f'_{co} = 2.4$. At confining stress ratios in excess of 2.4, Equation 8.7 will yield lower values for confined concrete strength enhancement than for $f'_l / f'_{co} = 2.4$.

This amount of lateral confining pressure is unlikely to be provided in a reinforced concrete column with the use of transverse steel reinforcement but the equation proposed by Mander et al. should be limited to maximum practical levels of lateral confining pressures around a confining stress ratio, f'_l / f'_{co}, less than 0.3.

In the laboratory concrete may be confined with the use of an active hydrostatic fluid pressure. Some early experimental results have attempted to establish the relationship between high levels of confining pressures and the resulting increase in concrete strength. Richart et al. [R1] tested cylinders actively confined with different lateral

pressures. They found that the increase in strength due to the confining pressure, f_l, is between 3.1 f_l for high levels of lateral confinement and 5.1 f_l for low levels of confinement and recommended using a value of 4.1 f_l to establish the increase in strength due to confining pressures. Balmer [B2] noted that earlier tests by the U.S. Bureau of Reclamation gave an average value for the strength increase of 5.6 f_l. Balmer also conducted tests on 12 x 6 inch diameter (305 x 152 mm diameter) cylinders with f_l / f'_{co} ratios up to 7.0. From these results an approximate relationship for the increase in the concrete compressive strength can be derived [D1],

$$\frac{f'_{cc}}{f'_{co}} = \left[\frac{9 f_l}{f'_{co}} + 1 \right]^{0.75} \tag{8.17}$$

These relationships for the amount of strength enhancement due to lateral confining pressures are shown in Figure 8.6 up to $f_l / f'_{co} = 0.5$. It can be seen that these relationships provide a similar level of strength enhancement due to lateral confinement up to about $f_l / f'_{co} = 0.3$. At very high confining stress ratios the relationships proposed by Richart et al., the U.S. Bureau of Reclamation and Balmer give results widely different from the equation proposed by Mander et al. Dodd and Cooke [D1] provide a comparison between these models and those from a number of different researchers and concluded that any of the relationships would provide satisfactory estimates for strength enhancement for normal strength concrete and reinforcing steel.

Results for the Mander et al. model must incorporate the efficiency factor, k_e, as the other models were derived from experiments conducted using active confining pressures on plain concrete. The Mander et al. model uses an effective lateral confining pressure reduced from the equivalent lateral confining pressure provided by yield of the transverse reinforcement to account for the effects of arching in the column. Models by Richart et al. and those reported by Balmer would have a confinement efficiency factor equal to 1.0 as arching does not occur due to the active confinement supplied to the concrete.

From Figure 8.6 it can be seen that the model proposed by Richart et al. closely matches the rather more complex equation proposed by Mander et al. over a practical range of confining stress ratios. The relationship in Equation 8.7 proposed by Mander et al. could be replaced by the following expression and still provide a satisfactory estimate for the confined concrete strength,

$$\alpha_1 = \left(1 + 4.1\frac{f'_{l2}}{f'_{co}}\right) \qquad \text{provided } \frac{f'_{l2}}{f'_{co}} \leq 0.3 \qquad (8.18)$$

where f'_{co} = unconfined concrete strength

f'_{l2} = maximum effective lateral confining pressure

= $k_e f_{l2}$

k_e = confinement efficiency factor

f_{l2} = maximum lateral confining pressure, f_{lx} or f_{ly}, from Equation 8.1 for rectangular columns or Equation 8.4 for circular columns

This simplification to establish the confined concrete strength would provide reasonable agreement up to a confining stress ratio, $f'_l / f'_{co} = 0.3$ as can be seen from Figure 8.6. Mander et al. [M4] proposed a simplified relationship suitable for design purposes for the strength enhancement of concrete which could be applied to columns, with typical levels of confinement, of the form,

$$\alpha_1 = \frac{f'_{cc}}{f'_{co}} = 1 + 5.5\frac{f'_l}{f'_{co}} \qquad \text{for } \frac{f'_l}{f'_{co}} \leq 0.1 \qquad (8.19)$$

Equation 8.18 would extend the simplified Mander et al. relationship over a wider range of confinement ratios to what would be approximately the maximum lateral confining stress ratio that could be provided to a normal strength reinforced concrete column with the use of mild steel transverse reinforcement. Although the relationship originally proposed by Richart et al. was for circular concrete cylinders the closeness to the relationship proposed by Mander et al. would allow it to be applied to circular and rectangular columns by accounting for the effects of arching through the

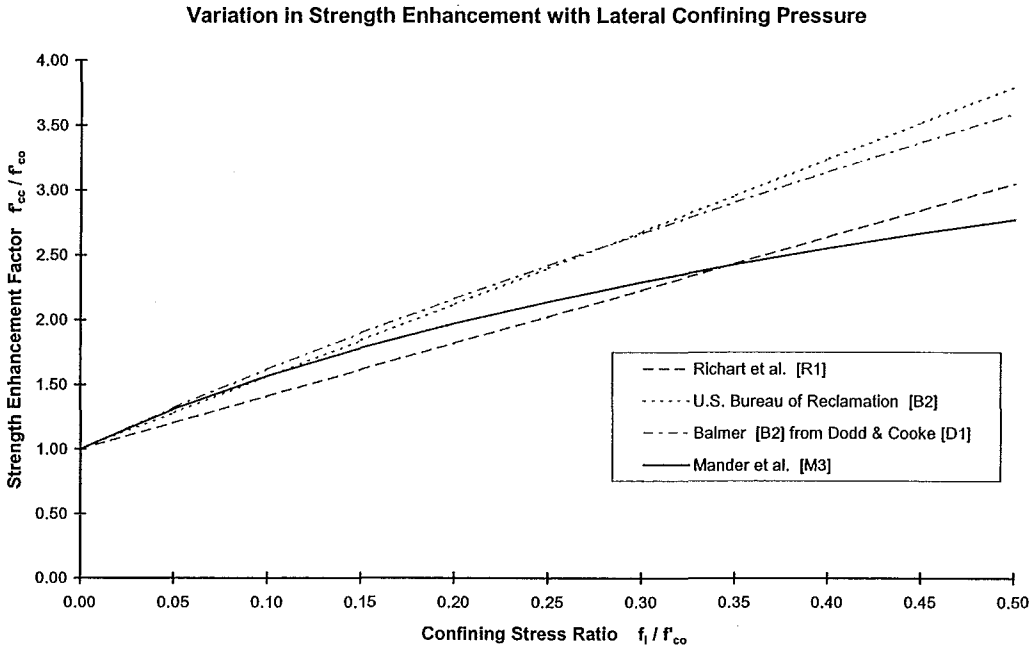

Richart et al. [R1]

$$\frac{f'_{cc}}{f'_{co}} = 1 + 4.1\frac{f_l}{f'_{co}}$$

U.S. Bureau of Reclamation reported by Balmer [B2]

$$\frac{f'_{cc}}{f'_{co}} = 1 + 5.6\frac{f_l}{f'_{co}}$$

Balmer as derived by Dodd and Cooke [D1]

$$\frac{f'_{cc}}{f'_{co}} = \left[\frac{9f_l}{f'_{co}} + 1\right]^{0.75}$$

Mander et al. [M3]

$$\frac{f'_{cc}}{f'_{co}} = \left[2.254\sqrt{1 + \frac{7.94f_l}{f'_{co}}} - 2\left(\frac{f_l}{f'_{co}}\right) - 1.254\right]$$

Figure 8.6 *Various Proposed Relationships for Confined Concrete Strength Enhancement due to Lateral Confining Pressure*

confinement efficiency factor, k_e, and unequal amounts of confinement through the reduction factor, α_2.

8.4 FACTORS INFLUENCING CONFINEMENT EFFICIENCY

8.4.1 Effectively Confined Concrete Core Area

The efficiency factors proposed by Mander et al. [M3], k_e, are derived from tests on short columns subjected to concentric axial load and is expressed as a ratio of the total effectively confined core area to the total core area.

Since the shape of the effectively confined core at the critical section may be cumbersome to evaluate, it is usual to assume that the area of confined concrete is the entire area enclosed by the centrelines of the peripheral hoops. The lateral confining pressure is then reduced by a confinement efficiency factor to give an effective confining pressure which is applied uniformly over the entire core area. Mander et al. reduce the lateral confining pressure, f_l, calculated assuming yielding of the transverse steel reinforcing, by an efficiency factor, k_e, which is based on the ratio of effectively confined concrete area to the area of concrete in the core.

The modified confinement efficiency factor, k^*_e, proposed by Zahn et al. [Z1] would ideally be taken about the neutral axis of the section. As the neutral axis varies in position the modified efficiency factor could be evaluated by taking the moments of each area about the centroidal axis to weight the efficiency factor to the strips further from the neutral axis. Zahn et al. presented an expression to calculate k^*_e for circular sections which has been further simplified by Dodd and Cooke [D1]. Watson and Park [W3] present an expression to determine k^*_e for rectangular shaped sections as a general expression for all rectangular shaped sections. This expression was derived by Zahn et al. for a specific worked example of a rectangular column section and is not applicable to all rectangular column sections. Derivation of a general expression to determine k^*_e for rectangular columns is not attempted in this study.

8.4.2 Influence of Strain Gradient Across Section

The models for the stress-strain behaviour of confined concrete have been calibrated against results obtained from concentrically loaded test specimens. Zahn et al. noted that assumptions made by Mander et al. for the shape of the effectively confined core, may be valid for columns which are loaded axially but may be conservative when applied to columns which are subjected to axial load and flexure.

Zahn et al. and Tanaka and Park [T1] discussed a number of factors which could affect the efficiency of lateral confinement in a column subjected to axial load and flexure including the effect of the strain gradient in a column and its influence on the stress-strain behaviour of confined concrete.

The compressive strain in a column subjected to flexure decreases as the location of each fibre is further from the extreme compressive fibre. The progress of concrete damage at the extreme compressive fibre is restrained due to the presence of adjacent compressive fibres which are subjected to lower strains. Lateral expansion of the core concrete varies with the strain gradient, being greater at the extreme compressive fibre and ideally non-existent at the neutral axis location. This results in the passive lateral confining pressure varying down the depth of the section. When the extreme compressive fibre reaches the peak strain, ε_{cc}, when the transverse steel is assumed to yield, the lateral expansion may not be great enough to have caused yielding of the transverse steel bar. Therefore the peak concrete compressive stress reached may be smaller than that assumed from analysis.

The comparison of results from eccentric and concentric load tests discussed by Tanaka and Park on confined columns has shown that the magnitude of hoop tensile strains in the extreme compressive fibre region in a column subjected to bending are lower than those attained in concentrically loaded columns for the same extreme fibre compression strain.

This would suggest that stress-strain models for confined concrete based on concentric loading of columns would overestimate the strength and ductility

enhancement, due to the lateral confining pressure provided by the transverse reinforcement, when applied to columns subjected to flexure.

The yield strength of the transverse reinforcement is used as the upper limit to determine the available lateral confining pressure. Dilation of the column core develops strains in the transverse reinforcement which cause the transverse steel to yield. If higher strength transverse reinforcement is used the strains developed through dilation of the column concrete core may not be large enough to develop the yield strength of the transverse reinforcement and the available lateral confining pressure will be somewhat lower. Satyarno et al. [S3] and Sato et al. [S4] tested a number of columns with ultra-high strength transverse reinforcement and found a maximum stress of around 800 MPa was developed in the transverse reinforcement during the tests. The New Zealand Concrete Structures Standard [X2] uses 800 MPa as the maximum strength of transverse reinforcement to be used in calculations for transverse reinforcement requirements in columns.

For columns with low axial load yielding of the transverse reinforcement may not occur until larger inelastic displacements are reached and sufficient dilation of the column core has taken place. For higher axial loads the transverse reinforcement yields around the same time as the nominal moment is attained in the column. Although the transverse reinforcement in low axial load columns does not yield until larger inelastic displacements are reached this does not tend to affect the ideal flexural strength of the column as the additional capacity provided in these columns, due to the effects of confinement at development of the ideal flexural strength, is small. Zahn et al. concluded that although there may be some effect of the delayed yielding of transverse reinforcement in columns subjected to a strain gradient, the overall effect on development of the flexural strength can be neglected.

The influence of a strain gradient will be important across a boundary between the effectively and ineffectively confined core areas as assumed to evaluate the confinement efficient factor. If the ineffectively confined concrete is assumed to act as unconfined concrete, the unconfined concrete stress-strain behaviour will vary greatly from confined concrete stress-strain behaviour, in the effectively confined core, at strains much higher than when the peak stress in unconfined concrete is

reached. Therefore the influence of the arches will be not be significant, with the presence of a strain gradient in a column, where the strains across the boundary between the effectively and ineffectively confined core areas are less than approximately ε_{co}. Arching of the concrete is required to transfer the confinement effects of the transverse reinforcement to the concrete core. The amount of confinement provided is dependent on the strains developed in the transverse reinforcement and these strains vary down the depth of the section due to the presence of the strain gradient.

8.5 MODELLING OF COLUMN CORE CONCRETE

8.5.1 Arching of Core Concrete

The concrete core of a column which is confined by transverse reinforcement can be defined as the area bound by the inside, centreline or outside of the peripheral hoops. Although the definition of core area has varied between different researchers and concrete design standards (Sargin et al. [S5], Sheikh and Uzumeri [S1], Mander et al. [M3], ACI 318 [X3], NZS 3101 [X2]) the differences in core area are fairly small and may be neglected.

The area of the effectively confined core between the layers of transverse reinforcement is recognised to be less than at the level of the hoops due to the effect of horizontal and vertical arching as seen in Figure 8.1 and Figure 8.2. Thus the critical section occurs midway between the layers of transverse reinforcement where the influence of horizontal and vertical arching results in the smallest area of effectively confined concrete in the core.

Many researchers have assumed the arching action produces a boundary between the confined core and the unconfined concrete in the form of an arc located between a triangle or a second degree parabola (Sargin et al., Watanabe et al. [W4], Sheikh and Uzumeri, Mander et al.). Figure 8.7 shows the various proposed arching profiles used by a number of researchers incorporated into various stress-strain models.

The effectively confined core area is evaluated by assuming arching occurs on all faces of the section, as would occur from a concentric axial load acting on the column. The effect of the arching on the lateral confining pressure is taken into account by the use of a confinement efficiency factor which is generally based on the ratio of the effectively confined core to the total concrete core areas.

8.5.2 Confinement Efficiency Factors

The definition of an efficiency factor recognises the difference in concrete stress-strain behaviour for different regions within the core due to the effects of arching. The use of this efficiency factor to reduce the lateral confining pressure to some effective lateral confining pressure neglects the assumed variation in concrete stress-strain behaviour for different regions within the core. This is often done to simplify the analysis of the critical section, by simplifying the shape of the effectively confined core area to be evaluated and to account for the influences of arching in the column and its effect on the strength and ductility enhancement in a column.

Values for the initial tangent angle of the arches are assumed or derived from regression analysis of experimental data to provide good agreement between the experimental results and the confined concrete stress-strain models. The angle of the arches influences the area of effectively confined core and the reduction in the lateral confining pressure used in calculation of the peak confined concrete stress. Direct measurement of the initial tangent angle of the arches and the area of ineffectively confined core during experiments is difficult and is therefore impossible to compare experimental results with the assumptions about the effectively confined core in a confined concrete stress-strain model.

Confined concrete stress-strain models by Sargin et al, Watanabe et al., Sheikh and Uzumeri, and Mander et al. are calibrated by determining the effective lateral confining pressure which is applied to a column, usually as some function of the transverse steel volumetric ratio, p_s, yield strength of the transverse reinforcement, f_{yh}, and a confinement efficiency factor in the form of the ratio of effectively

confined concrete core area to the total core area. These parameters are used to formulate a confining coefficient factor to represent the increase in concrete compressive strength due to the effects of confinement from transverse reinforcement.

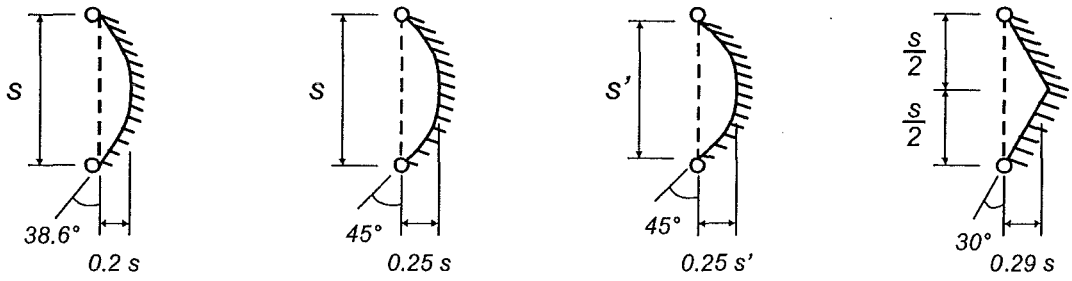

Sargin et al. [S5] | Sheikh and Uzumeri [S1] | Mander et al. [M3, M4] | Watanabe et al. [W4]

Figure 8.7 *Various Proposed Arching Profiles*

Agreement between the various stress-strain models and experimental results is achieved by calibration of the confining coefficients to provide theoretical results to match the experimental data. While the presence of the ineffectively confined core is included in these models the defined area of ineffectively confined concrete core is not involved in the determination of the strength of a column.

It would be logical to use the defined areas of effectively and ineffectively confined concrete core to determine the strength of a column. The effectively confined concrete core area would be subject to the full lateral confining pressure and the ineffectively confined core would possibly be confined by some lower pressure. Evaluation of the strength of a column would be no more computationally difficult than compared to current models. Evaluation of the effectively and ineffectively confined concrete core areas is more conceptually correct than the use of a lateral confining pressure which has been reduced and averaged over the entire core area to

account for the effects of arching. The effects of arching would be accounted for directly in the area of the ineffectively confined core area.

8.5.3 Application of Mander et al. Model to Columns with Flexure and Axial Load

Arching only occurs over the area of compressed concrete, between each of the transverse hoop sets and between each restrained longitudinal bar. When a column is subjected to flexure and axial compression the area of compressed concrete is reduced. The use of the efficiency factor, such as defined by Mander et al., does not reflect the reduction in compressed area that occurs in a column under low or moderate axial load levels and tends to overestimate the confinement efficiency for a column subjected to flexure and give poor comparison between experimental and theoretical moment-curvature results. Moment-curvature results from several researchers [A3, G1, P8, Z1] show better comparison could be obtained by altering the variable R to a value of R = 3, to determine the strain at which the peak stress occurred for the Mander et al. model, from the suggested value of R = 5.

The modified efficiency factor, k^*_e, proposed by Zahn et al. allows better theoretical and experimental result comparison to be obtained for columns subjected to flexure and axial load when using the original value of R = 5 in the Mander et al. model.

The concrete stress-strain model proposed by Mander et al. was determined from tests conducted on concentrically axially loaded column specimens. The modification to the efficiency factor proposed by Zahn et al. was required to recognise the change in the shape of the compressed area of the column and that arching of the concrete only occurs over this compressed region. Several concrete stress-strain models [S5, S1, M3, W4] use the concept of an effective lateral confining pressure which acts on a column. The effective lateral confining pressure involves taking average properties for the entire column cross section. The presence and behaviour of the ineffectively confined concrete in the arches is neglected as the entire core of the column is assumed to behave as concrete confined with the effective lateral confining pressure. As the ineffectively confined core concrete will

behave differently to the effectively confined core concrete the influence of the ineffectively confined core cannot be determined using this approach.

By separating the effectively and ineffectively confined concrete core areas, the effect of arching, occurring only over the compressed area of concrete, can be easily modelled and the influence of arching in the core of the column can be evaluated. The ineffectively confined concrete would represent the area of compressed concrete core which is affected by arching, the remaining area of compressed core concrete being effectively confined.

8.6 MODELLING OF EFFECTIVELY CONFINED CORE AND INEFFECTIVELY CONFINED CORE CONCRETE

8.6.1 Separation of Effectively and Ineffectively Confined Core Concrete

Modelling the effectively and ineffectively confined core areas separately, with a distinct boundary between the two, would result in a large change in stresses occurring across the boundary. On the boundary the effectively confined core area may be maintaining a stress close to the peak stress for confined concrete but the concrete which is not effectively confined will be supporting a much lower stress for the same strain. Although strain compatibility is maintained there is no stress continuity across the boundary. As the behaviour of each concrete fibre will influence the behaviour of adjacent fibres, some form of stress compatibility could be expected across the boundary between the effectively confined and ineffectively confined core areas.

The stress-strain relationship for concrete fibres in the ineffectively confined core area will vary depending on the location of the individual fibre within the region. Concrete fibres located immediately adjacent to the effectively confined core would be expected to behave in a similar manner to the fully confined concrete while concrete fibres close to the peripheral hoop will behave more like the cover concrete. Modelling the entire ineffectively confined area as unconfined concrete would take a

lower bound for the stress-strain behaviour and would be assumed to be the same for all fibres in the ineffectively confined core area.

To fully model the behaviour of the concrete core area and generate the stress compatibility which would exist across the boundary between the effectively and ineffectively confined core areas, each fibre within the ineffectively confined core area would be required to follow separate stress-strain relationships depending on the location of that fibre within the ineffectively confined area. This would require a finite element approach and the appropriateness of this type of model would depend on how the stress-strain relationships for the individual fibres were chosen to vary through the ineffectively confined core area.

Division of the concrete core into effectively and ineffectively confined regions reflects the difference in assumed concrete stress-strain behaviour of the two regions. However this is an artificial division of the core as in reality no distinct boundary exists defining and separating the behaviour of the two areas. A gradual change in the stress-strain relationship of concrete fibres exists through the concrete core and may be modelled by separating the areas of the core which can be regarded as effectively confined and the areas which may be regarded as ineffectively confined.

By using the previous definitions of effectively confined and ineffectively confined areas these two areas can be modelled separately, each following a different concrete stress-strain relationship. The effectively confined core area would be subjected to the full lateral confining pressure, due to yielding of the transverse reinforcement, and the ineffectively confined core would be subjected to a confining pressure reduced from the full lateral confining pressure to reflect the reduction in confinement efficiency and thus follow a different concrete stress-strain relationship, reflecting the transition between the two areas. This is referred to in this study as the segmented core model.

The stress-strain model for concrete developed by Mander et al. was used for this study taking a confinement efficiency factor, k_e, as a value $k_e = 1.0$ to establish the peak confined concrete stress for the effectively confined core. Concrete within the core which is not effectively confined was modelled as unconfined concrete.

Longitudinal steel stress-strain relations used in this study are based on the model proposed by Mander et al. [M4], and is of the form:

For $\varepsilon_s \leq \varepsilon_{sy}$

$$f_s = \varepsilon_s E_s \tag{8.20}$$

where $$\varepsilon_{sy} = \frac{f_y}{E_s} \tag{8.21}$$

For $\varepsilon_{sy} < \varepsilon_s \leq \varepsilon_{sh}$

$$f_s = f_y \tag{8.22}$$

For $\varepsilon_{sh} < \varepsilon_s \leq \varepsilon_{su}$

$$f_s = f_{su} + \left(f_y - f_{su}\right)\left[\frac{\varepsilon_{su} - \varepsilon_s}{\varepsilon_{su} - \varepsilon_{sh}}\right]^P \tag{8.23}$$

Equation 8.23 uses a power curve that describes the strain hardening portion of the stress-strain curve commencing at the point (ε_{sh}, f_y) at the onset of strain hardening and terminating at (ε_{su}, f_{su}) with zero slope at the ultimate load. The power term, P, is a function of the slope at the initiation of strain hardening – ie. the strain hardening modulus, E_{sh}, - and is given by:-

$$P = E_{sh}\left(\frac{\varepsilon_{su} - \varepsilon_{sh}}{f_{su} - f_y}\right) \tag{8.24}$$

Determining the strain hardening modulus, E_{sh}, from experimental data is difficult and the shape of the analytical curve is very sensitive to this value. By taking a point on the strain hardening curve, ($\varepsilon_{sh,1}$, $f_{sh,1}$), the term P can be determined by:

$$P = \frac{\log\left(\frac{f_{su} - f_{sh,1}}{f_{su} - f_y}\right)}{\log\left(\frac{\varepsilon_{su} - \varepsilon_{sh,1}}{\varepsilon_{su} - \varepsilon_{sh}}\right)} \qquad (8.25)$$

This stress-strain relationship for this study was assumed to be the same in tension as in compression, that is the monotonic skeleton curve of reinforcing steel in compression is equal and opposite to the curve in tension. Dodd and Cooke [D1] and Restrepo-Posada et al. [R3] found that the compression and tension curves are essentially the same up to the ultimate coordinates only when the stress and strain are changed to the natural coordinate system, which takes into account the instantaneous geometry of the specimen. By assuming equal and opposite stress-strain curves for tension and compression, the compressive stresses could be underestimated compared to the actual compressive stress-strain relation, but non-linear effects caused by incipient bar buckling can compensate for the difference.

8.6.2 Comparison of Moment-Curvature Results

Monotonic moment-curvature analyses were conducted for circular and square columns, using the segmented core model.

Figure 8.8 shows the areas of effectively and ineffectively confined concrete core and the stress-strain relationships assumed for the concrete in each region. The ineffectively confined concrete core represents the region of the compressed concrete core which is affected by arching between restrained longitudinal bars and transverse reinforcement sets. The boundary between the effectively and ineffectively confined concrete core areas were assumed to be second degree parabolas over the clear distance between restrained longitudinal bars and transverse hoop sets as assumed by Mander et al. [M3]. The initial tangent angle for the parabolas to describe the boundary between the effectively and ineffectively confined concrete areas was taken as 45° as assumed by Mander et al.

Monotonic moment-curvature results were generated for circular and square columns with varying axial load ratios and transverse hoop spacings using the original Mander et al. concrete stress-strain model and the segmented core model. Results for 800 mm diameter circular columns are shown in Figures 8.9 to 8.12 and for 800 mm by 800 mm square columns in Figures 8.13 to 8.16. Figures 8.17 to 8.20 show moment-curvature results for 400 mm diameter circular columns and Figures 8.21 to 8.24 show moment-curvature results for 400 mm by 400 mm square columns.

Moment-curvature response is calculated by incrementing the extreme concrete compressive fibre strain, evaluating the concrete and steel stresses at each point and calculating the resulting moment, from equilibrium of internal and external forces, and determining the curvature for each increment in strain. The analysis is halted when the concrete strain exceeds the ultimate concrete compressive strain, the extreme tension steel strain exceeds the specified ultimate steel strain or the moment drops to below 80% of the maximum moment capacity of the section, whichever occurs first.

Comparison of the moment-curvature results for circular columns showed reasonable agreement between the two models. Moment-curvature results for the square columns show a much wider variation, especially at higher curvatures, after developing the ideal flexural strength of the column.

Moment-curvature results for the 400 mm and 800 mm columns reflect the same trends. Response of the columns are very similar in both models up to development of the ideal flexural strength of the column. Increasing the axial load ratio shows a difference in the ideal flexural strength of the columns between the models, which increases as the axial load is increased from $0.1f'_cA_g$ to $0.3f'_cA_g$. The response of the columns modelled using the segmented core model gives maximum moments always below those predicted by the moment-curvature analysis using the Mander et al. model.

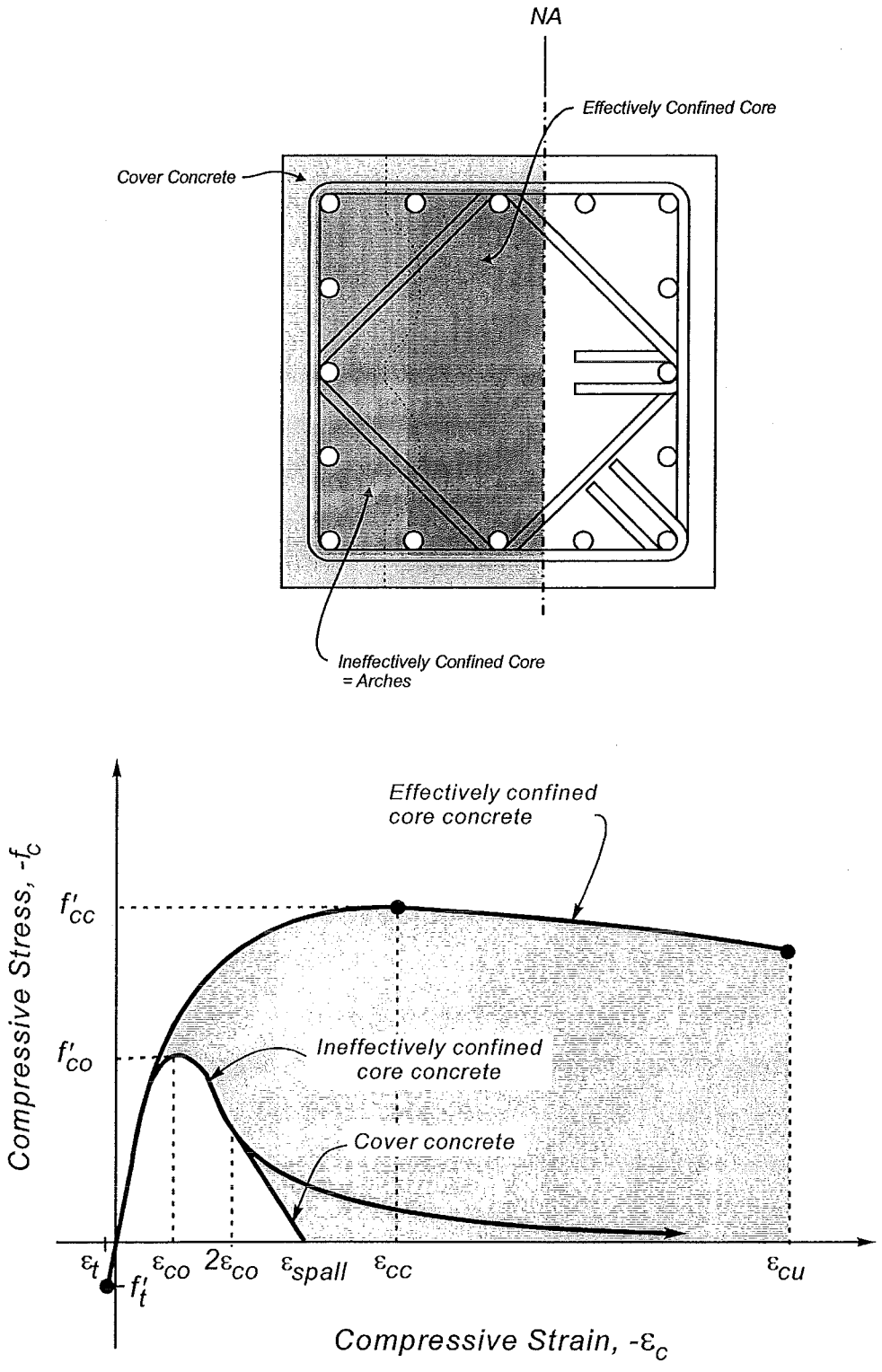

Figure 8.8 *Areas of Effectively and Ineffectively Confined Core and Assumed Concrete Stress-Strain Relationships for each Region*

Significant differences in the moment-curvature responses can be seen in the square columns after the ideal flexural strength is reached. Spalling of the cover concrete commences when the extreme concrete compressive fibre strain reaches 0.005, in the segmented core model. As the cover spalls the area of ineffectively confined concrete is supporting a very low stress, compared to the stresses carried in the core. This results in the large decrease in moment soon after the ideal flexural strength of the column is achieved as spalling of the cover concrete occurs. Figures 8.21 to 8.24 for the 400 mm square columns show a sharp drop in the moment after spalling of the cover concrete due to the relatively large cover concrete dimension. The decrease in curvature seen between the moment-curvature increments just prior to and after spalling of the cover concrete in the segmented core model is due to the increase in the neutral axis depth to maintain the compressive concrete force after spalling of the cover.

This decrease in moment capacity can lead to the moment-curvature response halting, in the segmented core model, as the moment drops below 80% of the maximum moment reached during the iterations, giving ultimate curvatures much less than achieved by the Mander et al. model moment-curvature response.

The reason for halting the moment-curvature iterations is influenced by increased transverse reinforcement spacing and increased axial load. The increased transverse reinforcement spacing gives a larger area of ineffectively confined concrete, which at higher compressive strains contributes less to the concrete compressive force. Increased axial load also places more reliance on the contribution of the concrete to resisting the applied forces on the column. As circular sections are only subjected to arching occurring between the transverse reinforcement there is a smaller area of ineffectively confined concrete within the core and the influence of the cover concrete spalling and the decrease in stress over the ineffectively confined core, with increased strain, is lessened.

Moment-curvature results from the Mander et al. model do not show the drop in moment after reaching the ideal strength of the column due to the cover spalling and influence of the arches. This is due to the way the Mander et al. stress-strain model for confined concrete accounts for the effects of arching within the column core. The

use of a uniformly applied equivalent lateral confining pressure across the entire concrete core does not result in different areas of the core behaving in different manners, following the stress-strain relationships assumed for each area.

The ultimate concrete strain, ε_{cu}, used in the model developed for this study is known to be a conservative estimate for the ultimate concrete compression strain [P2] and was formulated from considerations of confined sections under axial compression. When applied to evaluate the available ultimate compression strain of sections subject to bending or combined bending and axial compression, the evaluated strain tends to be even more conservative [P3]. As evaluation of the ultimate concrete compression strain is not investigated as part of this study the calculated ultimate concrete compression strain was only determined to provide a reasonable stopping condition for the moment-curvature iterations.

Results from the segmented core model show that the moment-curvature response does not reflect the same behaviour as show by the Mander et al. model and observed in experimental tests on columns under axial load and flexure. At the ideal flexural strength of the column, around an extreme compression fibre strain of 0.004, the moments and curvatures for columns modelled using the segmented core model and those using the Mander et al. model are similar.

With the influence of cover concrete spalling and the decrease in stress with increased strain for the ineffectively confined concrete core area the columns modelled with the segmented core do not quite achieve the same ideal flexural strength as the columns modelled using the Mander et al. model. The effect of the ineffectively confined concrete area can lead to greatly different moments and ultimate curvatures for the columns modelled using the segmented core. As this behaviour has not been observed in experimental results this may indicate that the 45° angle used to construct the parabolic arch boundaries between the effectively and ineffectively confined core in a column may be too large for columns subjected to axial load and flexure. The amount of arching may also be dependent on the level of axial load as is indicated by the larger variation in moment-curvature response between the two models for columns with higher axial loads.

The 45° parabolic arch boundaries between the effectively and ineffectively confined core has been calibrated for sections under concentric axial compression, where the strain conditions are the same across the entire section and stresses developed in each part of the section are identical. For columns under flexure the variation in strain down the depth of the section leads to different stresses developed in each concrete fibre. For the ineffectively confined core, modelled as unconfined concrete, after the peak strain is reached around $\varepsilon_c = 0.002$, the stress commences to decrease with increasing strain. Thus as the concrete force is summed up over the ineffectively confined core area the contribution of each fibre decreases the further it is from the neutral axis. Under concentric axial load the contribution of each fibre to the concrete force is the same, as all fibres are at the same strain. Therefore a reduced angle for the parabolic arches may be appropriate for columns subjected to flexure in order to reflect the decreased contribution to the concrete force from concrete fibres further from the neutral axis.

As the columns modelled with the segmented core do not achieve the same ideal flexural strength as the columns modelled using the Mander et al. model as the calibration of the Mander et al. concrete stress-strain model is done against experimental data from concentric axial load tests. Factors included in these equations to describe the increase in concrete compressive strength due to confinement, may over estimate the peak confined concrete stress in columns subject to axial load and flexure.

With the angle of arching reduced there would be a larger area of confined core within the column. This would result in reduced factors for the degree of strength enhancement in the Mander et al. model to offset the increased area of confined core contributing to the compressive force in the column. If arching in columns subjected to flexure is at an angle less than 45°, the Mander et al. model would be providing some degree of moment enhancement due to the over estimation of the confined concrete strength in the core for columns subjected to flexure.

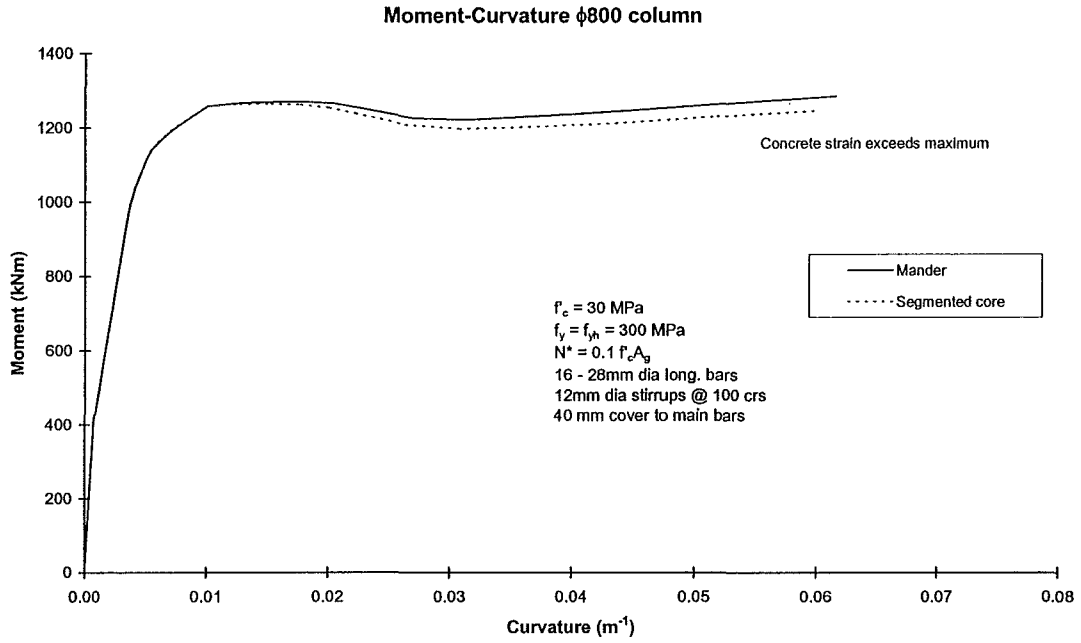

Figure 8.9 *Comparison of Moment-Curvature Results for 800 mm Circular Column, $N^* = 0.1 f'_c A_g$, Stirrups @ 100 mm crs*

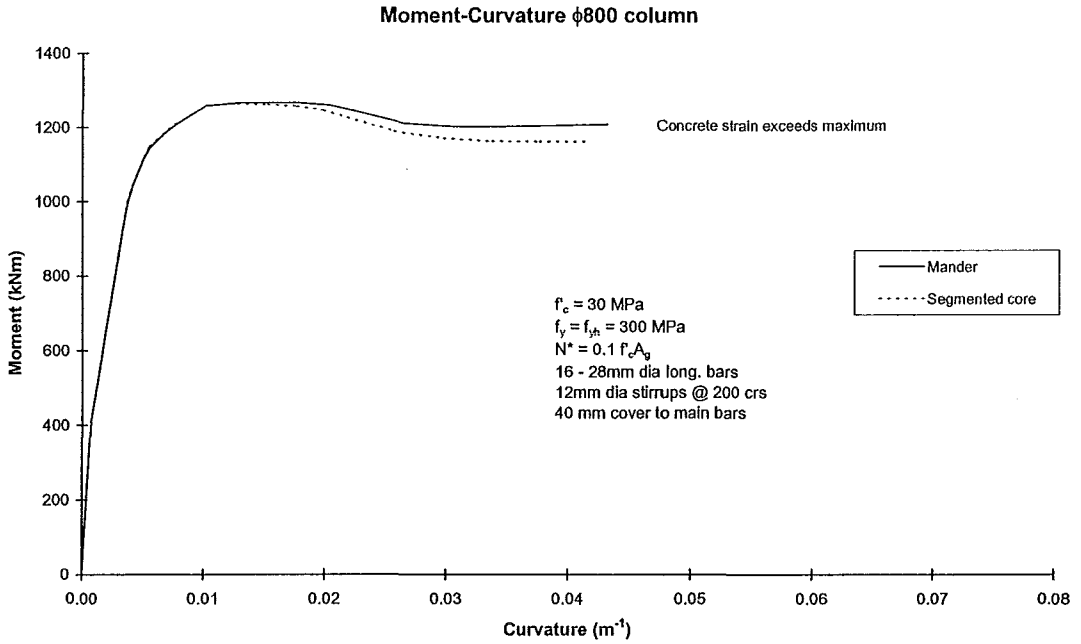

Figure 8.10 *Comparison of Moment-Curvature Results for 800 mm Circular Column, $N^* = 0.1 f'_c A_g$, Stirrups @ 200 mm crs*

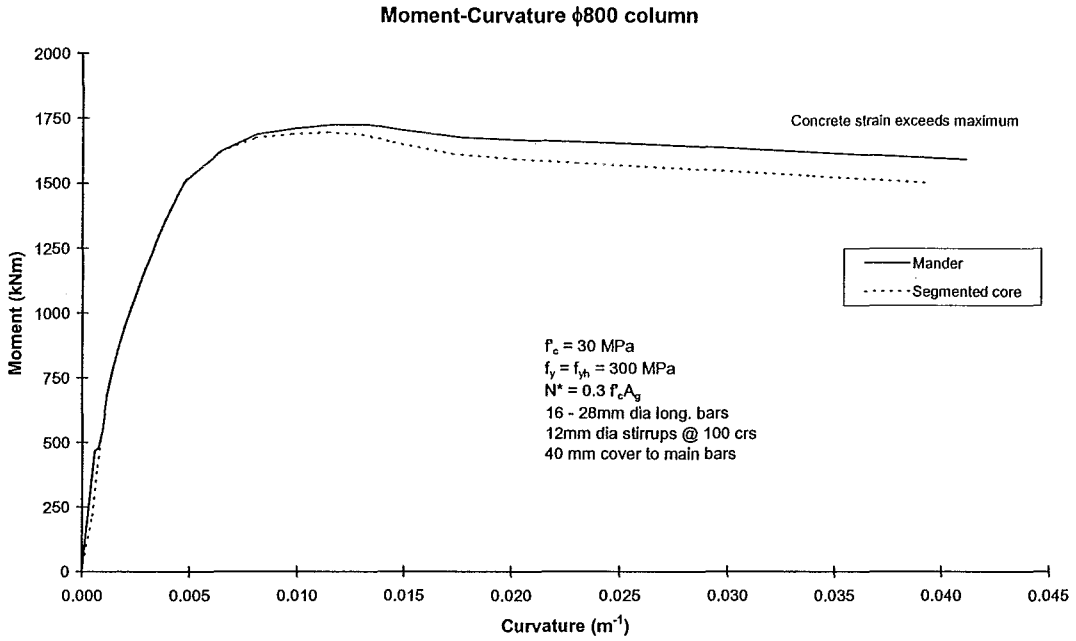

Figure 8.11 *Comparison of Moment-Curvature Results for 800 mm Circular Column, $N^* = 0.3 f'_c A_g$, Stirrups @ 100 mm crs*

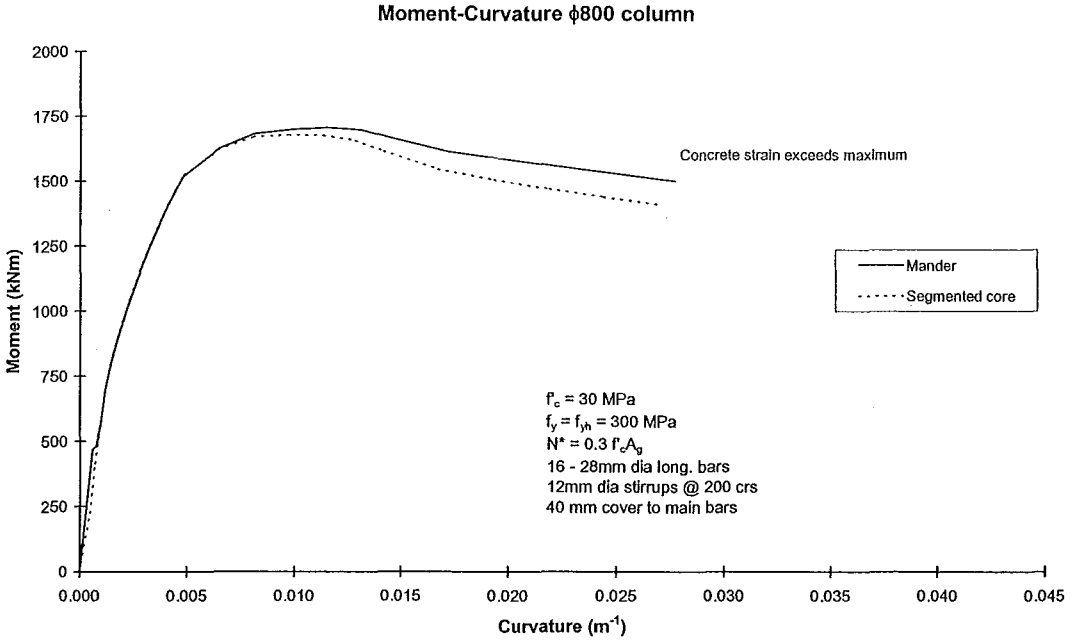

Figure 8.12 *Comparison of Moment-Curvature Results for 800 mm Circular Column, $N^* = 0.3 f'_c A_g$, Stirrups @ 200 mm crs*

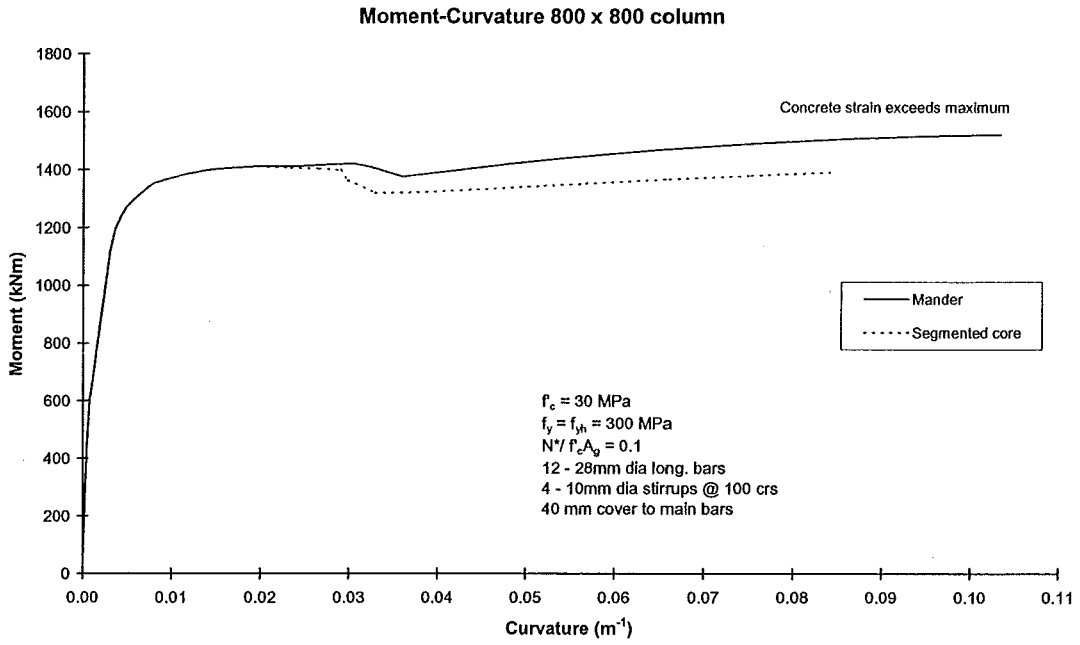

Figure 8.13 *Comparison of Moment-Curvature Results for 800 mm Square Column, $N^* = 0.1 f'_c A_g$, Stirrups @ 100 mm crs*

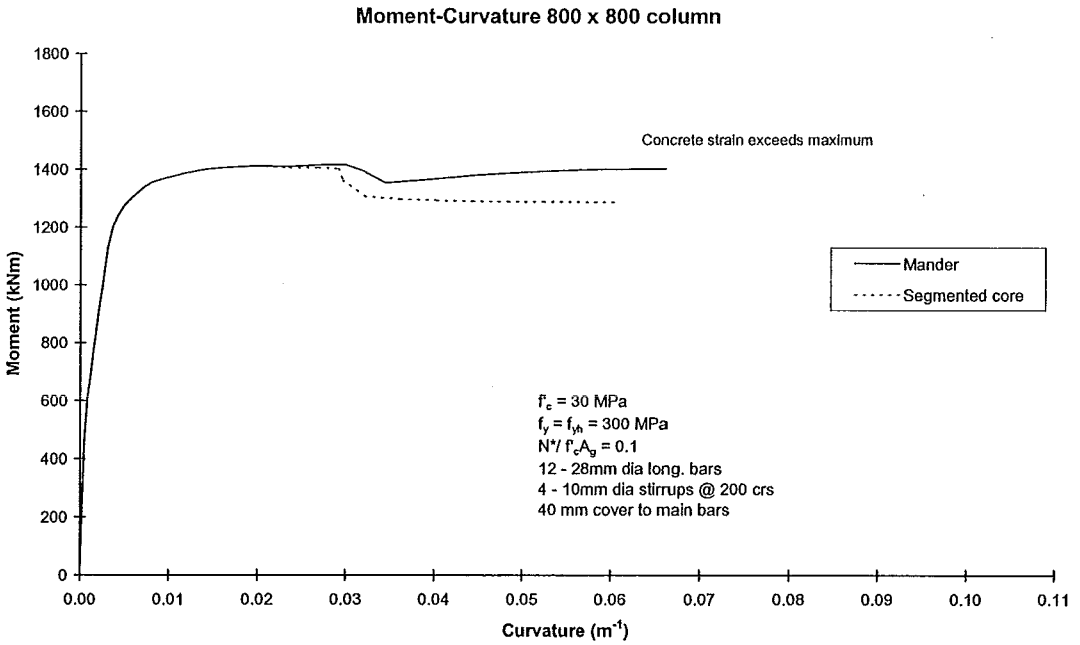

Figure 8.14 *Comparison of Moment-Curvature Results for 800 mm Square Column, $N^* = 0.1 f'_c A_g$, Stirrups @ 200 mm crs*

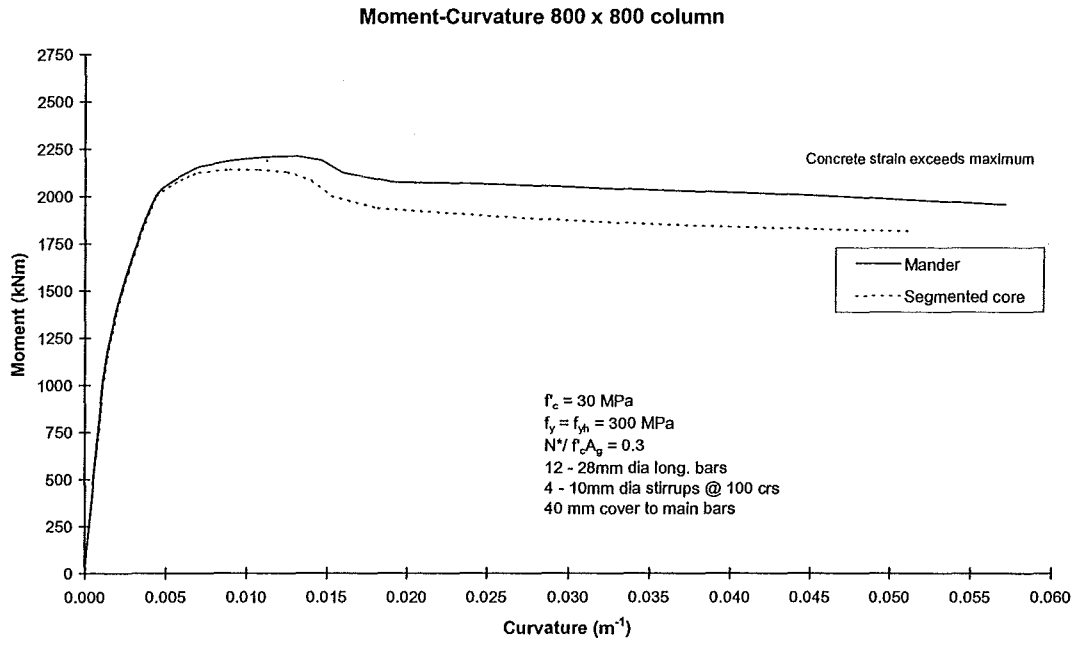

Figure 8.15 *Comparison of Moment-Curvature Results for 800 mm Square Column, $N^* = 0.3 f'_c A_g$, Stirrups @ 100 mm crs*

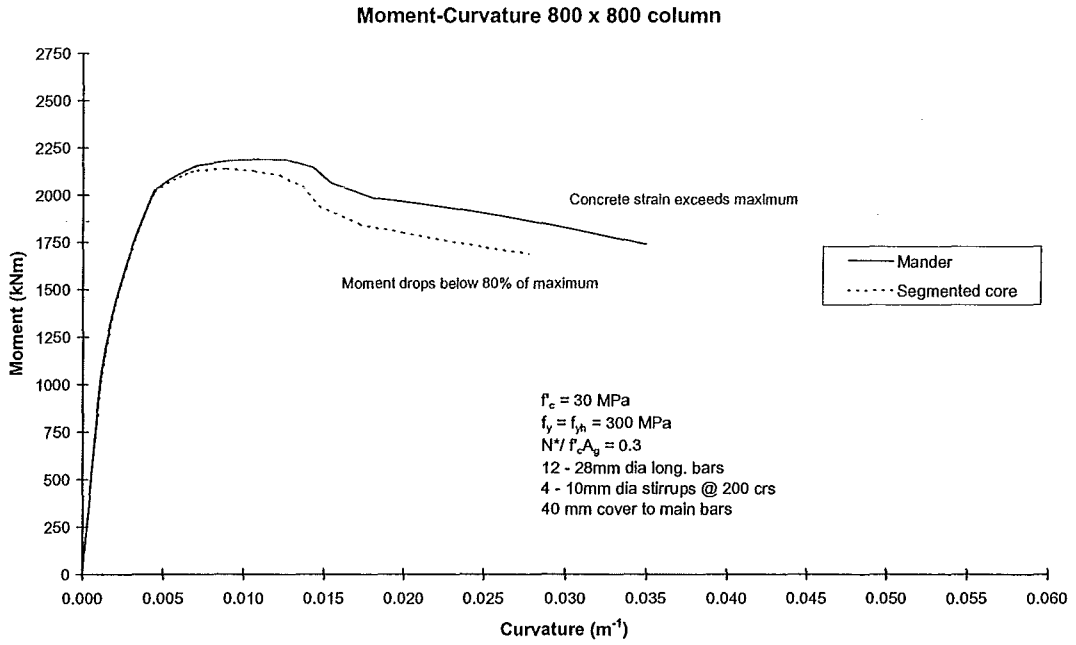

Figure 8.16 *Comparison of Moment-Curvature Results for 800 mm Square Column, $N^* = 0.3 f'_c A_g$, Stirrups @ 200 mm crs*

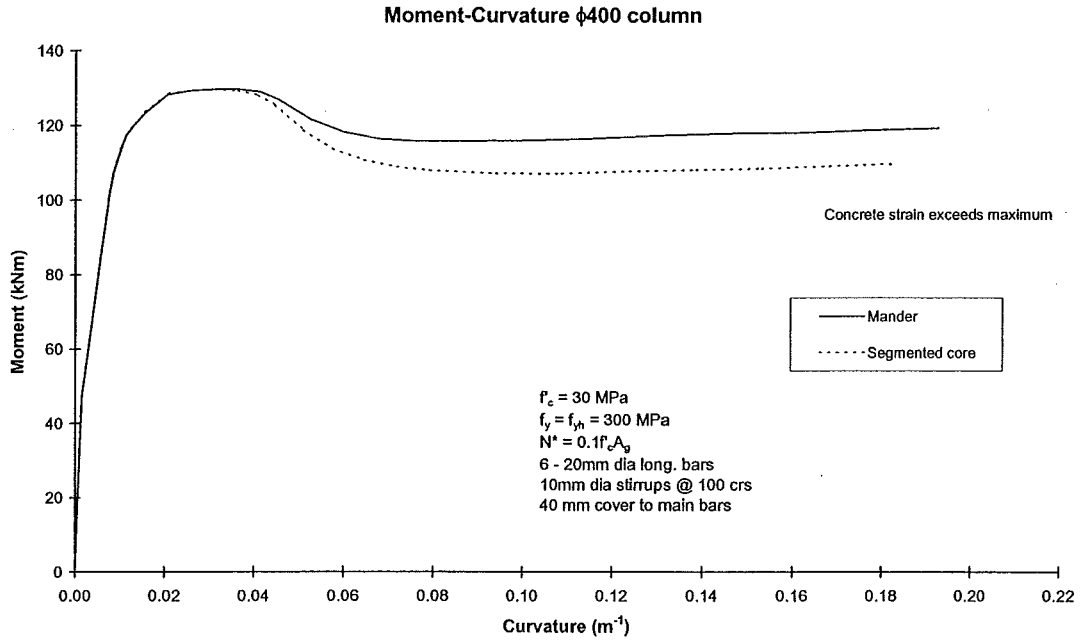

Figure 8.17 *Comparison of Moment-Curvature Results for 400 mm Circular Column, $N^* = 0.1 f'_c A_g$, Stirrups @ 100 mm crs*

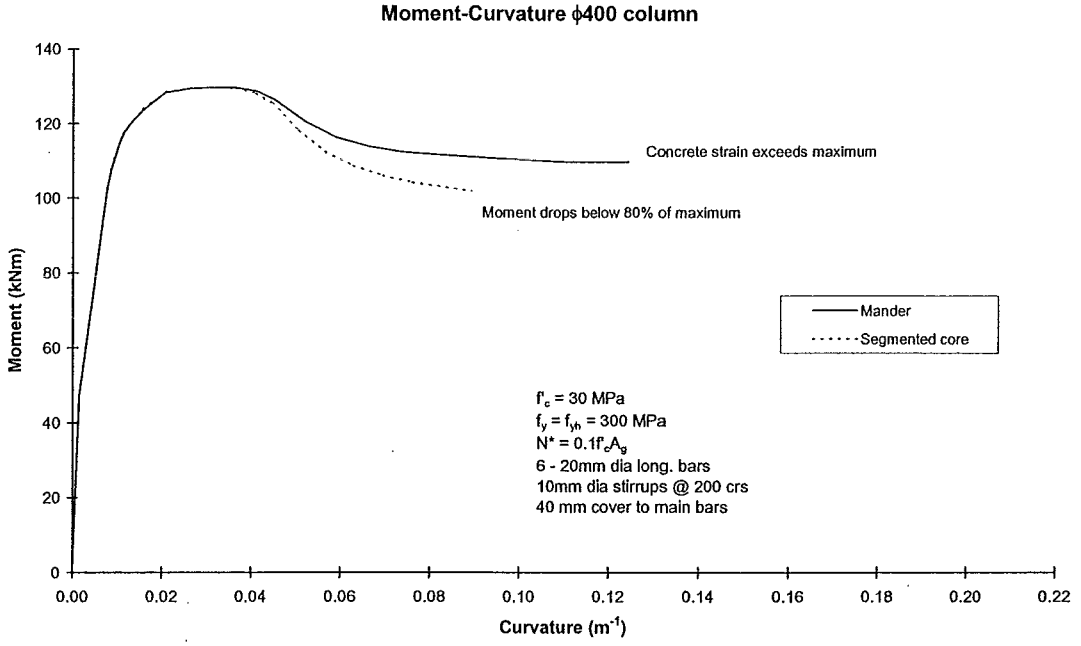

Figure 8.18 *Comparison of Moment-Curvature Results for 400 mm Circular Column, $N^* = 0.1 f'_c A_g$, Stirrups @ 200 mm crs*

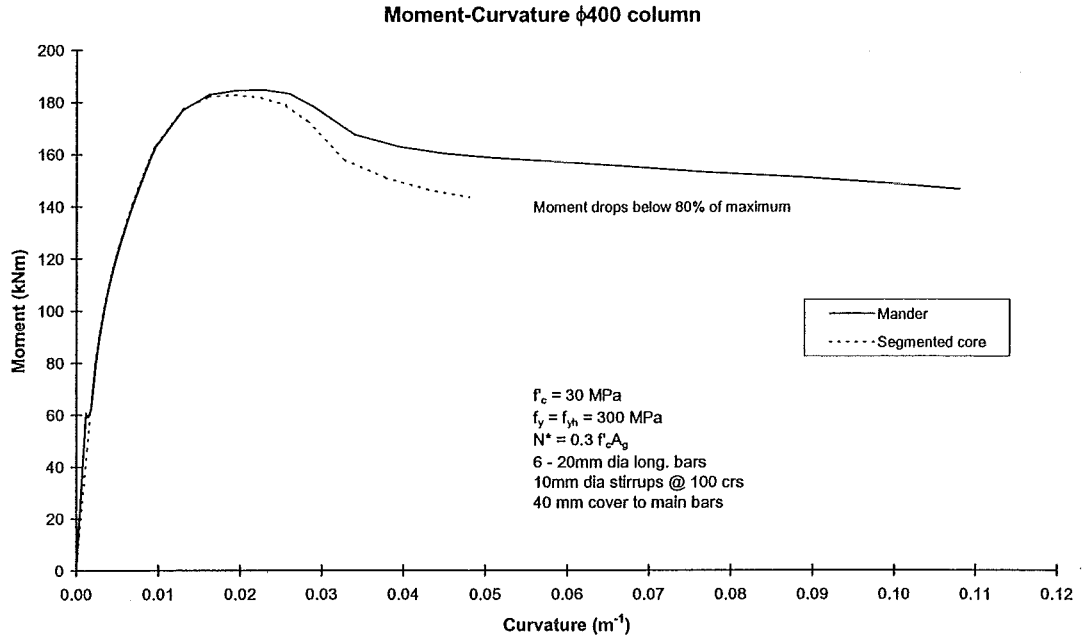

Figure 8.19 *Comparison of Moment-Curvature Results for 400 mm Circular Column, $N^* = 0.3 f'_c A_g$, Stirrups @ 100 mm crs*

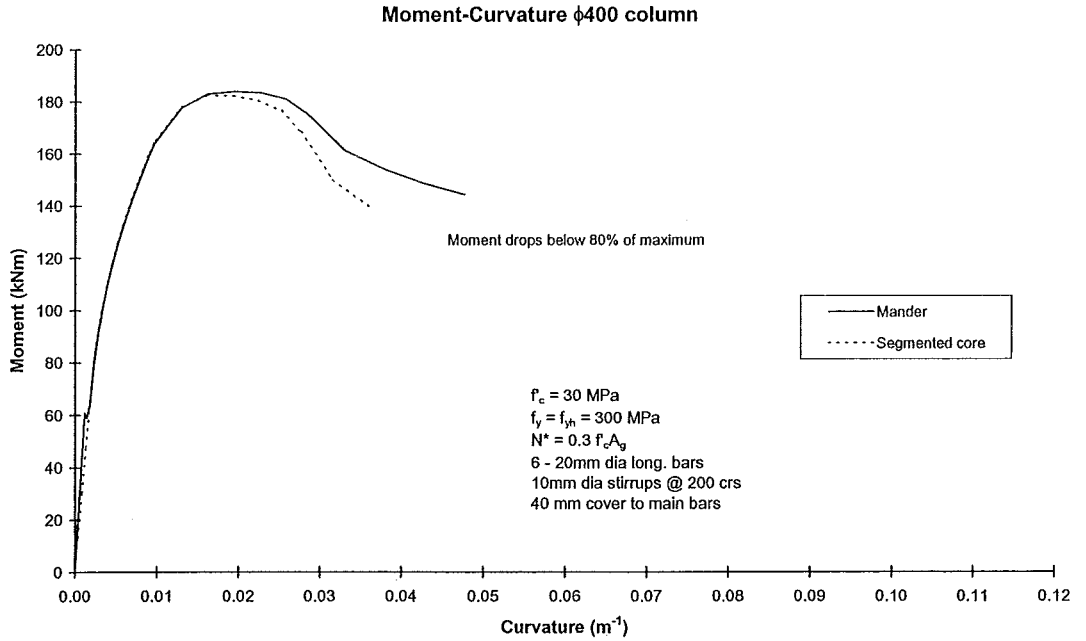

Figure 8.20 *Comparison of Moment-Curvature Results for 400 mm Circular Column, $N^* = 0.3 f'_c A_g$, Stirrups @ 200 mm crs*

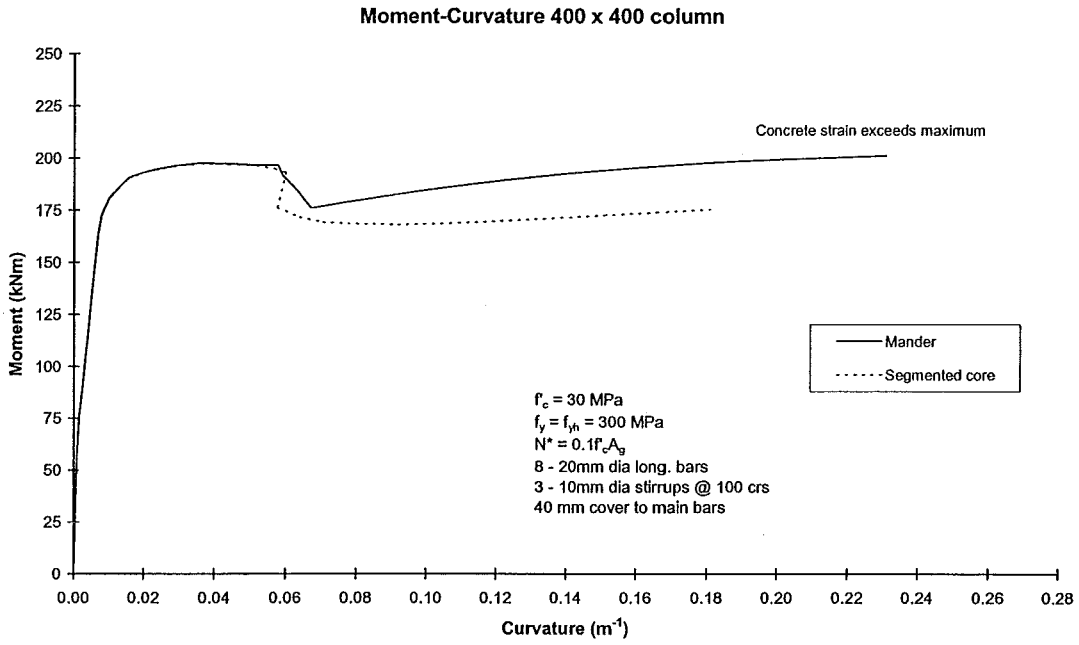

Figure 8.21 *Comparison of Moment-Curvature Results for 400 mm Square Column, $N^* = 0.1 f'_c A_g$, Stirrups @ 100 mm crs*

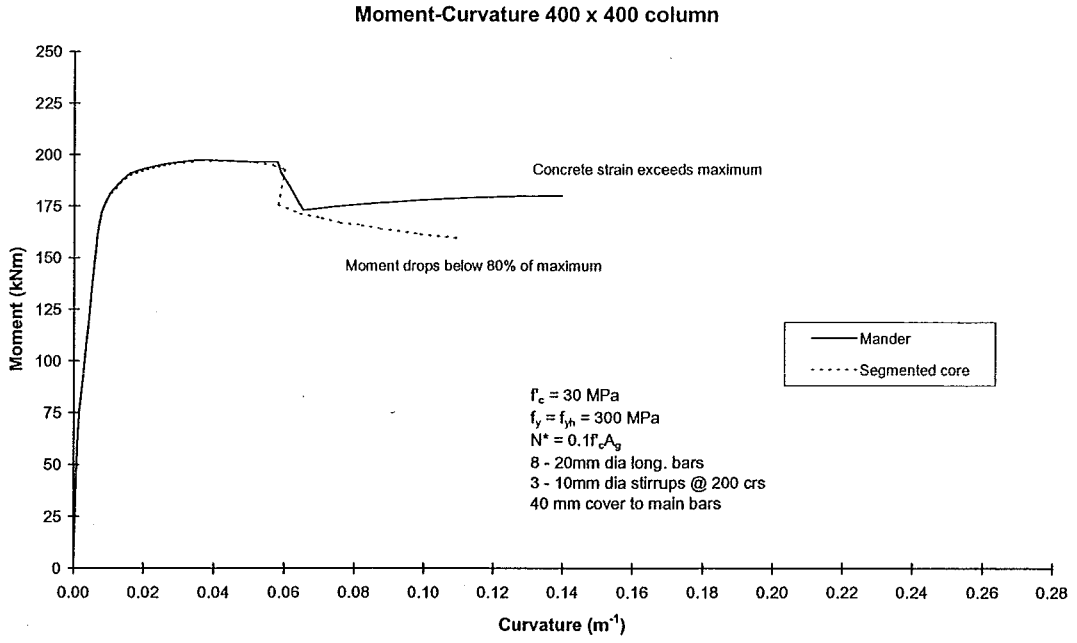

Figure 8.22 *Comparison of Moment-Curvature Results for 400 mm Square Column, $N^* = 0.1 f'_c A_g$, Stirrups @ 200 mm crs*

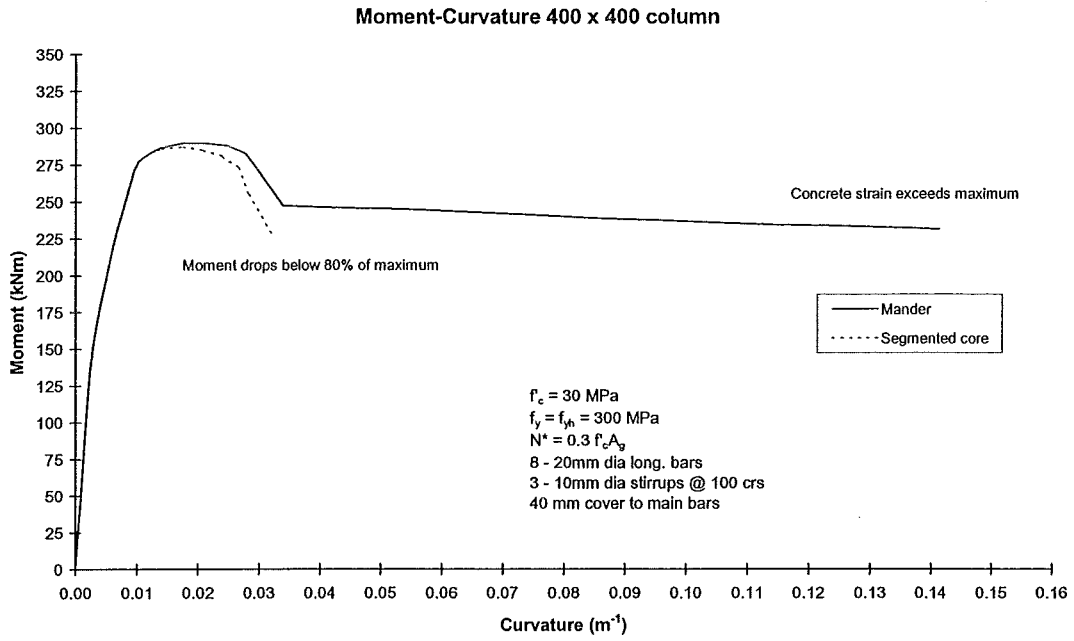

Figure 8.23 *Comparison of Moment-Curvature Results for 400 mm Square Column, $N^* = 0.3 f'_c A_g$, Stirrups @ 100 mm crs*

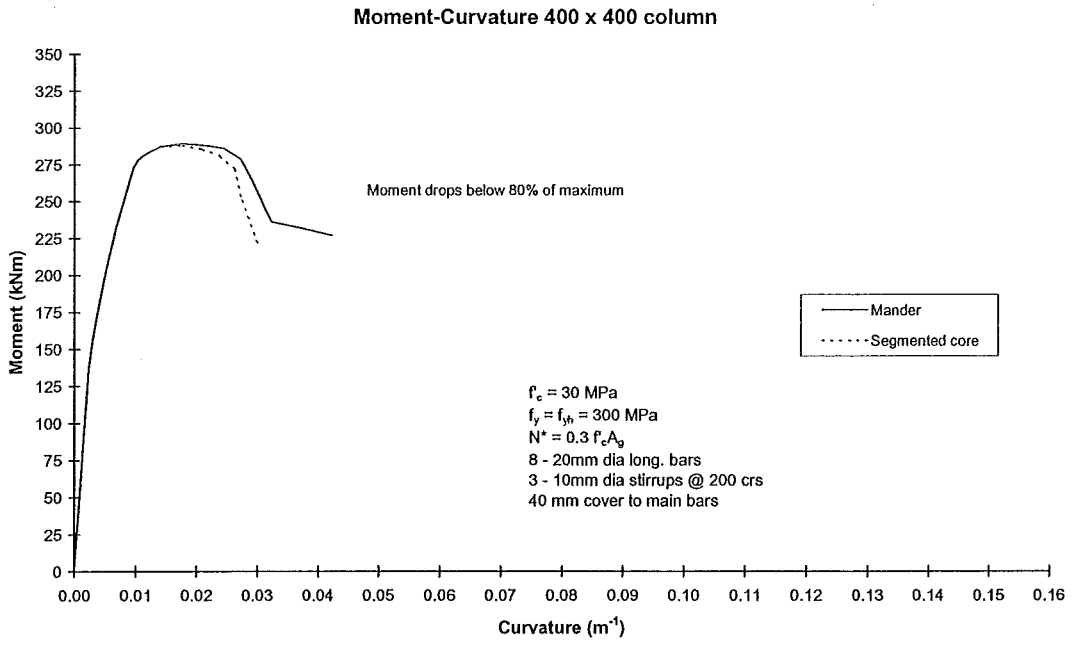

Figure 8.24 *Comparison of Moment-Curvature Results for 400 mm Square Column, $N^* = 0.3 f'_c A_g$, Stirrups @ 200 mm crs*

Moment enhancement arising from the increase in strength due to confinement of the concrete and strain hardening of the steel have already been accounted for in the monotonic moment-curvature analyses. Further moment enhancement may arise from cyclic loading of the column, dynamic loading strain rates and the observed shift in the critical section.

8.6.3 Cyclic Moment-Curvature Analysis

Reversed cyclic loading of a column can lead to stresses in the longitudinal reinforcement being much higher than those given by monotonic tension or compression tests. Due to the Bauschinger effect and strain hardening the stress developed in the steel at a given strain, in a cyclically loaded column, can be much greater than the stress given by the monotonic stress-strain response at the same strain, if the neutral axis is near mid section depth. Cyclic loading will also influence the stress-strain behaviour of confined concrete although it is reasonable to assume the monotonic curve will form an envelope to the cyclic loading stress-strain response [M3, M4].

The monotonic steel stress-strain curve can also be assumed to be a skeleton curve for cyclic loading stress-strain response by shifting the origin of the skeleton curve to account for the cyclic loading history [T2].

Cyclic moment-curvature analyses can be conducted by incorporating the cyclic stress-strain relations for both concrete and steel. The moment-curvature analysis is conducted in a similar manner by specifying the strain history for the extreme compressive fibre, establishing equilibrium of internal and external forces by determining the stresses in the concrete and steel from their respective cyclic stress-strain relations.

8.6.3.1 Steel Strain Relationship in Mander Model

To model the effects of cyclic loading on the enhancement of a column's flexural strength a pseudo-cyclic moment-curvature analysis was developed as part of this study. The steel stress-strain relation proposed by Mander et al. [M4], described in

Section 8.6.1, was used assuming behaviour in compression is equal and opposite to the tensile behaviour. To account for the increase in stress due to the Bauschinger effect and strain hardening, the origin of the monotonic stress-strain relation was shifted by an amount corresponding to the residual plastic strain remaining in the bar.

Under cyclic load reversals the extreme tension steel is subjected to compressive strains during the reversed cycle. By assuming the reverse cycle is to the same extreme compressive fibre strain as the previous cycle the tension steel will unload from the strain achieved during the original cycle and be subjected to the compressive strain resulting from the reverse cycle strain profile. This is illustrated in Figure 8.25 with the strain profile for the original and reverse cycle shown.

Unloading from the tension strain is assumed to be linear with a slope equivalent to the initial elastic modulus of the steel. The monotonic curve is only shifted if strains in the steel from loading during the first cycle have exceeded the yield strain. Once the yield strain has been exceeded the remaining residual strain in the steel is evaluated and added to the strain resulting from an equivalent cycle in the reverse direction. The steel is then subjected to a compressive strain which is reached by following the monotonic compressive steel stress-strain relationship, which has been offset by the amount of residual strain remaining in the steel after the first cycle.

The shifting of the origin of the monotonic stress-strain curves by an amount equivalent to the residual plastic strain in the steel after unloading determines the pseudo-cyclic strain. This is an approximation of the strains achieved in the reinforcement as a result of cyclic loading.

By incorporating pseudo-cyclic stress-strain relations for the longitudinal reinforcement in a column section the effects of a the cyclic response of the longitudinal steel can be included in a moment-curvature analysis. This pseudo-cyclic moment-curvature analysis, evaluating the stresses in the longitudinal reinforcement using the pseudo-cyclic strains, provides a good approximation for the increase in flexural strength which results from the cyclic loading of columns.

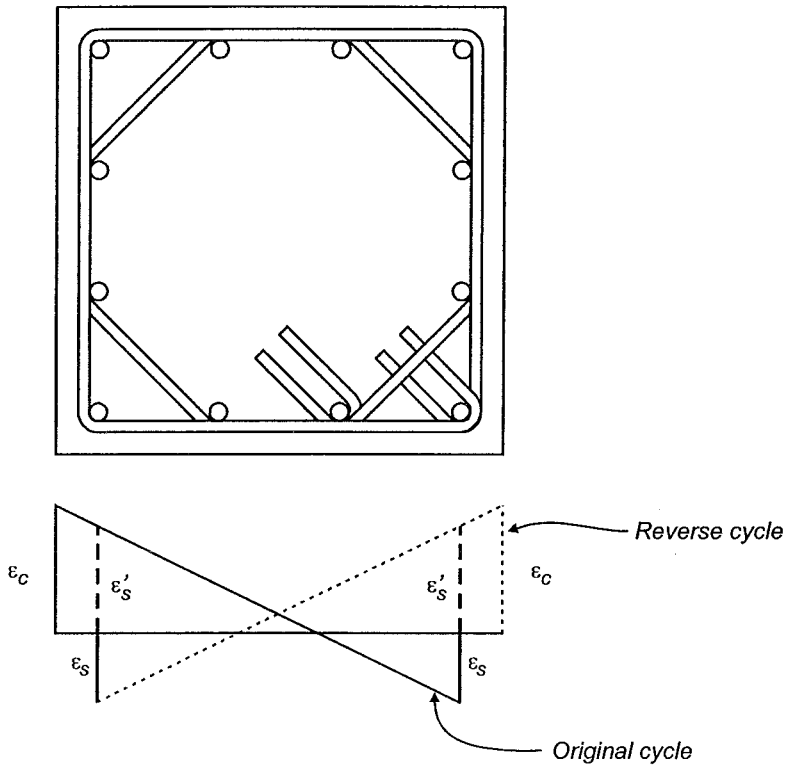

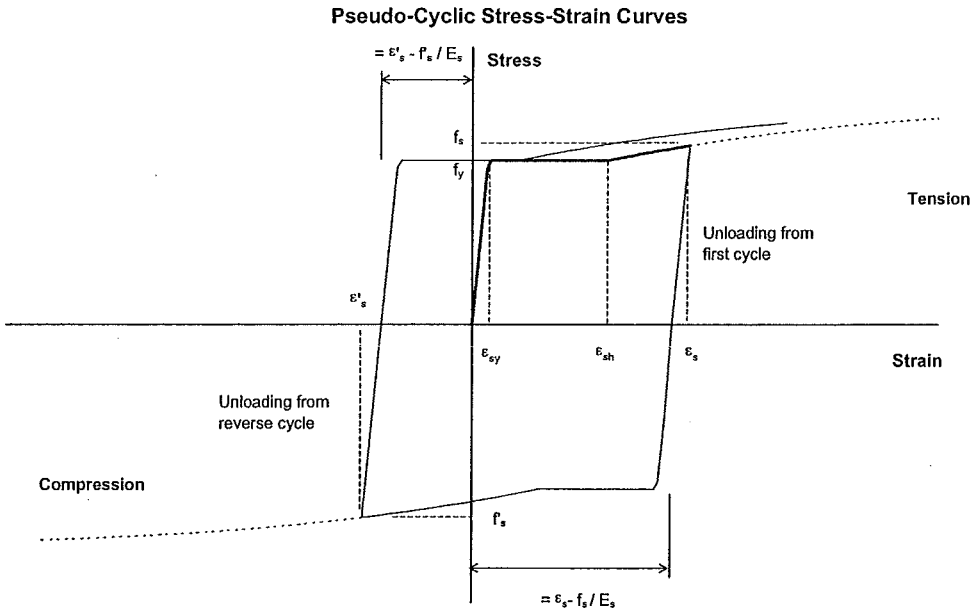

Figure 8.25 *Monotonic and Pseudo-Cyclic Stress-Strain Relations for Reinforcing Steel*

8.6.3.2 Dodd and Restrepo Steel Strain Model

A model for predicting the cyclic behaviour of reinforcing steel, calibrated against New Zealand manufactured steel grades 300 and 430, has been proposed by Dodd and Restrepo-Posada [D2]. This model has been shown to give a good prediction of experimental test results on these two grades of steel [D1, D2, R3, R4]. Analytical results using this model are compared to the shifted monotonic skeleton curves in Figure 8.26 where it can be seen that the cyclic stress-strain behaviour is closely matched by the shifted monotonic curve over the tensile (positive) region. As the compressive monotonic stress-strain curve is taken as equal and opposite to the tensile stress-strain curve the difference between the cyclic response and the shifted monotonic curve, as used in the pseudo-cyclic moment-curvature routine, is somewhat larger.

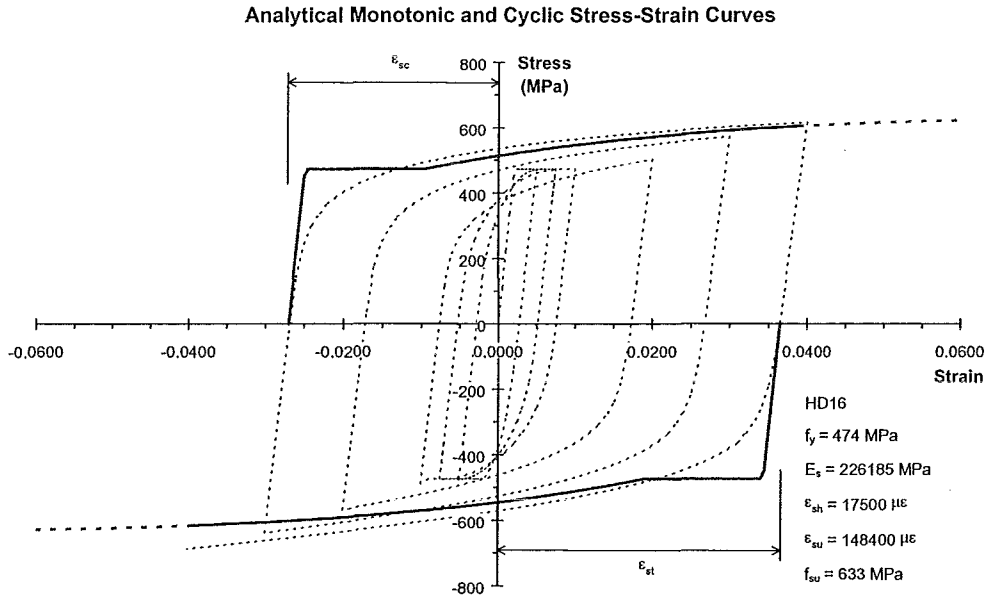

Figure 8.26 *Analytical Shifted Monotonic and Cyclic Stress-Strain Curves for Reinforcing Steel [W3]*

8.7 FLEXURAL STRENGTH ENHANCEMENT

8.7.1 Influence of Axial Load

Tests on columns subjected to constant axial load and cyclic lateral loading have indicated an increase in flexural strength with increasing axial load. Moments determined using actual material properties and taking the ACI stress block [X3] with $\varepsilon_c = 0.003$ and a strength reduction factor of unity give predicted flexural strengths which may be significantly lower than measured experimental moments. Some of this difference is due to the ACI method not accounting for increases in steel stresses as the steel enters the strain hardening region, a rather conservative assumption for the concrete strain at maximum moment and not accounting for the increase in concrete strength due to confinement from transverse reinforcement.

Ang et al. [A1] reviewed test data from a number of columns tested at the University of Canterbury under constant axial load and reversed cyclic lateral loading. Comparison of the ratio of M^*/M_i, where M^* is the maximum measured experimental moment and M_i is the predicted flexural strength, determined using the ACI method with actual material properties and strength reduction factor of 1.0, against axial load ratio, N^*/f'_cA_g, showed that flexural strength enhancement is strongly dependent on the axial load. This was attributed to the large contribution of the concrete compressive force to the flexural strength of a column at higher axial loads due to the influence of the enhanced concrete compressive strength, due to confinement.

At lower axial loads the increase in the ratio of experimental strength to the predicted strength, based on measured material strength properties, is primarily due to the effects of strain hardening in the flexural reinforcement. The average value of the experimentally obtained moment enhancement is given by:

$$\frac{M^*}{M_i} = 1.13 \qquad \frac{N^*}{f_c' A_g} > -0.1$$

$$\frac{M^*}{M_i} = 1.13 + 2.35\left(-\frac{N^*}{f_c' A_g} - 0.1\right)^2 \qquad \frac{N^*}{f_c' A_g} \leq -0.1 \tag{8.26}$$

where $N^* / f'_c A_g$ is taken as negative for compressive axial loads

The original experimental data used by Ang et al., shown in Figure 8.27, indicated that the points fall within ±15 % of this equation. The original data used to plot this graph was reviewed and additional experimental data points were included from subsequent tests on columns conducted at the University of Canterbury. It was found in this study that some of the points reported by Ang et al. [A1] did not compare with the measured experimental maximum moments determined by the original researchers. The experimental moments for the tests conducted by Davey and Park [D3], reported by Ang et al. for these tests, were the experimental moments measured at a concrete strain of $\varepsilon_c = 0.003$, not the maximum moments measured during the tests. Maximum moments were determined from the lateral load-lateral displacement plots measured by Davey and Park, including P-Δ effects, and are presented in Figure 8.28. The only experimental result which fell outside the ±15 % bounds of the proposed equation was determined by Ang et al. [A3]. The reported maximum moment for the column specimen with an axial load ratio of 0.56 does not agree with the reported lateral load-lateral displacement plots measured during the experiment. An experimental moment value has been determined from the reported lateral load-lateral displacement plots, including P-Δ effects and this point has been included in Figure 8.28.

It should be noted that the data point for the test conducted by Potangaroa et al. [P8] at an axial load ratio of 0.7 was determined by re-testing a column unit which had been previously tested at an axial load ratio of 0.35. The effect of excursions of the longitudinal reinforcing steel into the inelastic range during the initial test will have further increased the observed moment enhancement ratio for this column. Due to this the second experimental result cannot be directly compared with the other quasi-static test results. Test results from dynamically tested columns by Dodd and Cooke [D1] are shown in Figure 8.29.

Comparison of the corrected data points with further test results from a number of subsequent University of Canterbury column tests, shown in Figure 8.28, still show a trend for the increase in moment enhancement ratio with increased axial load. Also shown in Figure 8.28 are results reported by Sheikh and Yeh [S6] from tests conducted at the University of Houston. These tests differ from the column tests conducted at the University of Canterbury as loading is only applied monotonically and there is no stub adjacent to the critical section.

8.7.2 Influence of Confinement from Adjacent Members

Gill et al. [G1, P6] noted that the stub adjacent to the critical section provides additional confinement to the column and causes the critical section to move away from the face of the stub or adjacent member. They noted at large compressive strains an assumed 45° cone of influence from the compression region of the column could be taken. This would move the critical section 0.5 times the neutral axis depth away from the face of the stub and would account for a large part of the difference between theoretical and experimental flexural strengths.

From observations of column tests the critical section may be taken as 0.5 to 1.0 times the depth of the compressed region of the column away from the face of the adjacent member. This shift in the critical section results in an increase in the flexural strength of the column. The amount of shift is dependent on the axial load level and also the geometric properties of the column, namely the column's aspect ratio. Photographs from circular columns tested dynamically by Dodd and Cooke [D1], shown in Figure 8.30, clearly illustrate the shift in the critical section with increased axial load and increased column slenderness.

For columns in typical building frames and bridge structures it is usual to assume the critical section of a column occurs at the point of maximum moment, which is usually immediately adjacent to another member. The calculated flexural strength of the column, M_i, which can be determined using the ACI method or by using a moment-curvature analysis is assumed to be developed at this point. A moment-

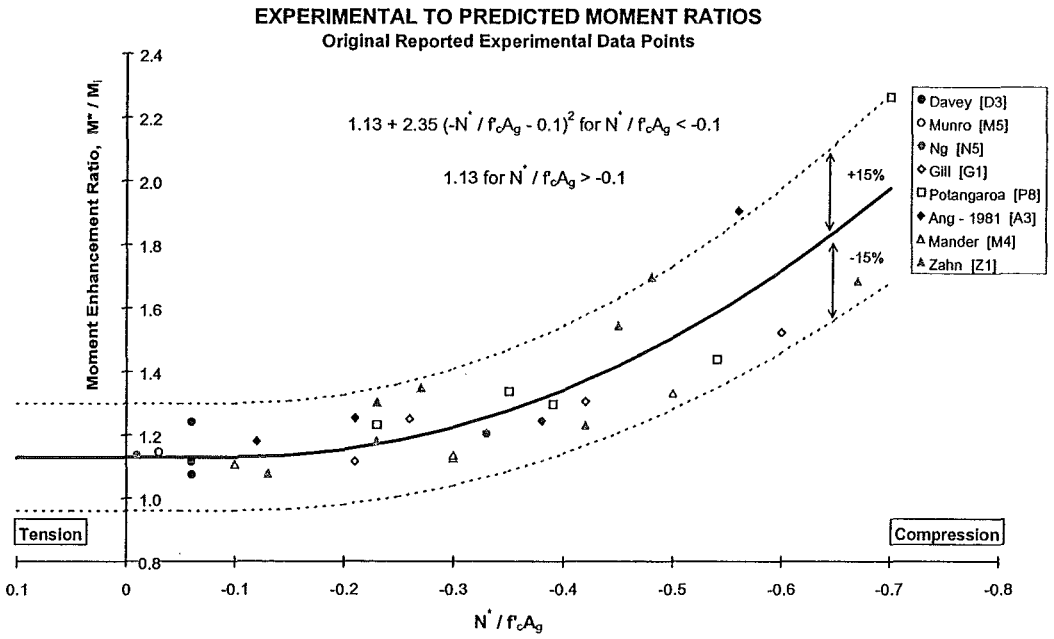

Figure 8.27 *Influence of Axial Load on Moment Enhancement Ratio from Ang et al. [A1]*

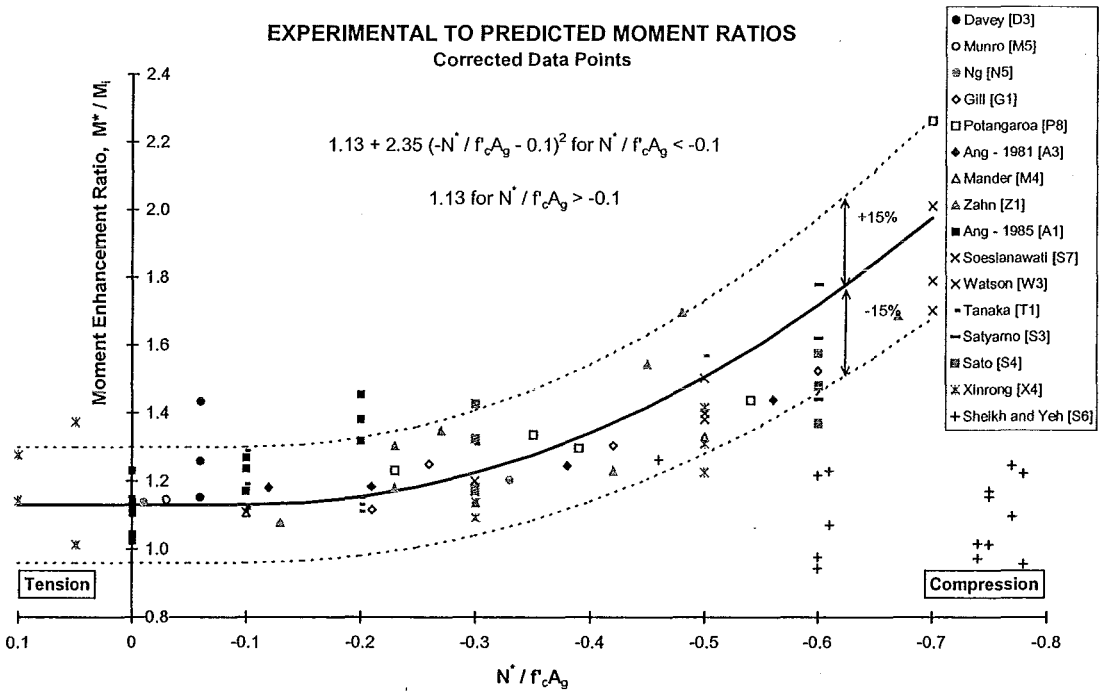

Figure 8.28 *Influence of Axial Load on Moment Enhancement Ratio with Corrected and Additional Data Points*

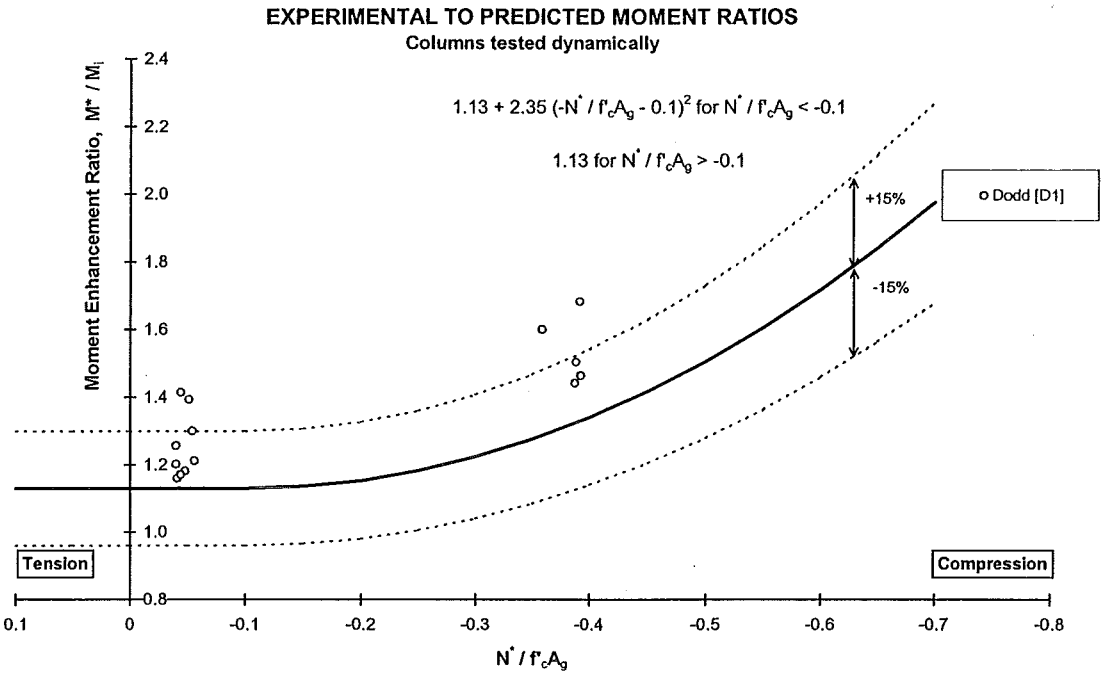

Figure 8.29 *Influence of Axial Load on Moment Enhancement Ratio for Dynamically Tested Columns*

curvature analysis has the advantage of being able to incorporate the effects of strain hardening in the reinforcement and the increase in concrete strength due to confinement by transverse reinforcement, depending on the stress-strain models incorporated into the analysis for each material. Figure 8.31 illustrates this effect showing the assumed and actual locations of the critical section and resulting bending moment diagrams. As the critical section moves some distance, x, from the base of the column the flexural strength of the column, M_i, is developed at this location, effectively increasing the moment in the column to $\alpha_{shift}M_i$ where:

$$\alpha_{shift} = \frac{l_c}{(l_c - x)} \qquad (8.27)$$

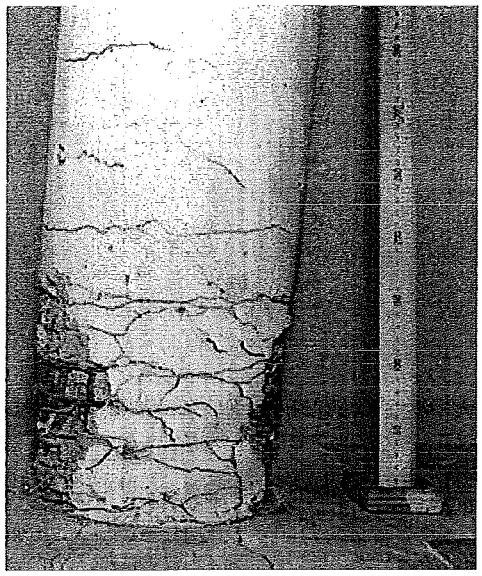

(a) Medium Pier with Low Axial Load, Aspect Ratio = 7, Pier 2b

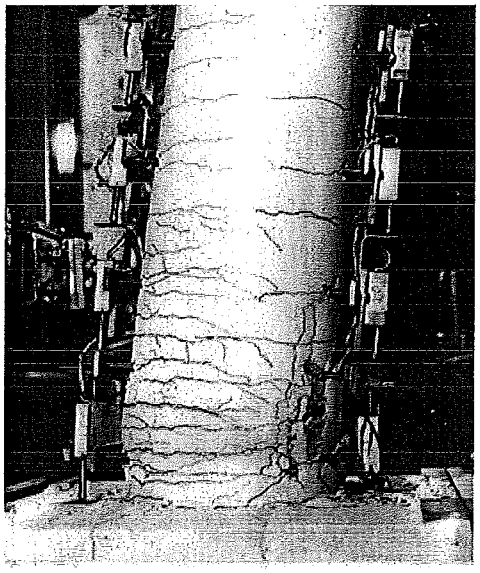

(c) Tall Pier with Low Axial Load, Aspect Ratio = 10, Pier 3b

(b) Medium Pier with High Axial Load, Aspect Ratio = 7, Pier 5

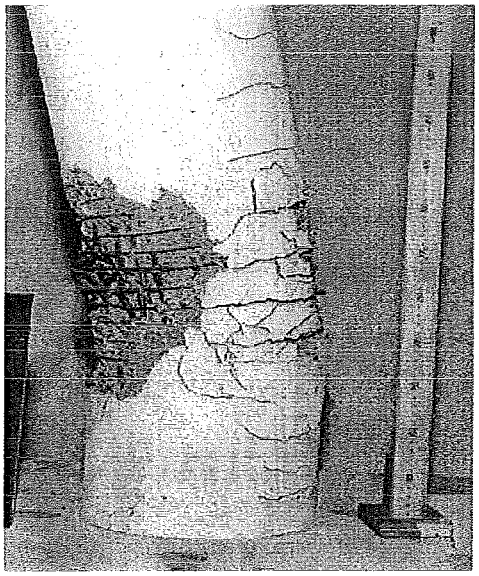

(d) Tall Pier with High Axial Load, Aspect Ratio = 10, Pier 6

Figure 8.30 Critical Sections of Columns with Varying Axial Load and Aspect Ratios from Dodd and Cooke [D1]

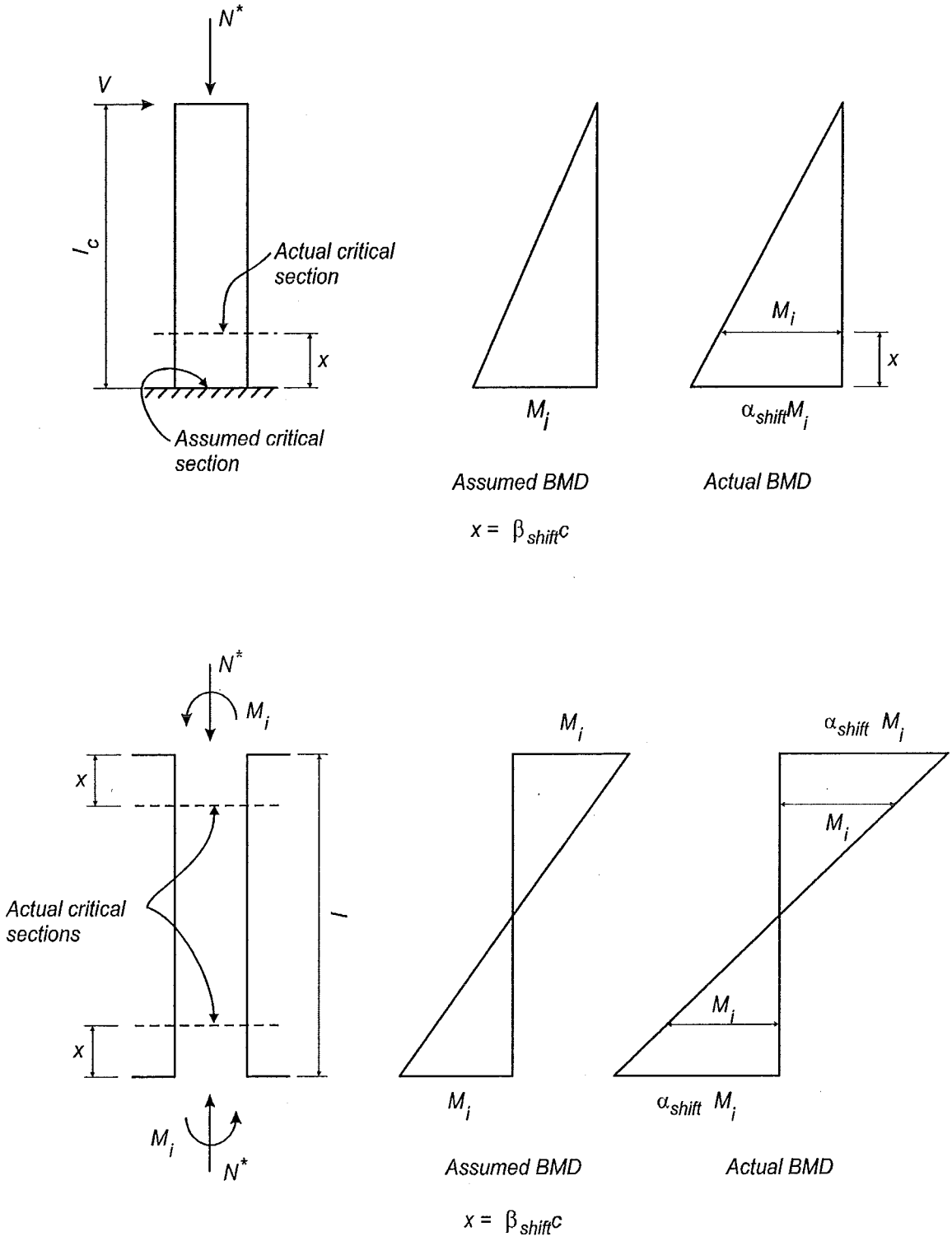

Figure 8.31 *Effect of Additional Confinement from Adjacent Member for a Column*

The distance for the shift of the critical section, x, is assumed to be between 0.5 and 1.0 times the neutral axis depth, which will vary with the axial load acting on the column. By including an expression for the neutral axis depth in Equation 8.27 an expression for the amount of moment enhancement due to the confining effects of adjacent members can be determined:

$$\alpha_{shift} = \frac{\frac{l_c}{D}}{\left(\frac{l_c}{D} - \beta_{shift} \frac{c}{D} \right)} \qquad (8.28)$$

where l_c = distance to point of contraflexure in column

D = depth of rectangular or square column or diameter of circular column

c = neutral axis depth taken at spalling of cover concrete

β_{shift} = ratio of shift in critical section to neutral axis depth, assumed to be between 0.5 and 1.0

As the position of the neutral axis varies in position throughout the moment-curvature response the neutral axis depth, c, should be taken at spalling of the cover concrete. When spalling occurs the critical section will form at this point and the flexural strength of the section will be developed at this location.

8.8 COMPONENTS OF FLEXURAL ENHANCEMENT

8.8.1 ACI Flexural Strength

The ACI method [X3] for determining the flexural strength of a confined column is based on unconfined concrete properties and is usually a conservative estimate for the actual strength. The flexural strength of a column is taken at a maximum concrete compressive strain of $\varepsilon_c = 0.003$ using the ACI concrete rectangular stress block, which assumes a mean stress of $\alpha_1 f'_c$ and neglects the effects of strain hardening in

the steel. This moment, M_i, the ACI ideal moment, will provide a lower bound for the flexural strength for a confined section, even if actual material strengths are used. This is conservative for flexural design purposes but is not conservative for shear design which is based on the flexural overstrength of a column when applying capacity design principles. Transverse reinforcement provided for confinement will enhance the compressive strength of the concrete and as a result of the increased ultimate curvature strain hardening in the longitudinal reinforcement will also contribute to moment enhancement.

The ACI ideal moment capacity can be obtained from considerations of strain compatibility through the column section and equilibrium of internal and external forces or may be determined from column interaction design charts prepared for various sections incorporating the same assumptions [C6].

An approximate closed form equation to predict the ACI ideal moment capacity for columns with rectangular sections can be expressed as:

$$M_n = \frac{1}{2}\left[\alpha_1\beta_1\frac{c}{D}\left(1-\beta_1\frac{c}{D}\right) + g\zeta\, p_t\left(\frac{f_s^{'}+f_s}{f_c^{'}}-\alpha_1\right)\right]BD^2 f_c^{'} \qquad (8.29)$$

where α_1 = factor defining effective stress in rectangular stress block

= 0.85 for $f'_c \le 55$ MPa

= $0.85 - 0.004\,(f'_c - 55) \ge 0.75$ for $f'_c > 55$ MPa

β_1 = factor defining effective depth of rectangular stress block

= 0.85 for $f'_c \le 30$ MPa

= $0.85 - 0.008\,(f'_c - 30) \ge 0.65$ for $f'_c > 30$ MPa

c = distance from extreme compressive fibre to position of neutral axis taken at spalling of cover concrete

D = depth of rectangular or square column

B = width of rectangular or square column

g = ratio of distance between reinforcing bars closest to faces of rectangular columns to section depth

ζ = factor depending on the distribution of longitudinal bars along the faces of the column

= $0.46\psi + 0.20$ for columns with distributed steel

= 0.5 for columns with longitudinal steel placed on opposite faces only

ψ = ratio of number of bars on one end face of the column to the total number of longitudinal bars in the column

p_t = longitudinal reinforcement ratio

f'_s = stress in longitudinal steel on compression face of column resulting from strain compatibility not taken greater than f_y

f_s = stress in longitudinal steel on tension face of column resulting from strain compatibility not taken greater than f_y

The first term within the square brackets evaluates the magnitude of the concrete compressive force assuming the ACI rectangular stress block of depth $\beta_1 c$ and an effective stress equal to $\alpha_1 f'_c$. This resultant force acts at the centroid of the rectangular stress block and moments are taken from the centreline of the section. The second term within the square brackets allows for the stress developed in the extreme tension and compression bars and for the distribution of the longitudinal steel through the ζ term. The strain profile through the section is set by the expression giving the neutral axis depth ratio, c / D, as:

$$\frac{c}{D} = \frac{N^*}{f_c' A_g}\left[6.9p_t + 0.015m + 0.24p_t m - 1.4\right] + 0.0025m + \gamma \qquad (8.30)$$

where γ = $(0.11m + 2.1)p_t + 0.03$ for $m \leq 25$

= $4.85p_t - 0.05$ for $m > 25$

$N^* / f'_c A_g$ is taken as negative for compressive axial loads

The derivation of Equation 8.29 is included in Appendix C along with comparisons of the moment – axial load interaction compared to results calculated using the ACI method. These comparisons show that Equation 8.29 will give results to ±5 % for

longitudinal steel ratios, p_t, up to 4 % and axial load ratios over the range $0.05 \leq N^* / f'_c A_g \geq -0.7$. The difference between the flexural strength determined using Equation 8.29 and the ACI method for higher tensile axial loads is due to Equation 8.30 not providing a good estimate of the actual neutral axis depth. The upper axial load limit of $-0.7\ f'_c A_g$ is often taken as the maximum design axial load for a column subjected to seismic actions.

For consideration of the nominal flexural strength of a column subjected to cyclic reversed loading the steel stresses f'_s and f_s in Equation 8.29 can be taken as equal to the yield stress f_y. Strains developed in the steel from the strain profile do not directly translate into stresses following the monotonic skeleton stress-strain curve. The stress developed in the longitudinal steel is a function of the amount of strain accumulated in the steel from the original and reversed cycle. Following Section 8.6.3 it can be shown that during cyclic reversed loading if the longitudinal steel has reached its yield strength in either tension or compression during one cycle, the steel will reach its yield strength during the cycle in the opposite direction.

8.8.2 Confined Concrete and Strain Hardening of Longitudinal Reinforcement

The ACI ideal moment capacity, M_i, or the predicted ACI moment capacity, M_n, from Equation 8.29 may not give the maximum flexural strength of a column as this strength will be influenced by the increase in concrete strength due to the presence of transverse reinforcement and strain hardening of the longitudinal steel. A refined calculation for the flexural strength can be made by incorporating the stress-strain relations for confined concrete, accounting for the enhancement in concrete strength and ductility due to confinement, and stress-strain relations for the longitudinal steel, including strain hardening. These are readily incorporated into a moment-curvature analysis from which the maximum moment attained during the moment-curvature response can be taken as the flexural strength of the column. Analytical stress-strain models for confined concrete are available and combined with actual or idealised relations for steel stress-strain behaviour the flexural strength of a column can be closely predicted.

As with the derivation of Equation 8.29 the concept of decoupling of the contribution to the flexural strength from the concrete compressive force resultant and the longitudinal steel couple can be applied.

From moment-curvature analyses the concrete compressive force, C_c, can be seen to remain reasonably constant through the moment-curvature response for curvatures beyond the yield curvature. Transverse reinforcement in the column will confine the concrete core and increase the peak compressive strength of the concrete. As the concrete compressive force is remaining constant and the peak compressive strength of the concrete has increased, the depth of compressed concrete required to carry the concrete compressive force is reduced. The shape of the compression block can also be taken to be rectangular in shape giving the depth of an assumed rectangular stress distribution equivalent to depth of the region supporting the compressive stresses.

Figure 8.32 shows the area of concrete assumed to be effective in supporting the concrete compressive force. Spalling of the cover concrete and the arching of the core concrete between the transverse hoop sets and restrained longitudinal bars reduce the region of concrete core. The arch region, or ineffectively confined core, can be assumed to be supporting no compressive stress at higher concrete compressive strains and therefore the effectively confined core must maintain the concrete compressive force. Figure 8.8 shows the assumed stress-strain relationships for the ineffectively confined and effectively confined core regions. At high compressive strains it can be seen that the ineffectively confined concrete stresses decrease close to zero while the concrete stresses in the effectively confined concrete stresses can be assumed to be close to the peak confined concrete compressive strength, f'_{cc}. This stress is maintained over a reasonable strain range and is assumed to be constant across the depth of the effectively confined concrete region.

By taking the components of the flexural strength due to the concrete compressive force and the longitudinal steel couple, the moment of resistance for rectangular sections after spalling of the cover concrete can be approximated as:

$$M_o = \left[\frac{\eta}{2}\frac{c}{D}\left(\sqrt{\lambda_e \frac{B}{B_c}} - \frac{f_c'}{f_{cc}'}\frac{c}{D}\right) + \frac{(\lambda_C + \lambda_T)\, g\zeta\, p_t f_y}{2 f_c'}\right] BD^2 f_c' \quad (8.31)$$

where η = 0.85

λ_e = confined concrete efficiency factor described in Section 8.8.2.1

f'_{cc} = confined concrete compressive strength

λ_C = overstrength factor of reinforcing steel in compression

λ_T = overstrength factor of reinforcing steel in tension

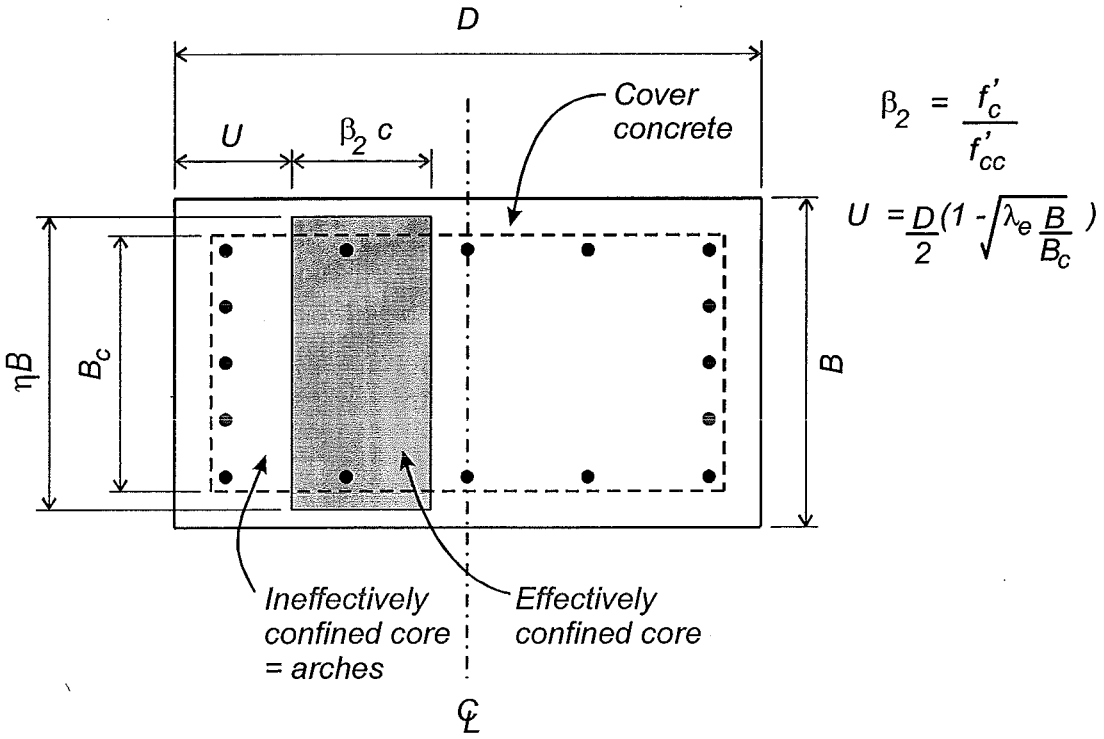

Figure 8.32 *Region to Support Confined Concrete Compressive Force After Spalling of Cover Concrete*

The term η accounts for a decreased width of section due to spalling of the cover concrete down the sides of the section toward the position of the neutral axis. The confined concrete efficiency factor, λ_e, reflects the influence of arching in the column due to the layout and spacing of the transverse reinforcement decreasing the area of the confined core capable of supporting the concrete compressive force.

The increase in concrete strength, due to confinement is reflected in the f'_c / f'_{cc} term, the more confinement the greater the strength enhancement and the smaller the

compressed area required. The confined concrete compressive strength, f'_{cc}, can be determined from Equation 8.18 taking the maximum lateral confining pressure, f_{l2}, as provided from the transverse reinforcement in the column.

The overstrength factors, λ_C and λ_T, are to reflect the increase in longitudinal stress with strain hardening of the steel. For cyclic loading of typical New Zealand reinforcing steels overstrength factors are taken as 1.25 which reflect the increase in the mean yield strength over the 5th percentile strength and the further increase in steel stress due to strain hardening. The overstrength factors, λ_C and λ_T, used in this study are applied to the measured steel yield strengths. The value of 1.25 reflects the increase in steel stress due to strain hardening only. For columns with high axial load the steel is subjected to high compressive strains during cyclic loading which lead to higher stresses being developed in the steel [P2]. Columns with low axial load are subjected to high curvatures during the cyclic load response which generate high tensile strains in the longitudinal reinforcement leading to higher steel stresses.

For columns with inefficient layout of transverse reinforcement, low λ_e values, and/or small levels of concrete compressive strength enhancement the maximum moment of resistance may be that given by Equation 8.29 rather than the flexural strength predicted by Equation 8.31.

At higher axial loads the contribution to the flexural strength of the column from the concrete compressive force decreases as the large neutral axis depth moves the position of the concrete force closer to the centreline of the column. The steel couple contribution will remain the same or increase due to the steel entering the strain hardening region. Columns with larger areas of the core affected by arching will have a reduced contribution to the flexural strength from the moment, due to the concrete compressive force, as the position of the centroid of this force will be restricted to the region between the neutral axis and the extent of the arching within the core. Low levels of confinement will give lower confined concrete compressive strengths, requiring a larger depth of compressed concrete to support the concrete compressive force, reducing the lever arm for the contribution of this force to the flexural strength.

The reduction in the contribution to the flexural strength from the concrete component, due to large arching or low levels of confinement provided in the column, despite any increase in the longitudinal steel couple contribution, in columns with high axial loads may give flexural strengths from Equation 8.31 which are less than that predicted by Equation 8.29. This indicates that the column will achieve the ACI ideal moment capacity with little or no increase in flexural strength due to the effects of confinement or strain hardening of the longitudinal reinforcement.

The ratio of the predicted flexural strength of the column, M_o, to the predicted ACI moment, M_n, may give a qualitative indication of the available curvature ductility of a particular column. Columns which possess predicted flexural strengths in excess of the predicted ACI moment or maintain this moment will have larger available curvature ductilities than columns which have predicted flexural strengths below the predicted ACI moment. No attempt has been made in this study to correlate the M_o / M_n ratio to the available curvature ductility of the section.

8.8.2.1 Confined Concrete Efficiency Factor

Mander et al. [M3] proposed a confinement efficiency factor, k_e, to reduce the lateral confining pressure from the transverse reinforcement to reflect the effects of arching occurring in the column core. Zahn et al. [Z1] modified the efficiency factor, k^*_e, for sections subjected to axial load and flexure as the ratio of the first moments of area of the effectively confined core to the concrete in the core. This reflected the increased contribution to flexure of fibres further from the neutral axis when a section is subjected to flexure.

These efficiency factors are both incorporated into the concrete stress-strain model when determining the confined concrete compressive strength due to the transverse reinforcement provided in the column. If the core of the column is modelled as two regions, ineffectively confined and effectively confined, the amount and effect of arching in the column are directly accounted for during the moment-curvature analysis.

A moment-curvature analysis will give a better estimation of the flexural strength of a column rather than the conservative estimate given by the ACI method [X3]. Using Equation 8.31 the flexural strength of a rectangular column can be better estimated by incorporating terms to account for strain hardening of the longitudinal steel and the increase in concrete compressive strength due to confinement from the transverse reinforcement. The influence of confinement is dependent on both the amount and arrangement of transverse reinforcement provided in a column.

When determining the flexural strength of a column after the cover concrete has spalled requires the compressed region of concrete be known, which is reduced by arching of the concrete within the core. The confined concrete efficiency factor, λ_e, reflects the efficiency of the transverse reinforcement arrangement, namely the influence of the arrangement on the amount of arching in the core.

Another section efficiency term, A_g / A_c, is often employed for columns as it is simple to determine and use and it reflects the efficiency of a section under concentric axial load. However this term does not reflect the influence of the transverse reinforcement arrangement and can be misleading for older columns not designed in accordance with NZS 3101 [X2].

The arching within the core is assumed to occur over the compressed region only as shown in Figure 8.33. The confined concrete efficiency factor is taken as the ratio of the first moments of area of the effectively confined core to the core area.

The dimensions of the core area in the column are taken to the centreline of the peripheral hoop. Vertical and horizontal arching is assumed to be parabolic in shape, similar to the arching profile proposed by Mander et al., starting at the centreline of the peripheral hoop over the clear distance between transverse hoop sets and the clear distance between restrained longitudinal bars.

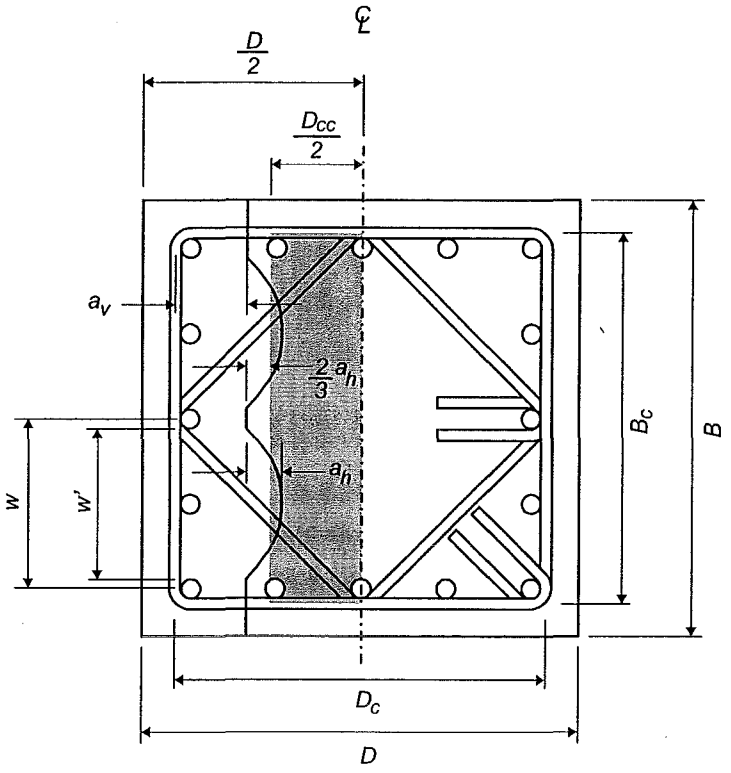

Figure 8.33 *Section Dimensions Used to Determine Confined Concrete Efficiency Factor, λ_e, for Rectangular Sections*

The extent of horizontal and vertical arching depends on the chosen arch profile, spacings between transverse hoop sets, distance between restrained longitudinal bars and the initial tangent angle of the parabolic arches.

The extent of vertical arching between transverse hoop sets is given by:

$$a_v = \frac{s'}{4\tan\theta} \tag{8.32}$$

where s' = clear distance between transverse hoop sets

θ = initial tangent angle of parabolic arches

The extent of horizontal arching is given by:

$$a_h = \frac{w'}{4\tan\theta} \tag{8.33}$$

where w' = average clear distance between restrained longitudinal bars

θ = initial tangent angle of parabolic arches

The horizontal and vertical arching form a hyperbolic paraboloid truncated surface. The projection of this surface, midway between the transverse hoop sets, determines the depth of the effectively confined core which can be expressed by a simple rectangle with a depth D_{cc} given by:

$$D_{cc} = D_c - 2\left(a_v + \frac{2}{3}a_h\right) \tag{8.34}$$

Converting the horizontal arching into an equivalent rectangular area maintains the position of the centroid of the area. This should have little influence on the result and with the simplification of the shape of the region allows a simpler evaluation of the confined concrete efficiency factor.

The confined concrete efficiency factor, λ_e, proposed in this study is given by the ratio of the first moments of area of the effectively confined area to the area of the column, taken about the centreline of the section. This definition is similar to that proposed by Zahn et al. for the modified efficiency factor, k^*_e, to reflect the increased contribution to flexure of fibres further from the neutral axis.

For a rectangular section the confined concrete efficiency factor is then given by:

$$\lambda_e = \frac{B_c D_{cc}^2}{B D^2} \tag{8.35}$$

The confined concrete efficiency factor, λ_e, provides a simple and easy to use method to compare the efficiency of a column's transverse reinforcement layout and incorporate its influence on the flexural strength of a column. Derivation of λ_e factors

for other section shapes can be done in a similar manner. Confined concrete efficiency factors for circular columns, square columns loaded across the diagonal and rectangular columns with rounded ends can be found in Appendix D.

8.8.2.2 Predicted Flexural Strength Example

Application of Equations 8.29 and 8.31 to predict the ACI moment capacity and the flexural strength of a column are illustrated with an example column shown in Figure 8.34. The column is 400 mm square with 12-D16 longitudinal bars and R10 transverse reinforcement at 75 mm centres between hoop sets.

The mechanical reinforcement ratio, m, for this column is:

$$\begin{aligned} m &= \frac{f_y}{0.85 f_c'} \\ &= \frac{300}{(0.85)(30)} \\ &= 11.76 \end{aligned} \tag{8.36}$$

The neutral axis depth of the column can be found from Equation 8.30 where $\gamma = (0.11\text{m} + 2.1)p_t + 0.03 = 0.081$:

$$\begin{aligned} \frac{c}{D} &= -0.5\left[(6.9)(0.0151) + (0.015)(11.76) + (0.24)(0.0151)(11.76) - 1.4\right] \\ &\quad + (0.0025)(11.76) + 0.081 \\ &= 0.649 \end{aligned} \tag{8.37}$$

Using this neutral axis depth, the strain profile for the column can be found using an extreme compressive fibre strain of -0.003 corresponding to the development of the ACI moment capacity. From this strain profile the compressive and tensile steel stresses can be determined:

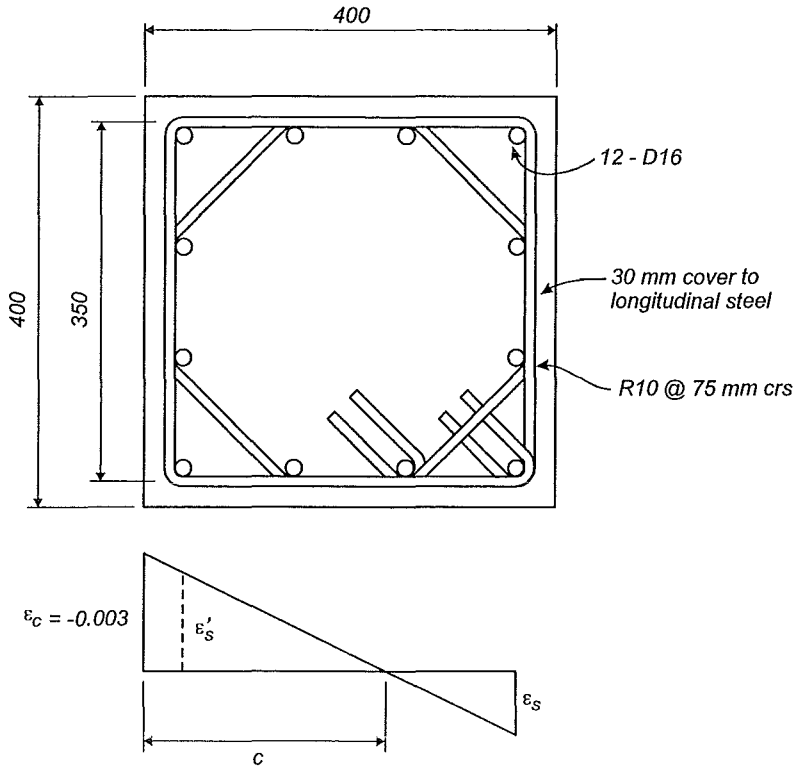

Figure 8.34 *Example Column Section*

$$\begin{aligned} f_s^{'} &= f_y = 300\,MPa \\ f_s &= 235\,MPa \end{aligned} \tag{8.38}$$

The arrangement of longitudinal steel in the column has four bars placed on each of the end faces of the column. Therefore the value of ψ is taken as:-

$$\begin{aligned} \psi &= \frac{4}{12} \\ &= 0.333 \end{aligned} \tag{8.39}$$

and:-

$$\begin{aligned} \xi &= (0.46)(0.333) + 0.20 \\ &= 0.353 \end{aligned} \tag{8.40}$$

Equation 8.29 predicts the ACI ideal moment capacity:

$$M_n = \frac{1}{2}\left[\begin{array}{l}(0.85)(0.85)(0.649)\left(1-(0.85)(0.649)\right)\\+(0.810)(0.353)(0.0151)\left(\frac{300+235}{30}-0.85\right)\end{array}\right](400)(400)^2(30)$$
$$= 272.2\,kNm \tag{8.41}$$

For predicting the ACI moment capacity where this column is subjected to cyclic loading, f'_s and f_s should be taken as equal to the yield stress of the steel, f_y. The predicted ACI moment from Equation 8.29 then becomes:

$$M_n = 281.2\,kNm \tag{8.42}$$

The clear spacing between transverse hoop sets, s′, is 65 mm. The average clear distance between restrained longitudinal bars, w′, is 92 mm. Assuming 45° parabolic arches the amount of vertical and horizontal arching can be found from Equations 8.32 and 8.33.

$$a_v = \frac{65}{4\tan 45°} = 16.25\,mm \tag{8.43}$$

$$a_h = \frac{92}{4\tan 45°} = 23.0\,mm \tag{8.44}$$

The confined concrete efficiency coefficient, λ_e, is given by Equation 8.35 where D_{cc} is given by Equation 8.34:

$$\lambda_e = \frac{(350)(336.8)}{(400)(400)} = 0.737 \tag{8.45}$$

The confined concrete strength can be taken as:

$$f'_{cc} = f'_c\left[1+4.1\frac{p_s f_{yh}}{2f'_c}\right]$$
$$= 30\left[1+4.1\frac{(0.0204)(300)}{2(30)}\right] \qquad (8.46)$$
$$= 42.5\ MPa$$

The steel overstrength factors, λ_C and λ_T, can be taken as 1.25 and the predicted flexural strength is given by Equation 8.31:

$$M_o = \left[\frac{0.85}{2}(0.649)\left(\sqrt{\frac{(0.737)(400)}{350}}-\frac{30}{42.5}(0.649)\right)+\frac{(1.25+1.25)(0.810)(0.363)(0.0151)(300)}{2(30)}\right](400)(400)^2(30) \qquad (8.47)$$
$$= 350.0\ kNm$$

8.8.3 Confinement From Adjacent Members

From Equations 8.29 and 8.31 the predicted flexural strength of a rectangular column can be determined as the larger of the flexural strengths predicted from the two equations. These equations take into account the contribution of the concrete and the longitudinal steel to the flexural strength, including the effect of confinement of the concrete and strain hardening of the longitudinal steel.

The predicted flexural strength of rectangular columns can be increased to account for the shift in the critical section, as noted by Gill et al. [G1, P6] and then compared to the flexural strength attained during the experimental testing of columns.

The flexural strength of a number of rectangular columns tested at the University of Canterbury, under cyclic reversed lateral loading and constant axial load, and monotonic lateral load column tests from the University of Houston [S6] were evaluated using Equations 8.29 and 8.31 and compared to the flexural strength attained during experimental testing of the columns. Overstrength factors, λ_C and λ_T,

of 1.25 were taken for both compression and tension for the cyclic tests conducted at the University of Canterbury. Overstrength factors of 1.25 for compression and 1.0 for tension were assumed for the monotonic column tests conducted at the University of Houston. The shift of the critical section was varied from zero to one times neutral axis depth as calculated from Equation 8.30.

The increase in flexural strength resulting from the shift in the critical section, α_{shift}, was determined from Equation 8.28. The shift of the critical section was varied from zero to one times neutral axis depth where the neutral axis depth at spalling of the cover concrete was determined from Equation 8.30. A plot of $M^* / \alpha_{shift}M_o$ against the shift in the critical section is shown in Figure 8.35 where M^* = maximum moment attained during testing and M_o = is the maximum flexural strength predicted from the maximum of Equations 8.29 and 8.31. Also shown in the same figure is the coefficient of variation of the data set. The graph shows that a minimum coefficient of variation of 9.8 % is reached with a shift in the critical section of approximately 0.75 times the neutral axis depth when the University of Houston tests are included. The coefficient of variation drops to 6.9 % with a shift in the critical section of 0.75 times the neutral axis depth if the University of Houston tests are excluded from the data set. This is due to the flexural strength of columns with high mechanical reinforcement ratios, m, not being predicted well by the proposed Equations 8.29 and 8.31.

The University of Houston tests all had mechanical reinforcement ratios, m, above 25 due to relatively high strength longitudinal reinforcement and low concrete compressive strengths. Typical values of m for design would be from 12 to 18 which will decrease as the concrete compressive strength increases over time.

The mean value of $M^* / \alpha_{shift}M_o$ decreases toward 1.0 with increasing shift in the critical section with a mean value of approximately 1.08 with a shift of 0.75 times the neutral axis depth.

Using a shift in the critical section of 0.75 times the neutral axis depth, the initial angle of the parabolic arches was varied to determine whether a better agreement

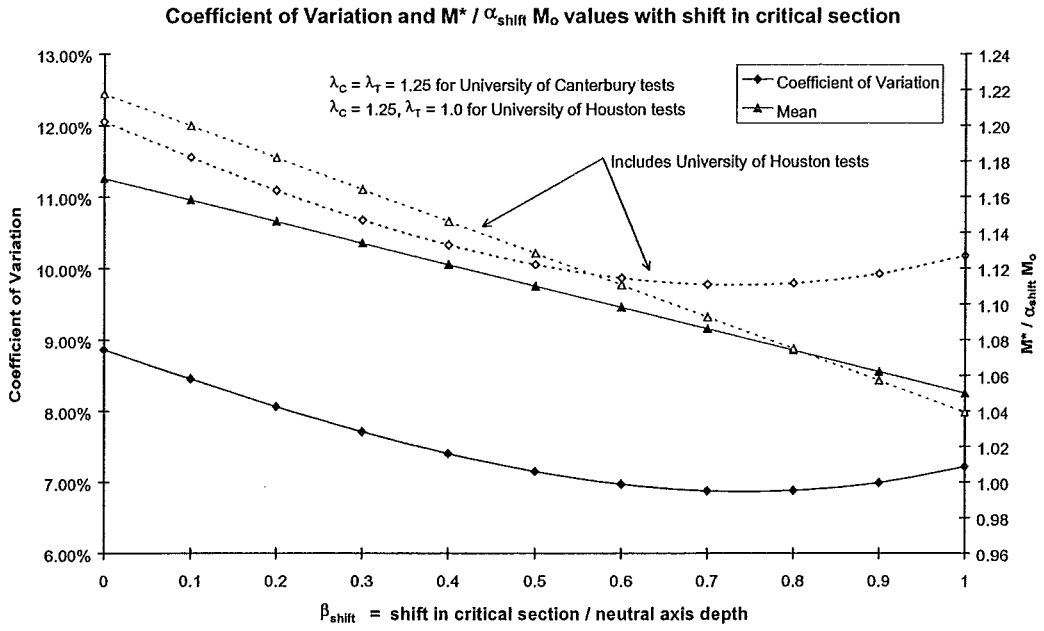

Figure 8.35 *Coefficient of Variation and $M^* / \alpha_{shift} M_o$ values for Rectangular Columns with Shift in Critical Section*

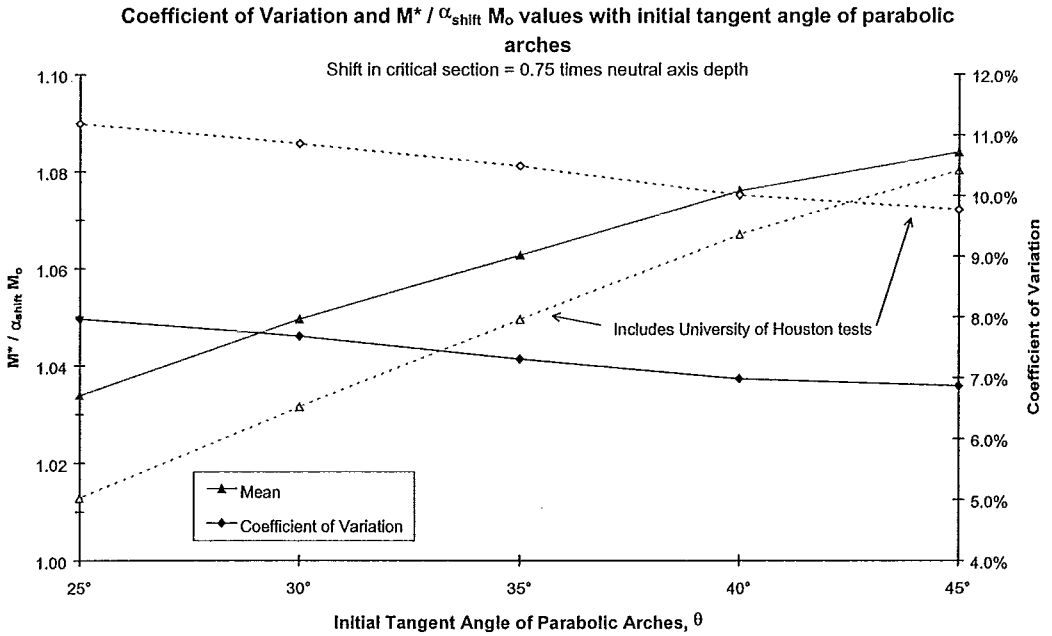

Figure 8.36 *Coefficient of Variation and $M^* / \alpha_{shift} M_o$ values for Rectangular Columns with Initial Angle of Parabolic Arches*

between the experimental and predicted flexural strengths for rectangular columns could be obtained. Decreasing the initial angle of the parabolic arches from 45° showed a decrease in the $M^* / \alpha_{shift} M_o$ values but with an increase in the coefficient of variation as shown in Figure 8.36. The initial angle of arching can be reduced from 45° to 40° to reflect a possible reduction in the angle of arching for columns subjected to flexure without affecting the prediction of the flexural strength of a rectangular column. Further experimental work could investigate the arching of columns subjected to axial load and flexure combined.

Figure 8.37 shows the experimental to the predicted ACI ideal moments for rectangular columns tested at the University of Canterbury and at the University of Houston. Also shown is the relationship proposed by Ang et al. [A1] which suggests moment enhancement with increased axial load. Square column units tested by Xinrong et al. [X4] with variable axial load have been omitted as the variable axial load will have reduced the strength of the columns preventing proper comparison of the results which assume constant axial load acting on the column. Columns tested by Sato et al. [S4] and Satyarno et al. [S3] which contained a mixture of ultra-high strength and normal strength longitudinal steel have also been omitted.

The same data points are shown in Figure 8.38 where the experimental moments, M^*, are compared to the predicted moments, M_o, which include the influence of confinement and strain hardening, from Equations 8.29 and 8.31. Predicted moments are evaluated assuming 40° parabolic arching in the columns.

University of Canterbury results shown in Figure 8.38 still show an increase in flexural strength over the predicted flexural strength with increasing axial load. Some of the scatter in these data points can be attributed to the prediction of the flexural strength of the tests specimens from Equations 8.29 and 8.31.

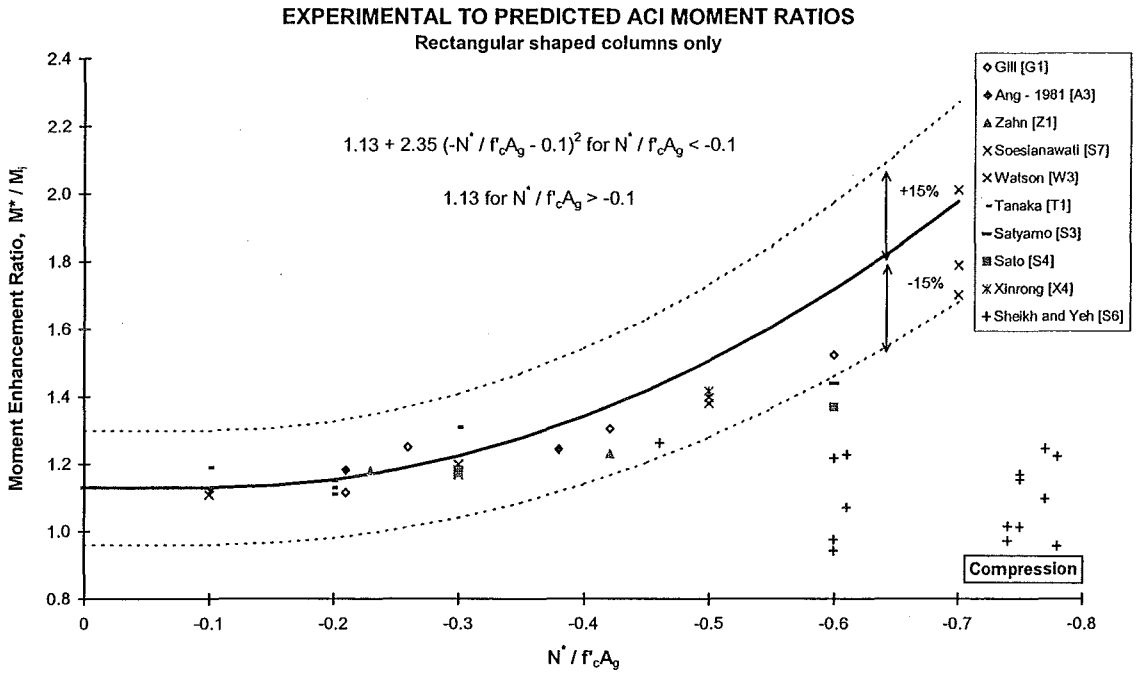

Figure 8.37 *M^* / M_i values for Rectangular Columns with Axial Load Ratio*

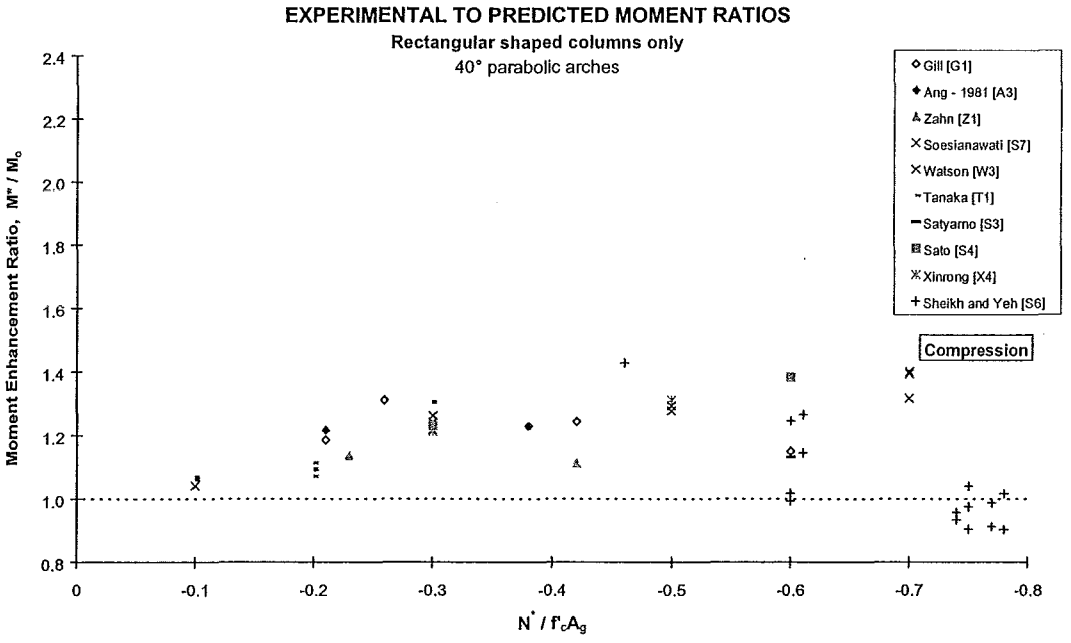

Figure 8.38 *M^* / M_o values for Rectangular Columns with Axial Load Ratio*

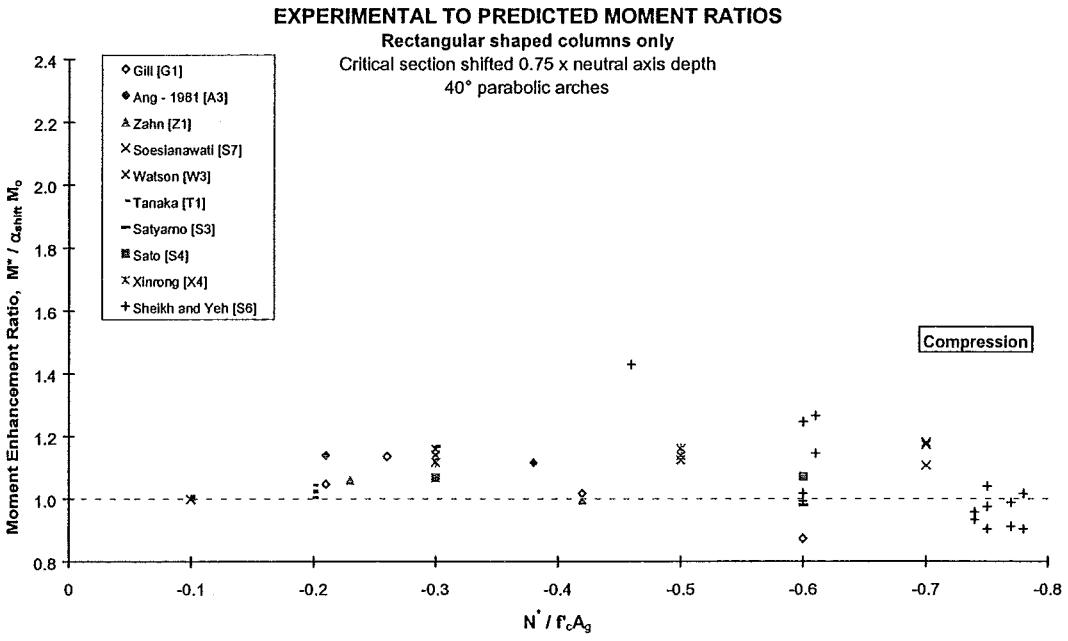

Figure 8.39 *$M^* / \alpha_{shift} M_o$ values for Rectangular Columns with Axial Load Ratio*

By accounting for the shift in the critical section, as noted by Gill et al., a better estimation of the flexural strength of a column can be obtained for the data points shown in Figure 8.38. These results are shown in Figure 8.39 where a shift in the critical section of 0.75 times the neutral axis depth has been taken.

Equation 8.31 has been proposed to evaluate the neutral axis depth for estimating the flexural strength of a rectangular concrete section. For calculating the neutral axis depth of a column, to determine the amount of flexural strength enhancement due to the shift in the critical section, α_{shift}, a simplified expression may be applied for use in practice:

$$\frac{c}{D} = 0.18 - 0.95\frac{N^*}{f_c' A_g} \qquad (8.48)$$

where $N^* / f'_c A_g$ is taken as negative for compressive axial loads.

The difference in neutral axis depth between Equation 8.31 and Equation 8.48 will not be significant when estimating the flexural strength of a column due to the shifted critical section.

8.9 QUANTIFYING COMPONENTS OF FLEXURAL ENHANCEMENT

The increase in the flexural strength over the ACI ideal moment can be determined by accounting for the various components which contribute to the observed flexural enhancement. The influence of confinement increasing the concrete strength and strain hardening of the longitudinal reinforcement have been estimated through Equation 8.31. A more refined means of accounting for these effects is to conduct moment-curvature analyses by incorporating appropriate stress-strain relations for each material. The influence of cyclic loading and dynamic strain rates can also be accounted for in a moment-curvature analysis if required by including the necessary relations to modify the monotonic or quasi-static stress-strain relations.

From the experimental results for rectangular columns shown in Figure 8.39 it can be seen that the additional confinement from an adjacent member, causing a shift in the critical section, can account for a considerable portion of the observed moment enhancement, especially for columns with high axial loads.

Example columns and actual case studies of columns tested at the University of Canterbury were taken to attain an estimate of the likely values for enhancement from cyclic loading and accounting for the shift in the critical section due to the confining effects of adjacent members.

8.9.1 Enhancement from Confinement and Strain Hardening

In order to evaluate to effects of confinement and strain hardening on the flexural strength of a column monotonic moment-curvature analyses were conducted for the selected columns modelling the concrete stress-strain behaviour in the column core using the method outlined in Section 8.6. The angle of arching between transverse

hoop sets and between restrained longitudinal bars was taken as 40° to reflect some possible reduction in the angle of arching which may occur for columns subjected to axial load and flexure.

8.9.2 Enhancement From Cyclic Loading

The monotonic moment-curvature analysis provides a lower bound solution to the flexural strength of a column but is unable to provide the maximum probable flexural strength for the critical section. A cyclic moment-curvature should be used to determine the maximum probable flexural strength of a section to be used in capacity design checks. Cyclic moment-curvature analysis routines have been developed and mainly used for research purposes [D1, M4] but the complexity of models to describe the cyclic stress-strain behaviour of steel and concrete often make the development of simple cyclic moment-curvature routines difficult for use and application in everyday practice. The pseudo-cyclic moment-curvature routine described in Section 8.6.3 is simple enough to understand and incorporate into moment-curvature routines to account for some of the influences of cyclic loading on the flexural strength of a section.

8.9.3 Enhancement From Dynamic Strain Rates

Structures are required to respond to the dynamic loadings imposed during an earthquake and the effects of these fast strain rates are known to alter the stress-strain response of both concrete and steel. Dynamic strain rates lead to a significant increase in the both the strength and stiffness of concrete over the values from loading at low strain rates. Increases in yield stress, ultimate stress and strain at the onset of strain hardening occur when steel is subjected to loading at increased strain rates [D1, P1, R3, R4].

A majority of columns tested at the University of Canterbury have been tested at quasi-static loading rates apart from a series of model columns which were tested by Dodd and Cooke [D1] to destruction on a shake table. The increase in strength of

dynamically loaded columns was found to be 10% - 20% over the flexural strength given by methods developed from quasi-static test methods.

8.9.4 Case Studies

Columns tested by Watson and Park [W3], Tanaka and Park [T1], Sato et al. [S4] and Sheikh and Yeh [S6] were used as case studies to conduct monotonic and pseudo-cyclic moment-curvature analyses and adjusting these results to account for the shift of the critical section to compare with measured experimental results. Actual measured material properties were used for the columns in each case study.

Table 8.1 shows the section properties of the columns tested by each researcher with the steel stress-strain properties for each column shown in Table 8.2.

The power term, P, in Equation 8.24 has been determined to match the measured stress-strain relations for the longitudinal steel reported by each researcher. Note that all the columns tested at the University of Canterbury used New Zealand manufactured reinforcing steel, Grade 275 or Grade 380, or the grades which subsequently replaced these two steels, Grade 300 and Grade 430 respectively. The columns tested by Sheikh and Yeh were conducted at the University of Houston using Grade 60 (414 MPa) longitudinal steel.

8.9.4.1 Columns Tested by Watson and Park [W3]

Two square column units, Units 8 and 9, tested by Watson and Park [W3], were selected for further study. These columns were subjected to reversed cyclic lateral loading and constant axial compressive load of $0.7\, f'_c A_g$. Moment-curvature analyses were conducted for each column using the Mander et al. [M3] monotonic model, monotonic and pseudo-cyclic analyses from the present study and accounting for the shift in the critical section. The critical section shift was taken as 0.75 times the neutral axis depth at spalling of the cover concrete as determined by Equation 8.48. Moments and curvatures were shifted to present the moment-curvature relationship

Table 8.1 *Column Section Properties*

Researcher	Unit	B mm	D mm	f'_c MPa	d_b mm	d_{bh} mm	s mm	p_t %	p_s %	N^*/f'_cA_g
Watson & Park [W3]	8	400	400	39.0	16	8	77	1.51	1.21	0.7
Watson & Park [W3]	9	400	400	40.0	16	12	52	1.51	4.10	0.7
Tanaka & Park [T1]	6	550	550	32.0	20	12	110	1.25	1.70	0.1
Sato et al. [S4]	4	400	400	71.6	20	9.2	80	3.14	1.56	0.6
Sheikh & Yeh [S6]	A3	305	305	31.8	19	9.5	110	2.44	1.68	0.61

Table 8.2 *Column Steel Stress-Strain Properties*

Researcher	Unit	f_y MPa	f_{su} MPa	f_{yh} MPa	E_s GPa	ε_{sy} %	ε_{sh} %	ε_{su} %	P
Watson & Park [W3]	8	474	633	372	226	0.225	1.75	14.8	3.83
Watson & Park [W3]	9	474	633	308	226	0.225	1.75	14.8	3.83
Tanaka & Park [T1]	6	511	675	325	200	0.256	1.70	13.1	4.79
Sato et al. [S4]	4	442	590	1368	200	0.221	1.83	15.9	3.80
Sheikh & Yeh [S6]	A3	516	823	490	207	0.249	0.85	10.7	3.85

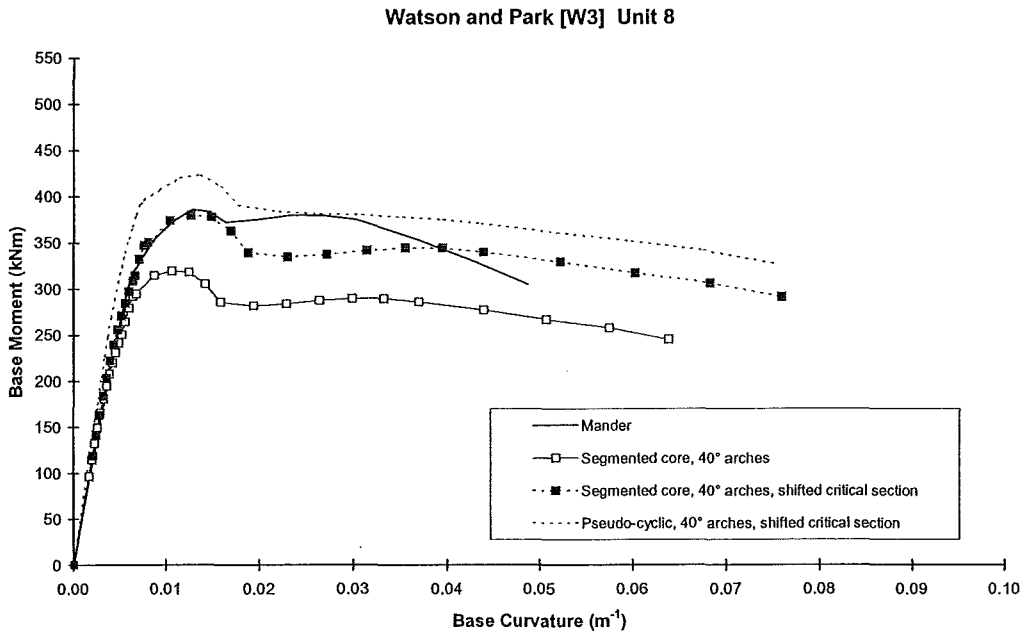

Figure 8.40 *Moment-Curvature Comparison for Watson and Park [W3] Unit 8*

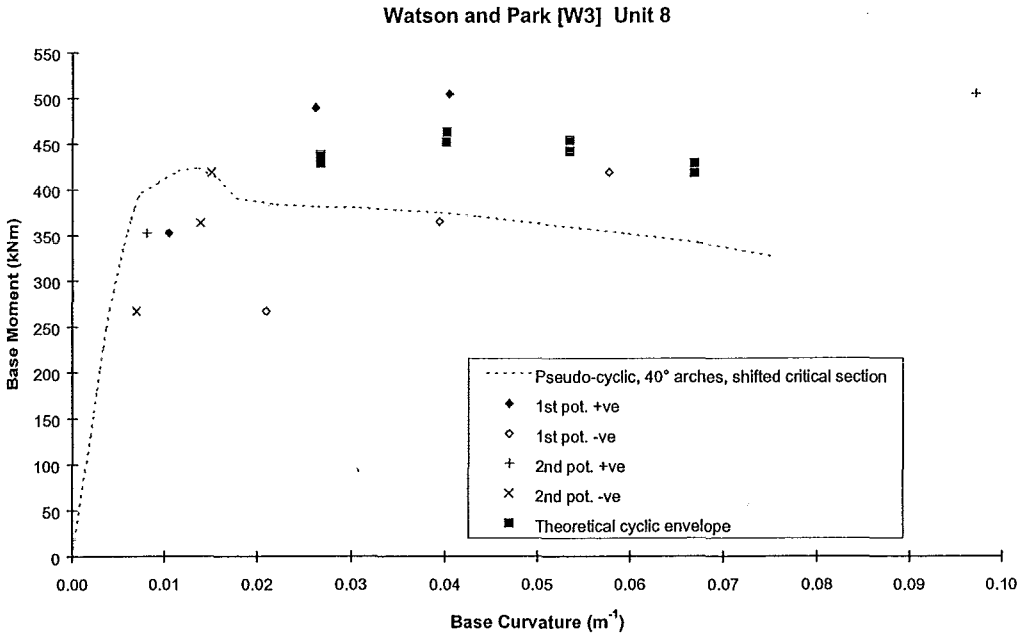

Figure 8.41 *Shifted Pseudo-Cyclic and Experimental Moment-Curvature Comparison for Unit 8*

at the base of the column, adjacent to the stub present in the tests, rather than the moment-curvature relation for the critical section.

Figure 8.40 shows the Mander et al. model monotonic response, the monotonic, pseudo-cyclic and shifted pseudo-cyclic moment-curvature response for Unit 8. The shifted pseudo-cyclic moment-curvature response has been compared to experimental moment-curvature results measured during the test in Figure 8.41. Curvatures were measured at several positions, in the original tests, over each plastic hinge location, above and below the central stub, for both the positive and negative loading directions. The first level of potentiometers were located 80 mm from the face of the central stub and the second level of potentiometers were located 160 mm from the face of the central stub.

From Figure 8.41 it can be seen that the predicted theoretical moment-curvature response, accounting for the shift in the critical section does not closely match the experimental data points. This is due to the unit showing some unsymmetrical rotations concentrating at one of the plastic hinges as can be seen by the larger curvatures recorded for the positive loading direction. A theoretical cyclic moment-curvature analysis was conducted by Watson and Park for this unit and the envelope points are shown in Figure 8.41. These points seem to approximate the experimental moment-curvature data points but are not matched by the shifted pseudo-cyclic moment-curvature response.

Figure 8.42 shows the Mander et al. model monotonic response, the monotonic, shifted monotonic and shifted pseudo-cyclic moment-curvature response for Unit 9. Experimental results are compared to the shifted pseudo-cyclic moment-curvature response in Figure 8.43. Experimental curvatures plotted were measured at the first level of potentiometers, located 100 mm from the face of the central stub and from the second level of potentiometers located 200 mm from the face of the central stub.

Figure 8.43 shows good agreement with the experimental moment-curvature results, the shifted pseudo-cyclic moment-curvature response and theoretical cyclic moment-curvature envelope points. The theoretical moment-curvature response has been terminated due to the extreme concrete compressive fibre strain being

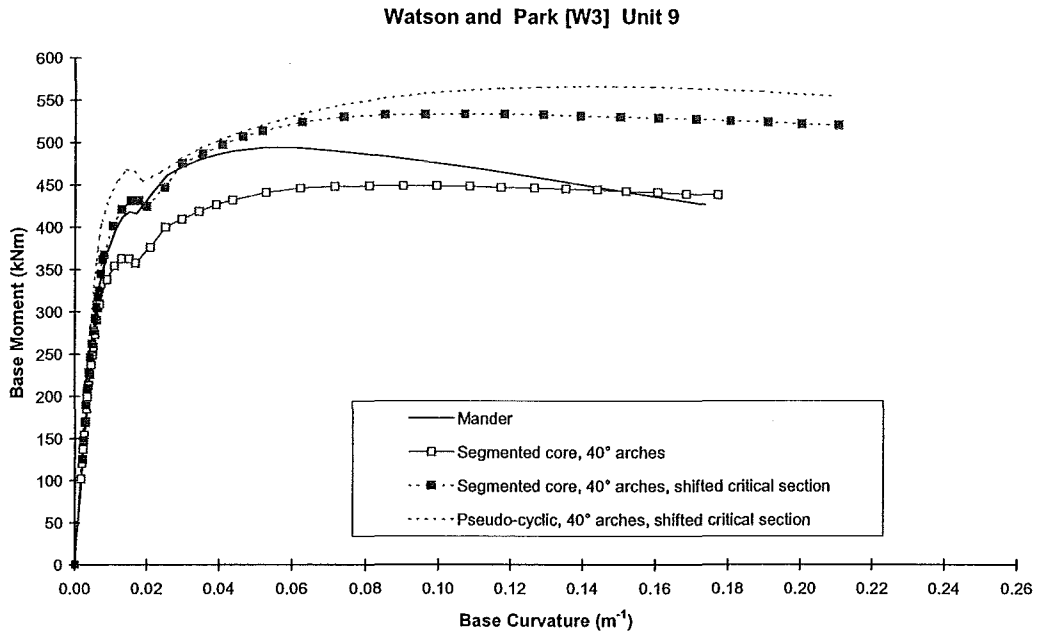

Figure 8.42 *Moment-Curvature Comparison for Watson and Park [W3] Unit 9*

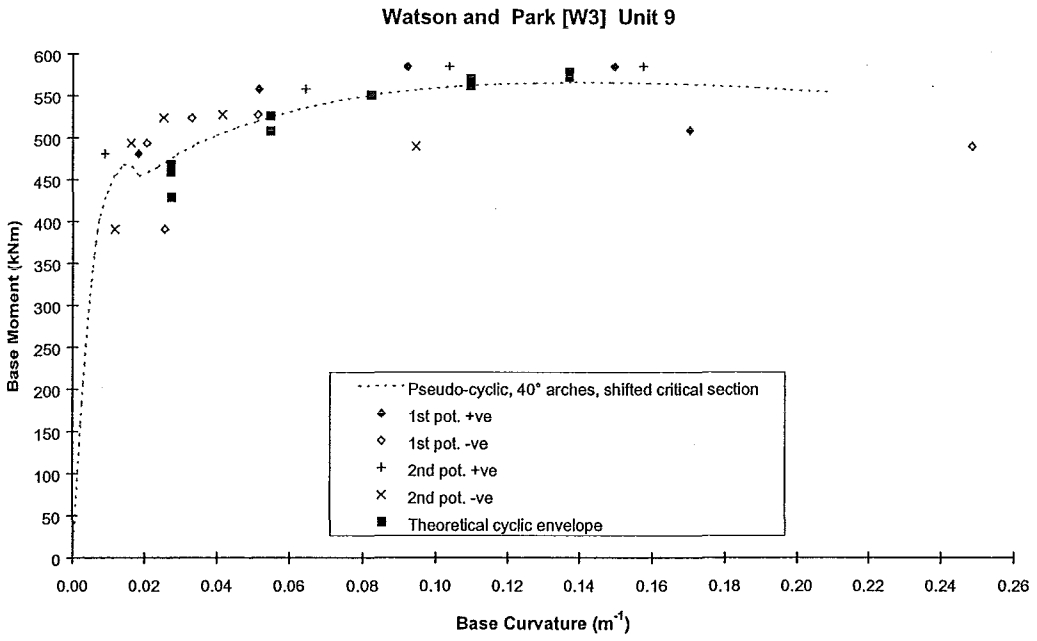

Figure 8.43 *Shifted Pseudo-Cyclic and Experimental Moment-Curvature Comparison for Unit 9*

exceeded. This stopping criteria is known to be conservative for sections subjected to axial load and flexure [P3] and a continued response should match the experimental moment-curvature data closely.

From Figures 8.40 and 8.42 the large increase in strength due to the shift in the critical section is apparent. The monotonic moment-curvature response, with 40° arches, for both units fall well below the moment-curvature response predicted by the Mander et al. model. By accounting for the shift in the critical section the two moment-curvature responses show better agreement between the nominal moments. The effect of the cyclic loading on the moment-curvature response can be seen between the shifted pseudo-cyclic and shifted monotonic moment-curvature curves, leading to a higher peak moment and increased response over the monotonic response at higher curvatures.

Unit 8 contains approximately 25 % of the amount of transverse reinforcement required by the current New Zealand Concrete Structures standard [X2] for a column to achieve full ductility. This low amount of confinement suggests the column would be unable to achieve any significant strength enhancement at large curvatures, as shown in the moment-curvature responses. Unit 9 contains approximately 85% of the amount of transverse reinforcement required for full ductility and maintains its strength at larger curvatures. Under cyclic loading, as modelled by the pseudo-cyclic moment-curvature analysis, this column is capable of achieving a degree of flexural strength enhancement over the monotonic response.

8.9.4.2 Column Tested by Tanaka and Park [T1]

Similar moment-curvature analyses were conducted for Unit 6 as tested by Tanaka and Park [T1]. The 550 mm square column was subjected to an axial load of $0.1\, f'_c A_g$.

Figure 8.44 shows the comparison for the Mander et al. monotonic moment-curvature response, the monotonic, shifted monotonic and shifted pseudo-cyclic responses. Due to the low axial load on the column the Mander et al. response and

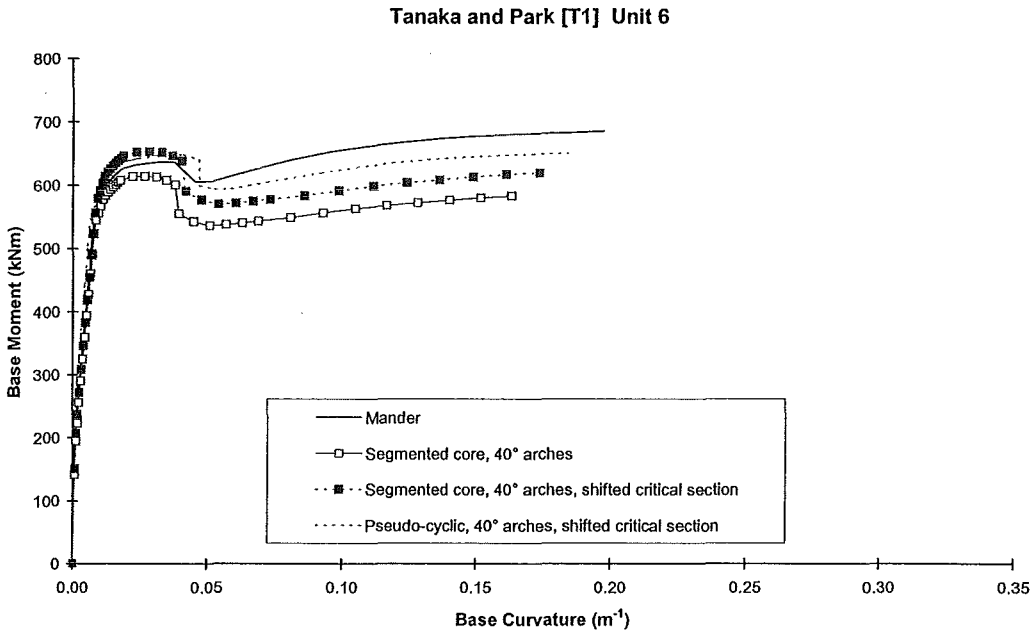

Figure 8.44 *Moment-Curvature Comparison for Tanaka and Park [T1] Unit 6*

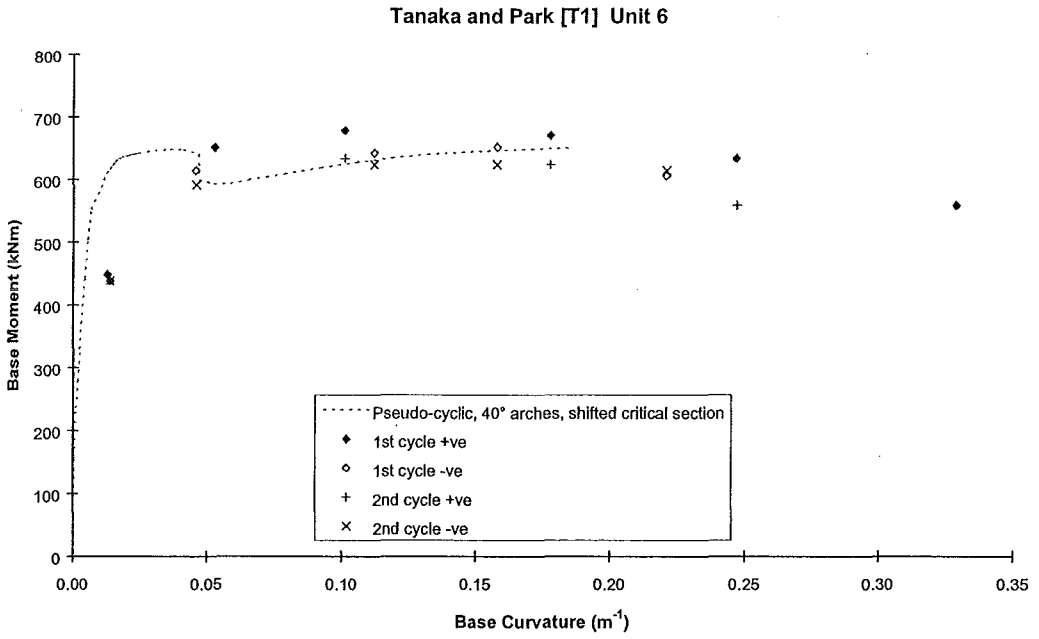

Figure 8.45 *Shifted Pseudo-Cyclic and Experimental Moment-Curvature Comparison for Unit 6*

the monotonic response are quite similar up to the ideal flexural strength of the column. Spalling of the cover concrete leads to the drop in the moment-curvature response in the Mander et al. model and the sharper drop in the 40° arch model due to the influence of the concrete stress-strain relationship assumed for the areas of the core influenced by arching.

The initial monotonic and pseudo-cyclic responses are very similar due to the low axial load and small neutral axis depth meaning larger tensile strains are developed in the longitudinal reinforcement with comparatively lower compressive strains.

Increased pseudo-cyclic moment-curvature response over the monotonic response is only seen after the tensile steel strains have reached strain hardening.

Figure 8.45 shows the comparison of the shifted pseudo-cyclic moment-curvature response and experimental moment-curvature results at the peaks of the first and second cycles to each level of ductility conducted during the test. Curvature measurements were taken from a set of linear potentiometers 90 mm above the face of the block at the base of the column unit. Again the shifted pseudo-cyclic moment-curvature response provides a good match to the experimental data points up to the point where the moment-curvature response is terminated upon reaching the ultimate concrete strain. The theoretical moment-curvature response can be extended to match the experimental moment-curvature points by taking a less conservative value for the available ultimate concrete compressive strain which is responsible for the termination of this analysis.

8.9.4.3 Column Tested by Sato et al. [S4]

Sato et al. [S4] tested a series of columns under varying axial loads containing a mixture of normal and ultra-high strength longitudinal reinforcement. Unit 4 was tested at an axial load of $0.6\, f'_c A_g$ and contained only normal strength longitudinal reinforcement. Ultra-high strength steel was also used for the rectangular transverse spiral reinforcement with a yield stress of 1368 MPa. The stresses developed in the transverse reinforcement remained low in all of the test units throughout the tests.

Yielding of the diagonal transverse spirals were recorded in the test units toward the end of the tests but an upper limit of approximately 800 MPa was reached in the perimeter spiral sets of some of the units before the end of the tests. The New Zealand Concrete Structures Standard [X2] allows the use of ultra-high strength steel as transverse reinforcement but limits the value of f_{yh} to be used in calculations to 800 MPa.

Attempts to generate monotonic moment-curvature results using an initial angle for the parabolic arches of 40° led to the moment-curvature routine terminating early due the moment dropping below 80% of the maximum. The Mander et al. monotonic moment-curvature response continues until termination upon reaching the ultimate concrete strain. In Figure 8.46 the Mander et al. moment-curvature and 40° monotonic moment-curvature response are shown using 800 MPa, the prescribed design standard limit for f_{yh}, for the yield stress of the transverse steel. The 40° monotonic moment-curvature response terminates early due to the decrease in moment caused by the influence of the ineffectively confined concrete in the core of the column. Unit 4 had a concrete strength of 71.6 MPa and the unconfined stress-strain behaviour of this concrete shows an almost immediate drop in strength after reaching the peak unconfined strength. In order to allow the monotonic moment-curvature response to be generated the arching was effectively removed by setting the initial tangent angle of the arches to 1° allowing the complete moment-curvature response to be generated for this column.

Early termination of the 40° moment-curvature response may indicate a limitation of the model used to generate these results or that the arching mechanism for high strength concrete is different to that assumed for normal strength concrete. It is recommended that the model used to generate these moment-curvature results be limited to concrete strengths below 55 MPa and further investigation is required into the arching mechanisms that form in columns with high strength concrete.

Due to the high concrete strength, large strains would have to be reached before sufficient micro-cracking of the concrete had occurred to lead to significant dilation of the concrete core to cause yield of the transverse reinforcement. Thus lower strains will have been developed in the transverse reinforcement. With the use of

ultra-high strength steel much lower stresses will have been developed in the transverse reinforcement giving much lower confining pressures being applied to the concrete core than would have occurred with normal strength transverse steel. As further dilation of the core occurred, with increasing compressive strains, the strains in the transverse reinforcement will have increased during the test, increasing the applied confining pressure to the column.

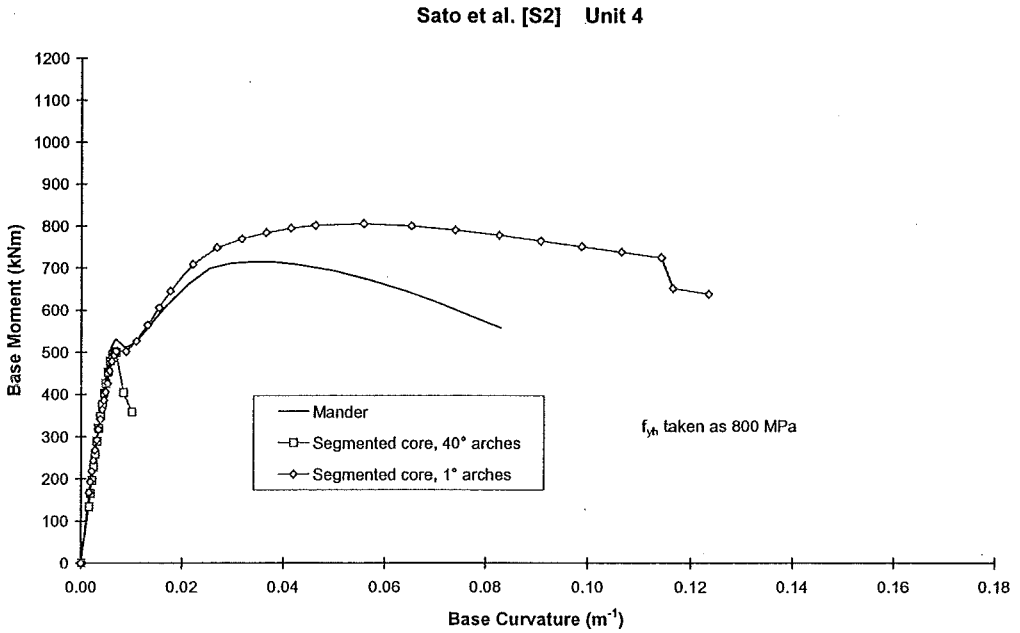

Figure 8.46 *Moment-Curvature Comparison for Sato et al. [S4] Unit 4 with 40° Arch and 1° Arch Monotonic Responses*

The brittle nature of high strength concrete will lead to a sudden loss of the cover and ineffectively confined concrete as the concrete spalls suddenly rather than crushing and spalling gradually. The plane of splitting between the cover and core concrete in columns with high strength concrete has been seen to be quite smooth [L2] indicating that there is little loss of concrete from within the core, between transverse hoop sets, due to arching. This lack of observed arching may indicate that the assumed arch mechanism, with parabolic arches, may not fully form in high strength concrete columns. By reducing the initial angle of the parabolic arches to 1° the influence of the ineffectively confined core can be removed. As there is little dilation of the

concrete core, due to its high strength, the arch mechanism may not fully form within the core, due to the low, passive, confining pressure being applied to the core, resulting in small areas of ineffectively confined concrete between the transverse hoop sets or restrained longitudinal bars. Figure 8.47 shows the comparison between the Mander et al. monotonic moment-curvature response and the moment-curvature response using 1° for the initial tangent angle for the parabolic arches and f_{yh} = 800 MPa.

Comparison of experimental moment-curvature results with the 1° shifted pseudo-cyclic moment-curvature response with f_{yh} = 800 MPa in Figure 8.48 shows the predicted moment-curvature response is higher than the experimental data points. As the test progresses dilation of the core continues resulting in increased strains induced in the transverse reinforcement, increasing the confining pressure being applied to the concrete core. Strains recorded in the transverse reinforcement in Unit 4 show stresses of 600 MPa were developed in the peripheral transverse spiral by the end of the test.

Figure 8.49 shows the comparison between shifted 1° pseudo-cyclic moment-curvature responses and the experimental data points for different values of f_{yh} up to 600 MPa. The experimental data points fall closer to the moment-curvature curves with higher values of f_{yh} as the column reaches higher curvatures and further dilation of the core increases the applied confining pressure. The moment-curvature response using f_{yh} = 600 MPa gives an envelope to all the experimental data points shown. As the test progressed to larger displacements, and hence larger curvatures, the moment-curvature response will shift from curve to curve as higher strains were developed in the transverse reinforcement.

Termination of this moment-curvature routine occurred with the moment dropping suddenly to below 80% of the maximum moment but there would be a close match between the trend of the theoretical moment-curvature results and the experimental moment-curvature points.

The poor agreement of the theoretical cyclic moment-curvature envelope points to the experimental and shifted pseudo-cyclic points may be due to the use of the

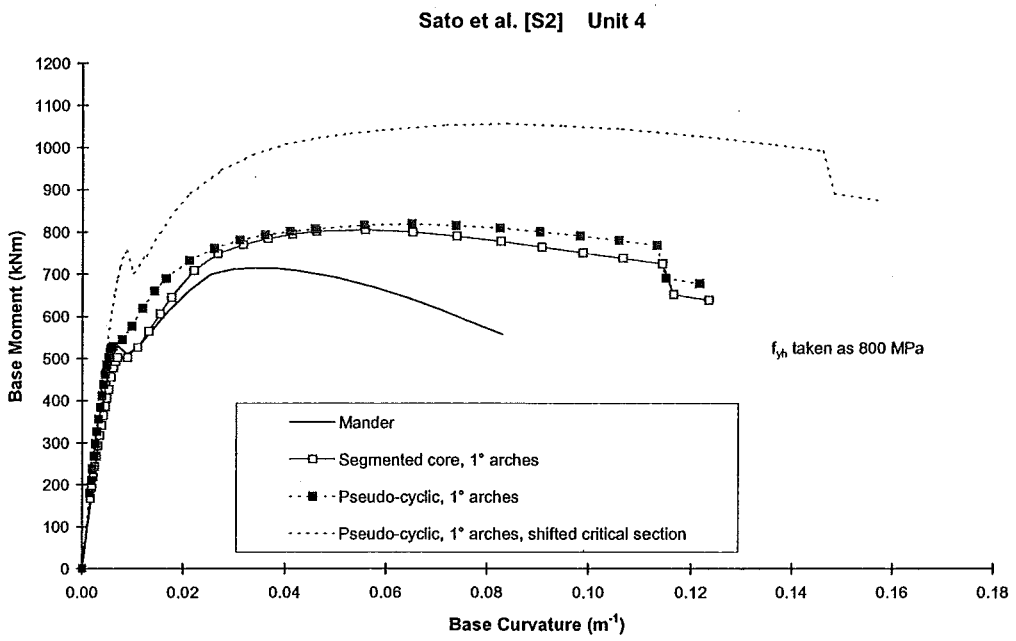

Figure 8.47 *Moment-Curvature Comparison for Sato et al. [S4] Unit 4 with 1° Parabolic Arches*

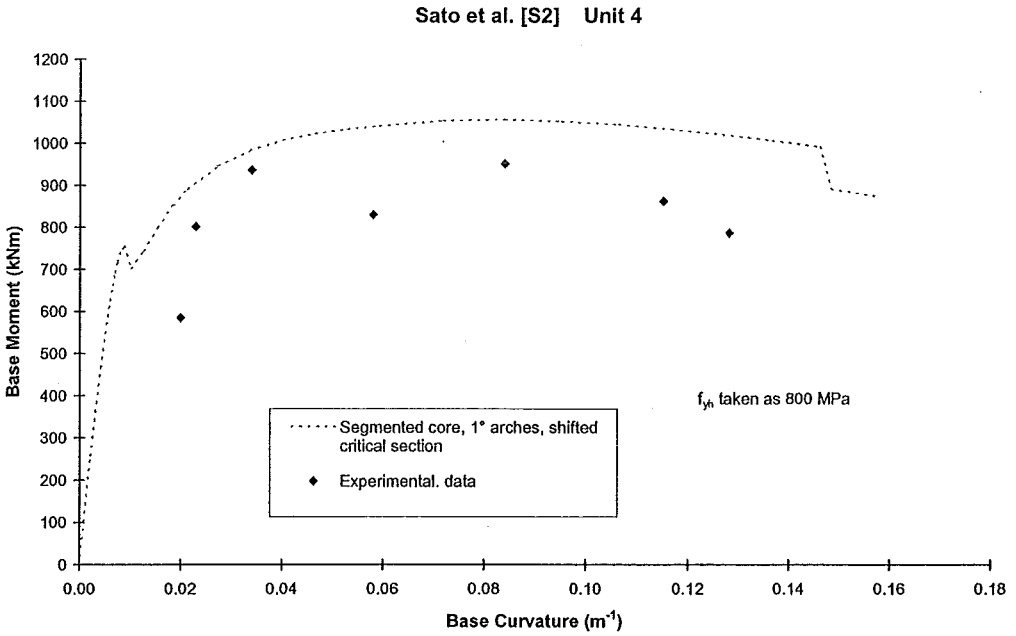

Figure 8.48 *1° Shifted Pseudo-Cyclic and Experimental Moment-Curvature Comparison for Unit 4 with f_{yh} = 800 MPa*

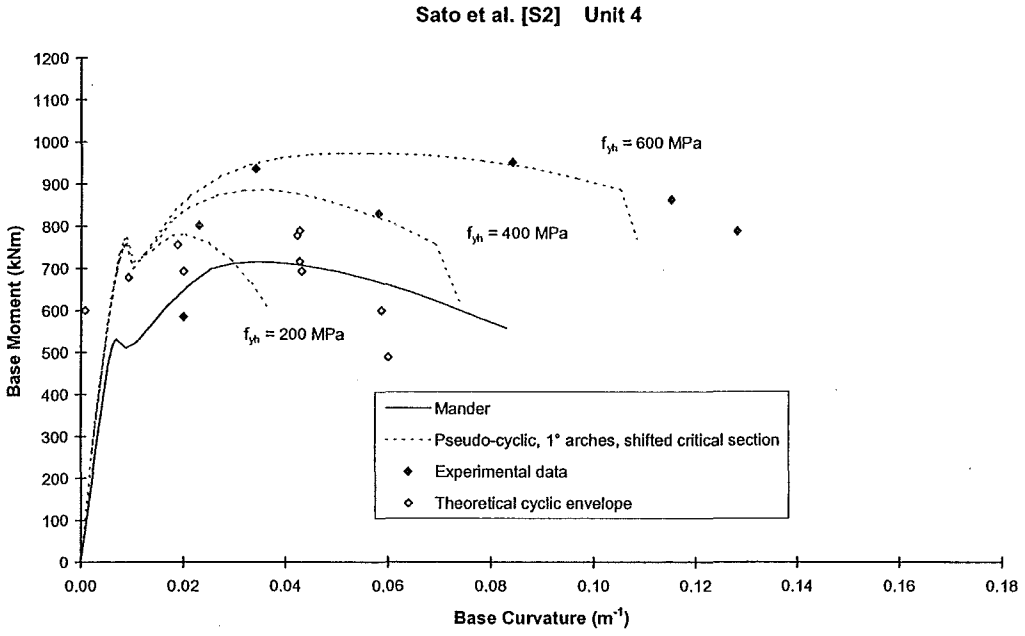

Figure 8.49 *Comparison of Moment-Curvature Response with Varying f_{yh} Values for Sato et al. [S4] Unit 4*

Mander et al. concrete stress-strain model to predict the response of a high strength concrete.

8.9.4.4 Column Tested by Sheikh and Yeh [S6]

Sheikh and Yeh [S6] tested a series of columns under constant axial load and monotonic lateral load at the University of Houston. These columns were subjected to two equal point loads applied at third points along the column to create a test region with zero shear. Columns with a range of axial loads, transverse steel configurations and volumetric ratios were tested to determine the effect of these variables on the performance of the columns. The major difference between these column tests and those conducted at the University of Canterbury is the absence of a stub adjacent to the critical section, to model the effects of members adjacent to the base of the column, and monotonic rather than cyclic loading.

Specimen A-3 consisted of 8 longitudinal bars with square peripheral and diagonal transverse hoop sets for confinement. Moment-curvature analyses using the Mander

et al. model and a monotonic moment-curvature analysis were conducted for this column. As there is no confining stub adjacent to the critical section there is no need to shift the moment-curvature response to account for the shift in the critical section and as loading was applied monotonically there is no requirement for a pseudo-cyclic analysis. Figure 8.50 shows the comparison of the moment-curvature analyses and the experimental data points.

The Mander et al. model over predicts the behaviour of this column specimen while the 40° monotonic moment-curvature analysis matches the experimental data points closely up to a curvature of about 0.07 m^{-1}. After this point the 40° monotonic analysis indicates a degree of strength enhancement probably due to strain hardening of the longitudinal steel which is not matched by the experimental data points, which show a reasonably constant moment up to the end of the test. At this point in the test the transverse hoops may have yielded allowing some buckling of the compressive longitudinal bars. This will lower the moment carried by the section as the couple carried by the compressive and tensile longitudinal steel bars contributes to a significant proportion of the moment for columns under high axial load.

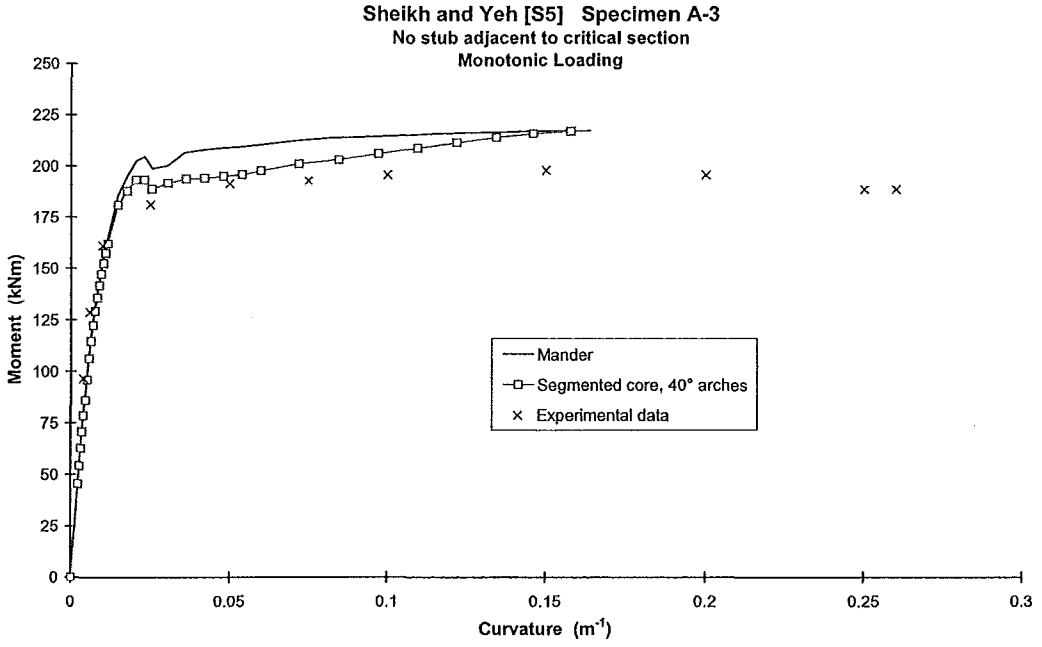

Figure 8.50 *Moment-Curvature Comparison for Sheikh and Yeh [S6] Specimen A-3*

8.9.5 Flexural Enhancement Component Summary

It is known that the ACI method [X3] to determine the flexural strength of a confined column section is a conservative method as it is based on the unconfined concrete properties. This method is usually used to establish the lower bound for the flexural strength of a section. The New Zealand Concrete Structures standard [X2] uses an equation similar to the equation proposed by Ang et al. [A1], shown in Equation 8.26, to account for the flexural overstrength developed in columns where plastic hinges are expected to form, such as at the base of ductile bridge piers, bottom storey columns in ductile frames or in one or 2 storey ductile frames where a strong beam-weak column mechanism design is permitted by the standard. In these situations the New Zealand Concrete Structures standard requires that the columns be detailed to achieve full ductility.

Previous studies [A1, P9] have indicated that there is a strong dependence of the flexural strength of a column on the axial load acting on the section. This has been attributed to the effects of confinement increasing the confined concrete compressive strength and the flexural strength of the column, especially for columns with axial loads higher than $0.3\ f'_c A_g$. In this study it can be seen that much of the flexural strength enhancement dependence on the axial load is due to the observed shift in the critical section. Strong and stiff members adjacent to the critical section in a column provide additional confinement to the column and cause the critical section to shift some distance away from the face of the adjacent member. This flexural strength enhancement is dependent on the column's aspect ratio and the column's neutral axis depth, which increases with axial load.

Figure 8.28 shows the results of experimental column tests plotting the ratio M^*/M_i against axial load ratio, where M^* is the maximum moment achieved during the experiment and M_i is the flexural strength of the column obtained using the ACI method using actual material properties and a strength reduction factor of 1.0. An improved prediction of a column's flexural strength can be made by considering the contribution to the flexural strength from the concrete compressive force and the longitudinal steel couple. The enhanced concrete compressive strength, due to the

presence of confinement, can be accounted as well as strain hardening of the longitudinal steel increasing the stresses in the longitudinal reinforcement. Equation 8.29 predicts the ACI ideal moment for a rectangular column and Equation 8.31 predicts the maximum flexural strength of a rectangular column by accounting for the effects of confinement and strain hardening. Figure 8.38 shows the ratio of M^* / M_o for rectangular columns tested at the University of Canterbury and the University of Houston, where M^* is the maximum experimental moment and M_o is the maximum flexural strength of the column as predicted by the maximum of Equations 8.29 or 8.31.

Moment-curvature analyses are capable of incorporating actual or idealised stress-strain relations of concrete and steel and can be used to establish a more refined calculation of the flexural strength of a column. By incorporating the material stress-strain relations the effects of enhancement of the concrete strength due to confinement and strain hardening of the longitudinal reinforcement on the flexural strength of the column can be evaluated. Cyclic moment-curvature analyses can also be conducted by incorporating the cyclic stress-strain relations for each material into the analysis.

Many of the column tests at the University of Canterbury have involved cyclic lateral loading of the columns which also influences the flexural strength of the columns. This could be accounted for by a cyclic moment-curvature analysis to include the influence of cyclic stress-strain behaviour of concrete and steel.

A pseudo-cyclic moment curvature analysis was developed by using an idealised steel stress-strain relationship and shifting the origin of the monotonic stress-strain curve to account for the residual strain remaining in the reinforcing due to symmetric strain cycles which would occur in a column with constant axial load. This pseudo-cyclic moment-curvature routine can be used to account for the increase in the flexural strength of a section due to cyclic loading effects. This enables the maximum probable flexural strength of a column to be determined for use with capacity design checks.

Structures subject to near-fault earthquake motions will be subjected to large ground velocities and displacements which may cause a large amplitude inelastic response. This may result in the structure having to dissipate energy over a single cycle of yielding response [M6]. This would mean that the structural response would be better modelled by the monotonic moment-curvature analysis rather than a cyclic analysis due to the structure not having to undergo multiple inelastic cycles over the duration of ground motions.

From Figure 8.38 there is still an apparent increase in flexural strength with axial load even with the influence of confinement and strain hardening accounted for. Gill et al. [G1, P6] noted that the critical section of a column moved away from the face of an adjacent member. This shift in the critical section can account for a significant amount of the difference between the predicted and experimental moments. Investigation of the amount of flexural enhancement due to the shift in the critical section indicates that a shift of 0.75 times the neutral axis depth of the column provides a good estimation of the flexural strength of a column. Results for rectangular columns are shown in Figure 8.39 with a shift of 0.75 times the neutral axis depth.

Figures 8.40 to 8.50 show comparison of various analytical moment-curvature results of columns tested by different researchers to the experimental moment-curvature response. The analytical moment-curvature responses are adjusted to account for the shift in the critical section for both the monotonic and pseudo-cyclic responses. Theoretical cyclic moment-curvature envelope points are also shown for units tested by Watson and Park [W3] and Sato et al. [S4]. Analysis of Unit 4 tested by Sato et al. only provided good comparison between the predicted response and experimental moment-curvatures by removing the influence of arching within the core. This unit had a high concrete compressive strength and this difference may be due to limitations of the proposed model for calculating moment-curvature response with high concrete strengths or the arching mechanisms for high strength concrete may not be the same as for normal concrete strengths.

8.10 SUMMARY

8.10.1 Modelling of Column Core Concrete

Research into the stress-strain behaviour of concrete confined by circular hoops, spirals or rectangular hoops has shown that the presence of transverse reinforcement can enhance the strength and ductility of the confined concrete. The amount, strength and configuration of the transverse reinforcement has considerable influence on the amount of confinement and the degree of enhancement provided. The amount and strength of steel provided sets the maximum confining pressure that can be provided due to yielding of the transverse reinforcement.

In the case of ultra-high strength transverse steel reinforcement, dilation of the confined concrete core may not be sufficient to develop yield of the transverse steel. In this case the maximum confining pressure is limited to the stress that is developed in the transverse steel. Tests by Satyarno et al. [S3] and Sato et al. [S4] with ultra-high strength transverse steel reinforcement have shown that maximum stress of approximately 800 MPa was developed in the transverse steel during the tests.

The configuration of the transverse reinforcement affects the confinement efficiency, the greater the efficiency, the greater the area of confined concrete. Circular hoops or spirals have greater efficiency as they apply a confining pressure through hoop tension uniformly over the cross section. Rectangular hoops can only apply effective confinement through the hoop corners or at restrained longitudinal bars. Arching of the concrete is necessary to transfer the confining pressure from the hoops into the core. Similar arching also occurs vertically between the transverse hoop sets so confinement efficiency is reduced with an increase in transverse hoop spacings.

The area of ineffectively confined core concrete determines the confinement efficiency. Concrete stress-strain models using a confinement efficiency factor, to model the effects of the ineffectively confined concrete in the core, apply a uniform confining pressure to the entire concrete core, reduced from the maximum confining

pressure applied to the concrete core. Application of a reduced confining pressure on the total core area using a confinement efficiency factor is a valid assumption for members loaded axially. Zahn et al. [Z1] proposed that the reduction of the confining pressure should be based on the ratio of first moment of areas for members which are subject to axial loads and flexure.

The relationship proposed by Mander et al. [M3] for the increase in concrete strength due to confinement should be limited to an effective confining stress ratio, f'_l / f'_{co}, of less than 0.3. The relationship proposed by Mander et al. in Equation 8.7 gives a strength enhancement factor, f'_{cc} / f'_{co} which reaches a maximum of 4.3 with an effective confining stress ratio of 2.4. At higher effective confining stress ratios the strength enhancement factor begins to decrease from this maximum. Limiting this equation to confining stress ratios less than 0.3 will not effect the application of this model to reinforced concrete columns as the proposed limit is approximately the maximum practical confining stress ratio that can be provided in a reinforced concrete column by mild steel transverse reinforcement to a normal strength concrete.

Over this range of confining stress ratios the strength enhancement given by Mander et al. can be adequately represented by a linear relationship proposed by Richart et al. [R1] which gives the increase in concrete strength over the unconfined concrete strength as 4.1 times the lateral confining pressure. This relationship would need to be modified to account for the effects of concrete arching that occur in reinforced concrete columns confined with the use of transverse steel reinforcement. Therefore the confined concrete strength would increase by 4.1 times the effective lateral confining pressure over the unconfined concrete strength.

The use of an efficiency factor assumes the ineffectively confined concrete remains within the core of the column and is able to carry stress at high strains. As the extreme concrete compression fibre strain is increased, some of the ineffectively confined concrete is actually lost, along with the cover concrete, reducing the area of concrete carrying load. The two areas of concrete within the core, effectively and ineffectively confined, can be modelled separately as it is computationally simple

and better reflects the behaviour of the concrete within the column and removes the assumptions involved with the use of a confinement efficiency factor.

By removing the confinement efficiency factor and modelling ineffectively confined concrete in the core as unconfined concrete similar moment-curvature analysis results can be achieved to those using the original Mander et al. [M3] concrete stress-strain model. The assumptions from the Mander et al. model are used with the boundary between effectively confined and ineffectively confined concrete in the core assumed to be parabolic in shape with an initial tangent angle of 45° over the clear spacing between bars. The segmented core model moment-curvature responses, modelling the effectively and ineffectively confined core, do not show the same flexural strength as the moment-curvature responses conducted using the original Mander et al. model. The difference between the flexural strengths of each model increases with increasing axial load acting on the column. For low axial loads the two models give similar flexural strengths but at higher axial loads the difference between the flexural strengths from the two models increases.

As the original concrete stress-strain model was calibrated against concentric axial load tests on columns the 45° parabolic arches may be too large for columns subjected to flexure. At low axial loads the contribution of the concrete compressive force to the flexural strength of the column is low and the influence of the arches will not be as significant. At high axial loads the concrete compressive force is a major contributor to resisting the applied forces on the column when subjected to flexure. With 45° arches the influence of the ineffectively confined concrete within the section is significant leading to a smaller flexural strength obtained for a column using this model. Therefore for columns subjected to axial load and flexure decreasing the initial tangent angle of the arches to 40° will improve the comparison of the flexural strength between the original Mander et al. model and the approach modelling the effective and ineffective regions within the column core.

8.10.2 Components of Flexural Enhancement

Flexural strength enhancement over the ACI ideal moment is due to the effects of confinement increasing the concrete compressive strength, strain hardening of the longitudinal steel, cyclic loading and the shift in the critical section due to the confining effects of members adjacent to the critical section. The effects of confinement, strain hardening and cyclic loading can be evaluated by using monotonic or cyclic moment-curvature analyses to determine a column's flexural strength. The flexural strength from a monotonic moment-curvature analysis can be adjusted to account for the effects of cyclic loading by assuming a pseudo-cyclic response which increases the strains in the longitudinal steel used to calculate the longitudinal steel compressive and tensile forces.

Expressions for rectangular columns have been developed to predict the ACI ideal moment and the maximum flexural strength of a column taking into account the effects of increased concrete strength due to confinement and strain hardening of the longitudinal steel. The maximum flexural strength of a column is dependent on the contribution of the concrete compressive force. Confinement increases the concrete compressive strength allowing it to maintain the concrete compressive force throughout the moment-curvature response with a reduced area of concrete core under compression. The concrete core area is reduced due to the influence of arching in the column. The ineffectively confined area of the core is not capable of supporting large compressive stresses at high compressive strains requiring the effectively confined core to resist the concrete compressive force. As confinement increases the compressive strength of the concrete the effectively confined core remains capable of maintaining the same concrete force.

The influence of the arching in a column is due to the layout of the transverse reinforcement in a column and can be expressed with a confined concrete efficiency factor, λ_e. This factor is taken as the ratio of the first moments of the ineffectively confined core to the concrete in the core and allows the influence of arching in the column and its effect on the maximum flexural strength of the column to be evaluated.

The ratio of the maximum flexural strength of a column, as obtained from the maximum of Equations 8.29 or 8.31, to the predicted ACI moment, from Equation 8.29, may give an indication of the available curvature ductility of a column.

Previous research [A1] has suggested that a major component of flexural enhancement can be expressed as a function of the axial load acting on the column. This is due to the increase in the required transverse reinforcement for confinement mobilising a larger concrete compressive force contribution to the flexural strength of a column. This study has shown that much of the observed moment enhancement dependence on axial load can be attributed to the shift of the critical section away from the face of an adjacent member, as documented by Gill et al. [G1, P6], once allowance has been made for the effects of confinement and strain hardening of the reinforcement. The amount of shift has been estimated to be between 0.5 and 1.0 times the neutral axis depth of the column. This study has shown that for rectangular columns, the shift can be taken as 0.75 times the neutral axis depth of the column at spalling of the cover concrete. The amount of flexural enhancement is dependent on the neutral axis depth, which is dependent on the axial load ratio, and the column's aspect ratio.

A pseudo-cyclic moment-curvature routine is proposed in lieu of full cyclic moment-curvature analysis. The pseudo-cyclic routine modifies the steel stresses to account for the cyclic strain history in the reinforcing steel by shifting the origin of the monotonic steel stress-strain curve to account for the residual strain remaining in the steel after symmetric strain cycles. The monotonic concrete stress-strain model is used as it provides an envelope to the cyclic stress-strain response of concrete.

Dynamic loading rates are also known to increase the flexural strength of columns due to different stress-strain response of concrete and steel under dynamic strain rates.

Comparison of experimental moment-curvature values and the predicted moment-curvature response, accounting for the shift in the critical section and cyclic

behaviour, where these effects need to be considered, has shown a good match for selected column case studies.

Chapter 9

CONCLUSIONS AND FUTURE RESEARCH

9.1 CONCLUSIONS

Testing of two scale model specimens, Units I-A and I-B, were carried out to determine the likely performance of the retrofitted Piers 68 and 46, respectively, of the Thorndon Overbridge. Reversed cyclic lateral load testing of each specimen revealed that the performance of the prototype retrofitted piers would likely be limited by the formation of a potentially brittle flexure-shear failure in the columns.

The occurrence of the tension shift effect, caused by the formation of diagonal flexure-shear cracking in the columns, led to the development of a failure in the columns where the longitudinal reinforcement had been curtailed. The curtailment of the longitudinal reinforcement in the columns of Piers 46 and 68 did not provide sufficient development length past the curtailed section to adequately anchor the bars after the development of diagonal flexure-shear cracking in the column leading to the failures at these locations.

Repair of each column with the fitting of full height steel jackets proved successful in increasing the available structural displacement ductility of each test specimen. The steel jackets also prevented the formation of shear failures around the curtailment points in each column and allowed each column to develop a large column overstrength. Design and provision of full height steel jackets for the columns of Piers 46 and 68 should prevent the premature column failures observed during the testing. The steel jackets should increase the available structural displacement ductility capacity of each pier beyond the expected structural displacement ductility demand for the chosen level of retrofit of the Thorndon Overbridge.

Design of the pilecap retrofit measures proved adequate to force inelastic action into the columns and prevent failure of the pilecap. The pilecaps and pilecap overlay retrofits were able to resist the applied forces from the column overstrength moments after repair of the columns with full height steel jackets.

As seen from the results of each test specimen the tension shift effect can limit the available strength and ductility of a column containing curtailed longitudinal reinforcement within the height of the column. Chapter 7 outlines the tension shift effect and proposes a procedure to assess the available strength and lateral deformation capacity of bridge columns containing curtailed longitudinal reinforcement. A parametric analysis was conducted for circular and rectangular columns which contained transverse reinforcement spacings that do not meet the current New Zealand Concrete Structures Standard, NZS 3101:1995 [X2], requirements for columns required to resist seismic actions. From this analysis expressions for the internal lever arm, neutral axis depth ratio, contribution of tension reinforcement and position of compression and tension force resultants have been proposed.

Investigations have shown that the amount of tension shift that occurs in a column may be up to half the value usually assumed for design purposes. Design standard requirements for development lengths and requirements for extension of reinforcement past the critical section are appropriate for the design of new structures as suitably conservative assumptions are used. Application of these same requirements to the assessment of existing structures may be too conservative and lead to the need for unnecessary retrofit of the structure.

The proposed expressions are intended to be applied to columns which were designed using earlier, less stringent, requirements for transverse reinforcement spacing and contain potential deficiencies with curtailment of the longitudinal reinforcement. From these the dependable flexural strength envelope can be drawn for the column without having to conduct moment-curvature analyses of the column or utilise column design charts. The bending moment demand, modified to include the tension shift effect and any dynamic effects if appropriate, can be compared to

the dependable flexural strength envelope to determine whether the flexural strength of the column will be reached at any point.

If a column contains curtailed longitudinal reinforcement the dependable flexural strength at the curtailment point may be exceeded due to the tension shift effect. The amount of flexural strength shortfall can be obtained from a graphical representation of the dependable flexural strength envelope, the bending moment demand and the "fictitious" bending moment demand due to the tension shift effect. Inelastic deformations will concentrate at the point(s) where the flexural strength is reached placing large curvature demands on the section. Moment-curvature analysis of the column and assessment of the shear strength capacity of the column are required to determine the available ductility capacity of the column for comparison against the expected ductility demand on the structure.

If the flexural strength and/or ductility capacity of a column are insufficient to meet the expected demands then retrofit is required to improve the performance to meet the expected levels of flexural strength and ductility corresponding to an acceptable chosen level of retrofit. Use of this procedure to assess Units I-A and I-B gave lower bound results for the failure load for Unit I-B and indicated the failure of Unit I-A at the curtailment points once the flexural strength at the base was reached. .

Chapter 8 summarises the stress-strain model proposed by Mander et al. [M3] for concrete confined with circular hoops, spirals or rectangular hoops. This model is reviewed as it is a widely accepted and used concrete stress-strain model in New Zealand research and design practice.

The Mander et al. concrete stress-strain model, along with other models [S3, S4, W4], assumes the effectively confined concrete within the core of the column is reduced from the core area by arching taking place between the transverse reinforcement. Mander et al. assumed the arches took the shape of second order parabolas with an initial tangent angle of 45°. The effect of the arching on the efficiency of the confining pressure provided by the transverse reinforcement is reflected through the use of a confinement efficiency factor.

The confinement efficiency factor is determined through calibration of the model to experimental results, from concentric axial load tests. The resulting stress-strain model is then incorporated into moment-curvature analyses to predict the behaviour and flexural strength of sections subjected to axial load and bending. Comparison of experimental and theoretical moment-curvature results, using the Mander et al. model, from several researchers [A3, G1, P8, Z1] have resulted in the proposed confinement efficiency factor being redefined for use with sections subjected to axial load and bending.

The definition of the confinement efficiency factor in many stress-strain models takes it as the ratio of the effectively confined core area to the total core area. The application of these stress-strain models then go on to effectively ignore the assumed area of ineffectively confined core by assigning uniform stress-strain properties to the entire core area. This assumes the ineffectively confined core is capable of supporting stresses at high strains.

Chapter 8 proposes separating the two areas of effectively and ineffectively confined core and modelling the stress-strain behaviour of each area. This reflects the assumed difference in behaviour of the two regions which was used to define the original confinement efficiency factors. Monotonic moment-curvature results were conducted for a range of circular and square columns separating the behaviour of the effectively and ineffectively confined regions and compared to the moment-curvature response obtained using the original Mander et al. stress-strain model. The Mander et al. model results show higher peak flexural strengths being obtained, especially for higher axial loads and increase transverse reinforcement spacings. This is due to the increase in contribution to flexure of the concrete compressive force resultant at higher axial loads and the inability for this force to be supported over the region of ineffectively confined concrete. With increase transverse reinforcement spacings the ineffectively confined concrete region is larger increasing its influence on the flexural strength.

With arching modelled as 45° parabolic arches the influence of the ineffectively confined region is significant leading to lower flexural strengths for the columns subjected to axial load and flexure modelled by separating the effectively and

ineffectively confined core regions. By reducing the initial tangent angle of the arches to 40° an improved comparison of flexural strengths between the Mander et al. model and the approach separating the effectively and ineffectively confined core regions is obtained.

A pseudo-cyclic moment-curvature routine is proposed in lieu of a full cyclic moment-curvature analysis. The pseudo-cyclic routine modifies the steel stresses to account for the cyclic strain history in the reinforcing steel by shifting the origin of the monotonic steel stress-strain relationship. This allows a pseudo-cyclic moment-curvature analysis to be conducted without requiring incorporation of complex cyclic concrete and steel stress-strain models into the moment-curvature routine.

Flexural strength enhancement over the ACI ideal moment is known to occur due to the effects of confinement, strain hardening, cyclic loading and the shift of the critical section due to the confining effects of members adjacent to the critical section. Expressions have been developed to predict the ACI ideal moment and the maximum flexural strength of a rectangular shaped column by taking into account the effects of confinement and strain hardening The maximum flexural strength of a column is influenced by the contribution of the concrete compressive force and the influence of arching within the column core. A confined concrete efficiency factor, λ_e, is proposed to allow the influence of arching in a column and its effect on the maximum flexural strength of the column to be evaluated. It is believed that the ratio of the maximum flexural strength to the ACI ideal moment may give an indication of the available curvature ductility of a column.

Previous research [A1] has shown that a major component of flexural strength enhancement can be expressed as a function of the axial load acting on a column. This study has shown that much of the observed moment enhancement dependence on axial load can be attributed to the shift of the critical section. This study has shown that for rectangular columns the shift can be taken as 0.75 times the neutral axis depth of the column at spalling of the cover concrete.

Comparison of experimental moment-curvature results and the predicted moment-curvature response, accounting for the shift of the critical section and cyclic behaviour, has shown a good match for the selected column case studies.

9.2 FUTURE RESEARCH

The proposed expressions in Chapter 8 to determine the maximum flexural strength of a rectangular column incorporate the confined concrete efficiency factor, λ_e. These expressions allow the influence of the amount and arrangement of the transverse reinforcement to the flexural strength of a section to be accounted for. Typically sections with larger λ_e values show maximum flexural strengths well above the ACI nominal flexural strength. It is believed the ratio of the maximum flexural strength to the ACI nominal strength could give an indication of the available curvature ductility of a section. Further investigation into the ultimate curvature achieved from experimental testing and the ratio between the maximum and ACI flexural strengths as determined from the expressions proposed in Chapter 8 is required. These ratios may give an indication as to whether a section is capable of limited or full ductility.

Derivations for the confined concrete efficiency factor, λ_e, for other sections shapes are included in Appendix D which may allow the extension of the concepts used for rectangular sections to other section shapes.

The proposed shift in the critical section of 0.75 times the neutral axis depth has been determined for rectangular column sections only. Extension of the concepts used to predict the flexural strengths of rectangular sections to other section shapes should allow the column database, included in Appendix B, to be extended and a value for the shift in the critical section to be determined for circular and rectangular section shapes.

Modelling the column core area separated into ineffectively and effectively confined regions indicates the assumed initial tangent angle for the parabolic arches, from the original Mander et al. model, of 45° may be too large for sections subjected to axial load and flexure. The presence of a strain gradient through the section and only part

of the column core being in compression may reduce the amount of arching that occurs in a column. Further experimental work could attempt to investigate the arching that occurs in columns subjected to axial load and flexure.

The expression used to determine the useable ultimate concrete compressive strain, as one stopping condition for a moment-curvature analysis, is derived from concentric axial load tests. The value for the ultimate compressive strain from this expression may be unnecessarily conservative when applied to columns subjected to flexure. A simple expression for the available ultimate concrete compressive strain for columns subjected to flexure is required to assess the ultimate curvature of existing sections. The existing expression, being conservative for columns subjected to flexure, may lead to an unnecessary need to retrofit an existing column based on inadequate curvature ductility capacity.

10 REFERENCES

[A1] Ang B.G., Priestley, M.J.N. and Paulay, T., "Seismic Shear Strength of Circular Bridge Piers", Research Report 85-5, Department of Civil Engineering, University of Canterbury, Christchurch, 1985, 408 pp.

[A2] Ang B.G., Priestley, M.J.N. and Paulay, T., "Seismic Shear Strength of Circular Reinforced Concrete Columns", ACI Structural Journal, Vol. 84, No. 1, Jan-Feb 1989, pp.45-59.

[A3] Ang B.G., Priestley, M.J.N. and Park, R., "Ductility of Reinforced Concrete Bridge Piers Under Seismic Loading", Research Report 81-3, Department of Civil Engineering, University of Canterbury, Christchurch, 1981, 113 pp.

[B1] Billings, I.J. and Powell, A.J., "Thorndon Overbridge Seismic Assessment", Proceedings of the Second International Workshop on Seismic Design and Retrofitting of Reinforced Concrete Bridges", R. Park editor, Queenstown, New Zealand, August 1994, pp. 535-559.

[B2] Balmer, G.G., "Shearing Strength of Concrete Under High Triaxial Stress - Computation of Mohr's Envelope as a Curve", Structural Research Laboratory Report No. SP-23, U.S. Bureau of Reclamation, 1943, 13 pp. plus tables and figures.

[C1] Chapman, H.E. and Kirkaldie, D.K., "Earthquake Resistance Evaluation and Upgrading of Bridges", New Zealand Concrete Society, Technical Report (TR) 13, October 1992, pp. 48-54.

[C2] Chapman, H.E., "Retrofitting - New Zealand", Proceedings of the International Workshop on Seismic Design and Retrofitting of Reinforced Concrete Bridges", G.M. Calvi and M.J.N. Priestley editors, Bormio, Italy, April 1991, pp. 505-527.

[C3] Chapman, H.E. and Kirkaldie, D.K., "Assessment of Highway Bridges in New Zealand", Proceedings of the Second International Workshop on Seismic Design and Retrofitting of Reinforced Concrete Bridges", R. Park editor, Queenstown, New Zealand, August 1994, pp. 561-566.

[C4] Chai, Y.H., Priestley, M.J.N. and Seible, F., "Seismic Retrofit of Circular Bridge Columns for Enhanced Flexural Performance", ACI Structural Journal, Vol. 88, No. 5, Sept-Oct 1991, pp. 572-584.

[C5] Chai, Y.H., Priestley, M.J.N. and Seible, F., "Analytical Model for Steel Jacketed RC Circular Bridge Columns", ASCE Journal of Structural Engineering, Vol. 120, No. 8, August 1994, pp. 2358-2376.

[C6] Cement and Concrete Association of New Zealand, "New Zealand Reinforced Concrete Design Handbook", Cement and Concrete Association of New Zealand, Porirua.

[D1] Dodd, L.L. and Cooke, N., "The Dynamic Behaviour of Reinforced Concrete Bridge Piers Subjected to New Zealand Seismicity", Research Report 92-4, Department of Civil Engineering, University of Canterbury, Christchurch, 1992, 460 pp.

[D2] Dodd, L.L. and Restrepo-Posada, J.I., "Model for Predicting Cyclic Behaviour of Reinforcing Steel", Journal of Structural Engineering, ASCE, Vol. 121, No. 3, March 1995, pp. 433-445.

[D3] Davey, B.E. and Park, R., "Reinforced Concrete Bridge Piers Under Seismic Loading", Research Report 75-3, Department of Civil Engineering, University of Canterbury, Christchurch, 1975, 100 pp.

[E1] Earthquake Engineering Research Institute, "Loma Prieta Earthquake Reconnaissance Report", Earthquake Spectra, Supplement to Volume 6, Earthquake Engineering Research Institute, Oakland, California, May 1990, 448 pp.

[E2] Earthquake Engineering Research Institute, "Northridge Earthquake of January 17, 1994, Reconnaissance Report - Volume 1", Earthquake Spectra, Supplement C to Volume 11, Earthquake Engineering Research Institute, Oakland, California, April 1995, 523 pp.

[E3] Earthquake Engineering Research Institute, "The Hyogo-Ken Nanbu Earthquake, Preliminary Reconnaissance Report", Earthquake Engineering Research Institute, Oakland, California, 1995, 116 pp.

[G1] Gill, W.D., Park, R. and Priestley, M.J.N., "Ductility of Rectangular Reinforced Concrete Columns with Axial Load", Research Report 79-1, Department of Civil Engineering, University of Canterbury, 1979, 136 pp.

[H1] Housner, G.W., "Competing Against Time", The Governor's Board of Inquiry on the 1989 Loma Prieta Earthquake, G.W. Housner, Chairman, State of California, Office of Planning and Research, May 1990, 264 pp.

[H2] Huizing, J.B.S., Bialostocki, R.J., Armstrong, I.C., Thornton, R.W., Wood, J.H. and Willberg, G.D. "Design of the Thorndon Overbridge", New Zealand Engineering, Vol. 23, No. 12, December 1968, pp. 484-504.

[J1] JSCE, "Preliminary Report on the Great Hanshin Earthquake, January 17, 1995", Japan Society of Civil Engineers, 1995, 346 pp.

[K1] King, D.J., Priestley, M.J.N. and Park, R., "Computer Programs for Concrete Column Design", Research Report 86-12, Department of Civil Engineering, University of Canterbury, 1986, 72 pp.

[L1] Lew, H.S., Editor, "Performance of Structures During the Loma Prieta Earthquake of October 17, 1989", NIST Special Publication 778, National Institute of Standards and Technology, Gaithersburg, MD, January 1990, 201 pp.

[L2] Li, Bing, Park, R. and Tanaka, H., "Strength and Ductility of Reinforced Concrete Members and Frames Constructed Using High Strength Concrete", Research Report 94-5, Department of Civil Engineering, University of Canterbury, 1994, 373 pp.

[M1] Maffei, J. and Park, R., "The Seismic Evaluation and Retrofit of Bridges", Research Report 96-2, Department of Civil Engineering, University of Canterbury, 1996, 312 pp.

[M2] Marsh, E.J. and Toan, D.V., "Geotechnical Aspects of the Thorndon Overbridge Seismic Retrofit, Wellington", New Zealand National Society of Earthquake Engineering, NZNSEE Conference, New Plymouth, pp. 161-168.

[M3] Mander, J.B., Priestley, M.J.N. and Park, R., "Theoretical Stress-Strain Model for Confined Concrete", Journal of Structural Engineering, ASCE, Vol. 114, No. 8, August 1988, pp. 1804-1826.

[M4] Mander, J.B., Priestley, M.J.N. and Park, R., "Seismic Design of Bridge Piers", Research Report 84-2, Department of Civil Engineering, University of Canterbury, Christchurch, 1984, 483 pp.

[M5] Munro, I.R.M., Park, R. and Priestley, M.J.N., "Seismic Behaviour of Reinforced Concrete Bridge Piers", Research Report 76-9, Department of Civil Engineering, University of Canterbury, Christchurch, 1976, 106 pp.

[M6] McVerry, G.H., "Near-Fault Earthquake Records and Implications for Design Motions", Proceedings NZNSEE Conference, Wairakei, Taupo, March 1997, pp. 88-95.

[N1] NIST, "1994 Northridge Earthquake, Performance of Structures, Lifelines, and Fire Protection Systems", NIST Special Publication 862, National Institute of Standards and Technology, Gaithersburg, MD, May 1994, 181 pp.

[N2] New Zealand National Society of Earthquake Engineering, "The Loma Prieta, California, Earthquake of October 17, 1989: Report of the NZNSEE Reconnaissance Team", Bulletin of the New Zealand National Society of Earthquake Engineering, Vol. 23, No. 1, March 1990, pp. 1-78.

[N3] New Zealand National Society of Earthquake Engineering, "Northridge Earthquake Reconnaissance Report", Bulletin of the New Zealand National Society of Earthquake Engineering, Vol. 27, No. 4, December 1994, pp. 235-344.

[N4] New Zealand National Society of Earthquake Engineering, "The Hyogo-ken Nanbu Earthquake of 17 January 1995", Bulletin of the New Zealand National Society of Earthquake Engineering, Vol. 28, No. 1, March 1995, pp. 1-98.

[N5] Ng, K.H., Priestley, M.J.N. and Park, R., "Seismic Behaviour of Circular Reinforced Concrete Bridge Piers", Research Report 78-14, Department of Civil Engineering, University of Canterbury, Christchurch, 1978, 129 pp.

[P1] Park, R. and Paulay, T., *Reinforced Concrete Structures*, John Wiley and Sons, New York, 1975, 769 pp.

[P2] Paulay, T. and Priestley, M.J.N., *Seismic Design of Reinforced Concrete and Masonry Buildings*, John Wiley and Sons, New York, 1992, 744 pp.

[P3] Priestley, M.J.N., Seible, F. and Calvi, G.M., *Seismic Design and Retrofit of Bridges*, John Wiley and Sons, New York, 1996, 686 pp.

[P4] Priestley, M.J.N., Verma, R. and Xiao, Y., "Seismic Shear Strength of Reinforced Concrete Columns", ASCE Journal of Structural Engineering, Vol. 120, No. 8, August 1994, pp.2310-2329.

[P5] Priestley, M.J.N., Seible, F., Xiao, Y. and Verma, R., "Steel Jacket Retrofitting of Reinforced Concrete Bridge Columns for Enhanced Shear Strength - Part 2: Test Results and Comparison with Theory", ACI Structural Journal, Vol. 91, No. 5, Sept-Oct 1994, pp. 537-551.

[P6] Park, R., Priestley, M.J.N. and Gill, W.D., "Ductility of Square-Confined Concrete Columns", Proceedings, ASCE, Vol. 108, ST4, April 1982, pp. 929-950.

[P7] Popovics, S., "A Numerical Approach to the Complete Stress-Strain Curves of Concrete", Cement and Concrete Research, Vol. 3, No. 5, September 1973, pp. 583-599.

[P8] Potangaroa, R.T., Priestley, M.J.N. and Park, R., "Ductility of Spirally Reinforced Concrete Columns Under Seismic Loading", Research Report 79-8, Department of Civil Engineering, University of Canterbury, Christchurch, 1979, 116 pp.

[P9] Priestley, M.J.N. and Park, R., "Strength and Ductility of Concrete Bridge Columns Under Seismic Loading", ACI Structural Journal, Vol. 84, No. 1, Jan-Feb 1987, pp. 61-76.

[R1] Richart, F.E., Brandtzaeg, A. and Brown, R.L., "A Study of The Failure of Concrete Under Combined Compressive Stresses", University of Illinios Engineering Experimental Station, Bulletin No. 185, 1928, 104 pp.

[R2] Restrepo, J.I. and Wang, Y.C., "Strength Enhancement of Reinforced Concrete Compression Members Retrofitted with Advanced Composite Materials", Third Canmet/ACI International Symposium on Advances in Concrete Technology, Supplementary Papers, August 1997, pp. 109-123.

[R3] Restrepo-Posada, J. I., Park, R. and Buchanan, A.H., "Seismic Behaviour of Connections Between Precast Concrete Elements of Moment Resisting

Frames", Research Report 93-3, Department of Civil Engineering, University of Canterbury, Christchurch, 1993, 385 pp.

[R4] Restrepo-Posada, J.I., Dodd, L.L., Park, R. and Cooke, N., "Variables Affecting Cyclic Behaviour of Reinforcing Steel", Journal of Structural Engineering, ASCE, Vol. 120, No. 11, November 1994, pp. 3178-3195.

[S1] Sheikh, S.A. and Uzumeri, S.M., "Analytical Model for Concrete Confinement in Tied Columns", Proceedings ASCE, Vol. 108, ST 12, December 1982, pp. 2703-2722.

[S2] Sakai, K. and Sheikh, S.A., "What Do We Know About Confinement in Reinforced Concrete Columns? (A Critical Review of Previous Work and Code Provisions)", ACI Structural Journal, Vol. 86, No. 2, Mar-Apr 1989, pp. 192-207.

[S3] Satyarno, I., Tanaka, H. and Park, R., "Concrete Columns Incorporating Mixed Ultra High and Normal Strength Longitudinal Reinforcement", Research Report 93-1, Department of Civil Engineering, University of Canterbury, Christchurch, 1993, 151 pp.

[S4] Sato, Y., Tanaka, H. and Park, R., "Reinforced Concrete Columns with Mixed Grade Longitudinal Reinforcement", Research Report 93-7, Department of Civil Engineering, University of Canterbury, Christchurch, 1993, 115 pp.

[S5] Sargin, M. Ghosh, S.K. and Handa, V.K., "Effects of Lateral Reinforcement upon the Strength and Deformation Properties of Concrete", Magazine of Concrete Research, Vol. 23, No. 75-76, June - September 1971, pp. 99-110.

[S6] Sheikh, S.A. and Yeh, C.C., "Tied Concrete Columns Under Axial Load and Flexure", Journal of Structural Engineering, ASCE, Vol. 116, No. 10, October 1990, pp. 2780-2800.

[S7] Soesianawati, M.T., Park, R. and Priestley, M.J.N., "Limited Ductility Design of Reinforced Concrete Columns", Research Report 86-10, Department of Civil Engineering, University of Canterbury, Christchurch, 1986, 208 pp.

[T1] Tanaka, H. and Park, R., "Effect of Lateral Confining Reinforcement on the Ductile Behaviour of Reinforced Concrete Columns", Research Report 90-2,

Department of Civil Engineering, University of Canterbury, Christchurch, 1990, 458 pp.

[T2] Thompson, K.J. and Park, R., "Stress-Strain Model for Grade 275 Reinforcing Steel with Cyclic Loading", Bulletin NZNSEE, Vol.11, No. 2, June 1978, pp 101-109.

[W1] Wang, Y.C. Restrepo, J.I. and Park, R. "Retrofitting of Reinforced Concrete Members Using Advanced Composite Materials", PhD. Thesis to be published, Department of Civil Engineering, University of Canterbury, Christchurch, 1999.

[W2] William, K.J. and Warnke, E.P., "Constitutive Model for the Triaxial Behaviour of Concrete", International Association for Bridge and Structural Engineering, Proceedings, Vol. 19, 1975.

[W3] Watson, S. and Park, R., "Design of Reinforced Concrete Frames of Limited Ductility", Research Report 89-4, Department of Civil Engineering, University of Canterbury, Christchurch, 1989, 232 pp.

[W4] Watanbe, F., Muguruma, H., Tanaka, H. and Katsuda, S., "Improving the Flexural Ductility of Prestressed Concrete Beam By Using the High Strength Lateral Hoop Reinforcement", Symposia on Partial Prestressing and Practical Construction in Prestressed and Reinforced Concrete, Proceedings: Part 2, FIP, September 1980, pp. 398-406.

[X1] Xiao, Y., Priestley, M.J.N. and Seible, F., "Seismic Assessment and Retrofit of Bridge Column Footings", ACI Structural Journal, Vol. 93, No. 1, Jan-Feb 1996, pp. 79-94.

[X2] Standards Association of NZ, *Concrete Structures Standard*, NZS 3101, Wellington, New Zealand, 1995.

[X3] ACI 318-89, *Building Code Requirements for Reinforced Concrete*, American Concrete Institute, Detriot, revised 1992.

[X4] Xinrong, Li, Park, R. and Tanaka, H., "Reinforced Concrete Columns Under Seismic Lateral Force and Varying Axial Load", Research Report 95-5, Department of Civil Engineering, University of Canterbury, Christchurch, 1995, 342 pp.

[Z1] Zahn, F.A., Park, R. and Priestley, M.J.N., "Design of Reinforced Concrete Bridge Columns for Strength and Ductility", Research Report No. 86-7, Department of Civil Engineering, University of Canterbury, Christchurch, 1986, 330 pp.

APPENDIX A

NUMERICAL EXAMPLES FOR ASSESSMENT OF BRIDGE COLUMNS WITH CURTAILED LONGITUDINAL REINFORCEMENT

A.1 EXAMPLE COLUMN 1

Pier 46 reinforcement layout is shown in Figure A.1. A pilecap overlay retrofit and post-tensioning cored through the pilecap is required to strengthen the existing pilecap and force all inelastic action to occur at the base of the column. The column is 8 feet (2.438 m) in diameter and the centre of mass of the bridge deck is 8.6 m above the top of the pilecap overlay retrofit. The axial load in the column from the superstructure load is 8,745 kN. A total of 76 longitudinal bars of 1 $^1/_2$ inch (38 mm) diameter are arranged bundled in pairs at the base of the column. Half of these bars are curtailed 4.34 m above the top of the proposed 375 mm pilecap overlay retrofit. This gives longitudinal reinforcement ratios, $p_t = 1.85\%$ for the base of the column and $p_t = 0.93\%$ for the column at the curtailment point. The cover to the transverse reinforcement is 2 inches (50 mm). The distance between the centreline of the transverse hoop is, $D_c = 2.325$ m. The pitch of the longitudinal reinforcement layout of 2.275 m gives a value for g of 0.933.

Transverse reinforcement consists of $^1/_2$ inch (12.7 mm) diameter circular hoops at 12 inch (305 mm) centres over the entire height of the column. The rotational inertia of the umbrella platform is assumed to increase the moment at the centre of mass of the umbrella platform by 10 % of the column base moment, due to dynamic effects in the first mode of vibration.

The concrete compressive strength is taken as $f'_c = 55$ MPa, giving an axial load ratio $N^* / f'_c A_g = -0.034$. Steel yield strengths of $f_y = 350$ MPa for the longitudinal steel and $f_{yh} = 286$ MPa are used for the analysis of this column.

The internal lever arm, tension force contribution and position of the compressive force resultant can be found for the "as-built" base of Pier 46 and the curtailed section of the column.

A.1.1 Base of Column

From Equation 7.8 the internal lever arm ratio is:-

$$\frac{jd}{D} = 0.593 \qquad \text{(A.1)}$$

Equation 7.10 gives the tension force resultant as a proportion of the total reinforcement yield force in the column.

$$\frac{T}{A_{st} f_y} = 0.694 \qquad \text{(A.2)}$$

The position of the compressive force resultant is given by the term α in Equation 7.12.

$$\alpha = 0.300 \qquad \text{(A.3)}$$

From Equation 7.6 the nominal flexural strength of the column at the base can be established as:-

$$\begin{aligned} M_n &= Tjd + (1-\alpha) jdN^* \\ &= 30{,}350 + 8850 \\ &= 39{,}200 \text{ kNm} \end{aligned} \qquad \text{(A.4)}$$

A.1.2 Curtailment Section

Above the curtailment point, Equation 7.8 indicates that the internal lever arm ratio for the column at the curtailment section remains as:-

$$\frac{jd}{D} = 0.593 \qquad \text{(A.5)}$$

Equation 7.10 gives the tension force resultant as a proportion of the total steel yield force in the column. With curtailment of half the longitudinal steel Equation 7.10 gives:-

$$\frac{T}{A_{st} f_y} = 0.75 \qquad \text{(A.6)}$$

For the curtailment section, using Equation 7.12 to find the position of the compressive force resultant, α, gives:-

$$\alpha = 0.257 \qquad \text{(A.7)}$$

From Equation 7.6 the nominal flexural strength of the curtailment point in the column can be established as:-

$$\begin{aligned} M_n &= Tjd + (1-\alpha) jdN^* \\ &= 16{,}400 + 9{,}395 \\ &= 25{,}795 \text{ kNm} \end{aligned} \qquad \text{(A.8)}$$

A.1.3 Pier 46 Structural Response

The flexural strength envelope and the bending moment demand can be plotted against the column height as shown in Figure A.2. The dependable flexural strength of the column sections is taken as $\phi[Tjd + (1-\alpha)jdN^*]$ where ϕ is a strength reduction factor less than or equal to 1.0. Some allowance for the development length of the

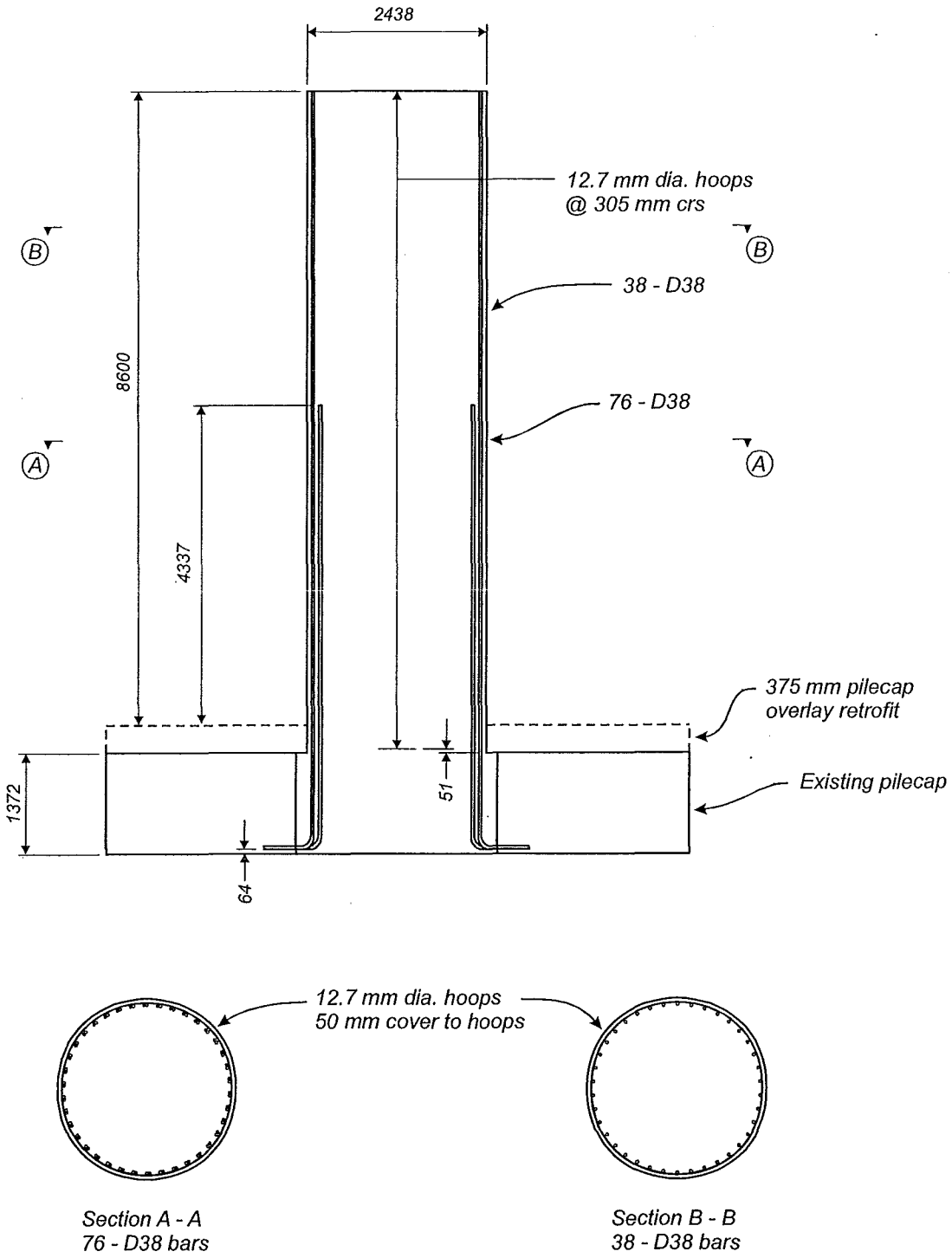

Figure A.1 *Pier 46 Longitudinal and Transverse Column Reinforcement*

longitudinal bars at the curtailment point is shown by gradually increasing the flexural strength envelope over a distance equal to the development length of the longitudinal bars. A strength reduction factor $\phi = 1.0$ has been used to plot the dependable flexural strength envelope for this column. Also shown in Figure A.2 is the moment demand due to the tension shift effect occurring in the column. This tension shift can be accounted for by increasing the bending moment above the base of the column by a moment equal to Ve_v, where V is the shear force in the column due to development of the flexural strength at the base of the column and $e_v = jd / 2\tan\theta$ where $\theta = 30°$.

The shear force, V, corresponding to the development of the dependable flexural strength at the base of the column is:

$$V = \frac{39{,}200 - (0.1)(39{,}200)}{8.600} = 4{,}100\ kN \qquad \text{(A.9)}$$

The tension shift is:

$$e_v = \frac{(0.593)(2.438)}{2\tan 30°} = 1.252\ m \qquad \text{(A.10)}$$

The fictional increase in bending moment due to the tension shift effect is then:-

$$Ve_v = (4{,}100)(1.252) = 5{,}135\ kNm \qquad \text{(A.11)}$$

From this diagram it can be seen that the shifted bending moment diagram corresponding to the moment demand including the tension shift effect exceeds the flexural strength envelope at the curtailment point. As a critical section is likely form at this point, the curtailed section will have to undergo inelastic deformations as these will concentrate at this point. Further refined analyses of the column, using moment-

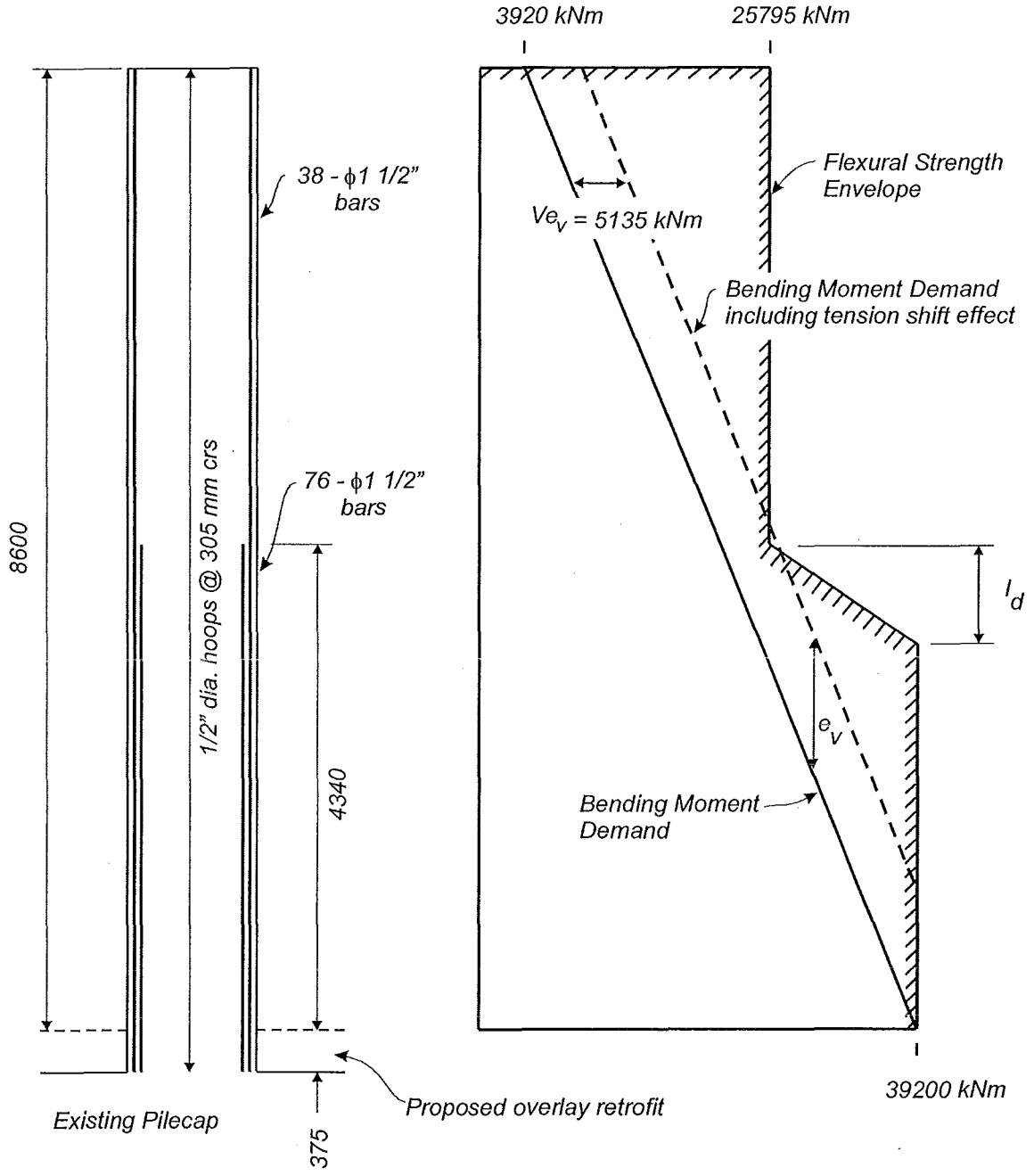

Figure A.2 *Pier 46 Dependable Flexural Strength Envelope and Bending Moment Demand due to the Tension Shift Effect*

curvature analysis of the column sections, can be conducted to determine the dependable flexural strength of the column up the height and account for the influences of confinement and strain hardening of the longitudinal reinforcement leading to overstrength of the column.

Moment-curvature analyses of the base of the column and the curtailment point give nominal flexural strengths at the base of 36,682 kNm at a yield curvature $\phi_y = 0.00154\ m^{-1}$ and 24,211 kNm for the curtailment point at a yield curvature of $\phi_y = 0.00147\ m^{-1}$. The dependable flexural strengths can be taken using a strength reduction factor of $\phi = 1.0$ and the dependable flexural strength envelope drawn for the column. As the dependable flexural strength envelope at the curtailment point is reached before the dependable flexural strength at the base of the column is reached, the bending moment demand must be redrawn so that the dependable flexural strength at the curtailment point is just reached when the tension shift is included.

The base moment corresponding to the development of the dependable flexural strength of the curtailment point is:-

$$M_b = \frac{M}{\left[\beta + (1-\beta)\left(\frac{x+e_v}{H}\right)\right]} \qquad \text{(A.13)}$$

where M = dependable flexural strength of curtailment point
= 24,211 kNm

β = ratio of moment at top of column due to rotational inertia of umbrella platform to base column moment
= 0.10

x = distance from centre of mass of umbrella platform to curtailment point
= 4.260 m

H = height of column to centre of mass of umbrella platform
= 8.600 m

e_v = tension shift

$= 1.252$ m

This gives a base moment of 35,770 kNm when the dependable flexural strength at the curtailment point is reached when the tension shift effect is included. The column shear force corresponding to this base moment is:-

$$V = \frac{35{,}770 - (0.1)(35{,}770)}{8.600} \qquad (A.14)$$
$$= 3{,}745 \ kN$$

The increase in bending moment due to the tension shift effect is:-

$$Ve_v = (3{,}745)(1.252) \qquad (A.15)$$
$$= 4{,}690 \ kNm$$

The elastic curvature distribution for the column can be established using the bi-linear moment-curvature approximation to determine the curvatures in the column according to the moment acting at each section. The bending moment demand and curvature distribution are shown in Figure A.3. The elastic flexural displacements at the top of the column can be found by integrating the curvature diagram. Further displacements through fixed end rotations of the column caused by strain penetration in the longitudinal reinforcement at the base and at the curtailment point have been neglected.

Further elastic displacements of the structure will occur through foundation compliance and will decrease the structural displacement ductility compared to the column displacement ductility.

As the dependable flexural strength at the curtailment point has been reached all further displacements at the top of the column can be assumed to occur through plastic rotation in the plastic hinge at the curtailment point. The available ultimate curvature of the curtailment point is limited by the lesser of the flexural curvature

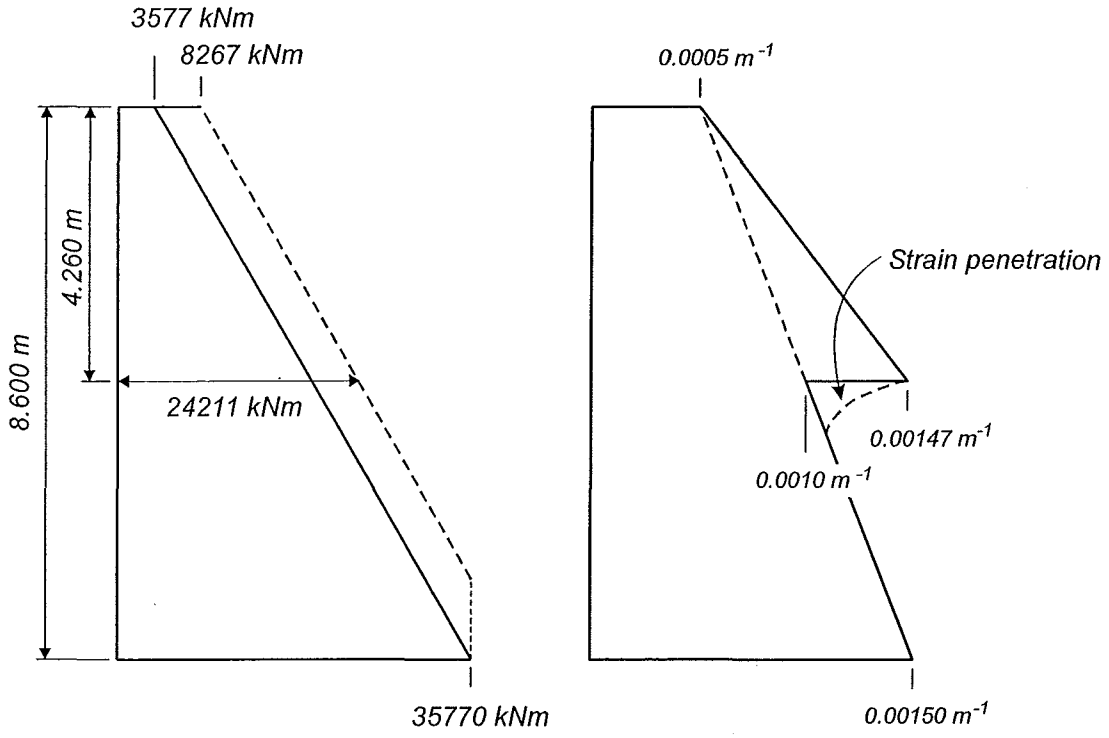

Figure A.3 *Bending Moment Demand and Curvature Distribution of Pier 46 at Development of Dependable Flexural Strength at the Curtailment Point Due to the Tension Shift Effect*

corresponding to the ultimate concrete compressive strain or the curvature at the development of a shear failure in the column.

The shear capacity of the column will have to be assessed to ensure that the shear strength of the column is sufficient to resist the imposed shear forces and to determine the ultimate curvature available form the critical section. This can be done following the method proposed by Priestley et al. [P3, P4] outlined in Section 7.4.2.

A.1.4 Pier 46 Shear Strength Assessment

Transverse reinforcement in Pier 46 consists of 12.7 mm diameter hoops placed at 305 mm centres over the entire height of the column. Assuming a yield strength for the transverse hoops of $f_{yh} = 286$ MPa, a concrete strength $f'_c = 55$ MPa and a

compressive axial load $N^* = -8{,}745$ kN the three components of shear resistance in the proposed model can be obtained.

The diameter to the centreline of the transverse hoops can be taken as $D_c = 2{,}325$ mm, the area of the transverse hoop as $A_{sp} = 127$ mm^2 and the angle of inclined flexure-shear cracking as $\theta = 30°$. The transverse steel contribution to the shear resistance is given by Equation 7.19(a):-

$$V_s = \frac{\pi}{2}\frac{127\times 286\times 2325}{(305)\tan 30°} = 785\ kN \qquad \text{(A.16)}$$

The contribution of the axial load to shear resistance is given in Equation 7.20. To determine the angle α at which the axial load is transferred from the top of the column to the base, as shown in Figure 7.7, the position of the compressive force resultant must be evaluated. From Equation 7.12 the term α gives the position of the compressive force resultant related to the centreline of the column and thus allows the distance from the extreme compressive fibre to the compressive force resultant to be found.

$$a = D\left(\frac{1}{2}-(1-\alpha)\frac{jd}{D}\right) = 2.438\left(\frac{1}{2}-(1-0.300)(0.593)\right) = 0.207\ m \qquad \text{(A.17)}$$

From Figure 7.7 it can be seen that:-

$$\tan\alpha = \frac{D - a}{2H} \qquad \text{(A.18)}$$

Thus from Equation 7.20:-

$$V_p = -(-8{,}745) \times \frac{2.438 - 0.207}{(2)(8.600)} \qquad \text{(A.19)}$$
$$= 1{,}135\ \text{kN}$$

As a plastic hinge develops at the curtailment point this component of shear strength will be ignored as the diagonal strut assumed to resist shear cannot develop between the top and bottom of the column.

The concrete contribution to shear resistance varies with curvature ductility in the column as shown in Figure 7.6. The column can be evaluated at k = 0.29, 0.10 and 0.05. The gross area of the column is $A_g = 4{,}676 \times 10^3$ mm^2 and from Equation 7.18:-

$$V_c = 0.8 \times 4{,}676 \times 10^3 \times k \times \sqrt{55}$$
$$= 8{,}030\ \text{kN} \qquad \text{for } k = 0.29$$
$$= 2{,}770\ \text{kN} \qquad \text{for } k = 0.10 \qquad \text{(A.20)}$$
$$= 1{,}385\ \text{kN} \qquad \text{for } k = 0.05$$

From Equations A.16 and A.20 the shear strength of the column can be found:-

$$V_n = V_c + V_s$$
$$= 8{,}815\ \text{kN} \qquad \text{for } k = 0.29$$
$$= 3{,}555\ \text{kN} \qquad \text{for } k = 0.10 \qquad \text{(A.21)}$$
$$= 2{,}170\ \text{kN} \qquad \text{for } k = 0.05$$

The base shear corresponding to development of the dependable flexural strength of the curtailment point is V = 3,745 kN. As the residual shear strength of the column corresponding to k = 0.05 is less than the shear force at development of the flexural strength of the column base it is possible that the column could fail in shear at some point. A moment-curvature plot will indicate the point at which the shear demand due to flexure will exceed the shear strength of the column and the likely development of a shear failure. Figure A.4 shows the moment-curvature relationship for the base and curtailment points expressed as the equivalent shear-curvature relationship. The shear force plotted is the column shear force required to develop the dependable flexural strength of the column at each point including the change in

bending moment demand due to dynamic effects and the tension shift effect. These are compared to the shear strength envelope of the column as it degrades with increasing curvature ductility.

As the critical section forms at the curtailment point due to the tension shift effect, the shear force-curvature relationship for this section of the column can be seen to intersect the shear strength envelope for the column. This limits the ultimate curvature of the column at this point due to the development of a flexure-shear failure. Further displacements from the column may be possible through shear deformations but the displacement capacity of this mode of deformation is likely to be limited before failure of the column.

A.1.5 Pier 46 Lateral Displacement Capacity

The elastic flexural displacement at the top of the column can be found by integrating the elastic curvature diagram as shown in Figure A.3. Neglecting fixed end rotations due to strain penetration, the elastic displacement at the top of the column is:-

$$\Delta_y = 46.1\,mm \qquad \text{(A.22)}$$

From Figure A.4 the available ultimate curvature capacity at the curtailment point is limited by the development of a shear failure in the column at this point. The ultimate curvature available is taken where the shear force-curvature diagram intersects the shear strength envelope. This gives an ultimate curvature of $\phi_{u,s} = 0.0110\ m^{-1}$ allowing the available plastic curvature to be established.

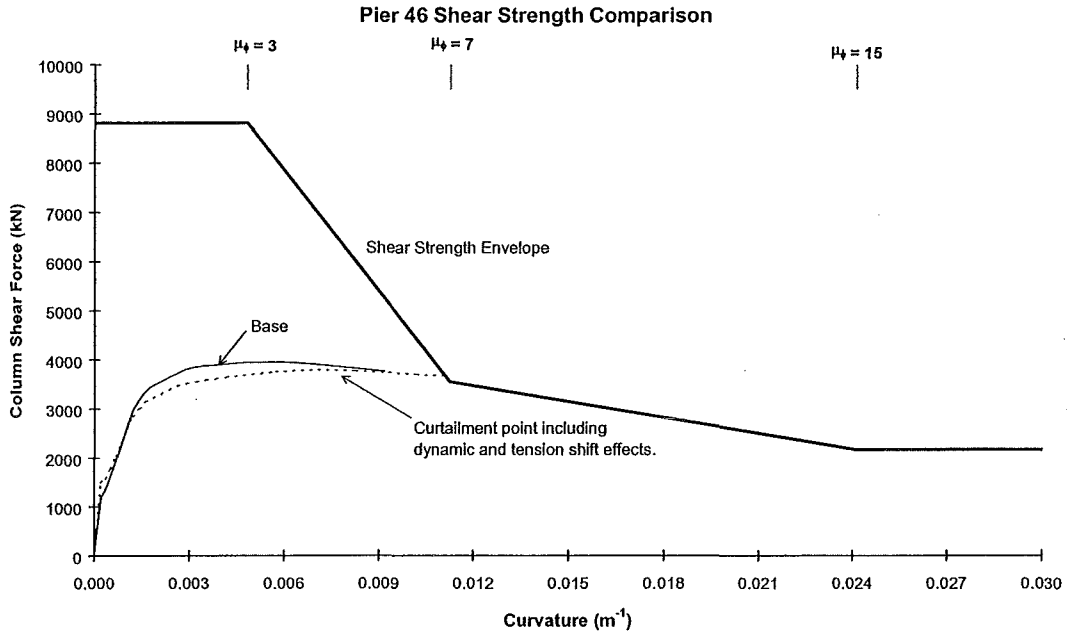

Figure A.4 *Pier 46 Base Shear-Curvature Demand against Column Shear Strength Envelope*

$$\begin{aligned} \phi_p &= \phi_{u,s} - \phi_y \\ &= 0.0110 - 0.00147 \\ &= 0.0095\, m^{-1} \end{aligned} \qquad \text{(A.23)}$$

The plastic displacement at the top of the column is due to rotation in the plastic hinge at the curtailment point. The plastic hinge length, L_p, for a plastic hinge which forms at a point which does not correspond to a point of maximum moment or adjacent to another member is assumed to be equal to the half the diameter, or depth, of the member. Taking $L_p = 0.5\,D$ for the length of the plastic hinge at the curtailment point gives a displacement at the top of the column equal to:-

$$\Delta_p = 42.8\, mm \qquad \text{(A.24)}$$

The lateral displacement capacity at the top of the column is the sum of the elastic displacements due to flexure and displacements through rotation in the plastic hinge.

$$\begin{aligned}\Delta_u &= \Delta_y + \Delta_p \\ &= 46.1 + 42.8 \\ &= 88.9\,mm\end{aligned} \qquad \text{(A.25)}$$

This gives a displacement ductility capacity for the column of:-

$$\begin{aligned}\mu_\Delta &= \frac{\Delta_u}{\Delta_y} \\ &= \frac{88.9}{46.1} \\ &= 1.93\end{aligned} \qquad \text{(A.26)}$$

If the elastic component of lateral deflection due to rotation and translation of the pilecap is assessed to be 80 mm, then the reference yield displacement and structural displacement ductility capacity for Pier 46 is:-

$$\begin{aligned}\Delta_y &= 46.1 + 80 \\ &= 126.1\,mm\end{aligned} \qquad \text{(A.27)}$$

$$\begin{aligned}\Delta_u &= 126.1 + 42.8 \\ &= 168.9\,mm\end{aligned} \qquad \text{(A.28)}$$

and:-

$$\begin{aligned}\mu_\Delta &= \frac{168.9}{126.1} \\ &= 1.34\end{aligned} \qquad \text{(A.29)}$$

Retrofit measures will have to be undertaken if the displacement ductility demand for this pier exceeds the structural displacement ductility capacity for the response spectra derived for the site for an accepted annual probability of exceedance.

A.2 EXAMPLE COLUMN 2

Pier 68 reinforcement layout is shown in Figure A.5. A pilecap overlay retrofit is required to force all inelastic action to occur at the base of the column. The column is 8 feet (2.438 m) in diameter and the centre of mass of the bridge deck, through which the lateral seismic force is assumed to act, is 10.92 m above the top of the 750 mm thick pilecap overlay retrofit. The axial load in the column from the superstructure load is -11,785 kN. A total of 93 longitudinal bars of 2 $^1/_4$ inch (57 mm) diameter are arranged bundled in threes at the base of the column. One third of these bars are curtailed 4.13 m above the top of the pilecap overlay retrofit. A further third of the longitudinal base are curtailed 7.18 m above the pilecap overlay. This gives longitudinal reinforcement ratios, $p_t = 5.11\%$ for the base of the column, $p_t = 3.41\%$ for the lower curtailment point and $p_t = 1.70\%$ for the upper curtailment point. The cover to the transverse reinforcement is 2 inches (50 mm). The distance between the centreline of the transverse hoop is, $D_c = 2.319$ m. The pitch of the longitudinal reinforcement layout is taken as 2.243 m giving a value for g of 0.920.

Transverse reinforcement consists of $^3/_4$ inch (19 mm) diameter circular hoops at 4 inch (102 mm) centres over the base of the column extending to 6 inch (152 mm) centres over the remainder of the column height.

Material properties of $f'_c = 55$ MPa, $f_y = 350$ MPa and $f_{yh} = 286$ MPa are assumed for use in the analysis which gives an axial load ratio of $N^* / f'_c A_g = -0.046$ for this column.

The internal lever arm, tension force contribution and position of the compressive force resultant can be found for the base of Pier 68, the lower and upper curtailment points in the column.

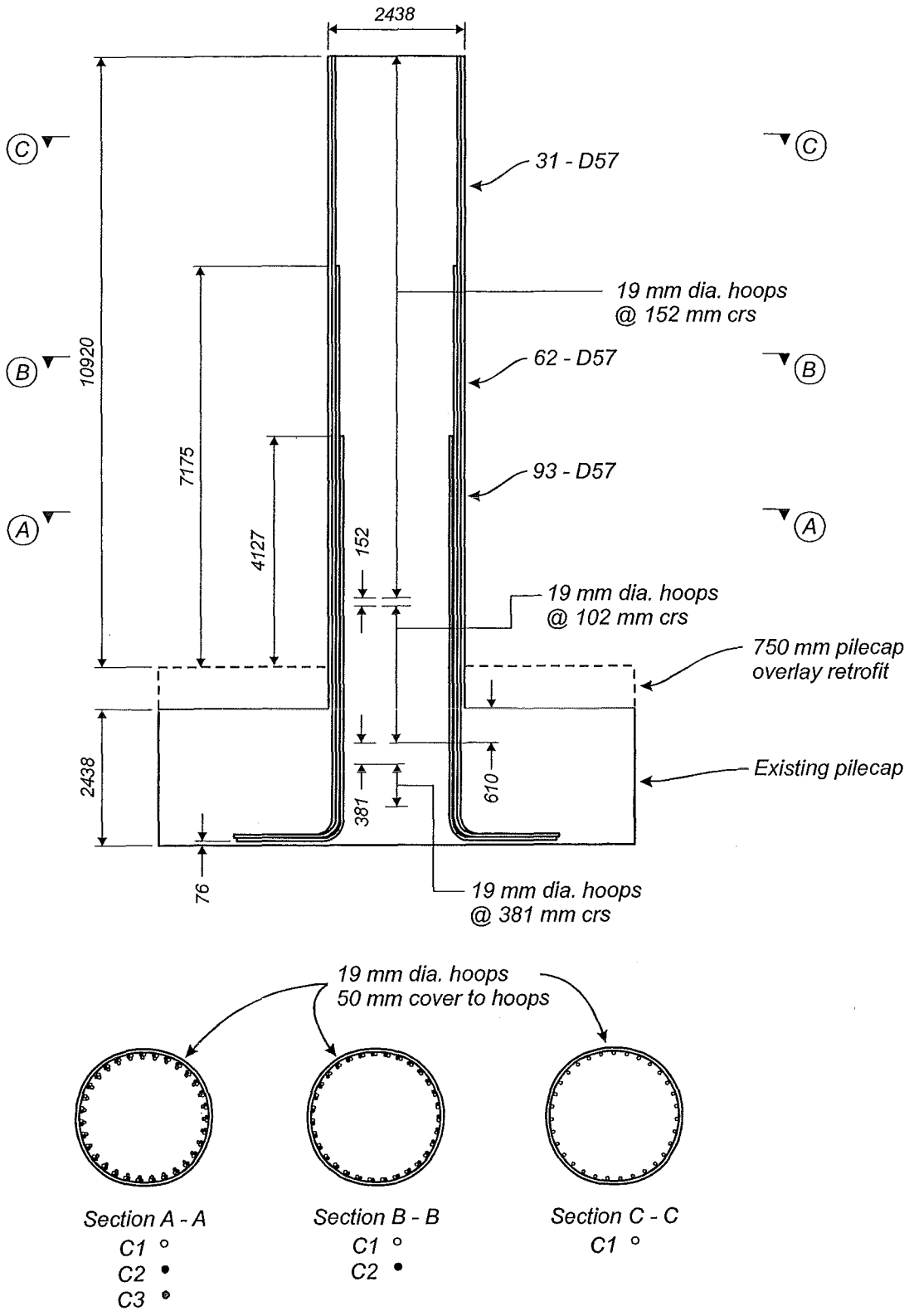

Figure A.5 *Pier 68 Longitudinal and Transverse Column Reinforcement Layout*

A.2.1 Base of Column

From Equation 7.8 the internal lever arm ratio is:-

$$\frac{jd}{D} = 0.588 \qquad \text{(A.30)}$$

Equation 7.10 gives the tension force resultant as a proportion of the total steel reinforcement force in the column.

$$\frac{T}{A_{st} f_y} = 0.580 \qquad \text{(A.31)}$$

The position of the compressive force resultant is given by the term α in Equation 7.12.

$$\alpha = 0.400 \qquad \text{(A.32)}$$

From Equation 7.6 the flexural strength of the column at the base can be established as:-

$$\begin{aligned} M_n &= Tjd + (1-\alpha) jdN^* \\ &= 69{,}425 + 10{,}135 \\ &= 79{,}560 \ kNm \end{aligned} \qquad \text{(A.33)}$$

A.2.2 Lower Curtailment

The internal lever arm ratio for the column at the curtailment sections remains as jd / D = 0.588 from Equation A.30.

At the lower curtailment with curtailment of one third the longitudinal steel Equation 7.10 gives:-

$$\frac{T}{A_{st} f_y} = 0.580 \qquad \text{(A.34)}$$

Equation 7.12 to find the position of the compressive force resultant, α, at the lower curtailment gives:-

$$\alpha = 0.400 \qquad \text{(A.35)}$$

The flexural strength of the column at the lower curtailment point can be established as:-

$$\begin{aligned} M_n &= Tjd + (1-\alpha) jdN^* \\ &= 46{,}285 + 10{,}135 \\ &= 56{,}420\ kNm \end{aligned} \qquad \text{(A.36)}$$

A.2.3 Upper Curtailment

The internal lever arm ratio for the column at the curtailment sections remains as jd / D = 0.588 from Equation A.30.

At the upper curtailment with the remaining one third the longitudinal steel, Equation 7.10 gives:-

$$\frac{T}{A_{st} f_y} = 0.685 \qquad \text{(A.37)}$$

Evaluation of Equation 7.12 to find the position of the compressive force resultant, α, at the upper curtailment gives:-

$$\alpha = 0.308 \qquad \text{(A.38)}$$

The flexural strength of the upper curtailment point can be established as:-

$$\begin{aligned} M_n &= Tjd + (1-\alpha) jdN^* \\ &= 27{,}330 + 11{,}690 \\ &= 39{,}020\ kNm \end{aligned} \tag{A.39}$$

A.2.4 Pier 68 Structural Response

A strength reduction factor of $\phi = 1.0$ is taken to establish the dependable flexural strength of each section. The shear force acting in the column, assuming that a plastic hinge will form at the base of the column, is:-

$$\begin{aligned} V &= \frac{79{,}560 - (0.1)(79{,}560)}{10.920} \\ &= 6{,}560\ kN \end{aligned} \tag{A.40}$$

The tension shift is:-

$$\begin{aligned} e_v &= \frac{(0.588)(2.438)}{2\tan 30^\circ} \\ &= 1.241\ m \end{aligned} \tag{A.41}$$

The increase in the flexural demand due to the tension shift is then:-

$$\begin{aligned} Ve_v &= (6{,}560)(1.241) \\ &= 8{,}140\ kNm \end{aligned} \tag{A.42}$$

The flexural strength envelope and the bending moment demand for Pier 68 has been plotted against the column height as shown in Figure A.6. Also shown is the moment demand due to the tension shift effect occurring in the column accounted for by increasing the bending moment above the base of the column by a moment equal to Ve_v.

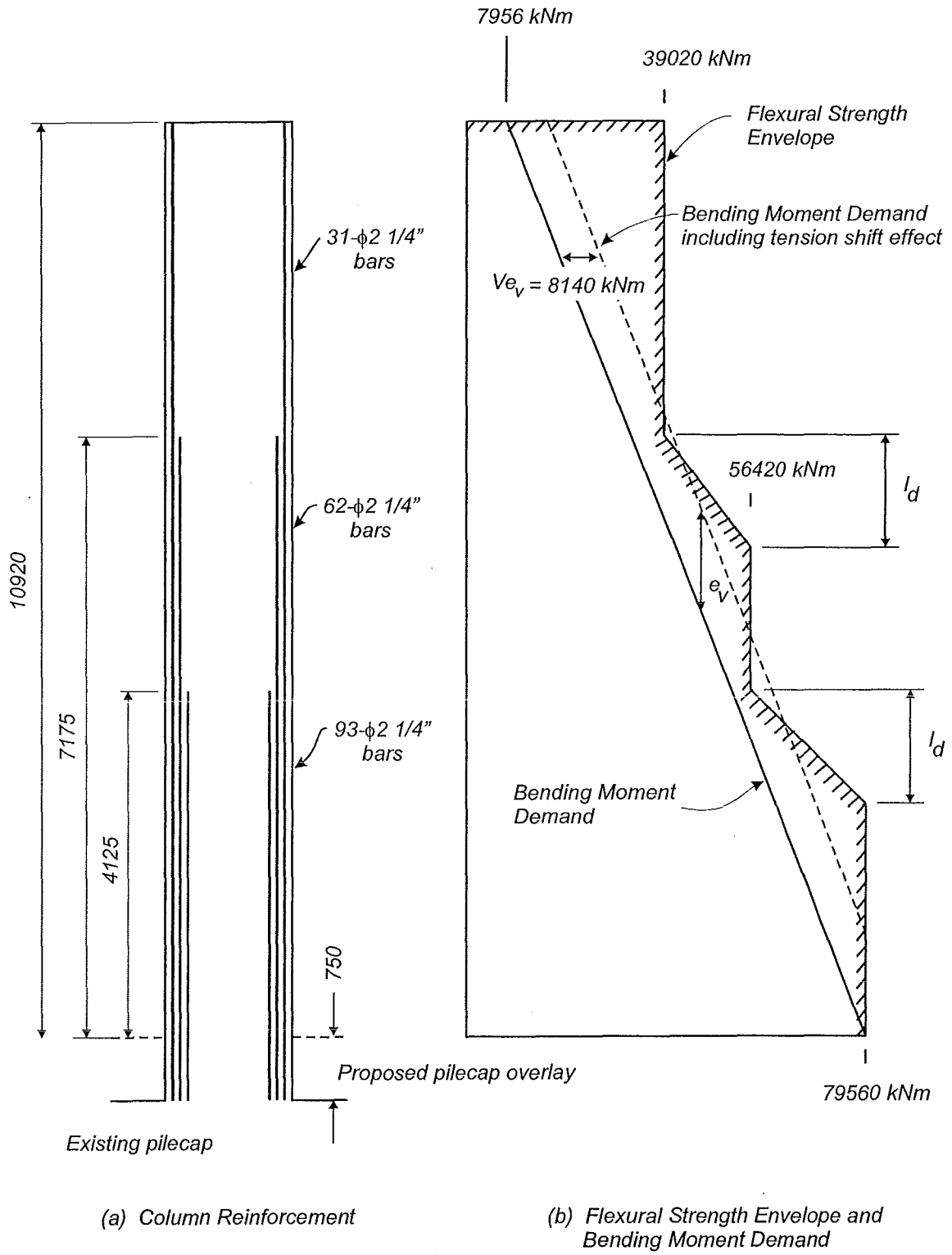

Figure A.6 *Pier 68 Flexural Strength Envelope and Bending Moment Demand due to the Tension Shift Effect*

From Figure A.6 it can be seen that the shifted bending moment diagram, corresponding to the moment demand including the tension shift effect, exceeds the flexural strength envelope for this column at the upper and lower curtailment points. Moment-curvature analyses for each section of the column give a more realistic value for the nominal flexural strength of each section by accounting for the effects of concrete confinement and strain hardening of the longitudinal reinforcement. The dependable flexural strength envelope can be redrawn using the flexural strengths obtained from the moment-curvature analysis.

Moment-curvature analyses for Pier 68 give nominal flexural strengths at the base of 81,826 kNm at a yield curvature $\phi_{y,b} = 0.00176\ m^{-1}$, 59,238 kNm for the lower curtailment at a yield curvature of $\phi_{y,l} = 0.00167\ m^{-1}$ and 37,119 kNm for the upper curtailment at a yield curvature of $\phi_{y,u} = 0.00157\ m^{-1}$. The dependable flexural strengths can be taken using a strength reduction factor of $\phi = 1.0$. As the dependable flexural strength envelope at the curtailment point is reached before the dependable flexural strength at the base of the column is reached, the bending moment demand must be redrawn so that the dependable flexural strength at the curtailment point is just reached when the tension shift is included.

Evaluation of the bending moment demand using the dependable flexural strengths obtained from the moment-curvature analyses indicates the upper curtailment point has the larger strength shortfall when the dependable flexural strength at the base of the column is developed. The base moment attained when the upper curtailment point reaches its dependable flexural strength can be determined from Equation A.13 giving a base moment of 72,469 kNm.

The column shear force corresponding to this base moment is:-

$$V = \frac{72{,}469 - (0.1)(72{,}469)}{10.920} = 5{,}970\ kN \qquad \text{(A.43)}$$

The increase in bending moment demand due to the tension shift effect is:-

$$Ve_v = (5{,}970)(1.241) = 7{,}410\,kNm \quad \text{(A.44)}$$

The elastic curvature distribution for the column can be established using the bi-linear moment-curvature approximations to determine the curvatures in the column according to the moment acting at each section. The bending moment demand and curvature distribution are shown in Figure A.7. The elastic flexural displacements at the top of the column can be found by integrating the curvature diagram. Further displacements through fixed end rotations of the column caused by strain penetration in the longitudinal reinforcement at the base and at the curtailment points have been neglected.

The shear capacity of this column will have to be evaluated to ensure that the shear strength of the column is sufficient to resist the imposed shear forces when the flexural strength of the column is reached and to determine the available ultimate curvature of this section.

A.2.5 Pier 68 Shear Strength Assessment

Pier 68 has $^3/_4$ inch (19 mm) diameter transverse hoops placed at 4 inch (102 mm) centres at the base of the column extending to 6 inch (152 mm) centres where the longitudinal bars are curtailed. Following the method proposed by Priestley et al [P3, P4] outlined in Section 7.4.2 the shear strength of Pier 68 at the base and over the curtailed sections of the column can be found assuming $f'_c = 55$ MPa, $f_{yh} = 286$ MPa and $N^* = -11785$ kN. Again the component of shear resistance provided by the axial load has been neglected as it cannot be transferred through the column where the critical section has formed.

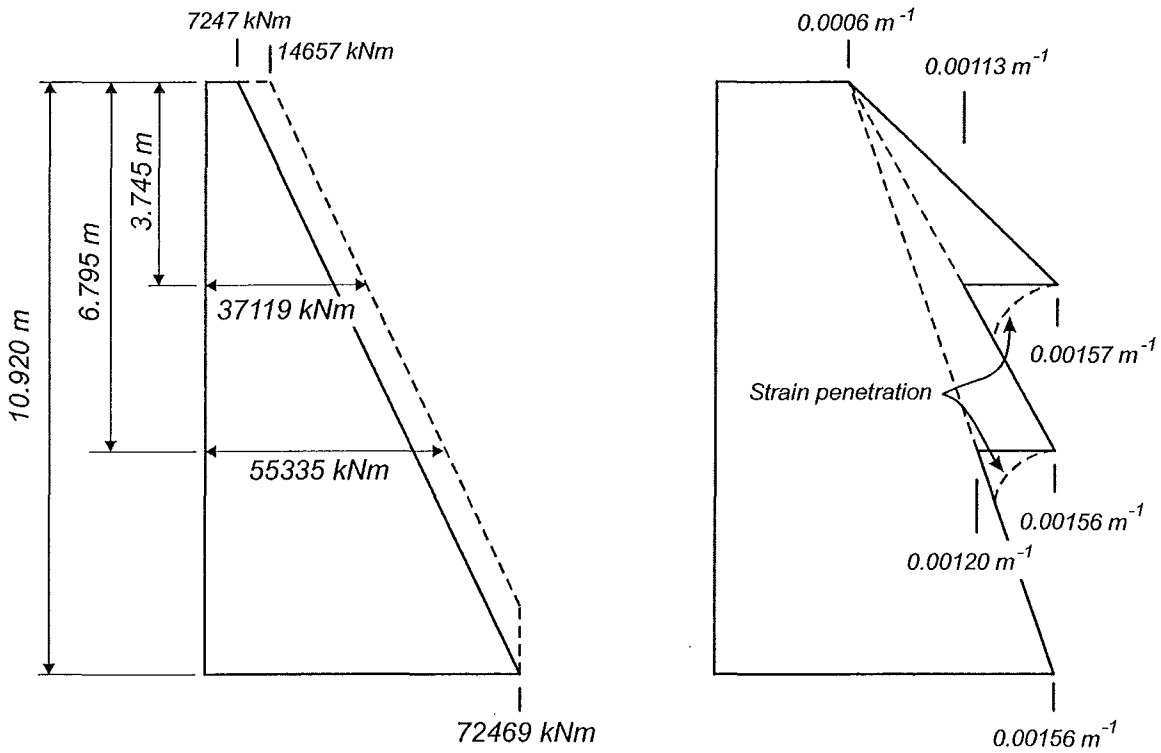

Figure A.7 *Bending Moment Diagram and Elastic Curvature Distribution for Pier 68 at Development of Flexural Strength of the Upper Curtailment Point due to the Tension Shift Effect*

At base of column:-

$$
\begin{aligned}
V_n &= V_s + V_c \\
&= 5{,}120 + 8{,}030 \\
&= 13{,}150\,\text{kN} \qquad \text{for } k = 0.29 \\
&= 5{,}120 + 2{,}770 \\
&= 7{,}890\,\text{kN} \qquad \text{for } k = 0.10 \\
&= 5{,}120 + 1{,}385 \\
&= 6{,}505\,\text{kN} \qquad \text{for } k = 0.05
\end{aligned}
\tag{A.45}
$$

At the upper and lower curtailment points in column:-

$$
\begin{aligned}
V_n &= V_s + V_c \\
&= 3{,}415 + 8{,}030 \\
&= 11{,}445\ \text{kN} && \text{for } k = 0.29 \\
&= 3{,}415 + 2{,}270 \\
&= 5{,}685\ \text{kN} && \text{for } k = 0.10 \\
&= 3{,}415 + 1{,}385 \\
&= 4{,}800\ \text{kN} && \text{for } k = 0.05
\end{aligned}
\qquad \text{(A.46)}
$$

The shear force at development of the flexural strength of the column at the base of Pier 68 is 5,970 kN which exceeds the residual shear strength of the column at the curtailment points. There is a possibility that the column could fail through shear around the upper curtailment point when the flexural strength of this section of the column is reached.

In Figure A.8 the equivalent shear-curvature relationship to develop the flexural strength at the base and each curtailment point are shown along with the shear strength envelope for the base and curtailment points. It can be seen that the shear-curvature relationship for developing the strength of the upper curtailment point meets the shear strength envelope for the curtailment points indicating that the available ultimate curvature of this section is limited by the development of a shear failure in the column.

A.2.6 Pier 68 Lateral Displacement Capacity

The elastic flexural displacement at the top of the column can be found by integrating the elastic curvature diagram as shown in Figure A.7. The elastic displacement at the top of the column is:-

$$\Delta_y = 81.7\,mm \qquad \text{(A.47)}$$

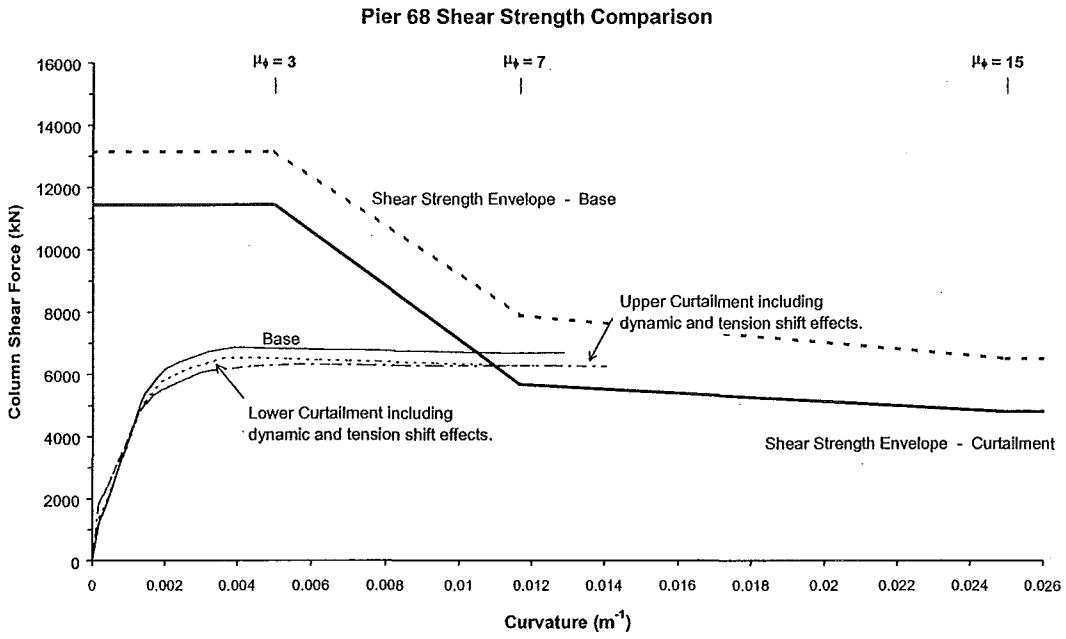

Figure A.8 *Pier 68 Shear-Curvature Demand against Column Shear Strength Envelope*

From Figure A.8 the available ultimate curvature capacity at the upper curtailment point is limited by the development of a shear failure in the column at this point. The ultimate curvature available is taken where the shear force-curvature diagram intersects the shear strength envelope giving an ultimate curvature of $\phi_{u,s} = 0.0109\ m^{-1}$ allowing the available plastic curvature to be established.

$$\begin{aligned} \phi_p &= \phi_{u,s} - \phi_y \\ &= 0.0109 - 0.00157 \\ &= 0.0093\, m^{-1} \end{aligned} \qquad \text{(A.48)}$$

The plastic displacement at the top of the column is due to rotation in the plastic hinge at the upper curtailment point. The plastic hinge length, L_p, for a plastic hinge which forms at a point which does not correspond to a point of maximum moment or adjacent to another member is assumed to be equal to the half diameter, or depth, of the member. Taking $L_p = 0.5\ D$ for the length of the plastic hinge at the curtailment point gives a displacement at the top of the column equal to:-

$$\Delta_p = 35.5\,mm \tag{A.49}$$

The lateral displacement capacity at the top of the column is the sum of the elastic displacements due to flexure and displacements through rotation in the plastic hinge.

$$\begin{aligned}\Delta_u &= \Delta_y + \Delta_p \\ &= 81.7 + 35.5 \\ &= 117.2\,mm\end{aligned} \tag{A.50}$$

This gives a displacement ductility capacity for the column of:-

$$\begin{aligned}\mu_\Delta &= \frac{\Delta_u}{\Delta_y} \\ &= \frac{117.2}{81.7} \\ &= 1.43\end{aligned} \tag{A.51}$$

If the elastic component of lateral deflection due to rotation and translation of the pilecap of this pier is assessed to be 165 mm, then the reference yield displacement and structural displacement ductility capacity for Pier 68 is:-

$$\begin{aligned}\Delta_y &= 81.7 + 165 \\ &= 246.7\,mm\end{aligned} \tag{A.52}$$

$$\begin{aligned}\Delta_u &= 246.7 + 35.5 \\ &= 282.2\,mm\end{aligned} \tag{A.53}$$

and:-

$$\begin{aligned}\mu_\Delta &= \frac{282.2}{246.7} \\ &= 1.14\end{aligned} \tag{A.54}$$

Retrofit measures will have to be undertaken if the displacement ductility demand for this pier exceeds the structural displacement ductility capacity for the response spectra derived for the site for an accepted annual probability of exceedance.

A.3 EXAMPLE COLUMN 3

The reinforcement layout for the example rectangular column is shown in Figure A.9. The column has overall dimensions of 1000 mm by 1800 mm. Material properties of $f'_c = 30$ MPa and $f_y = 300$ MPa were specified for the original design of this column. A total of 44 longitudinal bars of 32 mm diameter have been placed bundled in pairs at the base of the column arranged at equal spacing around the faces of the column. One half of the longitudinal bars have been curtailed 2.9 metres above the base of the column. The longitudinal steel ratio for the base of the column is 1.97% and for the curtailed section is 0.98%. Cover to the longitudinal bars is 50 mm.

A two column bent supports the bridge superstructure which will respond primarily as a cantilever when loaded longitudinally to the axis of the bridge with the lateral seismic force assumed to act 5.4 metres above the base of the column. The transverse response of the bridge will create moments in the fixed ends at the top and bottom of the column. The bottom of the cap beam supporting the superstructure is assumed to be 4.3 metres above the base of the column. The cap beam is assumed to have sufficient strength so that premature failure of the cap beam will not occur before the desired mechanism forms in the columns.

Transverse reinforcement placed in the column consists of 16 mm diameter hoops with four legs in the transverse and longitudinal directions. The transverse hoop layout does not satisfy the current New Zealand Concrete Structures Standard [X2] requirements to confine the concrete in the core. The transverse hoop sets are spaced at 200 mm centres which are approximately 6 times the longitudinal bar diameter, less than the 10 longitudinal bar diameter spacing specified to prevent premature buckling of column longitudinal reinforcement for columns detailed for limited ductility. The distance between longitudinal bars restrained by a corner of a hoop or

cross-tie exceeds the limit of one third the adjacent section dimension along the long face of the column.

A total axial load from the dead load of the superstructure of -8,000 kN is assumed to act on this bent.

A.3.1 Longitudinal Flexural Strength

The compressive axial load acting in each column of the bent is -4,000 kN. Only specified material strengths are known so realistic values for the probable material strengths must be used for the assessment. In lieu of destructive material testing to determine existing material strengths the following probable material strengths are suggested for assessment [P3]:-

$$\begin{aligned} f'_{ca} &= 1.5f'_c \\ f_{ya} &= 1.1f_y \end{aligned} \qquad \text{(A.55)}$$

This gives values for $f'_{ca} = 45$ MPa and $f_{ya} = 330$ MPa and an axial load ratio for this column of –0.049. With 50 mm cover to the main bars the value of g is 0.927 for this direction of loading.

A.3.1.1 Longitudinal Direction - Base

The internal lever arm ratio for this column is given by Equation 7.7.

$$\frac{jd}{D} = 0.671 \qquad \text{(A.56)}$$

Equation 7.9 gives the tension force resultant as a proportion of the total reinforcement yield force in the column.

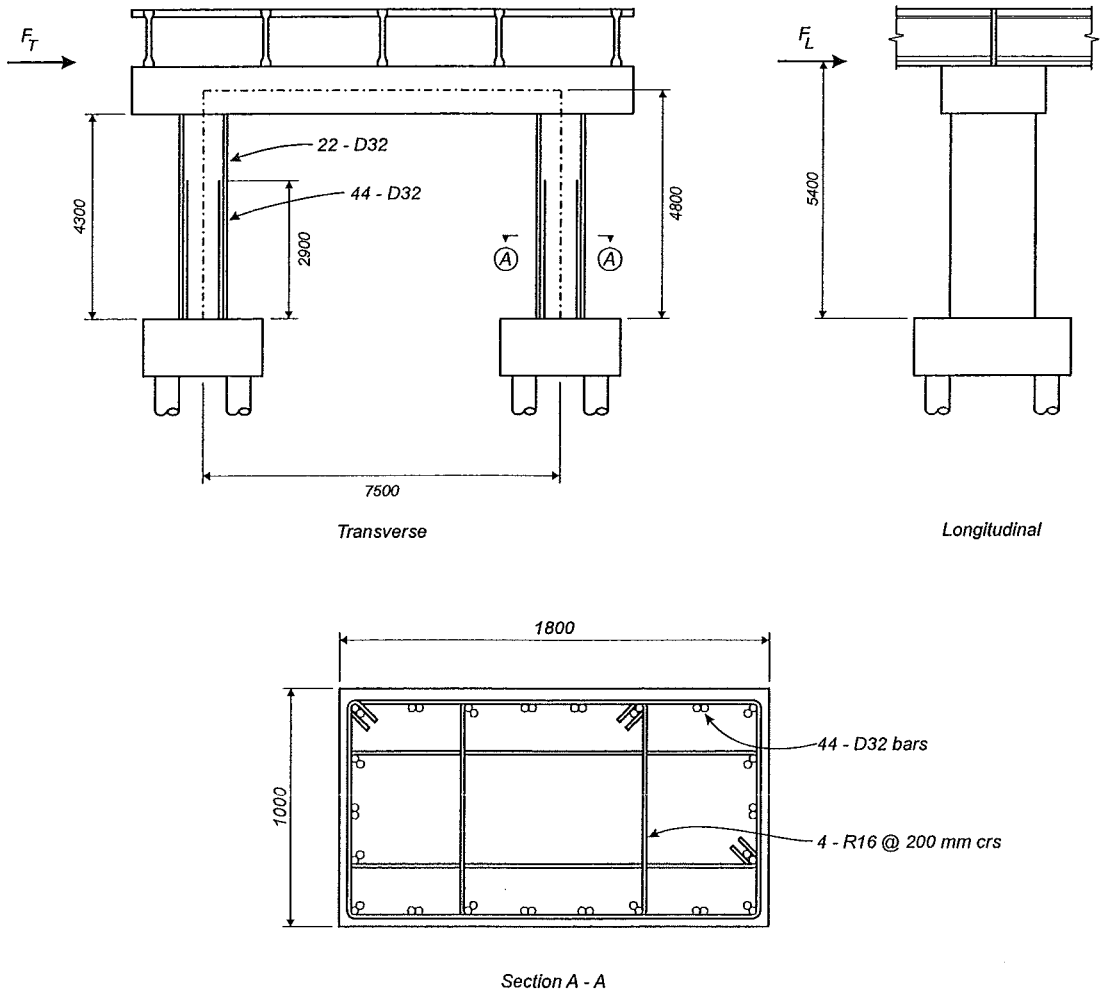

Figure A.9 *Example Rectangular Column Reinforcement Layout*

$$\frac{T}{A_{st} f_y} = 0.691 \tag{A.57}$$

Equation 7.11 gives the position of the compressive force resultant:

$$\alpha = 0.333 \tag{A.58}$$

The flexural strength of this section can now be determined from Equation 7.6:

$$
\begin{aligned}
M_n &= Tjd + (1-\alpha)jdN^* \\
&= 9{,}745 + 3{,}220 \\
&= 12{,}965\ kNm
\end{aligned}
\qquad \text{(A.59)}
$$

A.3.1.2 Longitudinal Direction - Curtailment Point

The values for the internal lever arm, the tension force resultant and position of the compression force resultant remain the same for the curtailment section as determined in Equations A.56 - A.58. The area of longitudinal steel at the curtailment point is halved and the flexural strength of the curtailment section can be determined from Equation 7.6:-

$$
\begin{aligned}
M_n &= Tjd + (1-\alpha)jdN^* \\
&= 4{,}870 + 3{,}220 \\
&= 8{,}090\ \text{kNm}
\end{aligned}
\qquad \text{(A.60)}
$$

A.3.2 Transverse Flexural Strength

The axial load acting in each column is increased or decreased due to the shear force carried in the cap beam. As the flexural strength of a column is influenced by the level of axial load a trial and error process is required to determine the levels of axial load and the amount of shear carried in each column. For transverse structural response the tension column has the axial load reduced from -4,000 kN to -2,500 kN and the compression column has the axial load increased to -5,500 kN due to the transverse seismic forces. This gives axial load ratios of -0.031 and -0.068 for the tension and compression columns respectively. The value of g for this direction of loading is 0.868.

A.3.2.1 Transverse Direction - Base

The internal lever arm for each columns is given by Equation 7.8:-

$$\frac{jd}{D} = 0.647 \qquad \text{(A.61)}$$

The tension force contribution and position of the compressive force resultant are dependent on the axial load ratio as shown in Equations 7.10 and 7.12 respectively.

For the tension column the contribution of the tension force resultant is:-

$$\frac{T}{A_{st} f_y} = 0.713 \qquad \text{(A.62a)}$$

and for the compression column:-

$$\frac{T}{A_{st} f_y} = 0.668 \qquad \text{(A.62b)}$$

The position of the compressive force resultant for the tension column is:-

$$\alpha = 0.320 \qquad \text{(A.63a)}$$

and for the compression column:-

$$\alpha = 0.345 \qquad \text{(A.63b)}$$

The nominal flexural strength for the base of the tension and compression columns can be found to be 6,485 kNm and 7,375 kNm respectively.

A.3.2.2 Transverse Direction – Curtailment Point

The values for the internal lever arm, tension force contribution and position of the compressive force resultant are the same for the curtailment point as for the base of the columns. The nominal flexural strength of the tension column is 3,795 kNm and 4,855 kNm for the compression column.

A.3.3 Rectangular Column Structural Response

A strength reduction factor of $\phi = 1.0$ is taken to establish the dependable flexural strength of each section of the column. Dynamic effects due to the rotational inertia of the superstructure are assumed to increase the moment at the centre of mass of the superstructure by 10 % of the moment at the base of the column for the longitudinal structural response. Due to a predominantly translatory response of the structure in the transverse direction dynamic effects will not change the bending moment demand on the structure in this direction.

A.3.3.1 Longitudinal Response

Taking the formation of a critical section at the base of the column, the shear force corresponding to this base moment is :-

$$\begin{aligned} V &= \frac{12{,}965 - (0.1)(12{,}965)}{5.400} \\ &= 2{,}160\,kN \end{aligned} \tag{A.64}$$

The tension shift is:-

$$\begin{aligned} e_v &= \frac{(0.671)(1.800)}{2\tan 30°} \\ &= 1.046\,m \end{aligned} \tag{A.65}$$

The increase in the bending moment demand due to the tension shift is:-

$$\begin{aligned} Ve_v &= (2{,}160)(1.046) \\ &= 2{,}260\,kNm \end{aligned} \tag{A.66}$$

The dependable flexural strength envelope and the bending moment demand for the rectangular column under longitudinal structural response been plotted against the column height in Figure A.10 including the tension shift effect.

From Figure A.10 it can be seen that the shifted bending moment diagram, corresponding to the moment demand including the tension shift effect, exceeds the flexural strength envelope at the position of the curtailment point. This indicates that the formation of a critical section at the curtailment point will occur before the dependable flexural strength at the base of the column is reached.

Further detailed assessment of the column, including moment-curvature analysis and assessment of the column's shear strength, are required to ensure these are sufficient to meet the expected force and inelastic displacement demands to be imposed on the column.

Moment-curvature analysis of the column in the longitudinal direction gives a yield moment for the base of the column of 12,126 kNm and for the curtailment of 8,022 kNm. The yield curvature for each section is 0.00200 m^{-1} and 0.00187 m^{-1} for the base and curtailment point respectively. Evaluation of the bending moment demand so that the flexural strength of the curtailment point is reached when the tension shift is included gives a base moment for the column of 11,610 kNm.

The column shear force corresponding to this base moment is:-

$$V = \frac{11{,}610 - (0.1)(11{,}610)}{5.400} = 1{,}935\,kN \qquad \text{(A.67)}$$

The increase in bending moment demand due to the tension shift effect is:-

$$Ve_v = (1{,}935)(1.046) = 2{,}025\,kNm \qquad \text{(A.68)}$$

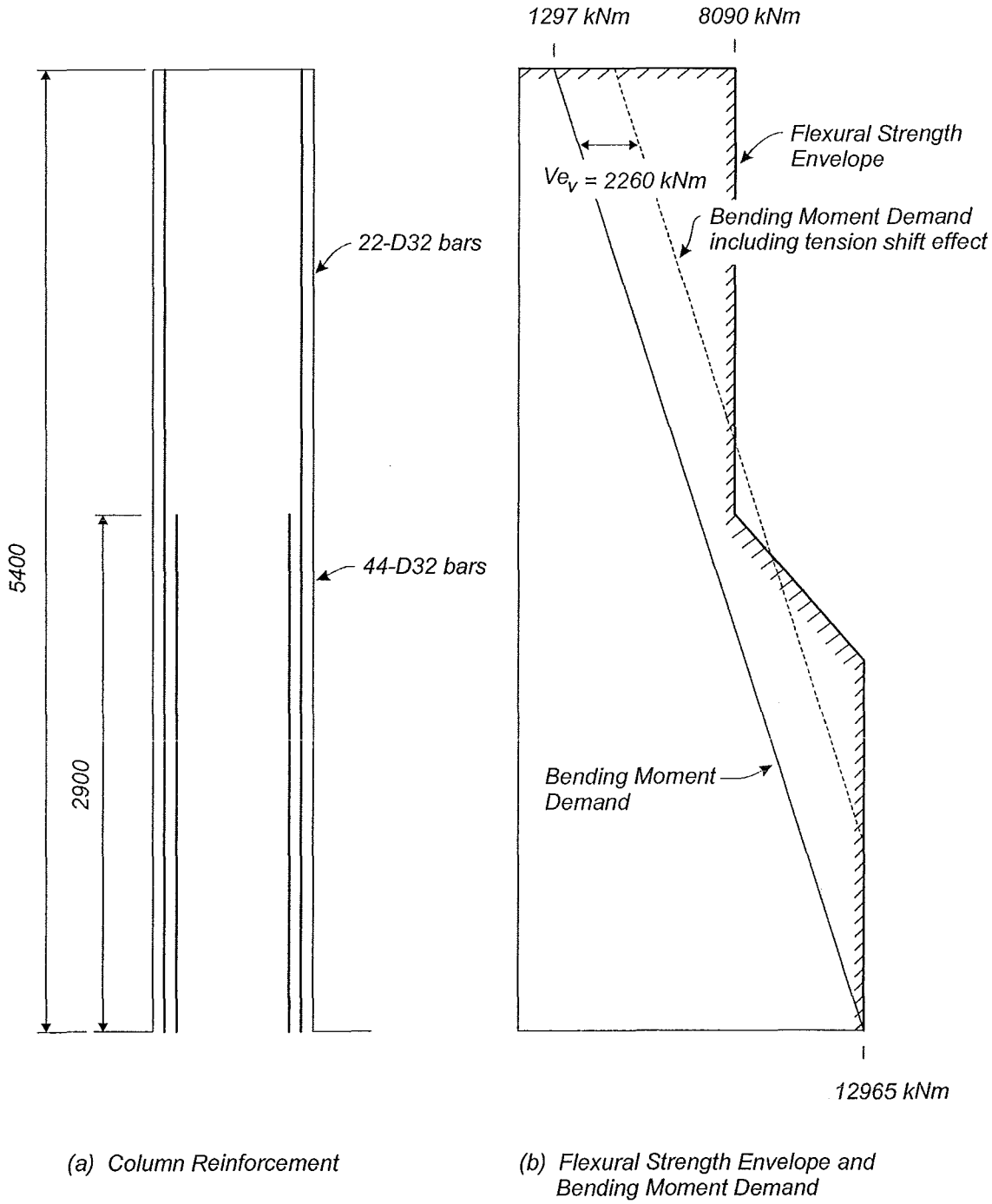

Figure A.10 *Rectangular Column Longitudinal Structural Response Flexural Strength Envelope and Bending Moment Demand*

The elastic curvature distribution for the column can be established using the bi-linear moment-curvature approximations to determine the curvatures in the column according to the moment acting at each section. The bending moment demand and corresponding elastic curvature distribution is shown in Figure A.11.

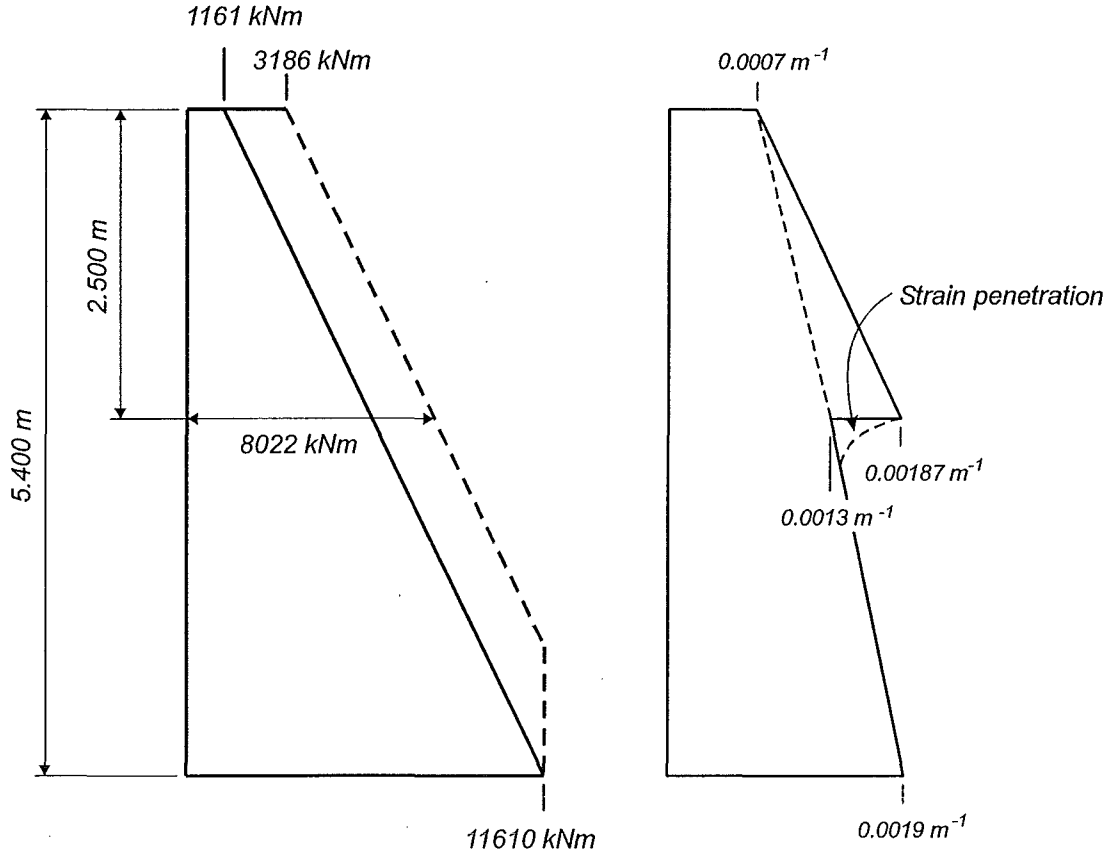

Figure A.11 *Rectangular Column Longitudinal Direction Bending Moment Demand and Elastic Curvature Distribution*

A.3.3.2 Transverse Response

Assuming the longitudinal structural response governs the flexural response of the structure, the transverse design moments will be equal to or less than the flexural capacity of the columns in this direction. Following capacity design principles, the design lateral force in the transverse direction must be taken at development of the nominal flexural strengths of the columns in the transverse direction.

The transverse shear force at development of the flexural strength of the tension column is:-

$$V_T = \frac{M_{T,T} + M_{T,B}}{L} = \frac{6{,}485 + 3{,}795}{4.300} = 2{,}390\ kN \qquad \text{(A.69a)}$$

and for the compression column:-

$$V_C = \frac{M_{C,T} + M_{C,B}}{L} = \frac{7{,}375 + 4{,}855}{4.300} = 2{,}845\ kN \qquad \text{(A.69b)}$$

The tension shift for both columns is:-

$$e_v = \frac{(0.647)(1.000)}{2\tan 30°} = 0.560\ m \qquad \text{(A.70)}$$

The increase in flexural demand due to the tension shift is:-

$$Ve_v = (2{,}390)(0.560) = 1{,}340\ kNm \qquad \text{(A.71a)}$$

for the tension column, and :-

$$Ve_v = (2{,}845)(0.560) = 1{,}595\ kNm \qquad \text{(A.71b)}$$

for the compression column.

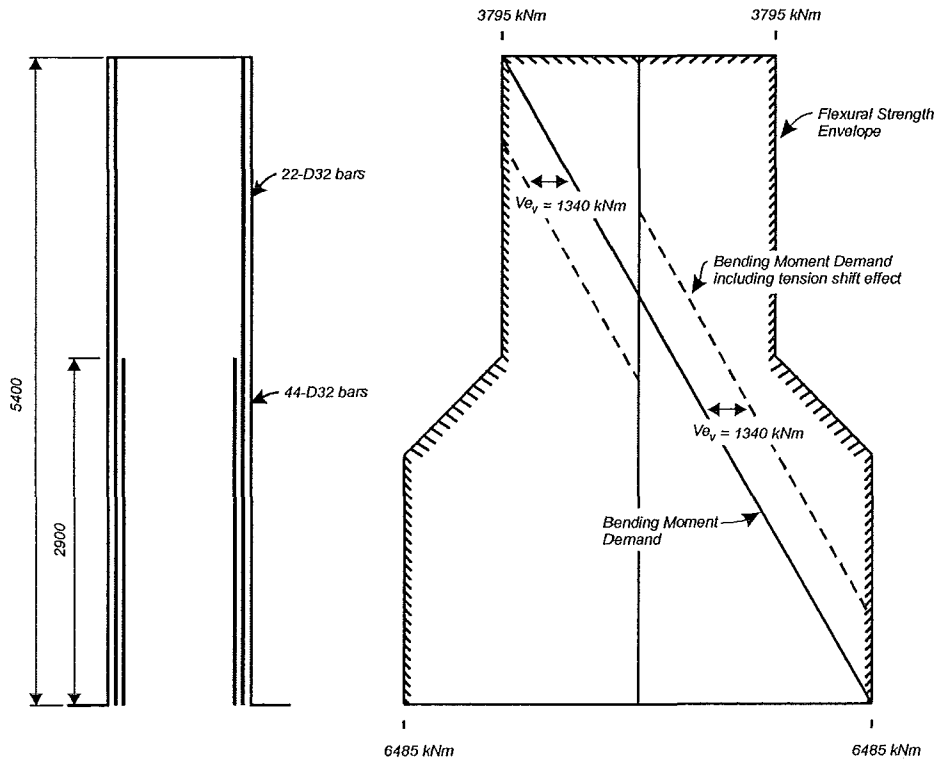

(a) "Tension" Column

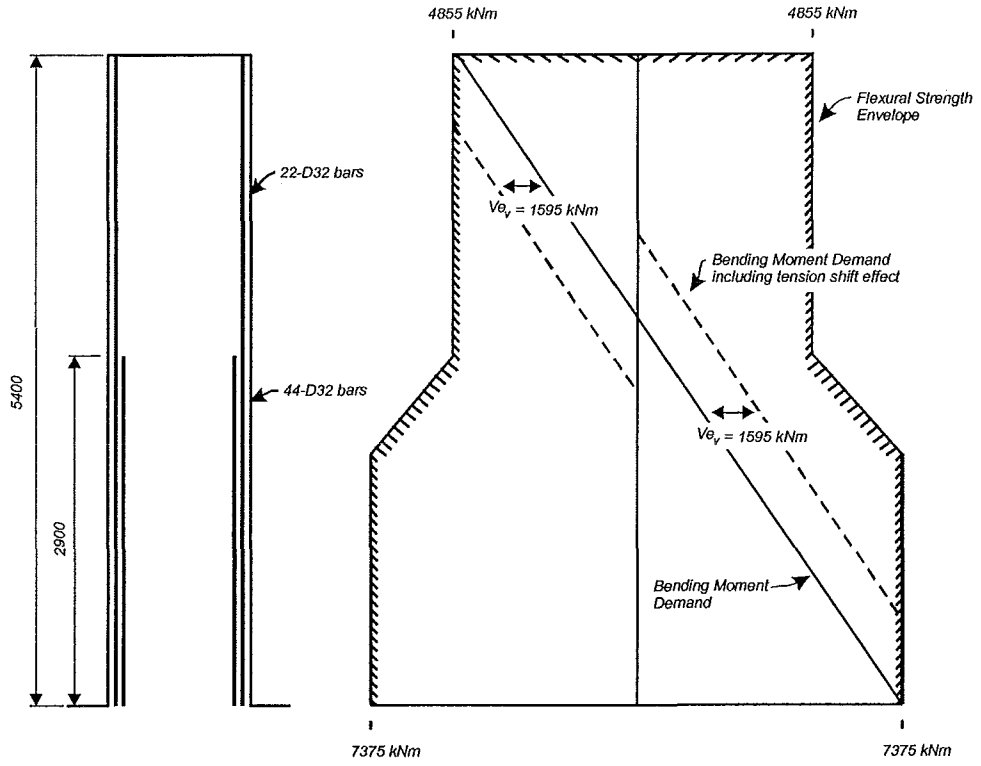

(b) "Compression" Column

Figure A.12 *Rectangular Column Transverse Response Flexural Strength Envelope and Bending Moment Demand*

The bending moment demand and dependable flexural strength envelope for each column for the transverse response is shown in Figure A.12 including the tension shift effect. It can be seen that the bending moment demand including the tension shift does not exceed the dependable flexural strength envelope for either column in this direction. A further check corresponding to the column overstrength moment should be carried out to ensure that development of the column overstrength does not lead to the formation of a critical section at the curtailment point.

A.3.4 Rectangular Column Shear Strength Assessment

A.3.4.1 Longitudinal Direction Shear Strength

The example rectangular column has four legs of 16 mm diameter hoops placed at 200 mm centres over the entire height of the column. Following the method proposed by Priestley et al. [P3, P4] outlined in Section 7.4.2 the shear strength of this column can be found assuming $f'_{ca} = 45$ MPa, $f_{yh} = 300$ MPa, taking the lower design strength value for the transverse reinforcement yield strength. The component of shear resistance provided by the axial load has been neglected as it cannot be transferred through the column when the critical section has formed above the base of the column.

Therefore the shear strength of the column in the longitudinal direction is:-

$$\begin{aligned} V_n &= V_s + V_c \\ &= 2{,}070 + 2{,}800 \\ &= 4{,}870\ \text{kN} \qquad \text{for } k = 0.29 \\ &= 2{,}070 + 965 \\ &= 3{,}035\ \text{kN} \qquad \text{for } k = 0.10 \\ &= 2{,}070 + 480 \\ &= 2{,}550\ \text{kN} \qquad \text{for } k = 0.05 \end{aligned} \tag{A.72}$$

The shear force required to develop the flexural strength at the curtailment point in

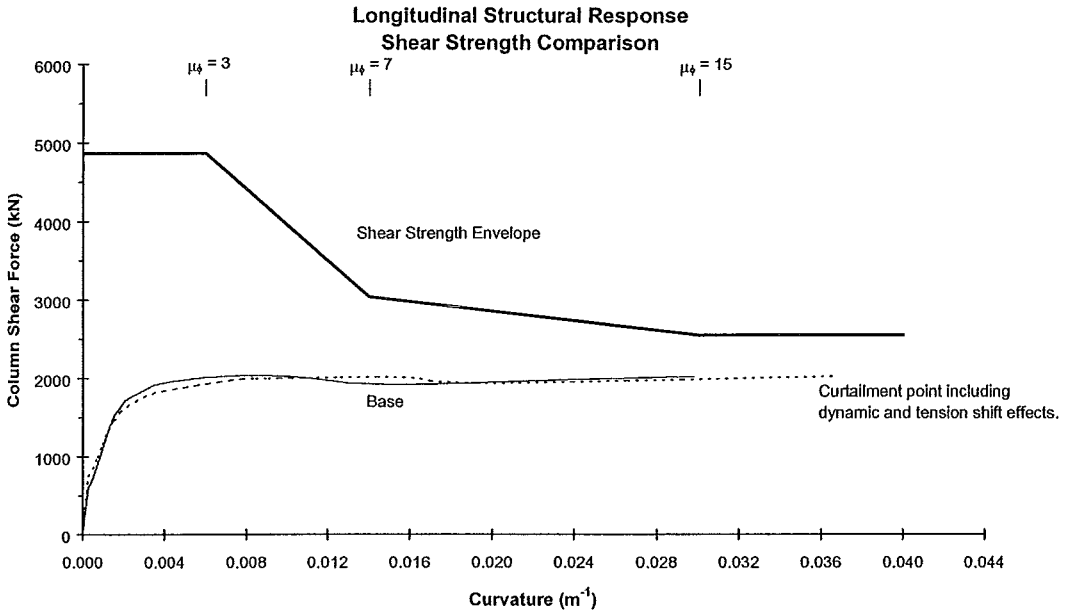

Figure A.13 *Rectangular Column Longitudinal Shear-Curvature Demand against Column Shear Strength Envelope*

the column is expressed as an equivalent shear force-curvature relationship in Figure A.13. Also shown is the shear force envelope for the column in the longitudinal direction. This indicates that the flexural strength at the base of the column will be reached sometime after development of the flexural strength is developed at the curtailment point due to a small degree of strain hardening occurring at the curtailment point. The available ultimate curvature for the column in this direction is not limited by the development of a shear failure in the column at the curtailment point and an ultimate curvature due to flexure of $\phi_{u,f} = 0.0368\ m^{-1}$ can be achieved.

A.3.4.2 Transverse Direction Shear Strength

The tension shift effect does not affect the response of the structure in the transverse Direction as the dependable flexural strength of the column is not reached. Moment-curvature analysis of the columns in the transverse direction indicate no significant overstrength moment is developed and assessment of the column for

tension shift effects at higher base moments is therefore not required. Assessment of the shear strength of the columns in this direction is carried out following the procedure outlined in Section 7.4.2. The contribution to the column shear strength due to the axial load component, due to the double bending of the column is included, as the critical section forms at the base of the column and the shear component from the axial load can be transferred through the entire column.

The shear strength of the columns in the transverse direction are assessed at:-

$$\begin{aligned} V_n &= V_c + V_s + V_p \\ &= 2{,}800 + 1{,}915 + 545 \\ &= 5{,}260\ kN \qquad \text{for } k = 0.29 \\ &= 965 + 1{,}915 + 545 \\ &= 3{,}425\ kN \qquad \text{for } k = 0.10 \\ &= 480 + 1{,}915 + 545 \\ &= 2{,}940\ kN \qquad \text{for } k = 0.05 \end{aligned} \tag{A.73a}$$

for the tension column and:-

$$\begin{aligned} V_n &= V_c + V_s + V_p \\ &= 2{,}800 + 1{,}915 + 1{,}180 \\ &= 5{,}895\ kN \qquad \text{for } k = 0.29 \\ &= 965 + 1{,}915 + 1{,}180 \\ &= 4{,}060\ kN \qquad \text{for } k = 0.10 \\ &= 480 + 1{,}915 + 1{,}180 \\ &= 3{,}575\ kN \qquad \text{for } k = 0.05 \end{aligned} \tag{A.73b}$$

for the compression column.

The shear strength envelope for both columns are shown in Figure A.14 along with the equivalent shear-curvature relationship corresponding to the development of the flexural strength of the base of each column. The available ultimate curvature for

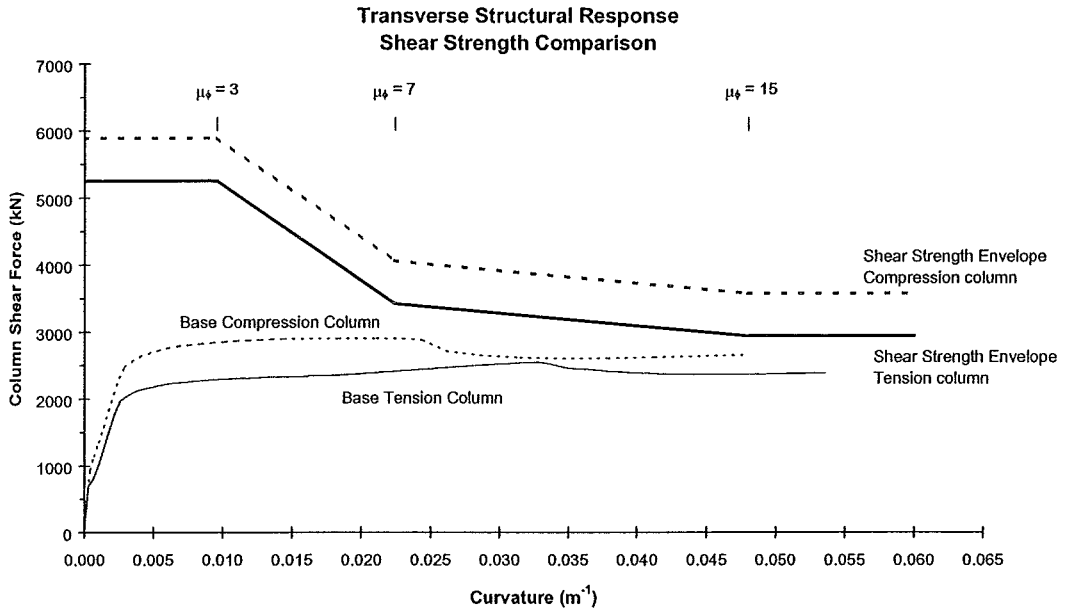

Figure A.14 *Rectangular Column Transverse Shear-Curvature Demand against Column Shear Strength Envelope*

both columns are limited by the ultimate flexural ductility indicating the shear strength of both columns in this direction is adequate to meet the expected demand.

A.3.5 Rectangular Column Lateral Displacement Capacity

A.3.5.1 Longitudinal Direction Displacement Capacity

The development of the critical section at the curtailment point in the longitudinal direction leads to the concentration of the inelastic displacements at this point in the column. The elastic displacements of the column can be obtained by integrating the curvature diagram shown in Figure A.11 to give:-

$$\Delta_y = 19.0\,mm \qquad \text{(A.74)}$$

The available ultimate curvature of this column is $\phi_{u,f} = 0.0368\ m^{-1}$. Therefore the available plastic curvature is:-

$$\begin{aligned}\phi_p &= \phi_{u,f} - \phi_y \\ &= 0.0368 - 0.00187 \\ &= 0.0349\ m^{-1}\end{aligned} \qquad \text{(A.75)}$$

The plastic displacement at the top of the column is due to rotation in the plastic hinge at the upper curtailment point. The plastic hinge length, L_p, for a plastic hinge which forms at a point which does not correspond to a point of maximum moment or adjacent to another member is assumed to be equal to the half diameter, or depth, of the member. Taking $L_p = 0.5\ D$ for the length of the plastic hinge at the curtailment point gives a displacement at the top of the column equal to:-

$$\Delta_p = 64.4\ mm \qquad \text{(A.76)}$$

The lateral displacement capacity at the top of the column is the sum of the elastic displacements due to flexure and displacements through rotation in the plastic hinge.

$$\begin{aligned}\Delta_u &= \Delta_y + \Delta_p \\ &= 19.0 + 64.4 \\ &= 83.4\ mm\end{aligned} \qquad \text{(A.77)}$$

This gives a displacement ductility capacity for the column of:-

$$\begin{aligned}\mu_\Delta &= \frac{\Delta_u}{\Delta_y} \\ &= \frac{83.4}{19.0} \\ &= 4.39\end{aligned} \qquad \text{(A.78)}$$

If elastic components of lateral deflection due to rotation and translation of the pilecap of this pier are assessed to be 60 mm, then the reference yield displacement

and structural displacement ductility capacity for the example rectangular pier in the longitudinal direction is:-

$$\begin{aligned}\Delta_y &= 19.0 + 60 \\ &= 79.0\,mm\end{aligned} \tag{A.79}$$

$$\begin{aligned}\Delta_u &= 79.0 + 64.4 \\ &= 143.4\,mm\end{aligned} \tag{A.80}$$

and:-

$$\begin{aligned}\mu_\Delta &= \frac{143.4}{79.0} \\ &= 1.82\end{aligned} \tag{A.81}$$

The available structural ductility capacity of the pier is substantially less than the column displacement ductility capacity due to the relatively flexible foundations contributing a significant component of elastic displacement to the structure in this direction. Retrofit measures for the pier in this direction will have to be undertaken if the displacement ductility demand for this pier exceeds the structural displacement ductility capacity for the pier at this site.

A.3.5.2 Transverse Direction Displacement Capacity

The displacement capacity of the structure in the transverse direction is not affected by the tension shift effect leading to the development of a critical section at the curtailment point. Determination of the lateral displacement capacity of the column bent in this direction will have to consider the sequence of formation of the plastic hinges in the bent when developing the collapse mechanism. A push over analysis will indicate the order of plastic hinge formation, the collapse mechanism formed and provide the overall lateral load-lateral deformation response for the column bent. This analysis may include the effects of foundation compliance through the inclusion of appropriate flexibilities in the structural model of the column bent. This will allow

evaluation of the structural displacement ductility capacity for comparison with the expected displacement ductility demand for the column bent.

APPENDIX B

COLUMN DATABASE

This Appendix contains the column data used in Chapter 8 to predict the ACI ideal moment, M_n, predict the maximum flexural strength, M_o, for square or rectangular shaped specimens and to determine the shift in the critical section.

The list is organised by researcher and includes information about each column specimen tested as reported by the original researchers. The data points presented in Figure 8.27 were originally compiled by Ang et al. [A1] and are included here along with subsequent research conducted at the University of Canterbury since 1985 and from tests at the University of Houston as published by Sheikh and Yeh [S6].

This database includes square, circular and octagonal specimens along with a small number of rectangular columns, hollow square columns and square columns loaded across the diagonal. Section dimensions, material strengths, reinforcement details and axial load ratios were sourced from the original references.

The data presented here is also contained in an Excel spreadsheet included with this thesis.

Researcher	Unit	Shape	D'	s' mm	w' mm	a_v mm	a_h mm	D_{oc} mm	D'_c	λ_e	α_1	β_1	n_{end}	n_{total}	ζ	Eqn 8.30 c / D	f'_s	f_s	Eqn 8.29 M_n monotonic	M_n cyclic	λ_C	λ_T
Davey [D3]	D1	O	441	58.5	0	12.3	0.0	435		0.881	0.850	0.824										
	D2	O	441	58.5	0	12.3	0.0	435		0.881	0.850	0.812										
	D3	O	441	58.5	0	12.3	0.0	435		0.881	0.850	0.820										
Munro [M5]	M1	O	423	26	0	5.5	0.0	433		0.875	0.850	0.770										
Ng [N5]	N2	O	215	9.6	0	2.0	0.0	228		0.931	0.850	0.809										
	N3	O	222	5.7	0	1.2	0.0	236		0.963	0.850	0.826										
Potangaroa [P8]	P1	O	516	65	0	13.6	0.0	523		0.882	0.850	0.850										
	P3	O	516	40	0	8.4	0.0	533		0.904	0.850	0.850										
	P4	O	516	60	0	12.6	0.0	525		0.886	0.850	0.827										
	P5-1	O	510	39	0	8.2	0.0	534		0.904	0.850	0.830										
	P5-2	O	510	39	0	8.2	0.0	534		0.904	0.850	0.830										
Gill [G1]	G1	S	426	70	134	14.7	28.1	393		0.427	0.850	0.850	4	12	0.353	0.389	375	375	659	659	1.25	1.25
	G2	S	426	63	134	13.2	28.1	398		0.440	0.850	0.759	4	12	0.353	0.340	375	375	852	852	1.25	1.25
	G3	S	426	65	134	13.6	28.1	395		0.432	0.850	0.850	4	12	0.353	0.529	375	375	673	673	1.25	1.25
	G4	S	426	50	134	10.5	28.1	404		0.452	0.850	0.850	4	12	0.353	0.700	375	160	610	698	1.25	1.25
Ang - 1981 [A3]	A1	O	338	34	0	7.1	0.0	346		0.873	0.850	0.850										
	A2	O	336	45	0	9.4	0.0	343		0.864	0.850	0.850										
	A3	S	313	88	89	18.5	18.7	279		0.415	0.850	0.850	4	12	0.353	0.492	427	427	268	268	1.25	1.25
	A4	S	311	80	89	16.8	18.7	279		0.409	0.850	0.850	4	12	0.353	0.339	403	427	247	250	1.25	1.25
Mander [M4]	MA	SH	58	54	66	11.3	13.8	33			0.850	0.850										
	MB	SH	58	24	66	5.0	13.8	45			0.850	0.850										
	MC	SH	58	34	66	7.1	13.8	41			0.850	0.850										
	MD	SH	58	54	66	11.3	13.8	33			0.850	0.850										
Zahn [Z1]	Z1	SD	338	74	97	15.5	20.3	306		0.821	0.850	0.800	4	12	0.353							
	Z2	SD	338	55	97	11.5	20.3	314		0.851	0.850	0.850	4	12	0.353							
	Z3	SD	338	62	97	13.0	20.3	311		0.840	0.850	0.832	4	12	0.353							
	Z4	SD	338	45	97	9.4	20.3	318		0.865	0.850	0.850	4	12	0.353							
	Z5	O	338	125	0	26.2	0.0	312		0.753	0.850	0.832										
	Z6	O	338	65	0	13.6	0.0	337		0.843	0.850	0.850										
	Z7	S	338	107	97	22.4	20.3	292		0.485	0.850	0.850	4	12	0.353	0.358	440	440	286	286	1.25	1.25
	Z8	S	338	82	97	17.2	20.3	302		0.520	0.850	0.769	4	12	0.353	0.559	440	391	382	389	1.25	1.25
Ang - 1985 [A1]	1	C	348	54	0	11.3	0.0	347		0.878	0.850	0.790										
	2	C	348	54	0	11.3	0.0	347		0.878	0.850	0.792										
	3	C	348	54	0	11.3	0.0	347		0.878	0.850	0.802										
	5	C	348	34	0	7.1	0.0	356		0.904	0.850	0.841										
	8	C	348	24	0	5.0	0.0	360		0.917	0.850	0.850										
	9	C	348	24	0	5.0	0.0	360		0.917	0.850	0.850										
	10	C	342	108	0	22.7	0.0	325		0.801	0.850	0.840										
	12	C	348	24	0	5.0	0.0	360		0.917	0.850	0.850										
	13	C	348	24	0	5.0	0.0	360		0.917	0.850	0.800										
	14	C	340	54	0	11.3	0.0	347		0.878	0.850	0.820										
	15	C	348	54	0	11.3	0.0	347		0.878	0.850	0.812										
	17	C	348	54	0	11.3	0.0	347		0.878	0.850	0.816										
	23	C	342	148	0	31.0	0.0	308		0.740	0.850	0.832										
	24	C	344	100	0	21.0	0.0	328		0.813	0.850	0.825										
Soeslanawati [S7]	SW1	S	344	78	99	16.4	20.8	307		0.539	0.850	0.716	4	12	0.353	0.217	407	446	286	292	1.25	1.25
	SW2	S	342	70	98	14.7	20.6	309		0.547	0.850	0.738	4	12	0.353	0.433	446	446	385	385	1.25	1.25
	SW3	S	344	84	99	17.6	20.8	304		0.530	0.850	0.738	4	12	0.353	0.433	446	446	386	386	1.25	1.25
	SW4	S	346	88	99	18.5	20.8	303		0.529	0.850	0.770	4	12	0.353	0.432	446	446	368	368	1.25	1.25
Watson [W3]	SW5	S	342	73	98	15.3	20.6	308		0.542	0.850	0.762	4	12	0.353	0.640	474	270	382	412	1.25	1.25
	SW6	S	346	90	107	18.9	22.4	300		0.519	0.850	0.770	4	12	0.353	0.638	474	277	378	407	1.25	1.25
	SW7	S	334	84	95	17.6	19.9	300		0.510	0.850	0.754	4	12	0.353	0.851	474	47	332	393	1.25	1.25
	SW8	S	344	69	98	14.5	20.6	312		0.558	0.850	0.778	4	12	0.353	0.842	474	63	314	374	1.25	1.25
	SW9	S	334	40	95	8.4	19.9	319		0.574	0.850	0.770	4	12	0.353	0.845	474	51	317	378	1.25	1.25
	SW10	O	342	76	0	15.9	0.0	334		0.881	0.850	0.770										
	SW11	O	338	47	0	9.9	0.0	344		0.881	0.850	0.778										
Tanaka [T1]	T1	S	276	68	115	14.3	24.1	247		0.294	0.850	0.850	3	8	0.373	0.332	320	474	241	261	1.25	1.25
	T2	S	276	68	115	14.3	24.1	247		0.294	0.850	0.850	3	8	0.373	0.332	320	474	241	261	1.25	1.25
	T3	S	276	68	115	14.3	24.1	247		0.294	0.850	0.850	3	8	0.373	0.332	320	474	241	261	1.25	1.25
	T4	S	276	68	115	14.3	24.1	247		0.294	0.850	0.850	3	8	0.373	0.332	320	474	241	261	1.25	1.25
	T5	S	426	98	120	20.6	25.2	383		0.404	0.850	0.834	4	12	0.353	0.227	302	511	570	630	1.25	1.25
	T6	S	426	98	120	20.6	25.2	383		0.404	0.850	0.834	4	12	0.353	0.227	302	511	570	630	1.25	1.25

Researcher	Unit	Shape	l mm	D mm	B mm	l / D	$N^* / f'_c A_g$	f'_c MPa	f_y MPa	f_{yh} MPa	d_b mm	d_{bh} mm	ρ_t	ρ_s	m	s mm	w mm	g	M_i ACI kNm	M^* Reported kNm	M^* P-Δ Included kNm	B_c mm	D_c mm	A_g / A_c
Davey [D3]	D1	O	2000	500		2.75	-0.06	33.2	373	312	13	6.5	2.58%	0.42%	13.2	65	0	0.881	421	470	530	0	460	1.18
	D2	O	2000	500		1.75	-0.06	34.8	371	312	13	6.5	2.58%	0.42%	12.5	65	0	0.881	419	520	601	0	460	1.18
	D3	O	2000	500		3.25	-0.06	33.8	373	342	13	6.5	2.58%	0.42%	13.0	65	0	0.881	428	460	493	0	460	1.18
Munro [M5]	M1	O	2000	500		2.73	-0.03	40.0	305	389	13	8	2.58%	0.42%	9.0	34	0	0.846	323	370	370	0	444	1.27
Ng [N5]	N2	O	1000	250		1.34	-0.01	35.1	305	263	13	4.4	2.58%	1.50%	10.2	14	0	0.858	44	50	50	0	232	1.16
	N3	O	930	250		3.7	-0.33	33.0	294	207	12	4.3	2.30%	2.44%	10.5	10	0	0.887	59	71	71	0	238	1.10
Potangaroa [P8]	P1	O	1200	600		2.0	-0.23	28.4	303	300	24	10	2.56%	0.76%	12.6	75	0	0.860	723	890	890	0	550	1.19
	P3	O	1200	600		2.0	-0.54	26.6	303	300	24	10	2.56%	1.14%	13.4	50	0	0.860	672	966	966	0	550	1.19
	P4	O	1200	600		2.0	-0.39	32.9	303	423	24	10	2.56%	0.82%	10.8	70	0	0.860	803	1041	1041	0	550	1.19
	P5-1	O	1200	600		2.0	-0.35	32.5	307	280	24	16	2.56%	2.69%	11.1	55	0	0.850	807	1079	1079	0	550	1.19
	P5-2	O	1200	600		2.0	-0.7	32.5	307	280	24	16	2.56%	2.69%	11.1	55	0	0.850	564	1276	1276	0	550	1.19
Gill [G1]	G1	S	1200	550	550	2.18	-0.26	23.1	375	297	24	10	1.79%	1.46%	19.1	80	158	0.775	691	864	864	460	460	1.43
	G2	S	1200	550	550	2.18	-0.21	41.4	375	316	24	12	1.79%	2.22%	10.7	75	158	0.775	905	1010	1010	462	462	1.42
	G3	S	1200	550	550	2.18	-0.42	21.4	375	297	24	10	1.79%	1.82%	20.6	75	158	0.775	646	843	843	460	460	1.43
	G4	S	1200	550	550	2.18	-0.6	23.5	375	294	24	12	1.79%	3.26%	18.8	62	158	0.775	598	911	911	462	462	1.42
Ang - 1981 [A3]	A1	O	1600	400		4.0	-0.12	26.0	308	308	16	6	2.56%	0.77%	13.9	40	0	0.845	222	262	262	0	360	1.23
	A2	O	1600	400		4.0	-0.56	28.5	308	280	16	10	2.56%	1.57%	12.7	55	0	0.840	219	417	315	0	362	1.22
	A3	S	1600	400	400	4.0	-0.38	23.6	427	320	16	12	1.51%	2.64%	21.3	100	105	0.783	270	336	336	341	341	1.38
	A4	S	1600	400	400	4.0	-0.21	25.0	427	280	16	10	1.51%	2.04%	20.1	90	105	0.778	257	322	304	337	337	1.41
Mander [M4]	MA	SH	3200	750	750	4.3	-0.1	30.0	335	320	10	6	1.55%	1.00%	13.1	60	76	0.077	815	902	902		74	1.62
	MB	SH	3200	750	750	4.3	-0.5	30.0	335	320	10	6	1.55%	2.05%	13.1	30	76	0.077	1194	1587	1587		74	1.62
	MC	SH	3200	750	750	4.3	-0.3	29.0	335	320	10	6	1.55%	1.55%	13.6	40	76	0.077	1178	1328	1338		74	1.62
	MD	SH	3200	750	750	4.3	-0.3	29.0	335	320	10	6	1.55%	1.00%	13.6	60	76	0.077	1178	1338	1338		74	1.62
Zahn [Z1]	Z1	SD	1600	400	400	4.0	-0.27	36.2	423	318	16	10	1.51%	2.24%	13.7	84	113	0.845	273	368	368	364	364	1.21
	Z2	SD	1600	400	400	4.0	-0.45	28.8	423	318	16	10	1.51%	2.89%	17.3	65	113	0.845	259	400	400	364	364	1.21
	Z3	SD	1600	400	400	4.0	-0.23	32.3	423	318	16	10	1.51%	2.14%	15.4	72	113	0.845	274	357	357	364	364	1.21
	Z4	SD	1600	400	400	4.0	-0.48	27.0	423	318	16	10	1.51%	2.80%	18.4	55	113	0.845	234	397	397	364	364	1.21
	Z5	O	1600	400		4.0	-0.13	32.3	337	466	16	10	2.43%	0.61%	12.3	135	0	0.845	217	234	234	0	364	1.21
	Z6	O	1600	400		4.0	-0.67	27.0	337	466	16	10	2.43%	1.09%	14.7	75	0	0.845	193	325	325	0	364	1.21
	Z7	S	1600	400	400	4.0	-0.23	28.3	440	466	16	10	1.51%	1.56%	18.3	117	113	0.845	284	335	335	364	364	1.21
	Z8	S	1600	400	400	4.0	-0.42	40.1	440	466	16	10	1.51%	1.99%	12.9	92	113	0.845	352	433	433	364	364	1.21
Ang - 1985 [A1]	1	C	800	400		2.0	0	37.5	436	328	16	6	3.20%	0.51%	13.7	60	0	0.870	245	256	*256*	0	370	1.17
	2	C	800	400		2.0	0	37.2	296	328	16	6	3.20%	0.51%	9.4	60	0	0.870	176	182	*182*	0	370	1.17
	3	C	1000	400		2.5	0	36.0	436	328	16	6	3.20%	0.51%	14.2	60	0	0.870	242	298	*298*	0	370	1.17
	5	C	800	400		2.0	0	31.1	436	328	16	6	3.20%	0.76%	16.5	40	0	0.870	241	272	*272*	0	370	1.17
	8	C	800	400		2.0	-0.2	28.7	448	372	16	6	3.20%	1.02%	18.4	30	0	0.870	285	380	394	0	370	1.17
	9	C	1000	400		2.5	-0.2	29.9	448	372	16	6	3.20%	1.02%	17.6	30	0	0.870	281	385	409	0	370	1.17
	10	C	800	400		2.0	-0.2	31.2	448	332	16	12	3.20%	1.02%	16.9	120	0	0.855	288	360	380	0	370	1.17
	12	C	600	400		1.5	-0.1	28.6	436	328	16	6	3.20%	1.02%	17.9	30	0	0.870	262	316	324	0	370	1.17
	13	C	800	400		2.0	-0.1	36.2	436	328	16	6	3.20%	1.02%	14.2	30	0	0.870	290	354	368	0	370	1.17
	14	C	800	400		2.0	0	33.7	424	326	24	6	3.24%	0.51%	14.8	60	0	0.850	243	249	*249*	0	370	1.17
	15	C	800	400		2.0	0	34.8	436	326	16	6	1.92%	0.51%	14.7	60	0	0.870	163	184	*184*	0	370	1.17
	17	C	1000	400		2.5	-0.1	34.3	436	326	16	6	3.20%	0.51%	15.0	60	0	0.870	281	329	329	0	370	1.17
	23	C	800	400		2.0	0	32.3	436	308	16	12	3.20%	0.76%	15.9	160	0	0.855	236	271	*271*	0	370	1.17
	24	C	800	400		2.0	0	33.1	436	310	16	10	3.20%	0.77%	15.5	110	0	0.860	244	270	*270*	0	370	1.17
Soesianawati [S7]	SW1	S	1600	400	400	4.0	-0.1	46.5	446	364	16	7	1.51%	0.84%	11.3	85	115	0.860	302	335	335	367	367	1.19
	SW2	S	1600	400	400	4.0	-0.3	44.0	446	360	16	8	1.51%	1.20%	11.9	78	114	0.855	405	486	486	366	366	1.19
	SW3	S	1600	400	400	4.0	-0.3	44.0	446	364	16	7	1.51%	0.78%	11.9	91	115	0.860	406	479	479	367	367	1.19
	SW4	S	1600	400	400	4.0	-0.3	40.0	446	255	16	6	1.51%	0.56%	13.1	94	115	0.865	383	448	448	368	368	1.18
Watson [W3]	SW5	S	1600	400	400	4.0	-0.5	41.0	474	372	16	8	1.51%	1.16%	13.6	81	114	0.855	381	526	526	366	366	1.19
	SW6	S	1600	400	400	4.0	-0.5	40.0	474	388	16	6	1.51%	0.54%	13.9	96	123	0.865	376	526	526	368	368	1.18
	SW7	S	1600	400	400	4.0	-0.7	42.0	474	308	16	12	1.51%	2.22%	13.3	96	111	0.835	304	517	517	362	362	1.22
	SW8	S	1600	400	400	4.0	-0.7	39.0	474	372	16	8	1.51%	1.21%	14.3	77	114	0.860	293	524	524	368	368	1.18
	SW9	S	1600	400	400	4.0	-0.7	40.0	474	308	16	12	1.51%	4.10%	13.9	52	111	0.835	298	599	599	362	362	1.22
	SW10	O	1600	400		4.0	-0.5	40.0	474	372	16	8	1.92%	1.30%	13.9	84	0	0.855	259	389	389	0	366	1.19
	SW11	O	1600	400		4.0	-0.7	39.0	474	338	16	10	1.92%	3.02%	14.3	57	0	0.845	214	364	364	0	364	1.21
Tanaka [T1]	T1	S	1600	400	400	4.0	-0.2	25.6	474	333	20	12	1.57%	2.55%	21.8	80	135	0.690	251	279	279	308	308	1.69
	T2	S	1600	400	400	4.0	-0.2	25.6	474	333	20	12	1.57%	2.55%	21.8	80	135	0.690	251	284	284	308	308	1.69
	T3	S	1600	400	400	4.0	-0.2	25.6	474	333	20	12	1.57%	2.55%	21.8	80	135	0.690	252	290	290	308	308	1.69
	T4	S	1600	400	400	4.0	-0.2	25.6	474	333	20	12	1.57%	2.55%	21.8	80	135	0.690	252	285	285	308	308	1.69
	T5	S	1650	550	550	3.0	-0.1	32.0	511	325	20	12	1.25%	1.70%	18.8	110	140	0.775	601	673	673	458	458	1.44
	T6	S	1650	550	550	3.0	-0.1	32.0	511	325	20	12	1.25%	1.70%	18.8	110	140	0.775	601	679	679	458	458	1.44

Researcher	Unit	Shape	f'_{cc} / f'_c = $1+4.1p_s f_{sh} / 2f'_c$	Eqn 8.31 M_o	Reported M^* / M_i	A M^* / M_i	A / Eqn 8.26	α_{shift}	$\alpha_{shift} M_i$ kNm	$M^* / \alpha_{shift} M_i$	$\alpha_{shift} M_o$ kNm	$M^* / \alpha_{shift} M_o$	Notes
Davey [D3]	D1	O	1.081		1.116	1.259	1.11		0				Loading controlled to give different M / V ratios
	D2	O	1.077		1.241	1.434	1.27		0				M_u reported when ε_c = 0.003 during test
	D3	O	1.087		1.075	1.152	1.02		0				
Munro [M5]	M1	O	1.084		1.146	1.146	1.01		0				
Ng [N5]	N2	O	1.230		1.136	1.136	1.01		0				Munro's 1/6 scale model
	N3	O	1.314		1.203	1.203	1.06		0				
Potangaroa [P8]	P1	O	1.165		1.231	1.231	1.09		0				
	P3	O	1.264		1.438	1.438	1.27		0				
	P4	O	1.216		1.296	1.296	1.15		0				
	P5-1	O	1.475		1.337	1.337	1.18		0				
	P5-2	O	1.475		2.262	2.262	2.00		0				
Gill [G1]	G1	S	1.385	658	1.250	1.250	1.11	1.15	798	1.083	761	1.136	
	G2	S	1.347	851	1.116	1.116	0.99	1.13	1025	0.986	965	1.047	
	G3	S	1.518	678	1.305	1.305	1.15	1.22	790	1.068	829	1.017	
	G4	S	1.836	792	1.523	1.523	1.35	1.32	788	1.157	1043	0.873	
Ang - 1981 [A3]	A1	O	1.187		1.180	1.180	1.04		0				Axial load ratio varied from 0.12 to 0.2 during test
	A2	O	1.316		1.904	1.438	1.27		0				P-Δ effects large for unit A2. ?? for M_u reported
	A3	S	1.734	273	1.244	1.244	1.10	1.10	297	1.130	301	1.115	
	A4	S	1.468	249	1.253	1.183	1.05	1.07	274	1.108	267	1.139	
Mander [M4]	MA	SH	1.219		1.107	1.107	0.98		0				Hollow columns, wall thickness = 120 mm
	MB	SH	1.448		1.330	1.330	1.18		0				Transverse steel volumetric ratios averaged for
	MC	SH	1.351		1.128	1.136	1.01		0				both directions
	MD	SH	1.226		1.136	1.136	1.01		0				
Zahn [Z1]	Z1	SD	1.403		1.348	1.348	1.19		0				
	Z2	SD	1.654		1.544	1.544	1.37		0				
	Z3	SD	1.432		1.303	1.303	1.15		0				
	Z4	SD	1.676		1.697	1.697	1.50		0				
	Z5	O	1.180		1.078	1.078	0.95		0				
	Z6	O	1.386		1.684	1.684	1.49		0				
	Z7	S	1.527	295	1.180	1.180	1.04	1.07	304	1.101	316	1.059	
	Z8	S	1.474	389	1.230	1.230	1.09	1.12	393	1.101	435	0.996	
Ang - 1985 [A1]	1	C	1.091		1.045	1.045	0.92		0				Specimens which failed in brittle shear have
	2	C	1.092		1.034	1.034	0.92		0				been excluded
	3	C	1.095		1.231	1.231	1.09		0				
	5	C	1.165		1.129	1.129	1.00		0				
	8	C	1.271		1.333	1.382	1.22		0				
	9	C	1.260		1.370	1.456	1.29		0				
	10	C	1.222		1.250	1.319	1.17		0				
	12	C	1.240		1.206	1.237	1.09		0				
	13	C	1.188		1.221	1.269	1.12		0				
	14	C	1.101		1.025	1.025	0.91		0				
	15	C	1.098		1.129	1.129	1.00		0				
	17	C	1.099		1.171	1.171	1.04		0				
	23	C	1.149		1.148	1.148	1.02		0				
	24	C	1.148		1.107	1.107	0.98		0				
Soesianawati [S7]	SW1	S	1.135	322	1.109	1.109	0.98	1.04	315	1.064	335	0.999	
	SW2	S	1.201	377	1.200	1.200	1.06	1.09	441	1.102	419	1.159	
	SW3	S	1.132	359	1.180	1.180	1.04	1.09	442	1.084	420	1.141	
	SW4	S	1.073	332	1.170	1.170	1.04	1.09	417	1.075	401	1.118	
Watson [W3]	SW5	S	1.216	347	1.381	1.381	1.22	1.14	433	1.215	468	1.124	
	SW6	S	1.107	296	1.399	1.399	1.24	1.14	427	1.232	462	1.138	
	SW7	S	1.334	278	1.701	1.701	1.51	1.19	362	1.429	467	1.106	
	SW8	S	1.237	262	1.788	1.788	1.58	1.19	348	1.506	444	1.180	
	SW9	S	1.647	430	2.010	2.010	1.78	1.19	354	1.692	511	1.173	
	SW10	O	1.248		1.502	1.502	1.33		0				
	SW11	O	1.537		1.701	1.701	1.51		0				
Tanaka [T1]	T1	S	1.680	250	1.112	1.112	0.98	1.07	268	1.042	278	1.004	
	T2	S	1.680	250	1.131	1.131	1.00	1.07	268	1.061	278	1.022	
	T3	S	1.680	250	1.151	1.151	1.02	1.07	269	1.079	278	1.044	
	T4	S	1.680	250	1.131	1.131	1.00	1.07	269	1.061	278	1.026	
	T5	S	1.354	635	1.120	1.120	0.99	1.06	637	1.056	673	1.000	
	T6	S	1.354	635	1.130	1.130	1.00	1.06	637	1.066	673	1.009	

Researcher	Unit	Shape	l mm	D mm	B mm	l / D	$N^* / f'_c A_g$	f'_c MPa	f_y MPa	f_{yh} MPa	d_b mm	d_{bh} mm	ρ_t	ρ_s	m	s mm	w mm	g	M_t ACI kNm	Reported M^* kNm	P-Δ included M^* kNm	B_c mm	D_c mm	A_g / A_c
	T7	S	1650	550	550	3.0	-0.3	32.1	511	325	20	12	1.25%	2.08%	18.7	90	140	0.775	796	1043	1043	458	458	1.44
	T8	S	1650	550	550	3.0	-0.3	32.1	511	325	20	12	1.25%	2.08%	18.7	90	140	0.775	798	1045	1045	458	458	1.44
	T9	R	1784	600	400	2.97	-0.1	26.9	432	305	24	12	1.88%	2.17%	18.9	80	168	0.840	598	712	712	342	540	1.30
	T10	RE	1784	600	400	2.97	-0.1	21.2	485	308	20	10	2.14%	1.29%	26.9	80	0	0.853	429	553	553		342	1.20
	T11	RE	1784	600	400	2.97	-0.3	29.7	485	308	20	10	2.14%	1.03%	19.2	100	0	0.853	554	737	737		342	1.20
	T12	RE	1784	600	400	2.97	-0.5	24.6	485	308	20	10	2.14%	1.38%	23.2	75	0	0.853	471	739	739		342	1.20
Satyarno [S3]	S1	S	1600	400	400	4.0	-0.6	50.0	497	800	20	7.4	3.51%	1.00%	11.7	80	160	0.832	507	793	902	360	360	1.23
	S2	S	1600	400	400	4.0	-0.6	50.0	497, 997	800	20	7.4	3.32%	1.00%	11.7	80	160	0.832	500	710	810	360	360	1.23
	S3	S	1600	400	400	4.0	-0.6	50.0	497, 997	800	20	7.4	3.14%	1.00%	11.7	80	160	0.832	482	583	694	360	360	1.23
Sato [S4]	YS1	S	1000	400	400	2.50	-0.3	59.8	442	800	20	9.2	3.14%	1.56%	8.7	80	160	0.827	647	759	759	360	360	1.23
	YS2	S	1000	400	400	2.50	-0.3	59.8	442, 1033	800	20	9.2	3.32%	1.56%	8.7	80	160	0.827	681	902	902	360	360	1.23
	YS3	S	1000	400	400	2.50	-0.3	59.8	442, 1033	800	20	9.2	3.51%	1.56%	8.7	80	160	0.827	698	996	996	360	360	1.23
	YS4	S	1000	400	400	2.50	-0.6	71.6	442	800	20	9.2	3.14%	1.56%	7.3	80	160	0.827	692	948	948	360	360	1.23
	YS5	S	1000	400	400	2.50	-0.6	71.6	442, 1033	800	20	9.2	3.32%	1.56%	7.3	80	160	0.827	716	1060	1060	360	360	1.23
	YS6	S	1000	400	400	2.50	-0.6	71.6	442, 1033	800	20	9.2	3.51%	1.56%	7.3	80	160	0.827	728	1147	1147	360	360	1.23
Xinrong [X4]	X1	S	1650	400	400	4.13	-0.3	33.2	450	362	20	10	1.57%	2.13%	15.9	70	160	0.800	345	408	408	350	350	1.31
	X2a	S	1650	400	400	4.13	-0.3	32.0	460	362	20	10	1.57%	2.13%	16.9	70	160	0.800	356	389	389	350	350	1.31
	X2b	S	1650	400	400	4.13	0.05	32.0	460	362	20	10	1.57%	2.13%	16.9	70	160	0.800	150	206	206	350	350	1.31
	X3a	S	1650	400	400	4.13	-0.3	32.0	460	362	20	10	1.57%	2.13%	16.9	70	160	0.800	356	405	405	350	350	1.31
	X3b	S	1650	400	400	4.13	0.05	32.0	460	362	20	10	1.57%	2.13%	16.9	70	160	0.800	150	152	152	350	350	1.31
	X4	S	1650	400	400	4.13	-0.5	35.7	460	362	20	10	1.57%	2.70%	15.2	55	160	0.800	348	493	493	350	350	1.31
	X5a	S	1650	400	400	4.13	-0.5	35.5	460	362	20	10	1.57%	2.70%	15.2	55	160	0.800	348	456	456	350	350	1.31
	X5b	S	1650	400	400	4.13	0.1	35.5	460	362	20	10	1.57%	2.70%	15.2	55	160	0.800	105	134	134	350	350	1.31
	X6a	S	1650	400	400	4.13	-0.5	35.7	460	362	20	10	1.57%	2.70%	15.2	55	160	0.800	348	427	427	350	350	1.31
	X6b	S	1650	400	400	4.13	0.1	35.7	460	362	20	10	1.57%	2.70%	15.2	55	160	0.800	105	120	120	350	350	1.31
Sheikh and Yeh [S6]	UH-E2	S	3050	305	305	10.00	-0.61	20.2	516	312	19	13	2.44%	1.69%	30.0	115	235	0.770	158	169	169	267	267	1.30
	UH-A3	S	3050	305	305	10.00	-0.61	20.5	516	316	19	10	2.44%	1.68%	29.6	110	119	0.780	161	198	198	267	267	1.30
	UH-F4	S	3050	305	305	10.00	-0.6	20.8	516	316	19	10	2.44%	1.68%	29.2	95	119	0.780	163	198	198	267	267	1.30
	UH-D5	S	3050	305	305	10.00	-0.46	20.2	436	316	16	10	2.58%	1.68%	25.4	115	80	0.790	162	205	205	267	267	1.30
	UH-F6	S	3050	305	305	10.00	-0.75	17.6	516	312	19	13	2.44%	1.68%	34.5	175	118	0.770	126	145	145	267	267	1.30
	UH-D7	S	3050	305	305	10.00	-0.78	16.9	436	303	16	6	2.58%	1.62%	30.3	55	80	0.803	109	133	133	267	267	1.30
	UH-E8	S	3050	305	305	10.00	-0.78	16.7	516	312	19	10	2.44%	0.84%	36.3	125	238	0.780	135	129	129	267	267	1.30
	UH-F9	S	3050	305	305	10.00	-0.77	17.1	516	316	19	10	2.44%	1.68%	35.5	95	119	0.780	122	152	152	267	267	1.30
	UH-E10	S	3050	305	305	10.00	-0.77	17.0	516	316	19	10	2.44%	1.68%	35.8	65	238	0.780	121	133	133	267	267	1.30
	UH-A11	S	3050	305	305	10.00	-0.74	18.0	516	303	19	6	2.44%	0.77%	33.7	110	121	0.793	139	135	135	267	267	1.30
	UH-F12	S	3050	305	305	10.00	-0.6	21.6	516	298	19	6	2.44%	0.82%	28.1	85	80	0.793	165	161	161	267	267	1.30
	UH-E13	S	3050	305	305	10.00	-0.74	17.6	516	312	19	13	2.44%	1.69%	34.5	115	235	0.770	126	128	128	267	267	1.30
	UH-D14	S	3050	305	305	10.00	-0.75	17.4	436	298	16	6	2.58%	0.81%	29.6	110	80	0.803	115	117	117	267	267	1.30
	UH-D15	S	3050	305	305	10.00	-0.75	16.9	436	316	16	10	2.58%	1.68%	30.3	115	80	0.790	115	135	135	267	267	1.30
	UH-A16	S	3050	305	305	10.00	-0.6	21.9	516	360	19	6	2.44%	0.77%	27.7	110	121	0.793	167	157	157	267	267	1.30
Dodd [D1]	LD1a	C	800	200		4.0	-0.04	40.7	450	260	6	4	0.0162	0.92%	13.0	30	0	0.860	20.7	26	26	0	182	1.21
	LD1b	C	800	200		4.0	-0.051	32.0	450	260	6	4	0.0162	0.92%	16.5	30	0	0.860	20.1	28	28	0	182	1.21
	LD2a	C	1400	200		7.0	-0.048	34.5	450	260	6	4	0.0162	1.11%	15.3	25	0	0.860	20.3	24	24	0	182	1.21
	LD2b	C	1400	200		7.0	-0.054	30.3	450	260	6	4	0.0162	1.11%	17.5	25	0	0.860	20.0	26	26	0	182	1.21
	LD3a	C	2000	200		10.0	-0.044	37.4	450	250	6	3.15	0.0162	0.69%	14.2	25	0	0.864	20.5	29	29	0	182	1.21
	LD3b	C	2000	200		10.0	-0.056	29.1	450	250	6	3.15	0.0162	0.69%	18.2	25	0	0.864	19.8	24	24	0	182	1.21
	LD4	C	800	200		4.0	-0.391	39.4	450	260	6	4	0.0162	0.99%	13.4	28	0	0.860	30.9	52	52	0	182	1.21
	LD5	C	1400	200		7.0	-0.388	37.2	450	260	6	4	0.0162	1.06%	14.2	26	0	0.860	29.9	45	45	0	182	1.21
	LD6	C	2000	200		10.0	-0.387	38.6	450	250	6	3.15	0.0162	0.82%	13.7	21	0	0.864	30.5	44	44	0	182	1.21
	LD7	C	800	200		4.0	-0.04	41.3	450	250	6	3.15	0.0162	0.48%	12.8	36	0	0.864	20.8	25	25	0	182	1.21
	LD8	C	800	200		4.0	-0.392	40.1	450	260	6	4	0.0162	0.99%	13.2	28	0	0.860	31.4	46	46	0	182	1.21
	LD9	C	1400	200		7.0	-0.041	40.4	450	250	6	3.15	0.0162	0.48%	13.1	36	0	0.864	20.7	24	24	0	182	1.21
	LD10	C	800	200		4.0	-0.044	36.9	450	260	6	4	0.0162	0.92%	14.3	30	0	0.860	20.5	24	24	0	182	1.21
	LD11	C	800	200		4.0	-0.358	43.0	450	260	6	4	0.0162	0.99%	12.3	28	0	0.860	32.5	52	52	0	182	1.21

Researcher	Unit	Shape	D'	s' mm	w' mm	a_v mm	a_h mm	D_{oc} mm	D'c	λ_s	α_1	β_1	n_{end}	n_{total}	ζ	Eqn 8.30 c / D	f'_s	f_s	Eqn 8.29 M_n monotonic	M_n cyclic	λ_C	λ_T
	T7	S	426	78	120	16.4	25.2	392		0.422	0.850	0.833	4	12	0.353	0.422	440	511	780	800	1.25	1.25
	T8	S	426	78	120	16.4	25.2	392		0.422	0.850	0.833	4	12	0.353	0.422	440	511	780	800	1.25	1.25
	T9	R	504	68	144	14.3	30.2	471		0.527	0.850	0.850	3	10	0.338	0.246	405	432	585	595	1.25	1.25
	T10	RE	312	70	0	14.7	0.0	313	400	0.905	0.850	0.850										
	T11	RE	312	90	0	18.9	0.0	304	400	0.893	0.850	0.850										
	T12	RE	312	65	0	13.6	0.0	315	400	0.908	0.850	0.850										
Satyamo [S3]	S1	S	333	72.6	140	15.2	29.4	290		0.474	0.850	0.690	5	16	0.344	0.708						
	S2	S	333	72.6	140	15.2	29.4	290		0.474	0.850	0.690	5	16	0.344	0.713						
	S3	S	333	72.6	140	15.2	29.4	290		0.474	0.850	0.690	5	16	0.344	0.717	530	166	527	613	1.25	1.25
Sato [S4]	YS1	S	331	70.8	140	14.9	29.4	291		0.477	0.831	0.650	5	16	0.344	0.444	442	442	565	565	1.25	1.25
	YS2	S	331	70.8	140	14.9	29.4	291		0.477	0.831	0.650	5	16	0.344	0.445						
	YS3	S	331	70.8	140	14.9	29.4	291		0.477	0.831	0.650	5	16	0.344	0.445						
	YS4	S	331	70.8	140	14.9	29.4	291		0.477	0.784	0.650	5	16	0.344	0.751	442	130	596	685	1.25	1.25
	YS5	S	331	70.8	140	14.9	29.4	291		0.477	0.784	0.650	5	16	0.344	0.747						
	YS6	S	331	70.8	140	14.9	29.4	291		0.477	0.784	0.650	5	16	0.344	0.743						
Xinrong [X4]	X1	S	320	60	140	12.6	29.4	286		0.446	0.850	0.824	3	8	0.373	0.428	450	450	337	337	1.25	1.25
	X2a	S	320	60	140	12.6	29.4	286		0.446	0.850	0.834	3	8	0.373	0.427						
	X2b	S	320	60	140	12.6	29.4	286		0.446	0.850	0.834	3	8	0.373	0.086						
	X3a	S	320	60	140	12.6	29.4	286		0.446	0.850	0.834	3	8	0.373	0.427						
	X3b	S	320	60	140	12.6	29.4	286		0.446	0.850	0.834	3	8	0.373	0.086						
	X4	S	320	45	140	9.4	29.4	292		0.466	0.850	0.804	3	8	0.373	0.631	460	256	345	376	1.25	1.25
	X5a	S	320	45	140	9.4	29.4	292		0.466	0.850	0.806	3	8	0.373	0.630						
	X5b	S	320	45	140	9.4	29.4	292		0.466	0.850	0.806	3	8	0.373	0.027						
	X6a	S	320	45	140	9.4	29.4	292		0.466	0.850	0.804	3	8	0.373	0.631						
	X6b	S	320	45	140	9.4	29.4	292		0.466	0.850	0.804	3	8	0.373	0.026						
Sheikh and Yeh [S6]	UH-E2	S	235	102	216	21.4	45.3	164		0.252	0.850	0.850	3	8	0.373	0.513	466	435	148	148	1.25	1.00
	UH-A3	S	238	100	100	21.0	21.0	197		0.365	0.850	0.850	3	8	0.373	0.513	472	440	151	151	1.25	1.00
	UH-F4	S	238	85	100	17.8	21.0	203		0.389	0.850	0.850	3	8	0.373	0.508	470	452	152	152	1.25	1.00
	UH-D5	S	241	105	64	22.0	13.4	205		0.396	0.850	0.850	4	12	0.353	0.421	436	436	143	143	1.25	1.00
	UH-F6	S	235	162	99	34.0	20.8	171		0.276	0.850	0.850	3	8	0.373	0.589	483	301	129	129	1.25	1.00
	UH-D7	S	245	49	64	10.3	13.4	229		0.492	0.850	0.850	4	12	0.353	0.607	436	292	125	125	1.25	1.00
	UH-E8	S	238	115	219	24.1	45.9	157		0.233	0.850	0.850	3	8	0.373	0.603	491	286	127	127	1.25	1.00
	UH-F9	S	238	85	100	17.8	21.0	203		0.389	0.850	0.850	3	8	0.373	0.599	490	292	129	129	1.25	1.00
	UH-E10	S	238	55	219	11.5	45.9	183		0.314	0.850	0.850	3	8	0.373	0.598	490	293	128	128	1.25	1.00
	UH-A11	S	242	104	102	21.8	21.4	195		0.357	0.850	0.850	3	8	0.373	0.585	494	320	136	136	1.25	1.00
	UH-F12	S	242	79	61	16.6	12.8	217		0.442	0.850	0.850	3	8	0.373	0.509	478	457	158	158	1.25	1.00
	UH-E13	S	235	102	216	21.4	45.3	164		0.252	0.850	0.850	3	8	0.373	0.583	482	310	130	130	1.25	1.00
	UH-D14	S	245	104	64	21.8	13.4	205		0.397	0.850	0.850	4	12	0.353	0.591	436	316	129	129	1.25	1.00
	UH-D15	S	241	105	64	22.0	13.4	205		0.396	0.850	0.850	4	12	0.353	0.589	436	312	126	126	1.25	1.00
	UH-A16	S	242	104	102	21.8	21.4	195		0.357	0.850	0.850	3	8	0.373	0.509	478	457	159	159	1.25	1.00
Dodd [D1]	LD1a	C	172	26	0	5.5	0.0	171		0.861	0.850	0.764										
	LD1b	C	172	26	0	5.5	0.0	171		0.861	0.850	0.834										
	LD2a	C	172	21	0	4.4	0.0	173		0.875	0.850	0.814										
	LD2b	C	172	21	0	4.4	0.0	173		0.875	0.850	0.848										
	LD3a	C	173	21.85	0	4.6	0.0	173		0.873	0.850	0.791										
	LD3b	C	173	21.85	0	4.6	0.0	173		0.873	0.850	0.850										
	LD4	C	172	24	0	5.0	0.0	172		0.867	0.850	0.775										
	LD5	C	172	22	0	4.6	0.0	173		0.872	0.850	0.792										
	LD6	C	173	17.85	0	3.7	0.0	175		0.883	0.850	0.781										
	LD7	C	173	32.85	0	6.9	0.0	168		0.842	0.850	0.760										
	LD8	C	172	24	0	5.0	0.0	172		0.867	0.850	0.769										
	LD9	C	173	32.85	0	6.9	0.0	168		0.842	0.850	0.767										
	LD10	C	172	26	0	5.5	0.0	171		0.861	0.850	0.795										
	LD11	C	172	24	0	5.0	0.0	172		0.867	0.850	0.746										

Researcher	Unit	Shape	f'_{cc}/f'_c = $1+4.1\rho_s f_{yh}/2f'_c$	Eqn 8.31 M_o	Reported M^*/M_l	A M^*/M_l	A / Eqn 8.26	α_{shift}	$\alpha_{shift} M_l$ kNm	$M^*/\alpha_{shift} M_l$	$\alpha_{shift} M_o$ kNm	$M^*/\alpha_{shift} M_o$	Notes
	T7	S	1.432	763	1.310	1.310	1.16	1.12	890	1.172	895	1.166	
	T8	S	1.432	763	1.310	1.310	1.16	1.12	892	1.171	895	1.168	
	T9	R	1.504	667	1.191	1.191	1.05	1.07	638	1.117	711	1.001	Rectangular specimen
	T10	RE	1.384		1.289	1.289	1.14		0				Rounded end columns
	T11	RE	1.219		1.330	1.330	1.18		0				"
	T12	RE	1.354		1.569	1.569	1.39		0				"
Satyamo [S3]	S1	S	1.328		1.564	1.779	1.57	1.15	585	1.543			Specimens contain some ultra-high strength longitudinal
	S2	S	1.328		1.420	1.620	1.43	1.15	577	1.403			and transverse steel f_y = 997 MPa Units 1, 2
	S3	S	1.328	538	1.210	1.440	1.27	1.16	557	1.246	709	0.979	P-Δ effects not included in reported experimental moments
Sato [S4]	YS1	S	1.428	617	1.173	1.173	1.04	1.15	746	1.017	711	1.067	Specimens contain some ultra-high strength longitudinal
	YS2	S	1.428		1.325	1.325	1.17	1.15	786	1.148			and transverse steel
	YS3	S	1.428		1.427	1.427	1.26	1.15	806	1.236			f_{yh} = 800 MPa from code limits and experimentally
	YS4	S	1.357	571	1.370	1.370	1.21	1.29	893	1.061	884	1.072	measured maximum stresses
	YS5	S	1.357		1.480	1.480	1.31	1.29	923	1.149			f_y = 442 and 1033 MPa Units 2,3,5,6
	YS6	S	1.357		1.576	1.576	1.39	1.29	937	1.225			
Xinrong [X4]	X1	S	1.476	332	1.183	1.183	1.05	1.08	374	1.091	365	1.117	Specimens were subjected to varying axial load
	X2a	S	1.494		1.093	1.093	0.97	1.08	386	1.008			during testing. Coupled and uncoupled axial load
	X2b	S	1.494		1.373	1.373	1.22	1.02	152	1.352			history used during testing.
	X3a	S	1.494		1.138	1.138	1.01	1.08	386	1.049			
	X3b	S	1.494		1.013	1.013	0.90	1.02	152	0.998			
	X4	S	1.561	372	1.417	1.417	1.25	1.13	393	1.254	425	1.161	
	X5a	S	1.564		1.310	1.310	1.16	1.13	393	1.160			
	X5b	S	1.564		1.276	1.276	1.13	1.00	106	1.270			
	X6a	S	1.561		1.227	1.227	1.09	1.13	393	1.086			
	X6b	S	1.561		1.143	1.143	1.01	1.00	106	1.137			
Sheikh and Yeh [S6]	UH-E2	S	1.533	141	1.072	1.072	0.95	1.00	158	1.072	148	1.145	Tests at University of Houston
	UH-A3	S	1.530	156	1.229	1.229	1.09	1.00	161	1.229	156	1.266	No stub adjacent to critical section
	UH-F4	S	1.524	159	1.217	1.217	1.08	1.00	163	1.217	159	1.246	Monotonic loading only
	UH-D5	S	1.540	141	1.263	1.263	1.12	1.00	162	1.263	143	1.428	Zero shear force at critical section
	UH-F6	S	1.610	140	1.154	1.154	1.02	1.00	126	1.154	140	1.040	
	UH-D7	S	1.594	148	1.223	1.223	1.08	1.00	109	1.223	148	0.903	
	UH-E8	S	1.321	124	0.957	0.957	0.85	1.00	135	0.957	127	1.016	
	UH-F9	S	1.637	154	1.246	1.246	1.10	1.00	122	1.246	154	0.988	
	UH-E10	S	1.642	145	1.097	1.097	0.97	1.00	121	1.097	145	0.912	
	UH-A11	S	1.265	141	0.973	0.973	0.86	1.00	139	0.973	141	0.957	
	UH-F12	S	1.232	158	0.976	0.976	0.86	1.00	165	0.976	158	1.018	
	UH-E13	S	1.614	137	1.015	1.015	0.90	1.00	126	1.015	137	0.934	
	UH-D14	S	1.285	128	1.013	1.013	0.90	1.00	115	1.013	129	0.904	
	UH-D15	S	1.643	138	1.170	1.170	1.04	1.00	115	1.170	138	0.975	
	UH-A16	S	1.260	150	0.943	0.943	0.83	1.00	167	0.943	159	0.993	
Dodd [D1]	LD1a	C	1.121		1.256	1.256	1.11		0				Circular columns tested dynamically
	LD1b	C	1.153		1.393	1.393	1.23		0				
	LD2a	C	1.171		1.182	1.182	1.05		0				
	LD2b	C	1.194		1.300	1.300	1.15		0				
	LD3a	C	1.094		1.415	1.415	1.25		0				
	LD3b	C	1.121		1.212	1.212	1.07		0				
	LD4	C	1.133		1.683	1.683	1.49		0				
	LD5	C	1.152		1.505	1.505	1.33		0				
	LD6	C	1.108		1.443	1.443	1.28		0				
	LD7	C	1.059		1.202	1.202	1.06		0				
	LD8	C	1.131		1.465	1.465	1.30		0				
	LD9	C	1.061		1.159	1.159	1.03		0				
	LD10	C	1.133		1.171	1.171	1.04		0				
	LD11	C	1.122		1.600	1.600	1.42		0				

APPENDIX C

Derivation of Equations 8.29 to 8.31

C.1 INTRODUCTION

Equations 8.29 to 8.31 are presented to enable approximation of the ACI ideal moment and maximum flexural strength of a rectangular section to be found. The expressions to determine the flexural strengths are based on taking moments about the column centreline due to the internal forces acting in the column from the concrete compressive force resultant and longitudinal steel forces.

Equation 8.29 uses the same assumptions as the ACI method [X3] to determine the flexural strength, using an equivalent rectangular stress block, neglecting the influence of increased concrete strength due to confinement and strain hardening of the longitudinal steel. Equation 8.31 allows the maximum flexural strength of a rectangular section to be predicted accounting for the beneficial effects of confinement and strain hardening of the longitudinal steel. Equation 8.30 presents an expression to predict the neutral axis depth of a rectangular section to enable the strain profile for the section to be established. This allows internal longitudinal steel forces to be determined for incorporation into Equation 8.29 to determine the ACI ideal moment.

C.2 EQUATION 8.29 - PREDICTION OF ACI IDEAL MOMENT

Inclusion of the axial load ratio in this expression allows the neutral axis depth to be determined for any axial load acting in the column giving a closed form solution to determine the flexural strength of the column section. Figure C.1 shows a rectangular column section with an arbitrary longitudinal steel layout and the strain profile acting in the section. The longitudinal steel assumed to be arranged on all faces of the column with an equal spacing between longitudinal bars on each face. Figure C.2

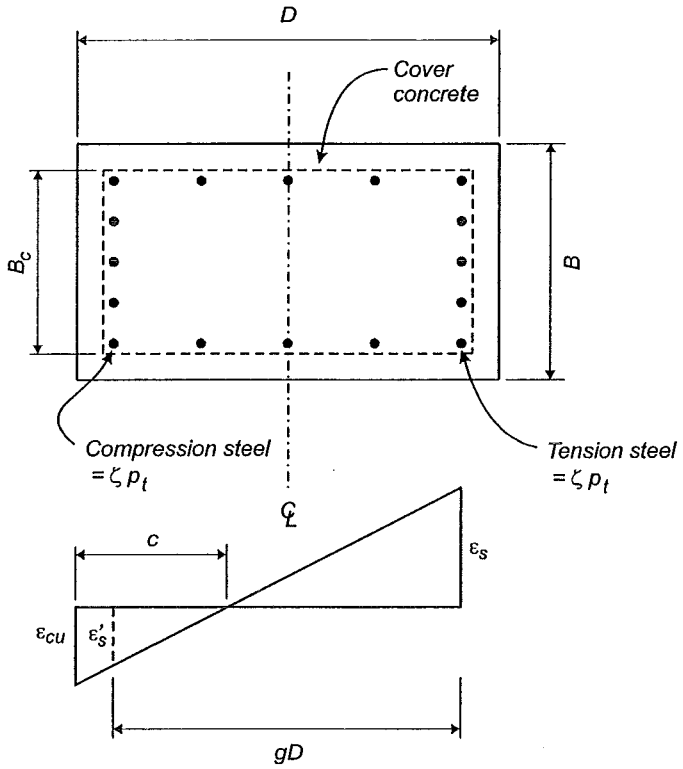

Figure C.1 *Rectangular Column Section Layout for Prediction of ACI Ideal Moment*

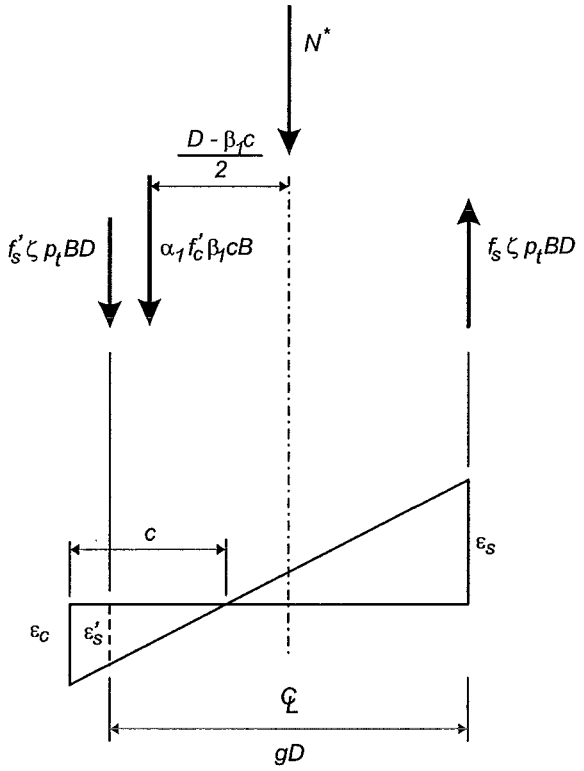

Figure C.2 *Components of Flexure from Concrete Compressive Force Resultant and Longitudinal Steel Couple*

illustrates the components of flexure from the concrete compressive force resultant and the longitudinal steel force couple.

The contribution of the concrete compressive force resultant can be determined by taking an equivalent rectangular stress block with an effective stress of $\alpha_1 f'_c$ and a depth of $\beta_1 c$ where c is the neutral axis depth which can be determined from Equation 8.30. Taking moments about the centreline of the column section gives-

$$\begin{aligned} M_{n,c} &= \alpha_1 \beta_1 f_c' cB \left(\frac{D}{2} - \frac{\beta_1 c}{2} \right) \\ &= \frac{1}{2} \alpha_1 \beta_1 f_c' \frac{c}{D} BD^2 \left(1 - \frac{\beta_1 c}{D} \right) \end{aligned} \qquad \text{(C.1)}$$

where α_1 = factor defining effective stress in rectangular stress block

= 0.85 for $f'_c \leq 55$ MPa

= $0.85 - 0.004 (f'_c - 55) \geq 0.75$ for $f'_c > 55$ MPa

β_1 = factor defining effective depth of rectangular stress block

= 0.85 for $f'_c \leq 30$ MPa

= $0.85 - 0.008 (f'_c - 30) \geq 0.65$ for $f'_c > 30$ MPa

f'_c = unconfined concrete compressive strength

c = distance from extreme compressive fibre to position of neutral axis

B = width of rectangular or square section

D = depth of rectangular or square section

The contribution from each column longitudinal bar can be determined individually from the strain profile in the section to determine the stress acting in each bar. The contribution of each bar to the flexural strength can then be found by taking moments of each resultant longitudinal bar force about the centreline of the section.

The longitudinal steel contribution to flexure can be determined as:-

$$M_{n,s} = \frac{\zeta p_t BD}{2}\left(f_s^{'} - \alpha_1 f_c^{'}\right)\frac{gD}{2} + \frac{\zeta p_t BD}{2} f_s \frac{gD}{2}$$
$$= \frac{1}{2} g\,\zeta p_t\, BD^2 f_c^{'}\left(\frac{f_s^{'} + f_s}{f_c^{'}} - \alpha_1\right) \qquad \text{(C.2)}$$

where
- g = ratio of distance between reinforcing bars closest to faces of rectangular column to section depth
- ζ = factor depending on distribution of longitudinal bars along faces of the column
- p_t = longitudinal steel ratio
- f'_s = stress in longitudinal steel on compression face of column resulting from strain compatibility, not taken greater than f_y
- f'_s = stress in longitudinal steel on tension face of column resulting from strain compatibility, not taken greater than f_y

In this approach the contribution to flexure of the longitudinal steel is assumed to come from a compressive and tensile steel force couple due to the longitudinal steel lumped at the extreme faces of the section. A parameter, ζ, accounts for the distribution of the longitudinal bars around the faces of the column, specifically the area of longitudinal steel located on each of the extreme faces of the column.

The stresses in the extreme compression and tension longitudinal bars, f'_s and f_s respectively, are determined from the strain profile in the section and are taken no greater than the yield strength of the longitudinal steel, f_y.

The compressive steel stress is reduced by $\alpha_1 f'_c$ to account for the area of concrete occupied by the compressive longitudinal steel bars. The lever arm at which the steel force couple acts is equal to gD / 2 taken from the centreline of the section.

The area of steel located at the extreme faces of the column is equal to $\zeta\, p_t BD$. For a simple case where the longitudinal steel is lumped at the extreme faces of the column the value for ζ is equal to 0.5. Where longitudinal steel is distributed on all faces of the column the contribution of the bars on the side faces is dependant on the ratio of

numbers of bars on the extreme faces of the column to the total number of longitudinal bars, ψ. In order to determine the relationship between ψ and ζ interaction diagrams were drawn up using Equation 8.29 and using the ACI method varying the value of ψ in the column. The value of ζ was varied to give a good fit between Equation 8.29 and the interaction diagram using the ACI method and a linear relationship was found to exist between ψ and ζ. Figure C.3 shows the linear relationship fit between ψ and ζ.

$$\zeta = 0.46\psi + 0.20 \qquad \text{(C.3)}$$

where ψ = ratio of number of bars on one end face of the column to the total number of longitudinal bars

Combining Equations C.1 and C.2 gives the predicted ACI ideal moment:-

$$M_n = \frac{1}{2}\left[\alpha_1\beta_1\frac{c}{D}\left(1-\beta_1\frac{c}{D}\right)+g\zeta\ p_t\left(\frac{f_s^{'}+f_s}{f_c^{'}}-\alpha_1\right)\right]BD^2f_c^{'} \qquad \text{(C.4)}$$

Figures C.4 to C.7 show the comparison between interaction diagrams determined using Equation 8.29 and the ACI method. These show that the difference between the two methods is approximately ±5 % for axial load ratios between 0.05 in tension and -0.7 in compression. The interaction diagrams using Equation 8.29 incorporate an expression for the neutral axis depth as determined from Equation 8.30.

C.3 EQUATION 8.30 - NEUTRAL AXIS DEPTH RATIO

Equation 8.30 presents an expression for the neutral axis depth of a section in terms of the section geometry, axial load ratio and longitudinal steel ratio. This expression was determined from a parametric study of rectangular columns, similar to that conducted to determine the proposed expressions presented in Chapter 7. This gives

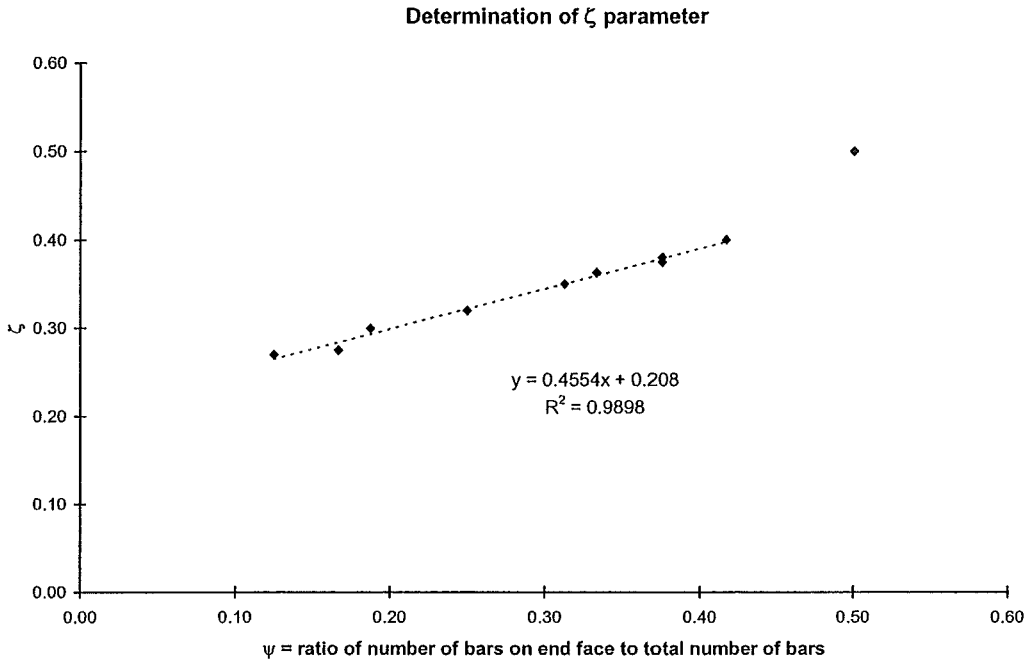

Figure C.3 *Linear Relationship Fit Between ψ and ζ*

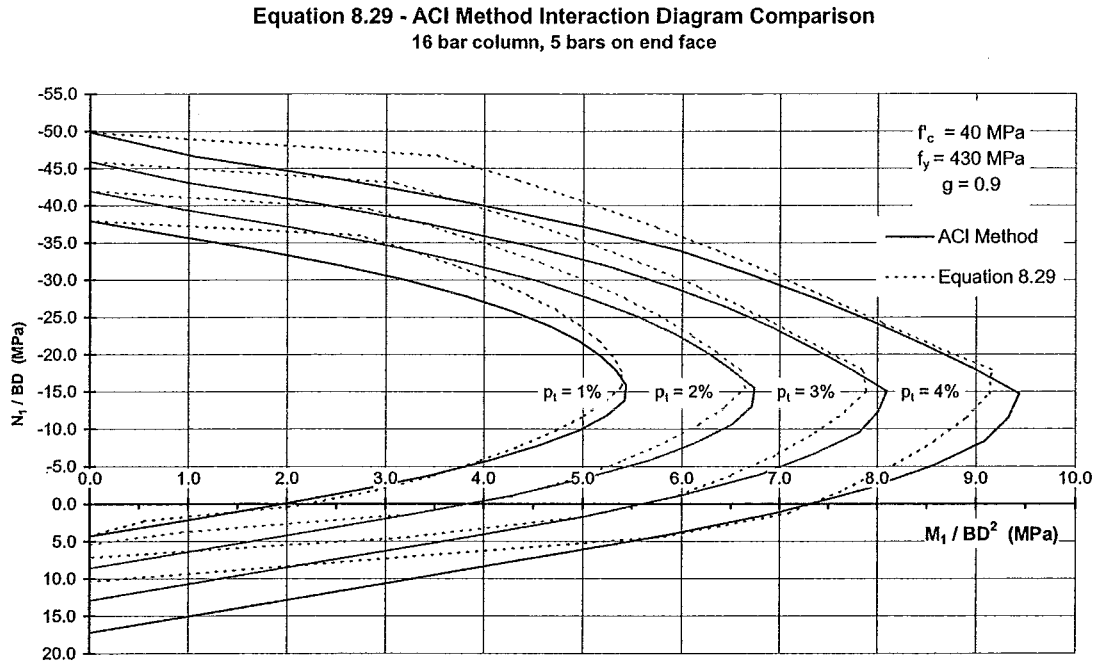

Figure C.4 *Interaction Diagram Comparison Between Equation 8.29 and ACI Method for f_y = 430 MPa, f'_c = 40 MPa and g = 0.9*

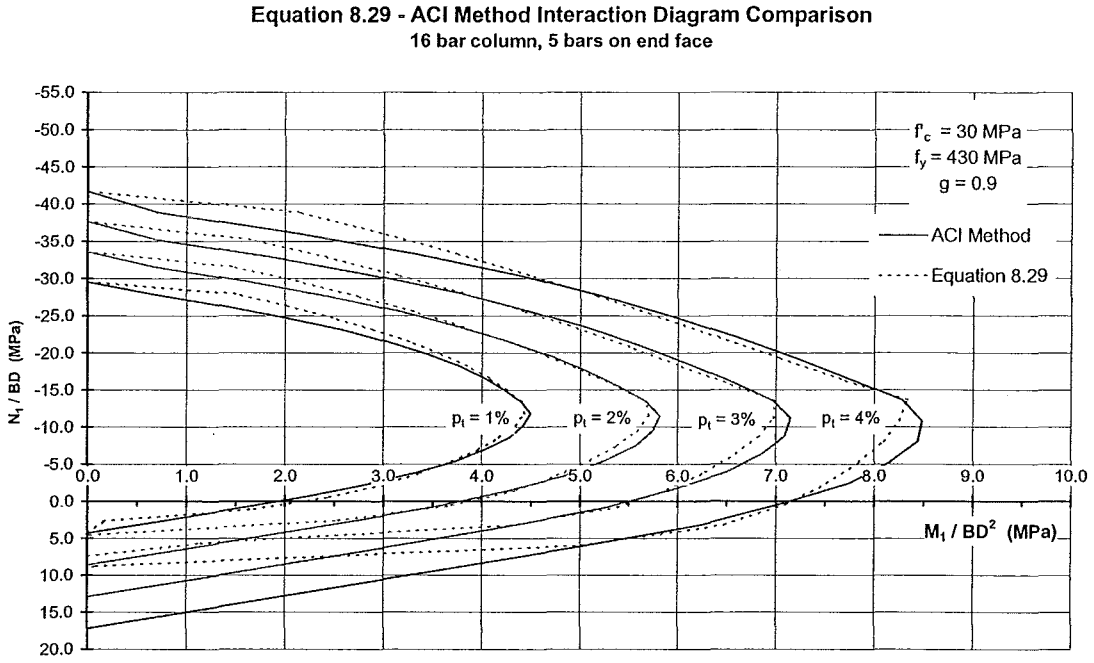

Figure C.5 *Interaction Diagram Comparison Between Equation 8.29 and ACI Method for f_y = 430 MPa, f'_c = 30 MPa and g = 0.9*

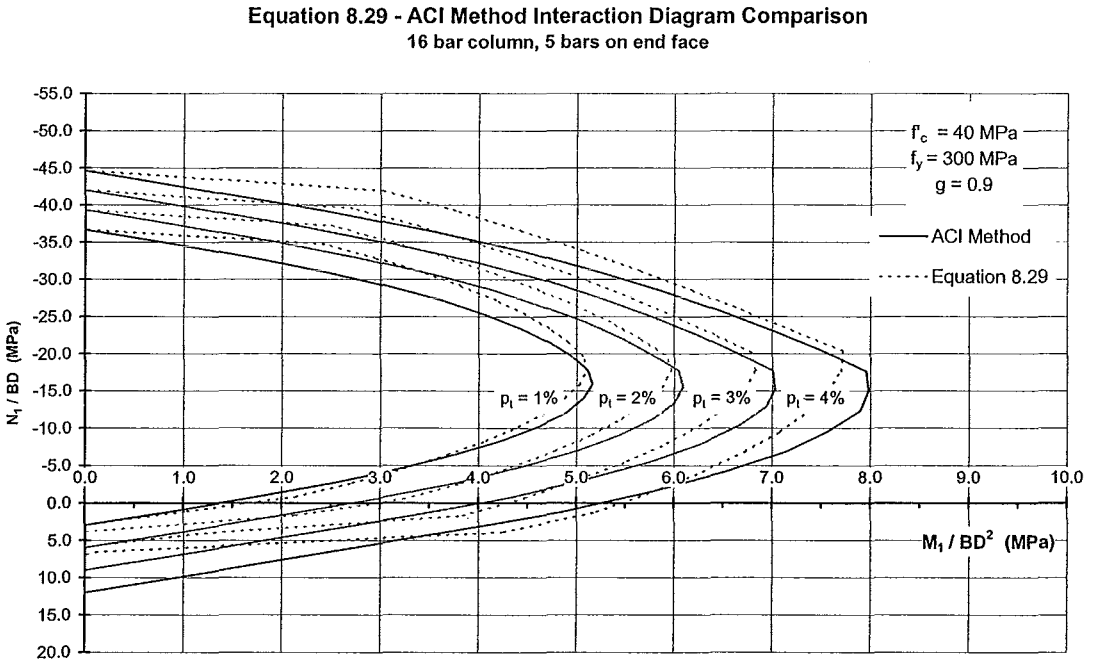

Figure C.6 *Interaction Diagram Comparison Between Equation 8.29 and ACI Method for f_y = 300 MPa, f'_c = 40 MPa and g = 0.9*

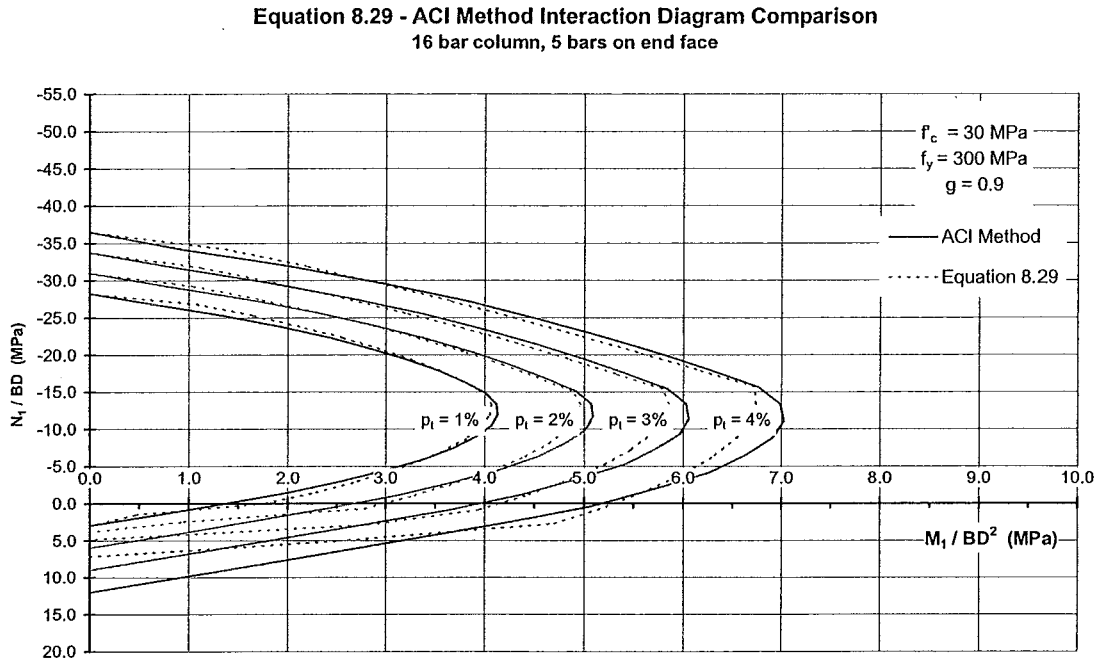

Figure C.7 *Interaction Diagram Comparison Between Equation 8.29 and ACI Method for f_y = 300 MPa, f'_c = 30 MPa and g = 0.9*

the neutral axis depth for a section at an extreme compressive fibre strain, $\varepsilon_c = -0.003$, the strain usually assumed to correspond to development of the ACI nominal moment, balancing the internal concrete and steel forces to the applied, external, axial load. The axial load ratio was varied from 0.05 in tension to -0.7 in compression, longitudinal steel ratios from 0.8 % to 4 %, values for g taken as 0.8, 0.9 and 1.0, and mechanical ratios were investigated from m = 6 to m = 30.

The neutral axis depth was found to vary linearly with axial load ratio as a function of both p_t, m and $p_t m$. Figure C.8 shows typical results from the parametric study for a section containing a longitudinal steel ratio of 1.5 %. A simplified linear relationship was used to determine the coefficient of the axial load ratio term as a function of p_t, m and $p_t m$. The constant of the linear term with axial load ratio for neutral axis depth was also found to depend on p_t, m and $p_t m$.

The expression for the neutral axis depth ratio was found to be:-

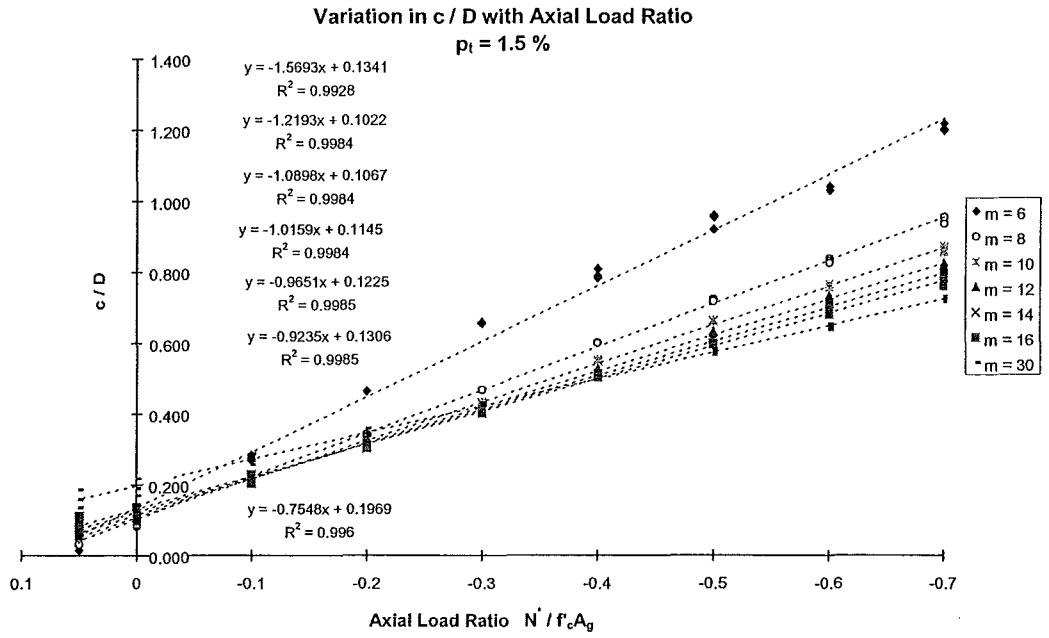

Figure C.8 *Variation in c / D with Axial Load Ratio for Rectangular Column with* $p_t = 1.5\ \%$

$$\frac{c}{D} = \frac{N^*}{f_c' A_g}\left[6.9p_t + 0.015m + 0.24p_t m - 1.4\right] + 0.0025m + \gamma \qquad \text{(C.5)}$$

where $\gamma = (0.11m + 2.1)p_t + 0.03$ for $m \le 25$

$\gamma = 4.85p_t - 0.05$ for $m > 25$

$N^* / f'_c A_g$ is taken as negative for compressive axial loads

The term γ is required to give better correlation between the predicted ACI moment, M_n, and the ACI moment, M_i, for higher values of m. Once the neutral axis depth of a section is determined strains and stresses can be determined for the longitudinal steel placed in the section based on the strain profile with an extreme compressive fibre strain of $\varepsilon_c = -0.003$.

C.4 EQUATION 8.31 - PREDICTION OF MAXIMUM FLEXURAL STRENGTH

The maximum flexural strength of a column section will be influenced by the increase in concrete compressive strength due to confinement from the transverse reinforcement and strain hardening of the longitudinal steel. Derivation of Equation 8.31 attempts to account for the effects of confinement and strain hardening increasing the flexural strength of a section. The same concept of determining the contributions to flexure due to the concrete compressive force resultant and the longitudinal steel couple are applied in this equation.

Figure C.9 shows the distribution of the concrete stresses at different curvature ductilities for Unit 9 tested by Watson and Park [W3]. The column cross section is modelled defining the areas of ineffectively and effectively confined concrete core within the column as presented in Section 8.6. This reflects the influence of arching in the column between transverse hoop sets and restrained longitudinal bars. At higher strains, and curvature ductilities, the region of ineffective concrete at the compression edge of the column can be seen to be supporting close to zero stress. The stress distribution has become rectangular in shape with the peak stress remaining reasonable constant across the compressed region of the column.

The concrete compressive force resultant remains reasonably constant during the moment curvature response for curvatures beyond the yield curvature. Due to the increased concrete compressive strength due to confinement from the transverse reinforcement the depth of the region to support this concrete force can be reduced. The region supporting compressive stresses is reduced by the region of ineffectively confined concrete, which can be expressed in terms of the confined concrete efficiency factor, and through the reduction due to the increased concrete compressive strength which can be expressed in terms of the ratio of the peak confined concrete compressive strength, f'_{cc}, to the unconfined strength, f'_c. Figure C.10 shows the region of a column cross section which is assumed to support the

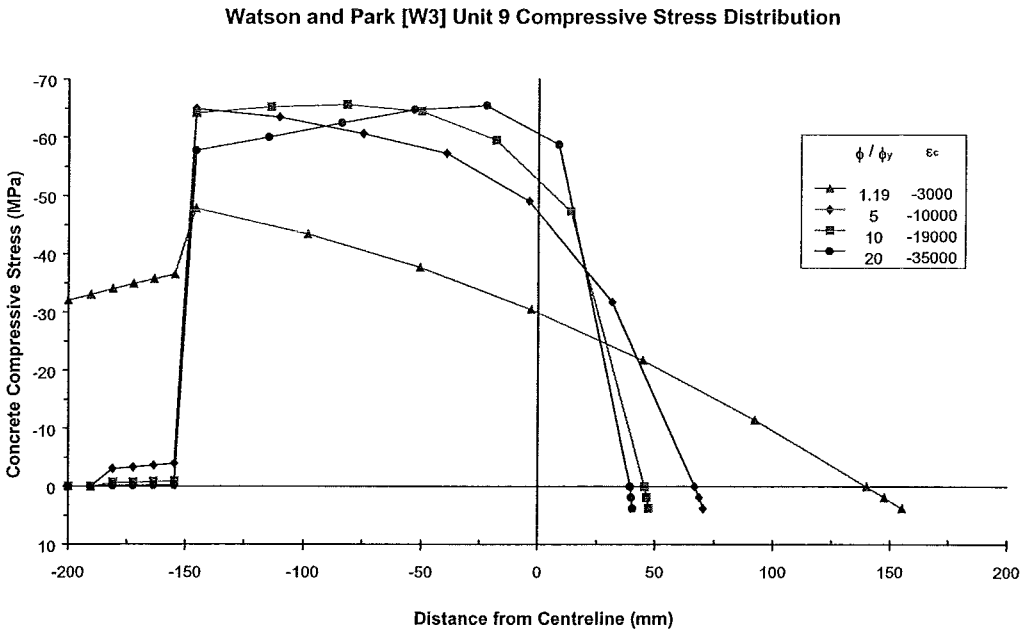

Figure C.9 *Concrete Compressive Stress Distribution in Unit 9 by Watson and Park [W3]*

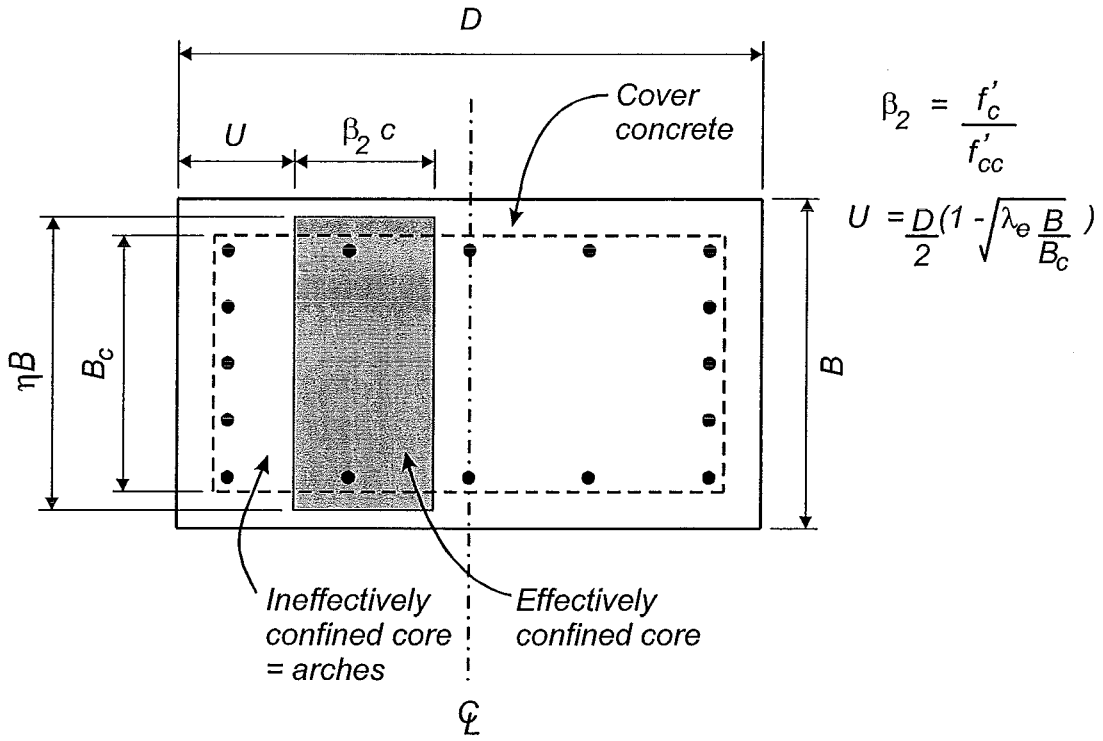

Figure C.10 *Region to Support Confined Concrete Compressive Force in Rectangular Column After Spalling of Cover Concrete*

concrete compressive force after spalling of the cover concrete. Expressing the reduction in depth of the compression zone due to the ineffectively confined region can be expressed as:-

$$U = \frac{D}{2} - \frac{D_{cc}}{2} \qquad \text{(C.6)}$$

This can be expressed in terms of the confined concrete efficiency factor as:-

$$\lambda_e = \frac{B_c D_{cc}^2}{BD^2} \qquad \text{(C.7a)}$$

$$D_{cc} = \sqrt{\frac{\lambda_e BD^2}{B_c}} \qquad \text{(C.7b)}$$

so that:-

$$U = \frac{D}{2}\left[1 - \sqrt{\frac{\lambda_e B}{B_c}}\right] \qquad \text{(C.8)}$$

where λ_e = confined concrete efficiency factor described in Section 8.8.2.1

B_c = core width dimension of rectangular or square section taken to the centreline of peripheral hoop

Derivation of λ_e is included in Appendix D along with formulations for other section shapes. The reduction in the depth of the compression zone due to the increased concrete compressive strength can be expressed as:-

$$\beta_2 = \frac{f_c'}{f_{cc}'} \qquad \text{(C.9)}$$

Referring to Figure C.10 and taking moments about the centreline of the section the contribution to flexure from the concrete compressive force resultant can be evaluated.

$$M_{o,c} = f_{cc}^{'} \eta B \beta_2 c \left(\frac{D}{2} - U - \frac{\beta_2 c}{2} \right) \qquad \text{(C.10)}$$

Substituting Equations C.8 and C.9 into Equation C.10 gives:-

$$M_{o,c} = \frac{\eta}{2} f_c^{'} B D^2 \frac{c}{D} \left(\sqrt{\frac{\lambda_e B}{B_c}} - \frac{f_c^{'}}{f_{cc}^{'}} \frac{c}{D} \right) \qquad \text{(C.11)}$$

At development of the maximum flexural strength the longitudinal steel is assumed to have yielded and entered the strain hardening region. The couple provided by the longitudinal steel at the extreme faces can be evaluated as:-

$$\begin{aligned} M_{o,s} &= \frac{\zeta\ p_t BD}{2} \left(\lambda_C f_y - f_c^{''} \right) \frac{gD}{2} + \frac{\zeta\ p_t BD}{2} \lambda_T f_y \frac{gD}{2} \\ &= \frac{1}{2} \left(\lambda_C + \lambda_T - \frac{f_c^{''}}{f_y} \right) g\zeta\ p_t BD^2 f_y \end{aligned} \qquad \text{(C.12)}$$

The term f''c is the compressive stress in the concrete at the location of the longitudinal bars on the compression face of the column to account for the area of concrete occupied by the longitudinal bars in the compression region of the column. As these bars are located within the region of the column core which is ineffectively confined the stress carried in the concrete, after spalling of the cover concrete, can be taken as zero. This gives:-

$$M_{o,s} = \frac{1}{2} \left(\lambda_C + \lambda_T \right) g\zeta\ p_t BD^2 f_y \qquad \text{(C.13)}$$

Combining Equations C.11 and C.13 gives the predicted maximum flexural strength of a section:-

$$M_o = \left[\frac{\eta}{2} \frac{c}{D} \left(\sqrt{\frac{\lambda_e B}{B_c}} - \frac{f_c'}{f_{cc}'} \frac{c}{D} \right) + \frac{(\lambda_C + \lambda_T) g\zeta \; p_t f_y}{2 f_c'} \right] BD^2 f_c' \quad \text{(C.14)}$$

For sections with low values of λ_e or with low values of f'_c / f'_{cc} the maximum flexural strength given by Equation C.14 may be less than that given by Equation C.4. This is due to the inefficient layout of transverse reinforcement, low λ_e values, or a low amount of transverse reinforcement provided in the column for confinement, low of f'_c / f'_{cc} values.

APPENDIX D

Derivation of λ_e, Confined Concrete Efficiency Factor

D.1 INTRODUCTION

The objective of defining the confined concrete efficiency factor, λ_e, is to derive a term which is simple and easy to determine and reflects the transverse reinforcement arrangement, namely the influence of the arrangement on the arching that occurs within the core of a column subjected to axial load and flexure.

Core dimensions of the column, B_c and D_c, are taken to the centreline of the peripheral hoop. This assumes the region of cover concrete extends to the peripheral hoop centreline. Arching only occurs over the compressed region of the column and is assumed to take place on the compression face of the column only. Any arching that occurs down the sides of the column between the compression edge of the column and the neutral axis is ignored.

Vertical and horizontal arching is assumed to commence at the centreline of the peripheral hoop over the clear distance between transverse hoop sets or the clear distance between restrained longitudinal bars. This follows the same assumptions of arch profile as used by Mander et al. [M3, M4]. The extent of horizontal and vertical arching depends on the chosen arch profile, spacings between transverse hoop sets, distances between restrained longitudinal bars and the initial tangent angle of the arches.

Figure D.1 shows the parabolic arch profile assumed in this study. Mander et al. assumed parabolic arch profiles with an initial tangent angle of $\theta = 45°$. Arching was assumed to take place over the clear distance between each transverse hoop set, s', and the clear distance between restrained longitudinal bars, w'.

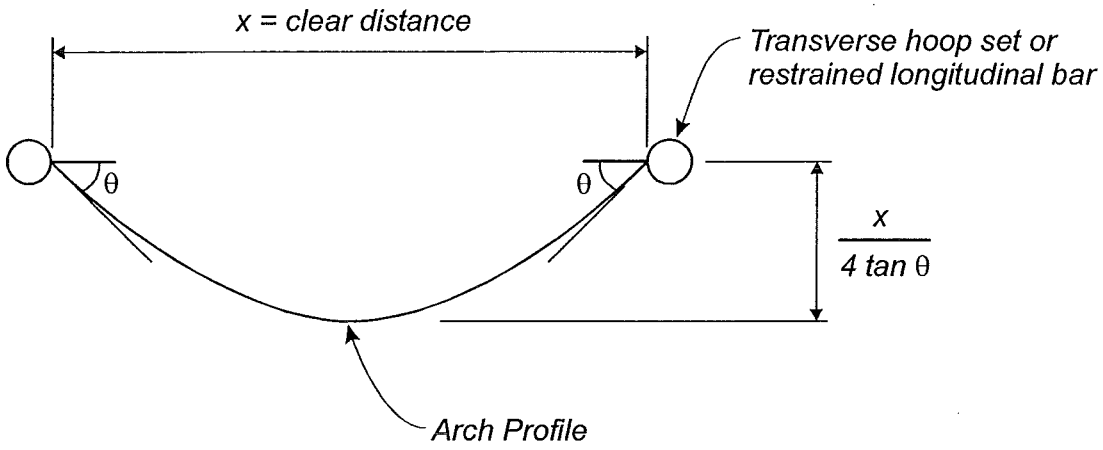

Figure D.1 *Profile for Horizontal and Vertical Arching*

This gives the extent of vertical arching as:-

$$a_v = \frac{s'}{4 \tan\theta} \qquad \text{(D.1)}$$

where s' = clear distance between transverse hoop sets

θ = initial tangent angle of parabolic arches

The extent of horizontal arching is given as:-

$$a_h = \frac{w'}{4 \tan\theta} \qquad \text{(D.2)}$$

where w' = average clear distance between restrained longitudinal bars

θ = initial tangent angle of parabolic arches

The term D_{cc} / 2 is the distance from the centreline of the column to the extent of arching within the column core, from the compression edge of the column. The confined concrete efficiency factor is taken as the ratio of the first moment of area of the effectively confined core area to the area of the column, taken about the centreline of the section. This follows the definition of the modified confinement efficient factor, k^*_e, by Zahn et al. [Z1] to reflect the greater contribution to the moment from the fibres further from the neutral axis.

Calculation of the confined concrete efficiency factor does not take into account the area of longitudinal steel in the compressed region of the column. This factor is determined to reflect the transverse reinforcement arrangement and its influence on the degree of confinement provided to the column section.

D.2 RECTANGULAR SECTIONS

Figure 8.33 is reproduced as Figure D.2 and illustrates the section dimensions used for determining the confined concrete efficiency factor, λ_e, for rectangular sections.

Rectangular sections are subjected to both vertical arching, between transverse hoop sets and horizontal arching between restrained longitudinal bars. The combined horizontal and vertical arching forms a hyperbolic paraboloid truncated surface. The projection of this surface, midway between transverse hoop sets, determines the size of the effectively confined core region which can be expressed as a simple rectangle with a depth D_{cc} given by:-

$$D_{cc} = D_c - 2\left(a_v + \frac{2}{3}a_h\right) \qquad \text{(D.3)}$$

This simplifies the parabolic projection of the horizontal arching into an equivalent rectangular area to allow simpler evaluation of the effectively confined core region.

The confined concrete efficiency factor is given by:-

$$\lambda_e = \frac{\left(\frac{B_c D_{cc}}{2}\right)\left(\frac{D_{cc}}{4}\right)}{\left(\frac{B D}{2}\right)\left(\frac{D}{4}\right)} = \frac{B_c D_{cc}^2}{B D^2} \qquad \text{(D.4)}$$

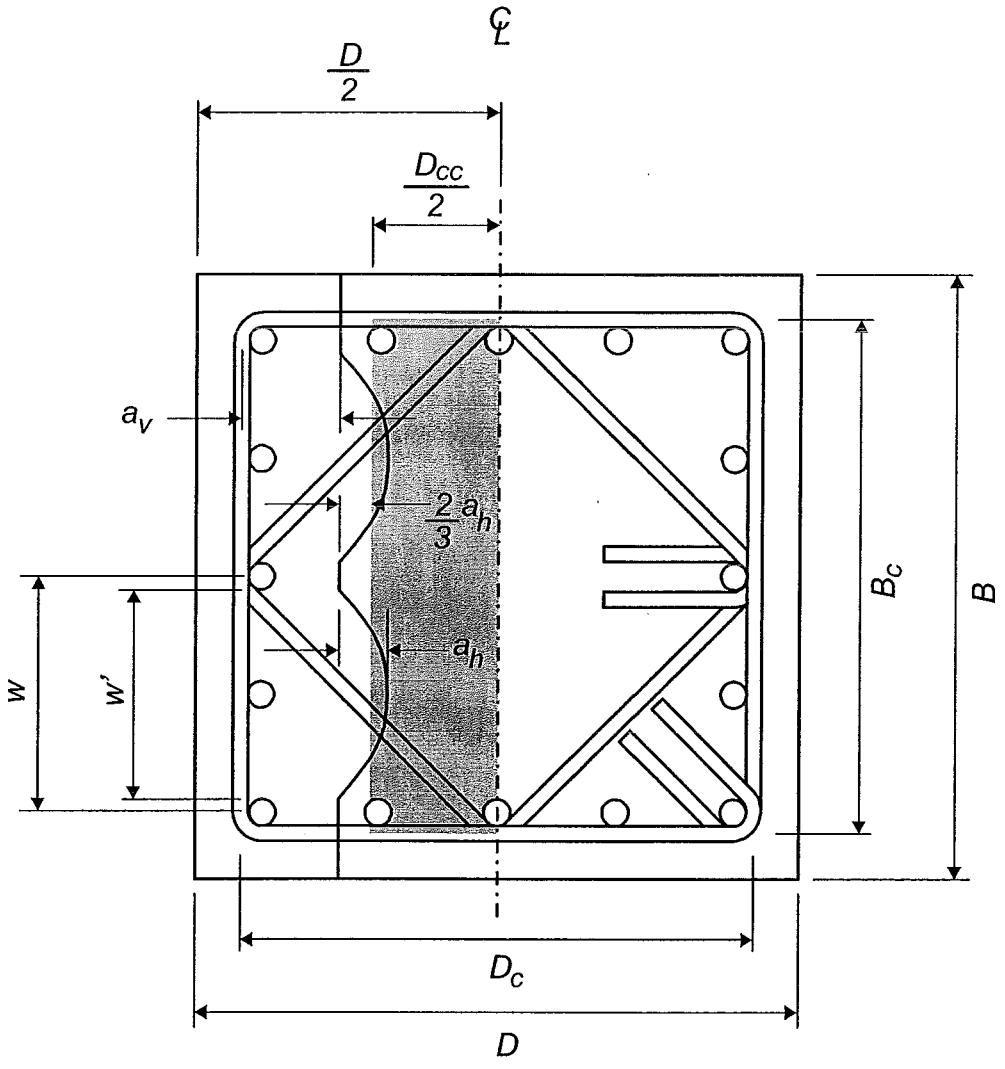

Figure D.2 *Section Dimensions Used to Determine λ_e for Rectangular Sections*

D.3 CIRCULAR SECTIONS

Figure D.3 shows the geometry of circular sections for determination of the confined concrete efficiency factor. The column core is only affected by vertical arching between transverse hoop sets as shown by the dashed line inside the column core. Arching for circular columns reinforced with circular hoops is assumed to apply for columns reinforced with spirals. The region of ineffectively confined core within the compressed concrete in the column is assumed to be bounded by a line parallel with the neutral axis of the column. Therefore midway between transverse hoop sets the ineffectively confined core is given by a line parallel to the neutral axis of the column extending to the point where the projection of the vertical arching encroaches on the column core. The extent of vertical arching is given by Equation D.1 and the depth of the effectively confined core is given by:-

$$D_{cc} = D_c - 2a_v \tag{D.5}$$

The confined concrete efficiency factor is then given by:-

$$\lambda_e = \frac{A_1\bar{x}_1 - A_2\bar{x}_2}{A_1\bar{x}_1} \tag{D.6}$$

where

$$A_1 = \frac{\pi D^2}{8}$$

$$\bar{x}_1 = \frac{2D}{3\pi}$$

$$A_2 = \frac{D^2}{8}(\alpha - \sin\alpha)$$

$$\bar{x}_2 = \frac{\left(D^2 - D_{cc}^2\right)^{3/2}}{12\,A_2}$$

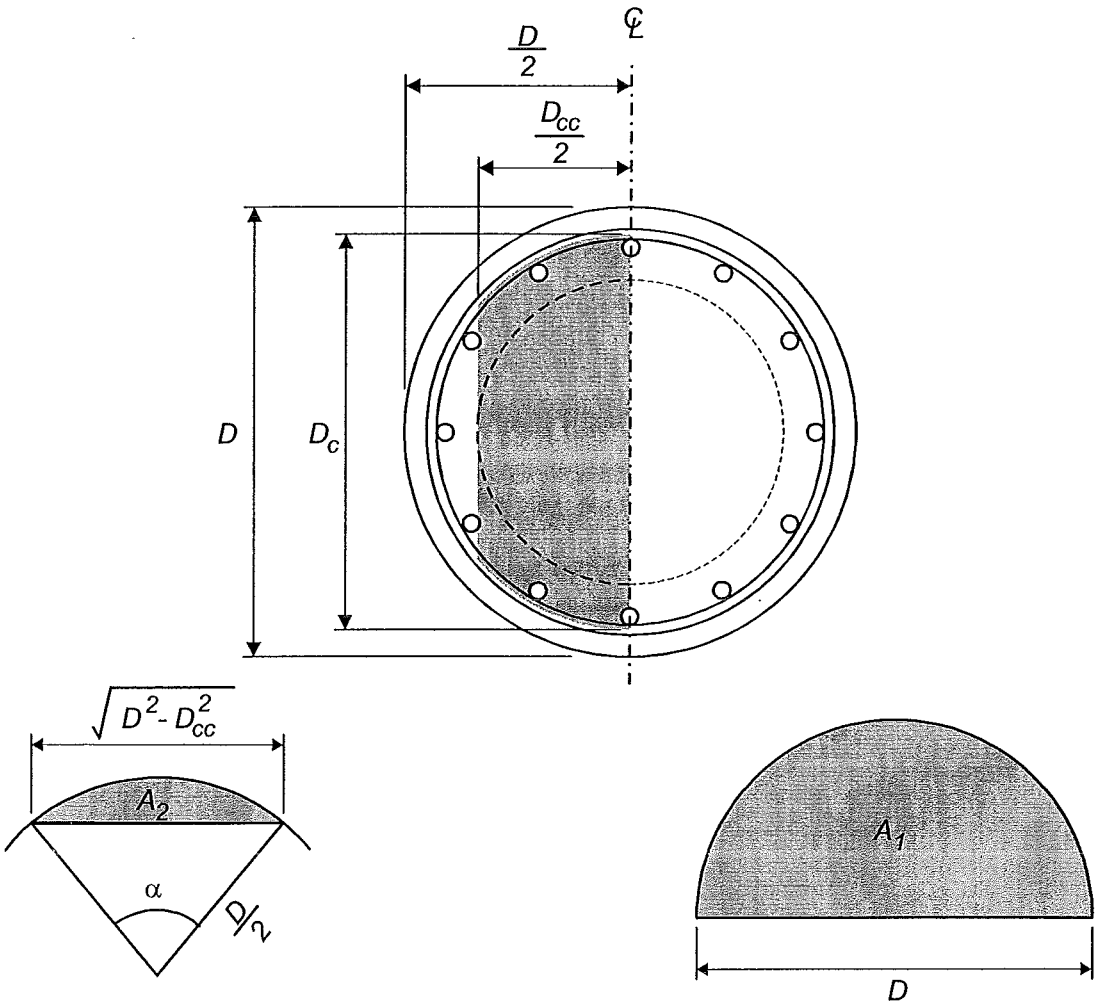

Figure D.3 *Section Dimensions Used to Determine λ_e for Circular Sections*

$$\lambda_e = 1 - \left[1 - \left(\frac{D_{cc}}{D} \right)^2 \right]^{3/2} \qquad \text{(D.7)}$$

D.4 SQUARE SECTIONS LOADED ACROSS DIAGONAL

Figure D.4 shows the section geometry and dimensions for square sections which are loaded from corner to corner across the diagonal of the cross section.

The depth of the effectively confined core is taken as for rectangular sections given by Equation D.3. The confined concrete efficiency factor is then given by Equation D.6 where:-

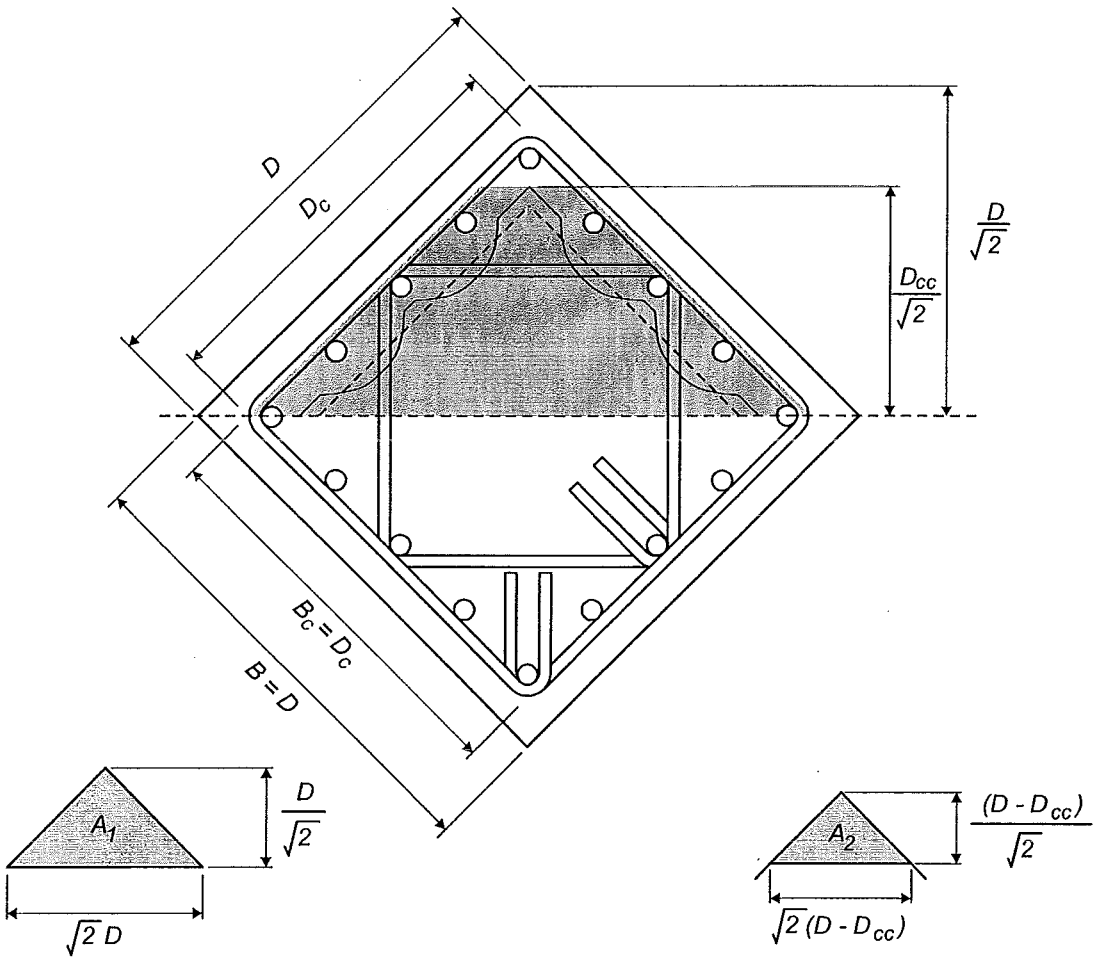

Figure D.4 *Section Dimensions Used to Determine λ_e for Square Sections Loaded Across the Diagonal*

$$A_1 = \frac{D^2}{2}$$

$$\bar{x}_1 = \frac{D}{3\sqrt{2}}$$

$$A_2 = \frac{(D - D_{cc})^2}{2}$$

$$\bar{x}_2 = \frac{(4D - D_{cc})}{3\sqrt{2}}$$

The confined concrete efficiency factor is then:-

$$\lambda_e = 1 - \left[\frac{(D - D_{cc})^2 (4D - D_{cc})}{D^3} \right] \qquad \text{(D.8)}$$

D.5 RECTANGULAR COLUMNS WITH ROUNDED ENDS

Rectangular columns with rounded ends were tested by Tanaka and Park [T1] studying the behaviour of column reinforced with interlocking transverse spiral reinforcement. This type of section may also be encountered in bridge piers as an alternative to a rectangular shaped column so that confinement can be efficiently provided to the section and all column longitudinal bars can benefit from the restraint provided by the transverse spirals. Figure D.5 illustrates the section dimensions for this type of column. The rounded ends of the column are taken as circular so the diameter of the rounded end, D_c', is equal to the overall width of the section, B.

Assuming only arching occurs in the vertical plane between the transverse spirals the effectively confined core shape can be approximated as the same shape as the overall column as indicated by the dashed line within the column core. The actual effectively confined core shape will be in a "Figure 8" shape due to vertical arching in both transverse spiral sets.

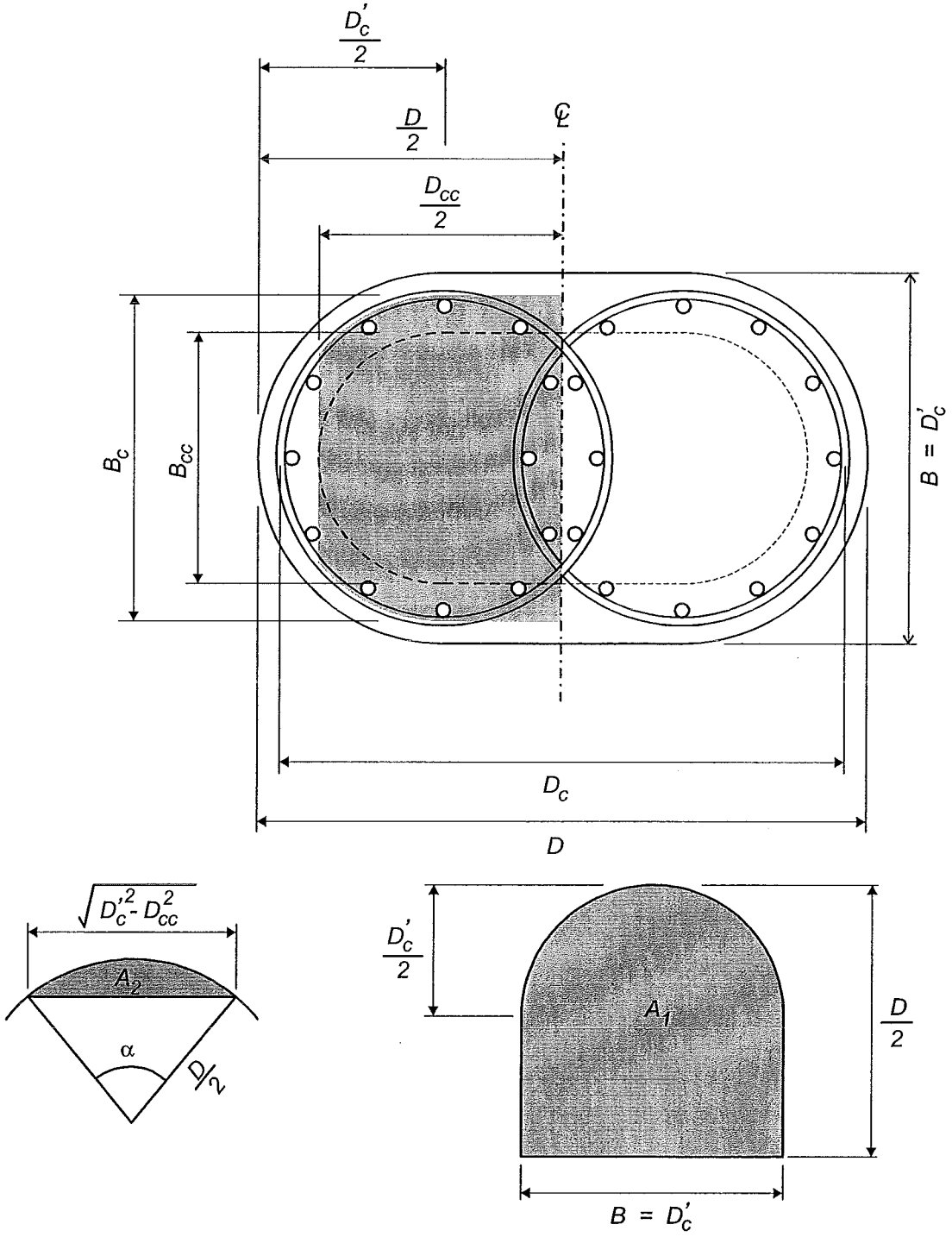

Figure D.5 *Section Dimensions Used to Determine λ_e for Rectangular Sections with Rounded Ends*

The depth of the effectively confined core region is given by Equation D.5 where D_c is taken as the distance between centrelines of the two sets of spiral or hoop reinforcement provided in the column as shown in Figure D.5. Again Equation D.6 gives the confined concrete efficiency factor with:-

$$A_1 = \frac{\pi D_c'^2}{8} + \frac{D_c'(D - D_c')}{2}$$

$$\bar{x}_1 = \frac{\left[\frac{(D - D_c')^2}{2D_c'} + \frac{\pi}{4}(D - D_c') + \frac{D_c'}{3}\right]}{\left[\frac{2(D - D_c')}{D_c'} + \frac{\pi}{2}\right]}$$

$$A_2 = \frac{D_c'^2}{8}(\alpha - \sin\alpha)$$

$$\bar{x}_2 = \frac{(D_c'^2 - D_{cc}^2)^{3/2}}{12 A_2}$$

This gives an expression for the confined concrete efficiency factor of:-

$$\lambda_e = 1 - \frac{\left[\frac{\pi}{2} + \frac{2(D - D_c')}{D_c'}\right]\left[\frac{(D_c'^2 - D_{cc}^2)^{3/2}}{12}\right]}{\left[\frac{\pi D_c'^2}{8} + \frac{D_c'(D - D_c')}{2}\right]\left[\frac{(D - D_c')^2}{2D_c'} + \frac{\pi}{4}(D - D_c') + \frac{D_c'}{3}\right]} \qquad \text{(D.9)}$$

Equation D.9 for λ_e can be shown to reduce to the same as Equation D.7 when $D_c' = D$, which would be the case for a circular column.

APPENDIX E

Variation of f_y in Equations 7.7 to 7.14

E.1 INTRODUCTION

Equations 7.7 to 7.14 presented in Chapter 7 were derived from a parametric study using constant values of longitudinal yield strength $f_y = 300$ MPa. Details of the study are contained in Chapter 7. These expressions are intended to be used for a quick, hand calculation assessment, of potential problems due to the tension shift effect. Included here are plots of the data points for each variable presented against the proposed equations to demonstrate the degree of fit. Comparison of the proposed expressions with analyses conducted with $f_y = 250$ MPa and 350 MPa are also included.

E.2 RECTANGULAR COLUMNS

Figures E.1 to E.4 show plots of the proposed equations from the parametric study, discussed in Chapter 7, for rectangular columns with a constant longitudinal yield strength of $f_y = 250$ MPa and $g = 0.9$. Figures E.5 to E.8 compare the data points for the proposed equations using $f_y = 300$ MPa, the initial data points used to fit the equations. Figures E.9 to E.12 compare the data points for the proposed equations using $f_y = 350$ MPa.

From the data plotted the fit between the proposed equations, derived from analyses with $f_y = 300$ MPa, remains a reasonable fit for the data points obtained from analyses conducted with longitudinal yield strengths at the lower and upper bounds recommended. Similar results are obtained for $g = 0.8$ and 1.0. For longitudinal yield strengths significantly different from these values, $f_y = 250 - 350$ MPa, a moment-curvature analysis can be used to obtain the appropriate values.

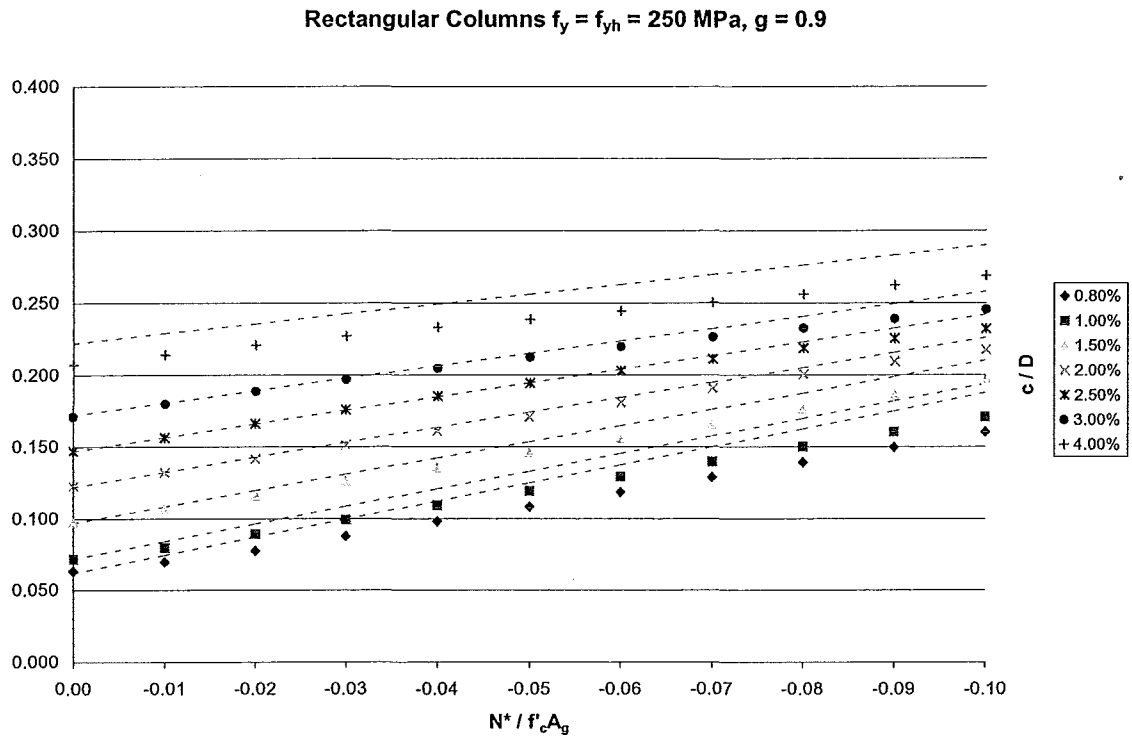

Figure E.1 *Rectangular Column, f_y = 250 MPa, Comparison with Eqn 7.13*

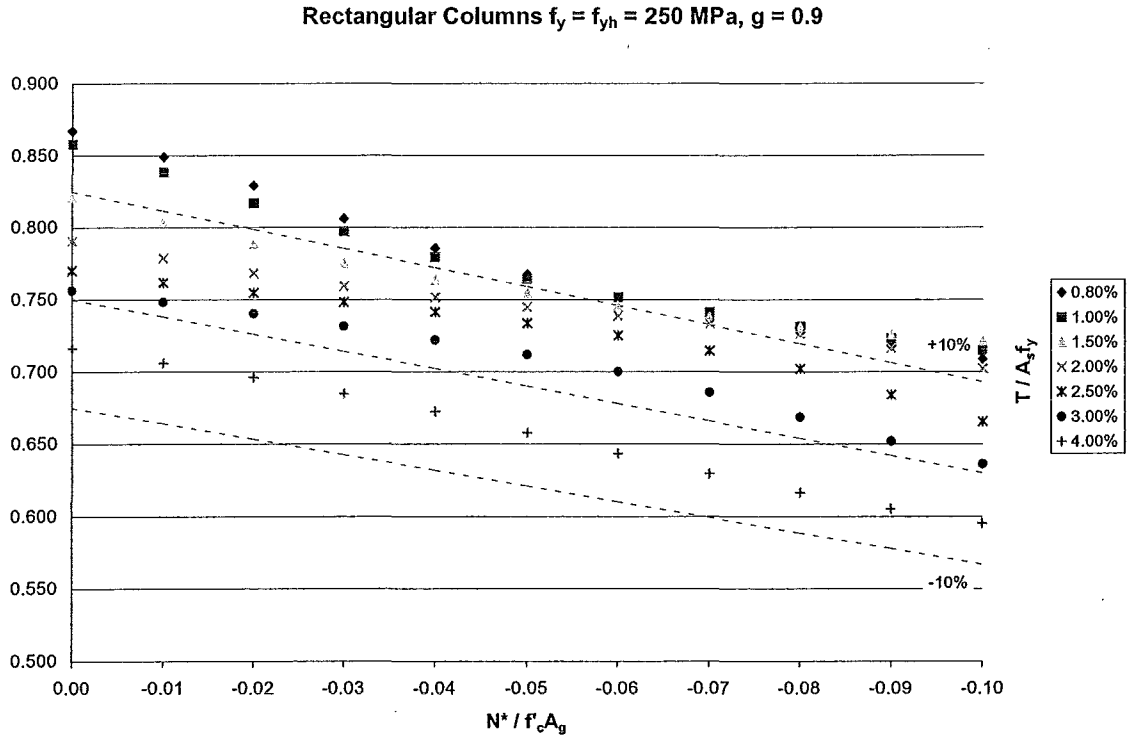

Figure E.2 *Rectangular Column, f_y = 250 MPa, Comparison with Eqn 7.9*

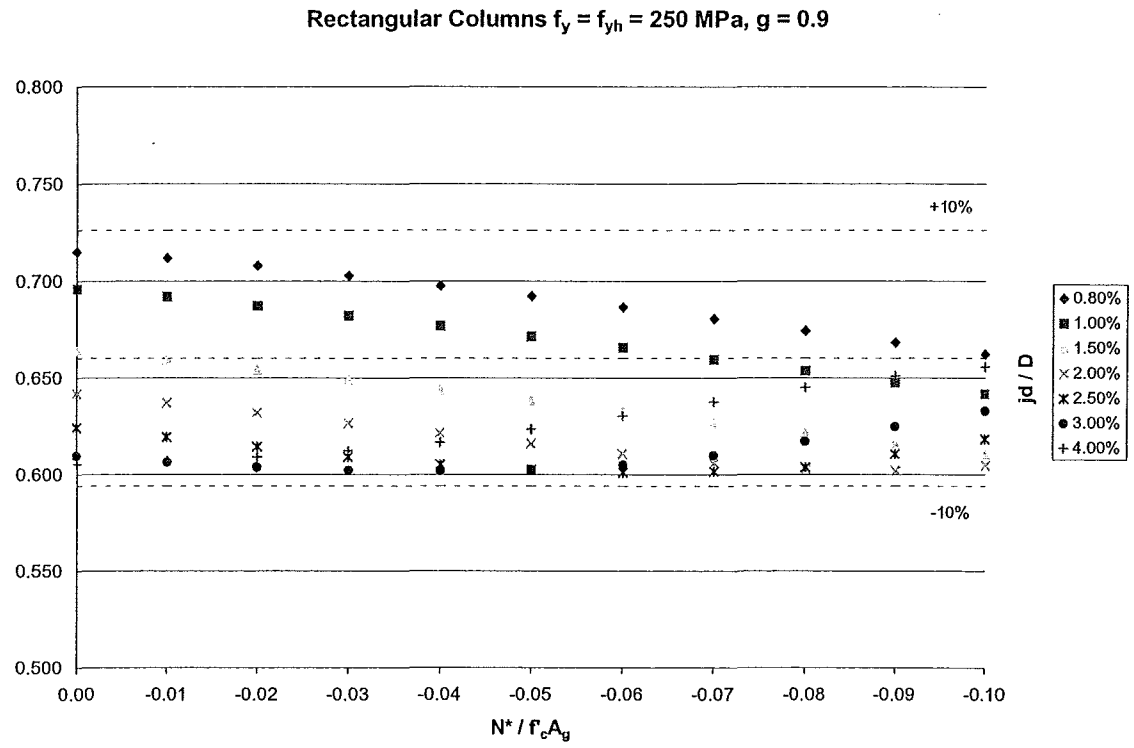

Figure E.3 *Rectangular Column, f_y = 250 MPa, Comparison with Eqn 7.7*

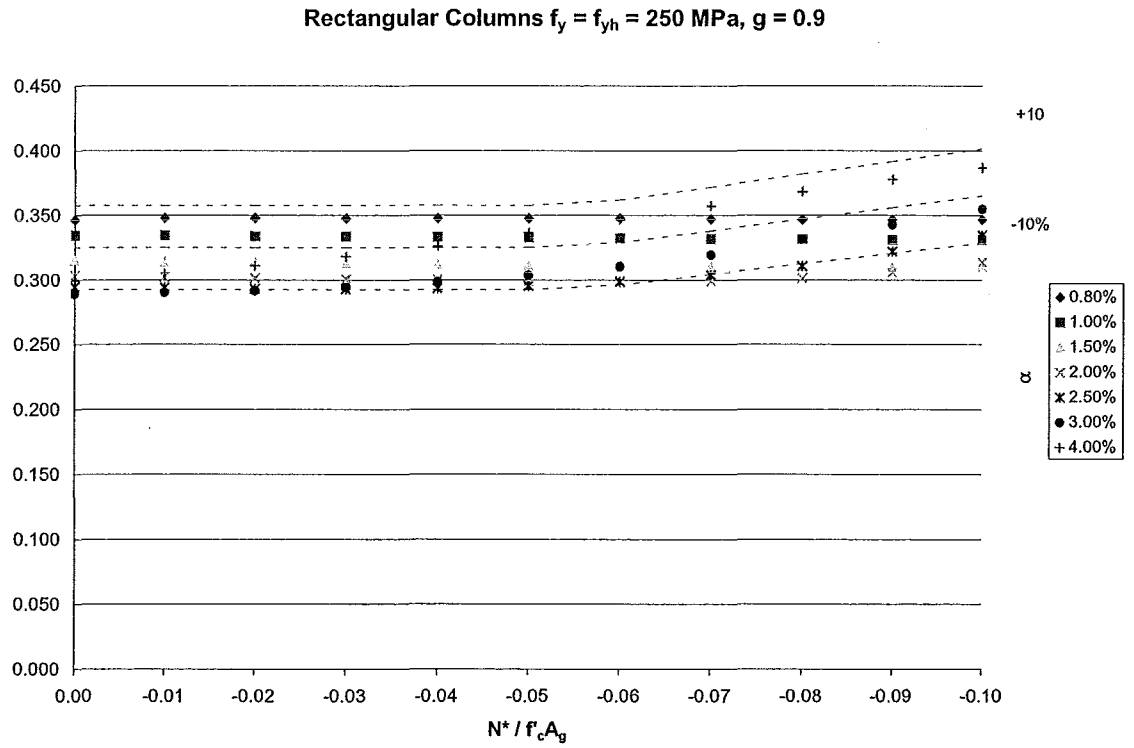

Figure E.4 *Rectangular Column, f_y = 250 MPa, Comparison with Eqn 7.11*

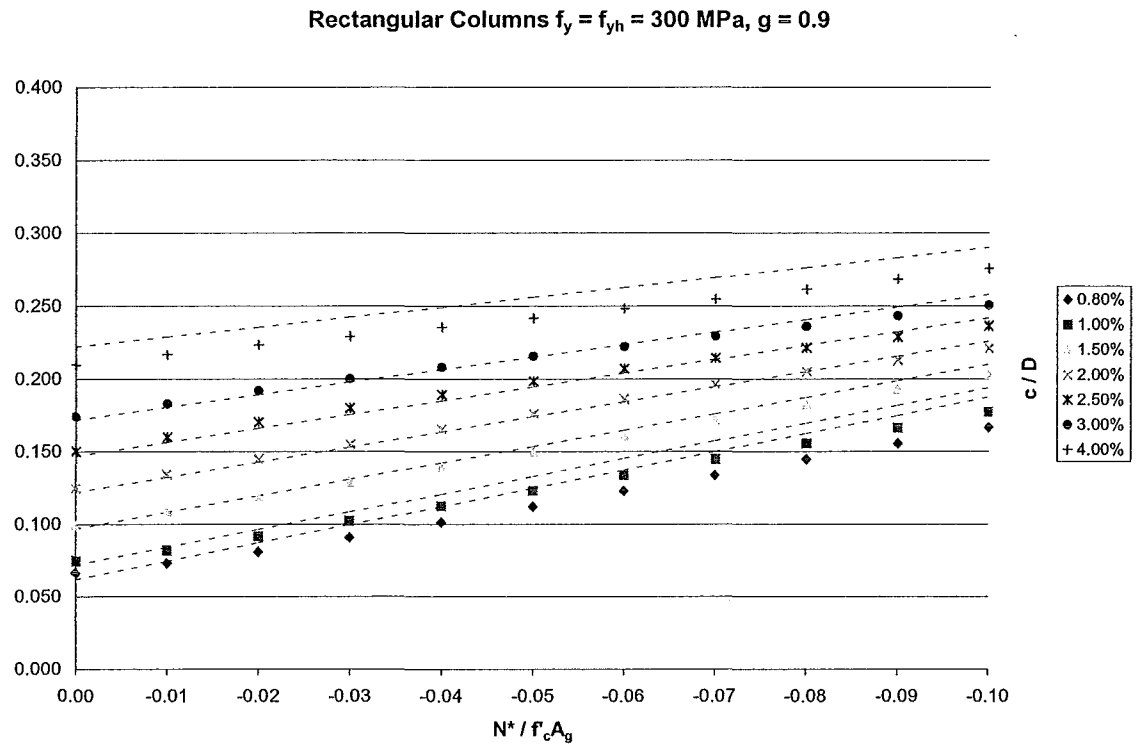

Figure E.5 *Rectangular Column, f_y = 300 MPa, Comparison with Eqn 7.13*

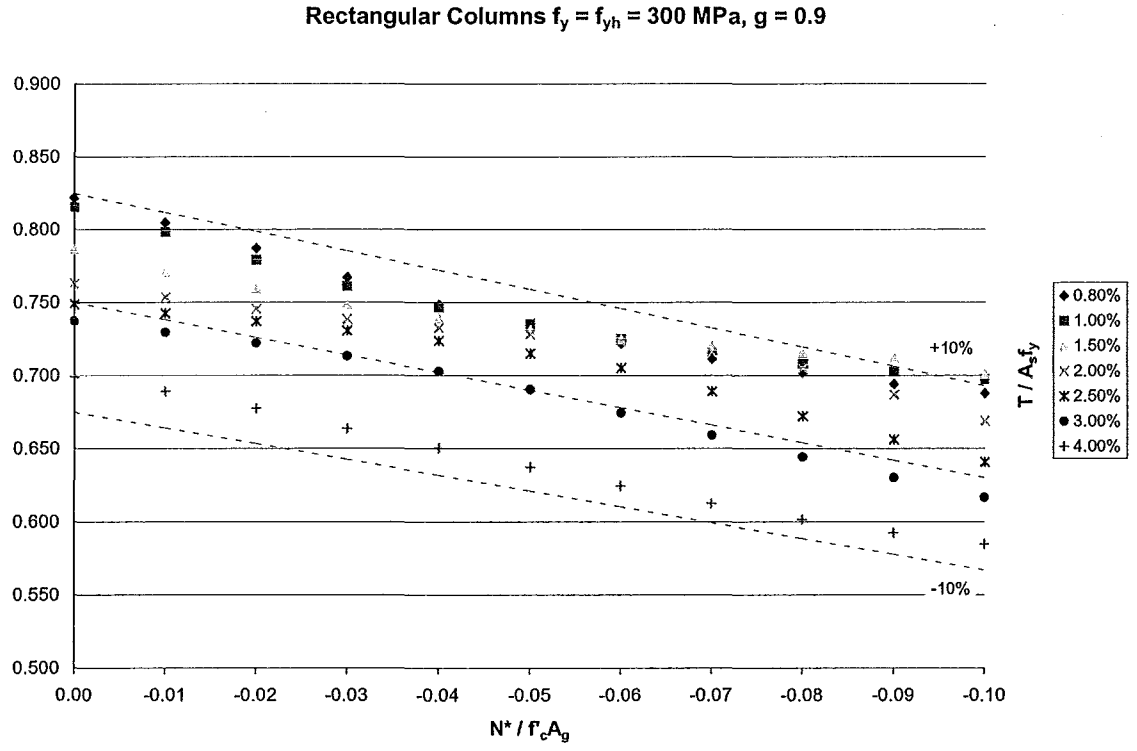

Figure E.6 *Rectangular Column, f_y = 300 MPa, Comparison with Eqn 7.9*

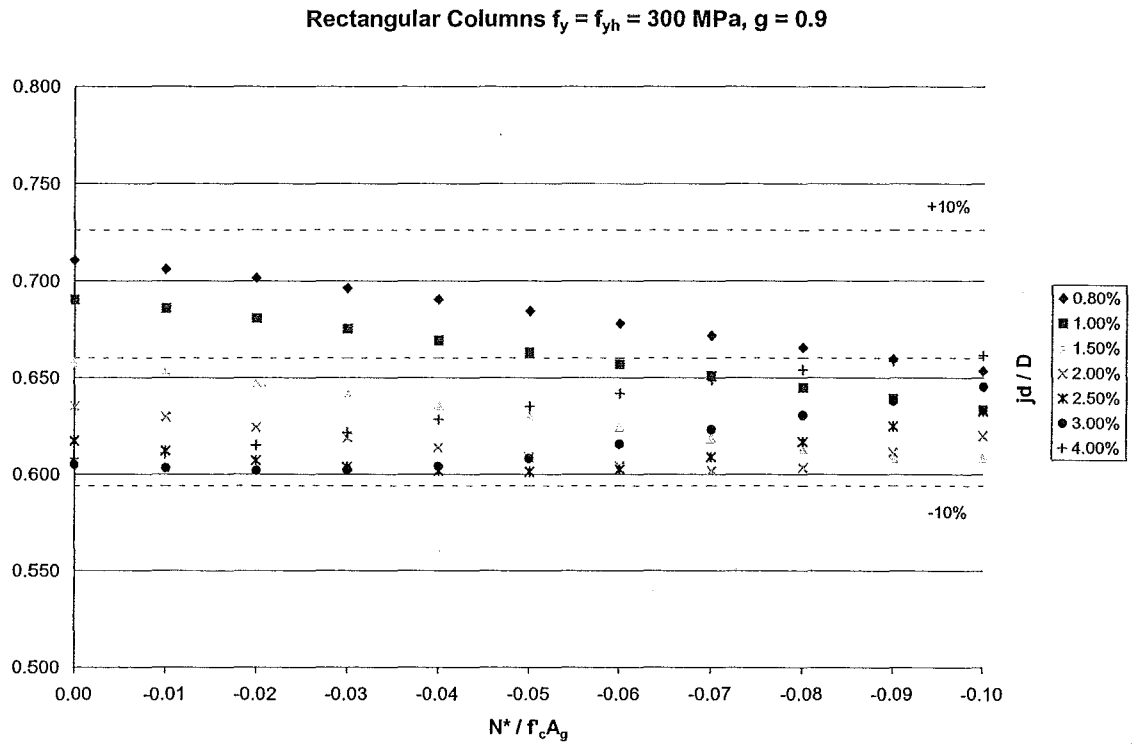

Figure E.7 *Rectangular Column, f_y = 300 MPa, Comparison with Eqn 7.7*

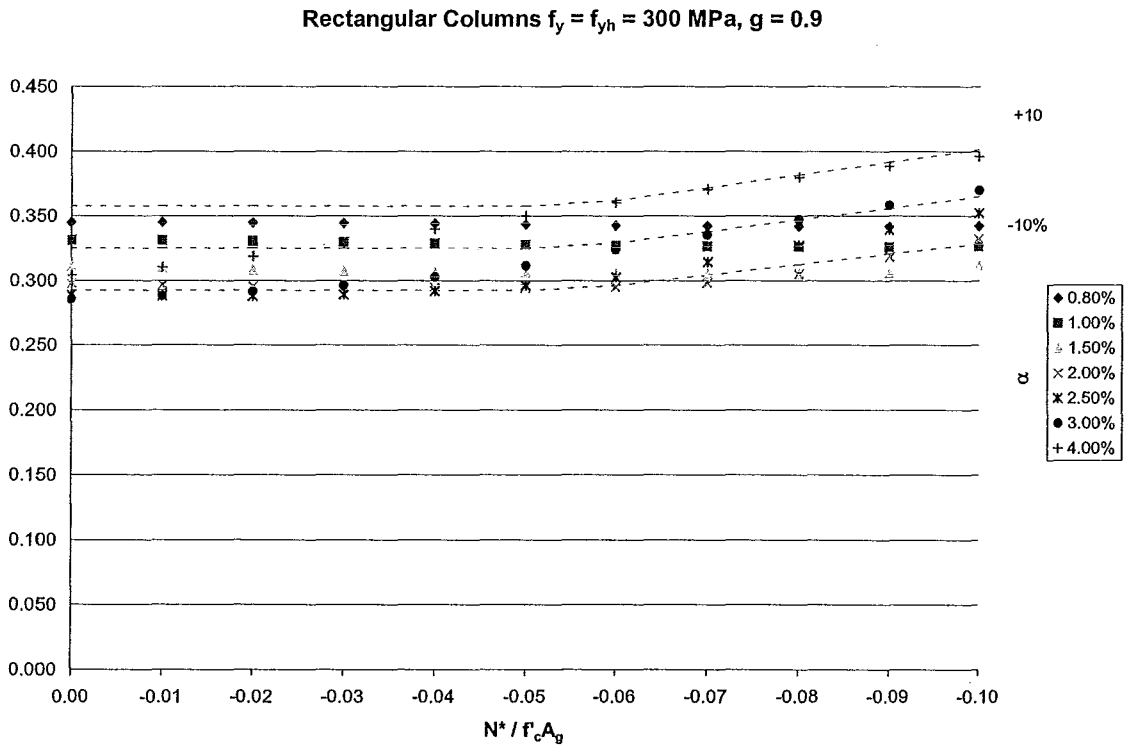

Figure E.8 *Rectangular Column, f_y = 300 MPa, Comparison with Eqn 7.11*

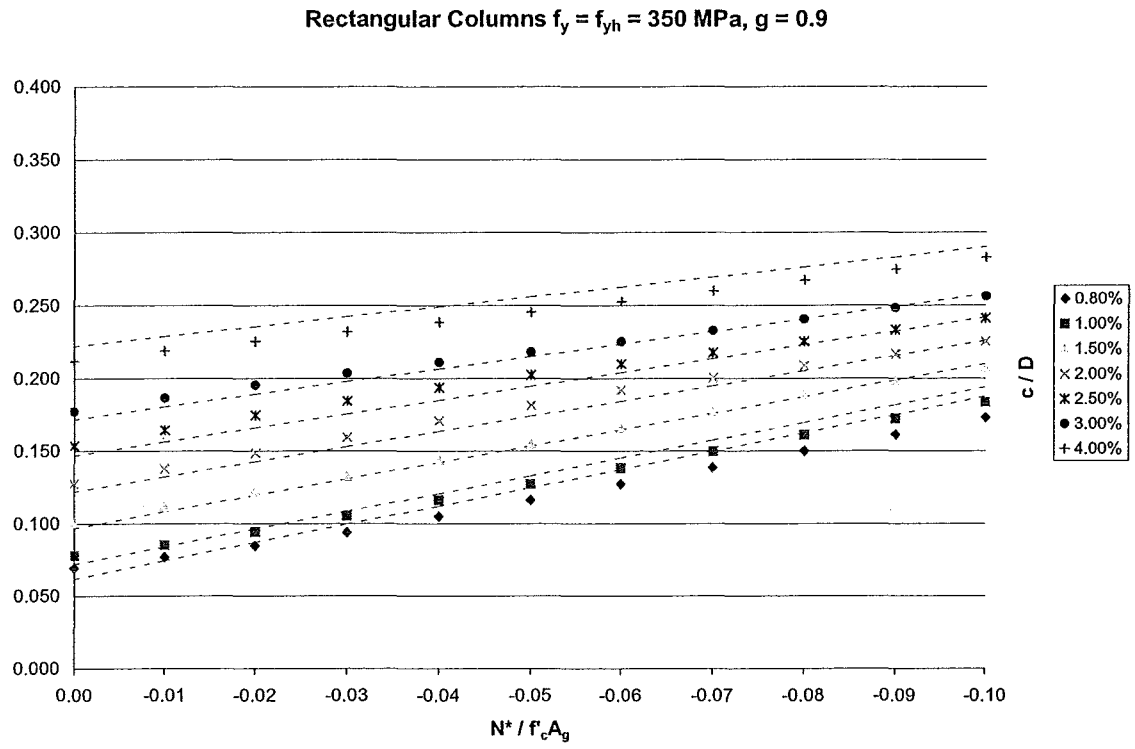

Figure E.9 *Rectangular Column, f_y = 350 MPa, Comparison with Eqn 7.13*

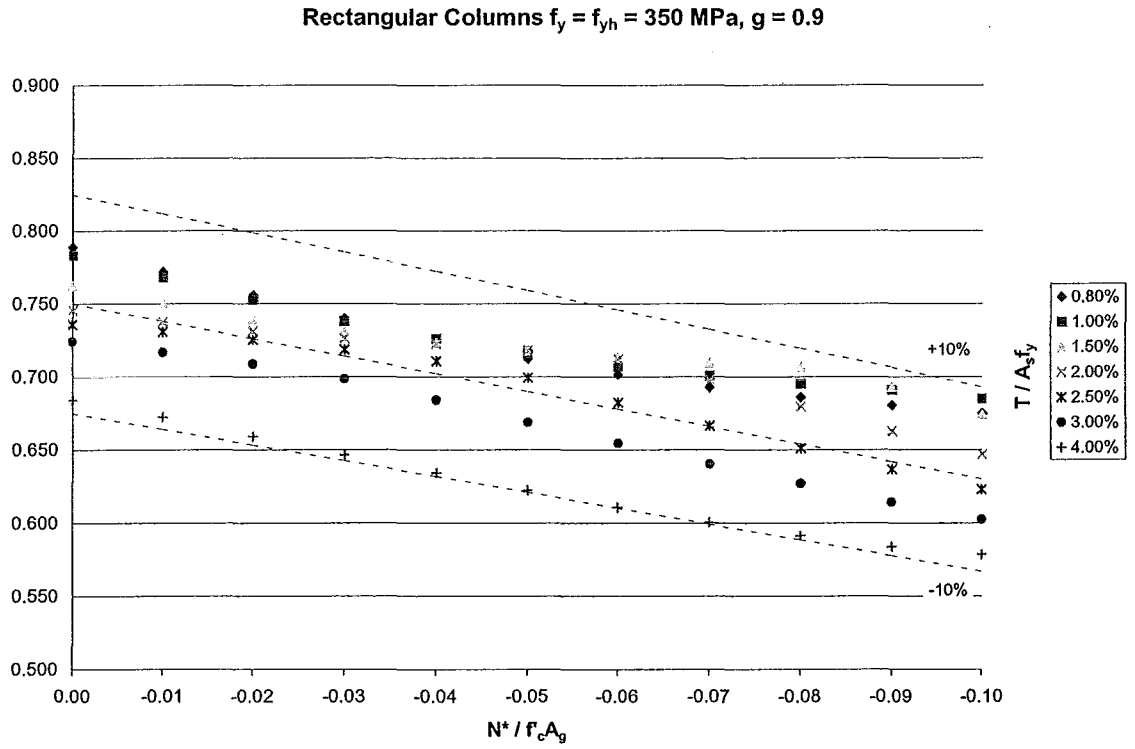

Figure E.10 *Rectangular Column, f_y = 350 MPa, Comparison with Eqn 7.9*

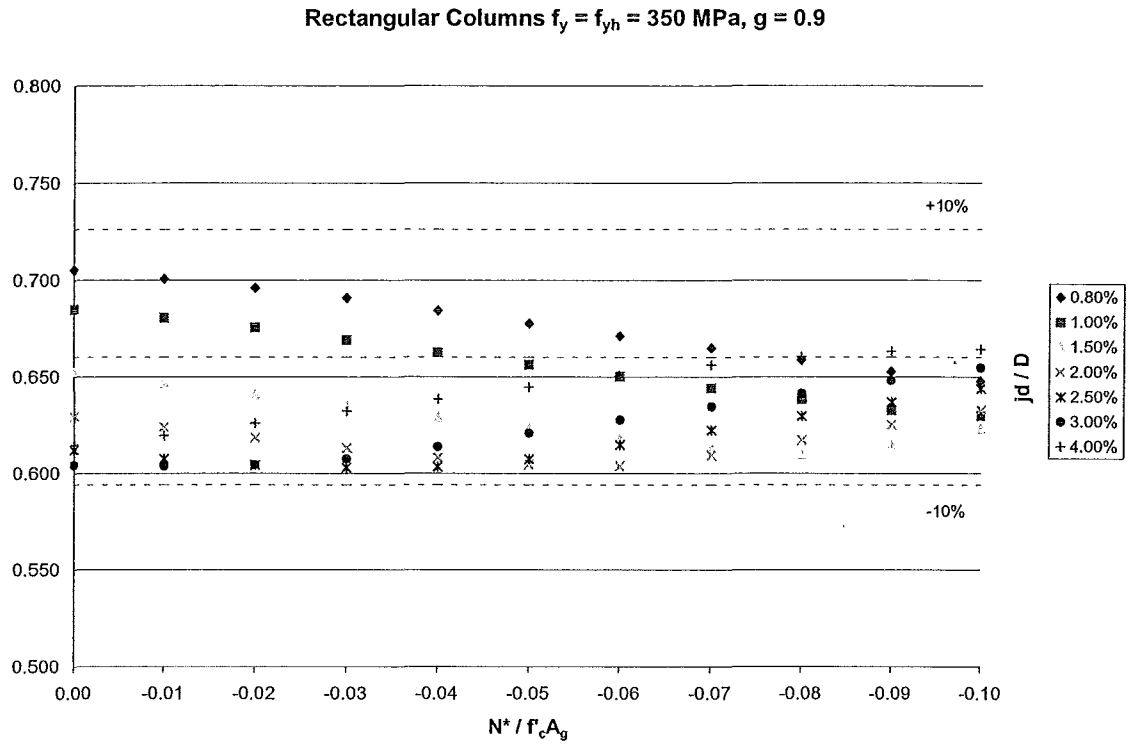

Figure E.11 *Rectangular Column, f_y = 350 MPa, Comparison with Eqn 7.7*

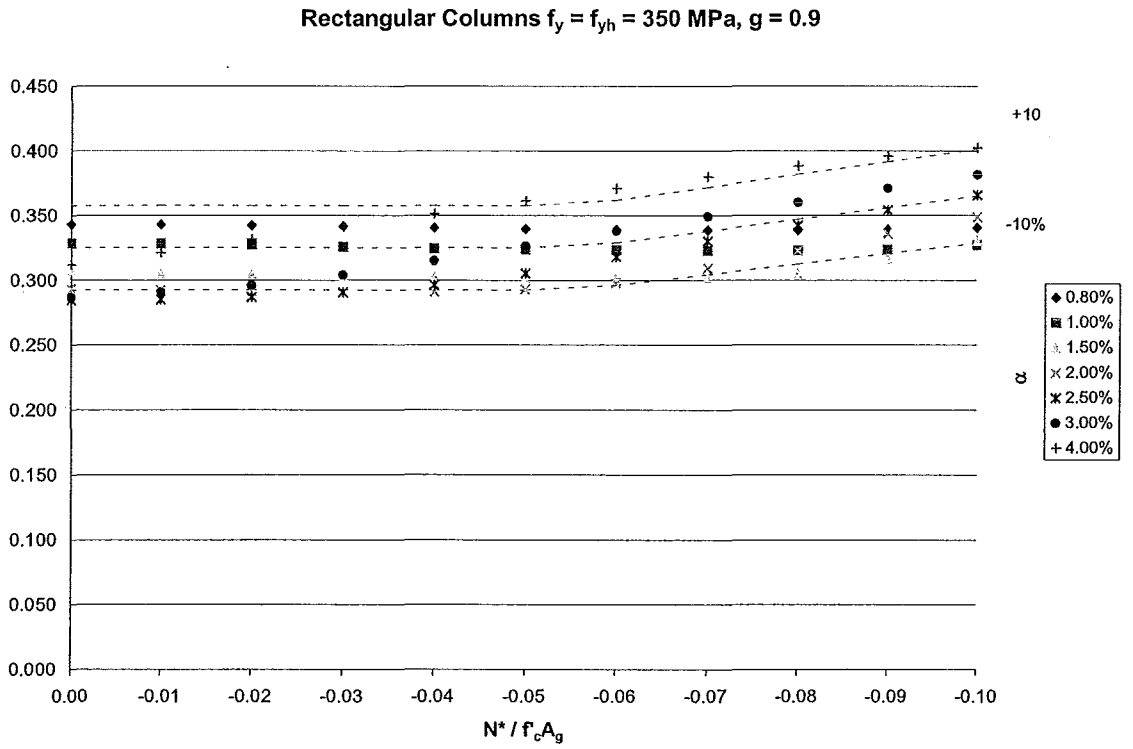

Figure E.12 *Rectangular Column, f_y = 350 MPa, Comparison with Eqn 7.11*

E.3 CIRCULAR COLUMNS

Figures E.13 to E.24 show plots of the proposed equations from the parametric study, discussed in Chapter 7, for circular columns with constant longitudinal yield strengths of f_y = 250 MPa, 300 MPa and 350 MPa and g = 0.9.

Again the data points plotted fit the proposed equations, derived from analyses with f_y = 300 MPa, reasonably well. Similar results are obtained for g = 0.8 and 1.0. For longitudinal yield strengths significantly different from these values, f_y = 250 - 350 MPa, a moment-curvature analysis can be used to obtain the appropriate values.

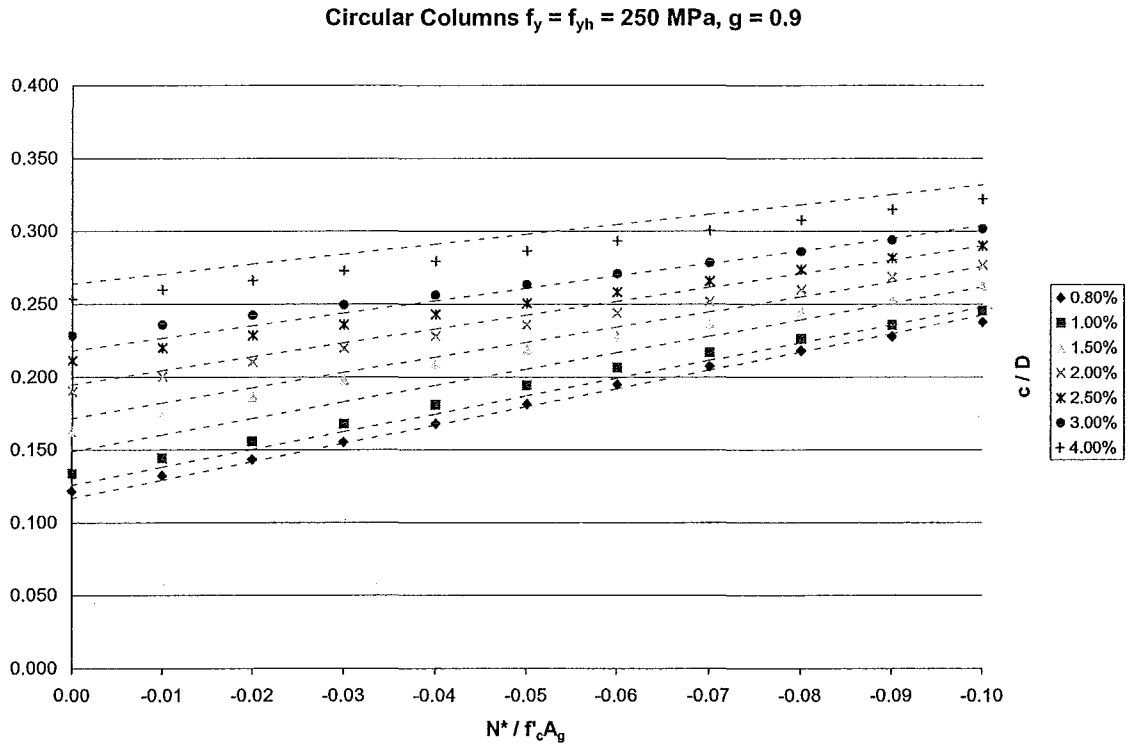

Figure E.13 *Circular Column, f_y = 250 MPa, Comparison with Eqn 7.14*

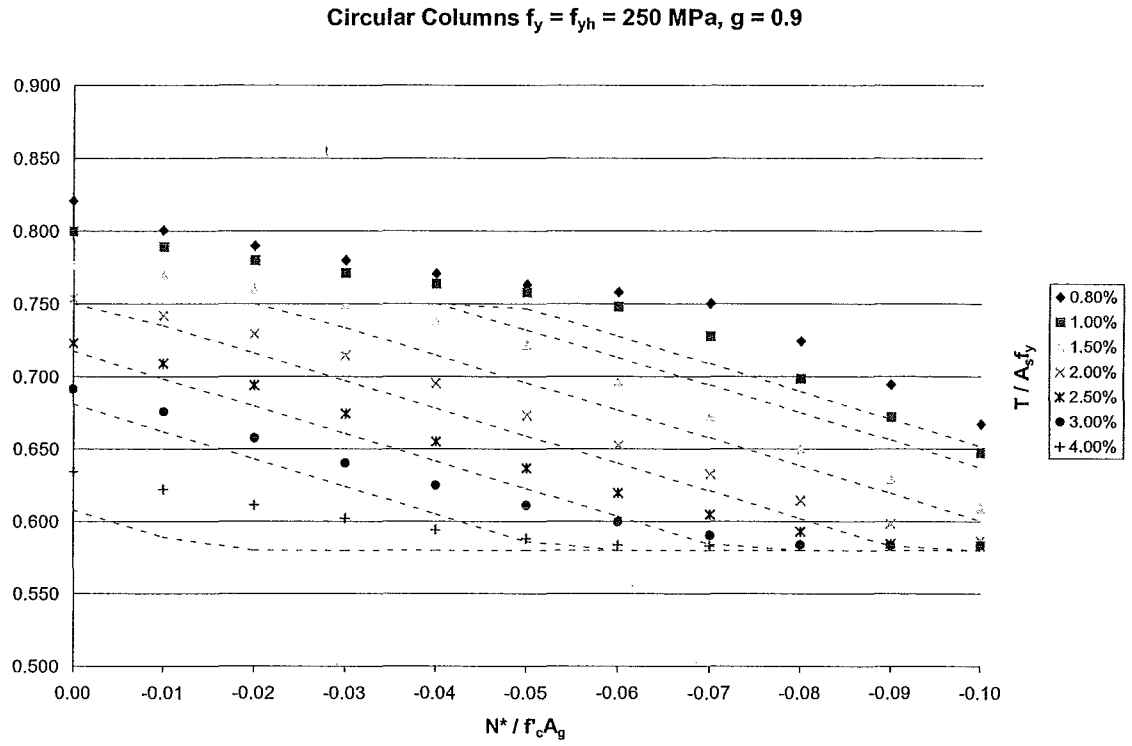

Figure E.14 *Circular Column, f_y = 250 MPa, Comparison with Eqn 7.10*

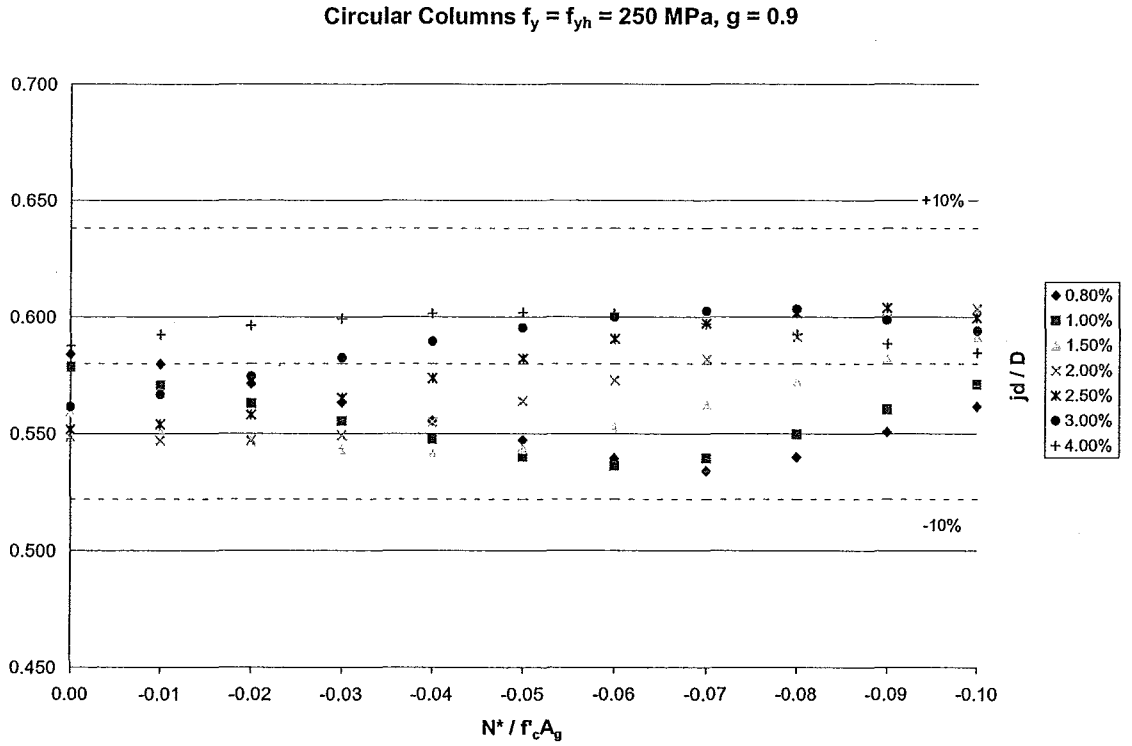

Figure E.15 *Circular Column, f_y = 250 MPa, Comparison with Eqn 7.8*

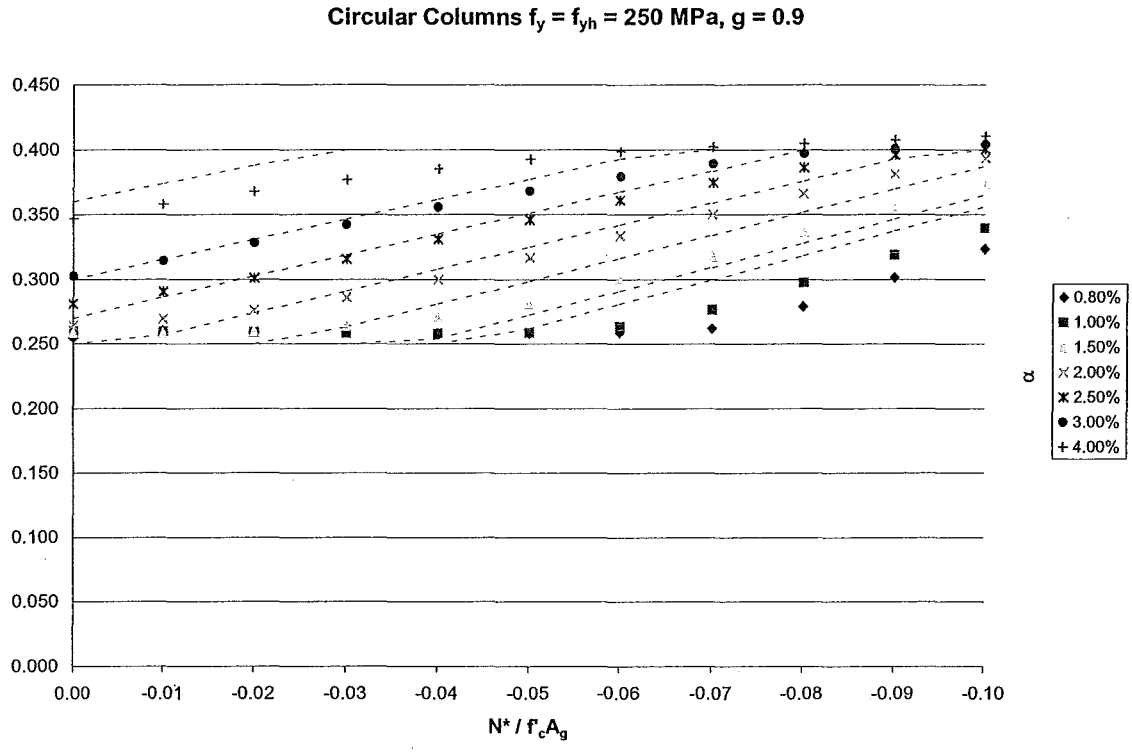

Figure E.16 *Circular Column, f_y = 250 MPa, Comparison with Eqn 7.12*

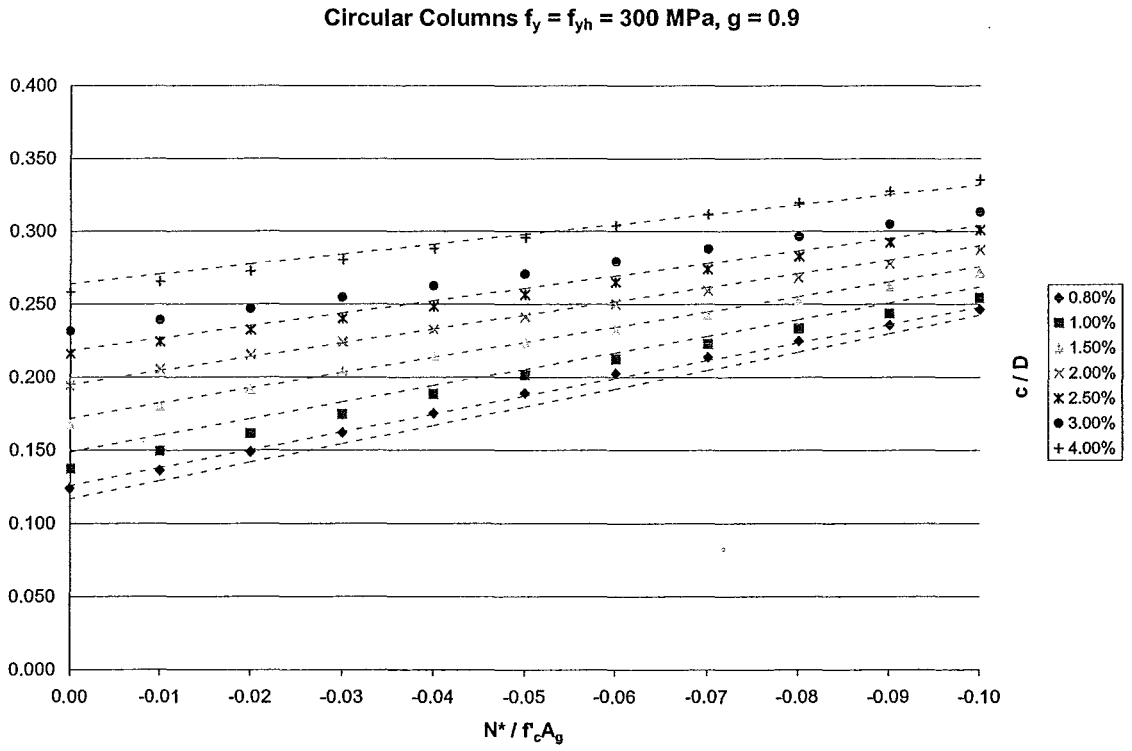

Figure E.17 *Circular Column, f_y = 300 MPa, Comparison with Eqn 7.14*

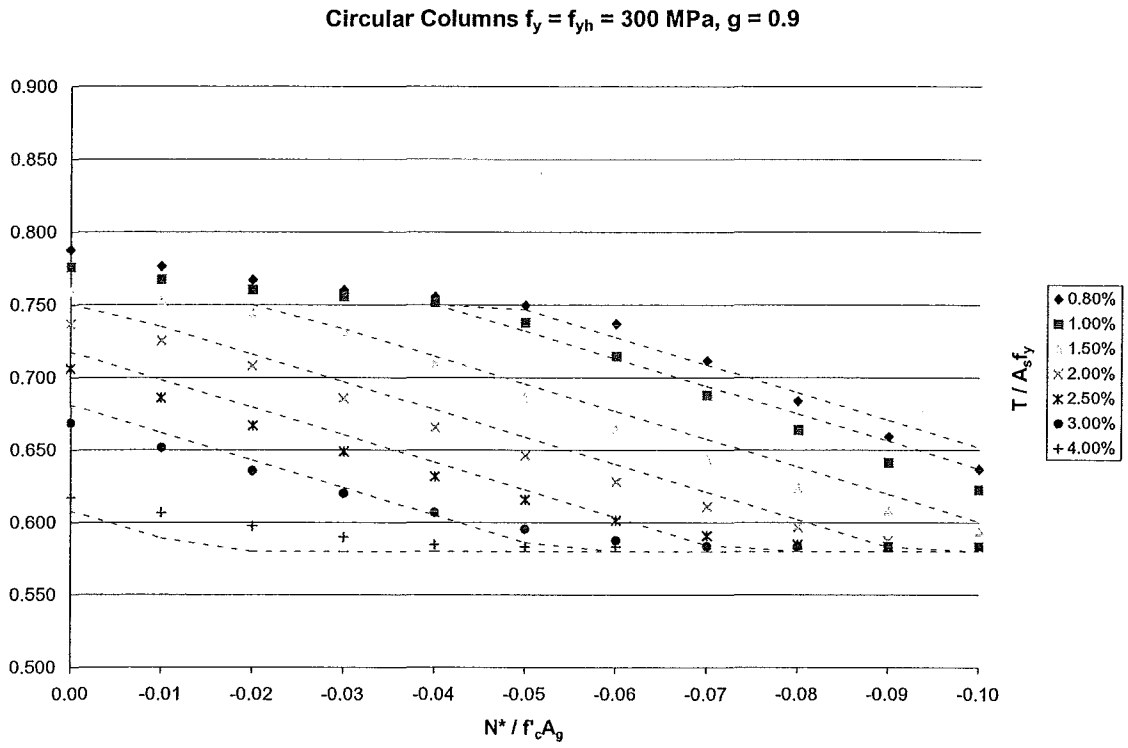

Figure E.18 *Circular Column, f_y = 300 MPa, Comparison with Eqn 7.10*

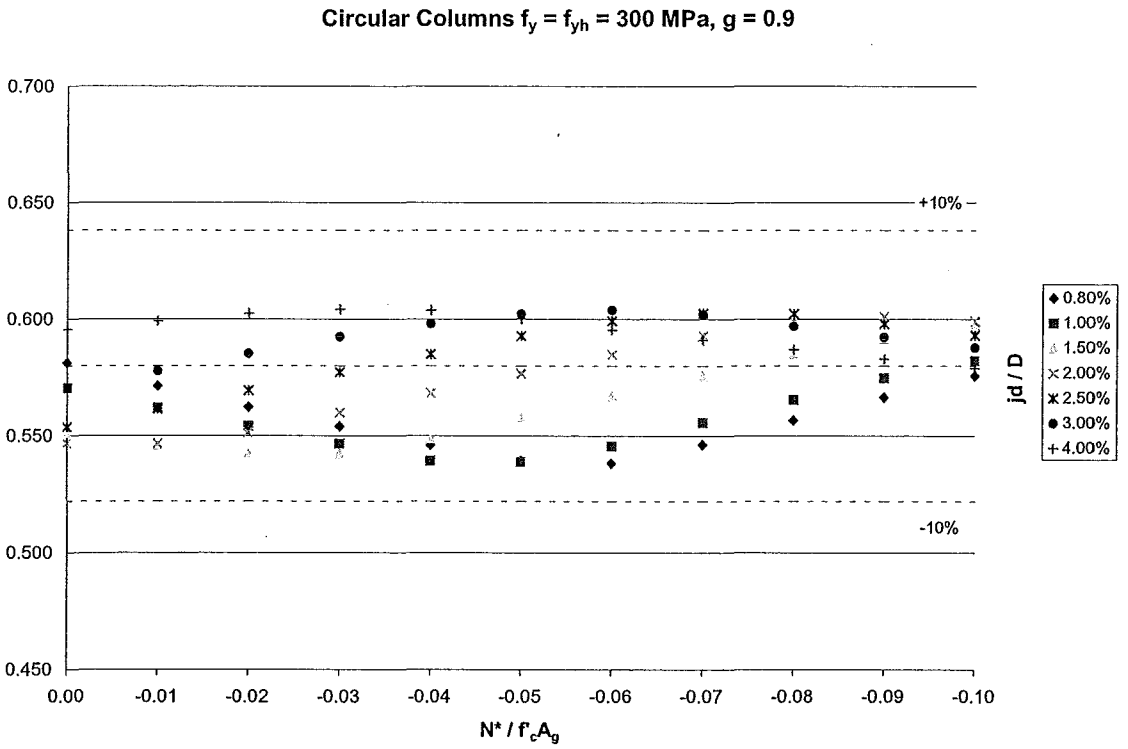

Figure E.19 *Circular Column, f_y = 300 MPa, Comparison with Eqn 7.8*

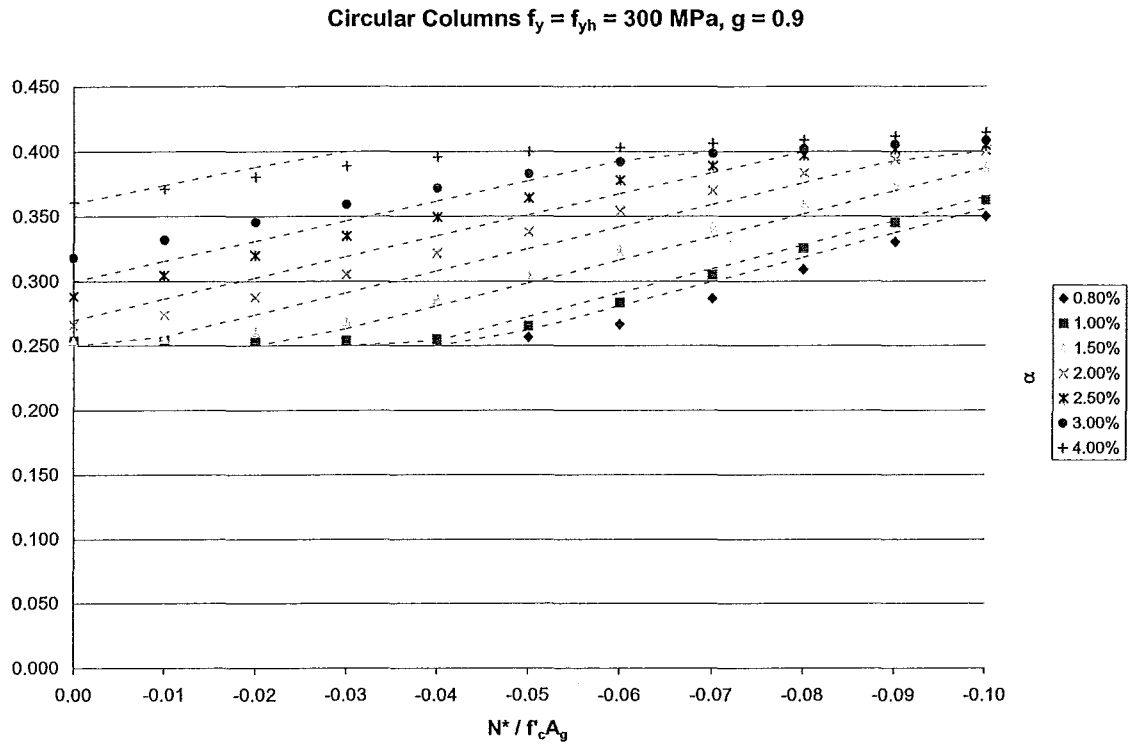

Figure E.20 *Circular Column, f_y = 300 MPa, Comparison with Eqn 7.12*

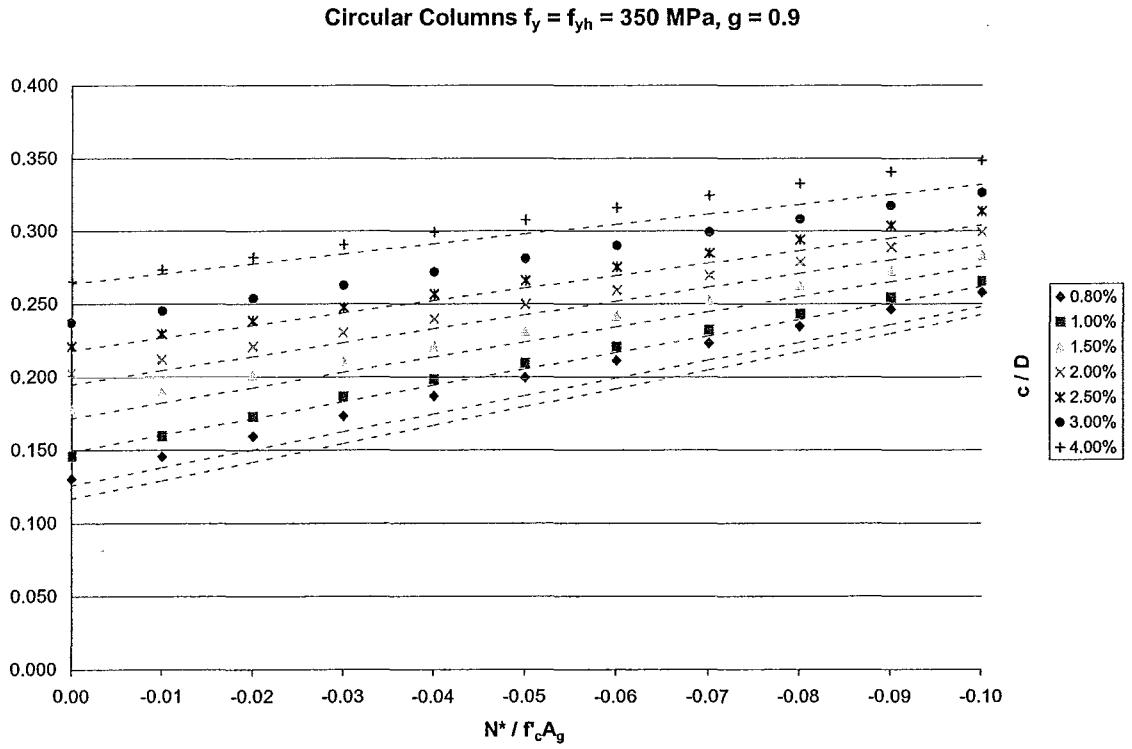

Figure E.21 *Circular Column, f_y = 350 MPa, Comparison with Eqn 7.14*

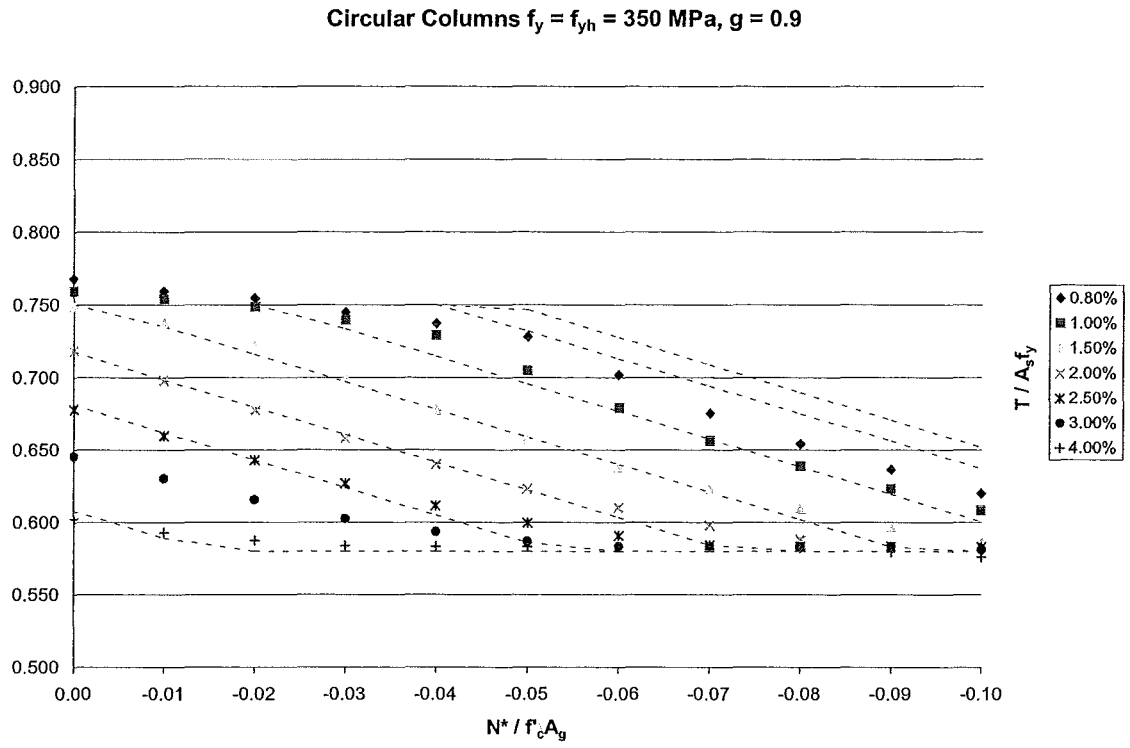

Figure E.22 *Circular Column, f_y = 350 MPa, Comparison with Eqn 7.10*

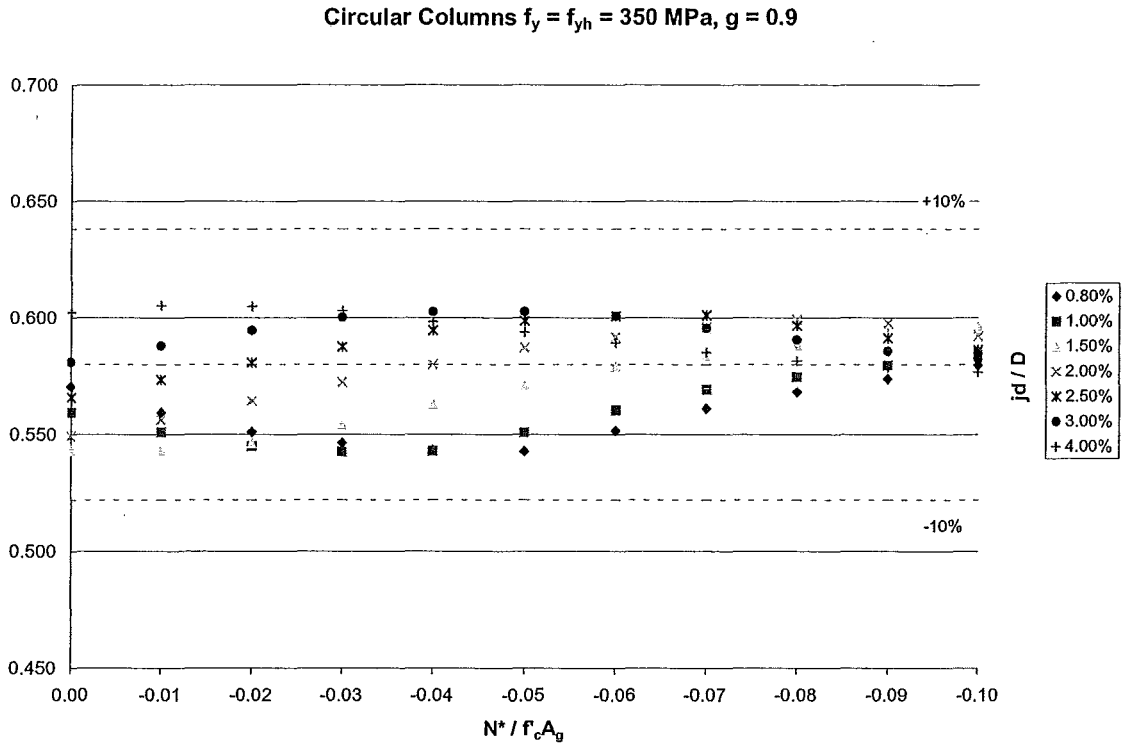

Figure E.23 *Circular Column, f_y = 350 MPa, Comparison with Eqn 7.8*

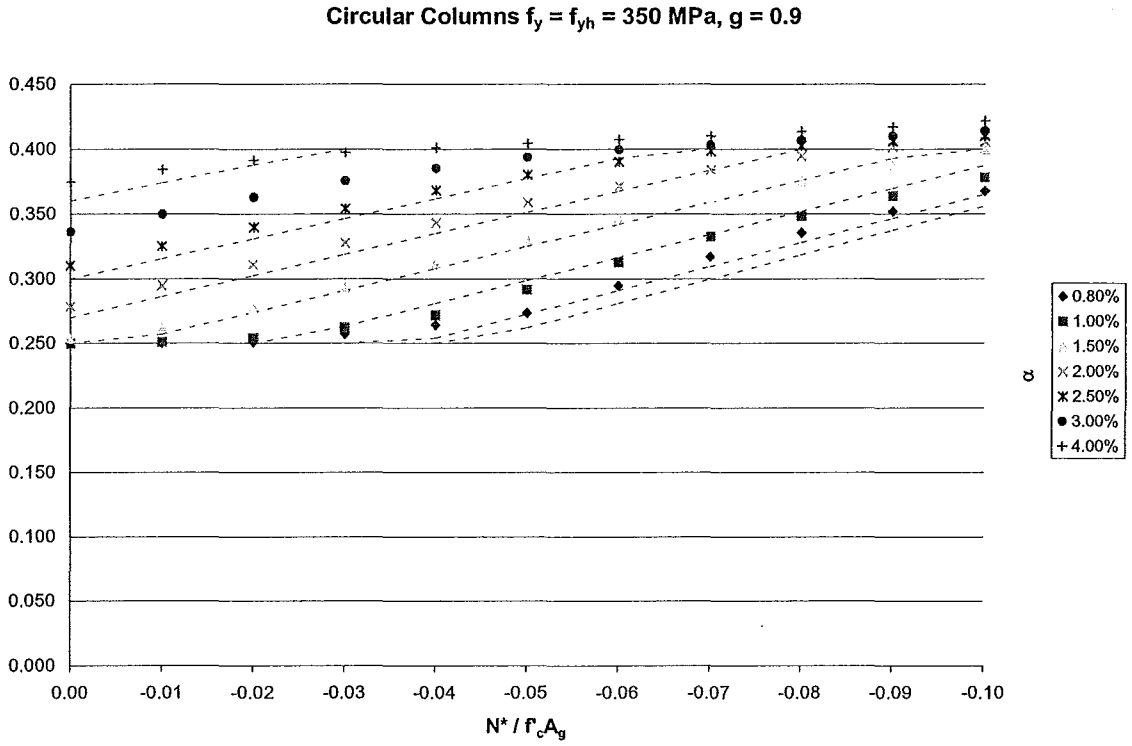

Figure E.24 *Circular Column, f_y = 350 MPa, Comparison with Eqn 7.12*

APPENDIX F

TEST RIG DETAILS

This Appendix contains fabrication drawings for the test rig used in the testing of Units I-A and I-B. Also included are details for the fabrication of the vertical springs for Units I-A and I-B and the lateral springs used in both tests.

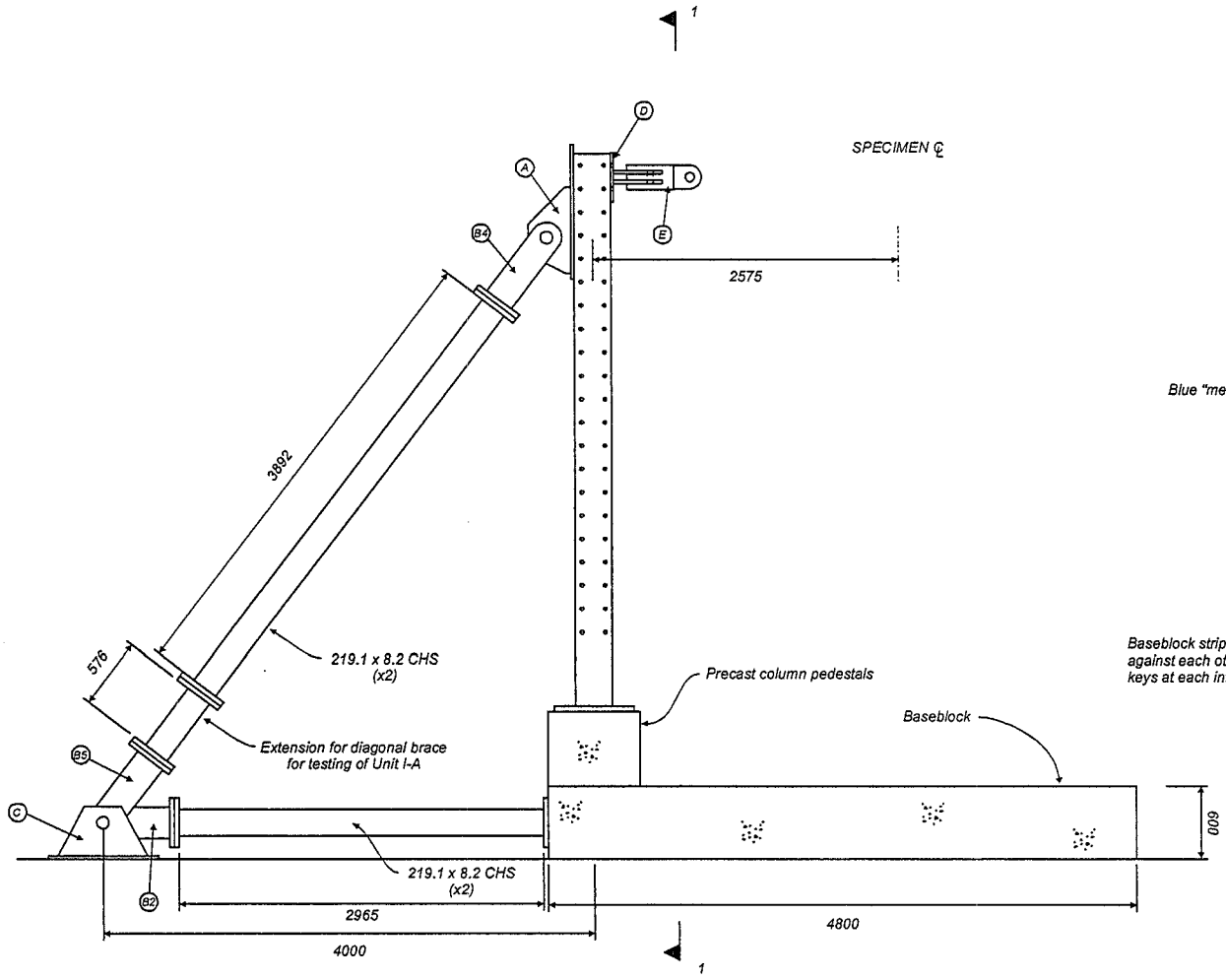

750 mm deep Concrete Laboratory Strong Floor

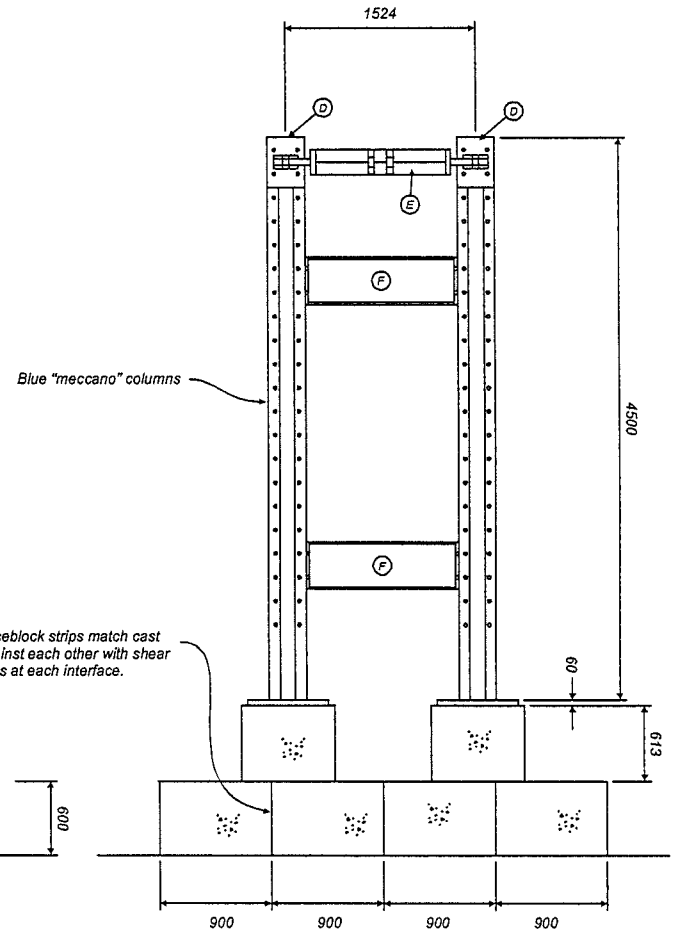

SECTION 1 - 1

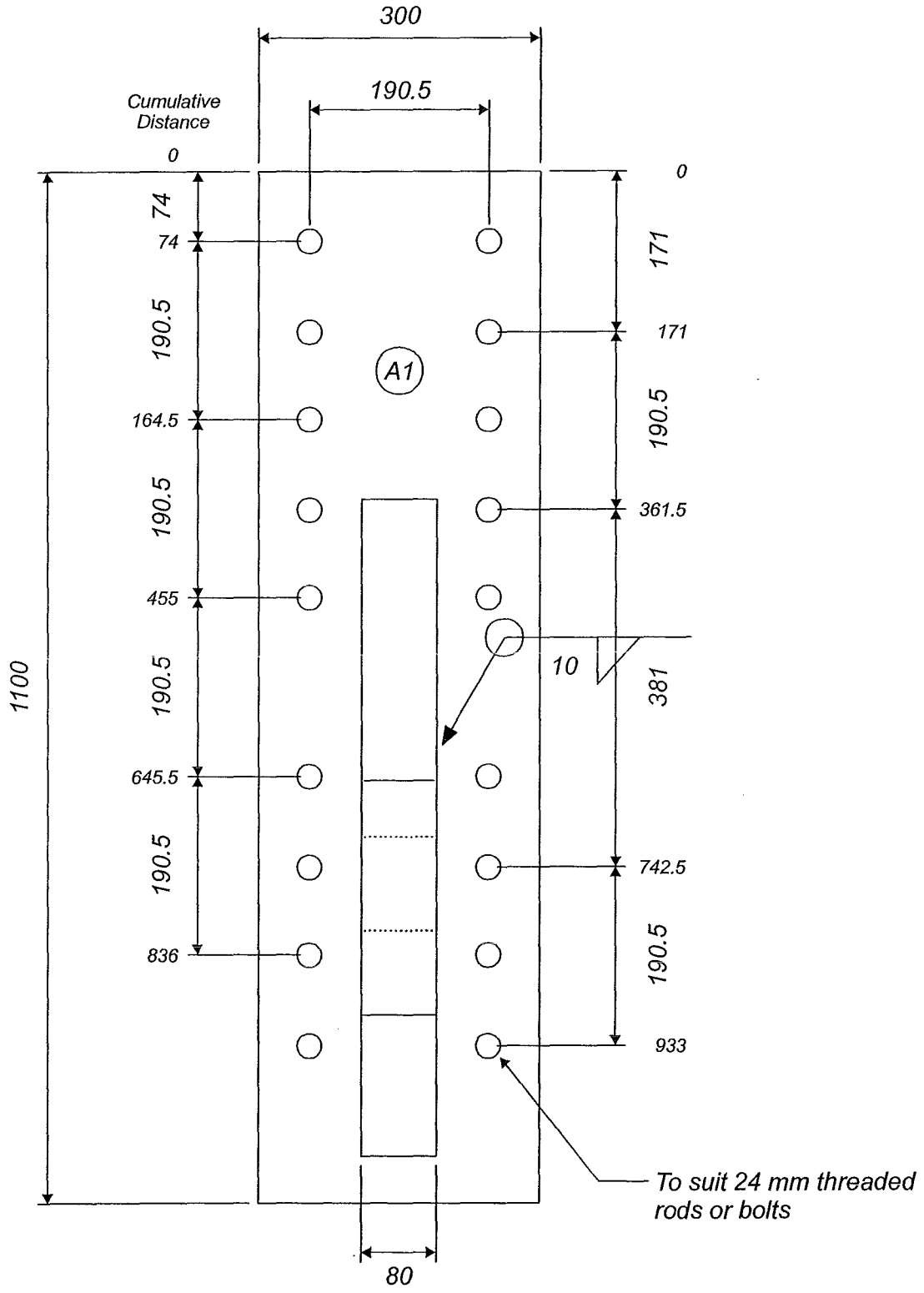

Diagonal Brace Connection A
(Two required)

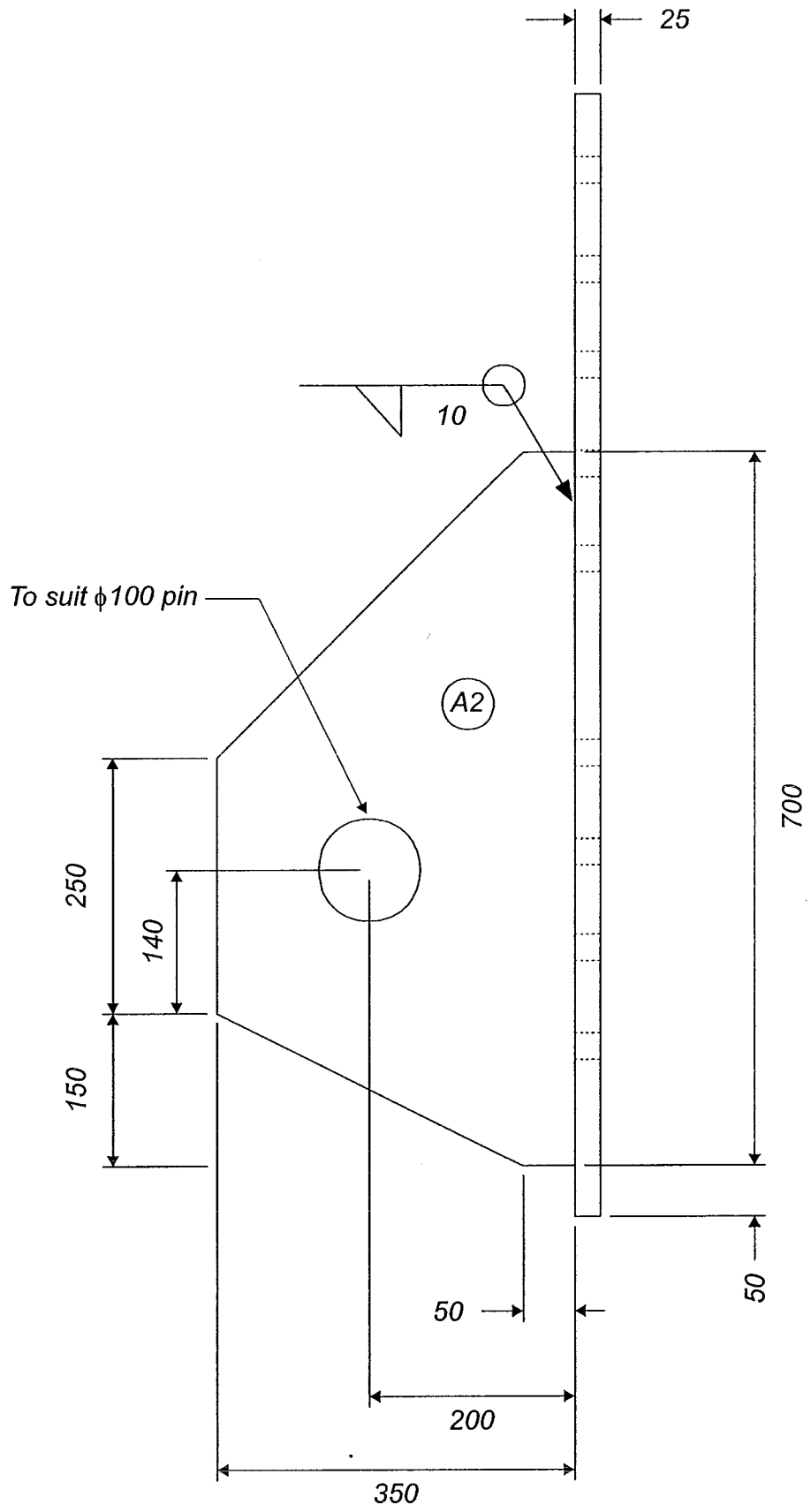

Diagonal Brace Connection A
(Two required)

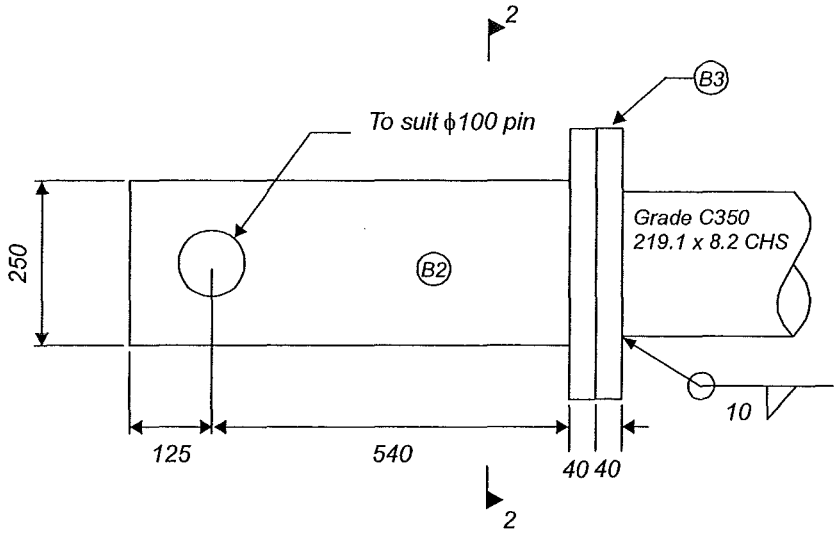

Horizontal Tie

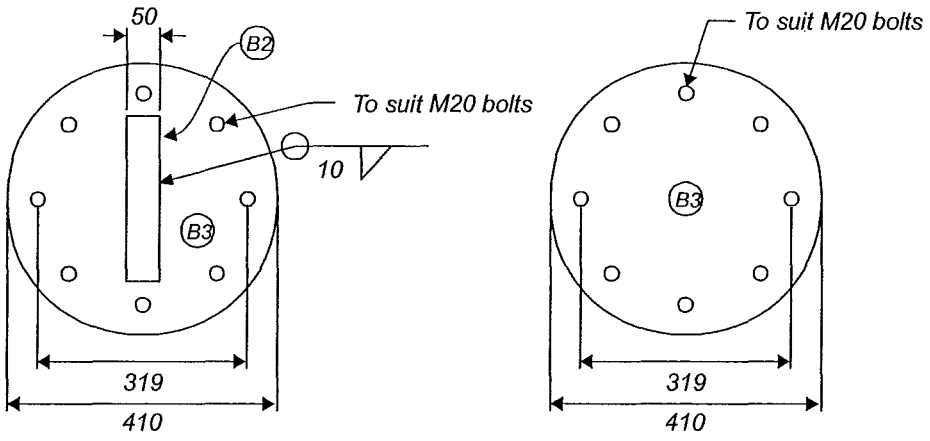

Section 2 - 2

Flange Detail

Diagonal Brace Connection Plates

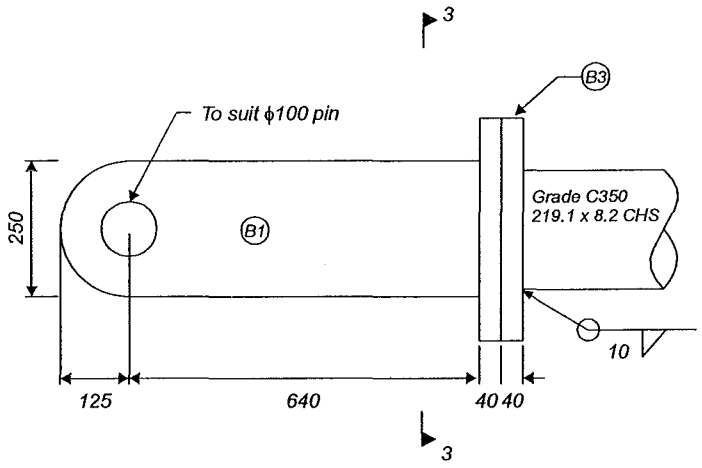

Diagonal Brace

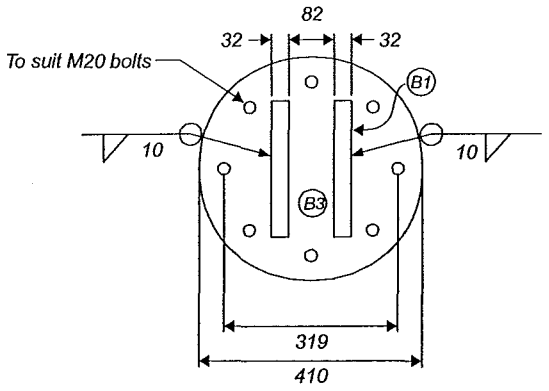

Section 3 - 3
Top Connection
B4

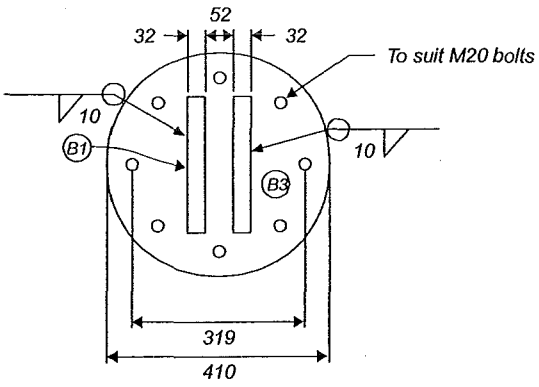

Section 3 - 3
Bottom Connection
B5

Diagonal Brace Connection Plates

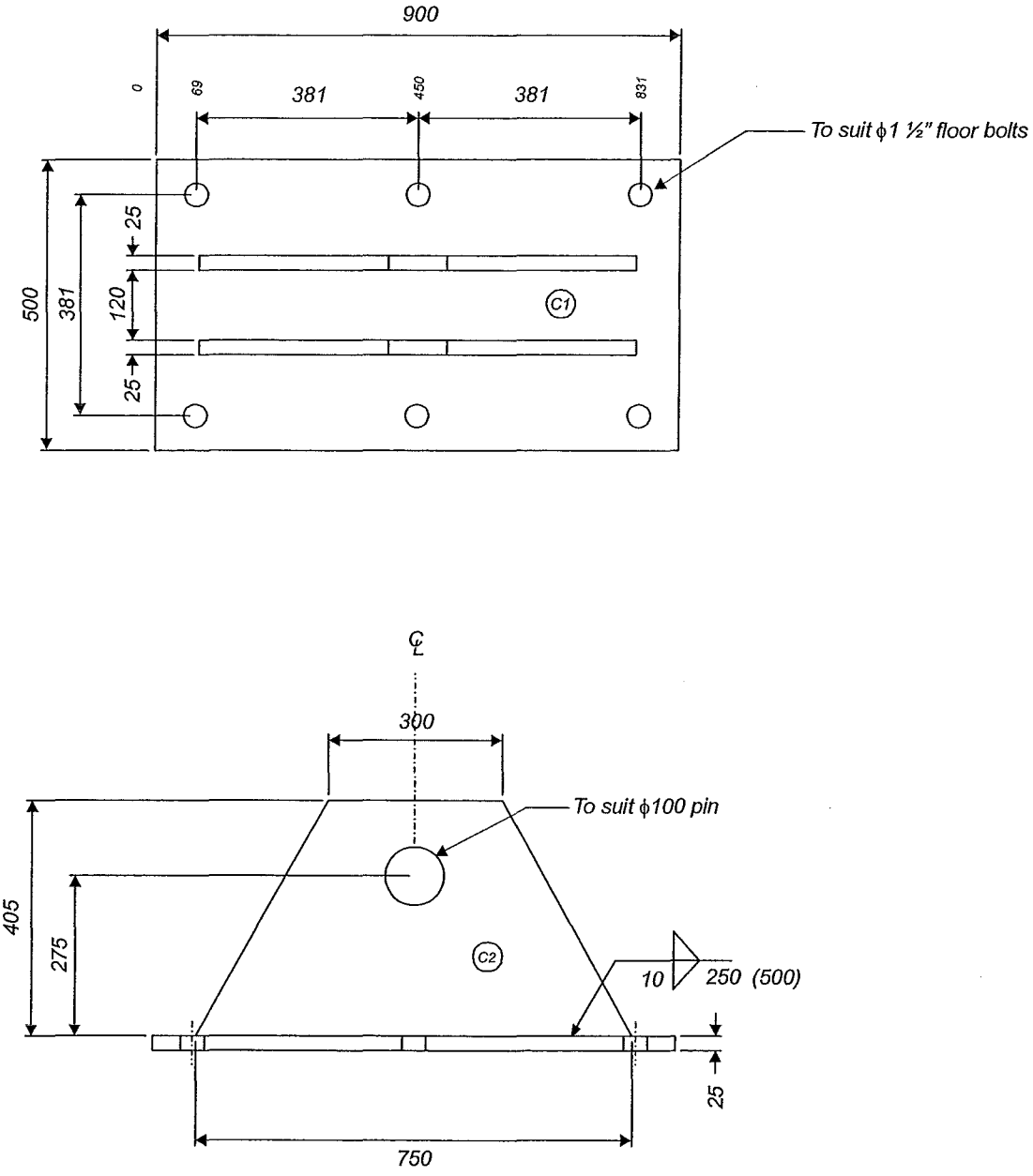
900
0
69
381
450
381
831
To suit ϕ1 ½" floor bolts
500
381
25
120
25
C1
℄
300
To suit ϕ100 pin
405
275
C2
10
250
(500)
25
750

Base Plate C

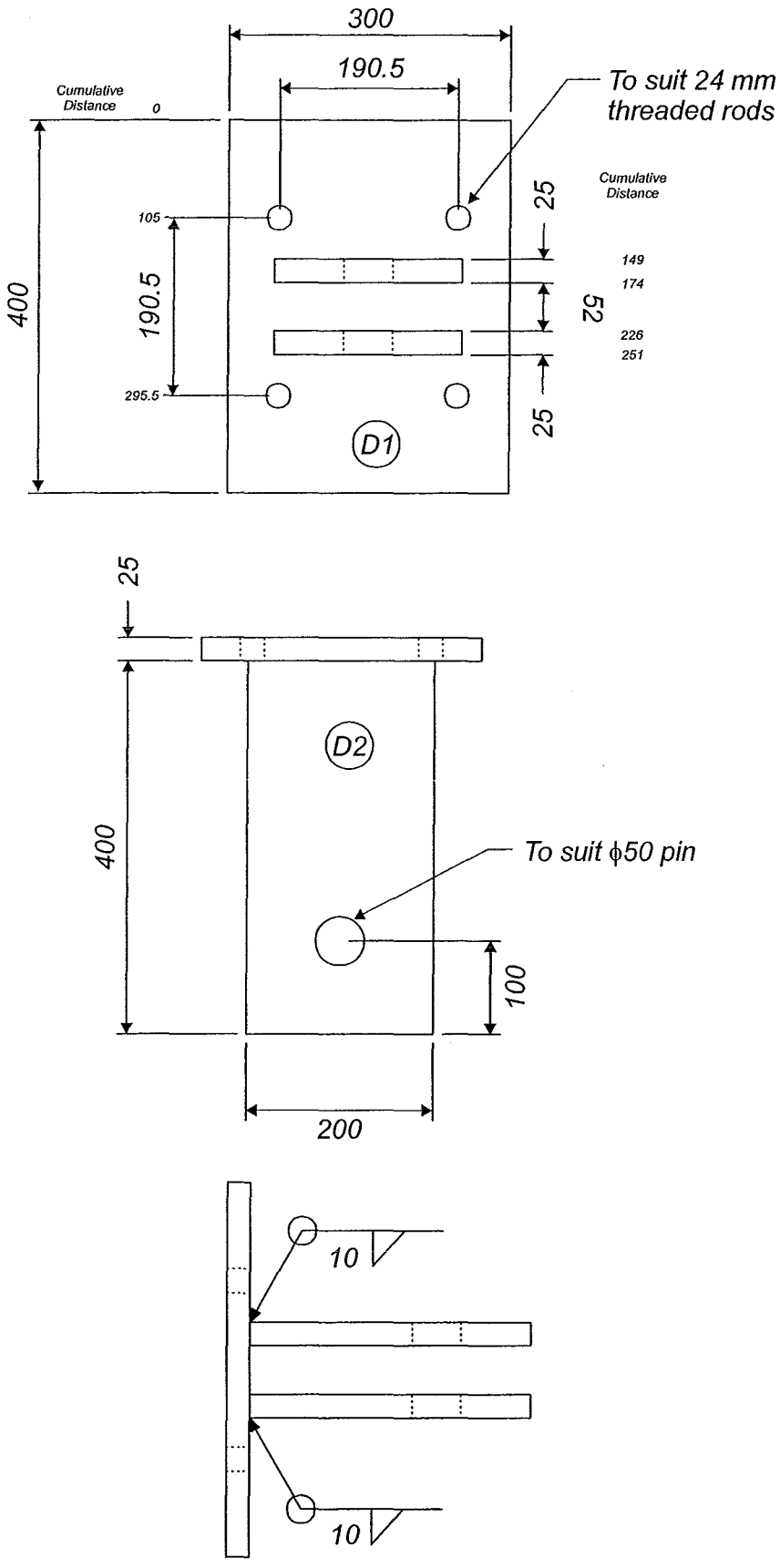

Actuator Mounting Bracket D

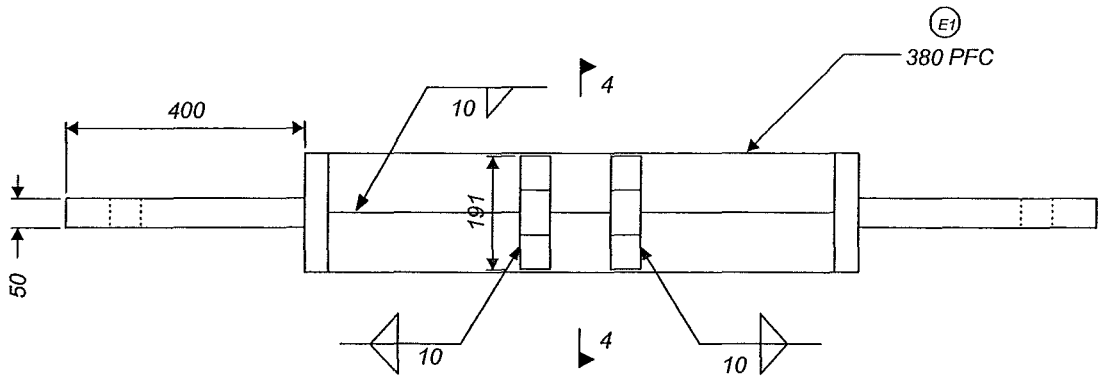

Elevation

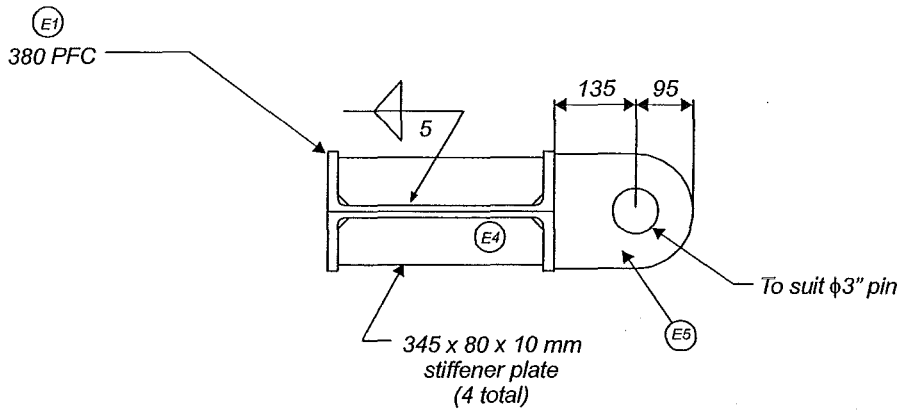

Section 4 - 4

Actuator Reaction Beam E

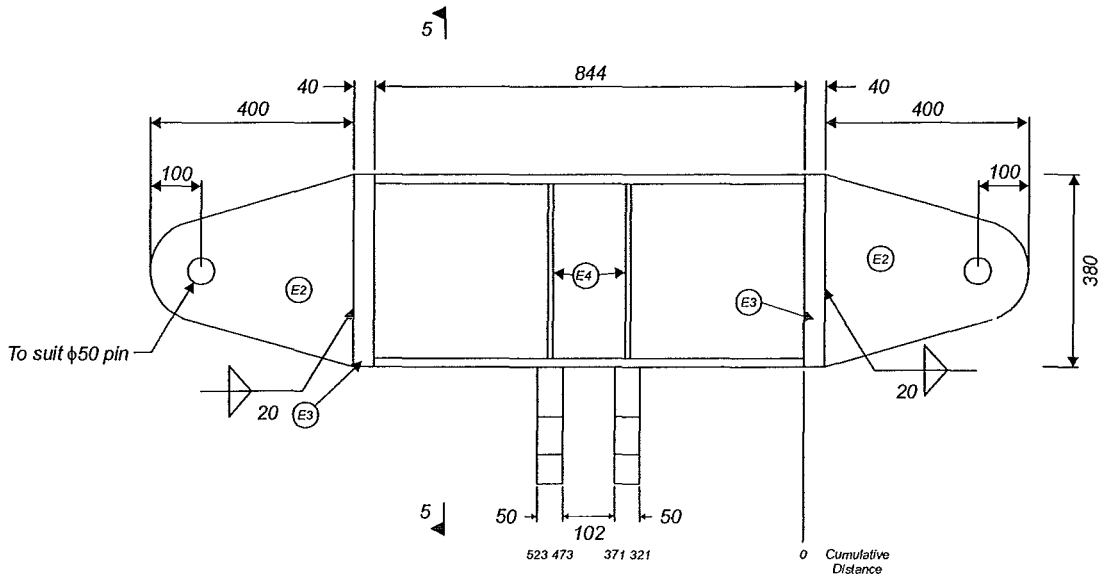

Plan

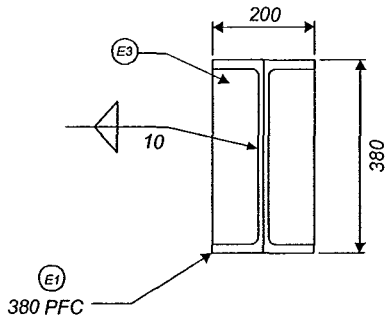

Section 5 - 5

Actuator Reaction Beam E

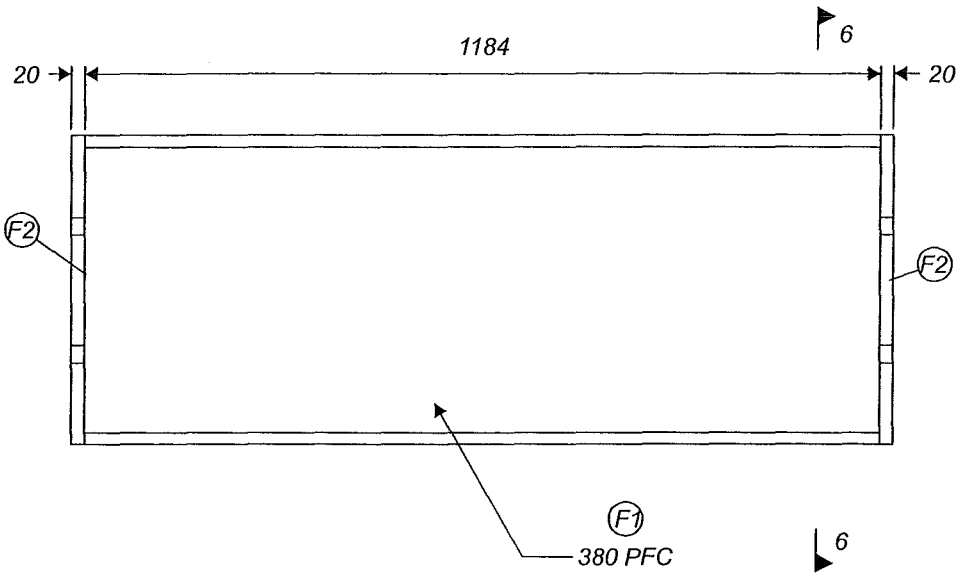

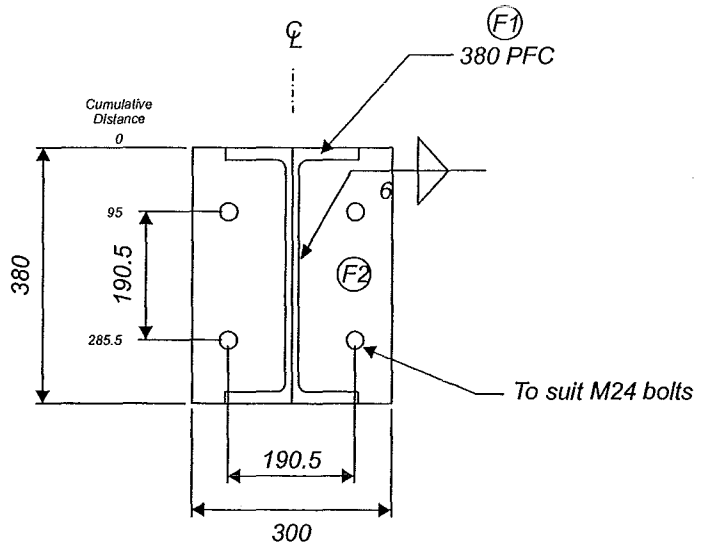

Section 6 - 6

Transverse Bracing Beam F

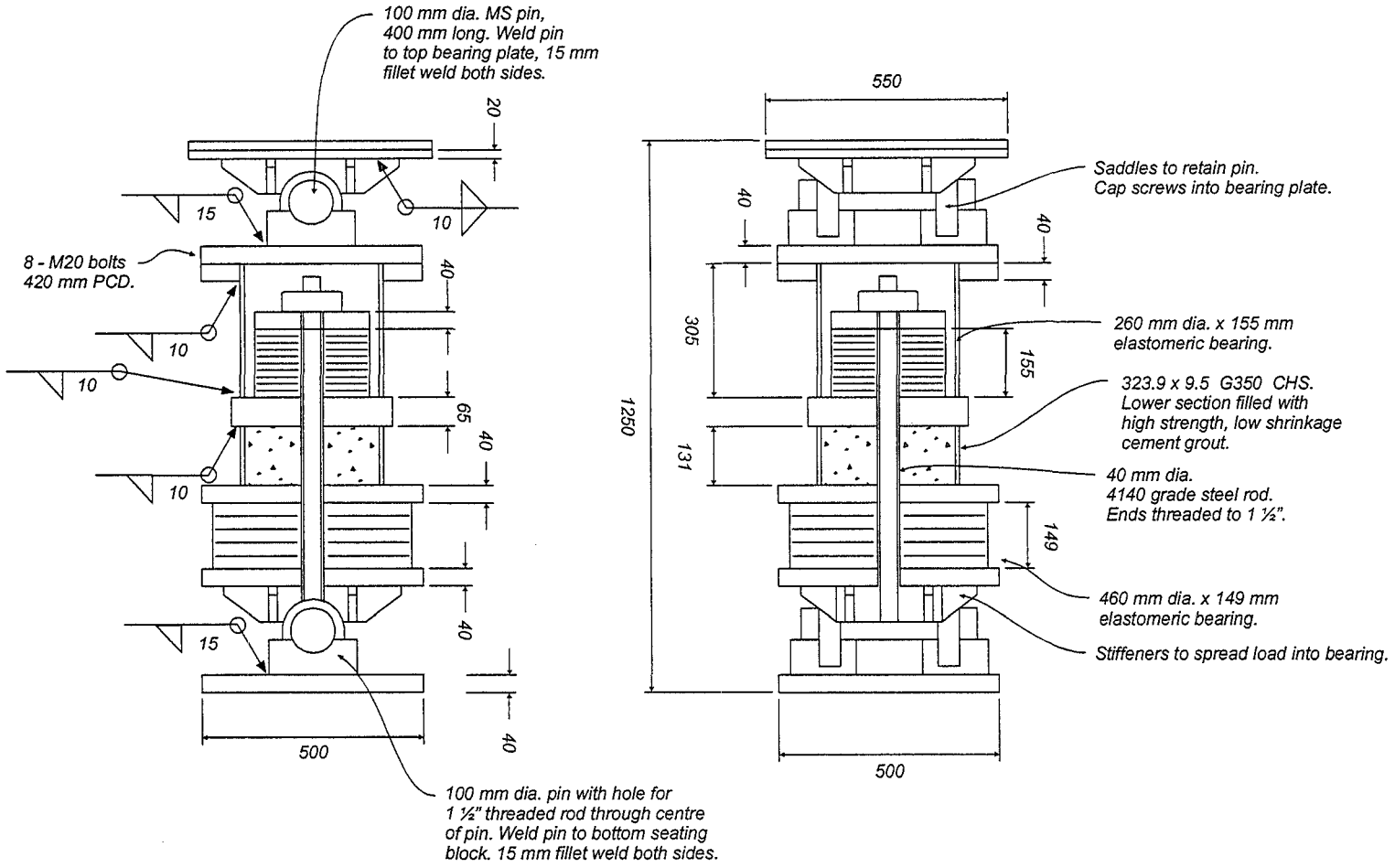

Unit I-A Outer Springs
(2 required)

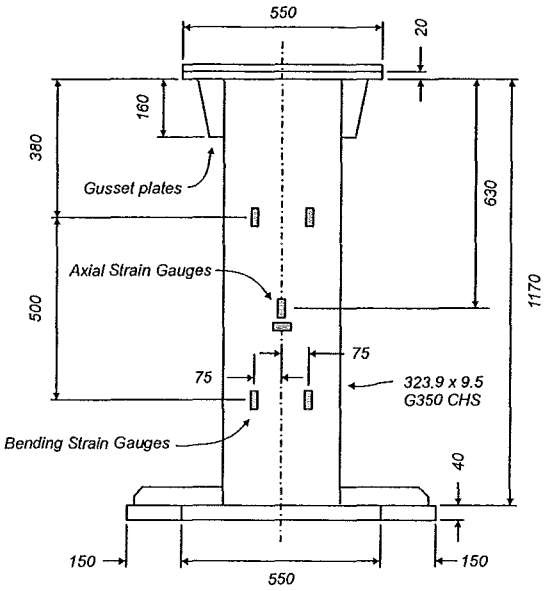

Elevation

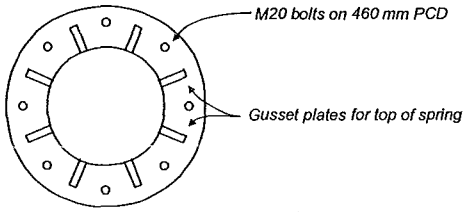

Top Plate Detail

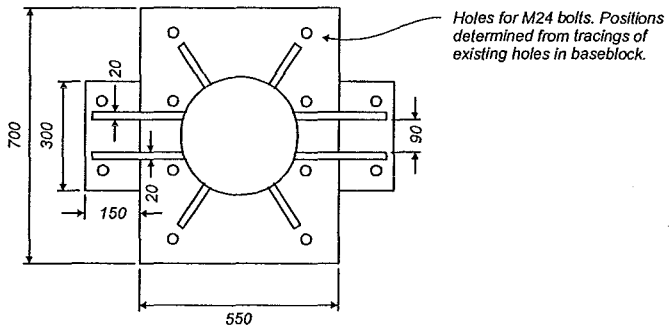

Bottom Plate Detail

Unit I-A Central Springs
(2 required)

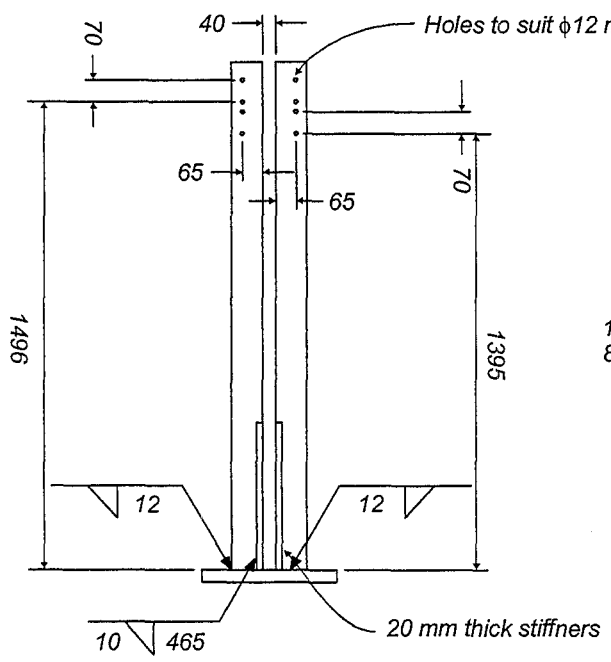

Lateral Spring End Elevation

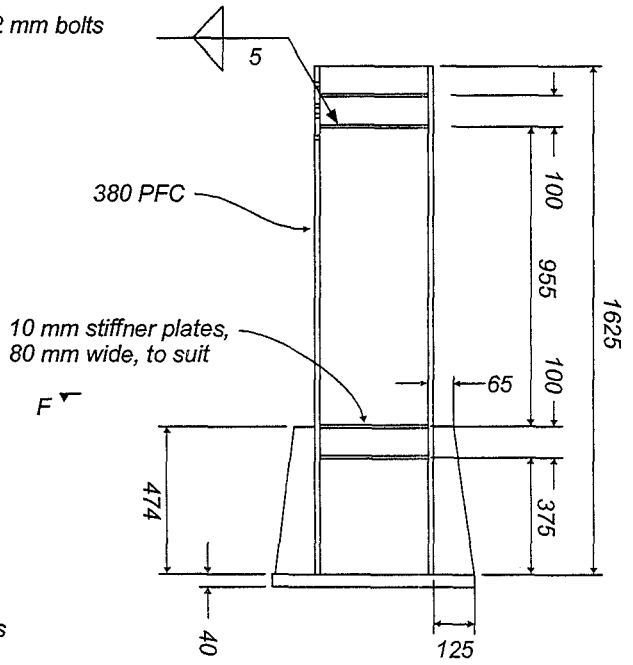

Lateral Spring Elevation

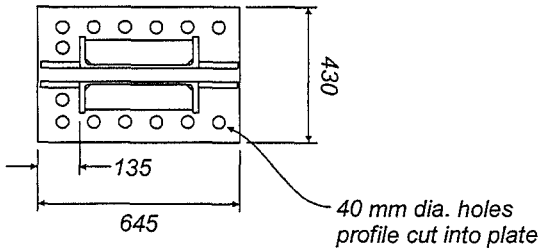

Section F - F

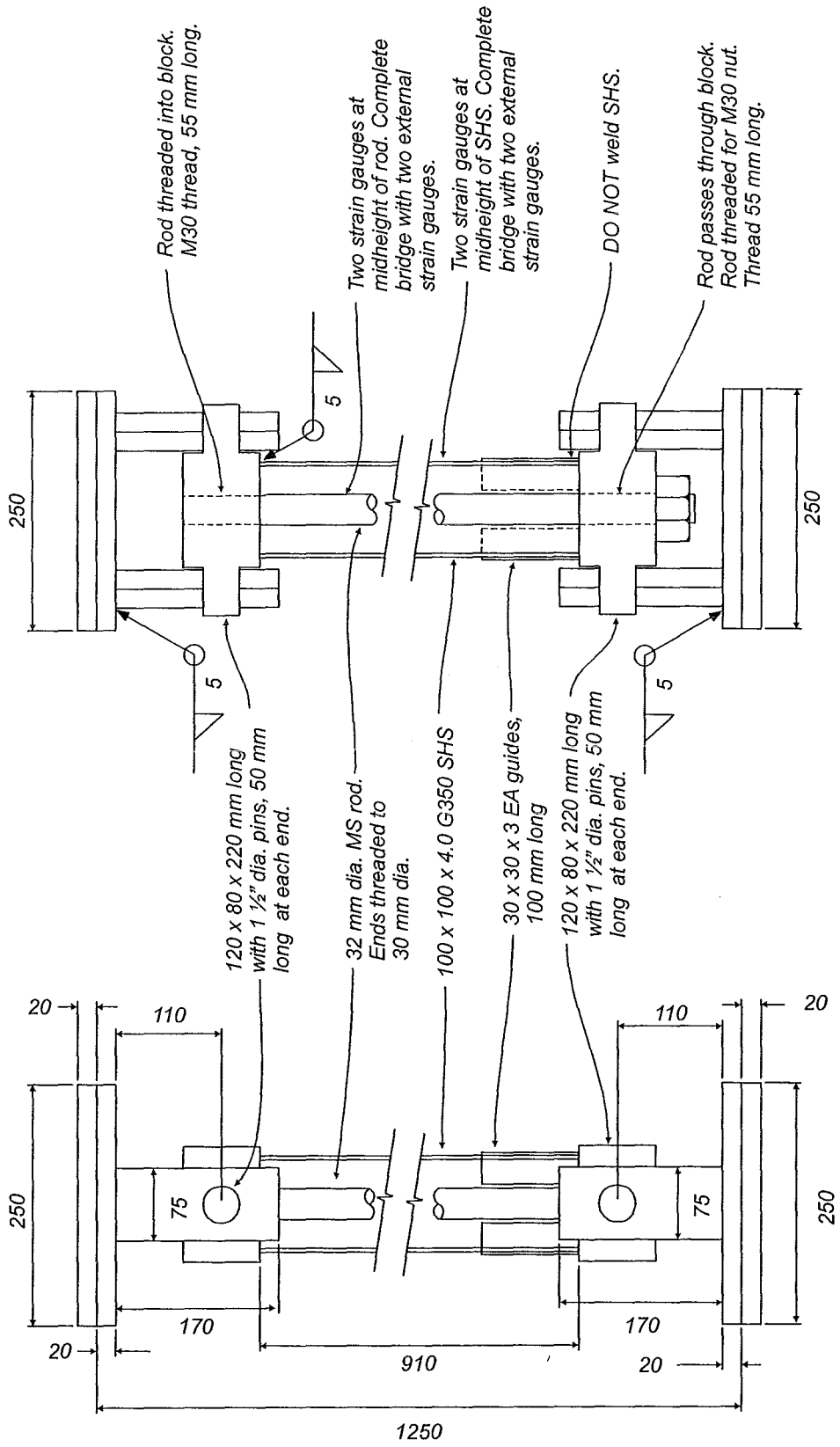

Unit I-B Vertical Springs
(12 required)

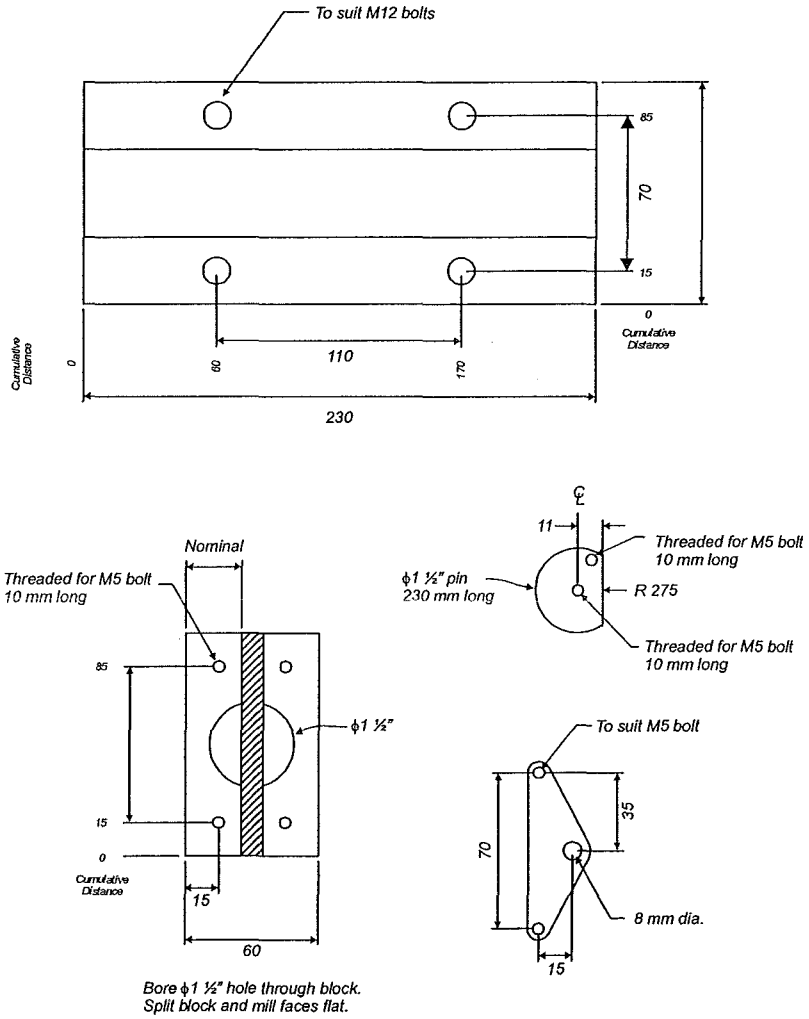

Roller Assembly for Lateral Springs
(Four required)

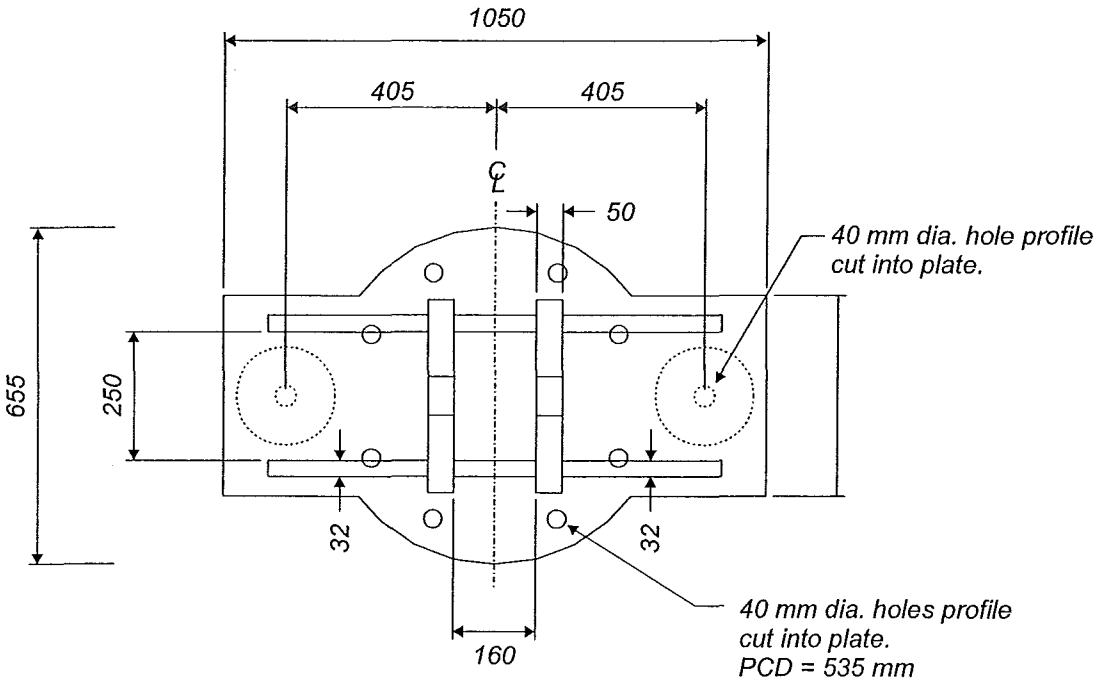

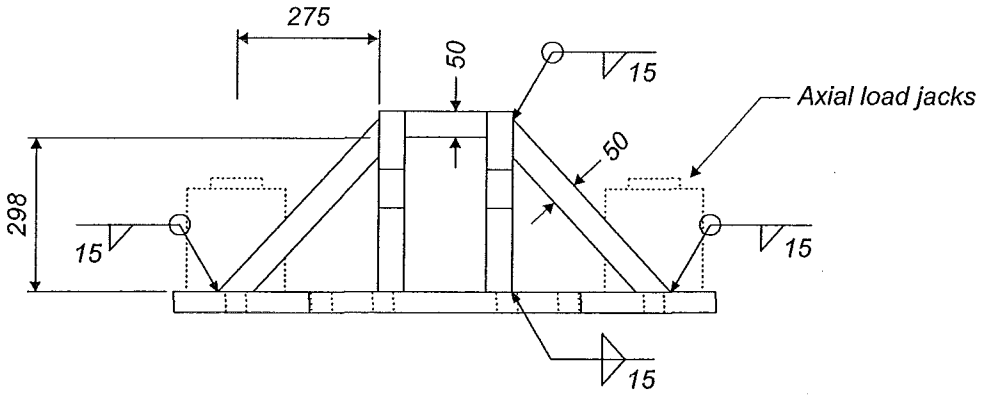

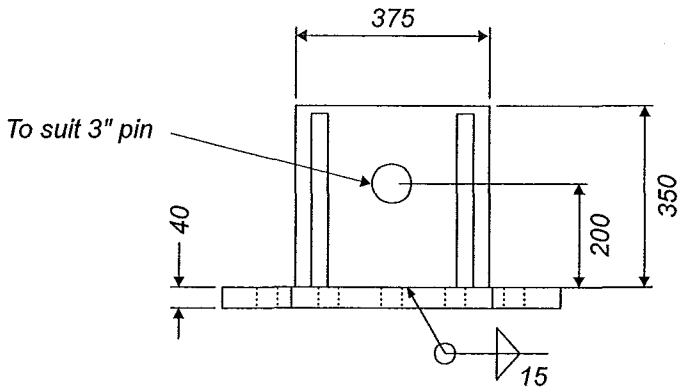

Fitting for top of column